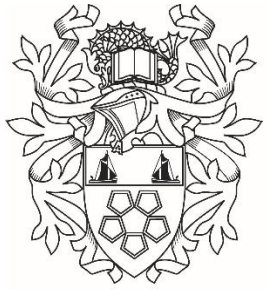

London South Bank University

EST 1892

# EXPERIMENTAL STUDY OF CHEMICAL ENHANCED OIL RECOVERY (CEOR) IN SANDSTONE CORE SAMPLES: EFFECT OF SALINITY AND DIVALENT CATIONS


**Maria Astrid Centeno Camino**

https://orcid.org/0000-0001-7237-9126


Thesis submitted in partial fulfilment of the requirements of London South Bank University for the degree of Doctor of Philosophy


School of Engineering, London South Bank University


July 2019

## DECLARATION OF AUTHORSHIP

I declare that the information presented in this document is based on the original work I have completed as result of my research.

# DEDICATION

I dedicate this thesis to my husband Jose Antonio and my children Jose Miguel and William Daniel. Thanks for all the support and apologize for the time and important activities I had to miss to complete this important project.

## ACKNOWLEDGEMENT

I would like to express my deep gratitude to London South Bank University for sponsoring my studies. A very special thanks to the director of my research Dr Pedro Diaz for his guidance and encouragement throughout this research project. A huge gratitude to Mr Steve Jones for his support on the assembling of experimental equipment and all his assistance during critical stages of this research. I also would like to take this opportunity to thank my colleagues at the division of Chemical and Petroleum Engineering who have supported, encouraged and guided me on the completion of this project.

I also would like to give a special acknowledge to all my acquaintance reservoir engineering specialists in my networking group and good friends who have made my learning journey in the speciality of reservoir engineering so pleasing. A special thanks to Dr Eduardo Manrique who provided me with an excellent introduction into the area of Enhanced Oil Recovery and screening methods. Also, for sharing his practical experience and for his donation of samples used in this research. I also acknowledge the support from Carmen Morataya, Carlos Rodriguez and Dr Anna Karin Axelsson with feedback and corrections.

I also would like to thank all the oil and gas companies that have contributed with donations of samples of materials and computer software I have used on this project, such as Maersk North Sea UK Limited, Nalco, SNF Floeger, Beijing Hengju, and Computer Modelling Group (CMG).

## ABSTRACT

Chemical Enhanced Oil Recovery (CEOR) is defined as the injection of chemical slugs into the reservoir with the object to increase the oil recovery factor (RF). Optimal combinations of chemicals, alkali (A), surfactant (S) and polymer (P) for an ASP CEOR have shown being an effective recovery method. However, due to high salinity and hardness (defined as the concentration of divalent cations $Ca^{2+}$ and $Mg^{2+}$) existing in the brine of some reservoirs, numerous and complicated physicochemical interactions such as adsorption, retention, and formation of emulsions are triggered.

This research project frames problems associated with the design of ASP CEOR for sandstone reservoirs under high salinity and hard brine. The fluid-fluid and fluid-rock interactions for the brine/oil, surfactant-brine/oil, alkali-surfactant-brine-oil, surfactant-polymer/oil, and alkali-surfactant-polymer/oil systems were evaluated at laboratory scale using Bentheimer sandstone core samples.

Results from the study were aiming to understand the various mechanisms that favour the oil displacement efficiency of the ASP CEOR processes in sandstone.

A sample of crude oil from the North Sea was used in this research and synthetic brines were prepared to reproduce the original brine composition. The first part of the research consisted of the study of the effect of brine salinity and hardness on the fluid-fluid and fluid-rock interactions for the brine/oil system.

Further studies were required on the microemulsion formation using different surfactant formulations with alcohol alkoxy -sulfate (APS), alcohol ethoxy sulfate (AES), and internal olefin sulfonate (IOS) surfactants for the system surfactant-brine/oil. The effect of sodium hydroxide and sodium metaborate on the microemulsion formation for alkali-surfactant-brine-oil system and interactions with polyacrylamide based polymers in surfactant-polymer/oil and alkali-surfactant-polymer/oil systems were also investigated.

Polymer viscosity exhibited shear thinning and Newtonian behaviour as a function of shear rate. The rheological behaviour was also associated with salinity, divalent cations, and the polymer size and structure in aqueous solution. These interactions were modelled adjusting experimental results to correlations proposed in the literature.

A comparative study of the displacement efficiency of waterflooding, P, AS, SP and ASP CEOR methods under a salinity gradient was completed to understand the different chemicals interactions.

It was found that the brine salinity and hardness affected the brine surface tension (ST) and the brine/oil interfacial tension (IFT). The brine ST and brine/oil IFT showed three well defined regions at different salinities. At low salinity (< 5,000 ppm TDS), the surface tension decreases with the salinity; between 5,000 ppm and 30,000 ppm TDS the ST and IFT slightly increase with salinity. In a third region the ST and IFT do not change with salinity exhibiting a plateau behaviour. Results from core-flooding tests showed that by creating a multicomponent salinity gradient that promotes the cationic exchange between divalent ($Ca^{2+}$ and $Mg^{2+}$) and monovalent ($Na^{+}$) ions, an additional 5% of oil recovery was obtained.

Alcohol alkoxy sulfate $C_{13-14}$—7APS surfactant promotes microemulsion formation and tolerate divalent cations $Ca^{2+}$ and $Mg^{2+}$ at salinity higher than 28,000 ppm and lower than 48,000 ppm. Alcohol ethoxy sulfate $C_{06-10}$-AES as co-surfactant moves the range of salinity for micoremulsion formation towards higher salinity (34,000 to 52,000 ppm) and enhance the stability of $C_{13-14}$—7APS surfactant. While salinity restricts the use of surfactant alcohol ethoxylated (AEO) due to instability and precipitation formation, the combination of this surfactant with surfactant alcohol alkoxy sulfate ($C_{13-14}$—7APS) increases its solubility and also promotes the microemulsion formation at salinity from 20,000 to 38,000 ppm.

Surfactants reduce the surfactant-brine/oil IFT to ultra-low values and increase the oil displacement efficiency by 15% compared with waterflooding. Surfactant absorption increases with its concentration and with salinity; this effect is increased for brine with divalent ions. Co-surfactant alcohol ethoxy sulfate $C_{06-10}$-AES reduces the adsorption of surfactant alcohol alkoxy sulfate $C_{13-14}$—7APS.

Divalent cations $Ca^{2+}$ and $Mg^{2+}$ react with alkali to form insoluble divalent hydroxides ($Ca(OH)_2$ and $Mg(OH)_2$); this effect limits the application of alkali for brines with divalent cations. However, the use of ethylene-diamine-tetracetic acid (EDTA) at controlled pH ≤ 9 prevents the precipitation of hydroxides by forming a complex between EDTA and divalent cations. The concentration of alkali should be controlled to reach a pH ≤ 9 in the formulation of alkali-surfactant slugs to prevent that a displacement reaction between the alkali in excess and divalent cations complexed with EDTA initiates. However, at pH ≤ 9 the formation of natural naphthenic surfactant from the oil is not favourable. The use of alkali-surfactant-brine increases the oil displacement efficiency by 12% compared with the use of surfactant.

High salinity also affects the interactions between polymers molecules in aqueous solution and reduces the viscosity of polymers; the effect is more marked by the presence of divalent cations. Polymers reduce the mobility of the displacing fluid and mobility ratio by permeability

reduction and viscosity augmentation. The effect is reflected in an increment of the displacement efficiency $E_D$.

Polymer CEOR increases the recovery factor by 25% for PHPA-6 and 16% for PHPAM-3. The addition of surfactants for SP CEOR adds 19% oil recovery in comparison with water flooding, whereas ASP CEOR adds 31% for blend of surfactant with sodium metaborate, and 33% for the blend of surfactant with sodium hydroxide/EDTA. The polymer HMPAM-3 is more effective in increasing the oil displacement efficiency than PHPA-6 polymer in formulations for SP and ASP CEOR.

The advantages of the synergy of ASP CEOR were demonstrated on the displacement efficiency with an increase up to 33% for ASP using NaOH and EDTA. Stoichiometry calculations are required to complete desired equilibrium reactions involved in the process and avoid hydroxide precipitation. While the mechanism of polymer flooding is associated with mobility ratio, it was demonstrated that the predominant effect of IFT on the displacement efficiency of SP and ASP systems for CEOR, which indicates the mechanism is dominated by the changes in the capillary number Nc.

It was found that the stability of chemicals is affected in a larger extent by the concentration of divalent ions $Ca^{2+}$ and $Mg^{2+}$ than by the total salinity. The surfactant stability in solution determines the optimal conditions for the microemulsion formation. Therefore, the selection of the surfactant formulation and controlling its stability are the main steps on the design of a successful ASP CEOR process.

This research presents a detailed study of the fluid-fluid and fluid-rock interactions that affect the design of SP and ASP CEOR at a microscopic scale. The results from the study provide a systematic analysis of standalone methods and the synergy of combined methods on a fluid-fluid–rock system. Henceforward, the range of applicability and conditions of CEOR at laboratory scale for oilfield applications can be established.

# TABLE OF CONTENTS

# LIST OF FIGURES

# LIST OF TABLES

# LIST OF NOMENCLATURE

| | |
|---|---|
| $E_o$ | Overall displacement efficiency (fraction) |
| $E_D$ | Displacement efficiency (fraction) |
| $E_V$ | Volumetric sweeping efficiency (fraction) |
| $E_A$ | Areal displacement (fraction) |
| $E_I$ | Vertical displacement (fraction) |
| Φ | Porosity (%, fraction) |
| Σ | Interfacial tension between the displaced and the displacing fluids (mN/m) |
| P | Density (gr/cm$^3$) |
| MW | Molecular weight (gr/mol) |
| *v* | Fluid velocity (cm/seg) |
| Q | Flow rate (cm$^3$/sec) |
| A | Cross-sectional area of the rock (cm$^2$) |
| $\mu p$ | Polymer viscosity (mPas) |
| $\mu_o$ | Oil viscosity (mPas) |
| $\mu_w$ | Water viscosity (mPas) |
| $\mu_{p0}$ | Zero shear polymer viscosity (mPa·s) |
| γ | Shear rate (1/sec) |
| $\gamma_{1/2}$ | Shear rate at which viscosity is the average of $\mu_w$ and $\mu_p^0$, (1/sec) |
| $\mu_p$ | Apparent polymer viscosity, Pa·s |
| $\mu_m$ | Microemulsion viscosity (mPas) |
| $\mu_s$ | Surfactant viscosity (mPas) |
| $C_{sep}$ | Effective salinity for polymer (eq/m$^3$) |
| $C_{11}$ | Water concentration in the aqueous phase, fraction |
| $C_{61}$ | Concentration of divalent cations in the aqueous phase, Eq/m$^3$ |
| $C_{51}$ | Concentration of anions in the aqueous phase, Eq/m$^3$ |
| Pα | Empirical parameter obtained by matching laboratory data |
| $R_k$ | Reduction factor for the aqueous phase due to polymer retention (fraction) |
| $R_f$ | Resistance factor (fraction) |
| λ | Fluid mobility |
| GOR | Gas Oil Ratio (scf/stb, m$^3$/m$^3$) |

| | |
|---|---|
| WOC | Water/Oil contact (cm) |
| BHP | Bottom Hole Pressure (Pa) |
| OOIP | Original oil in place (stb, $cm^3$) |
| IFT | Interfacial Tension (mN/m) |
| ST | Surface Tension (mN/m) |
| k | Absolute permeability (md) |
| $k_{ro}$ | Oil relative permeability (dimensionless) |
| $k_{rw}$ | Water relative permeability (dimensionless) |
| $k_w$ | Water effective permeability (mD) |
| $k_o$ | Oil effective permeability (mD) |
| $N_c$ | Capillary Number (dimensionless) |
| $N_T$ | Trapping Number (dimensionless) |
| $N_b$ | Bond Number (dimensionless) |
| Pc | Capillary pressure (Pa) |
| M | Mobility ratio (dimensionless) |
| $\theta$ | Contact angle between the wetting phase and the rock. |
| Pref | Reference pressure (psi) |
| RF | Recovery factor (%) |
| SG | Specific gravity of water= 1.0 |
| $f_w$ | Fraction of produced water or water cut (dimensionless) |
| L | Length of the rock sample (cm) |
| g | Gravitational acceleration ($cm/seg^2$) |
| $\Delta\rho$ | Difference on density between water and oil ($gr/cm^3$) |
| α | Formation dipping angle (degree) |
| $N_b$ | Bond number (dimensionless) |
| IPV | Inaccessible pore volume (fraction) |
| PV | Pore volume (fraction) |
| BV | Bulk volume ($cm^3$) |
| GV | Grain volume ($cm^3$) |
| $S_{or}$ | Residual oil saturation (%, fraction) |
| $S_{wc}$ | Connate water saturation (%, fraction) |
| $S_{wir}$ | Irreducible water saturation (%, fraction) |
| $\tau = \left({L_t}/{L}\right)^2$ | Ratio between the length of the capillary tube and the length of the representative elementary volume REV of the permeable medium. |

| | |
|---|---|
| Dp | Pore diameter. |
| dP/dL | Pressure gradient in the direction of the flow, (atm/cm). |
| L | Length of the rock sample (cm). |
| N | Number of components. |
| $D_{xx}$, $D_{yy}$, $D_{zz}$ | Components of dispersion in the directions x, y and z. |
| $C_i$ | Concentration of chemicals in the aqueous solution (gr/m$^3$). |
| $\overline{C_{is}}$ | Concentration of chemicals adsorbed on the rock surface (gr/m$^3$). |
| TAN | Total acidic number (mg KOH/gm oil) |
| CMC | Critical Micelle Concentration (% m/v) |
| CAC | Critical association concentration (% m/v) |

# LIST OF ABBREVIATIONS

| | |
|---|---|
| RF | Recovery Factor |
| REV | Representative elementary volume |
| RCA | Conventional or routine core analysis |
| SCAL | Special core analyses |
| IOS | Internal olefin sulfonate |
| APS | Alcohol propoxylated sulfate |
| AES | Alcohol etoxylated sulfate |
| ASP | Alkaline, surfactant and polymer |
| CDC | Capillary Desaturation Curve |
| EOR | Enhanced Oil Recovery |
| CEOR | Chemical Enhanced Oil Recovery |
| EDTA | Ethylenediaminetreataacetic acid |
| HEDTA | Hydroxyethylenediaminetetracetic acid |
| DTPA | Diethylenetriaminepentaacetic acid |
| PVT | Pressure, volume, temperature |
| HB | Hard Brine |
| SB | Soft Brine |
| Hardness | Concentration of divalent cations $Ca^{2+}$ and $Mg^{2+}$in the brine |
| Hard brine | Brine with divalent cations $Ca^{2+}$ and $Mg^{2+}$ |
| Soft Brine | Brine with only monovalent cations $Na^{+}$, $K^{+}$ |

# CHAPTER ONE: INTRODUCTION

## 1.1 Introduction

The production of oil is initially driven by the energy naturally existing in the reservoir rock (pressure) and this method of production is called primary recovery (Dake, 2001). However, after a period, the reservoir pressure declines and also oil production. At this stage, some methods called “secondary recovery methods” are used to supply additional energy to maintain the reservoir pressure and enhance fluid displacement. Common secondary recovery methods include injection of water (water flooding) or gas (gas flooding).

Water flooding is the most used recovery method by the industry because the high recovery factors that can be achieved compared to natural depletion (Craig, 1971; Dake, 2001). Besides, water resources are naturally available in the field location which makes the process economically attractive (Muggeridge *et al.*, 2014).

Water flooding is able to displace part of the oil left behind inside the rock making oilfield production rate economically viable for longer periods. Yet, water flooding can only displace some additional oil increasing recovery factors between 30 and 50% and a substantial amount is still left in the reservoir. The amount of oil remaining in the reservoir after primary and secondary production in mature oilfields has been reported to be about two third (~60%) of the original oil in place (OOIP) (Al-Mjeni *et al.*, 2010). For example, recovery factors reported for the North Sea are about 50% which are slightly higher than in the US with an average of 40% (Sandrea and Dharod, 2016).

Tertiary recovery methods such as Enhanced Oil Recovery (EOR) are required at that point to enhance the overall displacement efficiency. EOR, as defined by Lake (1989), is a way of improving oil recovery by the injection of materials not normally present in the reservoir. Depending on the fluid used for injection, a series of oil recovery methods have been classified. The use of tertiary methods can increase recovery factors between 50 to 70% (Muggeridge *et al.*, 2014; Kokal and Al-Kaabi, 2010). A summary of recovery methods is presented in Figure 1.1.

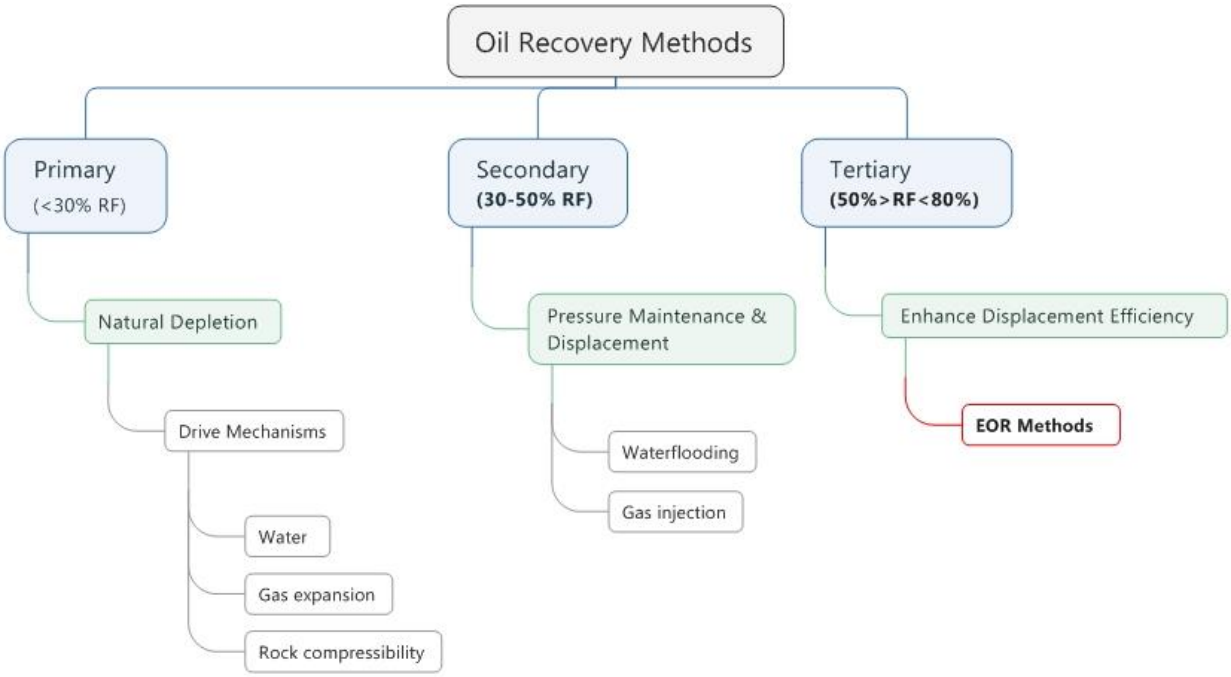


**Figure 1-1: Recovery Methods**
Adapted from (Thomas, 2008; Gurgel *et al.*, 2008)

EOR methods include thermal, gas injection, and chemical flooding methods within others (Thomas, 2008; Gurgel *et al.*, 2008). A schematic classification of EOR methods is shown in Figure 1.2. The effectiveness of EOR methods, in general, is based on creating favourable interactions on the fluid-fluid and fluid-rock systems to enhance the overall displacement of crude oil remaining in the reservoir aiming to increase the oil recovery factor.

With the current reduction of exploration projects and oil price, methods for production optimization directed to increase the recovery factor of existing mature reservoirs are in demand. EOR methods look like an excellent alternative to fulfil the current demand for hydrocarbon. As reported by the Oil and Gas Authority (OGA) for the EOR strategy for United Kingdom Continental Shelf (OGA, 2016), EOR methods will play an important role in the requirement to increase the recovery factor of those mature oilfields, making them more economically attractive and delay costly decommissioning processes.

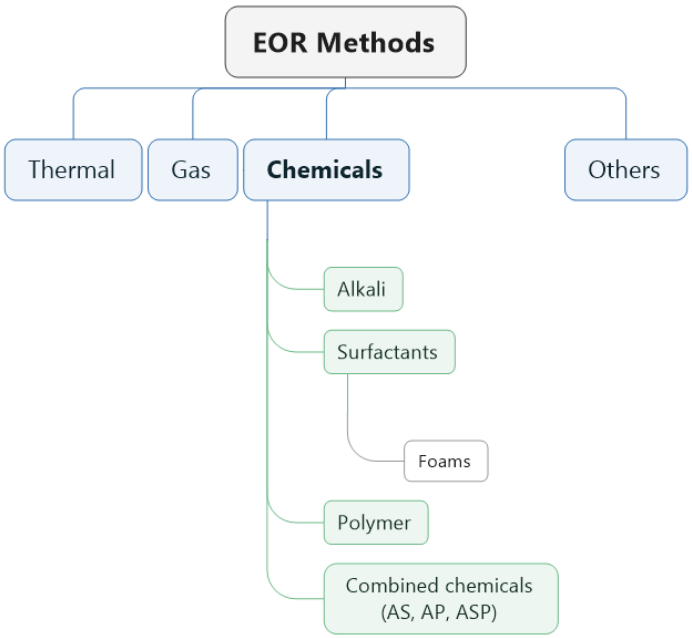


**Figure 1-2: Enhanced Oil Recovery Methods**
(Thomas, 2008; Gurgel *et al.*, 2008)

Chemical Enhanced Oil Recovery (CEOR) methods are defined as the injection of chemical slugs into the reservoir with the object to increase the oil recovery factor. These methods can consist on the addition of chemicals such as alkali (A), surfactant (S) and polymer (P) to the water used for injection. The use of CEOR methods is not new and date from 1927 when the ability of surfactant to reduce the interfacial tension between the oil and the reservoir rock was found (Sheng, 2010a). Review of publications on field applications of CEOR indicated the method, despite being relatively old, has the lowest number of applications and mainly in sandstone reservoirs (Manrique *et al.*, 2007; Sheng, 2013a), as showed in Figures 1.3 and 1.4.

CEOR methods can be applied as standalone method or as a combination of chemicals AS, AP or ASP. The larger number of reported applications and research for ASP and SP CEOR corresponds to China, with the development and application of surfactants and polymers to suit reservoir conditions of temperature and salinity (Sheng, 2013a).

CEOR methods have a high potential to increase oil recovery factors of existing mature reservoirs; yet the technology is not as well stablished as thermal and gas EOR methods. The mechanisms that favour the increase in oil recovery for CEOR processes are object of

increase research due to the complexity of the interactions that occurs, especially in conditions of high salinity and with concentration of divalent cations which are part of the composition of the water available for injection.

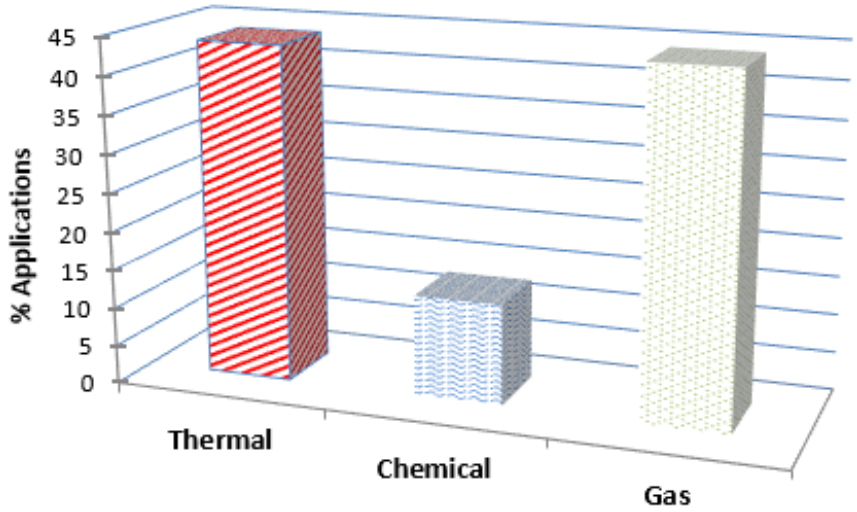


**Figure 1-3: Percentage of oilfield applications of EOR**
(data taken from Oil and Gas Statistic report, 2014)

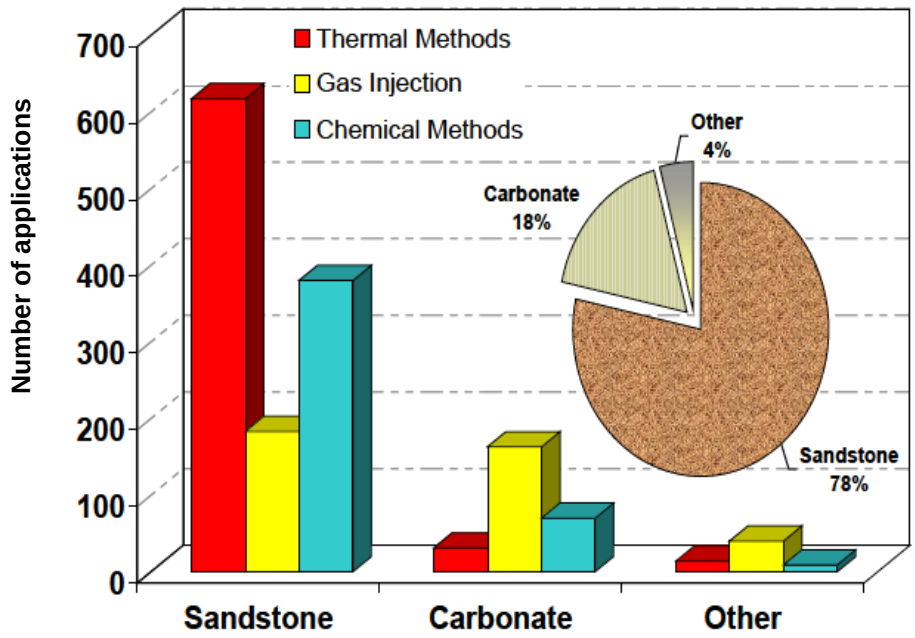


**Figure 1-4: Review of EOR applications**
(Manrique *et al.*, 2007)

The area of research presented in this report is CEOR, specifically using Alkali, Surfactant, and Polymer (ASP) under high salinity, and hardness given by the concentration of divalent cations as existing on a typical North Sea reservoir, as discussed below.

## 1.2 Background and statement of the problem

Alkaline-surfactant-polymer (ASP) is a method characterized by the synergy between these chemicals and the rock. The alkali has two functions, the first is the reduction of absorption of surfactant and polymer to the rock thus reducing chemical loss; and the second is the generation of in-situ natural surfactants (soaps) by reacting with naphthenic acids naturally present in the crude oil. The extent of the latter depends on the acidic number of the crude oil, which is indicated by the acidic number. A minimum acidic number of 0.3 mg KOH/gr crude oil is required for the formation of the natural surfactant. However, the amount of natural surfactant generated by the reaction of alkali during ASP processes is still uncertain as there are several equilibrium reactions involved with the use of alkali.

The functions of surfactants in ASP flooding are:

a) Reducing the interfacial tension (IFT) between oil and water.
b) Decreasing the capillary forces that keep the oil trapped inside the rock.
c) Changing the wettability of the rock in order to create an oil bank.

The polymer in APS flooding is used to modify the viscosity of the aqueous phase, thus reduce the movement of the displacing fluid (water), enhancing the displacement profile (Gregersen *et al.*, 2013). Another mechanism attributed to polymers is the “push and pull” effect of the oil trapped in the porous medium and this behaviour is related with the viscoelastic behaviour of polymers (Wang, J. and Dong, 2009).

The combination of the above mentioned effects enhances the sweeping efficiency of the injecting fluids and the displacement of discontinuous trapped crude oil remaining in the porous medium. Research published by Olson et al (1990) as referred by Sheng (2013) demonstrated higher increase in oil recovery using ASP than any chemical; alkali, surfactant or polymer, used separately. A summary of the ASP synergy is presented in Figure 1.5.

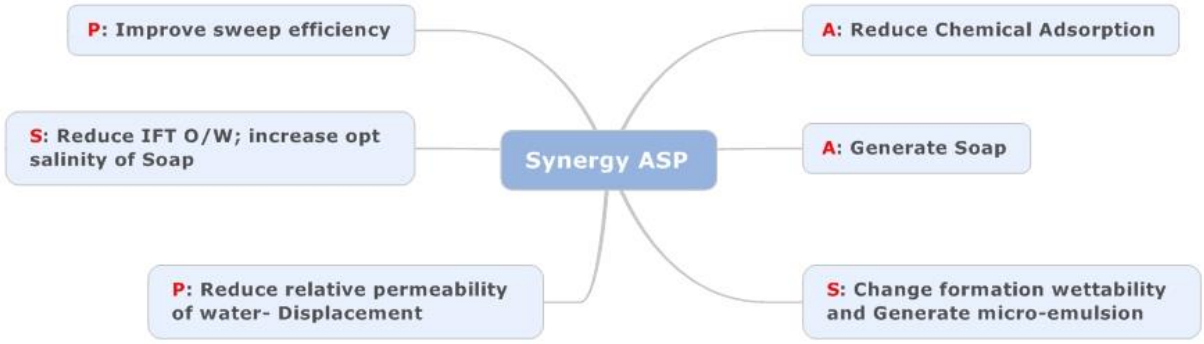


**Figure 1-5: Effect of ASP chemical EOR methods in the reservoir**
Adapted from (Gregersen *et al.*, 2013; Al-Mjeni *et al.*, 2010; Sheng, 2013a)

The effectiveness of ASP CEOR is highly affected by different parameters existing in the reservoir, such as temperature, oil viscosity, clay content, formation permeability, formation water salinity, and concentration of divalent cations among others (Sheng, 2010a; Sheng, 2013b; Olajire, 2014). Most of the applications of ASP CEOR reported the use of a pre-flush of low salinity and limitations on the concentration of divalent cations to avoid undesirable chemicals interactions (Muggeridge *et al.*, 2014). High salinity (given by the content of total dissolved solids (TDS)) and hardness in the brine used for injection cause several problems, such as chemical instability of the chemical slug, scaling and precipitation of insoluble hydroxide, and surfactants precipitation (Sheng, 2013b; Olajire, 2014). Brine salinity and hardness also affect the selection of the alkali used in ASP CEOR due to precipitation of insoluble hydroxides.

While the use of alkali in ASP flooding is reported as the main reason for many of the problems found for ASP applications; such as chemical dissolution, scaling, and precipitation; the use of alkali in ASP CEOR reduces chemical adsorption, thus chemical lost. The use of sequester agents may widen the range of applications for ASP CEOR to a reservoir with hard conditions; such as existing offshore. However, more study is required to evaluate the possibility to use production water with its original hardness for the preparation of the chemical slug. Besides, it seems to be important to find the right balance between the advantages of using ASP chemical flooding with the use of softened brine or use SP method, free of alkali.

The design of the chemical formulations for ASP CEOR requires the determination of the optimal salinity for microemulsion formation and ultra-low IFT between oil and brine. This optimal salinity is defined as the salinity where the surfactant is equally solubilized between the oil and aqueous phase and a three phase microemulsion is formed. The optimal salinity is usually lower than the salinity of the production water available for injection. Consequently, ASP applications normally require the use of desalination processes and/or softener additives for the preparation of the ASP chemical slugs which may not always be available in the place. These requirements have limited the use of ASP for offshore applications (Bataweel and Nasr-El-Din, 2012; Olajire, 2014).

Best practices for composition of water used for ASP flooding are not established yet; some research reported the total brine hardness limited to a maximal concentration of divalent cations ($Ca^{2+}$ and $Mg^{2+}$) of 10 ppm for offshore applications (Hernandez *et al.*, 2001), while Taber et al (1997) recommended a maximum of 1000 ppm and published executed ASP projects reported a maximum of 178 ppm (Sheng, 2013a). Most of the ASP projects have reported salinities of about 10,000 ppm TDS (Sheng, 2013a; Muggeridge *et al.*, 2014; Olajire, 2014).

Ongoing research on ASP chemical EOR has been focused on the development of chemicals, testing of novel surfactants or the design of slugs able to resist high salinity and concentration of divalent cations, and high temperature (Jamaloei, 2009; Flaaten *et al.*, 2010; Sharma *et al.*, 2015).

Previous research reports the use of chemicals to sequester divalent cations ($Ca^{2+}$ and $Mg^{2+}$) such as sodium metaborate (Flaaten *et al.*, 2008), ethylendiaminetetraacetic acid (Mahmoud and Abdelgawad, 2015) and sodium acrylate (Kalwar and Elraies, 2014) to prevent the precipitation of divalent hydroxides. These chemicals have been tested at a laboratory scale; however, there is not field application reported until now. Recently research by Mahmoud (2015) reported successful results with brine with concentration of divalent cations up to 600 ppm by using ethylenediaminetetraacetic acid (EDTA) as a sequester of $Ca^{2+}$ and $Mg^{2+}$. Bataweell (2011) also presented the successful use of a novel organic acid sodium salt of poly aspartic acid using seawater with 230,000 ppm (TDS) and formation connate water with a high content of divalent cation $Ca^{2+}$ at 29,700 ppm, results showed good solubility and low permeability loss when tested in sandstone core.

Salinity and brine hardness also affect requirements for surfactants for ASP CEOR in terms of the optimal conditions of microemulsion formation and ultra-low IFT. Anionic surfactants are more sensitive to divalent ions than monovalent ions at low surfactant concentrations (Nelson,

R., 1982). Most of the reported applications require the use of brine with divalent cations concentration limited to 1000 ppm (Sheng, 2015c). Requirements for surfactants to be more resistant to salinity and temperature have motivated more research on this area. The use of blends of surfactants type internal olefin sulfonate (IOS) with alcohol propoxylated sulfate (APS) or ethoxylated sulfates (AES) (Levitt, 2006; Liu et al., 2008; Hirasaki et al., 2011) is able to shift the optimal salinity of the system towards higher concentrations. However, divalent cations decrease optimal salinity for microemulsion formation and promote surfactant precipitation.

Polymers required for ASP CEOR are also subject of research as their stability under high salinity and hardness has been evaluated by Levitt et al (2011). Salinity affects the viscosity, the rheological behaviour and the viscoelasticity of polymeric solutions, and these effects are more prominent in the presence of divalent cations. Partially hydrolysed polyacrylamide polymer (PHPA) is the most common polymer used for ASP chemical flooding. Co-polymers and hydrophobically modified polymers have been developed for applications that involve high salinity (Olajire, 2014).

Synergy mechanisms in ASP chemical EOR have been widely studied considering brines containing mainly monovalent ions such as $Na^+$, $K^+$; and $Cl^-$ (Shen *et al.*, 2009; Arihara *et al.*, 1999), and the optimal conditions for the chemical slug considers the use of softened brine at optimal salinity conditions for microemulsion formation (usually lower than the salinity existing at reservoir conditions).

Successful ASP CEOR has been designed so that the surfactant is kept at optimal salinity conditions during the displacement process (Sheng, 2010a). However, more recently published research recognizes the effect of divalent anions and cations $Ca^{2+}$ and $Mg^{2+}$ existing on the connate formation water on the increase of oil recovery observed during low salinity flooding (Aghaeifar et al., 2018; Law et al., 2015; RezaeiDoust et al., 2010). Several mechanisms have been proposed, including multi-component ion exchange (MIE); and expansion of ionic double layer, among others (Khanamiri *et al.*, 2015; Strand *et al.*, 2016; Kakati and Sangwai, 2017).

It is apparent that the injection of a brine with low salinity, as required for the optimal salinity for microemulsion formation, can also affects the final recovery factor of ASP CEOR. Besides, the effect of the salinity gradient created between the existing reservoir salinity (connate water) and the injected preflush and the ASP slug at low salinity need to be evaluated for ASP CEOR.

These two aspects should be considered to evaluate whether or not a salinity gradient is beneficial for oil recovery.

Fluid-fluid and fluid-rocks interactions involved in ASP CEOR processes are complex and the drive mechanisms are still objected. The effect of divalent cations, high salinity and salinity gradient on the oil recovery of ASP CEOR still needs to be better elucidated to consider ionic interactions. This research is focused on the study of Chemical Flooding Enhanced Oil Recovery (CEOR) under high salinity and concentration of divalent cations as found offshore such as in the North Sea.

### 1.3 Rationale of the research

ASP CEOR involves different interactions between chemicals which make the process more effective as a recovery method. However, due to high salinity and hardness existing in some reservoirs, numerous and complicated physicochemical interactions such as adsorption, retention, and formation of emulsions, that are part of the mechanisms, are triggered.

Important research has been done on chemical flooding (Arihara *et al.*, 1999; Bataweel, 2011; Olajire, 2014; Shen *et al.*, 2009) however, the mechanisms in which reservoir properties such as wettability, capillary pressure in porous media are affected by salinity and the effect of divalent cations on ASP chemical flooding are still object of research. The use of softened water is a requirement for ASP CEOR, however the study of the physical-chemical interactions within the rock-oil-chemical fluid system are not completely elucidated yet, especially on aspects such as ionic interactions with the chemical slug, with the formation water under high salinity with monovalent and divalent cations $Ca^{2+}$ and $Mg^{2+}$ which are present in the reservoir.

### 1.4 Research questions

Despite the synergy of ASP chemical flooding offers higher recovery than any of the standalone chemical methods, the technology has not been extensively used yet. There are still problems and limitations that have emerged from fluid-fluid and fluid-rock interactions, which need to be elucidated, to understand the following aspects:

- How optimal conditions for chemicals used for CEOR are affected by the existing brine salinity and hardness given by divalent cations?
- How the composition of the brine affects the design of ASP CEOR?
- What is the performance of ASP versus SP for high salinity and concentration of divalent cations?

## 1.5 Aims and Objectives of the research

The research project aims to study the mechanisms and fluid-fluid and fluid-rock interactions of ASP CEOR under high salinity and concentration of divalent cations $Ca^{2+}$ and $Mg^{2+}$ (hardness) experimentally for a homogenous sandstone reservoir.

The objectives of the research are the study of the following aspects:

- The effect of high salinity and hardness on ASP chemical EOR processes for sandstone reservoirs.
- The stability of fluid systems under high salinity and with divalent cations.
- The optimal conditions of microemulsion formation.
- The rheological behaviour of acrylamide based polymers.
- The effect of sequester agents for divalent cations on the optimal conditions of ASP systems.
- The oil displacement efficiency of SP and ASP in Bentheimer sandstone rocks using core flooding tests.

## 1.6 Deliverables and Outcomes

The research proposes a systematic method to evaluate the mechanisms for CEOR processes using alkali (A), surfactant (S), and polymer (P). The study of the fluid-fluid and fluid-rock interactions and their effect on the design of SP and ASP CEOR at the microscopic scale is analysed considering the effect of salinity and divalent cations. The proposed systematic analysis identifies the range of applicability and conditions of salinity and divalent cations for CEOR at laboratory scale for oilfield applications.

## 1.7 Limitations of the research

For this study reservoir conditions of temperature similar to an offshore, sandstone reservoir, with a medium-heavy crude oil (21 ºAPI) and with a high acidic number and reservoir temperature of 60 ºC (140 ºF) were used. The study case considered a homogenous reservoir, represented by Bentheimer sandstone core samples. Core flooding tests at a laboratory scale were used to evaluate the microscopic displacement efficiency of CEOR. The effect of reservoir heterogeneities and high temperature on the behaviour of chemicals at a macroscopic scale are not part of this study.

## 1.8 Outline of chapters

This report has been organized in different chapters, following a sequence of a research project. In this chapter one, the introduction of the area of the research CEOR has been presented; including the background of CEOR and statement of the problem object of this research, the rationale, and research questions, expected deliverables and objectives.

Chapter two frames CEOR and discusses fundamentals principles of displacement efficiency and associated mechanisms that favor CEOR processes. Moreover, technical fundamentals and problems encountered for the design of the different methods alkali (A) flooding, surfactant (S) flooding, polymer (P) flooding, SP and ASP CEOR are also studied, with an emphasis in environments of brine with high salinity and hardness.

In chapter three, the materials and methods used to complete the research have been presented and explained in detail. Due to the complexity of the interactions in the ASP system for CEOR processes under salinity and divalent cations, the strategy used was to study the different fluid-fluid and fluid-rock interactions for each chemical system as standalone method with brine and oil, and then integrated as alkali-surfactant (AS), surfactant -polymer (SP) and alkali-surfactant-polymer (ASP).

Chapter four presents the methodology and results of the study of the effect of brine salinity and hardness on the displacement efficiency with water injection. This part of the study is aiming to capture the effect of brine salinity and hardness in the injected brine on the oil recovery factor of water flooding.

Chapter five focusses on the study of the behaviour of surfactants and the conditions for microemulsion (ME) formation, the effect of brine salinity and hardness on the conditions for ME, and the effect of interactions of surfactants with alkali in the oil displacement efficiency.

Chapter 6 emphasises on study of the behaviour of polymers and co-polymers acrylamide type, recommended for application at high salinity, and the effect of interactions within A-S for S-P and A-S-P on the oil displacement efficiency. Besides, relative permeability curves and oil displacement efficiency obtained by history match core-flooding tests with a laboratory-scale simulation model are compared.

Chapter seven presents the conclusions and recommendations product of this research, and finally in chapter eight a list of references used to support this work is presented.

# CHAPTER TWO: LITERATURE REVIEW

## 2.1 Introduction

This chapter presents a review of the research publications on the principles and mechanisms of CEOR using alkali, surfactant, and polymer, with emphasis on the effect of brine salinity and the hardness given by the concentration of divalent cations ($Ca^{2+}$ and $Mg^{2+}$). The mechanisms of alkali, surfactant, and polymer as standalone methods are studied, to frame all the aspects that need to be considered for the design of the chemical slug, the issues associated with high salinity and divalent cations and the variables controlling the process to the ASP CEOR system.

Enhanced oil recovery (EOR) methods involve the use of components or materials that are not originally present in the reservoir (Lake, 1989). The main objective of EOR is to increase the recovery factor to values above the obtained by primary recovery thus depletion and secondary methods, such as water flooding. EOR methods include several processes such as the injection of miscible gas, water alternating gas; liquids, steam, combustion, etc.

To increase the recovery factor, EOR methods must increase the overall displacement efficiency $\mathrm{E_o}$, which is defined as the amount of movable oil that has been recovered from the swept zone at any given time. $\mathrm{E_o}$ is the product of the displacement efficiency ($E_D$) at a microscopic or porous level and the volumetric sweeping efficiency ($E_V$) at the macroscopic or reservoir level (equation 2-1).

$$E_o = E_D x E_V \tag{2-1}$$

$\mathrm{E_D}$ describes the mobilization of oil from the porous media at pore scale; it measures the effectiveness of the displacing fluid to mobilize oil trapped in the porous medium, reducing the initial oil saturation ( $S_{oi}$) to the residual oil saturation ($S_{or}$) (Olajire, 2014), (equation 2-2).

$$E_D = \frac{S_{oi} - S_{or}}{S_{oi}} \tag{2-2}$$

$E_D$ depends on several variables such as temperature, pressure, time, PVT properties of the oil, saturation and relative permeability of fluids in the reservoir, interfacial tension, rock properties, wettability of the rock and capillary pressure, as is summarized in Figure 2-1 (Olajire, 2014; Liu, 2008).

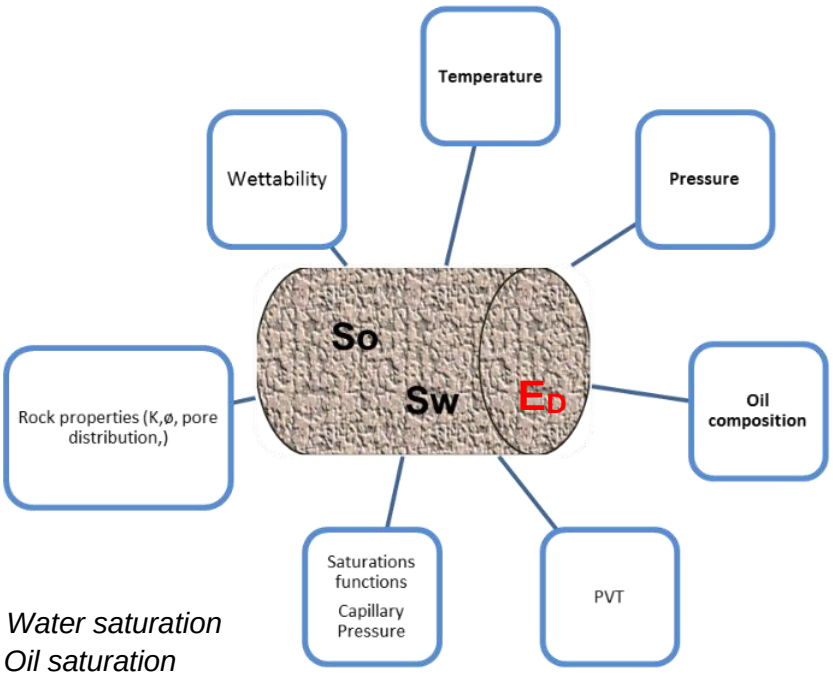


**Figure 2-1: Variables that affect microscopic displacement efficiency $E_D$**
(Liu, 2008)

The macroscopic displacement or sweeping efficiency $E_V$ represents the volumetric displacement and it measures the grade of effectiveness of displacing fluid to sweep the oil towards the production wells. $E_V$ is affected by the areal $E_A$ and the vertical $E_I$ displacement (equation 2-2) . A schematic representation of the areal and vertical swept zones for the calculation of displacement volume is represented in Figure 2-2.

$$E_V = E_A \times E_I \tag{2-3}$$

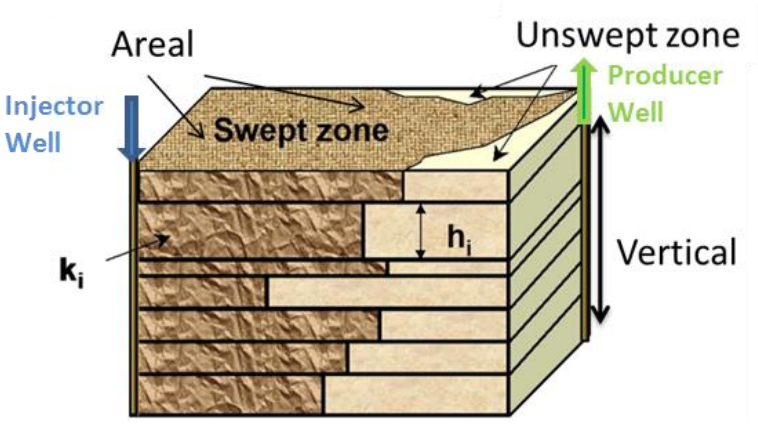


**Figure 2-2: Schematic representation of arear and vertical swept zones of a section of a Reservoir**
(Bataweel, 2011)

$E_A$ is the relationship between the swept area and the total reservoir area; whereas $E_v$ is the relationship between the porous volume displaced by the injected fluid and the total porous space between injector and producer wells, including all layers. It is understandable that $E_V$ is affected by reservoir aspects such as layering, geology heterogeneities and fluid properties such as viscosity and density which are linked to mobility ratio between displaced and displacing fluids, and flow patterns between injector and producer well.

The use of EOR increases the complexity of the fluid flow behaviour in the porous media, hence the mathematical representation of the process as additional physical-chemical interactions need to be considered. Mechanisms for EOR methods are complex and usually involve modifications on pressure gradient, interfacial tension, and wettability of the rock, fluids mobility and rock permeability between others (Muggeridge *et al.*, 2014).

## 2.2 Chemical enhanced oil recovery (CEOR)

CEOR is the injection of a pre-designed chemical slug or solution into the reservoir aiming to increase the oil recovery factor after the field has been in production by water flooding. Both effects, microscopic and macroscopic displacement, need to be achieved to optimize a CEOR method (Muggeridge *et al.*, 2014). The effectiveness of CEOR is mainly attributed to a combination of effects:

- Reduction of the interfacial tension (IFT) between the displaced fluid (oil) and displacing fluid (water).
- Consecutive change of the different interactions between fluids-rock, affecting the wettability of the rock thus oil distribution in the porous space.
- Enhancement of the displacement profile of discontinuous trapped crude oil that remains in the porous medium by affecting the mobility ratio between displacing and displaced fluid.

The chemical slug used for CEOR can be composed by a single or a combination of chemical compounds, such as alkali, surfactant, and polymer. According to the type of chemicals in the chemical slug, the process can be classified as alkali (A) or caustic flooding, alkali-surfactant (AS) or micellar flooding, surfactant-polymer (SP) or micellar/polymer, or alkali-surfactant-polymer (ASP).

ASP CEOR method can improve the recovery factor by the combined effect of different chemicals, improving both microscopic and macroscopic efficiencies. The first one is achieved by the reduction of the interfacial tension (IFT) between water and oil and, the later one is attained by adding polymer to match water and oil mobility during fluid displacement.

CEOR is not new, some studies dated before 1980 (Chang, 2013; Hirasaki et al., 1983; Mayer et al., 1983) reporting research and applications of alkali, surfactant flooding and combinations with polymer flooding. Afterward, with the findings of the advantages of combinations between alkali and surfactant, and the benefit of adding polymer to improve displacement efficiency, the process was transformed to alkaline, surfactant, and polymer (ASP) flooding process (Hirasaki et al., 2011).

CEOR has been classified as a promising technology that will increase applications in the future based on successful experiences and better understanding gained from China applications (Manrique et al., 2010; Wang, F. et al., 2017)

. Furthermore, the UK OGA government report for the EOR strategy (OGA, 2016), indicates that the activity of chemical flooding EOR will play a crucial role in maximising economic recovery from the UKCS, extending the productive life of oilfields and deferring expensive decommissioning processes.

The number of published CEOR field applications (based on the review of 148 publications), separated by the different methods, is presented in Figure 2-3. According to that distribution, polymer flooding has a higher number of applications 51% and is considered as a well-known technology (Manrique et al, 2010; Kan et al, 2014; Romero-Zeron, 2012). Alkali- surfactant-polymer (APS) presents 18% of the applications followed by alkali with 13%. Surfactant and alkali-surfactant (AS) as a standalone method have barely been used.

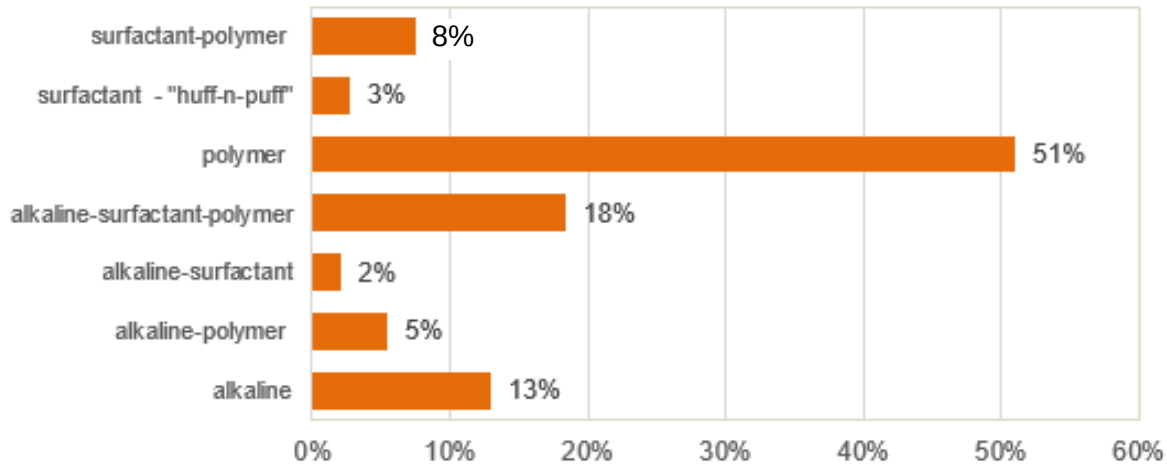


**Figure 2-3: Percentage distribution of CEOR field applications out of published papers of each CEOR method**
(Based on a review of 148 field applications 1983-2017)

Combined methods ASP and SP CEOR processes have not been extensively applied (18% and 8% respectively in figure 2-3). The technology is still under research aiming to understand the mechanisms that favour one or another method to optimize oil recovery.

For a CEOR project to be applied in the field, an exhaustive study and preliminary evaluation are required. Such a study involves several defined stages, where an example of stages is presented in Figure 2-4 (Kaminsky *et al.*, 2007). The first stage comprises a screening process to define whether CEOR or any other EOR method applies to the reservoir according to different conditions. In this respect, several variables have been considered for the screening of CEOR processes and have been published by different researchers (Taber *et al.*, 1997a; Taber *et al.*, 1997b; Alvarado and Manrique, 2010).

However, the number of variables studied has changed in the last years as a result of experience from field applications and laboratory studies. While only nine parameters were suggested by Taber et al. (1997) as enough to select an EOR method; later publications (Gharbi, 2000) included six more parameters such as connate water saturation and salinity, crude oil acidic number and swelling properties, and dipping angle of layers in the reservoir. Nowadays, there are still discussions about the required screening parameters for the stages; however, most of them consider the variables proposed by Taber (1997).

Screening criteria reported in the literature for CEOR applications based on the oil and reservoir properties are summarized on table 2-1 (Sheng, 2013a; Taber *et al.*, 1997b; Taber *et al.*, 1997a; Lake, 1989; Al-Bahar *et al.*, 2004; Saboorian-Jooybari *et al.*, 2015). It can be noticed that CEOR has mains applications on sandstone reservoirs. There is no clear limitation on the range of oil gravity, as there are applications from heavy to medium crude oil for polymer CEOR, while for applications of SP and ASP oil gravity needs to be higher than 20 $^{o}$API. Permeability range is another variable; however, most of the applications reported permeability values higher than 50 millidarcys. There is a threshold on brine salinity and hardness of 200,000 ppm and 1,000 ppm respectively, for temperatures up to 140 $^{o}$F. These limits decrease with the increase of temperature. An average of maximal temperature for all applications was about 200 $^{o}$F. Polymer flooding is the most applied process under different reservoir conditions and has expanded the range of conditions of heavy oil reservoirs summarized by Saboorian-Jooybari et al. (2015).

The second phase in a typical EOR process (step 2 in Figure 2-4) is crucial to evaluate in-depth the selected method to use (Kaminsky *et al.*, 2007). This stage requires laboratory studies to design the chemical formulation, the optimal salinity conditions for microemulsion

formation and, optimize displacement mechanisms of CEOR using core-flooding tests and simulation modelling. Important considerations and possible problems to look at this stage are the stability of the different systems; especially when mixing with the existing fluids in the reservoir; temperature dependence, chemical properties required for the slug, and displacement efficiency in terms of oil recovery factor.

Step 3 involves a pilot test of the chosen CEOR method in a well to evaluate the effectiveness of the system and identify possible problems or uncertainties identified in the previous stage. In the last stage, step four is the plan and implementation of the recovery method in the whole field.

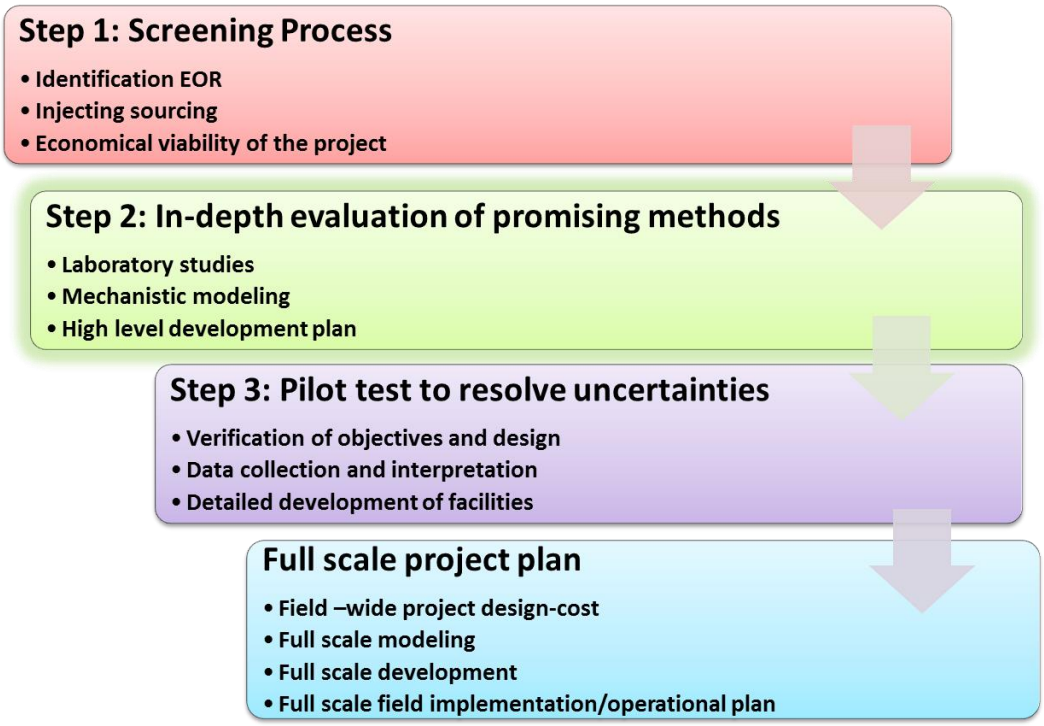


**Figure 2-4: Phases for an EOR project**
(Kaminsky *et al.*, 2007)

## Table 2-1: Screening criteria for Chemical EOR

(Taber *et al.*, 1997b; Lake, 1989; Al-Bahar *et al.*, 2004; Al Adasani and Bai, 2011; Sheng, 2013a; Saboorian-Jooybari *et al.*, 2015; Dickson *et al.*, 2010)

| Method | Oil Properties | | | Reservoir Properties | | | | |
|---|---|---|---|---|---|---|---|---|
| | Gravity ºAPI | Viscosity (cp) | Soil (%PV) | Form Type | Average Perm (mD) | Depth | Temp (ºF) | Salinity (TDS) ($Cl^-$) [Divalent cations] (ppm) |
| **Taber et al (1983) and Lake et al (1989)** | | | | | | | | |
| **Alkali** | 13 -35 | <200 | >35 | Sandstone | >20 | <9000 | 200 | < 20,000 [< 500] |
| **SP** | >25 | <30 | >30 | Sandstone | >20 | <8000 | <175 | |
| **Polymer** | >25 | <150 | >10 | Sand/Carb | >10 | <9000 | <200 | |
| **ASP** | | <200 | | | | | | |
| **Taber et al (1997)** | | | | | | | | |
| **Alkaline** | >20 | <35 | >35 | Sandstone | >10 | <9000 | <200 | <20,000 [<500] |
| **SP** | >20 | <35 | >35 | Sandstone | >10 | <9000 | <200 | <20,000 [<500] |
| **Polymer** | >15 | 10-150 | >50 | Sandstone | >10 | <9000 | <200 | |
| **APS** | >20 | <35 | >35 | Sandstone | >10 | <9000 | <200 | <20,000 [<500] |
| **Al-Bahar et al (2004)** | | | | | | | | |
| **Alkali** | | <150 | | Sandstone | >50 | <9000 | <158 | 50,000 [<1000] |
| **SP** | | <150 | >35 | | >50 | | <158 | <50,000 [<1000] |
| **AP** | 35 | <150 | >50 | Sandstone | >50 | | <158 | |
| **Polymer** | | <150 | >60 | | >50 | | <158 | 100,000 [<1000] |
| **APS** | 35 | <150 | >35 | Sandstone | >50 | | <158 | <50,000 [<1000] |
| **Dickson et al (2010)** | | | | | | | | |
| **Polymer** | >15 | <1000 | >30 | | >100 if (10<μ<100) >1000 if (100<μ<1000) | 800-9000 | <170 | <3000 if (10<μ<100) <1000 if (100<μ<1000) |
| **ASP** | >20 | <35 | >45 | Sandstone | >100 | 500-9000 | <200 | <200,000 if T<140 F <50,000 if T>140 F |
| **Adasani et al(2011)** | | | | | | | | |
| **S +P/A** | 31.75 | <16 | >44 | Sandstone | 57 | 625-5300 | 155-122 | |
| **ASP** | 23-34 | 11-6,500 | 68-75 | Sandstone | 596-1520 | 2985-3900 | 118-158 | |
| **Polymer** | 13-42.5 | >4000 | 34-82 | Sandstone | 5500 | >9460 | 167 | |
| **Sheng (2013)** | | | | | | | | |
| **ASP projects** | | 12.9 | 30 | Sandstone | 473 | | <126 | 7993 [178] |
| **ASP new** | | <50 | 30 | Sandstone | >50 | | <203 | <50,000 |
| **Saboorian et al (2015)** | | | | | | | | |
| **Polymer** | >11 | <5,400 | >50 | Sandstone | >1,000 | <5250 | <149 | <46,000 |

Most of the difficulties reported for CEOR are related to high salinity and divalent cations (Sheng, 2014a; Sheng, 2013a). Reported problems include chemical instability of the chemical slug, scaling and precipitation of insoluble hydroxide, and surfactant precipitation (Sheng, 2013a; Sheng, 2014a; Olajire, 2014). These problems have limited the application of CEOR technology, especially offshore (Muggeridge *et al.*, 2014).

From the analysed information, it can be seen that ASP CEOR is complex and is a technology on developmental stages. Additional studies are still required to overcome limitations found in applications where for example high salinity and divalent cations are present. This research is mainly focused on the deep evaluation of ASP chemical flooding (step 2, Figure 2-4).

### 2.3 Mechanisms involved in CEOR methods

During the CEOR process, the chemical slug designed based on laboratory studies and mechanistic modelling, is injected into the reservoir through the injector well. Figure 2-5 shows a schematic representation for CEOR flooding. The injection of the chemical slug containing surfactants reduces the interfacial tension between oil and water producing more oil. The injection of polymers modifies the viscosity of the displacing fluid which provides mobility control to the interfaces, reducing fingering effect and achieving piston-like displacement, which will lead to a better sweep efficiency (Kotlar *et al.*, 2007).

The main mechanisms reported for CEOR are the reduction of the interfacial tension IFT between oil and water and the increase of viscosity of the displacing fluid (Al-Mjeni *et al.*, 2010; Sheng, 2010a). During the injection of the chemical slug, properties such as interfacial tension, mobility, viscosity, wettability, and oil composition (swelling) among other properties, can be altered (Al-Mjeni *et al.*, 2010).

The sequence of injecting fluids normally includes the use of a pre-flush slug or scavenger with salinity close to the optimal salinity for microemulsion formation, followed by the chemical slug and finally displacement with water flooding (Zerpa *et al.*, 2005). As a result, an oil bank will be developed ahead of the displacing chemical slug. This oil bank will be eventually displaced either by additional post flush of chemicals or by water flooding injected behind the chemical slug.

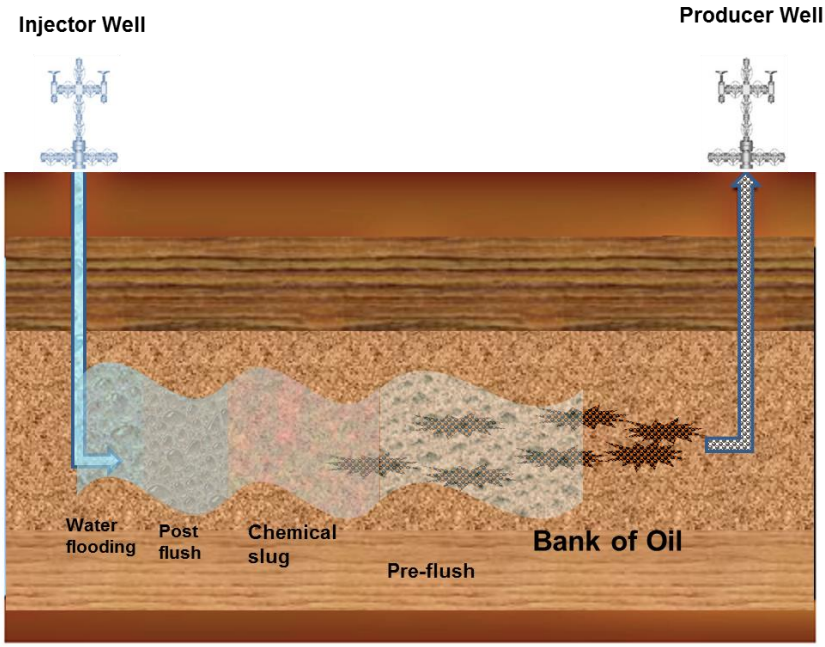


**Figure 2-5: Schematic representation of CEOR process**
Adapted from (Zerpa *et al.*, 2005)

The nature of the CEOR process promotes different interactions between fluids with different compositions, different phases (oil, aqueous, microemulsion), and between fluids and the rock surface. A summary of the performance, issues, and challenges of CEOR methods is presented in table 2-2. Larger incremental oil recovery has been obtained with ASP CEOR compared to standalone methods. Alkali based methods are not preferred in carbonate type reservoirs, as there are many problems with dissolution and precipitation. All CEOR processes are affected by high salinity and divalent cations. Common issues are high chemical adsorption, retention, and precipitation of insoluble divalent salts and hydroxides.

The mechanisms presented in table 2-2 are still under research due to the complexity of the reservoirs, the variety of crude oils, and location conditions, and the amount of chemicals available for applications. In the following section, a review of the relevant aspects and properties associated with each of the mechanisms will be presented.

**Table 2-2: Summary of chemical EOR methods**
(Taber *et al.*, 1997b; Sheng, 2013a; Muggeridge *et al.*, 2014)

| Method | Mechanism | Effect | Issues | Typical incremental oil recovery |
|---|---|---|---|---|
| **Alkali** | React with crude oil to generate Natural surfactant<br>Adsorb on rock surface | - Reduce IFT<br>- Reduce surfactant loss<br>- Modify wettability | Anhydrite, gypsum ($CaSO_4$) or clay are unwanted Precipitation with divalent cations, critical in carbonate rocks | 5-10% |
| **Surfactant** | Interact with oil and water at the surface and form micelles | -Reduce IFT<br>-Modify wettability | Chemical retention<br>High salinity | --- |
| **Polymer** | Increases displacing fluid viscosity<br>Modify relative permeability | -Mobility reduction<br>-Improve sweeping efficiency | -Injectivity stability<br>-Effect of high salinity<br>-Degradation | 5-11.6% |
| **Surfactant /Polymer** | Combine surfactant and polymer effects | | Same as Polymer and Surfactant | 15% |
| **Alkali/Polymer** | Combine Alkali and Polymer effect | | Same as alkali and Polymer | 5% |
| **ASP** | Synergetic effect of Alkali, surfactant and Polymer | | Same as Alkali, Surfactant and Polymer | 21.8 % |

From these results is evident that the synergetic effect of chemical alkali, surfactant, and polymer in ASP CEOR increases the oil recovery factor compared with standalone methods. However, ASP CEOR has not been extensively applied due to problems associated with complex interactions and undesirable precipitation related to high salinity and divalent cations.

## 2.4 Reservoir properties and principles associated with flow in the porous medium

To understand the principles and mechanisms associated with CEOR, and the effect of brine salinity and hardness, it is important to review the principles that govern the distribution and movement of fluids in the porous medium and their relevance on CEOR methods.

The amount and distribution of oil remaining trapped inside the pore structure is affected by a balance between gravity, viscosity and capillary forces (Karpan *et al.*, 2011; Olajire, 2014). Resultant gravity forces are present in the reservoir due to the difference in density between

the existing fluids in the porous media and these forces are more important as the density difference is larger.

Viscosity forces govern the behaviour of the fluid flow in the porous media and pressure drop profile obtained by Darcy's Law (Lake, 1989). The more viscous the fluid, the higher the viscous forces are. Capillary forces determine how fluids are distributed on the porous space, and their interfacial tension; they are also affected by the pore structure and interactions fluid-fluid and fluid-rock.

A crucial part of reservoir studies is gathering reliable reservoir data such as permeability, porosity, and capillary pressure to characterize the reservoir and distribution of fluids on the porous media. Typically, this data is obtained from well-logging and core analysis.

Core-analyses are defined by the integration of field and production data (Unalmiser and Funk, 1998). Conventional or routine core analysis (RCA) in the laboratory includes: core handling, sampling, cleaning process, and measurements of porosity, permeability and fluids saturation among others, while wettability, interfacial tension, capillary pressure, relative permeability, and chemical flooding tests are classified as special core analyses (SCAL) (Keelan, 1972).

In the following sections, parameters controlling the fluid displacement efficiency in porous media (Figure 2-6) will be defined and discussed with special attention to the effect of salinity and divalent cations.

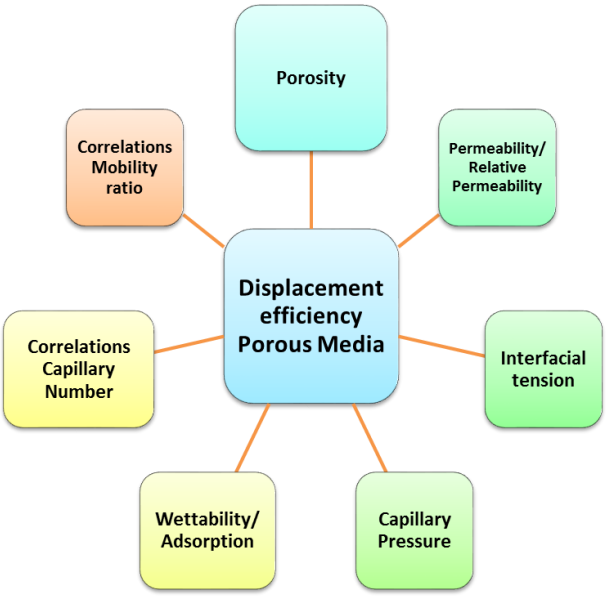


**Figure 2-6: Parameters that affect the displacement efficiency of Chemical EOR**

### 2.4.1 Porosity

Reservoir porosity (ø) represents the capacity of the rock to store fluids; it is a measure of the fraction of void space in a rock or reservoir (Nimmo, 2004; Lake, 1989) and it can be calculated as the ratio of the pore space volume (PV) to the bulk volume (BV) of the rock (equation 2-4). The reservoir porosity is crucial in the calculation of the initial oil in place OOIP in a reservoir (American Petroleum Institute, 1998). Porosity can be measured in the laboratory by different methods: Measurements of bulk volume (BV), grain volume (GV), direct measurement of pore volume (PV) between others. Depending on the method used, porosity can be calculated using the following equations:

$$\text{Porosity } (ø) = PV/BV \tag{2-4}$$

$$PV = (BV-GV) \tag{2-5}$$

$$\text{Porosity } (ø) = PV/(PV+GV) \tag{2-6}$$

$$\text{Porosity } (ø) = (BV-GV)/BV \tag{2-7}$$

There are two types of porosities determined in a rock**,** total porosity which is the measured value of the total void space (connected and isolated) in a rock sample, and effective porosity which is the measurement of the connected voids in the pore space and can be calculated as total porosity minus the porous volume occupied by shale or clay. Both, total and effective porosity are the same for clean sands. While porosity is not part of the screening for EOR methods; pore size distribution and effective porosity affect properties such as capillary pressure and permeability.

CEOR methods have been mainly applied to sandstones; in a range of porosity from 13 to 39% (Al Adasani and Bai, 2011). It is well known the permeability increases and capillary pressure decreases with increasing pore size (Lake, 1989).

Effective porosity and pore size distribution affect the grade of inaccessible pore volume (IPV)**,** which is a variable relevant to CEOR processes, especially for polymer flooding. IPV is defined as the portion of the porous space that cannot be accessed by the polymer (Lake 1989). The value of IPV is affected by the relation between the effective size of polymer molecules and the porous size. Depending on variables such as salinity and polymer concentration, the effective size of polymers in aqueous solution is between 0.3 µm and 2.0 µm (Shah *et al.*, 1978). The range of pore throat diameter or porosity that can be found in a reservoir is wide, where examples of reservoir rocks are presented in the table showed in Figure 2-7. The range

of pore size can be from 0.895 µm to 17,000 µm, these changes in pore size affect the value of IPV.

| Source of Samples | No.** | Pore-Throat Diameter (µm) | | | Method** | Model** | Statistic** | Porosity (%) | Permeability |
|---|---|---|---|---|---|---|---|---|---|
| | | Min. | Max. | Avg. | | | | | |
| Medium-grained sandstones, various, worldwide | 3 | 9.000 | 23.000 | 16.667 | Hg | C | ET | 14 | 25.5 md |
| Fine-grained sandstones, various, worldwide | 12 | 4.000 | 30.000 | 15.500 | Hg | C | ET | 18.1 | 19.6 md |
| Very fine-grained sandstones, various worldwide | 6 | 8.000 | 13.000 | 9.667 | Hg | C | ET | 24.2 | 109.7 md |
| Coarse siltstones, various, worldwide | 6 | 4.000 | 7.000 | 5.667 | Hg | C | ET | 26.3 | 22.3 md |
| Upper Cretaceous Lance Formation, Greater Green River Basin | 7 | 0.362 | 2.520 | 0.895 | Hg | C | ET | 7.5 | 17.7 µd |

**Figure 2-7: Pore throat diameter for sandstone and shales**
(Nelson, P., 2009)

The description of the pore space is considerably related to porosity, permeability, relative permeability, tortuosity, capillary pressure, connectivity, adsorption and wettability (Askarinezhad, 2010).

### 2.4.2 Permeability

Permeability measures how a fluid will be displaced through the porous medium in the reservoir, in other words, the transmissibility of fluids (Lake, 1989). The correlation that represents this process is the Darcy law (Lake, 1989) which states the velocity of a fluid through a porous medium is directly proportional to the pressure gradient along with the porous medium and inversely proportional to the fluid viscosity, in only one dimension it can be written as:

$$v_j = -\frac{kA}{\mu}\frac{dp}{dL} \tag{2-8}$$

Where:

$v_j$ is the fluid velocity (cm/s).

k is the absolute permeability of the porous rock (mD).

A is the cross-sectional area of the rock ($cm^2$).

µ is the viscosity of the fluid, centipoises (cP).

L is the length of the rock sample (cm).

dP/dL = pressure gradient in the direction of the flow (atm/cm).

The constant of proportionality in equation 2-8 is the permeability, which has Darcy units. The term absolute permeability is used when only one homogeneous single-phase fluid is flowing

in the rock sample (American Petroleum Institute, 1998) while effective permeability is the value obtained for a specific phase in a multi-phase fluid-saturated rock sample. Effective permeability is dependent on the saturation of the fluids in the rock and it is always lower than the absolute permeability. Permeability is strongly linked to the pore size distribution and effective porosity.

Karmen- Kozeny correlation representing the flow of fluids through a capillary tube (representing the porosity in the reservoir) is an important correlation that corroborates the relationship between permeability and porosity (equation 2-9). This correlation is very useful in CEOR to estimate the pore size from permeability, to evaluate mobility for polymer flooding.

$$k = \frac{1}{72\tau}\frac{\emptyset^3 D_p^2}{(1-\emptyset)^2} \tag{2-9}$$

Where:

$\tau = \left({}^{L_t}/_{L}\right)^2$: is the ratio between the length of the capillary tube and the length of the representative elementary volume (REV) of the permeable medium.

Ø= Porosity

Dp= pore diameter

$\frac{\emptyset}{a_v(1-\emptyset)}$: Hydraulic ratio to consider the tortuosity of the pore.

Another form of the Karmen –Kozeny correlation was reported by Lake (1989) to estimate the local shear rate $\gamma_{eq}$ of the flow of Non-Newtonian fluids in a permeable medium (equation 2-10). The equation has been used by many researchers to study the rheological properties of polymer flooding.

$$\gamma_{eq} = 4v\left(\frac{\emptyset}{8k}\right)^{1/2} = \frac{4q}{A\sqrt{8k\emptyset}} \tag{2-10}$$

Permeability is one of the screening parameters for EOR; Sheng (2011). High permeability is required for CEOR methods. Polymer injectivity and permeability reduction are part of properties that need to be evaluated, and these properties are important for the effectiveness of polymer flooding.

### 2.4.3 Wettability and relevance for CEOR

Wettability is the preference of a solid for a liquid (water or oil) rather than for another and can be measured by the contact angle $\theta$ between the fluid and the surface of the rock (Sheng, 2010a). The wettability of the rock can be water wet, oil wet or mixed wet.

The principle used to define the wettability based on the contact angle $\theta$, is defined as follow:

- If this angle between the fluid and the rock is small (<< 90°), that means the fluid extends on the surface and the wettability of the rock is favourable.
- If the contact angle is higher (> 90°) the surface has low wettability.
- If the angle is in between those extremes the rock is mixed wet.

An example of water-wet (a) and oil-wet (b) is presented in Figure 2-8. While sandstones rocks are mainly water-wet, carbonate rock tends to be oil-wet or mixed wet (Mohammed and Babadagli, 2015)

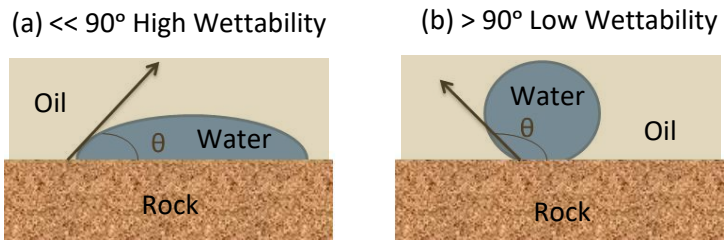


**Figure 2-8: Scheme of contact angle for wettability**

Wettability is an important parameter in oil recovery by chemical flooding (Wu, Y. *et al.*, 2005) as it affects the mobility of the fluids in the porous medium. The wettability of a formation can be altered after the migration of hydrocarbons and consequently, it will affect the profile of saturation of the porous matrix besides production profile.

The displacement of oil by water flooding in the porous matrix of lower mix-wet rocks is more difficult than in water-wet rocks. Some studies have reported an increase in oil recovery by changing the wettability of carbonate rocks to water-wet using surfactants (Wu, Y. *et al.*, 2005). Moreover, some published research in low salinity EOR in Berea core samples showed that oil recovery increases when wettability moves from water-wet to neutral wet, and the wettability is affected by salinity (Hadia *et al.*, 2013).

The determination of solid-fluids wettability at pore level has been an object of extensive research due to the complexity of the interactions between two or more fluids. A recent review

on wettability (Mohammed and Babadagli, 2015) report several cases of wettability changes by the effect of alkali, alkali/surfactants, low/high salinity water flooding, and high temperature. All those variables that affect wettability have been summarized in Figure 2-9. The injection of low salinity water flooding changes the wettability of sandstone to more water-wet, whereas high salinity changes the wettability of carbonate rocks to water-wet (Ayirala et al., 2017). Surfactants reduce the interfacial tension between oil/water and the capillary forces that keep the oil trapped inside the pore. Alkali interacts with the rock surface and changes the wettability (water-wet to oil-wet and oil-wet to water-wet). Temperature shifts the wettability to more water-wet for sandstones and to water-wet for carbonate rocks.

There are several methods to measure wettability, however spontaneous inhibition has been more used to compare wettability changes (Hirasaki et al., 2011; Mohammed and Babadagli, 2015).

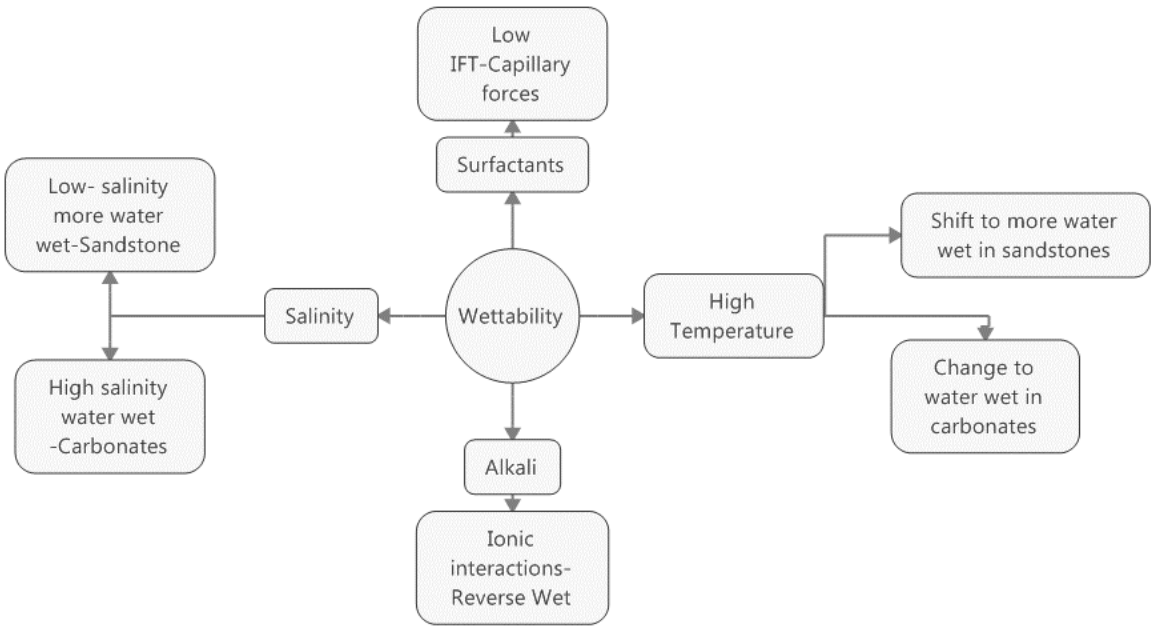


**Figure 2-9: Variables that affect wettability in sandstone and carbonate rocks by CEOR adapted from** (Mohammed and Babadagli, 2015)

Despite wettability is recognized to be one important parameter that affects the majority of CEOR processes such as alkali, surfactant, polymer, ASP and for low salinity CEOR, the area objects of research. For example, the high salinity and hardness existing in the formation brine play an important role in fluid-rock interactions that need more study. The effect of chemicals on the wettability is also affected by the type of rock.

### 2.4.4 Relative Permeability

Relative permeability ($k_{rj}$) is the relationship between the effective permeability ($k_j$) of a fluid in a multi-phase fluids system and the absolute permeability ($k$).

$$k_{rj} = \frac{k_j}{k} \tag{2-11a}$$

Relative permeability measures the flow performance of two or more immiscible fluids in the porous medium. The distribution of the fluids flowing in a porous medium depends on their relative permeability, as a result, it is one of the most relevant tests for CEOR (Lake, 1989).

The cross-sectional velocity of individual fluids flowing in multiphase flow in the reservoir with a dip angle (α) at steady-state conditions is estimated using Darcy law (equation 2-11b).

$$v_j = -k\left(\frac{k_{rj}}{\mu_j}\right)\left(\frac{\partial P_j}{\partial L} + g\rho sen(\alpha)\right) \tag{2-11b}$$

Darcy equation needs to be solved in three dimensions x, y, and z. The relative mobility of each fluid ($\lambda_{rj}$) is directly proportional to the absolute permeability $k$, and the relative permeability ($k_{rj}$) of that fluid and inversely proportional to its viscosity ($\mu_j$).

$$\lambda_j = k\left(\frac{k_{rj}}{\mu_j}\right) \tag{2-12}$$

Where:

$\left(\frac{k_{rj}}{\mu_j}\right) = \lambda_{rj}$: Relative Mobility

Another important correlation is the one between effective permeability ($k_j$) and relative permeability ($k_{rj}$).

$$k_j = kk_{rj} \tag{2-13}$$

A detailed curve of relative permeability for the flow of oil and water inside a rock with relevant parameters is presented in Figure 2-10. The relative permeability of a phase decreases as the saturation of that phase decrease until zero, which means that the phase cannot flow, leaving a residual amount of the phase trapped in the porous space.

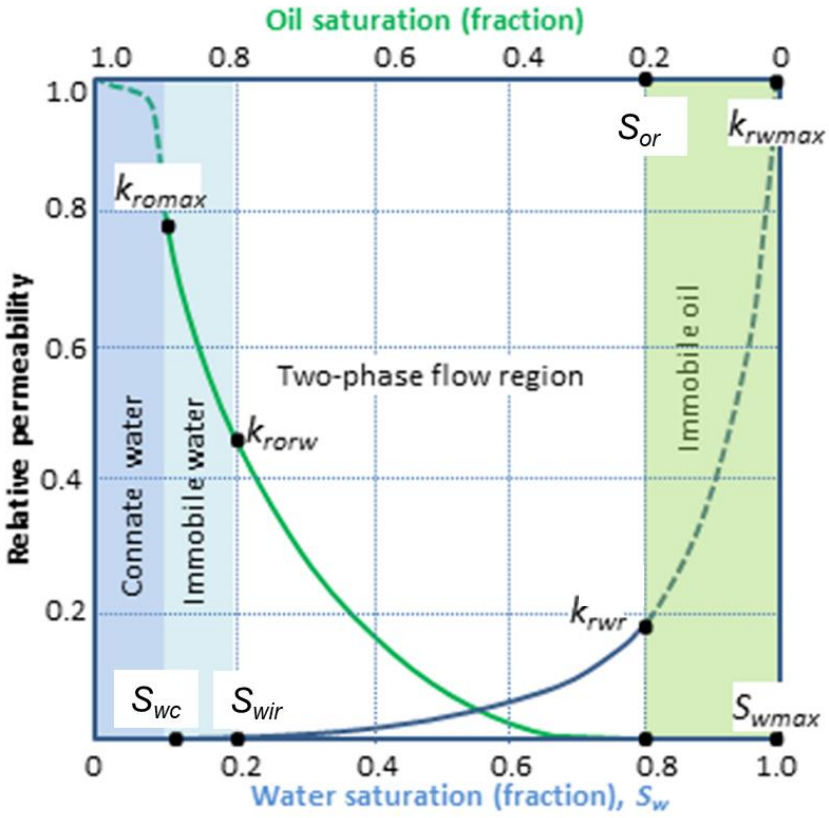


**Figure 2-10: Relative Permeability Curves**
Adapted from Schlumberger (2016)

The following parameters are characteristics of the oil-water-rock system:

- $S_{or}$: residual oil saturation (fraction) which represents the amount of oil that is left trapped in the porous space and is one of the main targets for CEOR methods.
- $S_{wc}$: connate water saturation (fraction) which is the water that was in the pore space before any water injection takes place.
- $S_{wir}$: irreducible water saturation (fraction) which is the fraction of water that is trapped in the porous space and cannot be removed.
- $K_{rorw}$: Relative permeability of oil at the $S_{wir}$ or endpoint oil relative permeability.
- $K_{rwr}$: Relative permeability of water at the $S_{or}$ or endpoint water relative permeability.

In a flow of two immiscible fluids inside the rock, one of them is wetting the rock and is called the wetting phase and the other one is called the non-wetting phase. The relative permeability curves also indicate the wettability of the fluid that is saturating the rock. For example, for the case of a water-wet rock, water is primarily located in the smaller porous space and is close to the rock surface as wetting the rock (as shown in Figure 2-11 first figure), and the oil is filling the pore space. The relative permeability of the oil (no-wetting phase on this example) is not going to be extremely affected by the flow of the wetting phase. The water flooding at a low flow rate tends to contact and displace most of the oil ahead until approaching to the residual oil saturation. The displacement is represented by small raise of the relative permeability of the wetting phase (Krw) by increase of water saturation ($S_w$) and small reduction of the relative permeability for the non-wetting phase (Kro) until approaching the residual oil saturation Sor (second and third figures in the sequence), a sequence of displacement is showed in Figure 2-11.

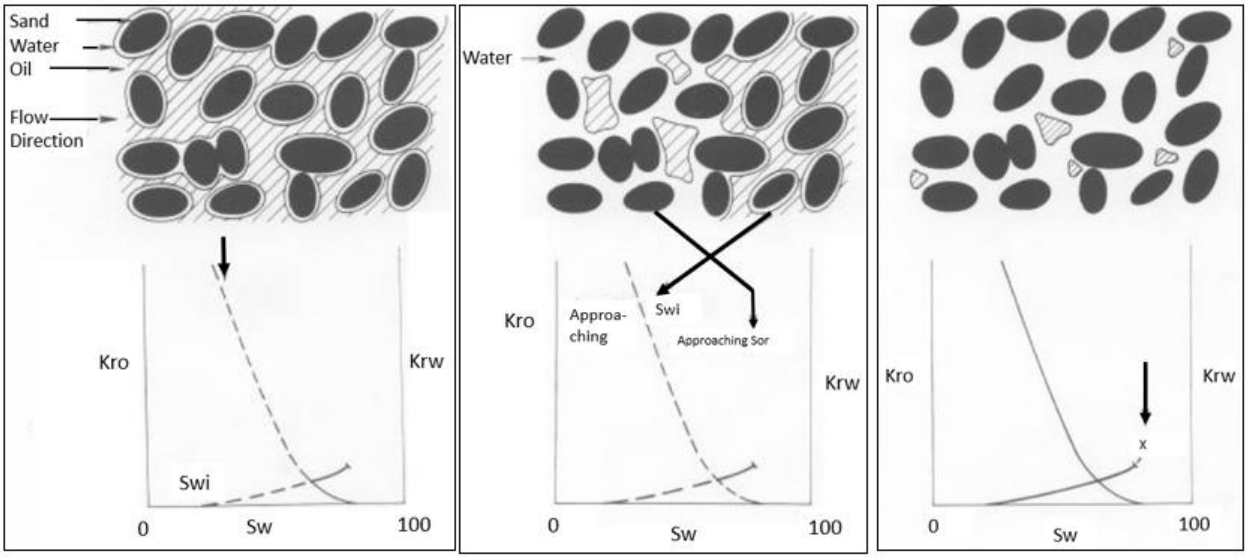


**Figure 2-11: Sequence of water flooding profile and relative permeability expected for a water wet rock**
(Anderson, W., 1986; Glover, 2002)

For the case of an oil-wet system the oil is located inside the smaller pore space and adsorbed on the rock and the non-wetting (water phase) is filling the pore space (first figure of the sequence presented in figure 2-12). The water flooding affects drastically the wetting phase (oil) relative permeability. Higher minimal pressure is required for the water to be able to displace the oil, compare with the water-wet system. The water will flow through large permeability channels; therefore, the relative permeability of oil decrease and water relative

permeability increase drastically with an early water breakthrough. An example of the sequence of water flooding for an oil-wet rock is showed in Figure 2-12.

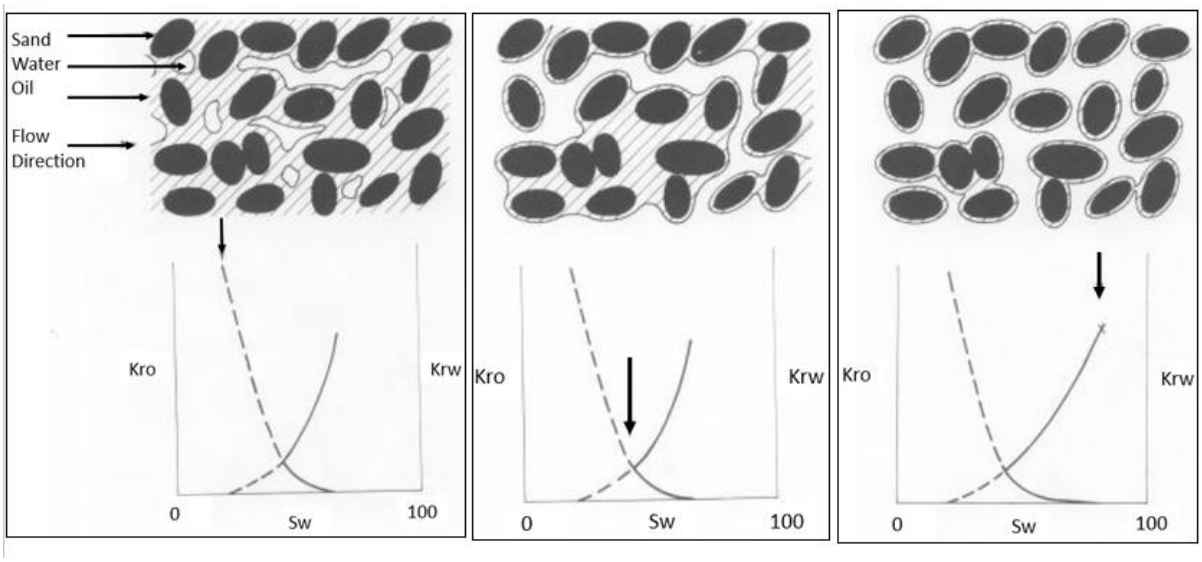


**Figure 2-12: Sequence of water flooding profile and relative permeability expected for an oil wet rock**
(Anderson, W., 1986; Glover, 2002)

The endpoints for each phase and the cross-point water saturation where both relative permeabilities are equal can also indicate the wettability of the rock (Lake, 1989). For example, as it is more difficult to displace the oil when is adsorbed on the rock and trapped inside small pores, the trapped non-wetting phase is expected to have a larger effect on the relative permeability of the wetting phase than on the non-wetting phase. Therefore, the ratio of the wetting phase to non-wetting phase endpoints relative permeability is higher than the value expected for a water-wet rock. This ratio is a good qualitative indication of the wettability of the rock. Moreover, for oil-wet systems, the cross-point water saturation where both relative permeabilities are equal is moved toward lower water saturation compared to water-wet rocks, due to the early water breakthrough. Figure 2-13 compares the relative permeability curves obtained for water flooding tests in an oil-wet in a water-wet rock sample.

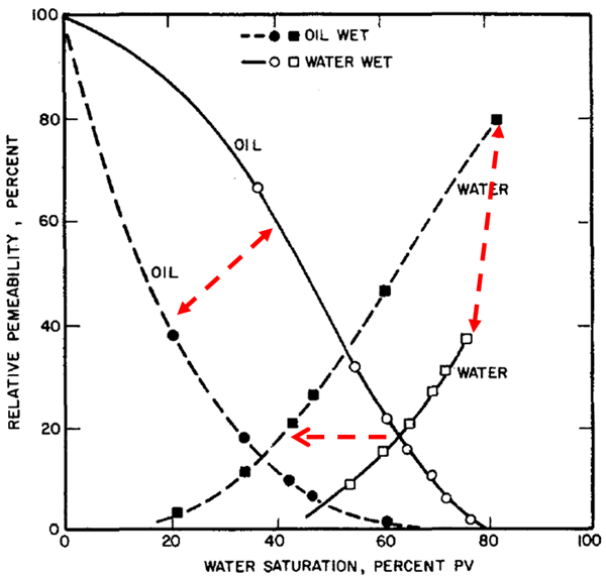


**Figure 2-13: Comparison of relative permeability curves for water wet and oil wet rocks** (Anderson, W., 1986)

The success of CEOR is therefore based on the wettability changes towards water wet using alkali and surfactants for non-wetting reservoirs and by reducing IFT between the phases. Both effects of wettability and IFT by CEOR can be identified by the relative permeability curves.

### 2.4.5 Surface and Interfacial Tension

The surface free energy between two immiscible fluids such as oil and water is known as the interfacial tension (IFT) (Anderson, D. R. *et al.*, 1976). Interfacial phenomena exist whenever there is direct interaction between two immiscible phases usually called surface or interface. The surface tension is the force presents on the interface curvature between a liquid phase and a vapour phase while IFT is the force between two non-gaseous phases. The units for surface tension are force per unit length (equation 2-14). Both ITF and surface tension can be measured in the laboratory by different methods. The value of IFT is very important for designing enhanced oil recovery applications.

$$\sigma = \frac{Force\ (mN)}{L\ (Perimeter\ m)} \qquad (2\text{-}14)$$

(1 dyne/cm = 1 mN/m)

CEOR methods rely on reducing IFT between displaced and displacing fluid to improve microscopic displacement efficiency (Anderson, D. R. *et al.*, 1976; Shen *et al.*, 2005), chemicals such as surfactants are either generated in situ by the reaction of alkali with the crude oil or by adding surfactants to the displacing fluid. The analysis of IFT between crude oil and chemical slug and the effect of reservoir conditions predict the behaviour of CEOR processes.

### 2.4.6 Capillary Pressure and effects on chemical EOR

The capillary forces are originated in a petroleum reservoir because of combined effects at the pore space such as interfacial tensions between the rock and fluids, and the wetting characteristics of the system. Due to the interaction between immiscible phases (oil and water, water and gas or oil and gas), a curved surface is present at the interface and tends to contract into the smallest possible area per unit volume. Capillary pressure Pc is the pressure difference between the non-wetting and the wetting face in a rock sample (Lake, 1989). The relationship for capillary pressure and the curvature of the interface fluid-fluid inside a capillary tube is given by the Laplace equation (equation 2-15).

$$P_c = (P_{in} - P_{out}) = = \frac{2\sigma cos\theta}{r} \quad (2\text{-}15)$$

Where σ is the interfacial tension between the two fluids, θ is the contact angle and r is the inner radius of the capillary tube. Capillary pressure is directly proportional to the IFT and inversely proportional to the radius of the pore throat. Capillary pressure is strongly affected by the wettability of the rock and saturation history (drainage and imbibition process).

Capillary pressure is a function of the water saturation in the porous media. The capillary pressure is extremely important to determine the fluids saturation distribution in the reservoir especially in the transition zone between the free water level and the oil-saturated zone.

The effect of the capillary pressure in CEOR processes is represented by two important correlations defined in the following section.

### 2.4.7 Capillary and Bond number

One of the main aims of CEOR processes is to overcome the capillary forces that keep the oil trapped inside the porous media. This can be achieved by modifying either capillary, viscous or gravity forces. Two relevant correlations represent capillary, viscous and gravity forces in the porous media which are the capillary number ( $N_c$) and the Bond number ($N_b$).

A capillary number is a dimensionless number that represents the relation between viscous and capillary forces. It is inversely proportional to interfacial tension (equation 2-16).

$$N_c = \frac{v}{\sigma cos\theta}\mu \tag{2-16}$$

$v$: Darcy Velocity (m/sec)

$\mu$: Viscosity of displacing fluid (Pa.s)

σ: Interfacial Tension (N/m)

$\theta$: The contact angle between the wetting phase and the rock.

The more effective method to increase the capillary number is by the reduction of the interfacial tension IFT between oil and water, and the effect is associated with the reduction of the residual oil saturation (Sheng, 2010a).

The capillary number is related to the residual oil saturation through the capillary desaturation curve CDC. A characteristic representation of the relation is presented in Figure 2-14. After water flooding, the residual saturation of the wetting phase $S_{nwr}$ is smaller than the residual saturation of the wetting phase $S_{wr}$. For a water-wet rock, where the wetting phase is water and the oil phase is oil. A capillary number higher than $10^{-5}$ is required to decrease the residual oil saturation and recovery additional oil left inside the porous media. For an oil-wet rock, a capillary number higher than $10^{-3}$ is required as water is the non-wetting phase and oil is the wetting phase. It is more difficult to recover oil from an oil wet condition.

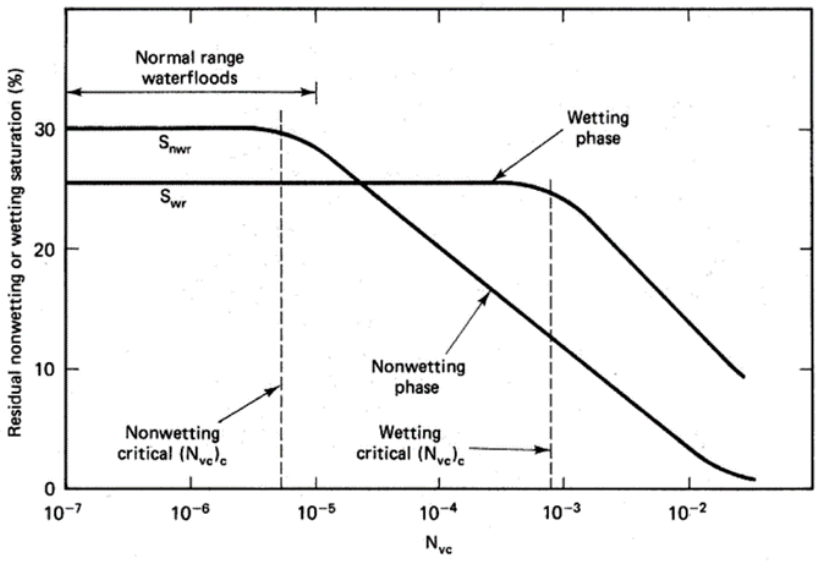


**Figure 2-14: Representation of Capillary Desaturation Curve**
(Lake, 1989)

Typical water flooding processes have capillary numbers of about $10^{-6}$ with a residual oil saturation of 0.30 (30%). To increase the oil recovery factor and minimize residual oil saturation, capillary number values have to be higher than $10^{-5}$ (Park *et al.*, 2015) so that the residual oil saturation is decreased.

In surfactants-based CEOR processes, the mechanisms of oil recovery are the reduction of the interfacial tension (IFT) between the oil and the displacing fluid (Sheng, 2010a; Lake, 1989) and rock wettability change (contact angle $\theta$). The decreases of IFT also increases the capillary number according to equation 2-16.

The Bond number ($N_b$) is defined as the ratio between gravity forces to capillary forces (equation 2-17)

$$N_b = \frac{\Delta\rho g k k_{rw} \cos\alpha}{\sigma cos\theta} \quad (2\text{-}17)$$

Where:

$\Delta\rho$: the density difference between water and oil (gr/m$^3$)
g : the gravitational acceleration (m/sec$^2$)
k : the absolute permeability (m$^2$)
σ: Interfacial Tension (N/m)
$k_{rw}$: is the water relative permeability. (fraction)
$\theta$: The contact angle between the wetting phase and the rock.
α: Angle formed between the direction of the flow and the gravity force.

The trapping number ($N_T$) is the combination of the capillary number (Nc) and the bond number ($N_b$) (equation 2-18).

$$N_T = N_c + N_b \quad (2\text{-}18)$$

The bond number is relevant when the gravity effect is important, such as in cases of gravity stabilized flow (Olajire, 2014). This number is used to analyse the effect of gravitational forces to study the fingering effect. A high value of the Bond number is an indication that gravitational forces are more important than capillary forces.

### 2.4.8 Mobility Ratio

Another important parameter that controls the effect of CEOR process is the mobility ratio, which is defined as the ratio of mobility between displacing fluid (water or chemical slug) and displaced fluid (oil). The mobility of a fluid is defined as a ratio of its relative permeability and viscosity. The correlation for mobility ratio is presented in equation 2-19.

$$M = \frac{\lambda_{displacing\ fluid}}{\lambda_{displaced\ fluid}} = \frac{\frac{k_{rj}}{\mu_j}}{\frac{k_{ri}}{\mu_i}} = \frac{k_{rj}\mu_i}{\mu_j k_{ri}} \qquad \lambda = \frac{k}{\mu} \qquad (2\text{-}19)$$

$k_{rj}$: Effective Permeability of fluid *j, i* ($m^2$)

$\mu_j$: Viscosity of fluid *j, i* (Pa.s)

Chemical flooding needs to be designed considering both mobility ratio (equation 2-19) and capillary number (equation 2-16). These are the key factors for CEOR. For instance, surfactants increase the capillary number by decreasing interfacial tension and polymers decrease mobility ratio by increasing viscosity of the displacing fluid. Figure 2-15 shows the effect of capillary number and mobility ratio in residual oil saturation (Thomas, 2008).

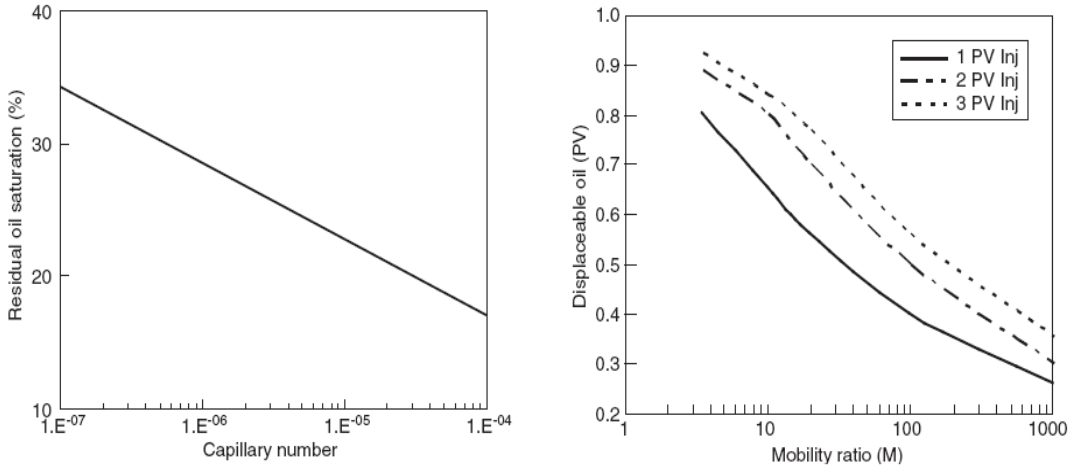


**Figure 2-15: Effect of mobility ratio and capillary number in residual oil saturation and displacement of oil response.**
(Thomas, 2008)

Chemical flooding has been described as a deep-formation fluids profile control where the mobility control process is based primarily on maintaining a favourable mobility ratio between displaced and displacing fluids to improve sweep efficiency (Sheng, 2010a). The mechanism predominant for polymers flooding is a reduction of the mobility of water modifying the viscosity of the fluid and therefore increasing the sweep efficiency.

### 2.4.9 Adsorption of chemicals in CEOR

Adsorption is the process where dissolved or dispersed components are removed from solutions by interphase transference to the surface or adsorbent substrate (Bera *et al.*, 2013). Depending on the nature of the interactions, adsorption can be classified as chemical or physical, being the former stronger than the later.

Physical adsorption interactions are due to the presence of weak electrostatic forces type “Van der Waals”. Chemical adsorption involves the formation of a strong chemical bonding between the surface and the adsorbate. Adsorption performance is therefore different for chemical and physical interactions. Physical adsorption is characterized by a high rate of adsorption and the presence of multiple layers, whereas chemical adsorption is usually limited to only one layer of adsorption (Somasundaran and Krishnakumar, 1997). As both types of adsorptions can be present in CEOR processes, the identification of the adsorption mechanism is more complex.

Adsorption of chemicals on the rock during CEOR processes can result in the reduction of chemical concentration, which makes the process less efficient in terms of keeping the required conditions of salinity and chemical concentration for microemulsion formation and ultra-low IFT for optimal oil recovery.

Adsorption is affected by different variables (as summarized in Figure 2-16), such as temperature, nature of the adsorbate, solvent and other chemical components, ions present in the solution, and chemical composition of the substrate or rock.

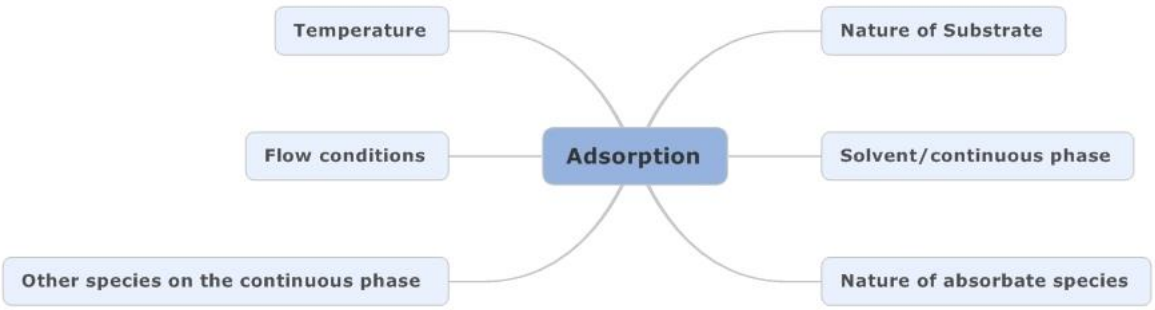


**Figure 2-16: Variables affecting adsorption of chemicals on the rock surface**

Adsorption of polymers and surfactants on the rock surface has been an object of many studies, as the cost of consumption of chemicals during CEOR affects the feasibility of the process (Liu *et al.*, 2008). Adsorption of surfactants is affected by its type and structure. The mineralogy of the rock and ionic composition of the solution also affects adsorption. Due to physical interactions, anionic surfactants present low adsorption on sandstone rocks and high adsorption in carbonate rocks (Sheng, 2010a; Sheng, 2010b).

Adsorption isotherms are commonly used to evaluate the adsorption behaviour of chemicals. This is the relationship between adsorbate density and adsorbate concentration. Freundlich and Langmuir are the most common adsorption isotherms used to represent the correlation

between adsorbate concentrations in equilibrium. Freundlich isotherm (Sheng, 2010a) presents the following correlation:

$$\overline{C_{is}} = K_F C_i^n \tag{2-20}$$

Where $C_i$ (g/m$^3$) represent the concentration of the chemical in the aqueous solution, $\overline{C_{is}}$ (g/m$^3$) is the concentration of the chemical on the rock surface, and $K_F$ and $n$ are factors determined by fitting the function of chemical concentration adsorbed and chemical concentration in the solution. Langmuir isotherm is represented by the following correlation (Sheng, 2010a; Lake, 1989):

$$\overline{C_{is}} = \frac{a_L C_i}{1+b_L C_i} \tag{2-21}$$

In this equation, $a_L$ is a dimensionless constant and the units for $b_L$ are the inverse value of concentration. The value of $b_L$ affects the curvature of the isotherm and the value of $a_L$ affects the adsorption at the plateau stage (Lake, 1989). A representation of the adsorption isotherm curve is presented in Figure 2-17 (Sheng, 2010a; Sheng, 2013a).

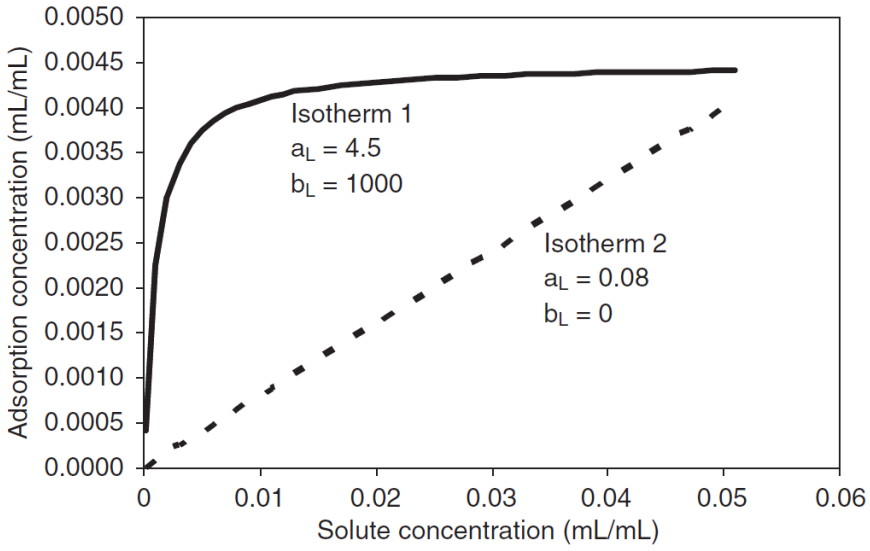


**Figure 2-17: Examples of isotherms for Langmuir with different values of $a_L$ and $b_L$** (Sheng, 2013a)

Assumptions for the two adsorption isotherm models are different. According to the Langmuir isotherm, adsorption will only take place on available sites on the substrate and not on places occupied by an adsorbate. Thus, the rate of adsorption is governed by gradient of adsorbent concentration and available on the substrate (Park *et al.*, 2015). Assumptions for the

Freundlich isotherm consider different places on the substrate and the amount of adsorbate able to occupy places on the substrate is proportional to the adsorbate concentration. Langmuir isotherm fits most of the adsorption behaviour of polymers and surfactants (Sheng, 2010a; Lake, 1989; Park *et al.*, 2015).

The reduction of chemicals during CEOR processes by adsorption represents a challenge for the application of CEOR. The use of alkali on ASP CEOR method supply negative ions for the adsorbate (rock surface) and reduce adsorption of surfactants.

Recent studies have included the use of chemicals as a pre-flush to modify adsorption and wettability of the rock. For instance, polyacrylate molecules are able to compete with anionic surfactants for adsorption places in the rock (ShamsiJazeyi *et al.*, 2014). Despite there are several successful ways to reduce chemical adsorption, the associated mechanisms are still under research.

### 2.4.10 Flow equations for CEOR

To predict the flow of CEOR processes, material balance equation, continuity equation, and Darcy Law are used. The material balance equation for the number of components present in the system can be expressed as in equation 2-22 (Sheng, 2010a).

$$\frac{\partial(\emptyset C_n^t)}{\partial t} + \frac{\partial}{\partial x}\sum_{j=i}^{n_p}\left[C_{nj}v_{xj} - \emptyset S_j\left(D_{xxnj}\frac{\partial C_{nj}}{\partial x} + D_{xynj}\frac{\partial C_{nj}}{\partial y} + D_{xznj}\frac{\partial C_{nj}}{\partial z}\right)\right] + \frac{\partial}{\partial y}\sum_{j=i}^{n_p}\left[C_{nj}v_{yj} - \emptyset S_j\left(D_{yynj}\frac{\partial C_{nj}}{\partial y} + D_{yznj}\frac{\partial C_{nj}}{\partial z} + D_{yxnj}\frac{\partial C_{nj}}{\partial x}\right)\right] + \frac{\partial}{\partial z}\sum_{j=i}^{n_p}\left[C_{nj}v_{zj} - \emptyset S_j\left(D_{zznj}\frac{\partial C_{nj}}{\partial z} + D_{zynj}\frac{\partial C_{nj}}{\partial z} + D_{zxnj}\frac{\partial C_{nj}}{\partial x}\right)\right] = q_n \quad (2\text{-}22)$$

Where n=1…. N: is the number of components; the number of phases is given by $\mathbf{n_p}$. $\mathbf{D_{xx}}$, $\mathbf{D_{yy}}$, $\mathbf{D_{zz}}$ are components of dispersion, $\boldsymbol{v}$ is Darcy velocity, ∅ is the porosity, $\boldsymbol{S_j}$ is the saturation of the phase **J** and $\boldsymbol{q_n}$ is the flow rate of that component (n) as an external source of energy.

The combination of material balance with Darcy equation gives the continuity equation for the transport of each component n and for each phase $n_p$ (equation 2-23).

$$\emptyset c_t \frac{\partial p}{\partial t} + \vec{\nabla}\cdot\sum_{j=1}^{n_p}\vec{v_j}\sum_{n=1}^{N_v}(1 + c_n\Delta p)\,C_{nj} = \sum_{n=1}^{N_v} q \quad (2\text{-}23)$$

Where $\mathbf{N_v}$ is the volume occupied by each component, $\boldsymbol{C_n}$ is the compressibility of each component on each element volume and q is the rate of injection or production of each component and $\boldsymbol{C_t}$ is the total compressibility.

Initially, pressure and fluid saturations are determined at a specific time, and then the concentration of components is calculated using a material balance equation. Afterward, according to chemicals interactions and the equilibrium reactions involved in the process, the concentration of reactants and products are calculated using equilibrium constants. Results allow getting new saturation distribution by using relative permeability correlations; and pressure calculation for the fluid distribution.

The complexity of mathematical calculations is higher for CEOR processes as they include equilibrium reactions, diffusion, and dispersion. The effect of interfacial tension and wettability changes is represented by chemical adsorption, relative permeability curves and capillary pressure (Delshad *et al.*, 2013).

The initial conditions usually include the setting of variables such as pressure and saturation of fluids at every point in the reservoir; boundary conditions are given by injection and production rates which determine the movement of the fluid through the porous medium. The displacement of fluids and determination of fluids saturation simplified to one dimension can be represented by the fractional flow theory developed by Leverett in 1941 and used for several researchers as reference equations (Craig, 1971; Lake, 1989). The derived equation from the application of Darcy law and capillary pressure is as follow:

$$f_w = \frac{1+\frac{Kk_{ro}}{v_t\mu_o}\left(\frac{\partial P_c}{\partial L}-g\Delta\rho sen(\alpha)\right)}{1+\frac{\mu_w k_o}{\mu_o k_w}} \tag{2-24}$$

Where:

$f_w$= Fraction of produced water or water cut (dimensionless)
$foil$=1 − $f_w$
$K$= Formation Absolute Permeability (Darcy)
$k_{ro}$= Oil Relative Permeability (dimensionless)
$k_o$= Oil Effective permeability (Darcy)
$\mu_o$= Oil viscosity (cp)
$\mu_w$= Water viscosity (cp)
$v_t$=total fluid velocity (cm/seg)
$P_c$= Capillary pressure (atm)
$L$= distance of the movement of fluids (cm)
g= gravity term cm/seg$^2$
Δρ= Difference on density between water and oil (gr/cm$^3$)
α = Formation dipping angle (degree)

Assuming capillary pressure is neglected and horizontal displacement, the following equations can be obtained:

$$f_w = \frac{1-N_b(1-S)^{n_w}}{1+\frac{(1-S)^{n_w}}{MS^{n_0}}} \quad (2\text{-}25)$$

Where $N_b = \frac{Kk_{rw}\Delta\rho g}{\mu_w v_t}$, is the Bond number and M is the mobility ratio obtained from permeability test. S is the reduced water saturation and is given by equation 2-26.

$$S = \frac{S_w - S_{wir}}{1-S_{or}-S_{wir}} \quad (2\text{-}26)$$

The simplifications taking into consideration to get the equation (2-25) are as follow:

a. Flow in one dimension and horizontal (not gravity effect).
b. The flow of oil and water in a homogenous reservoir, thus $f_{total} = f_w + f_{oil}$
c. Immiscible and Incompressible fluids.
d. Capillary pressure is neglected.

Lake (1989) demonstrated the effect of CEOR on the oil displacement efficiency by doing a sensitivity analysis of mobility ratio, gravity number, and relative permeability. Results showed that decreasing mobility ratio, increasing gravity number and changing wettability to more water-wet increase oil displacement efficiency. In the following sections, the relevant considerations and required correlations to simulate the flow of each chemical process; alkali, surfactant and polymer will be presented each as 2.5 alkalis, 2.6 surfactants, 2.7 polymers, and 2.8 combinations of chemicals.

From this part of the review, it is evidenced the need for the design and characterization of the chemicals for a CEOR process and a good understanding of the interactions within the fluid-fluid-rock system to avoid the triggering of undesirable reactions. The complexity is higher for CEOR than for water flooding, however, mathematical correlations are able to represent the process.

## 2.5 Alkali flooding

Alkali flooding is the injection of alkali solutions into the reservoir aiming to generate a natural surfactant, by the saponification reaction with organic acids (naphthenic acids) existing in the crude oil. This surfactant, or soap, reduces the interfacial tension between oil and water, hence enhances microscopic displacement efficiency. Alkali flooding is also called “caustic flooding”; where the injected alkali increases the pH of the chemical slug and reduces the adsorption of the surfactant to the rock surface.

Alkali or caustic flooding applications are dated back from 1920. A review of alkali applications (Mayer and Breit, 1986; Mayer *et al.*, 1983) as a standalone method revealed that most of the cases were in the USA following by Russia. Distributions of field applications of alkali and type of alkali based on publications are presented in Figures 2-18 and 2-19 (Graue and Johnson Jr, 1974; Mayer *et al.*, 1983; Mayer and Breit, 1986; Xie, J. *et al.*, 2008; Boardman *et al.*, 1982; Konopnicki and Zambrano, 1984; Goyal *et al.*, 1991).


**Figure 2-18: Distribution of published alkali flooding field applications by country**
(Based on a review of 19 field applications from 1983 to 2008)

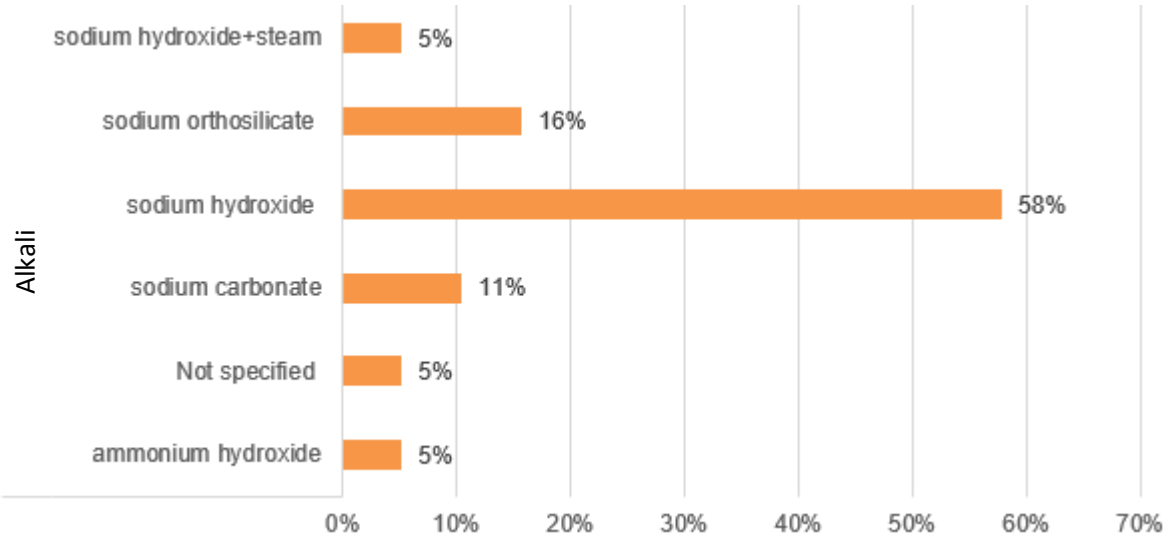


**Figure 2-19: Percentage distribution of publish alkali flooding field applications**
(Based on a review of 19 field applications from 1983 to 2008)

Several inorganic alkalis have been used, such as sodium hydroxide (NaOH), sodium carbonate ($Na_2CO_3$), sodium orthosilicate ($Na_4SiO_4$), ammonium hydroxide ($NH_4OH$) and sodium metaborate ($NaBO_2$). The most common alkali reported of field applications is sodium hydroxide NaOH, followed by sodium orthosilicate and sodium carbonate ($Na_2CO_3$) as shown in Figure 2-19.

Most of the applications of chemical flooding with alkali have been in sandstone reservoirs as is showed in Figure 2-20. Applications in carbonate reservoirs are limited by the presence of anhydrite or gypsum ($CaSO_4$) which promote dissolution and precipitation that cause excessive consumption of alkali and permeability modifications. The reaction between the natural occurring gypsum and the sodium hydroxide alkali to form precipitation is as follow, (Sheng, 2010a):

$$CaSO_4(s) + NaOH \longrightarrow Ca(OH)_2(s) + Na_2SO_4 \quad (2\text{-}27)$$

Alkali flooding has been applied as a standalone method but most of the applications are in combination with chemicals surfactant and polymer with better results due to the synergy between them. These methods are AP, and ASP and will be discussed later in this chapter. Some limitations and specific conditions for alkali flooding have been learned from applications on Chinese oilfields (Wang, F. et al., 2017), and can be summarized as follow:

- Well spacing to reduce alkali consumption, needs to be controlled
- Injection at early stages (So > 0.4),
- Lower than 15% clay content.
- Formation permeability >100 mD,
- Oil viscosity < 100 cp.

Alkali CEOR method has demonstrated to have the potential for heavy oil applications when thermal methods are not available (Pei *et al.*, 2013). There are limitations for salinity lower than 200,000 ppm TDS and the concentration of divalent cations lower than 4,000 ppm. Alkali can cause problems such as scaling and low injectivity, there are also problems associated with the production of emulsion and cost for treatments.

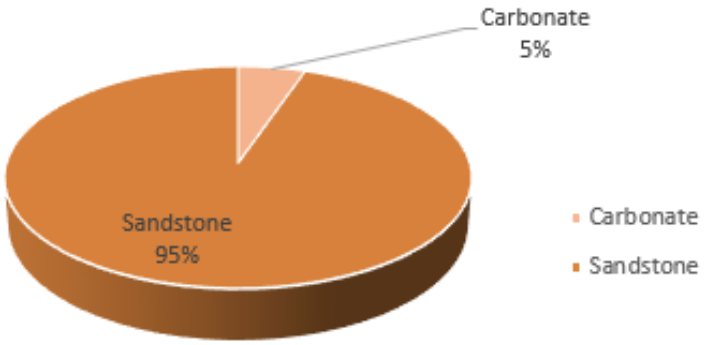


**Figure 2-20: Percentage distribution of field application of alkali flooding by type of rock**
(Based on a review of 19 field applications from 1983 to 2008)

### 2.5.1 Mechanisms of alkali flooding

Mechanisms associated with alkali flooding have been discussed by several authors and numerous mechanisms have been reported. The oldest recognized mechanisms were emulsification and entrapment, emulsification and entrainment and wettability reversal (water-wet to oil-wet and oil-wet to water-wet) (Graue and Johnson Jr, 1974). Then, later publications added combined mechanisms, such as emulsification with coalescence, wettability gradients, oil phase swelling with disruption of rigid films between oil and sand, and low interfacial tension by the in-situ generated surfactant (DeZabala *et al.*, 1982).

More recent publications of alkali flooding (Sheng, 2015b) still include the initial three mechanisms reported by Graue (1974) plus emulsification and coalescence reported by DeZabala (1982). There is an additional mechanism defined as “mobility control caustic flood” described as the permeability modifier effect of the injection of alkali due to the precipitation of divalent hydroxides by the reaction with existing divalent cations present in some rocks. The most common mechanisms from the review of different publications consider the following aspects:

a) Emulsification between oil and water triggered by a natural surfactant (soap).
b) Change of wettability of the rock by hydroxyl ions provided by the caustic flood.
c) Precipitation of hydroxide due to the presence of divalent cations in the formation brine and in the rock surface.

The dominance of one mechanism with respect to others is still under research. More than one mechanism can be existing for a particular application of alkali flooding. A detailed description of each mechanism is presented further in this section.

The mechanism of emulsification and entrainment is due to the effect of the natural surfactant formed by the alkali-oil reaction. The natural surfactant reduces the interfacial tension IFT and favours the formation of oil in water O/W emulsion. The effect is measured through the recovery of additional oil entrained in the porous media. The emulsion O/W formed also makes improvements on the displacement profile due to the high viscosity of the emulsion. This viscous emulsion acts as flow diverting of the displacing fluid, allowing the flow to sweep other areas thus improving volumetric sweeping efficiency.

The mechanism of emulsification and entrapment is explained as a dynamic process that occurs when the crude oil in the emulsion is re- trapped on small pores downstream of the displacement due to changes and possible destabilization of the O/W emulsion.

The mechanism of emulsification and coalescence is also a consequence of emulsion destabilization, which promotes the coalescence of oil drops to generate the oil bank downstream of the flow.

Wettability reversal mechanism refers to the change of the rock wettability from oil-wet to water-wet. This mechanism can be monitored by changes in the relative permeability of water. The wettability can be changed from oil-wet to water-wet by the injection of high pH water flooding. Although the mechanism associated with wettability changes from water-wet to oil-wet is more complex, it has been explained by Cook et al. (1974) as reported in the literature (Graue and Johnson Jr, 1974). The mechanism depends on the composition of the crude oil and the salinity. On this wettability reversal process, the oil drops change from discontinuous to continuous phase and changing the water relative permeability. Moreover, if the in-situ surfactant decreases the IFT low enough to create water in oil emulsion, this high viscosity emulsion will also generate a pressure gradient enough to overcome the capillary pressure that keeps the oil trapped in the porous media. Sodium carbonate has been extensively used to change the wettability of carbonate rocks from oil-wet to water-wet (Hirasaki et al., 2011)

The resultant of any of the mechanisms is the reduction of the residual oil saturation or increase of displacement efficiency. Moreover, each of the mechanisms is very sensitive to several variables existing in the reservoir, (DeZabala *et al.*, 1982; Graue and Johnson Jr, 1974) such as:

- The chemical characteristic of the rock.

- Composition of the crude oil, brine salinity and concentration of divalent cations.
- pH and temperature

The effect of all these variables is schematized in Figure 2-21.

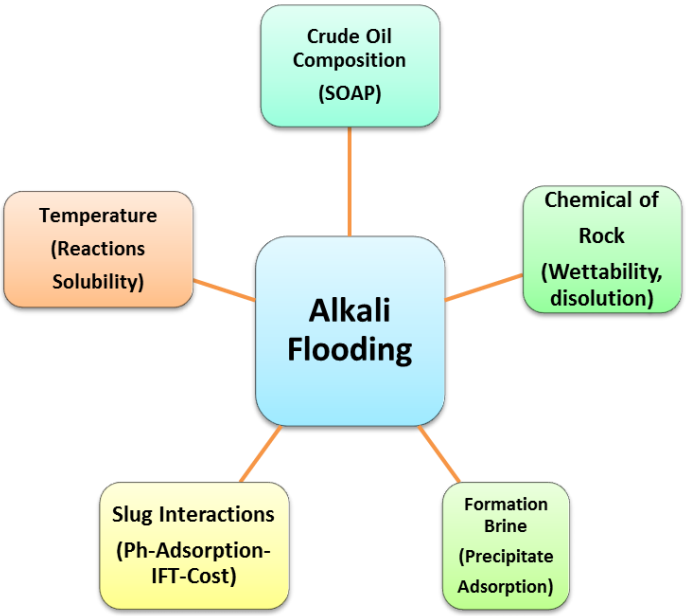


**Figure 2-21: Parameters affecting alkali flooding**

The effect of crude oil compositions on the mechanism of alkali flooding is mainly based on the presence of organic acids. The acidic number is a measure of the amount of organic acid in the crude oil composition and it is defined as the amount of potassium hydroxide (KOH), milligrams, required to neutralize one gram of crude oil. The value is reported as the total acidic number (TAN) (Sheng, 2011). The TAN number is usually measured using no aqueous potentiometric titration. The scale for oil acidity (Sheng, 2015b) classify the oil as follow:

- High acidity for oils with a TAN > 1,
- Intermediate acidity for oils with TAN > 0.3 <1 and,
- Low acidity for oils with TAN > 0.1 < 0.25.

The in-situ surfactant formation by alkali flooding requires a minimum TAN of 0.3 mg KOH/g.

For alkali flooding, the presence of divalent cations is not desirable as it promotes precipitation of hydroxides (Graue and Johnson Jr, 1974). These precipitation reactions can cause injectivity problems and they are the main source of problems for an application that combined alkali (A), surfactant (S) and polymer (ASP) CEOR applications (Sheng, 2014a). For

applications of ASP with brines with divalent cations, the use of a softened pre-flush and a softener or filtration equipment in place to remove or complex divalent cations is required.

Alkali reacts with divalent cations $Ca^{2+}$ and $Mg^{2+}$ to form, depending on the pH of the solution, insoluble hydroxides, silicates or carbonates. These salts and hydroxides will act as permeability modifiers to divert the flow of injected fluids, to zones of low permeability (Mayer *et al.*, 1983). The use of chelating agents to avoid precipitation of divalent ions has been reported by different authors. Sodium metaborate has been used as a sequester of divalent ions for a case of formation brine with salinity up to 157,000 ppm TDS and 8600 ppm of divalent ions, $Ca^{2+}$ and $Mg^{2+}$ (Flaaten *et al.*, 2010). The optimal salinity for the chemical slug with alkali, surfactant, and polymer was 6,000 ppm of divalent ions, 120,000 ppm TDS salinity and pH 11. Studies of comparison of different alkalis in high salinity and temperature reported the need to use a chemical compound able to form chelates with divalent ions (Bataweel, 2011).

Successful results of applications of organic acids have been reported with components such as poly-aspartic acid as a complexing agent of divalent ions, allow the use of alkali in the application of divalent ions (Berger and Lee, 2006). Also Ethylenediaminetetracetic acid (EDTA), hydroxyethylenediaminetetracetic acid (HEDTA) and diethylenetriaminepentaacetic acid (DTPA) have been used as chelating agents of divalent ions in applications on sandstone and carbonate rock samples; with a resultant incremental recovery of 20% using 5% of chelating agents in seawater (Mahmoud and Abdelgawad, 2015). In this last case, the EDTA is taking divalent ions adsorbed on the rock. Therefore, the mechanism for this alkali flooding CEOR process was rock dissolution. The mechanism was corroborated by the increase in the concentration of divalent ions in the effluent. The reduction of IFT was also reported as an effect of carboxylic groups present in the chelating agent.

From the analysis of the available literature, the complexity of alkali flooding is evident, with multiple reactions between fluids and fluids-rock. Several mechanisms were identified which include different chemical interactions with minerals existing in the rock, which can lead to a change of permeability, wettability, and flow behaviour. The dissolution of minerals also can occur during caustic flooding. In the next section the multiple reactions associated with alkali flooding are discussed.

### 2.5.2 Equilibrium reactions involved in alkali flooding

During alkali flooding, several interactions can occur between alkali-oil, alkali-rock, and alkali-formation water. Naphthenic acids are part of the crude oil composition and are defined as a

mixture of cyclic carboxylic acids. Naphthenic acids are represented as a pseudo component (denoted as HA), which is highly soluble in oil. The equilibrium reactions of naphthenic acid components between the oil and aqueous phase involve a sequence as shown in equations 2-28 to 2-31. There is a partition equilibrium of the acidic components between the oleic and aqueous phase (equations 2-28), then the dissociation of the acidic components in aqueous solution (2-29), and the water dissociation equilibrium takes place and the hydrolysis reaction of acidic components with alkali to produce the surfactants (equation 2-31). Naphthenic acids present in the oleic phase, denoted by (HAo) reacts with the alkali to produce an anionic surfactant ($A^-$), a schematic representation of the equilibrium reactions is displayed in Figure 2-22.

| | | | |
|---|---|---|---|
| $HA_o \leftrightarrow HA_w$ | $K_D = \frac{[HA_W]}{[HA_O]}$ | $K_D = 10^{-4}$ | (2-28) |
| $HA_w \leftrightarrow H^+ + A^-$ | $K_A = \frac{[H^+][A^-]}{HA_W}$ | $K_A = 10^{-10}$ | (2-29) |
| $H_2O \leftrightarrow H^+ + OH^-$ | $K_W = \frac{[H^+][OH^-]}{[H_2O]}$ | $K_w = 5 \times 10^{-14}$ | (2-30) |
| $HA_o + NaOH \leftrightarrow NaA + H_2O$ | $[A^-] = \frac{K_A K_D [HA_O]}{[H^+]} = \frac{K_A K_D [HA_O][OH^-]}{K_W} [A^-] = \frac{[HA_O]}{5x[H^+]}$ | | (2-31) |

The concentration of the natural surfactant [$A^-$] generated by the hydrolysis reaction is directly proportional to the concentration of the hydroxyl concentration, thus (–log [$OH^-$]), pOH, (DeZabala *et al.*, 1982), and also to the concentration of acidic components existing in the crude oil [HAo].

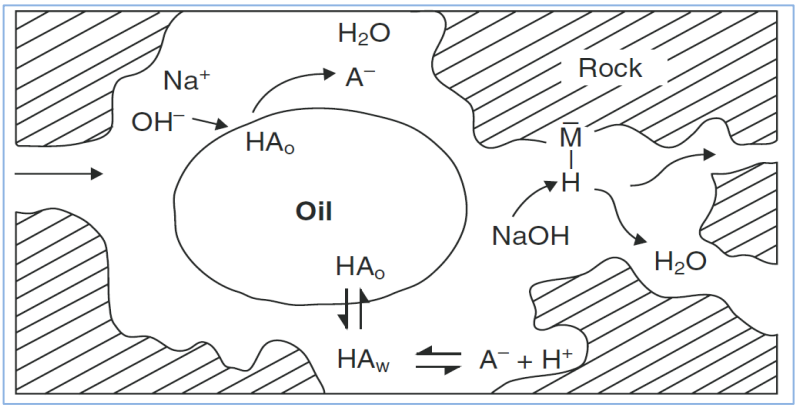


**Figure 2-22: Schematic model of interactions in alkali flooding**
(DeZabala *et al.*, 1982)

Reactions of alkali with rock depend on its mineralogy, the composition of formation water, pH and temperature (Sheng, 2014a). Alkali will be consumed as it interacts with fluids and mineral present in the rock, three main equilibrium reactions represent the process (Mohnot *et al.*, 1987):

a) Reversible ion exchange or adsorption with the rock surface (M-O-H): sodium –hydrogen exchange. Sodium ions replace hydrogen or calcium in the rock surface:

$$MO\text{-}H + Na^+ \leftrightarrow MO\text{-}Na + H^+ \qquad K_1 = \frac{[MO-Na][H+]}{[MO-H][Na^+]} \tag{2-32}$$

$$MO\text{-}H + Na^+ + OH^- \leftrightarrow MO\text{-}Na + H_2O \qquad K_2 = \frac{[MO-Na]}{[MO-H][Na^+][OH^-]} = \frac{K_1}{K_w} \tag{2-33}$$

The equilibrium is displaced to the right in both equations when there are more places in the rock to be replaced by sodium. For alkaline conditions and salinity, the total concentration of ions sodium that will be available for the adsorption equilibrium presented on equations 2-32 and 2-33, can be estimated by the following equation.

$$[Na^+] = [Na^+]_{Alkali} + [Na^+]_{brine} \tag{2-34}$$

The adsorption equilibrium has been demonstrated to behave like a Langmuir adsorption type curve with the plateau values that increase with salinity and temperature. When divalent ions are present on the rock surface, the following equilibrium reaction will take place and is favoured over the monovalent ions.

$$2MO\text{-}H + Ca^{2+} \leftrightarrow (MO)_2\text{-}Ca + 2H^+ \qquad K_1 = \frac{[(MO)_2-Ca][H+]^2}{[MO-H]^2[Ca^{2+}]} \tag{2-35}$$

$$2MO\text{-}H + Ca^{2+} + 2OH^- \leftrightarrow (MO)_2\text{-}Ca + 2H_2O \qquad K_2 = \frac{[(MO)_2-Ca]}{[MO-H]^2[Ca^{2+}][OH^-]^2} = \frac{K_1}{{K_w}^2} \tag{2-36}$$

One equivalent (or milli-equivalent) of divalent cations $Ca^{2+}$ or $Mg^{2+}$ will replace two equivalents hydrogens places on the surface of the rock (two negative charges); therefore,

the loss of hydroxide from alkali is double with divalent ions. Besides, if the concentration of divalent ions is high enough to overcome the solubility limit of calcium or magnesium hydroxide, the consumption of hydroxide will increase considerably. Another equilibrium reaction found in the exchange between $Ca^{2+}$ and $Na^{+}$:

$$MO_2\text{- Ca} + 2Na^{+} + 2OH^{-} \leftrightarrow 2(MO\text{- Na}) + Ca(OH)_2 \quad K_3 = \frac{[MO-Na]^2[Ca(OH)_2]}{[MO_2-Ca][Na^{+}]^2[OH^{-}]^2} \qquad (2\text{-}37)$$

b) <u>Mineral dissolution by reactions</u> are more complex and depend on the mineralogy of the rock. An example of mineral dissolution occurs with anhydrite ($CaSO_{4(s)}$) from carbonate rock reacts with alkali to generate insoluble hydroxide and dissolution of carbonate rocks, equations 2-38 and 2-39 represent the equilibrium reactions involved. Data on chemical loss of alkali in meq OH/kg of minerals is presented on the table in Figure 2-23. Alkali loss is higher in the presence of anhydrite and low to insignificant for sandstone (quartz) (Sheng, 2010a).

$$CaSO_{4(s)} + NaOH \leftrightarrow Ca(OH)_{2(s)} + Na_2SO_4 \qquad (2\text{-}38)$$

$$CaCO_{3(s).} + NaOH \leftrightarrow Ca(OH)_{2(s)} + Na_2CO_3 \qquad (2\text{-}39)$$

The consumption of alkali flooding at high temperatures for different mineral rocks is low for quartz sands and high values for kaolinite clay (Mohnot *et al.*, 1987). The dissolution of minerals from a rock can generate other minerals and promote precipitation of minerals when they exceed their solubility.

c) Precipitation of insoluble hydroxides $Ca(OH)_2$ and $Mg(OH)_2$ when dissolution constants are overcome by the presence of divalent ions as part of the mineral dissolution reactions.

| Minerals | Ehrlich and Wygal (1977) | Mohnot and Bae (1989)[2] |
|---|---|---|
| Calcite | Insignificant | Insignificant |
| Chlorite | | 110, 140 |
| Dolomite | Insignificant | 610, 930 |
| Gypsum (anhydrite) | 11600[1] | |
| Gypsum (selenite) | | 1180, 1180 |
| Illite | 1360 | 720, 900 |
| Kaolinite | 130 | 1250, 1270 |
| Labradorite (Ca-Na feldspar) | | 160, 210 |
| Montmorillonite | 2280 | 780, 1060 |
| Quartz, fine | | 220, 450 |
| Quartz, sand | Insignificant | Insignificant |
| Zeolite (Clinoptilolite) | | 670, 990 |

[1] *Calculated from stoichiometry assuming conversion to $Ca(OH)_2$.* **Units: meq OH / kg of minerals**
[2] *First value at pH 8.3, and second value at pH 10.*

**Figure 2-23: Alkali loss in meq of alkali/kg minerals**
(Sheng, 2010a)

It is evident that alkali flooding interacts not only with the oil to generate natural surfactant by saponification but also with the ions adsorbed on the rock leading to different equilibriums reactions. These multiple equilibrium reactions have adverse effects on the effective alkali concentration available to generate the natural surfactant or soap. Besides, salinity and divalent cations also react with alkali to form insoluble hydroxides, which can modify rock properties by dissolution and precipitation reactions.

### 2.5.3 Flow equations for alkali flooding

Alkali flooding can be described by the solution of the material balance, continuity equation and Darcy law equation, considering initial conditions of the pressure and fluid saturations given by the distribution of fluids. The concentration of each component is calculated using material balance and continuity equations (2-22) and (2-23). Then, depending on the equilibrium reactions involved in the alkali flow, the concentration of reactants and products is calculated using equilibrium constants of reactions.

The equilibrium reactions considered for alkali are the formation of the natural surfactant (equations 2-28 to 2-31), adsorption, and precipitation by reaction with divalent ions, represented by equations 2-32 to 2-37.

The generation of the natural surfactant includes the reduction of IFT, wettability changes by chemical adsorption, and permeability changes by precipitation of divalent hydroxides.

Results from this step allow the calculation of the new saturation distribution of fluids to calculate the new pressure. A flowchart of the sequence for calculations is represented in Figure 2-24.

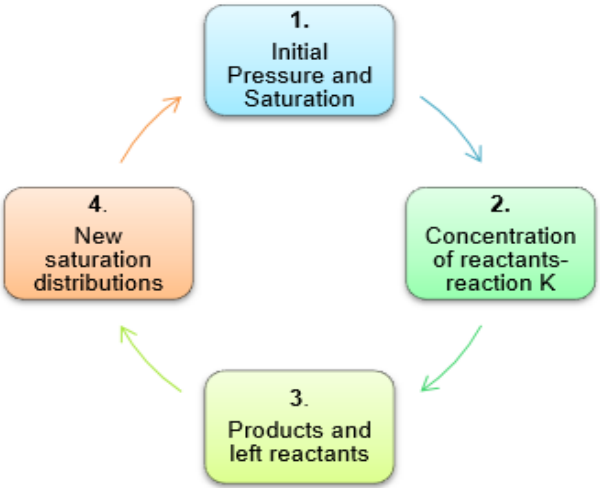


**Figure 2-24: Flow of mathematic calculation of alkali flooding**

From these findings in the literature, it can be noticed that the description of the process of alkali flooding is complex and require the analysis of multiple interactions between both fluid-fluid and fluid-rock. Besides, it is important to consider the effect of precipitation of hydroxides on properties of the porous media, such as porosity and permeability and possible formation dissolution by the effect of alkali flooding on the final fluid saturations and displacement efficiency.

## 2.6 Surfactant Flooding

Surfactants are chemical compounds, usually called surface agents because they have affinity by both organic compounds and water. Surfactants tend to be concentrated at the interface of fluid/ fluid, solid/fluid and reduce the interfacial tension (IFT). Surfactants also interact with contra-ionic at the surface layer to change the wettability of the rock (Sheng, 2010a; Sheng, 2013a).

Surfactant flooding is the injection of a pre-designed surfactant chemical slug into the reservoir with the objective of reducing the interfacial tension between oil and water. The injection of surfactants in the porous media aids to mobilize trapped oil in small pores by reducing capillary forces and increase capillary number which improves the microscopic displacement (Lake, 1989). Surfactant flooding is sometimes called micellar flooding because of the nature of the surfactant to form micelles. However, the difference between the surfactant and micellar flooding is the amount of surfactant used (Gogarty, 1976; Wang, F. et al., 2017). While micellar flooding consists of the injection of a small chemical slug with high surfactant concentration; surfactant flooding is the injection of a high volume of a chemical slug at low surfactant concentration.

The technology of surfactant flooding is not new (Gogarty, 1976) with some published evaluations on the field tests for surfactant and micellar flooding that date previous to 1976 with promise results of oil recovery with the use of micellar surfactant flooding. However, the use of micellar flooding was not economical attractive due to the cost and amount of chemical required, and some uncertainties on the time to obtain the incremental recovery.

The common aspect of the two methods (micellar and surfactant flooding) is that they are both based on the reduction of IFT and the generation of a microemulsion.

The design of a surfactant chemical slug should consider the following characteristics (Hirasaki et al., 2011):

- Reduce and maintain ultra-low values of interfacial tension between oil and water, below $10^{-3}$ dynes/cm,
- Be characterized by minimal adsorption on the rock surface;
- Be stable under salinity and hardness existing in the water to make the chemical slug and in the brine existing in the reservoir rock.
- Be compatible with other chemicals such as alkali and polymers.

The above requirements for a surfactant to be effective in chemical flooding have been an object of research aiming to make the process economically viable and developing surfactants compatible with different existing reservoir conditions.

Based on published research, surfactant flooding has only been used as a standalone method in a well stimulation process called “huff and puff”, which consists of the injection of a chemical enhancement slug into the well, with a soaking period and then the well is put back in production. This process has been successfully applied in carbonates (Yang, H. D. and Wadleigh, 2000; Zubari and Sivakumar, 2003; Xie, X. *et al.*, 2005; Rilian *et al.*, 2010).

Surfactant changes the wettability of the rock (Sheng, 2013a). These changes have been found as a great potential for carbonate reservoirs as they are mainly oil-wet (Alvarado and Manrique, 2010). The residual oil saturation of fractured chalk reservoirs is favourable affected by wettability changes.

Surfactant flooding applications have been mainly combined with other chemicals such as alkali (AS), polymer (SP) and alkali and polymer (ASP). Percentage distribution of publishing field applications of surfactants according to the type of rock is presented in Figure 2-25.

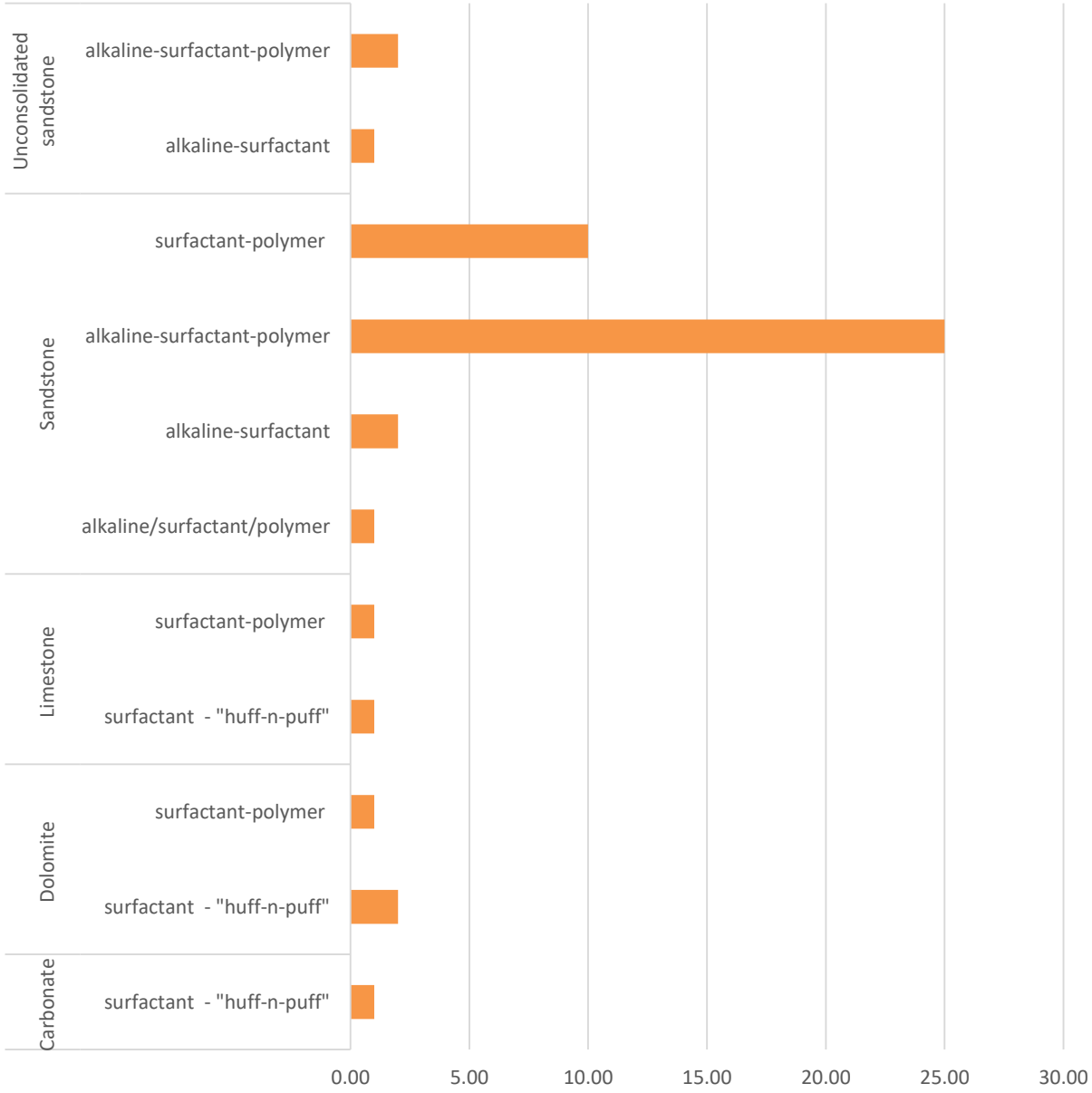


**Figure 2-25: Distribution of applications of CEOR method with surfactant according to rock type**
(Based on a review of 46 field applications from 1992 to 2017)

From the distribution, it is noticed that surfactant has been more used in sandstone reservoir rocks and combined as the ASP CEOR method. The high number of applications are reported from China (Wang, F. et al., 2017). While SP has been used in both sandstone and carbonate rocks, ASP has not been used in carbonate rocks with a lower number of applications.

The distribution of applications by country is showed in Figure 2-26, the higher numbers of applications are in China and the USA. Applications in the USA which involve surfactants are mainly SP and some ASP while in China applications are mostly ASP flooding (Alvarado and Manrique, 2010; Olajire, 2014; Manrique et al., 2010; Sheng, 2014a; Wang, F. et al., 2017).


**Figure 2-26: Distribution of applications of CEOR method with surfactant by country**

(Based on a review of 46 field applications from 1992 to 2017)

The high number of applications of surfactants is combined with alkali and polymer as ASP due to the advantage of the synergy of chemicals. However, as there are several complex mechanisms that can be present in an ASP COER process that still are an object of discussion. Most of the mechanisms reported for ASP CEOR are associated with fluid-fluid and fluid-rock interactions, therefore it is expected that for each chemical combination with crude oil, a different mechanism can dominate the process.

The design of surfactant slugs is complex and depends on the different conditions existing in the reservoir; some of them are summarized in Figure 2-27. The choice of surfactant is affected by different parameters such as:

- The type of formation rock (sandstone or carbonate). According to the mineralogy of the rock, there is a net charge on their surface, sandstone rocks are negatively charged whereas carbonate rocks have a positive charge. In order to minimize surfactant adsorption on the rock surface, anionic surfactants are recommended for sandstones, whereas no-ionic, cationic and amphoteric surfactants are recommended for carbonate rocks (Han et al., 2013; Hirasaki et al., 2011; ShamsiJazeyi et al., 2014).
- Temperature affects the behaviour of surfactant, its stability, and solubility in the chemical slug, the IFT and optimal salinity for microemulsion formation is also affected by the temperature. surfactants type sulfates are available on different structures for applications up to 60 ºC. For higher temperatures sulfonate types are more stable (Hirasaki et al., 2011).
- The minimal surfactant concentration has to be higher than the critical micellar concentration so the microemulsion formation is favourable.
- Salinity determines surfactant solubility and affects the choice of surfactant. At low salinity, the surfactant is soluble and will be mainly dissolved in the water because of its high solubility, therefore oil in water dispersion is favourable. As the salinity increases, the surfactant is driven out the aqueous solution toward the oil/water interface, more oil will be dispersed in water until the salinity reaches the “optimal salinity of microemulsion formation”, where the surfactant partition is equal in both phases, and a microemulsion Type III, w/o and o/w is formed. This salinity is defined as “optimal salinity”. At higher salinity the dispersion of water in oil is favourable. The formation of type III microemulsion is a mechanism of oil swelling because the oil solubilized into the emulsion makes the effective oil saturation higher and the resulting oil relative permeability increase (Healy et al., 1976; Wade et al., 1979; Sheng, 2010b).
- The adsorption of surfactants on the rock surface needs to be minimal to avoid chemical loss. However, the adsorption of the surfactant modifies the wettability of the rock to more water-wet (Ayirala et al., 2017). Surfactant adsorption increases with surfactant concentration until reaching a plateau (Azam *et al.*, 2013). Surfactant adsorption also increases by the effect of salinity until a maximal concentration (Saxena *et al.*, 2019; Azam *et al.*, 2013) . Increasing the pH modifies the net charge of the rock surface to more negative at pH > 8 and reduces surfactant adsorption (Azam *et al.*, 2013). The mechanism associated with adsorption seems to be highly dependable of ionic interactions within the

surfactant functional groups and the rock surface. However, the effect of the composition of oil and rock wettability is not well elucidated yet.

A zone of ultra-low IFT is required for the microemulsion formation. Once the optimal surfactant concentration is determined, phase separation tests with a salinity scan are required to define the optimal salinity for microemulsion formation, the range of salinity with ultra-low IFT, and the value of minimal IFT.

In order to achieve ultra-low IFT, it is necessary to use softened water (reduce $Ca^{2+}$ and $Mg^{2+}$). It is required to design a surfactant chemical slug with an optimal salinity or ultra-low IFT close to the salinity of the available water used for injection (either produced water or seawater), however there are also advantages in oil recovery using low salinity (Sheng, 2014b).

Despite there is a good understanding of interactions and conditions for surfactant formulations, the plan for the injection and displacement of CEOR is still in discussion (Hirasaki et al., 1983; Bourrel et al., 2011; Riswati et al., 2019). Some researchers recommend the injection of a pre-flush of brine at the optimal salinity followed by the surfactant chemical slug and displacement at the optimal salinity. In addition to the identification of the region of low IFT, it is important to evaluate the effect of the salinity gradient created during CEOR processes and find the optimal profile of salinity (Flaaten et al., 2008; Hirasaki et al., 1983; Chou and Shah, 1981; Aghaeifar et al., 2018) .

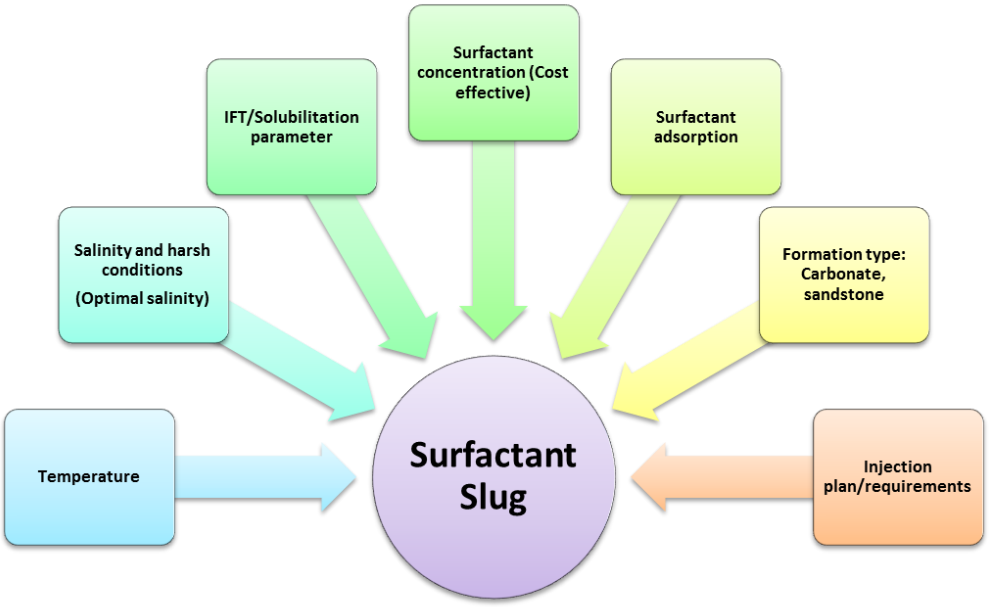


**Figure 2-27: Considerations for the design of surfactants chemical slug**

The review of the variables and mechanisms of surfactant flooding will be included further in this chapter.

### 2.6.1 Commons Surfactants used in EOR

Surfactants have been classified based on the type hydrophilic head (part of the molecule presenting affinity to water). According to this classification, they can be ionic (anionic, cationic), zwitterionic (both anionic and cationic) and non-ionic. The specific characteristics for each of them are summarized as follow:

- Anionic: Surfactants that have negatively charged head in aqueous solution. This type of surfactant is the most commonly used in chemical flooding for sandstone reservoirs because it has low adsorption in this type of rock. Examples of anionic surfactants are salts of alkylbenzene sulfonate, phosphates, carboxylic acids, xanthates, internal olefin sulfonate (IOS), phosphates, carboxylates, alcohol ester sulfate (alcohol Ethoxy AES or propoxy APS).
- Cationic: surfactants that have positively charged head in aqueous solutions, this type of surfactant is mainly used for carbonate type reservoirs. Examples are fatty amine and quaternary ammonium.
- Zwitterionic: Surfactants that have both cationic and anionic charged groups on the hydrophilic head. Examples are betaines and aminoacids.
- Non-ionic: Surfactants that do not have any resultant charge in aqueous solution, this type of surfactant is more used on carbonate reservoirs and also as co-surfactants for several applications. Examples are poly-ethoxylated alcohols, alkylphenols, acids, and esters. These types of surfactants are less sensitive to salinity.

Sheng (2015) reports a wide range of surfactants that have been evaluated such as petroleum sulfonates, synthetic carboxylates, ethyl sulfate, alkane sulfonate, ether sulfate, lignosulfonate, alkyl aryl sulfonate, alcohol propoxy sulfate, alcohol ethoxy sulfate, etc. Surfactants sulfobetaine were tested for high temperatures (30-90 ºC) and high salinity up to 120,000 ppm.

To control the effect of divalent ions the used of chelate agents has been proposed by Basin et al (2013). Table 2-3 presents the chemical formula of some commonly used surfactants with recommendations found in the literature.

There is a wide option of surfactants available for CEOR applications and the selection process is complex (Table 2-3). For example, surfactants type IOS are more sensitive to

salinity than surfactants type alcohol propoxy sulfate APS; however, blends of surfactants type IOS with surfactants type APS have shown high tolerance to salinity and divalent cations (Levitt, 2006; Kumar and Mandal, 2016). A combination of surfactants ionic and no-ionic has also been recommended to increase tolerance to high salinity (Shen, 2011).

**Table 2-3: Common surfactant applied on chemical EOR**
(Hirasaki et al., 2011; Sheng, 2015c; Bera et al., 2011)

| Surfactant Type | Chemical Formula | Recommendations |
|---|---|---|
| **Anionic olefin Sulfonate (IOS)** | R-CH-OH-$CH_2$-CH-$SO^-_3$-R<br>R-CH=CH-$SO^-_3$-R' | Unstable at high temp > 100ºC, sensible to divalent cations. |
| **Anionic Methyl Ester Sulfonated** | R-CH-($CO_2$-Me)$SO^-_3$Na ~20%<br>R -($CO_2$-Na)$SO^-_3$Na<br>Me-$OSO_3$Na | Hydrophilicity increases with the ester and make the surfactant less sensible to salinity. |
| **Non-ionic Alcohol Ethoxylate** | R-[$CH_2$-$CH_2$-O-]$_7$-OH ~ 55-65% | Stable at high temperature (105ºC), the number of ethoxy groups increases salinity tolerance and decrease IFT (Bera et al, 2011) |
| **Anionic Alcohol Ethoxy Sulfate** | R-O-[$CH_2$-$CH_2$-O-]$_n$-$SO_3^-$Na | Ethoxy groups add tolerance to divalent cations, stability at high salinity conditions and temperature up to 100 ºC |
| **Anionic Alcohol Propoxy Sulfate** | R-O-[$CH_2$-($CH_3$)-CH--O-]$_{13}$-$SO_3^-$ Na | Propoxy groups add tolerance to divalent cations stables at high salinity conditions and temperature up to 100 ºC |

For applications on temperature below 60 ºC, surfactants with ethylene oxide (EO) or propylene oxide (PO) or mixes of surfactant with different hydrophobic length are recommended; the use of branched hydrophobic chains of PO and EO segments was also successfully applied by Exxon (Maerker and Gale, 1992) as referred by Hirasaki et al (2008). For high temperatures and lower salinity sulfonates surfactant are found more stable. The stability order for surfactant is as follow (Shen, 2011):

Petroleum sulfonates < Alpha olefin sulfonates < Alkylarylsulfonates.

The presence of divalent cations makes sulfonate surfactants very unstable and precipitation is triggered, the use of ethoxylated or propoxylated sulfates increases tolerance to divalent cations as they do not precipitate.

Despite there is a wide variety of surfactants available in the market, still the process to select the best surfactant system is complex especially when high salinity, divalent cations, and high

temperatures are involved. Temperature restricts the stability of surfactant components. The surfactant formulation for CEOR is based on the microemulsion formation at salinities close to existing brine to avoid extra costs for soft water. The required concentration of surfactant is also an important issue considered for CEOR applications that need to be addressed.

### 2.6.2 Mechanisms of Surfactant flooding

The mechanism of surfactant flooding is based on the reduction of the interfacial tension IFT between oil and water to ultra-low values and the generation of a three-phase microemulsion. During surfactant flooding, the surfactant solution gets in contact with trapped oil and the oil is emulsified; drops of oil are dispersed in the microemulsion and displaced downstream. As the microemulsion changes with reservoir conditions, the oil drops in the emulsion will coalesce and form a continuous thread which will be able to deform and pass through pore throats to create an oil bank (Wang, F. et al., 2017).

The process used to evaluate surfactants and their ability to generate lower ITF tension starts with the determination of critical micellar concentration CMC (Shen, 2011), which is the concentration of surfactant required to form micelles and the point of minimal IFT, this test is represented in Figure 2-28.

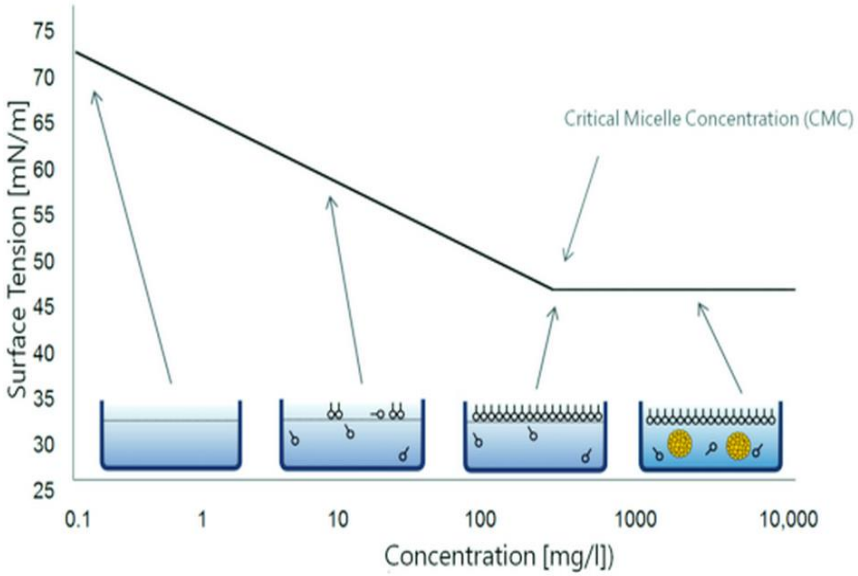


**Figure 2-28: Critical micellar concentration**
(Sanderson, 2012)

The CMC should be small, a maximal concentration of 10 ppm is common (Green and Willhite, 1998) as referred by Shen (2011). During the process of designing the chemical slug for CEOR, once the minimal surfactant concentration based on CMC results has been determined, phase behaviour tests need to be completed to determine the optimal salinity for microemulsion formation and ultra-low IFT; this test include aqueous stability and salinity scan, a flowchart of the process is presented in Figure 2-29.

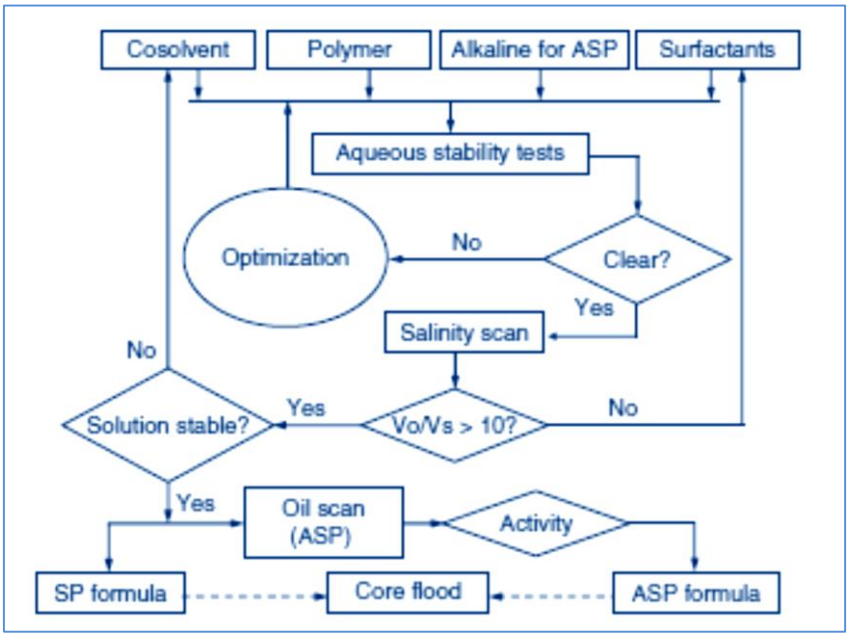


**Figure 2-29: Flow chart of phase behaviour test according to Sheng (2010a)**

The salinity scan will show how the surfactant system will perform under different salinity conditions and the development of the microemulsion at the optimal salinity. Salinity scan allows the evaluation of the microemulsion for the system oil, brine, and surfactant; the method was first described by Winsor (1954). The optimal salinity and type of microemulsion is a function of the surfactant structure, molecular weight (MW) and MW distribution, concentration and reservoir conditions of salinity, pressure, and temperature, oil phase characteristics. The effect of the different variables has been summarized in Figure 2-30.

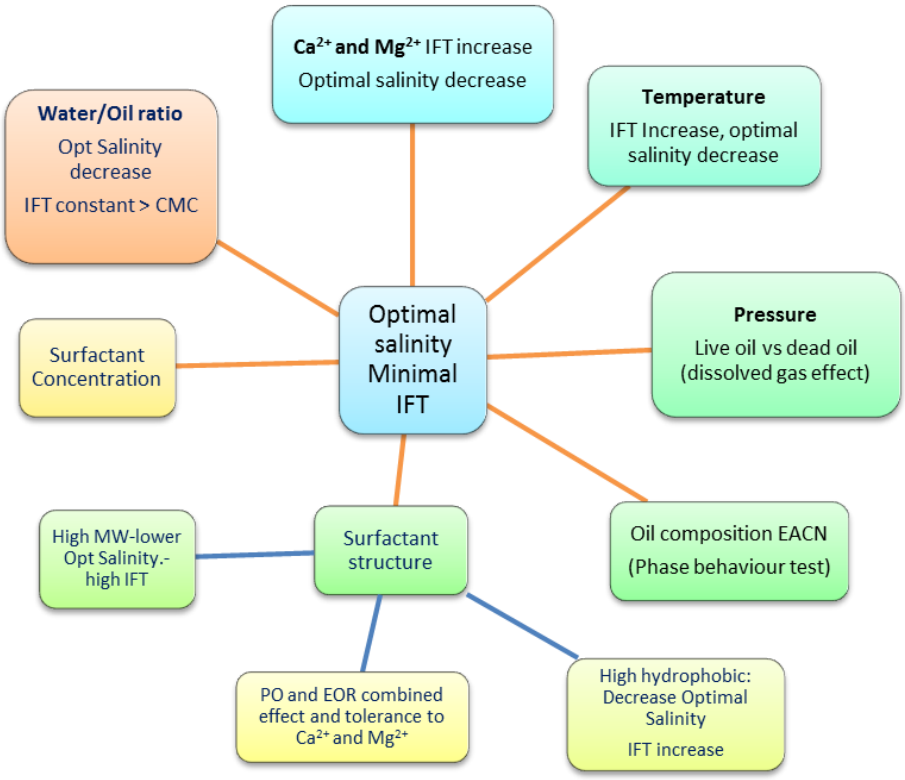


**Figure 2-30: Variables affecting IFT and optimal salinity**
summarized from Sheng (2010a)

Results from phase behaviour can be represented on ternary phase diagrams for a better representation of the multiphase system, (Nelson and Pope, 1978). An illustration of the salinity scan reported by Sheng (2010a) is presented in a ternary diagram in Figure 2-31. At low salinity, the surfactant is on the aqueous phase, and the oil is up, the system is called type $II^-$ or upper phase. As salinity increases, the surfactant solubility decreases, and it migrates to the interface and both oil and aqueous phase form the three-phase microemulsion. At high salinity, the surfactant is mainly in the oil phase and emulsion water in oil is form type $II^+$, leaving an aqueous phase at the bottom.

Phase behaviour allows the use of solubilisation ratio and estimation of IFT calculations according to the Huh method (1979).

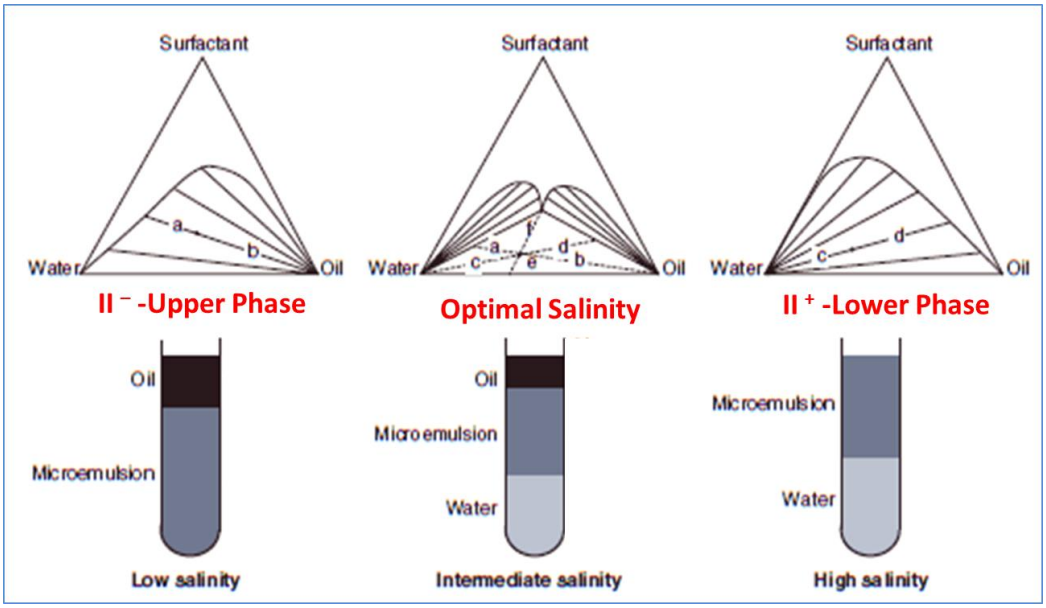


**Figure 2-31: Type of microemulsion and effect on phase behaviour on ternary graphs**
Adapted from (Sheng, 2010a)

The IFT ($\sigma$) is related with solubilisation ratio $\left(\frac{V_i}{V_s}\right)$ by the following expression, according to Hud (1979).

$$\sigma = \frac{C}{(V_i/V_s)^2} \tag{2-40}$$

Where C is equal to 0.3 mN/m and $V_i/V_s$ is the solubilisation ratio of the phase in the surfactant in the microemulsion, the optimal salinity is the point of minimal IFT. A representation of IFT values obtained from the phase behaviour test is shown in Figure 2-32.

The phase behaviour test will allow evaluating interactions fluid-fluid (oil, water, surfactant with salinity). Maximal oil recovery will be obtained when IFT is minimal, thus when solubilisation ratio is maximal, IFT values of water/microemulsion (me) and oil/microemulsion (me) as a function of salinity are presented in Figure 2-33. The optimal salinity is the point of salinity where the solubilisation ratio $V_i/V_s$ of both phases in the surfactant in the microemulsion are equal.

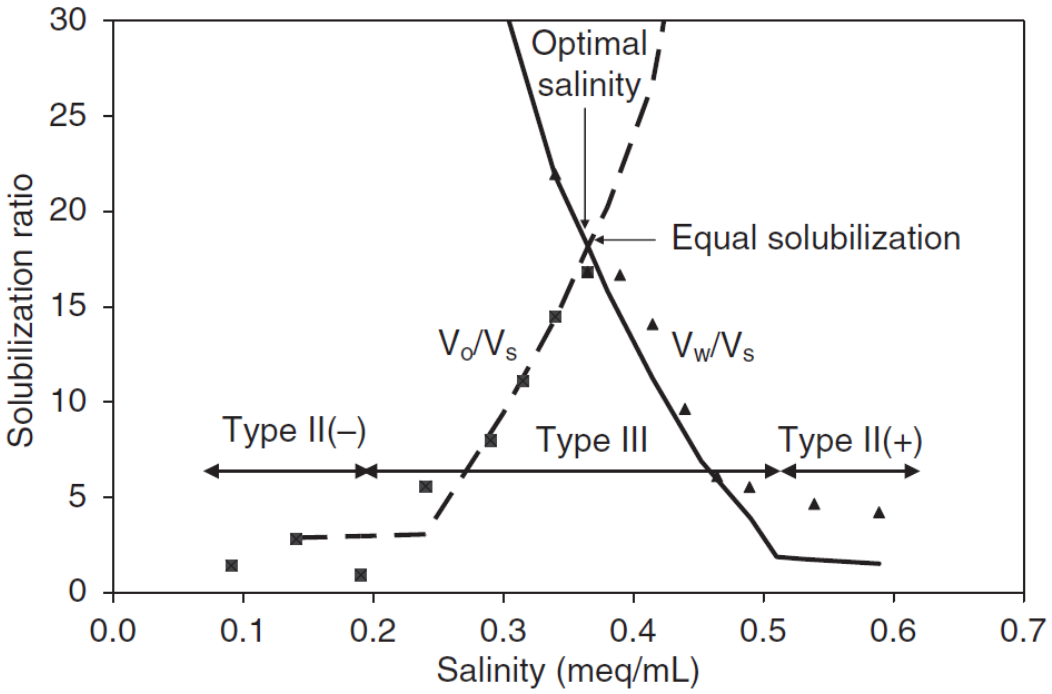


**Figure 2-32: Solubilisation ratio as function of salinity (Sheng, 2010a)**

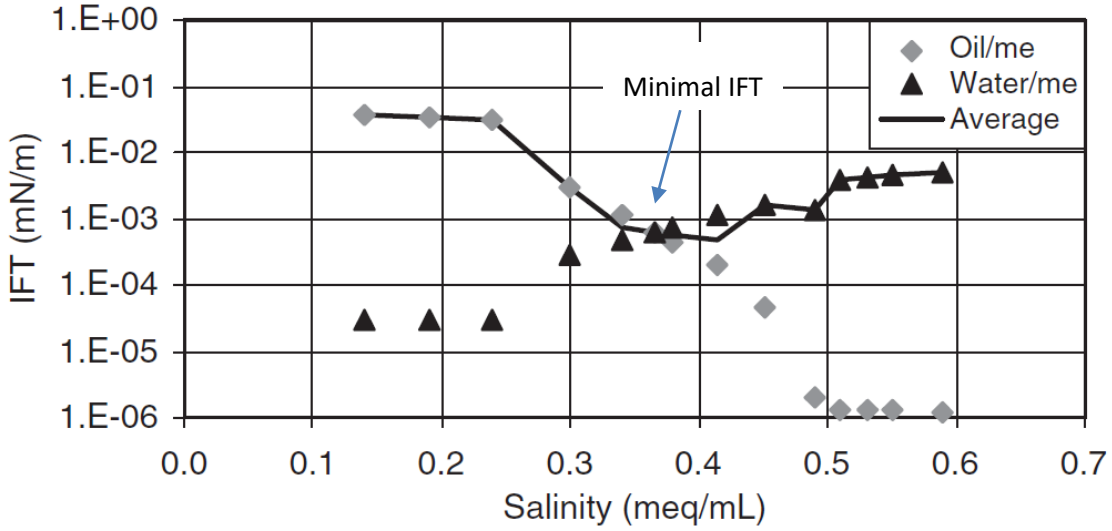


**Figure 2-33: IFT of (oil/me) and (water/me) as function of salinity**
(Sheng, 2010a)

The minimal interfacial tension coincides with optimal salinity showed in Figure 2-32. The surfactant also affects the relative permeability of the fluids and capillary pressure, thus the capillary number.

The presence of divalent cations decreases the optimal salinity of surfactants/oil due to a strong association between surfactants and divalent cations (Sheng, 2010a). However, recent studies (Tichelkamp *et al.*, 2015) indicate that the presence of $Ca^{2+}$ ions has a positive effect on IFT reduction during low salinity flow.

Another important mechanism of surfactant flooding that has been reported is wettability change; Ayirala et al. (2004) studied the effectiveness of low-cost surfactants in wettability and interfacial tension using Berea sandstones (permeability about 400 mD and porosity 23%) to represent the reservoir and crude oil from Yates Field Unit in Texas. They tested non-ionic surfactant (ethoxy alcohol) and anionic surfactant (ethoxy sulfate) and found that alteration of wettability to mixed-wettability was the principal mechanism for large enhanced oil recovery observed on their experiences. They proposed the following mechanisms: Firstly, a rupture of the water film from the rock surface, followed by the adsorption of molecules of surfactant on the rock surface.

From this part of the review, it can be identified the complexity of interactions between the system rock/fluids and fluids-fluids and how the selection of the appropriate surfactant requires the consideration of a series of variables existing in the reservoir. Moreover, it is critical to the planning of relevant laboratory tests to check the compatibility of the systems and effect of the composition of the brine exiting in the location, available for injection. The salinity and concentration of divalent cations affect optimal conditions of surfactants and interactions fluids-rock.

### 2.6.3 Flow equations for surfactant flooding

To represent the flow of surfactant it is important to consider that surfactants will affect the phase behaviour of the fluids as it was explained in the previous section. The presence of microemulsion with ultra-low IFT will create a range of salinity of miscible displacement. It is important to determine the correlations that involve interfacial tension, such as the capillary number and relative permeability. To describe the range of salinity where a microemulsion is present, partitioning of surfactant between oil and water phase according to results from phase separation tests are used. The distribution of surfactant between oil and brine for different salinity and IFT values are also calculated.

To describe the flow of surfactant flooding, initial conditions for pressure and fluid saturations are determined, and then the concentration of different components in the porous media is calculated using a material balance equation. Depending on the surfactant concentration and salinity, the IFT and the partition of the surfactant between oil and aqueous phase and

microemulsion are calculated. The value of IFT is considered in the calculation of the capillary number. Then, from the capillary desaturation curve CDC, relative permeability and saturations for wetting and non-wetting phase will be extrapolated and the new saturation distribution will allow calculating the new pressure distribution.

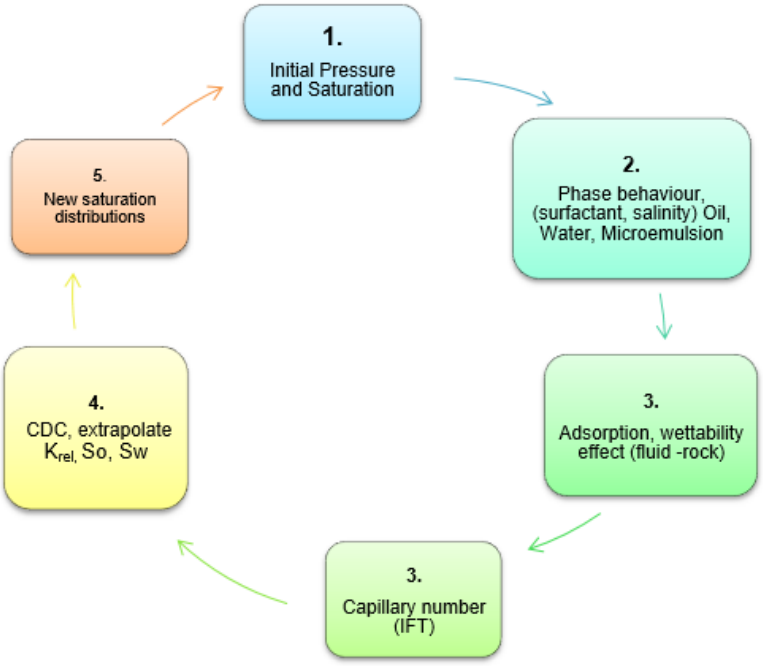


**Figure 2-34: Flow of mathematic calculation of surfactant flooding**

From the diagram shown in Figure 2-34, the minimal tests required for the analysis of surfactant flooding are:

- Fluids stability to select chemicals and concentration and stability under reservoir conditions and salinity,
- Phase separation tests to evaluate the range of low IFT and effect of salinity and, surfactant and fluid partition based on solubilisation ratio obtained from phase separation test;
- Analysis of capillary desaturation curve (CDC) to find a correlation between capillary number and saturation of wetting and non-wetting phases. Equivalent values of endpoints can be obtained by interpolation of relative permeability curves (Computer Modeling Group Ltd, 2015; Sheng, 2010a).

An example of the effect of surfactant on the relative permeability is presented in Figure 2-35. Surfactant flooding affect relative permeability curves, in term of the endpoints effective permeability for oil and water, the saturations of fluids and the Corey exponents.

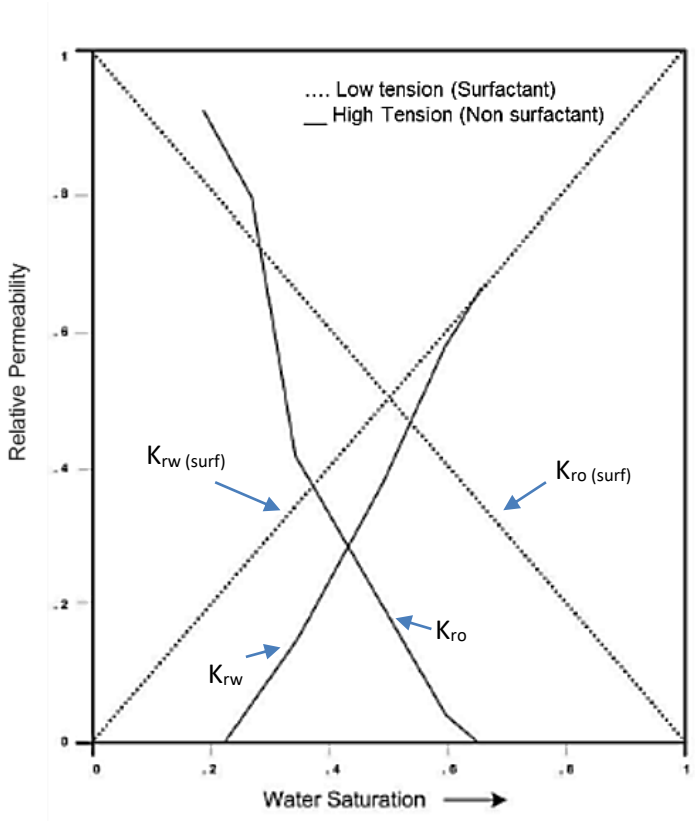


**Figure 2-35: Effect of surfactant on the relative permeability curves**
(Computer Modeling Group Ltd, 2015)

Additional fluids-rock interactions such as surfactant adsorption and wettability need also to be considered. Experimental adsorption isotherms need to be determined first. The capillary number is calculated based on relative permeability curves. CDC and saturation relationship can be fit from experimental values.

Then, adsorbed surfactant affects the displacement of fluids in the reservoir; this effect is considered on the new saturation distribution as surfactant loss. Wettability changes for oil-wet and water-wet considered relative permeability curves were presented previously in Figure 2-8.

## 2.7 Polymer Flooding

Polymer chemical flooding is the most used method in chemical flooding EOR (Manrique *et al.*, 2010). Most of the applications have been with water-soluble polymers such as polyacrylamides and biopolymers (polysaccharides and cellulose polymers). The most used polymers are PHPA (Partially hydrolysed polyacrylamides (Veerabhadrappa *et al.*, 2011). Distribution of applications by country is presented in Figure 2-36. The USA is leading the application of polymer flooding including applications in sandstone and carbonate reservoirs,

and China has a larger field-scale application of polymer flooding in the Daquing field (Zhang et al, 2016).

The success of polymer applications has been attributed to a profile control mechanism where properties such as viscosity, concentration, and molecular weight are important variables to adjust in the screening process. During chemical flooding, polymers are exposed to chemical, physical and mechanical degradation processes depending on reservoir characteristics, fluids, temperature, and pressure. Therefore, an extensive screening process that includes evaluation of variables such as polymer stability to pH, salinity, temperature, flow conditions needs to be considered in the selection of the best system for polymer flooding EOR for any particular application. Veerabhadrappa et al. (2011) studied rheological characteristics of polymers measuring viscosimetry and elasticity of different combinations of polymers and found higher oil recovery associated with higher elasticity (high poly-disperse index) and also degradation of the polymer as a result of the flooding process with a consequently declining in oil recovery.


**Figure 2-36: Distribution of applications of polymer flooding on chemical EOR methods**
(Based on a review of 75 field applications from 1982 to 2016)

### 2.7.1 Commons Polymers used in EOR

Polymers type HPAM (partially hydrolysed polyacrylamide) are the most common polymers applied in chemical EOR because of their cost and wide range of available molecular weight

for different applications (Sheng, 2010a). However, the viscosity of this polymer is highly affected by brine salinity and hardness.

Results from research about the type of polymers used for CEOR applications from existing publications are presented in Figure 2-37.

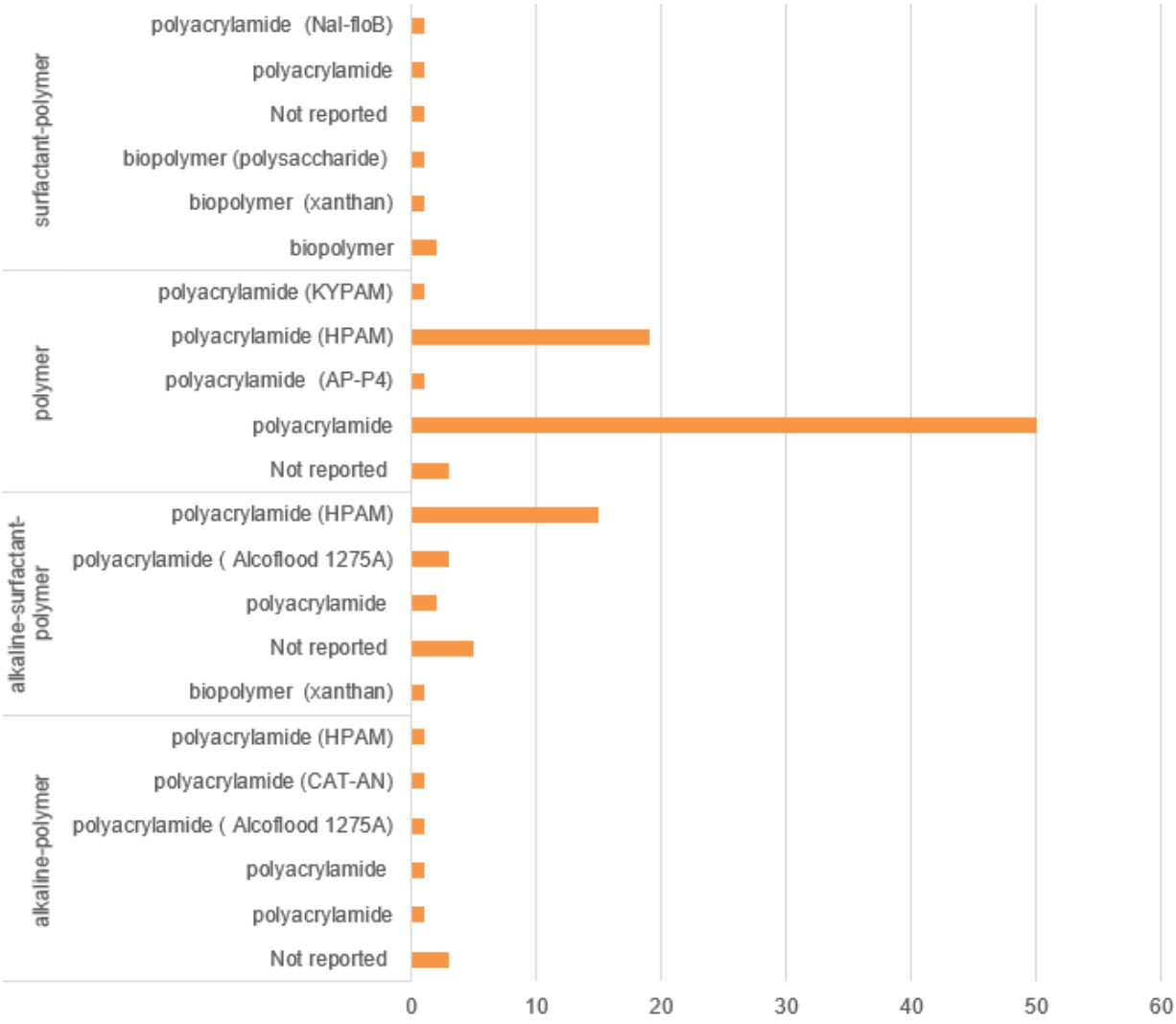


**Figure 2-37: Type of polymer applied on chemical EOR applications**
(Based on a review of 75 field applications from 1982 to 2016)

Despite the wide range of available acrylamide based polymers tolerant to high salinity, brine hardness and temperature for different applications, polyacrylamide PHPAM polymer is the more used for field applications (50% of publishing applications). Modified polyacrylamide

(Comb-polymers) based polymers have only been applied in polymer flooding as showed in figure 2-37.

The structure of the modified polyacrylamide based polymers has been tailored to enhance ionic interaction in aqueous solutions. For example, the resistance to salinity and divalent cations (hardness) has been improved by incorporating hydrophobic monomers C8-C12-alkyl, and monomers with a different functional group along the polyacrylamide chain in the composition of HPAM. Some polymers also have other monomers, such as 2-acrylamido-2-methyl-propane-sulfonate (AMPS), incorporated into its structure (Lewit, 2008). Examples of these copolymers are type AM-AMPS and AM-nVP respectively. Furthermore, there are also the comb-type polymers which are hydrophobic modified polyacrylamide (HMPAM) made by incorporating both hydrophobic and hydrophilic groups into the short side branches along with the main chain of the copolymer as is shown in Figure 2-38. A contains a hydrophilic group and R1, R2, R3 and R4 are hydrophobic groups (Sheng, 2011). These polymers have reported higher viscosity and better resistance to high salinity than HPAM.

These high resistance polymers can expand the possibility to use the produced water with high salinity to prepare polymer solution used for polymer flooding, which increases their potential for field applications with favourable economic consequences in saving freshwater and protecting the environment.

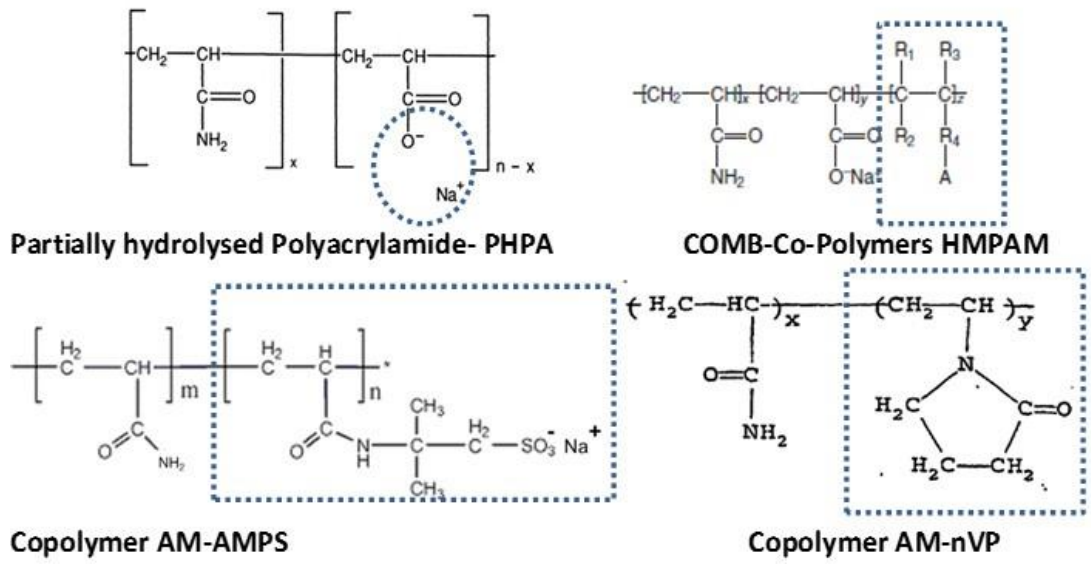


**Figure 2-38: Chemical structure of polymers and copolymers acrylamide**

Methods of polymers screening have been presented in many studies to determine the variables that affect their behaviour in aqueous brine solutions. For CEOR applications, polymer solutions are affected by different parameters; some of them are presented in Figure 2-39.

The main advantage reported for polymers is the increase of viscosity when added to the brine solution used as displacing fluid in CEOR processes (Sheng, 2010a). The viscosity of polymer solutions is controlled by several variables, such as:

- Polymer concentration, thus at high polymer concentration higher viscosity of polymer solutions can be obtained compared with the viscosity of water. However, a high concentration of polymer affects polymer adsorption on the rock and the relative permeability of the displacing fluid.
- The distribution of ions along the molecule of polymer and how these ions interact with existing ions in the brine used for the preparation of the polymer chemical slug define the viscosity of polymer solutions (Wever *et al.*, 2011).
- The salinity of polymer solutions affects the resultant viscosity. The viscosity of polymer solutions decreases by the increase of salinity. However, the resultant depends on polymer structure and hydrolysis degree. For example, while solutions of PHPA polymers increases the viscosity by charge repulsion and molecular elongation of the polymer. HMPAM polymer increase the viscosity by both repulsion and intermolecular association above a critical concentration (Levitt and Pope, 2008).
- The hydrolysis degree of the polymer defines the number of ions along the polymer molecule in aqueous solution. While non-hydrolysed polymers are less affected by salinity, they are less stable under temperature and alkali conditions. The optimal value of hydrolysis for polymers if between (25-35%).
- Optimal viscosity for polymer solutions depends on the type of crude oil and reservoir permeability aiming to obtain a favourable mobility ratio (M<1) (Wang, J. and Dong, 2009).
- Flow conditions affect the hydrodynamic size of the polymer molecule and its effective viscosity. In this area, additional consequences are important, such as polymer degradation and viscosity loss (Wever *et al.*, 2011).

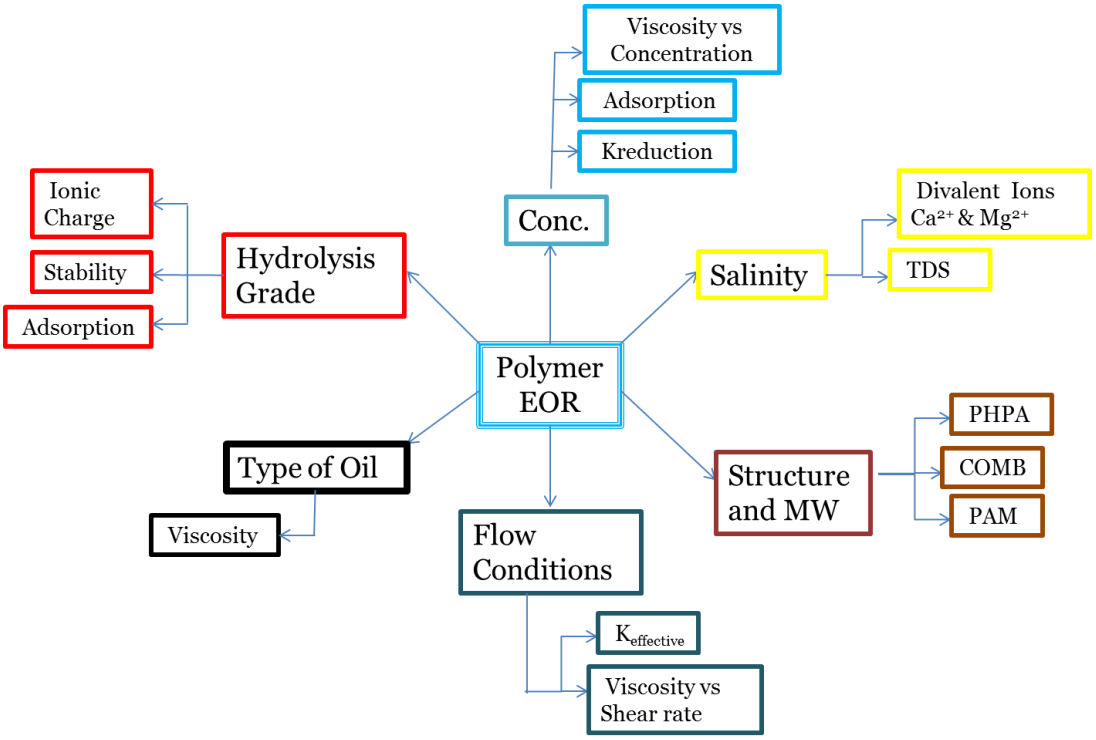


**Figure 2-39: Variables for screening polymers for CEOR applications**

As the properties of polymeric solutions are strongly linked to ionic interactions, variables such as the distribution of ionic charge along the polymer, the length of the hydrophobic monomers, the molecular weight of the polymer and polymer concentration are affected by the ionic composition and salinity of both the formation brine in the porous media and water used for injection.

One of the objects of this research is to study the behaviour of polymers as chemical flooding treatments on sandstones rocks under high salinity conditions, through the evaluation of HPAM (hydrolysed polyacrylamide) of different molecular weight (MW) and special co-polymers AM-AMPS, AM-nVP and HMPAM using concentration of divalent cations and brine salinity similar to the North Sea.

### 2.7.2 Mechanisms of polymer flooding

The principle behind polymer flooding is well understood and is based on the modification of the viscosity of the displacing fluid using polymers to travel through the reservoir rock, pushing the oil toward the production wells (Mansour *et al.*, 2014). There are several physical and chemical interactions involved in the process as polymer solutions will be in contact with

existing conditions in the porous media; the fluid will be deformed by the permeability and pore network of the reservoir. The success of an application depends on the appropriate selection of the polymer solution to be injected considering reservoir properties and location conditions (de Melo *et al.*, 2005).

The more important properties for a polymer to be evaluated before injecting into the reservoir are:

- Solubility and stability on the brine used for the preparation of polymer solution and reservoir conditions.
- Provide enough viscosity for oil displacement and tolerate brine salinity and hardness.
- Be stable under shear rate conditions given by flow conditions and permeability.
- Keep the high viscosity, and tolerance to salinity and calcium, mechanical and thermal stability, injectivity, and transport conditions (Levitt and Pope, 2008).

The effect of effective viscosity of the polymer in the oil recovery obtained for oil of different viscosities indicated that for each oil viscosity there is a minimum and maximum value of effective viscosity required for the polymer flooding to improve the oil recovery at constant permeability (Wang, J. and Dong, 2009). High polymer concentration was required for oil with high viscosity but there was an optimal polymer concentration for each oil viscosity. Polymer solutions were evaluated at a fixed shear rate. At polymer concentrations higher than the optimal, it seems other interactions prevent high polymer viscosity to increase oil recovery further.

The increase in the viscosity of an aqueous solution of polymers PHPA has been explained by the extension of the polymer due to repulsion of negatively charges existing on carboxylic groups distributed along the polymer chain (Sheng, 2010a). The number of negative charges along the polymer molecule is given by the grade of hydrolysis and by the size of the molecule or molecular weight.

The repulsion of charges along polymer solutions is shielded by the presence of ions in a brine solution with the consequent viscosity reduction. Divalent ions have a higher effect than monovalent ions on the decrease of viscosity.

For PHPA polymers, the higher the grade of hydrolysis the stronger the shielding effect on viscosity is for high salinity conditions. PHPA molecules interact to form self-complex molecules on the presence of $Ca^{2+}$, and the result is affected by the concentration of $Ca^{2+}$ and the anionic grade of HPAM (Wever *et al.*, 2011). The resultant interactions of polymers depend

on salinity, and intra-chain, interchange or formation of a complex of polymer with ionic interactions with $Ca^{2+}$.

Physical-chemical interactions are more complex for co-polymers and terpolymers because they have two types of charges, one from the carboxylic group and the other one given by the functional groups existing in the monomer. These charges can polarize the molecule and form complex structures by interaction with divalent ions. The resultant viscosity of polymers in aqueous solution depending on the type of interaction between polymer molecules and with divalent ions (Wever *et al.*, 2011).

Studies on performance of polymers under reservoir conditions reported limitations of temperature (70°C) for PHPA polymers and properties associated with the degree of hydrolysis (Shepherd *et al.*, 2013).

For hydrophobic modified polymers type comb HMPAM, hydrophobic and hydrophilic groups are introduced in the co-monomer to increase the rigidness of the molecule and to create stereo and electric repulsion between hydrophilic and lipophilic chains. There are also interactions between hydrophilic and carboxylic groups among the polymer. These electric and steric interactions increase the hydrodynamic radio of the molecule and therefore the viscosity (Zhu, You Yi *et al.*, 2012; Sheng, 2010a).

HMPAM polymer molecules form a series of entangled temporary network where both tangles and hydrophobic interactions are present in polymeric solutions (Wever *et al.*, 2011) with consequences on rheological behaviour. Because of these different interactions, the flow behaviour under high salinity conditions and shear rate need to be rigorously evaluated before any application. Adjust variables and mathematical correlations required to simulate polymer flooding EOR.

### 2.7.3 Flow equations for Polymer Flooding

To simulate the flow behaviour of polymer flooding into the reservoir some mathematics models have been developed to represent the dependence of viscosity with polymer concentration, salinity, shear rate, and reservoir permeability (Sheng, 2010a).

For the dependence of viscosity with polymer concentration and salinity different correlations have been used. For example, the viscosity of polymers for EOR has been represented by Flory-Huggins (Sheng, 2010a; Pope and Delshad, 2000; Computer Modeling Group Ltd, 2015). The correlation is presented in equation 2-41. This equation allows the estimation of polymer viscosity, $\mu_p^0$ considering polymer concentration $C_p$, salinity, and divalent ions $C_{sep}^{Sp}$.

$$\mu_p^0 = \mu_w\left(1+\left(A_{p1}C_p + A_{p2}C_p^2 + A_{p3}C_p^3\right)C_{sep}^{S_p}\right) \quad (2\text{-}41)$$

Where the factor $C_{Sep}^{Sp}$ represents the dependence with salinity and brine hardness (divalent ions), Sp can be estimated by the slope of the log-log plot of, $\frac{\mu_p^0 - \mu_w}{\mu_w}$ versus Csep and, βp is a parameter to adjust the correlation.

$A_{P1}$, $A_{P2}$, $A_{P3}$ are constants obtained through matching with experimental data,

μw is the brine viscosity, Pa·s

Cp is the polymer concentration in brine, kg/m$^3$

$\mu p_0$ – zero shear viscosity, Pa·s

The variable $C_{Sep}^{Sp}$ in equation 2-41 represents the effect of salinity and brine hardness on the viscosity of polymer solutions. The parameter $C_{sep}$ is called the "effective salinity" and represents the balance of ions available for cation exchange. $C_{sep}$ has units of concentration as Normality (N) in equivalent per litre eq/lt. The units equivalent per litre consider the valence of the divalent ions $Ca^{2+}$ and $Mg^{2+}$ and are relevant for cation exchange calculations. $C_{sep}$ considers the ionic composition, given by cations and ions concentration in the polymer solution. This parameter is mathematically calculated by using equation 6-6 (Pope and Nelson, 1978). $C_{sep}$ can be calculated by the equation 2-42;

$$C_{sep} = \frac{C_{51} + (\beta_p - 1)C_{61}}{C_{11}} \quad (2\text{-}42)$$

$C_{11}$ - water concentration in the aqueous phase, fraction

$C_{61}$ – divalent concentration in the aqueous phase, Eq/m$^3$

$C_{51}$ – anion concentration in the aqueous phase, Eq/m$^3$

The dependence of polymer viscosity on shear rate will be modelled using the power law shear thinning between viscosity and Darcy velocity as represented by equation 2-43 (Sheng, 2010a).

$$\mu_p = \mu_w + \frac{\mu_p^0 - \mu_w}{1+\left(\frac{\dot{\gamma}}{\dot{\gamma}_{1/2}}\right)^{(p\alpha-1)}} \quad (2\text{-}43)$$

Where

$\mu_w$ – brine viscosity, Pa·s

$\gamma$ – shear rate, $s^{-1}$

$\gamma_{1/2}$ - shear rate at which viscosity is the average of $\mu_w$ and $\mu_p^0$, $s^{-1}$

$\mu_p^0$ – zero shear viscosity, Pa·s

Pα - empirical parameter obtained by matching laboratory data

μp – apparent polymer viscosity, Pa·s

The effect of polymer on the mobility of the displacing fluid is accessed by the combined effect of the increase in viscosity and permeability reduction, and the term which combines these two effects is called “resistance factor”, ($R_F$). The permeability reduction factor is defined as the ratio between the effective permeability of brine and the effective permeability of the polymer and is represented in equation 2-44. The correlations used is to calculate the resistance factor is represented by equation 2-45, UTCHEM (Pope and Delshad, 2000).

$$R_k = \frac{Kw\ (effective{-}water)}{Kpolymer\ (effective{-}polymer)} \tag{2-44}$$

$$R_F = R_k x \frac{\mu_{polymer}}{\mu_{water}} \tag{2-45}$$

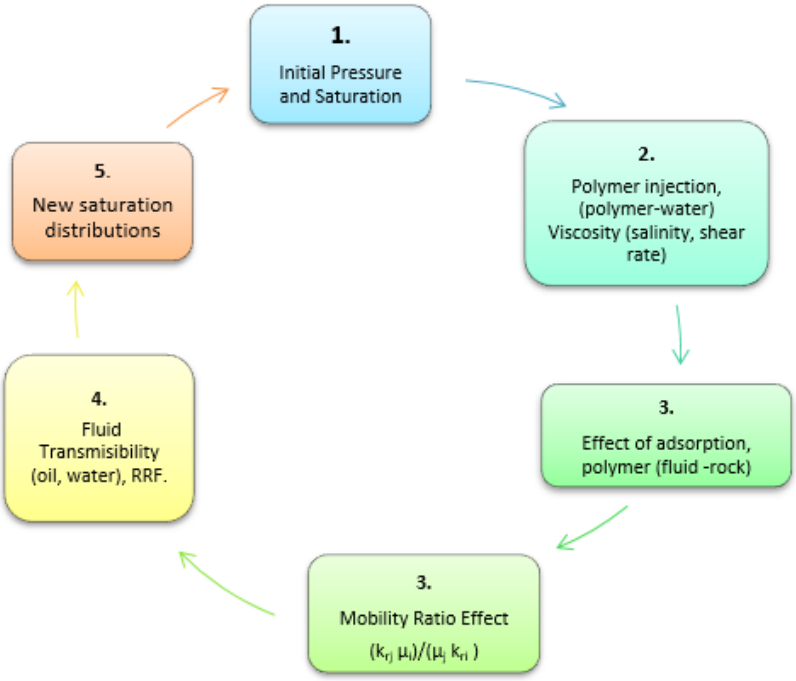


**Figure 2-40: Flow of mathematic calculation of polymer flooding**

From the diagram shown in Figure 2-40, it is important to mention the minimal required tests for evaluation of polymers are fluid stability, chemical retention, and adsorption tests, and rheological tests to evaluate the effect of viscosity with variables as polymer concentration, shear rate and salinity.

## 2.8 Interactions between chemicals, AP, SP and ASP

The success of CEOR processes is associated with the interaction of chemicals that form part of the chemical slug. Therefore, CEOR processes have evolved from alkali (Graue and Johnson Jr, 1974) or caustic flooding, to alkali-surfactant or co-surfactant-enhanced alkaline flooding (Nelson, R. et al., 1984). alkali-polymer (Sheng, 2017; Sheng, 2010a), surfactant - polymer (Pope et al., 1982) and alkali, surfactant-polymer (Demin *et al.*, 1999).

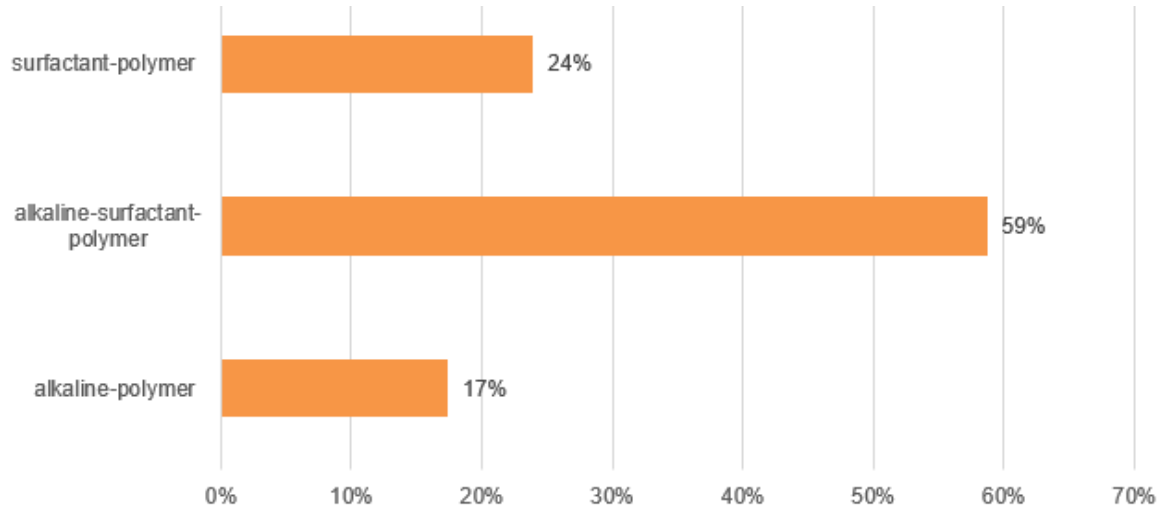


**Figure 2-41: Distribution of chemical applications of CEOR**
(Based on a review of 43 field applications from 1983 to 2015)

The distribution of applications for using combinations of chemical slug is presented in Figure 2-41 where ASP CEOR presents a higher number of applications (59%).

### 2.8.1 Alkali-Polymer

The use of alkali-polymer includes the advantage of the reduction of IFT by the natural surfactant formed from the reaction of the alkali with acidic components existing in the crude oil, plus the mobility control provided by the polymer (Sheng, 2013b; Sheng, 2010a; Sheng, 2017).

Alkali hydrolyses the polymer and increase the viscosity of polymer solution but the effect of ions in the solution reduce the viscosity of polymers (Sheng, 2010a). Applications of alkali-polymer have its major potential for acidic heavy oil that will react with alkali and form a natural surfactant. Alkali also reduces the adsorption of polymer o the rock. Field applications of alkali-polymer CEOR from published data includes heavy crude oil in Canada, USA and in China (Doll, 1988; Bala *et al.*, 1992; Zhang, J. *et al.*, 1999; Pitts *et al.*, 2004; Yang, D. *et al.*, 2010; Sheng, 2010a), the distribution of applications is showed in Figure 2-42.

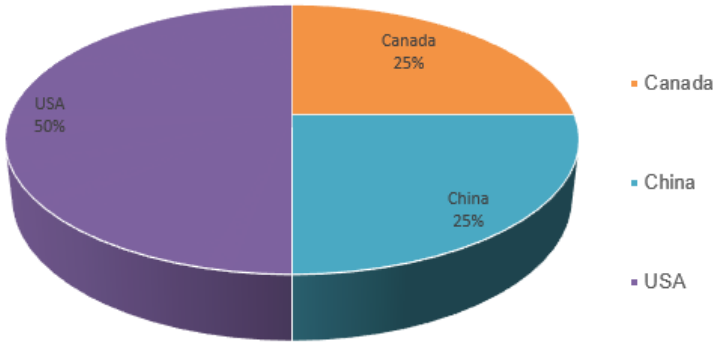


**Figure 2-42: Distribution of alkali-polymer (AP) applications by country**
(Based on a review of a total of 8 field applications from 1988 to 2014)

The use of alkali-polymer flooding increases the oil recovery in sandstone showing excellent performance compared with standalone CEOR methods using polymer or alkali (Pei *et al.*, 2014). However, the use of polymer affects the resultant IFT of alkali-polymer flooding. Experimental results comparing different sequences of alkali and polymer injection for CEOR, showed high oil recovery for concurrent injection of alkali and polymer (Sheng, 2010a). It also showed that a higher concentration of alkali is not beneficial, with a maximal of 0.5% with optimal of 0.25%.

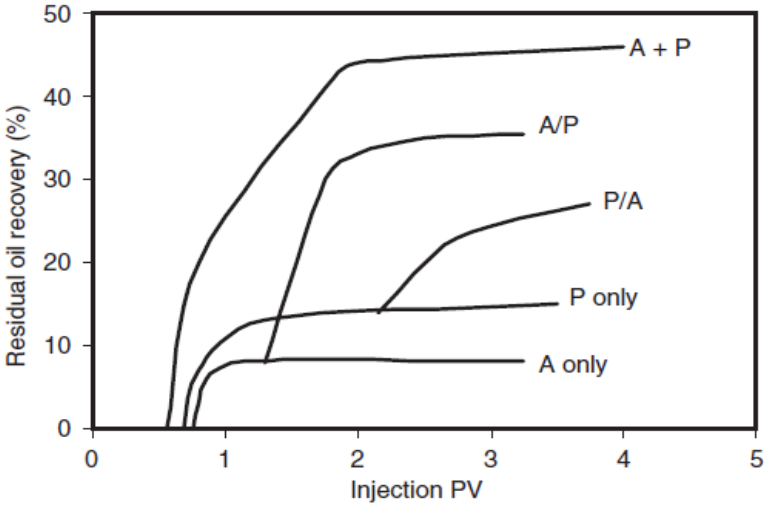


**Figure 2-43: Experimental results of oil recovery (%) by using different alkali-polymer injection** (Sheng, 2010a)

Moreover, the core-flooding test on micromodels showed advantages of organic alkali ethylenediamine over NaOH and $Na_2CO_3$ at low salinity (0.5% NaCl) on the incremental recovery of alkali-polymer flooding (Chen *et al.*, 2015).

Screening for AP CEOR based on published applications includes permeability higher of 50 mD, salinity lower than 50,000 ppm TDS and divalent ions lower than 110 ppm (Sheng, 2017). Alkali-polymer has the following advantages (Sheng, 2017):

- Alkali reduces polymer adsorption and polymer viscosity.
- Polymer increases the viscosity of alkali-polymer chemical slug and improve the sweeping efficiency.
- Polymer decreases the mobility of alkali and puts it more in contact with oil.
- The reduction of IFT and enhance on sweeping efficiency is achieved by alkali-polymer chemical slugs.

One of the limitations of alkali-polymer is related to the alkali, due to the formation of scales, which limit the use of strong alkali or high ph. Moreover, the formation of natural surfactant or soap from the reaction of alkali is favourable at low salinity. The maximal concentration of surfactant that can be formed from naphthenic acids is very small, with a maximal of 0.1% (Sheng, 2010a). There are only a few applications of this method and not conclusive results. However, the mechanism associated with each chemical and how the different combinations affect the oil recovery implies further investigation is required to verify the different interactions involved.

### 2.8.2 Interactions Alkali-Surfactant-Polymer AS, SP and ASP

ASP flooding is the injection of a pre-designed chemical slug composed of an alkali, one or more surfactants, a solvent which can be optional, brine and polymer; the composition of the slug is selected so that an ultra-low IFT microemulsion is achieved when contacted with crude oil, not chemical precipitation is observed in the compatibility tests, and this microemulsion is able to achieve high oil recovery in core flooding tests at reservoir conditions (Flaaten *et al.*, 2008; Flaaten *et al.*, 2010).

The interest on ASP date back to 1980's when Nelson et al (1984) proposed the use of a small amount of surfactant to alkali slugs to wider optimal conditions of alkali flooding, the synergy of surfactant and alkali, plus the mobility control given by a suitable polymer promoted the beginning of ASP flooding (Liu, 2008). Alkaline Surfactant Polymer (ASP) flooding involves the injection of specially designed slugs of alkali, surfactant, and polymer for mobilizing the remaining oil trapped in the reservoir.

ASP CEOR includes the combination of the three methods alkali, surfactant, and polymer considering the following aspects (Sheng, 2013a):

- Alkali reacts with crude oil to generate a natural surfactant carboxylic type and reduce the adsorption of injected surfactant.
- The natural surfactant and injected surfactant expand the range for lower IFT since they have different optimal salinities.
- The stability of the microemulsion is increased, because the high viscosity provided by the polymer reduces the time for the diffusion of chemicals through the emulsion, thus delay coalescence of oil drops in the microemulsion.
- ASP has a viscosity higher than an AS viscosity, therefore the sweeping efficiency is enhanced.
- There is a competition for adsorption on the surface of the rock between the polymer and surfactant which provide a dynamic interaction fluid-rock during the displacement of fluids.

Due to the different interactions that result from the mix of chemicals, the sequence in which slugs are injected and its impact on oil recovery are still under study. Slugs can be injected sequentially such as alkali A, surfactant S and polymer P, which is described as A/S/P or as a full mix ASP.

Usually the method consists in injecting a slug of alkali; surfactant, polymer first followed by a slug of polymer (Gurgel *et al.*, 2008), although it has been found that simultaneous injection

of alkali and polymer gives better results than sequential injections of the same solutions with not contact between them (Zhang, J. *et al.*, 1999). After water flooding, residual oil is left trapped in the smaller porous of the rock by capillary pressure; by injecting surfactant it is possible to remove the crude oil by reducing the interfacial tension between oil and water.

According to a review of publishing field applications, the major number of applications of ASP has been in China with applications in the Daqing, Shengli, Xinjiang, and Henan oilfields, among others (Wang, F. et al., 2017). ASP flooding has been researched, evaluated and applied in China for more than 20 years and ASP is classified as the most dominant technology in the Daqing oilfield, which is in the stage of industrial application.

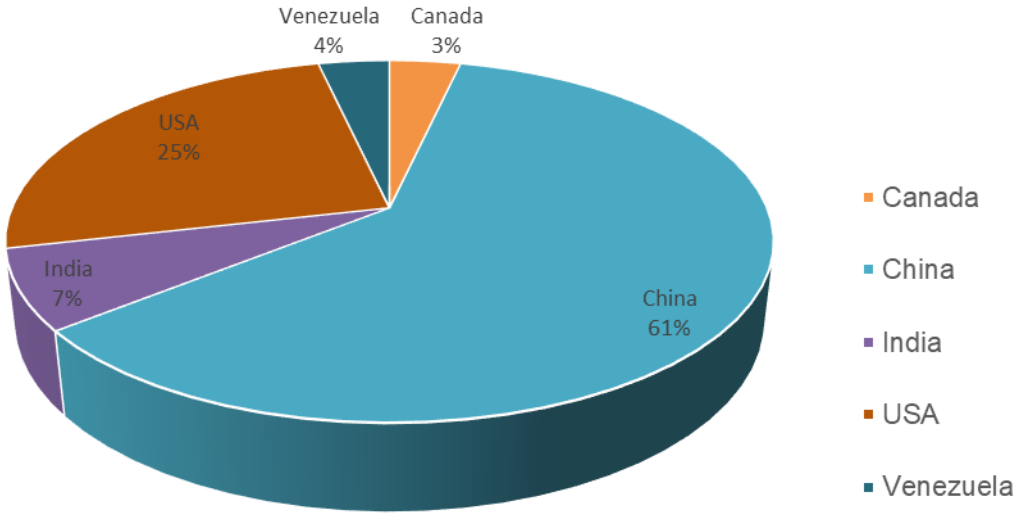


**Figure 2-44: Distribution of ASP applications by country**
(Based on a review of 28 field applications from 1992 to 2017)

ASP flooding has been applied mainly in sandstone reservoirs, and with permeability higher than 100 mD. and porosity higher than 0.25. The applications include light crude oil with API > 35 API. The distribution of screening parameters from existing publications on ASP is presented in Figures 2-45 to 2-47. Most of the applications of ASP are reported by Daqing oil field, in a range of permeabilities from 181 mD to about 600 mD and temperatures of 45ºC (Wang, F. et al., 2017). ASP CEOR applications have been in sandstones reservoirs with high porosity (>25%) and permeability (>1000 mD) and light crude oil (API >35), with viscosities lower than 100 cp. These results are presented in Figures 2-45 to 2-47.

The use of ASP has increased oil recovery until 30% OOIP in Daqing oilfield, and China has reported a learning curve from existing experience (Wang, F. et al., 2017; Zhang, D. et al., 2006). Several problems have been identified from ASP applications in China, such as the formation of scales using alkali. One of the proposed solutions was to replace NaOH by $Na_2CO_3$. Injectivity problems were also solved with fracturing and well spacing was reduced. Ongoing research in China is focused on ASP flooding using organic acid to replace inorganic alkali, also there is ongoing research aiming to understand mechanisms associated with the interaction between cationic and anionic surfactants. Existing challenges for applications are the reduction in the cost of surfactants, standardization of methods and better understanding of the criteria for IFT profile for chemical slugs.

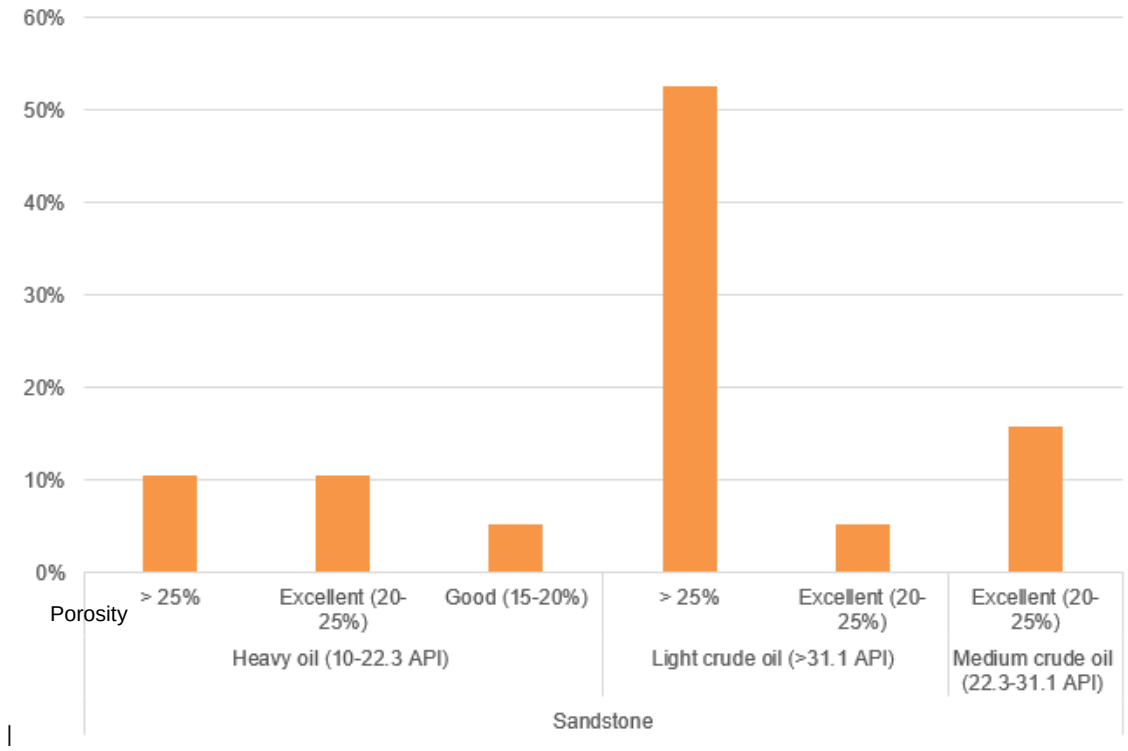


**Figure 2-45: Distribution of applications of ASP for type of crude oil and porosity**
(Based on a review of 28 field applications from 1992 to 2017)

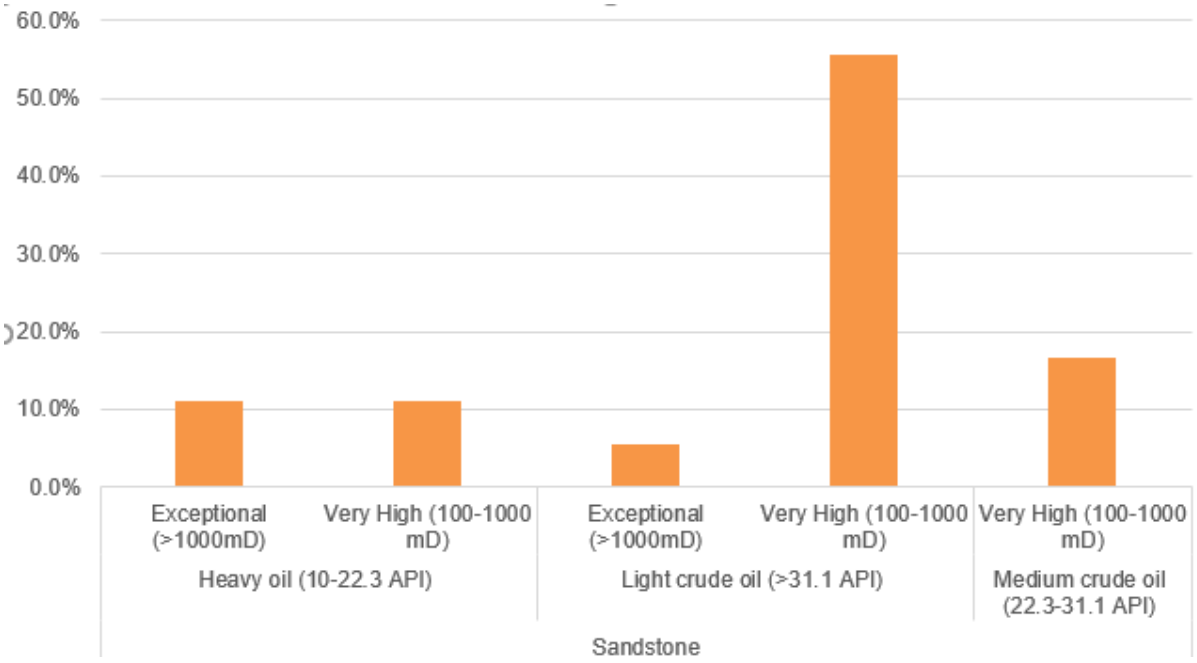


**Figure 2-46: Distribution of applications of ASP for type of crude oil and permeability**
(Based on a review of 28 field applications from 1992 to 2017)

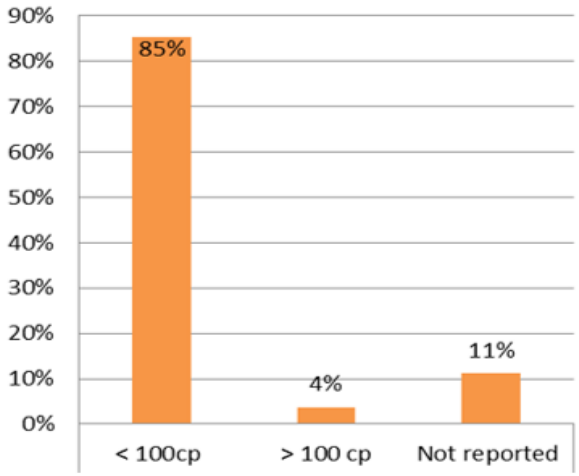


**Figure 2-47: Distribution of oil viscosity for ASP projects**
(Based on a review of 28 publications from 1992 to 2017)

Surfactant polymer SP CEOR is a process that requires the injection of a chemical slug of surfactant and polymer followed by a polymer chase slug. SP CEOR combines the effect of the surfactant and polymer, thus the reduction of IFT and change of wettability by the surfactant and the reduction of the mobility ratio due to augmented viscosity (Sheng, 2010a). SP CEOR is one of the most important processes for applications with high salinity and when

the use of ASP is not recommended. Most of the applications of SP CEOR have been reported in the USA, China, and Indonesia in sandstone reservoirs and some in carbonate rocks. SP is a simplification of ASP and has been applied in China due to problems for some ASP CEOR (Wang, F. et al., 2017; Hongyan et al., 2009).

### 2.8.3 Common systems used in SP and ASP flooding

ASP flooding combined different physical and chemical interactions between alkali, surfactant, polymer, oil and ions content in the formation brine. The design of the chemical slug and planning of the sequence of injection according to distributions of fluids in the porous medium is crucial in the success of field applications of ASP (Arihara *et al.*, 1999). During the displacement, alkali reacts with acids naturally present in crude oils (especially in case of acidic crude oils) generating natural surfactants. This surfactant acts as co-surfactant in ASP CEOR. The mechanism reported for alkali is based on the reduction of the interfacial tension between oil/water phases and adsorption of the main synthetic surfactant part of the chemical slug. Alkali, injected in the porous matrix, induces a negative charge in the rock surface.

A common mechanism for alkali and surfactant is the reduction of interfacial tension, therefore increasing the capillary number. The polymer will still control the mobility of the chemical slug by decreasing the mobility ratio thus improving sweep efficiency (Karpan *et al.*, 2011).

The mechanism predominant for polymers flooding is a reduction of the mobility of water modifying properties of the fluid hence increasing the sweep efficiency. In surfactant-based flooding, the mechanism is the reduction of interfacial tension (IFT) between the oil and the displacing fluid (Sheng, 2011; Lake, 1999) and changing formation wettability. The injection of polymer modifies the viscosity of the displacing fluid which will give more mobility control to the interfaces reducing the fingering effect and achieving piston-like displacement that will lead to a better sweep efficiency (Kotlar *et al.*, 2007).

The interactions between surfactant and polymer SP involve electrostatic and hydrophobic forces which affect IFT profile for surfactant and viscosity for polymers (Wu, X. *et al.*, 2015). The interfacial properties of the surfactant are affected by the interaction with polymer and the effect depends on the temperature (Wu, X. *et al.*, 2015). Variations on viscosity and IFT due to a combination of surfactants with polymers have been reported in previous research (Yan and Xiao, 2004; Wu, X. *et al.*, 2015; ZHU, Youyi *et al.*, 2012; Kwak, 1998).

The increase on the ITF by the addition of ionic polymer has been explained by two types of interactions that can occur between ionic polymers and surfactants, which are hydrophobic

and electrostatics (Kwak, 1998; Wu, X. *et al.*, 2015), the resultant effect on the IFT depends on the structure and ionic charge of polymer and surfactant, and also the ionic content of the solution, given by salinity and divalent cations $Ca^{2+}$ and $Mg^{2+}$. Surfactants tend to form aggregates with polymers rather than with other surfactant molecules when the surfactant concentration is at a point defined as critical association concentration CAC. At this point, the surfactant concentration is lower than the critical micellar concentration CMC. The surface tension at the CAC is slightly higher than the surface tension at the CMC. However, at a high concentration of surfactant, the effect may not be evidenced. The presence of electrolytes in solution debilitates the formation of aggregate surfactant –polymers and increases the point of CAC. A graphical representation of surface tension versus surfactant concentration for surfactant and surfactant-polymer is presented in Figure 2-48. The sequence of the formation of aggregates between surfactants and polymers is presented in Figure 2-49.

As a resultant of aggregates formation, the viscosity of blends surfactant-polymer can increase or decreases depends on the formation of aggregate polymer –surfactant given by the balance of charge between the molecule and counter ions existing in the solution. The shielding effect and net charges will govern the final orientation and hydrodynamic size of the polymer with resultant viscosity (Kwak, 1998). For example, the interactions between different hydrophobic chains existing along the polymer backbone for terpolymers or hydrophobically modified polymers with the surfactant can form complex structures which favour higher viscosities (Kwak, 1998).

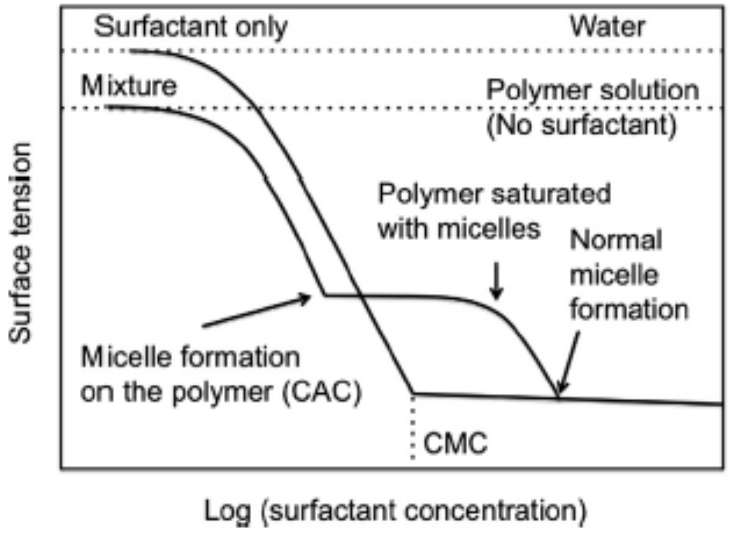


**Figure 2-48: Effect of interaction surfactant-polymers on the surface tension of aqueous solutions** (Kronberg *et al.*, 2014)

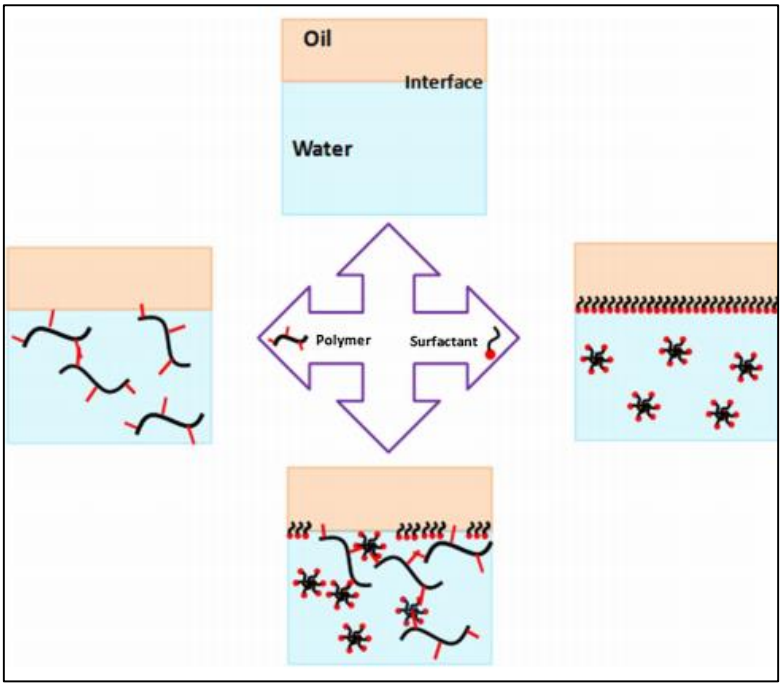


**Figure 2-49: Schematic representation of interaction surfactant-polymers on the IFT of aqueous solutions** (Wei *et al.*, 2017)

Chemicals used for SP and ASP have common surfactants and polymers. Alkali that provides strong pH, like NaOH will favour alkali reactions with naphthenic acids to generate soap, especially for low acidic crude oils. However, scale problems and damages of equipment reported by field applications in China support the use of weak alkali instead. Alkyl aryl sulfonates and petroleum sulfonate surfactants are the most applied surfactants for ASP and SP CEOR. Distribution of surfactants used for applications of SP and ASP CEOR is presented in Figure 2-50.

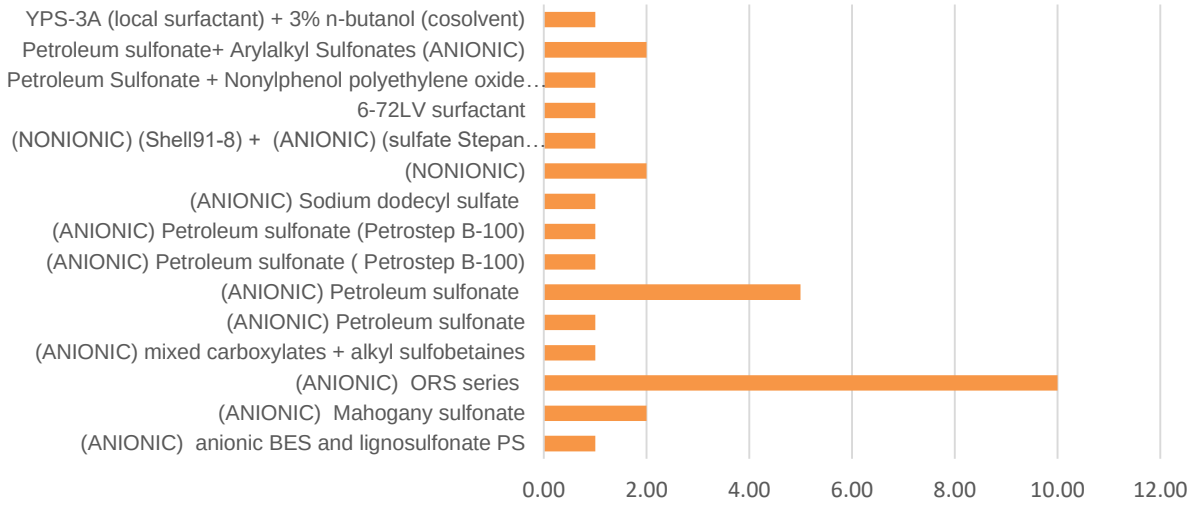


**Figure 2-50: Distribution of type of surfactant used in ASP and SP projects**
(Based on a review of 41 field applications from 1992 to 2017)

The limitations of chemicals used for SP and ASP are high salinity and temperature. These limitations have been driving forces for the development of new chemicals for CEOR applications.

Alkali such as sodium carbonate has displaced the use of NaOH. ASP CEOR flooding has limitations of salinity and divalent ions $Ca^{2+}$ and $Mg^{2+}$, if divalent ions are present in the brine, precipitation of the alkali to form $CaCO_3$ occurs, or hydroxides of divalent ions. A distribution of alkali used for ASP CEOR applications is presented in Figure 2-51.

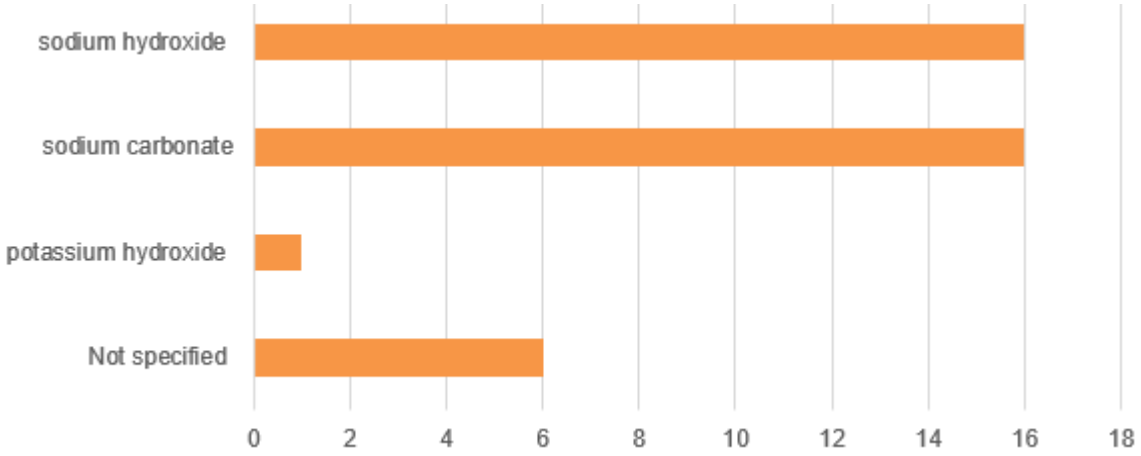


**Figure 2-51: Distribution of type of alkali used in ASP projects**
(Based on a review of 28 field applications from 1992 to 2017)

The use of sodium metaborate as a complex agent for $Ca^{2+}$ and $Mg^{2+}$ was reported by Zhang et al (2008), the system is sensitive to pH and more stable at pH> 10.5. Flatten et al (2010) also evaluated the alkali in conjunction with a mix of surfactant alcohol propoxy sulfate $C_{17-18}$-7PO-$SO_4$ and an internal olefin sulfonate $C_{15-18}$-IOS in a relation 1:1 the optimal salinity was maximal 160,000 mg/L TDS. However, the optimal salinity decreases with sodium metaborate, which demonstrates the alkali increases divalent tolerance but not high salinity tolerance.

The sequence of the injection of chemicals and salinity for ASP CEOR processes is an important aspect of the design. According to reported applications of ASP flooding, requirements for a low optimal salinity for microemulsion formation of chemical slugs define the sequence of injection of fluids for CEOR. Some applications have used a sequence that included the use of a pre-flush of low salinity soft water, followed by the chemical slug at the optimal salinity for microemulsion formation. This salinity is lower than the salinity of the water existing in the reservoir rock, therefore a salinity gradient is created during the displacement (Bourrel et al., 2011; Liu, 2008). The effect of the salinity gradient is still in discussion. For example, a negative salinity gradient was first proposed by Nelson (1982), with the following sequence: injection of a pre-flush at salinity higher than the optimal salinity for micro emulsion formation, following by the chemical slug at the optimal salinity and a post chemical slug at lower salinity. In opposition, Sheng (2010) proposed an optimal salinity profile with injection as follows: a pre-chemical slug at any salinity, followed by a slug and post slug at the optimal salinity for micro emulsion formation. A schematic representation of the sequence of the salinity of the fluids injected for the two displacement schemes is presented in Figure 2-52. It has been demonstrated by simulation how a salinity gradient can keep the surfactant at optimal conditions and will reduce chemical retention (Hirasaki et al., 1983). However, the best type of microemulsion for optimal oil recovery, not always result in the highest recovery (Sheng, 2010a).

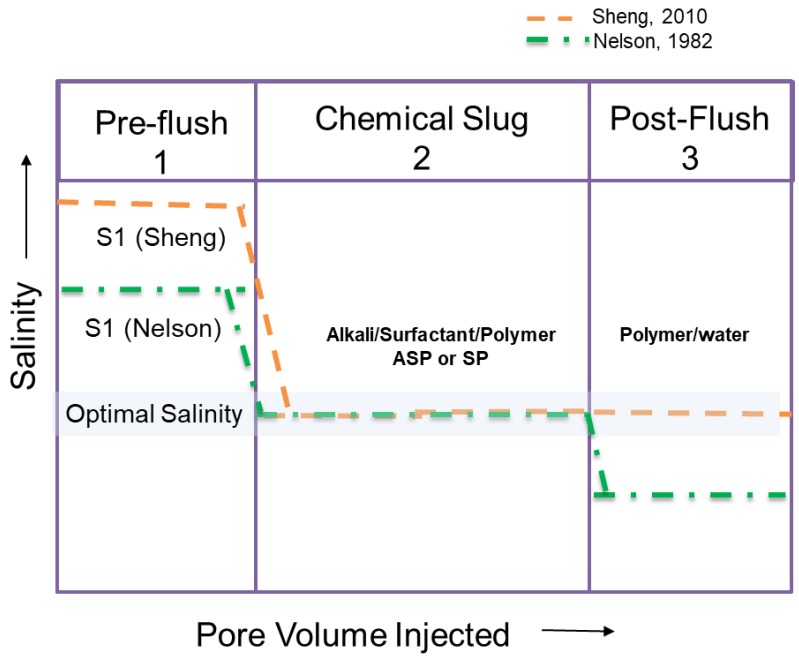


**Figure 2-52: Schematic representation of the salinity for the sequence proposed to keep chemicals at the optimal salinity for microemulsion**
(Sheng, 2010a; Nelson, R., 1982)

Based on these findings, the complexity of the interactions on CEOR processes is evident and increase from standalone to combined methods. Several ionic interactions can control the properties of the chemical slug and the effectiveness of the process. It is also evident that not only interactions fluid-fluid and the design of the chemical slugs in the laboratory are important but displacement tests using core-flooding and sensitivity analysis with simulation are also required to understand the different interactions and the complexity of the process.

### 2.8.4 Properties and correlations for ASP chemical flooding

The success of chemical ASP flooding relies on the ability of the system to recover more oil from the reservoir and increase displacement efficiency. As the ASP CEOR method was created as an evolution of alkali, surfactant, and polymer, the evaluation of properties described before is required for the design of the chemical slug.

The selection of the optimal ASP system is based on a series of tests, part of them following the flow chart presented in Figure 2-27, (Sheng, 2010a). The design can be divided into two stages, one stage is the evaluation of fluid-fluid interactions which include: stability test, phase separation tests, soap generation test and the relation between IFT and optimal salinity conditions. The second stage is the interactions fluids-rock which is represented by relative

permeability tests, chemical retention tests (absorption tests, wettability, permeability reduction factor) and the relationship between a capillary number and residual oil saturation. The final ASP slug will be then tested in a core flooding test to simulate dynamic conditions.

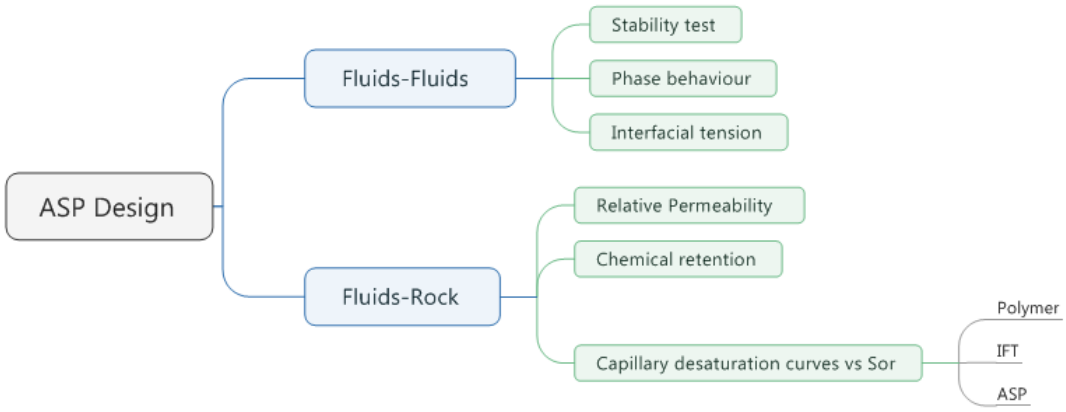


**Figure 2-53: Stages for the design of ASP slugs for CEOR**

The resultant synergy of ASP systems relies on the modification of both capillary number and mobility ratio. The optimal ASP slugs have to fulfil a series of requirements (Hirasaki et al., 2011; Bataweel, 2011):

- It should show compatibility with formation fluids to avoid any insoluble precipitate that could modify rock or fluid properties during displacement.
- Minimal chemical retention by adsorption on the rock surface or by internal interactions between surfactants and polymers existing in the chemical slug.
- Be able to generate an ultra-low IFT miscible zone of microemulsion during the displacement process.

The use of alkali increases the negative charge of the surface of the rock thus reduces the adsorption of chemicals. In the study surfactant and polymers are these chemicals in the ASP slug that compete for adsorption places on the rock surface. (Bataweel, 2011) studied adsorption from ASP systems and reported how intermolecular interactions between surfactant and polymer affect the optimal interfacial tension of the chemical slug (Bataweel, 2011), thus affect surfactant concentration. Chromatographic separation of ASP chemicals has been reported (Wang, Z. *et al.*, 2013) due to adsorption and retention during displacement inside a sand packed long slim tube, polymer adsorption was higher than surfactant adsorption. The design of ASP slug is complex and involved an optimal salinity to generate

ultra-low IFT miscible zone. Ideally, optimal salinity conditions must be closed to the conditions existing in the rock, otherwise soft water is required for the chemical slug.

### 2.8.5 Flow Equations for ASP flooding

The representation of the ASP CEOR process includes the use of appropriate correlations for the interactions of alkali, surfactant, and polymers as were discussed in previous sections. The modelling of APS CEOR is very complex as it must consider the concomitance of interactions described for alkali, surfactant, and polymer plus the effect of salinity and existing conditions in the reservoir.

The flow of fluids is affected by interactions fluid-fluid and fluids-rock. As the polymer is used, the viscosity of the slug will increase to control mobility; alkali will react with oil to generate natural surfactant that will add to the synthetic surfactant to modify the phase behaviour reducing IFT, alkali also will react with formation to change wettability and modify ionic distribution thus chemical adsorption. The schematic flow of mathematical calculations for ASP CEOR is presented in Figure 2-45. To represent the flow behaviour during ASP CEOR, the mathematical model needs to consider (Mohammadi and Jerauld, 2012) the following aspects:

- Generation of soap by the reaction of alkali with the crude oil, according to the equilibrium reactions (2-31) to (2-34).
- Changes in phase behaviour considering the partition of surfactant and soap concentration between oil and aqueous phase.
- IFT oil/water as a function of surfactant, soap concentration and salinity.
- Changes in adsorption, considering correlation (2-21) and effect of pH.
- Ionic interactions between fluids and rock given by the reaction equilibrium (2-35) to (2-39).

In addition to the points included above, the effect of salinity gradient generated during CEOR process and its effect on the oil recovery also needs to be considered when the optimal salinity or designed chemical slug includes the use of soft water as it was explained on section 2-7.1.

This research covers the collection of experimental data and simulation of interactions fluids-fluids and fluid-rock that occurs in CEOR process. The study is based on conditions existing in the North Sea for the formation brine composition, crude oil, and temperature conditions. The reservoir rock is simplified to homogenous at a laboratory scale.

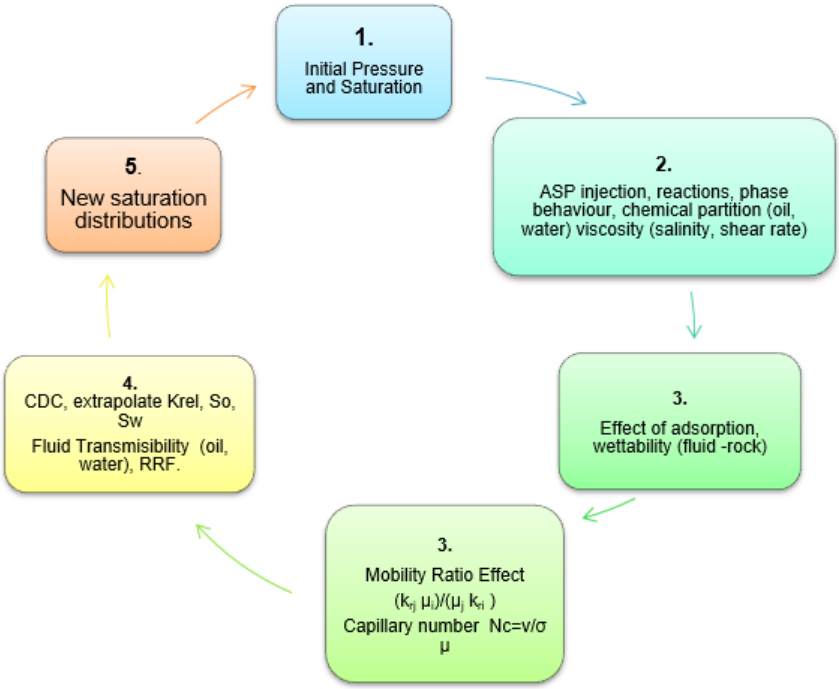


**Figure 2-54: Flow of mathematic calculation of ASP flooding**

### 2.8.6 The role of the brine salinity and hardness on CEOR processes

In this section, specific aspects of salinity and effects on EOR will be discussed. Salinity is usually represented by the total concentration of solids or total dissolved solids (TDS) in mass percentage. However, the content of divalent cations ($Ca^{2+}$ and $Mg^{2+}$), defined as hardness, in the brine is more critical for the selection of chemicals for CEOR processes than the total salinity (Lake, 1989).

The classification of water according to the salinity is presented in table 2-4. The range of salinity found in oilfields can go from low salinity (500 ppm to higher than 200,000 ppm).

A sample of the population of salinity and divalent ions concentration for oilfields brines is represented in Figure 2-55, salinity higher than 10,000 ppm TDS are classified as high salinity. The area of salinity and hardness used for this study is identified with a circle in the graph presented in figure 2-55.

**Table 2-4: Water classification according to salinity**
(Government of Western Australia. All rights reserved., 2017)

| Water classification | Salinity (ppm) |
|---|---|
| Fresh water | < 500 |
| Very low salinity | 500 –1 000 |
| Low salinity | 1 000 – 2 000 |
| Media salinity | 2 000 – 10 000 |
| **Highly salinity** | **10 000–35 000** |
| **Brine** | **> 35 000** |

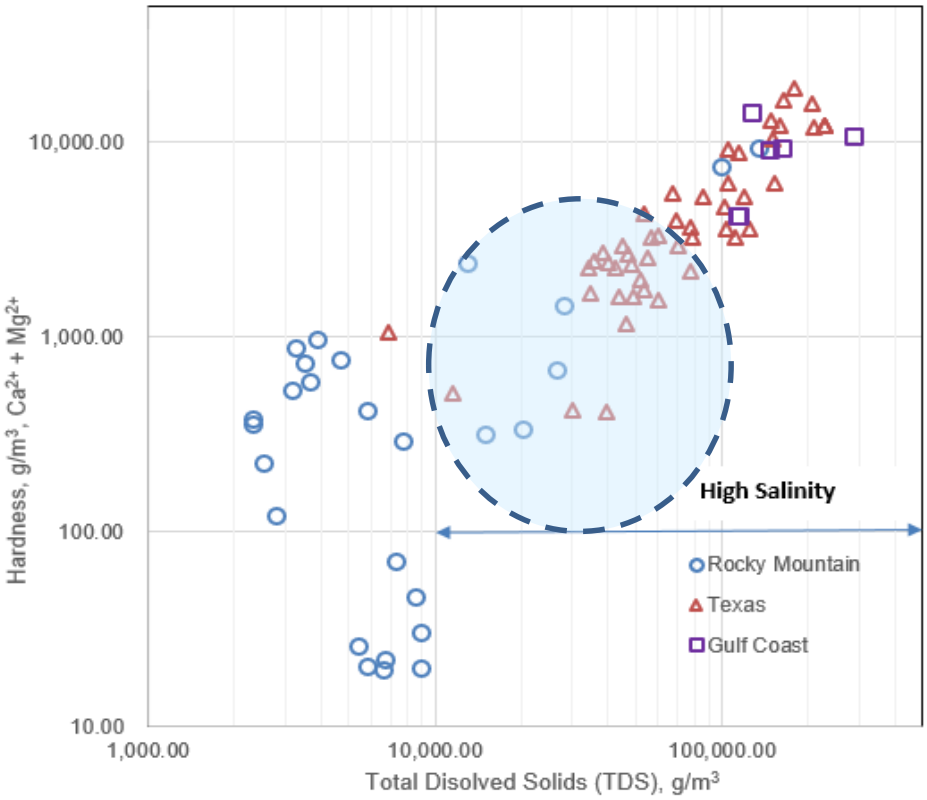


**Figure 2-55: Salinities from representative oilfield brines**
(Lake, 1989)

Water is injected in oil reservoirs as a secondary method of oil recovery and the salinity of the water is determined by the location conditions. Usually produced water or seawater available offshore are used for injection. The composition and salinity of the water used for injection is very relevant for CEOR processes (Sheng, 2014b; Ayirala and Yousef, 2014), due to the advantages found with the injection of low salinity, and the requirements for optimal salinity for surfactant applications.

Low salinity water flooding remarkable increases the oil recovery compare with high salinity water flooding (Tang and Morrow, 1997), however the mechanism that favour the process is not well understood yet. Low salinity is recognized as a CEOR method with economic advantages compare to the rest of the chemicals because is an extension of water flooding using engineered water and not many additional facilities are required in the oilfield (Sheng, 2014b).

Studies have demonstrated that there is an increase in the oil recovery factor by ionic effect, given by the interactions between the injected brine with the existing formation brine. This result is not new and dates back from 1997 (Tang and Morrow, 1997); however, the subject has recently been an object of growing research to understand the mechanisms that govern the process. There is a specific area of chemical EOR identified as low salinity technology which a patented technology called LoSal$^{TM}$ developed by BP (Lager *et al.*, 2007).

From the analysis of existing published research in low salinity water flooding, it was found a total population of 771 publications using an analytic search tool available in Scopus. The distribution of publications by country is presented in Figure 2-52. Most of the research has been done in the USA by the University of Texas followed by China and Norway. Universities are leading the research in low salinity with some pilot applications from oil companies.

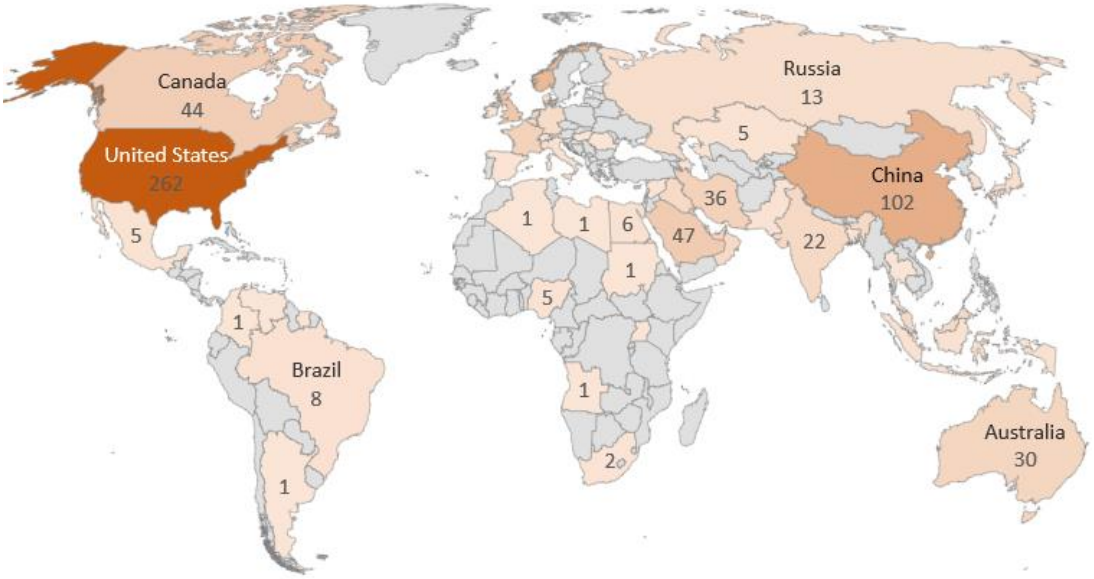


**Figure 2-56: Distribution of the number of publications in low salinity by country**
(Based on 771 publications of research and applications of low-salinity CEOR)

Field applications of low salinity are reported in Alaska by British Petroleum BP with the increase of oil recovery of 4 to 9% by the injection of low salinity from the composition of formation water. A summary of applications in low salinity is presented in table 2-5.

**Table 2-5: Field applications of low salinity water flooding**

(Dang *et al.*, 2013)

| Author | Reservoir | Injected Brine (ppm) | Formation Damage | Incremental Oil Recovery (%) |
|---|---|---|---|---|
| Webb (2004) | Sandstone | 3,000/ 220,000 | No | 20% -50% |
| McGuire (2005) | Sandstone <Alaska North Slope> | 150-1,500 /15,000 | No | 13% |
| Robertson (2007) | Sandstone <West Semlek Reservoir> <North Semlek Reservoir> <Moran Reservoir> | 10,000/60,000 3,304/42,000 7,948/128,000 | No | Recovery tends to decrease as the salinity ratio increases. |
| Lager (2008) | Sandstone <Alaskan Oil Field> | 2,600/ 16,640 | No | 10% |
| Veledder (2010) | Sandstone <Omar Oil Field> <Isa Oil Field> | 2,200/ 90,000 | No | 10% - 15% |
| Seccombe (2010) | Sandstone <Endicot Oil Field> | 12,000/ -- | No | 13% |
| Skrettingland (2010) | Sandstone <Snorre Oil Field> | 500/50,000 | No | No significant change. |

The effect of low salinity on the study and design of chemical enhanced oil recovery processes CEOR with alkali, surfactant, and polymer has been evident by the required optimal salinity for the chemical slug, which is usually a low salinity compare with the salinity of the connate water. However, chemical composition requirements for the salinity and ion composition of the brine are different for the different CEOR processes (Ayirala and Yousef, 2014).

Low salinity water flooding CEOR requires the injection of low salinity with a selective composition of divalent ions, such as sulfates, $Ca^{2+}$ and $Mg^{2+}$ (Manshad *et al.*, 2016). For alkali CEOR, the formation of petroleum sulfonates is favourable at very low salinity. Besides, alkali precipitates with divalent cations to form insoluble hydroxides. Surfactants also require optimal conditions of salinity to form the III phase microemulsion with ultra-low IFT.

Surfactant and polymer adsorption increase with divalent ions (Ayirala and Yousef, 2014). Salinity also affects the viscosity of polymer solutions and the effect is higher with divalent ions. Analysis of IFT of brines with different inorganic salts at different salinities reveals that there is a minimal IFT at 1,000 -2,000 ppm TDS, results are presented in Figure 2-48 (Manshad *et al.*, 2016). Similar behaviour has been published, with different salinity for minimal IFT (Kakati and Sangwai, 2017; Moeini *et al.*, 2014).

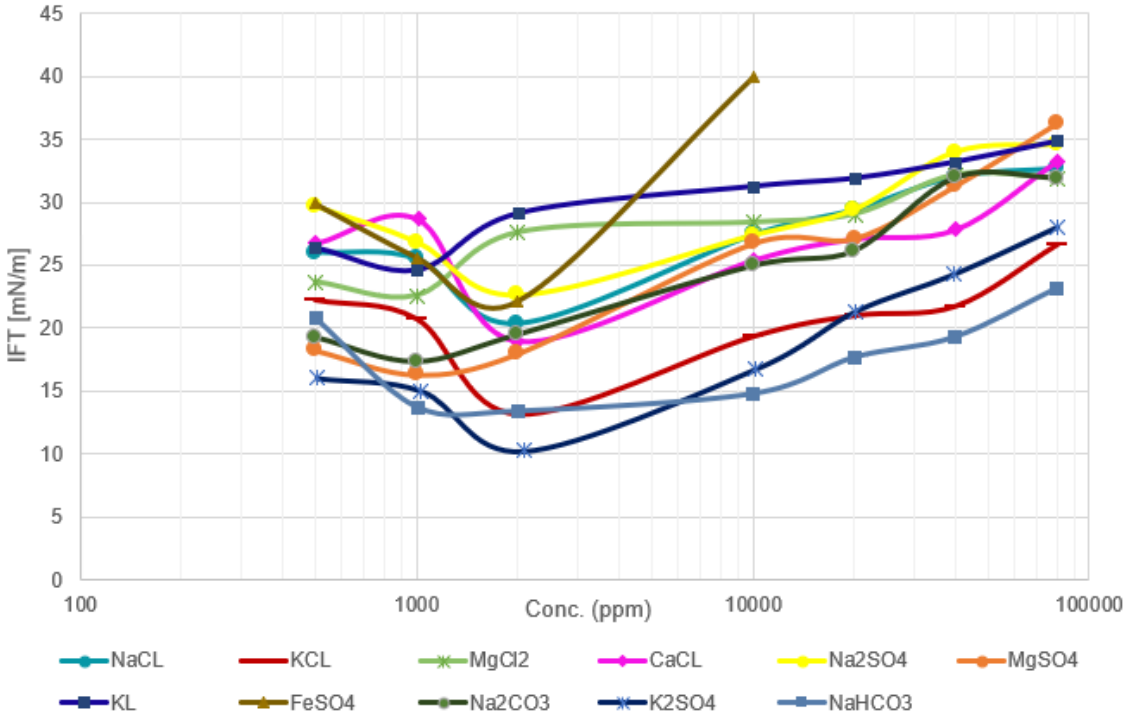


**Figure 2-57: Interfacial tension (IFT) of brines with different inorganic salts at different salinities**

(Manshad *et al.*, 2016)

The decrease in surface tension of saline solutions at lower concentrations has been an object of controversy, discussion, and research. Studies of the electrical potential at the interface air/water and the activity coefficient of ionic aqueous solutions, containing 1:1 electrolyte at high salinity revealed that the activity coefficient factor of the ionic solution has a great effect on the surface tension, especially for electrolytes containing hydrogen and nitrate (Leroy *et al.*, 2010).

Cations in the solution act as “structure–breaking” ions which can be positively absorbed at the air/water interface and effectively reduce the surface tension. As a result of interactions between positively charged ions with the dipole of water molecules, intermolecular interactions

are affected. This effect can cause a weakening of the net force produced by the water dipole moment and thus decrease the Gibbs free energy. As the Gibbs free energy is directly proportional to the surface tension, a reduction of surface tension is observed.

Anions have the opposite effect and they can act as “structure making” migrating to the bulk water and makes the water dipole interact through the hydrogen. As a result, the surface tension increases by the accumulation of negative charge at the interface air/water (Leroy *et al.*, 2010).

Similar results obtained for surface tension have been observed for interfacial tension. The IFT between oil/brine decreases with the increase of salinity until a minimal value and increases with a further increase of salinity. The composition of the crude oil and brine affects the salinity for the minimal interfacial tension for each system. The following trends have been found (Kakati and Sangwai, 2017):

- For aliphatic or saturated oils, the dilution of brine with sodium ions $Na^+$ reduces the IFT oil/brine more than with divalent ions $Mg^{2+}$ and $Ca^{2+}$. The effectiveness of IFT reduction follows the sequence: $Na^+ > Mg^{2+} > Ca^{2+}$. And the sequence for hydrocarbon is C5 > C6> C7.
- For aromatic oils, the dilution of divalent cations $Mg^{2+}$ and $Ca^{2+}$ reduces the IFT oil/brine more than with $Na^+$ and the sequence is $Mg^{2+} > Ca^{2+} > Na^+$.

The resultant surface tension of aqueous solutions containing electrolytes, $\sigma_E$, is thought to be the combination of the interfacial tension of pure water ($\sigma_W$) and the resultant in surface tension increment due to interactions of electrolytes ($\Delta\sigma$). This increment is related to the electronic radii and concentration of the electrolyte and can be positive or negative (Marcus, 2016).

At the moment, there are 17 mechanisms reported to explain the favourable effect of low salinity water flooding (Sheng, 2014b), some of them are very similar to mechanisms reported for alkali, surfactant, and polymer, such as wettability alteration, reduction of IFT, mineral dissolution, and emulsification. Wettability modifications by low salinity have been one of the most investigated mechanisms aiming to understand how ionic composition and salinity gradient affect the enhanced oil recovery process. According to proposed mechanisms, the acidic components in crude oil plays an important role in the results obtained by low salinity water flooding (Hua *et al.*, 2016). Besides, divalent ions in the formation water can act as a bridge between negative charges on the rock surface and the acidic components of the crude oil (represented as carboxylic acids), making the surface more hydrophobic. Wettability modification has been explained by two ionic interactions, one is the mechanisms is the multi-

component ion exchange (MIE) and the other is the double layer expansion (DLE) in sandstone reservoirs.

The DLE mechanism considers there is debilitation of the forces between rock-ions and oil/ion at the interface rock-fluid. The resultant forces and interactions in the rock-brine-oil system can change the wettability of the rock to more water-wet. Therefore, injection of the brine at low salinity can modify the forces holding the oil in the reservoir in a way that it can be removed easily from the pore space with a resultant increase in oil recovery (Hua *et al.*, 2016). The MIE mechanism considers the system crude oil, brine and rock is disturbed by the injection of brine solutions of different ionic concentration or salinity. For example, the injection of brine at low salinity with a composition 1:1 electrolyte (NaCl % TDS brine) will promote the displacement of divalent ions initially adsorbed to the rock by the injected sodium and this effect can release the bonding between calcium and oil.

The different possible interactions between rock-brine-oil are presented in Figure 2-58.

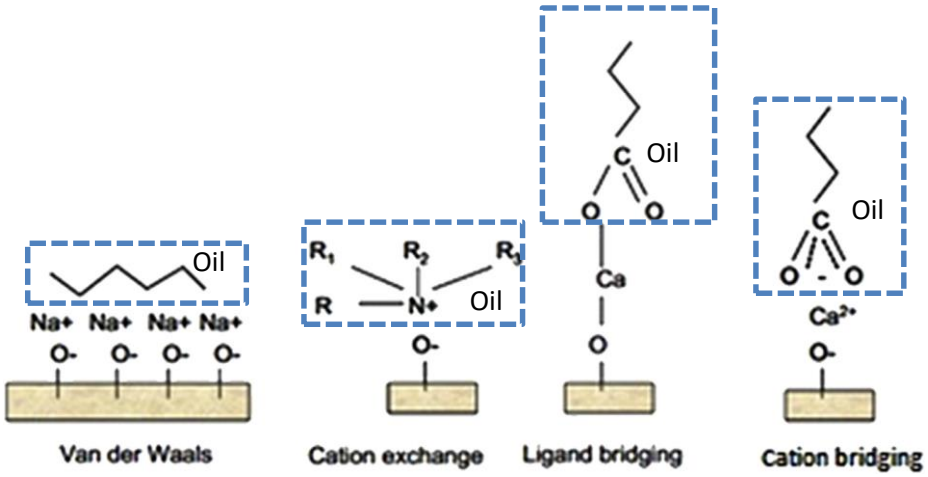


**Figure 2-58: Mechanisms of interaction between rock surface, brine and crude oil** (Lager *et al.*, 2007)

The weak Van der Walls interactions are found between a hydrocarbon and monovalent cations. The cation exchange interaction is one of the strongest interactions and occurs between aromatics oil components and the rock surface. The ligand bridging and cation bridging interaction can be found in acidic crude oils and reservoirs rock with formation brine with a high content of divalent cations. The cation bridging is the weakest interaction between oil and rock so divalent ions can be replaced by the injection of monovalent ions (Kakati and Sangwai, 2017).

Interesting, similar mechanisms have been reported by alkali flooding for interactions rock/brine/oil and the surfactant-like behaviour tends to be like surfactant flooding. The relevance of the salinity and ionic composition on the mechanisms of CEOR is demonstrated in low salinity water flooding. However, it is still not clear the effect of the brine composition (monovalent or divalent ions) on the effectiveness of the process. Some research reported an increase in oil recovery by injection of diluted monovalent salts (Hua *et al.*, 2016) but not change have been obtained for some cases. The injection of low salinity brine with a diluted concentration of divalent ions also reported an increase in oil recovery (Kakati and Sangwai, 2017).

This effect of low salinity is relevant for the design of the displacement of the chemical slug for SP and ASP CEOR processes, because of the determination of an optimal salinity to get ultra-low IFT for surfactants and the plan of injection and displacement of fluids to control those conditions. Besides, to minimize the precipitation of divalent ions during ASP CEOR processes, the injection of a pre-flush and post flush of water with low salinity is required as part of the CEOR process (Lake, 1989). However, the effect of the injection of that low salinity and the salinity gradient created between the formation brine and the injected low salinity brine as part of the sequence for CEOR is not clear yet. This salinity gradient also needs to be considered on the mechanism of the CEOR process.

There are several studies on the design of the displacement of CEOR flooding to evaluate the effect of the salinity gradient created, aiming to maintain the optimal conditions of salinity for ultra-low IFT microemulsion longer during the displacement of fluid in the porous media, however there is no clear indication of the mechanism that favour an increase of oil recovery. A negative salinity gradient was recommended during the injection and displacement of surfactant flooding to keep the surfactant/oil IFT on the salinity zone for microemulsion formation, or Windsor Type III (Nelson, R., 1982)

. The negative salinity gradient can be achieved by injecting a pre-flush of water at salinity higher than the optimal salinity, followed by the chemical slug at optimal salinity and then further post-flush of brine at salinity lower than the optimal salinity. This sequence of negative salinity gradient follows an arrangement of phases in the following order: II III I on the Windsor phase separation diagram for surfactant versus salinity test. Further studies (Hirasaki et al., 1983) confirmed several advantages of the use of the negative salinity gradient compared to the constant salinity flood. The design of displacement for optimal conditions of salinity for surfactant, polymer SP CEOR was to inject the surfactant slug at optimal salinity and the polymer at lower salinity. This plan was aiming to keep the salinity conditions for ultra-low IFT

for the surfactant slug and then reduce the adsorption of surfactant with the injection of the polymer at low salinity. Later studies of different cases of salinity gradient demonstrated that the negative salinity gradient was not applicable for reservoirs with existing formation brine at low salinity (Bourrel et al., 2011). The use of a non-negative gradient with a sequence of phase I III I increased the recovery factor. The non-negative gradient is achieved by injecting a low salinity ahead of the chemical slug follow by optimal salinity and a post slug of low salinity, higher than the pre-slug. Results suggested that a non-negative gradient will have better oil recovery than a negative gradient for low salinity reservoir conditions; however, the simulation was not able to match experimental results (Bourrel et al., 2011). The injection of surfactant at salinity lower than the optimal salinity was recommended to avoid retention of surfactant in the rocks surface, thus keeping a Windsor phase I, (Spildo *et al.*, 2014).

From these results, the importance of the salinity and ionic composition on the design of CEOR processes is evident. However, if the injection of low salinity can improve the oil recovery factor, the contribution of the chemical slug to the resultant increase in oil recovery and the involved mechanisms that prevail with the different sequences of injection are not clear yet.

## 2.9 The effect of the crude oil on CEOR processes

Crude oils can be classified according to their chemical composition in paraffinic, naphtenic or aromatics base oils. Paraffinic oils have a high content of saturates, they are usually light oils with high API and content of naphthenes in the range 15%–25%. Naphthenic oils contain saturates and aromatics hydrocarbons in a range of 25-30%, they are classified as medium oils. Aromatic oils are mainly composed of aromatics hydrocarbons and high content of sulphur; they are classified as heavy oil. A ternary diagram of the crude oil classification based on the chemical composition is presented in Figure 2-59 (Pabón and de Souza Filho, 2019). The crude oil composition distribution based on the amount of saturated (non-polar paraffin compounds), aromatic (aromatic and slightly polarizable hydrocarbons), resins and asphaltenes (polar compounds) in the crude oil is determined by an analysis method called SARA.

The crude oil composition and its interactions with brine play an important role in the mechanism associated with wettability changes. Studies on the effect of the type of salt on the interfacial tension of brine/oil suggested monovalent salts are effective to increase the oil recovery of aliphatic hydrocarbons and brines with monovalent salts are more effective for aromatics hydrocarbons (Kakati and Sangwai, 2017). It has been reported a high reduction in IFT for crude oils with high aromatic content (Kakati and Sangwai, 2017).

It is also believed that polar components on the crude oil, which are associated with the acidic components, are also responsible for the decrease of interfacial tension of low salinity brine/crude oil. The effect of different crude oils and with a different type of salinity are presented in table 2-6. Higher IFT values were obtained for divalent salts compared with monovalent.

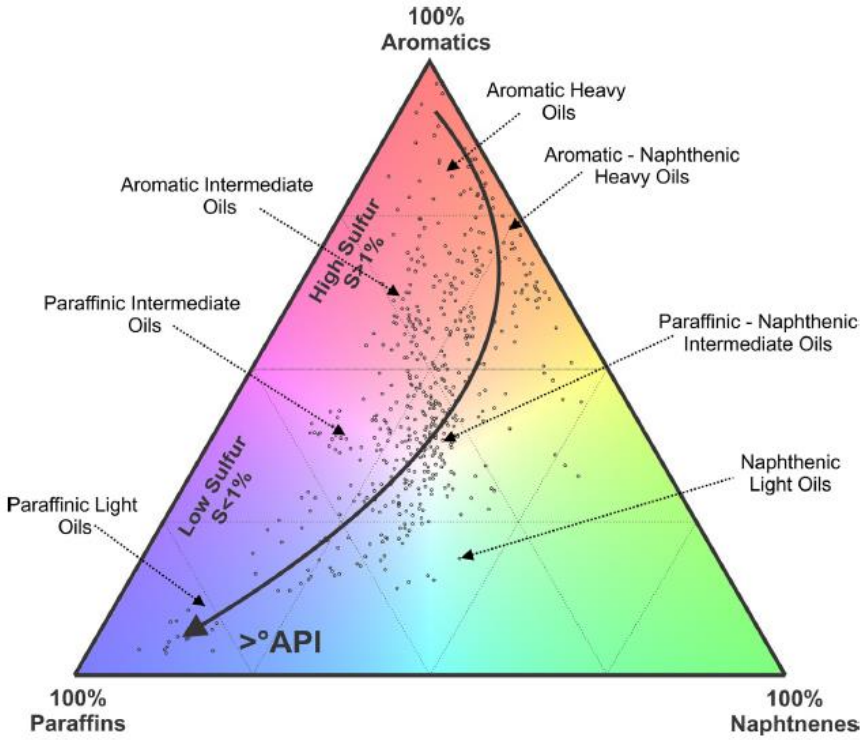


**Figure 2-59: Crude oil classification based on SARA distribution, API and sulphur content**
(Lager *et al.*, 2007)

**Table 2-6: Effect of brine salinity and composition on the IFT for different crude oils**
(Kakati and Sangwai, 2017)

| Crude type | Brine type and concentration range | Effect on IFT |
|---|---|---|
| Yates crude | Yates reservoir brine | Minimum IFT at 50% dilution |
| Iranian crude, 20° API, TAN 1.5 | NaCl 0-45000 ppm | Minimum IFT at 15,000 ppm |
| | $CaCl_2$ 0-45000 ppm | IFT decreases with increase in salt concentration |
| | $MgCl_2$ 0-45000 ppm | Minimum IFT at 30,000 ppm |
| | $Na_2SO4$ and $MgSO_4$ 0-45000 ppm | Minimum IFT at 15,000 ppm |
| Iranian crude, 20.2° API, TAN 0.06 | NaCl 0-200000 ppm | Minimum IFT at 30000 ppm |
| | $CaCl_2$ 0-200000 ppm | Minimum IFT at 40,000 ppm |
| Asmari crude (Iran) | NaCl, KCl, $MgCl_2$, $CaCl_2$, $Na_2SO_4$, $MgSO_4$, KI, $FeSO_4$, $Na_2CO_3$, $K_2SO_4$ and $NaHCO_3$ 0-100000 ppm | Minimum IFT between 1 000 and 2000 ppm |

All previous results suggested that oil recovery for CEOR is also associated with changes in the chemistry of the water (Hilner *et al.*, 2015; Pouryousefy *et al.*, 2016; Kakati and Sangwai, 2017). There is a growth in research and publications that demonstrated that low-salinity water injection increases the oil recovery factor (Sheng, 2014b; Jerauld et al., 2006; Vledder et al., 2010; Mohammad Salehi et al., 2017; Pouryousefy et al., 2016). However, the optimal conditions and mechanisms of the process still are in a discussion (Nasralla and Nasr-El-Din, 2014). There are several mechanisms reported such as wettability change, multicomponent ionic exchanges, electric double layer and, pH modifications and fine migration (Dang *et al.*, 2013). These mechanisms may also occur during ASP CEOR due to the salinity gradient created which is not fully understood yet. The effect of divalent ions and salinity on the optimal conditions for CEOR still need to be evaluated in order to control the design parameters and mechanisms that govern ASP CEOR processes and minimize associated problems of precipitation that occurs under unfavourable conditions.

In this research, the role of divalent ions and salinity and the effect on the ASP CEOR process is studied.

# CHAPTER THREE: MATERIALS AND METHODS

## 3.1 Introduction

This chapter describes the stages developed to pursue the study of the mechanisms of chemical enhanced oil recovery CEOR and the effect of brine salinity and hardness, the required materials and methods utilized to collect the data for the objectives of the research.

## 3.2 Stages of the research

To study the effect of brine salinity and hardness on mechanisms of CEOR with alkali, surfactant and polymer ASP CEOR, the following assumptions were taken into consideration:

- Homogeneous sandstone reservoir of the Bentheimer sandstone rock samples for laboratory-scale study.
- Reservoir conditions similar to the Gryphon oilfield, which is an offshore, sandstone reservoir, with crude oil 21 ºAPI and with high acidic number and temperature of 60 ºC (140 ºF).
- Reservoir formation water salinity with a composition like the production water of the Gryphon oilfield. This water is available to be reinjected and used to prepare chemical slugs or seawater can also be considered. The special conditions existing in that oilfield that are relevant for this research are existing brine salinity and content of divalent cations $Ca^{2+}$ and $Mg^{2+}$ (hardness) in the produced water and the high salinity of the seawater naturally available for injection.
- CEOR systems study based on a selection of available commercial alkali, surfactant, and polymers normally used in oilfield applications.
- The use of ethylene diamine tetra-acetic acid EDTA as a sequestering agent for divalent ions is also going to be evaluated.
- CEOR systems are injected in the reservoir rock as a tertiary recovery method (EOR) after water flooding.
- The simulation model of laboratory experiments will be matched to study microscopic displacement.

Four stages were defined for the study of the effect of brine salinity and hardness on mechanisms of CEOR with alkali, surfactant and polymer ASP CEOR which can be described as follow:

1. Study of the effect of brine salinity and hardness on the effectiveness of water flooding: aiming to capture the effect of ionic distribution existing in the injected fluid on the oil recovery factor.
2. Study of the behaviour of different surfactants and their interactions with alkali for optimal conditions of microemulsion formation and the effect of brine salinity and hardness.
3. Study of the behaviour of acrylamide polymers and their interactions with alkali and surfactants for SP and ASP CEOR systems with the effect of brine salinity and hardness.
4. Consideration for reservoir simulation of the effect of brine salinity and hardness for SP and ASP CEOR

Research stages are presented schematically in Figure 3.1:

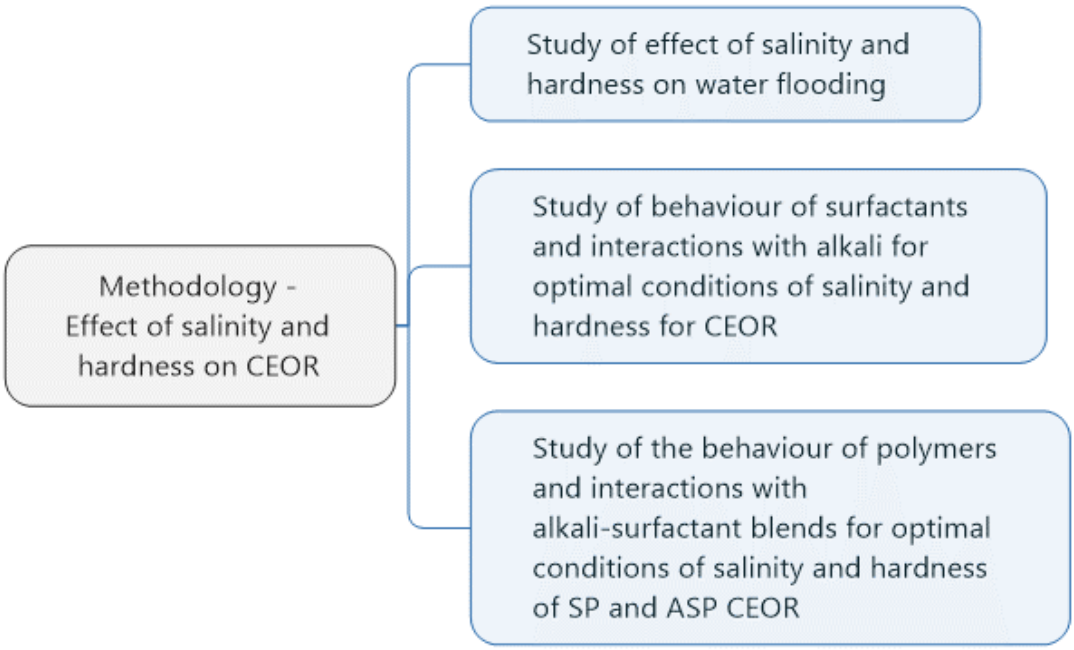


**Figure 3-1: Stages defined for the research**

Each stage of the research has been developed and discussed in the following chapters. Details of the methodology followed for each stage are also included in each of them. In the following sections, materials and methods used are described.

## 3.3 Material required for the research

To collect the required data to complete this research, a series of materials were required to represent the system crude oil/ brine/reservoir rock and ASP CEOR.

A list of materials required for the research and suppliers are shown in table 3.1.

**Table 3-1: Materials and suppliers**

| Representing System | Material | Company Supplier |
|---|---|---|
| Crude Oil (Oil) | Crude Oil from North Sea | Maersk North Sea UK limited |
| Rock samples (Reservoir) | Bentheimer Sandstone | Kocurek Industries |
| Synthetic Brine (Brine) | NaCl (Sodium Chloride) | Sigma- Aldrich |
| | KCl (Potassium Chloride) | Sigma- Aldrich |
| | $Ca_2Cl$ (Calcium Chloride) | Sigma- Aldrich |
| | $Mg_2Cl$ | Sigma- Aldrich |
| Alkalis (A) | NaOH (Sodium Hydroxide) | Sigma- Aldrich |
| | $NaBO_2$ (Sodium-Metaborate) | Sigma- Aldrich |
| | $NH_4OH$ (Ammonium Hydroxide) | Sigma- Aldrich |
| | $NaHCO_3$ (Sodium Hydrogen Carbonate) | Sigma- Aldrich |
| | $NaO_2C_2H_3$ (Sodium Acetate) | Sigma- Aldrich |
| Surfactants (S) | Anionic Olefin Sulfonate $C_{20-24}$-IOS | Nalco (USA) |
| | Anionic Olefin Sulfonate $C_{15-18}$-IOS | Nalco (USA) |
| | Anionic Methyl Ester Sulfonate $C_{12-18}$-MES | Nalco (USA) |
| | Non-ionic Alcohol Ethoxylate $C_{12-15}$-7EO | Nalco (USA) |
| | Anionic Alcohol Ethoxy Sulfate $C_{06-10}$-AES | Nalco (USA) |
| | Anionic Alcohol Ethoxy Sulfate $C_{12-14}$-AES | Nalco (USA) |
| | Anionic Alcohol Alkoxy Sulfate $C_{16-17}$-13APS | Nalco (USA) |
| | Anionic Alcohol Alkoxy Sulfate $C_{16-17}$-7APS | Nalco (USA) |
| | Anionic Alcohol Alkoxy Sulfate $C_{13-14}$—7APS | Nalco (USA) |
| Polymers (P) | Partially hydrolyzed poly acrylamide PHPA -6 | SNF Floeger (France) |
| | Partially hydrolyzed poly acrylamide PHPA-5 | SNF Floeger (France) |
| | Partially hydrolyzed poly acrylamide PHPA-4 | SNF Floeger (France) |
| | Partially hydrolyzed poly acrylamide PHPA-3 | SNF Floeger (France) |
| | 2-acrylamido-2-Methyl propane Sulfonate- AM-AMPS | SNF Floeger (France) |
| | 2-acrylamido-2-Methyl- Vinyl- Pyrrolidone - AM-n-VP | SNF Floeger (France) |
| | Hydrophobic modified Comb-Co-Polymers HMPAM-1 | Beijing Hengju |
| | Hydrophobic modified Comb-Co-Polymers HMPAM-2 | Beijing Hengju |
| | Hydrophobic modified Comb-Co-Polymers HMPAM-3 | Beijing Hengju |
| | Hydrophobic modified Comb-Co-Polymers HMPAM-4 | Beijing Hengju |
| Solvents to clean core sample | Toluene | Sigma- Aldrich |
| | Acetone | Sigma- Aldrich |
| | 2- Propanol | Sigma- Aldrich |
| Chemicals required for the crude oil acidic number titration | Potassium hydrogen phthalate (KHP) | Sigma- Aldrich |
| | Potassium hydroxide (KOH) alcohol based 0.1 M | Sigma- Aldrich |
| Compound to complex divalent ions | EDTA (Ethylene-diamine-tetracetic acid) | Sigma- Aldrich |

A sample of stock tank crude oil from an offshore reservoir, located at the North Sea was obtained from a Petroleum company. Bentheimer sandstone rocks with homogenous properties were used as reservoir rock samples.

Synthetic brine was prepared using commercial salts. Also, commercial samples of alkali analytic grade were used for alkaline chemical slugs. Samples of special surfactants and polymers used in CEOR processes were donated by service companies. Organic Solvents were required to clean rock samples, they were purchased at analytic grade as well as the complexing agent, Ethylene-diamine-tetraacetic acid (EDTA).

More details about the methods applied for the research are included in the next section.

## 3.4 Experimental methods used to collect required data

In this section, the experimental methods used for the research are described. A series of tests were required to measure fluid stability and properties, fluid-fluid and fluid-rock interactions. A summary of the required experiments, the purpose of the test and the name of the equipment used are presented in table 3.2.

**Table 3-2: Summary of experiment and equipment required**

| Test | Objective of the test | Equipment |
|---|---|---|
| Density | Measurements of density of liquids (Oil, brine, chemical solutions) | Pycnometer |
| IFT | IFT of fluid-fluid, oil-brine, brine-air, CMC of surfactant systems, oil-air using the ring method or pendant drop method | DCA-100 Tensiometer Pendant drop equipment |
| Viscosity | Viscosity of fluids, rheology behavior of polymer solutions | Rheometer Bohlin Gemini |
| Phase separation test | Salinity scan to determine the optimal salinity for ultra-low IFT | Glass Pipettes |
| Porosity | Measurement of pore volume by saturation method and NMR | Caliper, electronic balance and Low Frequency NMR |
| Permeability | Measurement of Absolute permeability | Core flooding |
| Relative Permeability | Relative permeability of oil and brine on the porous medium | Core flooding |
| Chemical Flooding | Effect of chemical flooding on oil recovery | Core flooding |
| Adsorption | Chemical retention | Core flooding |

The density of the fluids required for the CEOR process was determined by using a pycnometer. The value of the density of the different fluids involved in a CEOR process allowed the evaluation of the effect of gravity forces on the saturation distribution of fluids during displacement.

An in-house assembled core flooding equipment was required to measure absolute permeability, relative and effective permeability, and for chemical flooding and adsorption tests. Details of each of the methods used are described in the following sections.

### 3.4.1 Surface and interfacial tension IFT

To measure the surface tension of the liquids, oil, brine, and surfactant solutions, the ring method; Du Noüy Ring for Liquid/Gas & Liquid/Liquid Interfaces, using a contact angle tensiometer apparatus model (DCA 100) was applied. The method measures the force exerted by the ring to break through the liquid surface. Initially, the ring is submerged into the solution and then pulled through the interface. The maximal force is directly proportional to the surface tension. The force is related to the weight as the sensor of the equipment is an electronic balance; therefore, weight is monitored during the test and converted to force. A schematic representation of the test is presented in Figure 3.2, (a) and a representation of the obtained results is showed in Figure 3.2 (b).

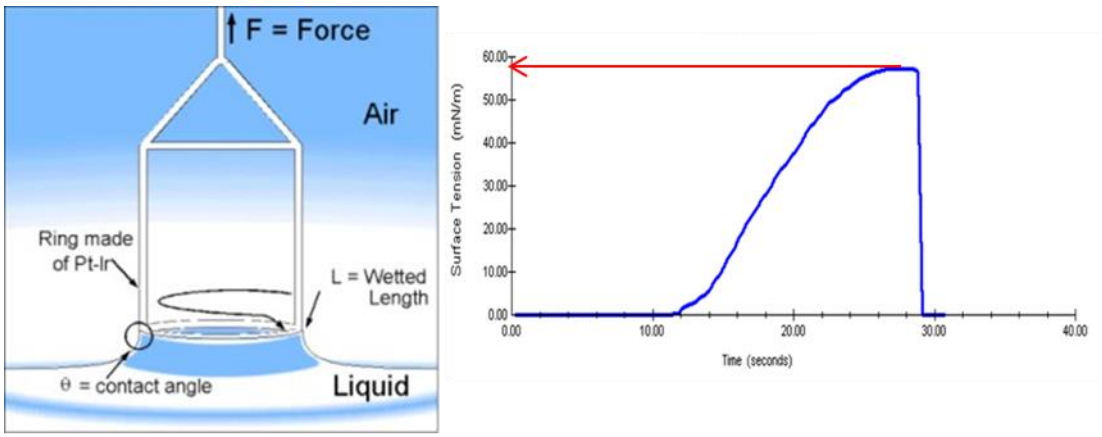


(a) Ring test variables

(b) Surface tension result

**Figure 3-2: Schematic representation of the ring method**
(Drelich *et al.*, 2002)

The method assumes the contact angle $\theta$ between the fluid and the ring is zero when the liquid surface is broken, the wetted length of the ring is calculated as L = 4$\pi$R, considering both internal and external circumference of the ring. The surface tension $\sigma$ is calculated according to the following equation 3-1:

$$\sigma = \frac{F}{L\cos(\theta)} \quad (3\text{-}1)$$

The interfacial tension IFT between the aqueous solution of brine, surfactant and alkali and oil was measured by using **the pendant drop method**. For this method, an in-house experimental setting was used; the oil drop was pumped at 0.2 ml/min through a 0.7846 mm needle inserted inside a hollowed glass test tube filled with the aqueous solution. The system was monitored with a video camera connected to a microscope so that the formation of the drop of oil was recorded. The video was processed by using an image captured just before the drop was released from the needle, and the best images were analysed by a microscopic image processing program to measure the parameters required to calculate the shape factor (Guo, B. and Schechter, 1997; Misak, 1968).

In the pendant drop method, IFT can be obtained by measurements of shape parameters of the drop of oil inside the aqueous solution. These parameters are the equatorial diameter (D) and the distance at the diameter equivalent to a spherical drop (d) as represented in Figure 3.3.

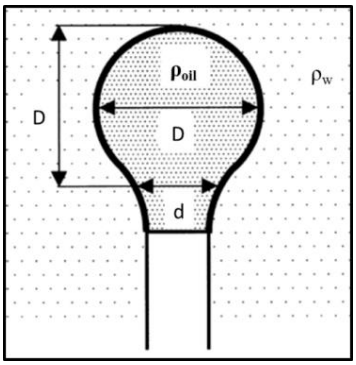


**Figure 3-3: Schematic representation of the Pendant drop method to measure IFT between oil and water**

(Drelich *et al.*, 2002)

The correlation between IFT and the drop shape parameters is as follow:

$$IFT = \frac{\Delta \rho g D^2}{H} \tag{3-2}$$

Where H is a correlation which considers the drop shape parameter D/d and is giving by the following equation:

$$H = \frac{1}{\left(0.31270\,(d/D)^{-2.6444}\right)} \tag{3-3}$$

The limitations of the pendant drop method are associated with the difference in density of the oil and brine and possible gravity effects. Vibrations and evaporation of the sample during the test also affect the measurements. The analysis of the shape of the drop also presents a source of error, due to the determination of the shape parameters (D and s), specifically determining the transition zone which separates the drop formation from the needle used for the test. Besides, the precision of the shape parameters is limited by the qualities of the images taking by the video camera.

From the test, the shape parameters were calculated based on the number of pixels estimated by the diameter of the needle. This value was used as a conversion factor from pixels to millimetres. The experiment was repeated three times to estimate the repeatability of the method and error calculations.

### 3.4.2 Qualitative pre-selection of surfactants using the pendant drop method

Interfacial tensions lower than 0.1 Nm/m cannot be quantitatively determined using the pendant drop method. However, the method was useful to determine the concentration of surfactants able to generate ultra-low interfacial tension (<0.1 Nm/m) and to select surfactants able to form ultra-low IFT when in contact with oil.

The criteria used for the qualitative screening of surfactant based on the generated ultra-low IFT was assuming that if a drop of oil was able to grow inside the brine solution during the test, the IFT value was not ultra-low as required for chemical flooding. On the other hand, if the oil was able to freely flow through the brine during the test and was not able to grow a drop inside the brine solution it means that the IFT between oil and brine was ultra-low. The schematic procedure is shown in Figure 3.4.

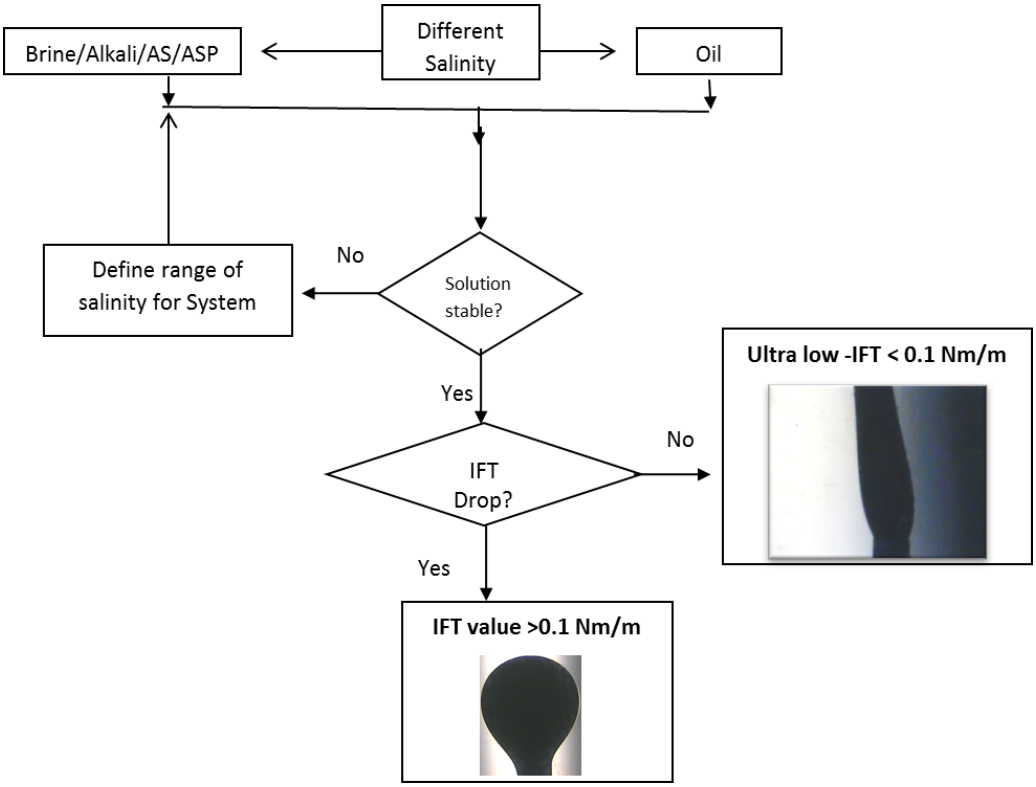


**Figure 3-4: Liquid-Liquid stability tests**

A representation of a drop of oil at high interfacial tension (left image) and the oil flowing through the brine without any drop (right image) is presented in Figure 3-5. The effect of surfactant concentration on the drop shape is presented in Figure 3-6.

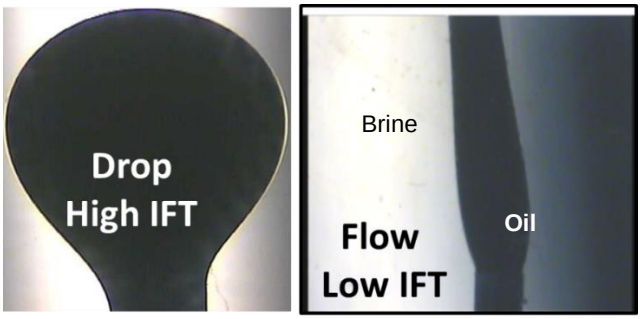


**Figure 3-5: Criteria to select surfactants for chemical EOR using the pendant drop method**

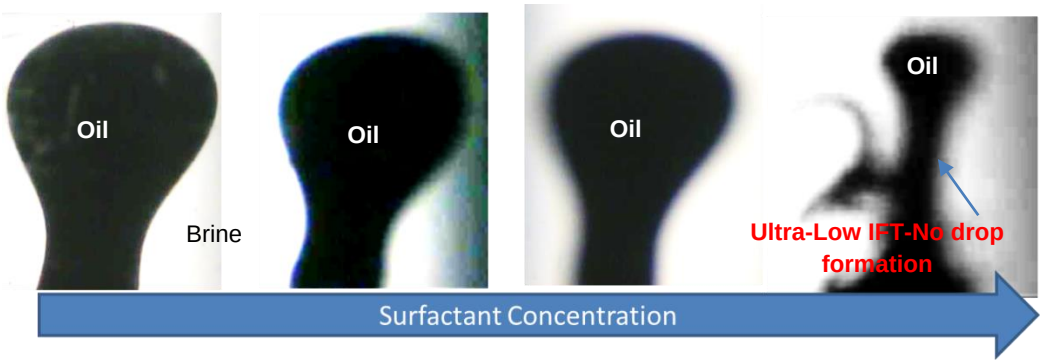


**Figure 3-6: Example of reduction of the oil drop shape with the increase of surfactant concentration**

The method was used to measure IFT of mixtures brine/oil at different salinities and scan IFT between combinations of chemicals in brine at different salinities and oil phases. The method allowed a preselection of main surfactants as able to reduce IFT aqueous/oil to values lower as 0.1 Nm/m.

### 3.4.3 Preparation of polymer solutions

The procedure used to prepare polymer solutions was according to recommended practices provided by the manufacturer of the polymer, with special consideration for the mixing rate and time and considering the active fraction of polymer, given for each polymer.

The amount of polymer and brine solution required to prepare solutions 0.5% m/v polymer concentration in brine. The amount of polymer in grams required, considering the active fraction (x) is 1/x grams, the amount of brine to is (200-1/x) grams.

The mixing procedure is important to get homogeneous solutions. The following protocol was used for the preparation of polymer solutions:

- After the amount of polymer and brine were weighted. The paddle stirrer was set at a rate of 700 rpm. A strong vortex was created in the stirred brine.
- The amount of polymer was slowly sprinkled into the walls of the vortex to get a homogeneous mix.
- After all the polymer was added and mixed, the stirring rate was reduced to 500 rpm and continue mixing for 2 hours to allow the polymer to hydrate.

The required amounts of polymer and brine were weighted using an electronic balance with an accuracy of 0.001 g. A representation of the mixing procedure is presented in Figure 3-7.

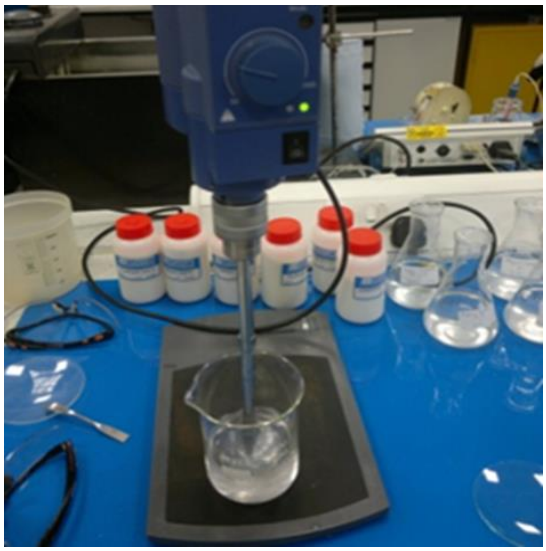

**Figure 3-7: Mixing procedure for the preparation of polymer solutions**

### 3.4.4 Viscosity and rheological behaviour of solutions

The rheometer was used to measure the viscosity profile of crude oil, brine, polymers and 3 phase microemulsions generated at optimal salinities for the fluid-fluid analysis. A representation of the test and geometry system is presented in Figure 3.8.

The geometry for the test using the Bohlin Gemini rotational rheometer was cone and plate type, with a fixed lower plate of 6·cm diameter, with a thermal regulated jacket and upper cone of 4 cm diameter, the cone angle was 4°.

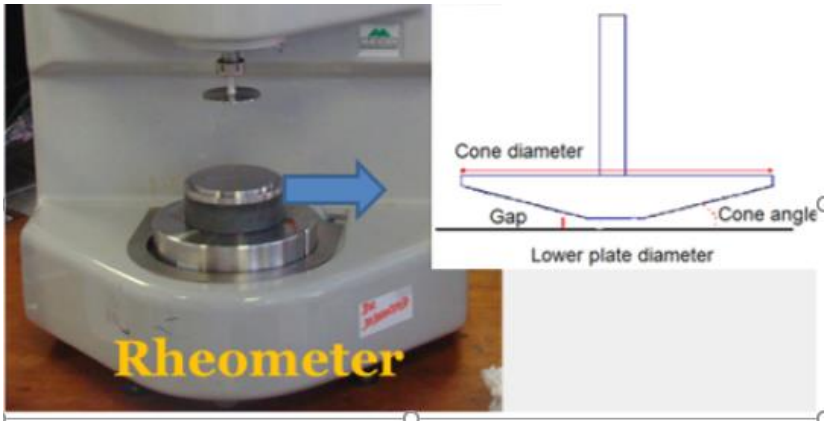


Figure 3-8: Rheometer test and geometry

### 3.4.5 Fluid Stability for oil and brine

#### 3.4.5.1 Properties of the crude oil

The chemical composition of the crude oil, tests for viscosity and formation volume factor as a function of pressure, and temperature, included in the PVT report were analysed to determine the phase diagram and the correlations of properties with pressure. The phase envelope pressure versus temperature was calculated using the software WinPro (Computer Modeling Group Ltd., 2015), from the computer modelling group.

Properties such as density, viscosity, acidic number and surface tension of the crude oil sample were measured in the laboratory. A schematic representation of the analysis followed for this stage is shown in Figure 3.9


Figure 3-9: Sequence used for the analysis of the crude oil

#### 3.4.5.2 Synthetic brine composition and properties

Two synthetics brines of different ionic compositions and salinity were prepared in the laboratory. One hard brine (HB) had an ionic composition similar to the produced water for the Gryphon oil field (Mansell and Dean, 1994), and the other brine, prepared as soft brine (SB),

with a similar composition of monovalent ions, and without divalent ions. Details of the salts used to prepare both brines are presented in tables 3-3 and 3-4.

**Table 3-3: Composition used for synthetic brine labelled HB**

| Hard Brine (HB) Composition | | | | | | |
|---|---|---|---|---|---|---|
| **Element** | **mg/L** | **Atomic W (g/mol)** | **g/L** | **mol.** | **Compound** | **g/L** |
| **Na** | 22,330 | 22.99 | 22.33 | 0.97 | NaCl | 56.77 |
| **K** | 295 | 39.10 | 0.30 | 0.01 | KCl | 0.56 |
| **Ca** | 1,860 | 40.08 | 1.86 | 0.05 | $CaCl_2$ | 6.82 |
| **Mg** | 975 | 24.31 | 0.98 | 0.04 | $MgCl_2$ | 3.82 |
| **Cl** | 40,830 | 35.45 | 40.83 | 1.15 | Total Cl (gr) | **40.8** |
| **Total dissolved solids TDS (ppm)** | | | | | | 66,290 |
| **Salt Concentration based on NaCl &KCl (ppm)** | | | | | | 57,336 |
| **TDS (%)** | | | | | | 6.63 |
| **Salt Concentration ($CaCl_2$ & $MgCl_2$) ppm** | | | | | | 8,894 |

**Table 3-4: Composition used for synthetic brine labelled SB**

| Soft Brine (SB) Composition | | | | | | |
|---|---|---|---|---|---|---|
| **Element** | **mg/L** | **Atomic W gr/mol.** | **g/L** | **mol.** | **Compound** | **gr.** |
| **Na** | 22,330 | 22.99 | 22.33 | 0.97 | NaCl | 56.77 |
| **K** | 295 | 39.10 | 0.30 | 0.01 | KCl | 0.56 |
| **Ca** | ----- | 40.08 | | | --- | |
| **Mg** | ------ | 24.31 | | | --- | |
| **Cl** | 34,741 | 35.45 | 34.74 | 0.98 | Total Cl (gr) | 34.741 |
| **Total dissolved solids (TDS)** | | | | | | 57,366 |
| **Salt Concentration (NaCl &KCl) ppm** | | | | | | 57,366 |
| **TDS (%)** | | | | | | 5.736 |
| **Salt Concentration ($CaCl_2$ & $MgCl_2$) ppm** | | | | | | 0 |

The HB has a cationic relation 20:2:1 Na: Ca: Mg. Moreover, the HB contains 2,835 ppm of divalent ions ($Ca^{2+}$ and $Mg^{2+}$), and total dissolved solids TDS of divalent salt $CaCl_2$ and $MgCl_2$ of about 9,000 ppm and 56,336 ppm of monovalent salts based on NaCl & KCl.

Both synthetic brines were diluted with distilled water at different salinities to cover a salinity range between 66,290 and 0 TDS (ppm) for HB and between 57,366 and 0 TDS (ppm) for SB. Properties such as stability, density, and surface tension were evaluated.

### 3.4.6 Fluid Stability for alkali, surfactant, polymers, and ASP with brine

When ions are present in the aqueous solution with alkali, surfactant or polymer the chemicals become less soluble. This reduction in solubility promotes the formation of precipitation or cloudiness.

To evaluate the stability of mixtures fluid-fluid between brine, alkali, alkali-surfactant, and alkali-surfactant-polymer with oil, mixes of 1:1 at different salinities were prepared in test tubes, kept at reservoir temperature conditions (60 ºC or 140 ºF) and monitored for a month and observations were recorded. Solutions that developed any type of precipitation or cloudiness were reformulated.

The presence of cloudiness or precipitate was defined as a distinctive indication of instability. This test is useful to check the compatibility of the chemical with the formation/injection water and determine the range of salinity where the surfactant can be used. The formation of precipitation (PPT) or cloudiness (CLD) in the aqueous solution was recorded as an indication of incompatibility as that condition could affect the reservoir properties by pore volume blockage or permeability modifications.

A clear (CLR) aqueous solution was classified as compatible and stable. As result of the stability tests, the range of salinity and concentration under reservoir conditions of temperature were determined for each chemical system. Only stable samples were selected for further tests.

The stability of surfactant solutions in brine was evaluated for a range of salinity, between 5,000 to 60,000 ppm (TDS). The range of alkali concentrations used was 0.25 -0.02 mol/lt, and constant salinity for different salinities, covering a salinity range from 5000 to 60000 ppm total dissolved solids (TDS).

### 3.4.7 Phase separation and optimal salinity for microemulsion formation

The chemical systems that passed preliminary stability tests and generated low IFT were selected for the phase separation test. The test is designed to determine the optimal salinity for microemulsion formation, the range of salinity for the three-phase microemulsion or miscible zone and the estimation of IFT versus salinity.

For the phase separation test 1:1 (2.5 ml: 2.5 ml) mixes of chemical slugs with oil are transferred to pre-sealed 5 ml glass pipettes. The samples are stirred by hand-shaking and put in a water bath at 60 °C. They are observed under temperature and observations are

recorded. Important observations are related to changes at the interface oil/aqueous solution, which are required to calculate the solubilisation parameters.

IFT from phase separation tests is calculated using Huh correlation (1978) as referred by Sheng (2011). According to this relationship, the IFT (γ) is inversely proportional to the square of the solubilisation ratio (σ) given as:

$$\gamma = \frac{C}{\sigma^2} \tag{3-4}$$

In this correlation, the value of C is approximately 0.3 dynes/cm for most EOR surfactants with crude oil. The solubilisation ratio (σ) is defined as the volume of solubilized oil or water divided by the volume of surfactant in the microemulsion and this value is obtained from the graph of solubilisation ratio for each surfactant system. The optimal salinity is determined as the point of salinity where the solubilisation ratio of oil and water are equal.

Schematic representation of the method used to measure aqueous stability of surfactant under salinity, range of salinity for microemulsion formation and optimal salinity (define as the point where the values of solubilisation of the surfactant in the oil and aqueous phases are equal) is showed in Figure 3-10.

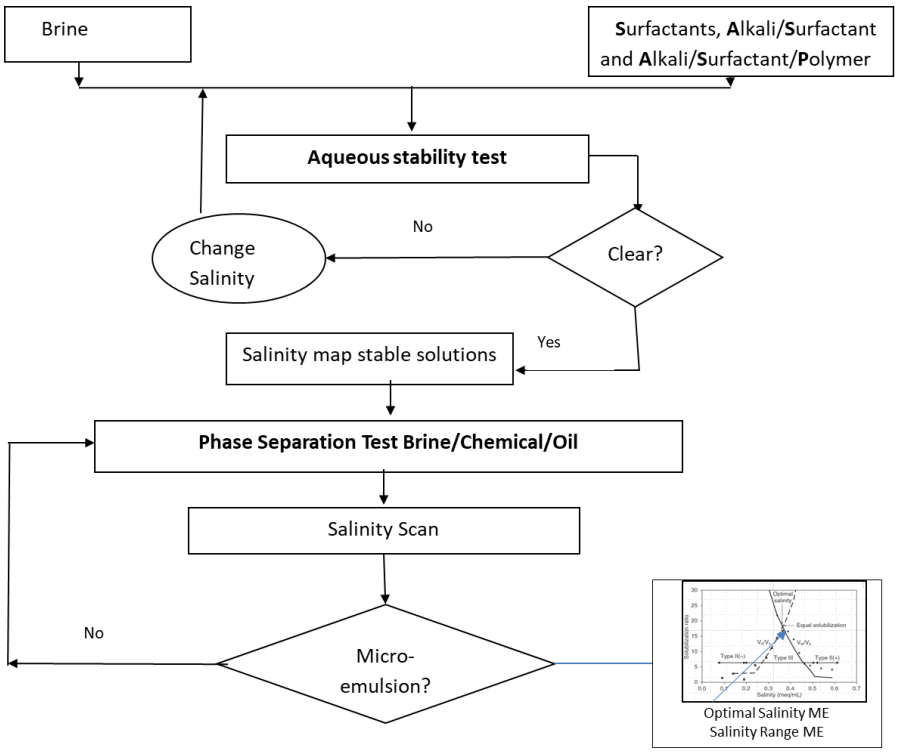


**Figure 3-10: Method used to determine aqueous stability of chemical systems, salinity range and optimal salinity for microemulsion formation**

(Sheng, 2010a)

### 3.4.8 Cleaning and preparation of core samples

Chemical and mineral composition of the Bentheimer rock samples provided by the supplier are included in tables 3.5 and 3.6.

**Table 3-5: Characteristics of Bentheimer sandstone core samples**

| Component name | Formula | Composition (%) |
|---|---|---|
| Silica | $SiO_2$ | 86.47 |
| Alumina | $Al_2O_3$ | 7.31 |
| Iron Oxide | $FeO/Fe_2O_3$ | 1.14 |
| Titanium Oxide | $TiO_2$ | 0.70 |
| Calcium Oxide | CaO | 1.21 |
| Magnesium Oxide | MgO | 0.11 |
| Alkalies | $OH^-$ | 1.65 |
| Water | $H_2O$ | 1.20 |
| Undetermined | | 0.21 |

**Table 3-6: Mineral composition of Bentheimer Sandstone core samples**

| Component name | Formula | Composition (%) |
|---|---|---|
| Quartz | $SiO_2$ | 97.5 |
| Feldspar | $KAlSi_3O_8$ | 2 |
| Kaolinite | $Al_2Si_2O_5(OH)_4$ | 0.5 |
| Calcite | $CaCO_3$ | Traces |
| Dolomite | $CaMg(CO_3)_2$ | Traces |
| Siderite | $FeCO_3$ | Traces |
| Specific Gravity | 2.24 | |
| Porosity % | 0.20 | |
| Permeability (mD) | 500 | |

The main chemical component is silica in the mineral form of quartz, the content of clay minerals such as kaolinite is low. The amount of clay minerals affects chemical adsorption and wettability changes by ionic interactions. The core samples were cleaned with solvents such as toluene, acetone and ethanol, these solvents removed any impurity of residual fluid inside the porous medium. For this purpose, a Soxhlet extractor system was set-up in the laboratory (American Petroleum Institute, 1998). A picture of a Soxhlet extractor and a schematic representation of the test are presented in Figures 3.11 and 3.12 respectively.

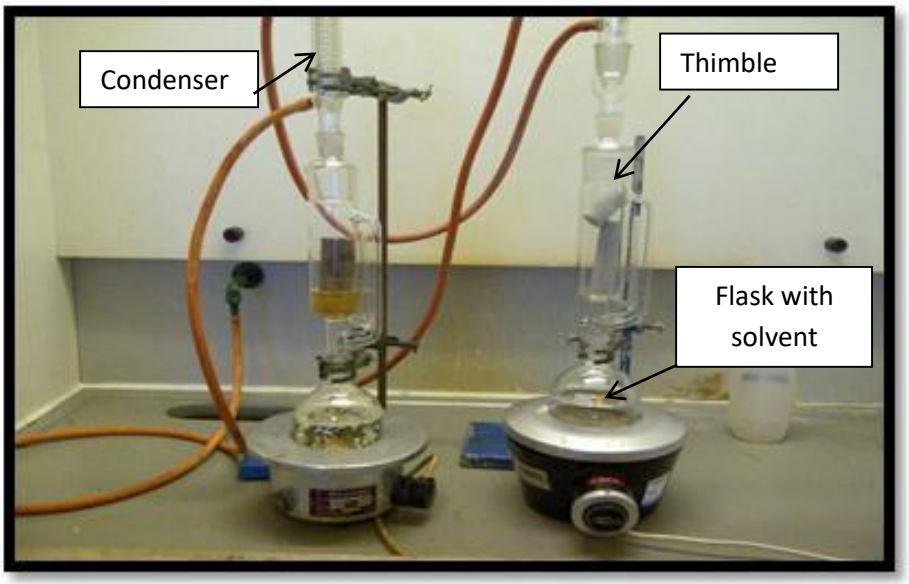


**Figure 3-11: Soxhlet extractor used to clean core samples**

Ultraviolet (UV) light was used to quality check whether rock samples were clean from oil after cleaning with toluene in the soxhlet. Any presence of oil in the sample can be detected as green spots under UV light. After cleaning with toluene to remove oil, the solvent was changed to acetone or alcohol, these two solvents will remove salts from the rock. Then, the samples were put inside the oven at 60º C and let dry until constant weight, once dried there were kept in a desiccator under vacuum to avoid adsorption of any moisture.

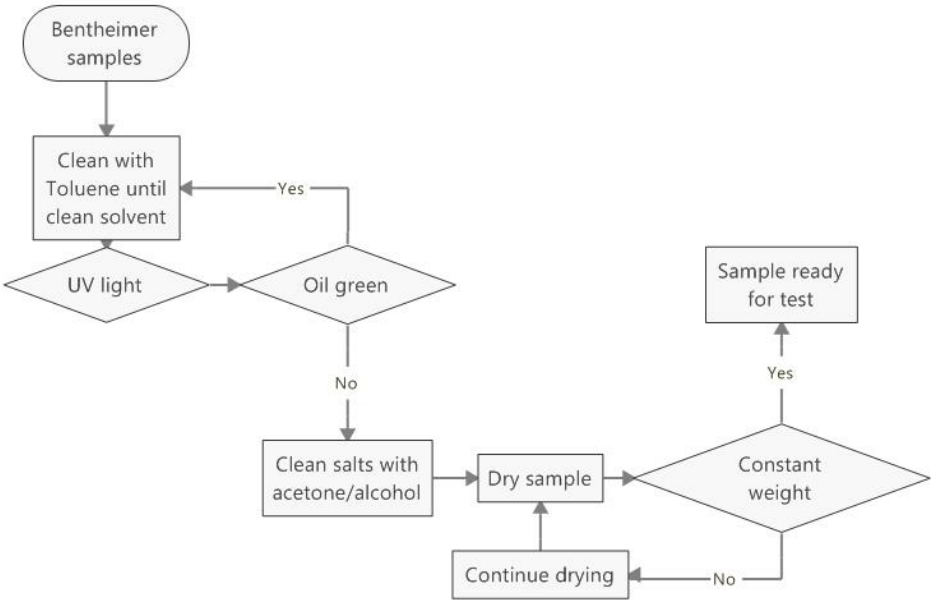


**Figure 3-12: Procedure for cleaning and drying core samples**

### 3.4.9 Porosity

The porosity of sandstone samples was measured by using the saturation method and Archimedes principle. Laboratory tests were designed following recommended practices RP40 (American Petroleum Institute, 1998).

For the saturation method, the dry samples are weighted on a scale, the dimensions of the core sample are measured using a calliper and bulk volume is calculated. Then, the sample is saturated with the brine under pressure using a vacuum chamber for a minimal of 12 hours, afterward the saturated sample is weighed again. The pore volume is calculated by subtracting the weight of the saturated sample minus the weight of the dry sample, divided by the density of the brine used to saturate the sample. The porosity can then be calculated using the equation 3-4:

$$\emptyset = \frac{Pore\ volume}{Bulk\ Volume} = \frac{(Wsaturated - Wdry)/\rho_{satfluid}}{BV} \quad (3\text{-}4)$$

### 3.4.10 Absolute permeability

Absolute liquid permeability was measured using the core flooding equipment (American Petroleum Institute, 1998). By this method, core samples are saturated in brine under vacuum pressure before being transferred into the core holder. Once the core holder is set up, an overburden pressure of 500 psi is applied. Once the core is pressurized, brine is circulated at different flow rates from 1 to 6 ml/min and values of stabilized delta pressure are captured, only low flow rates were used to avoid the developing of turbulent flow which limits the validity of Darcy law equation. The absolute permeability is defined as the constant of proportionality between flow rate and pressure drop. Absolute permeability values for a rock sample can be experimentally obtained by plotting delta pressure readings as a function of flow rates, represented by equation 3-5:

$$Q = \frac{kA}{\mu}\frac{\Delta P}{L} \quad (3\text{-}5)$$

The units for this equation are atmosphere for pressure, $cm^3/s$ for flow rate, cm for L (length of the core sample), $cm^2$ for the transversal area of the core sample, centipoise for viscosity μ and milli Darcy for permeability *k*.

### 3.4.11 Relative Permeability

The behaviour of the fluids inside the porous media is well represented by relative permeability curves. An unsteady state water flood experiment was used to determine the two-phase relative permeability as well as oil recovery. The schematic representation of the core flood test is presented in Figure 3.13.

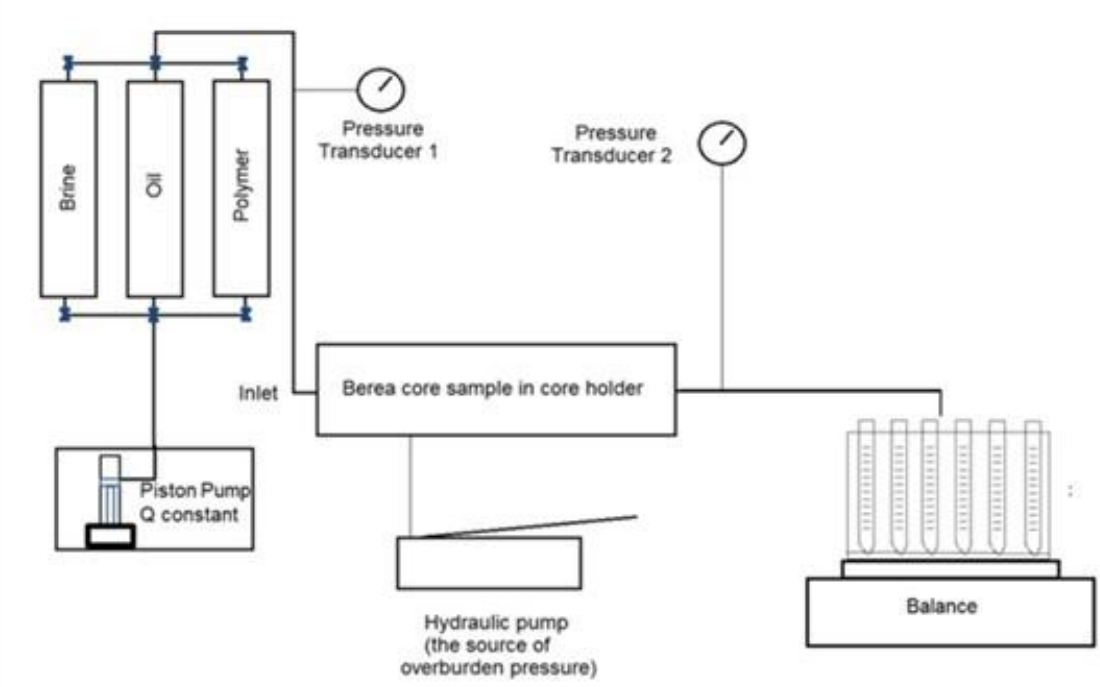


**Figure 3-13: Diagram of core flooding equipment**

The method to estimate relative permeability curves using experimental data obtained by core-flooding tests was as follow:

1) The absolute permeability was determined through the values of pressure at different flow rates through core samples 100% saturated with synthetic brine (HB) and using Darcy law correlation.
2) The core was displaced by oil until there was not more production of brine; this process is called drainage. From volume calculation, the estimation of experimental values of irreducible water saturation $S_{wi}$ left in the porous media was possible.
3) The endpoint effective permeability of oil can be calculated using the dynamic constant pressure measured at irreducible water saturation $S_{wi}$. This calculation is done using the

modified Darcy correlation for the determination of effective permeability of one fluid when another fluid is in the porous media $S_{wi}$ as follow:

$$K_{eff} = \frac{Q\mu_i L}{AxΔP} \quad (3\text{-}7)$$

Where:

Q = is the flowrate ($cm^3/s$)

L = is the length of the core sample (cm)

A = is the transversal area of the core sample ($cm^2$)

ΔP =is the pressure drop (atm)

$\mu_i$ = is the viscosity of fluid i (cp)

4) After the core sample was saturated with oil until the irreducible water saturation $S_{wi}$ was obtained, the core was kept aging under pressure 330 KPa and temperature (60 °C or 140 °F) for 20 days.
5) Afterward, the aged core saturated with oil is flooded with brine until the residual oil saturation Sor was reached, this process is called imbibition. The oil recovery and residual oil saturation were estimated from produced fluids. The effective permeability of water at residual oil saturation Sor was calculated using a modified Darcy law correlation.

The completed procedure for a core flooding test is shown in Figure 3-14.

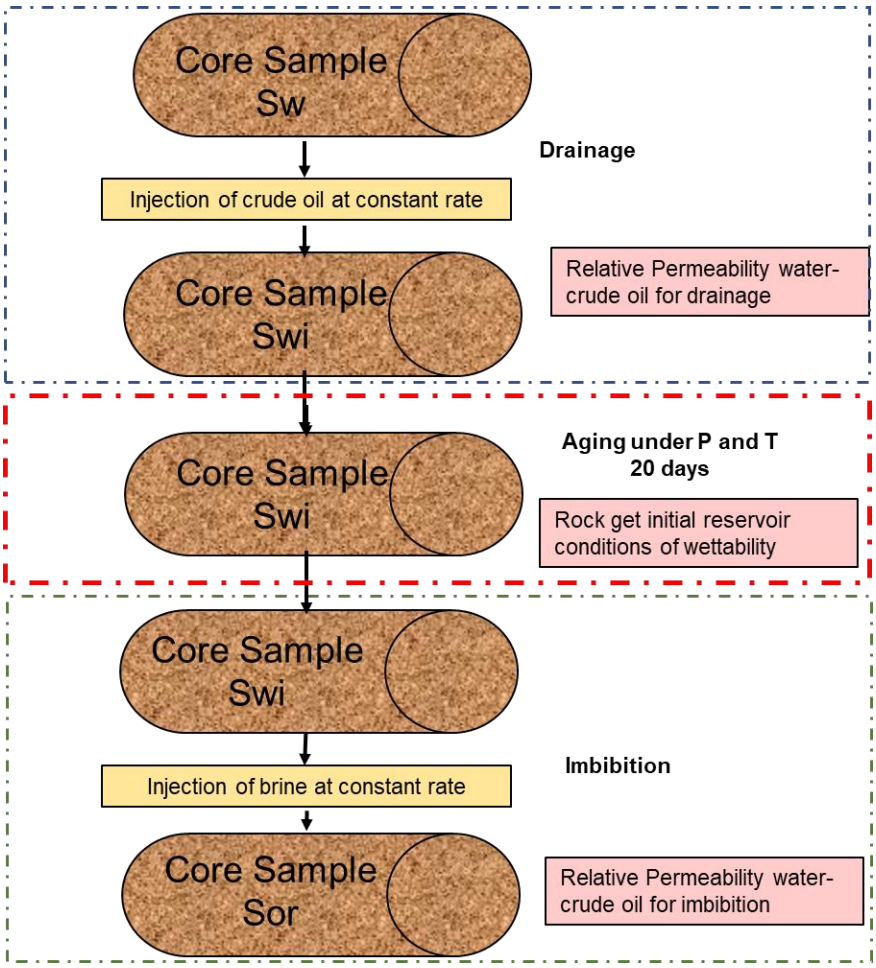


**Figure 3-14: Method applied to measure the relative permeability of fluids by core flooding test**

Relative permeability curves for water and oil phase $k_{rw}$ and $k_{row}$ as a function of water saturation, were adjusted using calculated values of endpoints effective permeability and experimental values of $S_{wi}$ and $S_{ro}$ from core flooding tests, and by using Corey correlation, the exponent $n_0$ and $n_w$ are adjusted to match the production of fluids (oil and brine) and pressure (equation 3-6).

$$k_{rw} = k_{rw}^{o}\left(\frac{S_w - S_{iw}}{1 - S_{iw} - S_{or}}\right)^{n_w} \qquad k_{ro} = k_{ro}^{o}\left(1 - \frac{S_w - S_{iw}}{1 - S_{iw} - S_{or}}\right)^{n_o} \tag{3-6}$$

Where:

$S_w$ – is the saturation of water, fraction

$S_{iw}$ – is the residual saturation of water, fraction

$k_{rw}^{o}$ – is the relative permeability endpoint of water, fraction

$k_{ro}^{o}$ – is the relative permeability endpoint of oil, fraction

$S_{or}$ – is the residual saturation for oil, fraction

$k_{rw}$ – is the relative permeability of water, fraction

$k_{ro}$ – is the relative permeability of oil, fraction

$n_0$ – is the curvature of the relative permeability curve for oil, dimensionless

$n_w$ – is the curvature of the relative permeability curve for water, dimensionless

### 3.4.12 Capillary number

In addition to the relative permeability curves, capillary numbers for the different tests were calculated using equation 3-7 and experimental data from core-flooding tests. The relevance of the analysis of capillary number was the interpretation of the variables affecting the flow of fluids in the porous media.

$$N_c = \frac{v\mu}{\sigma} \tag{3-7}$$

Where v is the Darcy velocity which represents the flow in the porous media, μ is the viscosity of the fluid and σ is the interfacial tension between aqueous and oil phase. Usual values of velocity are close to 1 ft/day (0.3 m/day), the viscosity of the brine = 1 cp and interfacial tension σ = 30 dynes/cm. Replacing the values in the formulae, the capillary number for water-flooding is about is approximately $1x10^{-7}$.

### 3.4.13 Fractional flow

Fractional curves for water-flooding and polymer flooding were studied aiming to analyse the effect of changes in water relative permeability on the water production profile. Fractional curves for water-flooding and polymer flooding were calculated by applying Buckley and Leverett fractional flow theory for displacement during water- flooding, simplified for horizontal displacement, as explained by Lake (Lake, 1989), and using data from relative permeability curves for water-flooding and polymer injection, fluids viscosity, and equation (3-8).

$$f_w = \frac{1}{1+\frac{\mu_w k_{ro}}{\mu_o k_{rw}}} \tag{3-8}$$

Where:

$f_w$= is the fraction of produced water or water cut (dimensionless)
$k_{ro}$= is the oil relative permeability (dimensionless)
$k_o$= is the oil effective permeability (Darcy)
$\mu_o$= is the oil viscosity (cp)
$\mu_w$= is the water viscosity (cp)

### 3.4.14 Chemical flooding evaluation

The effect of interactions fluid-rock between the chemicals surfactant, alkali-surfactant and alkali-surfactant-polymer, with brine, and oil was studied by using results from core-flooding tests. On this method, chemical slugs were injected, after the water flooding stage using the core flooding equipment as explained in the previous section.

For this purpose, a volume equivalent to 0.5 porous volume PV of the chemical slug was injected in the core sample followed by the displacement with brine.

Different chemical slugs were tested to investigate the effect of salinity and divalent cations $Ca^{2+}$ and $Mg^{2+}$ on the effectiveness of the CEOR process and to compare the different chemical formulations using a brine at optimal conditions of microemulsion formation.

### 3.4.15 Polymer mobility, permeability reduction, and resistance factor

The effect of polymer on the mobility of the displacing fluid is assessed by the combined effect of the increase in viscosity and permeability reduction $R_k$, and the term is called "resistance factor", ($R_f$). (UTCHEM, 2009).

$$R_F = R_k x \frac{\mu_{polymer}}{\mu_{water}} \tag{3-9}$$

The permeability reduction factor $R_k$ is defined as the ratio between the effective permeability of brine and the effective permeability of the polymer and represents the performance of polymer changing the relative permeability of the displacing fluid.

$$R_k = \frac{Kw\ (effective{-}water)}{Kpolymer\ (effective{-}polymer)} \tag{3-10}$$

### 3.4.16 Surfactant adsorption tests

The concentration of surfactant adsorbed on Bentheimer sandstone cores was estimated by measuring surfactant concentration in collected samples of the injected fluids from core flooding tests.

Calibration curves of UV surfactant absorbance versus surfactant concentration were required for each salinity for HB and SB. These calibration curves are used to calculate the surfactants concentration of collected samples based on results from the UV test.

The UV spectrometer method was used to measure the concentration of surfactants. The method used to determine surfactant concentration by absorbance was as follows:

a. A battery of solutions with different concentrations of surfactants was prepared, keeping constant salinity and for different salinities.
b. Absorbance for all solutions was measured.
c. Graph of absorbance versus surfactant chemical concentration was plot and the best linear fitting was found using Microsoft Excel, the linear correlation was obtained for each surfactant.
d. Then these calibration curves were used to determine the surfactant concentration of samples collected from the test shown in Figure 3.15.
e. Absorption isotherms using Langmuir and Freundlich (Bera *et al.*, 2013) correlations were adjusted for each surfactant.

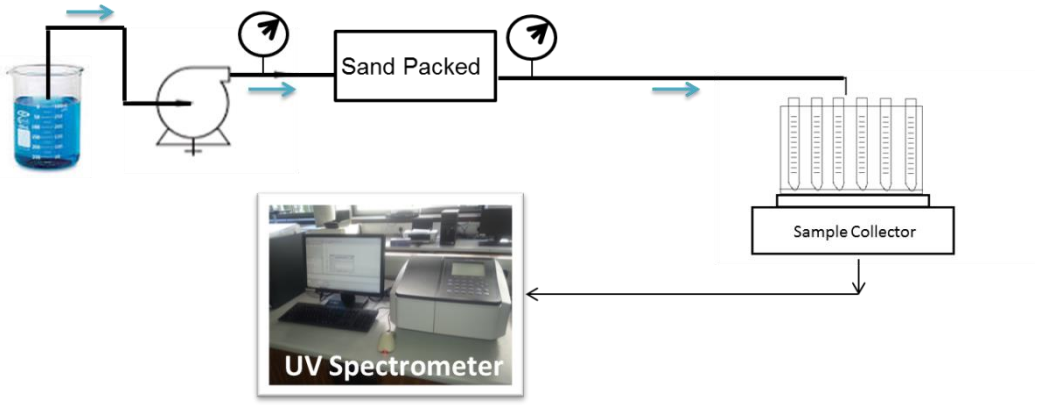


**Figure 3-15: Procedure used for adsorption tests**

### 3.4.17 Laboratory scale 2D core-flooding simulation model

The software used to simulate the process was CMG Starts, which is a compositional simulator that includes advances processes such as ASP chemical flooding with geochemical reactions, adsorption, and effect of brine composition gradient during the injection. The grid was a cartesian grid with dimensions defined according to the dimensions of the reservoir to be simulated.

A 2D simulation model at a laboratory scale was designed using the dimensions of the Bentheimer core. The model allowed matching laboratory results obtained from core flooding tests and evaluated the effect of CEOR process.

The characteristics of the 2D model are presented in Figure 3-16. The model had a total of 100 nodes, 20 in x-direction, 1 in y-direction and 5 in z-direction. The dimensions of the grid

were defined according to the dimensions of the core sample, thus 0.010 m length and 0.0025 m diameter.

After the grid is defined, then properties were assigned to each discrete volume, required properties such as porosity, permeability. Then, fluids present in the reservoir at initial conditions were defined. Fluid properties such as density, viscosity, oil, water and gas formation volume factors, saturation functions, and rock compressibility function are defined. The initialization process used for the core flooding was an enumeration, which consists of the allocation of initial saturation and pressure conditions to each grid cell; the included data was based on the initial oil saturation and water saturation obtained from experimental results.

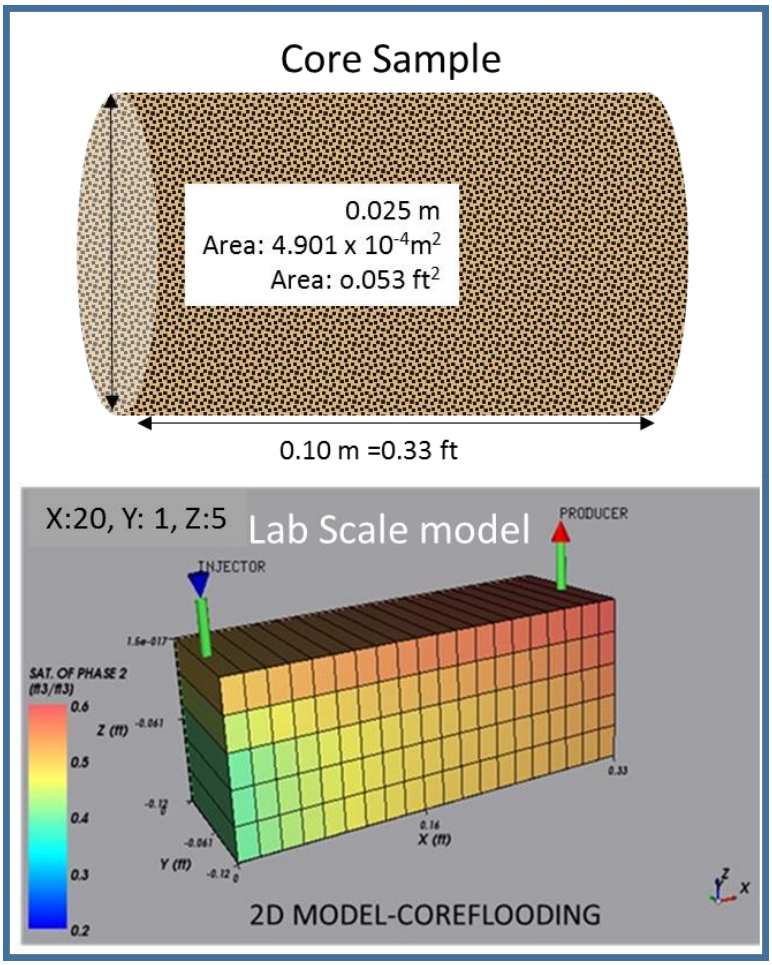


**Figure 3-16: Laboratory scale 2D Model**

Once initial saturation of fluids was found and checked by initialization of the reservoir model, the reservoir was put in production with a producer and an injector well, control and constraints were applied as follow:

- Constant velocity 0.0244 cm/min, equivalent to 1.15 ft./day
- Reference Pressure Pref of 330 KPa

The simulation was run considering identical conditions used in the laboratory and the simulation results were history matched against oil recovery factor and produced water. As a result, the relative permeability curves for the process were adjusted using the Corey correlation.

The assumptions taken into considerations for the models were as follow:

- A sandstone homogeneous reservoir.
- There is no presence of clay.
- Only two phases are present (dead oil); Oil phase and aqueous phase.
- Total equilibrium.
- There are 11 components: water, surfactant, polymer, sodium, magnesium, calcium, alkali, soap, hydrogen, chloride and oil

For CEOR processes, parameters obtained from laboratory tests are used as input, such as:

- Interfacial tension oil/aqueous phase as a function of brine composition.
- Changes in relative permeability oil/water as the effect of salinity, surfactant injection, etc.
- Viscosity, density, and saturations of injection fluid as a function of concentration and brine composition.
- Adsorption correlations as a function of concentration and brine composition.

# CHAPTER FOUR: EFFECT OF BRINE SALINITY AND HARDNESS ON THE OIL RECOVERY

## 4.1 Introduction

This chapter presents the methodology and results for the study of the effect of brine salinity, salinity gradient and concentration of divalent cations $Ca^{2+}$ and $Mg^{2+}$ (hardness) on the oil recovery of crude oil during water flooding on Bentheimer sandstone core samples.

The study was aiming to:

- Understand how optimal salinity conditions required for the chemical slug for CEOR processes are related to the formation water existing in the rock, and
- Evaluate the additional effect of the salinity gradient created by the injection of the low optimal salinity required for CEOR processes, on the surface tension, relative permeability and oil recovery on a sandstone core sample.

The approach taken was the analysis of the effect of salinity and divalent ions on the interfacial tension and relative permeability curves. Changes in the capillary number and fractional flow curves are also analysed to elucidate the mechanisms involved in the process.

Results from this study can provide a better understanding of the additional effect of the salinity gradient generated between formation and injection brine at low salinity on the oil recovery factor. The relevance of these findings for CEOR processes is associated with the effect of the use of a low salinity brine required for optimal conditions of CEOR on the total oil displacement efficiency.

## 4.2 Methodology

The study has been subdivided into three stages.

1. Analysis of fluid stability and determination of key fluid properties for oil and brine samples such as density, aqueous stability of brine solutions to salt concentration, and surface tension.
2. Study of interactions fluid-fluid between oil and brine with different salinities, based on the interfacial tension of oil/water mixes at different salinities.
3. Study of interactions fluids-rock through the behaviour of relative permeability, oil recovery factor and capillary number of water flooding using optimal conditions of salinity required for CEOR processes.

The methodology followed for this part of the research is presented in Figure 4-1.

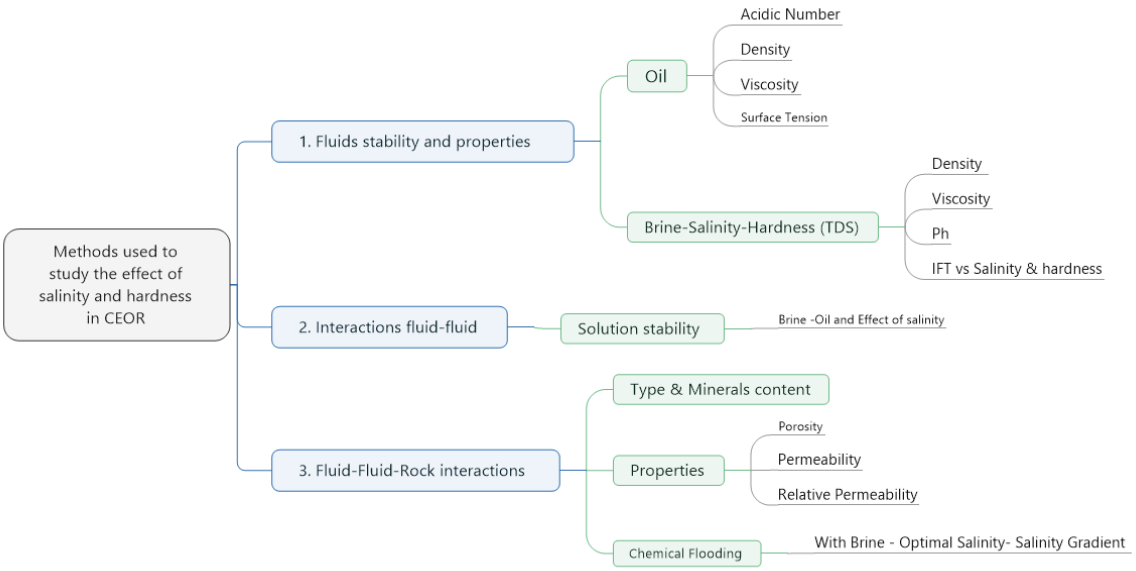


**Figure 4-1: Methodology for the study of the effect of brine salinity and hardness on the oil recovery factor of sandstone core samples**

## 4.3 Results and discussion

### 4.3.1 Study of fluids stability and properties

In this section, the results from the analysis of the stability of brine solutions and oil are presented and discussed.

#### 4.3.1.1 Crude oil properties

The chemical composition of the crude oil, viscosity, and formation volume factor as a function of pressure, and temperature were provided from the PVT analysis report (included in the appendix). Some relevant properties are presented in table 4-1.

The phase envelope pressure versus temperature was calculated using WinPro (Computer Modeling Group Ltd., 2015). The graph is presented in Figure 4-2. According to the behaviour of pressure versus temperature, the crude oil is moderate-low volatile and therefore the fluid

can be modelled as “black oil” (Dake, 2001), as the chemical composition of the oil is not substantially changed by pressure.

**Table 4-1: PVT properties of the North Sea crude oil given by the supplier**

| Pressure (psig) | Temperature (°F) | Gas-Oil Ratio (scf/bbl) | Oil Density ($g/cm^3$) | Formation Volume Factor (BOFB) | Gas Gravity |
|---|---|---|---|---|---|
| 2430 | 140 | - | 0.8576 | 1.114 | |
| 140 | 113 | 221 | 0.9136 | | 0.592 |
| 0 | 60 | 20 | 0.9269 | | 0.608 |
| API gravity | | 21.0° | | | |
| Acidic Number TAN (mg KOH/gr) | | 3.1 | | | |
| Surface tension mN/m | | 35.9 | | | |
| Viscosity @ 20 ºC- Dead Oil (cp) | | 367 | | | |
| Viscosity @ 60 ºC—Dead Oil (cp) | | 26 | | | |
| Viscosity @ 60 ºC—Live oil (cp) | | 6 | | | |

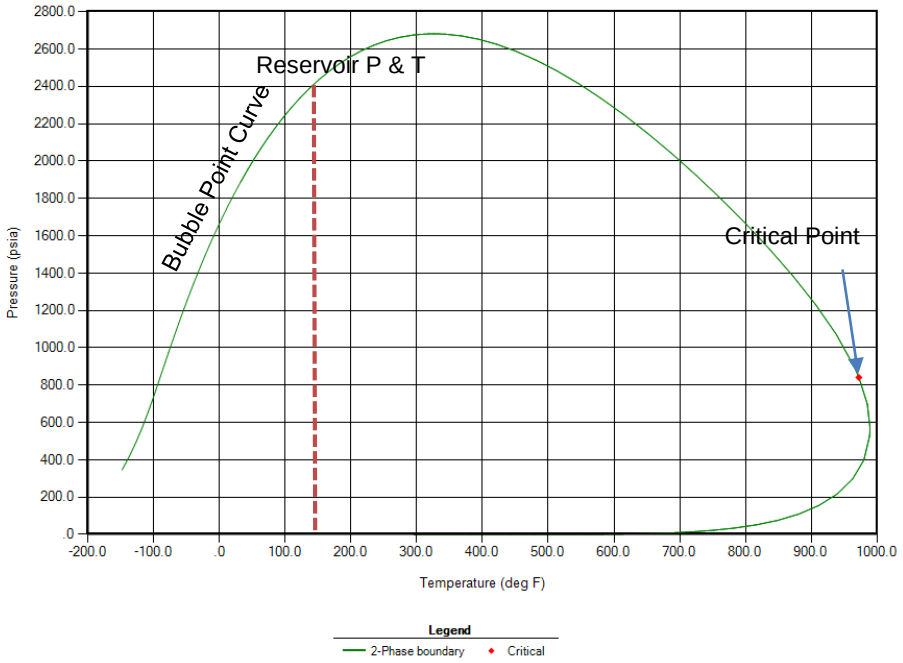


**Figure 4-2: Pressure versus temperature diagram for the crude oil calculated using WinPro (Computer Modelling Group Ltd., 2015)**

The analysis of the chemical composition of the crude oil based on the content of saturates, aromatics, resins and asphaltenes, SARA, is presented on the plot shown in Figure 4-3.

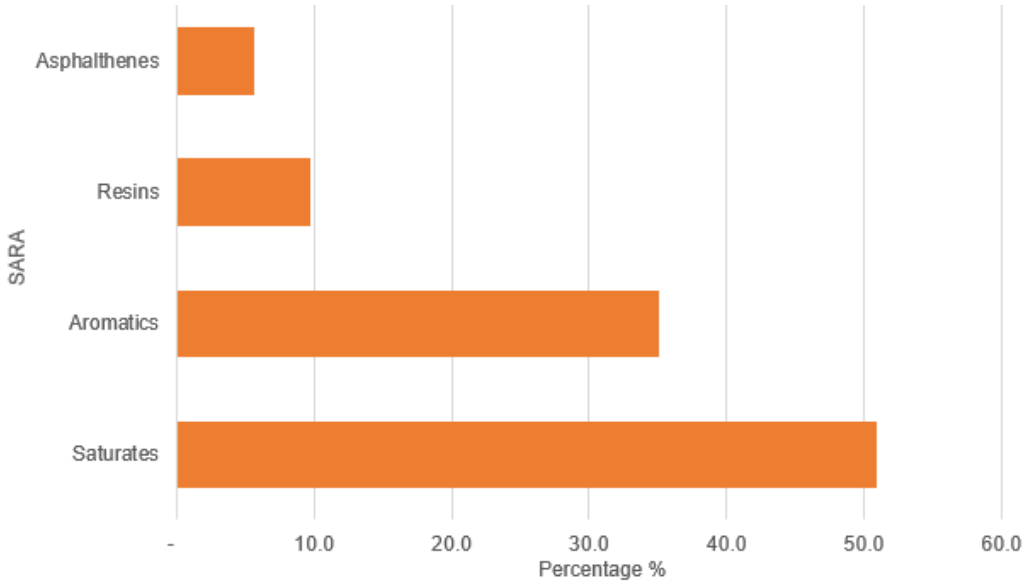


**Figure 4-3: Chemical composition of the crude oil according to SARA analysis** (Aliyu, 2009)

The content of saturates is 51%, aromatics 35%, resins 9.7%, and asphaltenes 5.6%. The crude oil is an aromatic based according to the content of aromatics (higher than 30%) (Pabón and de Souza Filho, 2019). The content of polar components in the crude oil; which is defined by the content of asphaltenes, resins, and some aromatics compounds; is 53% of the total components.

The screening of the properties of the crude such as API°, density, viscosity, and the acidic number indicates a favourable case for the study of ASP CEOR. The high content of polar components should favour the formation of natural surfactants (SOAP) by reactions with alkali.

#### 4.3.1.2 Brine- Salinity-Hardness

Density and surface tension measured for the different brines are reported in table 4-2 and Figures 4-4 and 4-5. The density of the brine increases with salinity and the effect is more noticeable for HB. Both brines, present the same trend with slightly higher values for HB. Those differences found for HB are related to the higher total dissolved solids due to the presence of divalent ions $Mg^{2+}$ and $Ca^{2+}$ and associated chloride ions.

**Table 4-2: Measurements of density and surface tension for SB and HB solutions**

| SB | | | HB | | |
|---|---|---|---|---|---|
| Salinity (ppm) | Density ($gr/cm^3$) | Surface Tension (mN/m) | Salinity (ppm) | Density ($gr/cm^3$) | Surface Tension (mN/m) |
| 57,366 | 1.06 | 61.5 | 66,290 | 1.07 | 57.3 |
| 50,000 | 1.05 | 61.5 | 50,000 | 1.07 | 57.2 |
| 40,000 | 1.04 | 63.1 | 40,000 | 1.06 | 58.1 |
| 30,000 | 1.03 | 62.8 | 30,000 | 1.05 | 56.7 |
| 20,000 | 1.03 | 59.0 | 20,000 | 1.04 | 52.5 |
| 10,000 | 1.02 | 54.0 | 10,000 | 1.03 | 48.4 |
| 5,000 | 1.01 | 45.1 | 5,000 | 1.02 | 41.2 |
| 0 | 0.97 | 72.0 | 0 | 0.97 | 72.0 |

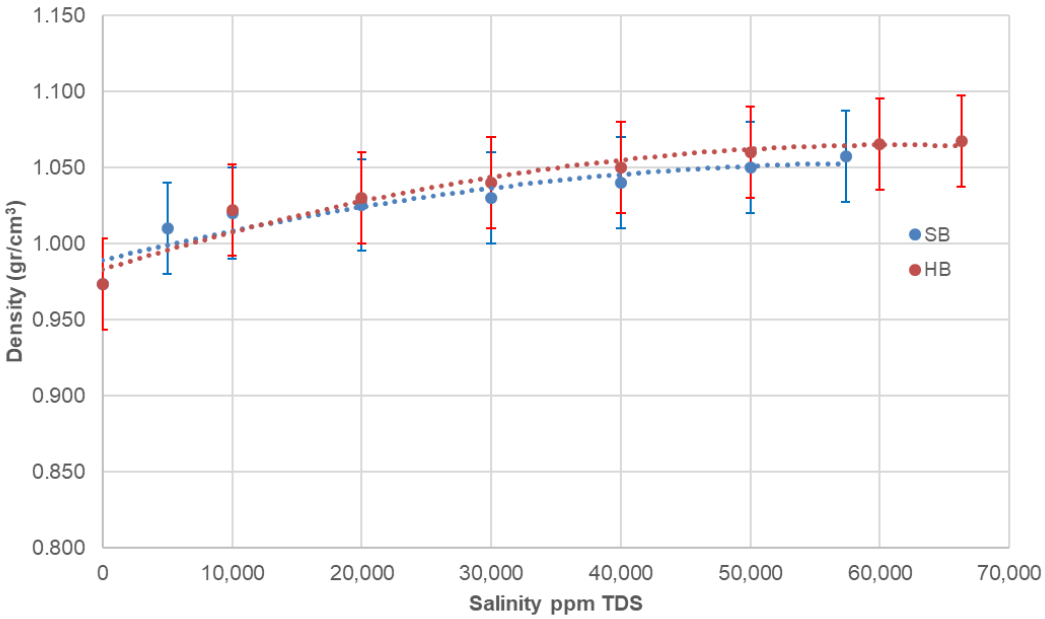


**Figure 4-4: Density of brine versus salinity for SB and HB**

Results for surface tension versus salinity for HB and SB show three defined regions, a region I where the surface tension decrease with salinity at lower TDS, follow by another region II where surface tension increase with salinity until a third region III with a plateau behaviour, where not more relevant changes are observed. Results for surface tensions for both brines are presented on the graph in Figure 4.5. While both brines, soft and hard showed the same trend, the effect is more noticeable for the HB.

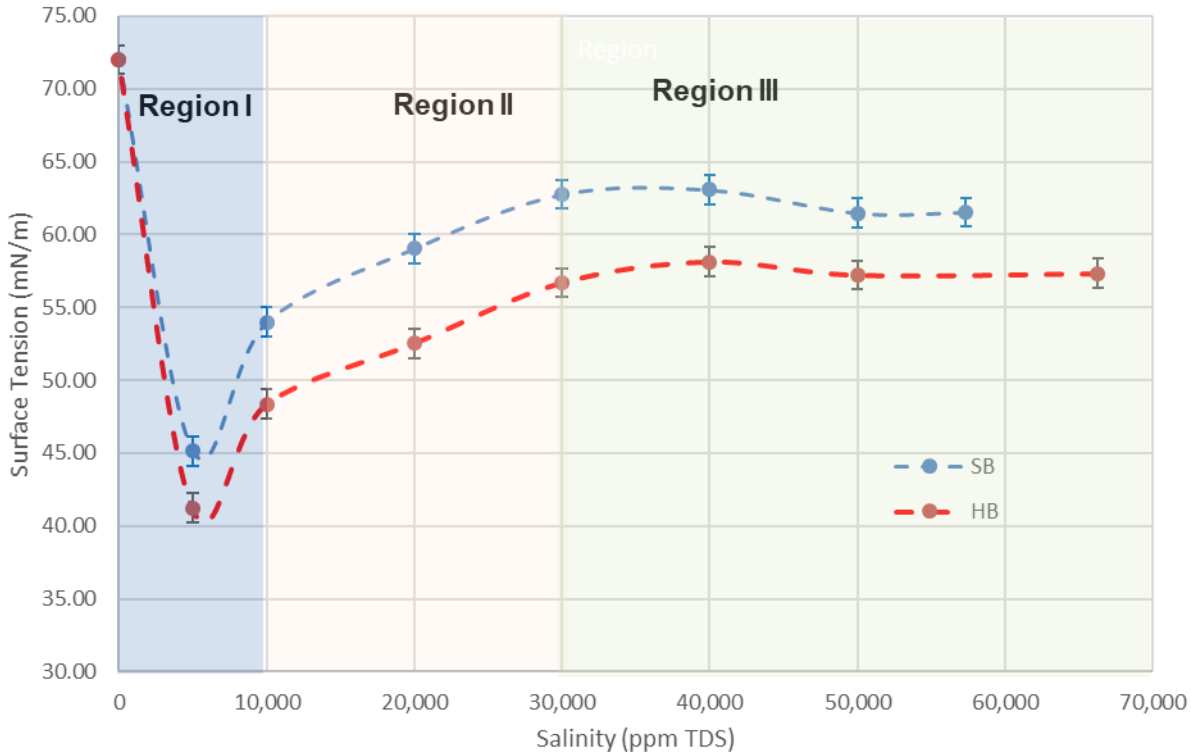


**Figure 4-5: Surface tension of brine versus salinity**

A similar effect of reduction of surface tension of brine at low salinity was observed in previous research (Petersen and Saykally, 2005; Petersen and Saykally, 2004) and was explained as "Jones Ray Effect" for 1:1 electrolytes solutions. The differences observed for divalent cations $Ca^{2+}$ and $Mg^{2+}$ are opposite to previous findings. While the type and concentration of ions affect the surface tension, it is believed that cations only have a small influence (dos Santos *et al.*, 2010). However, as the HB is a multicomponent brine, it is possible that at low salinity ionic interactions favour the migrations of cations to the interface air/water acting as "structure–breaking" ions and reduce the surface tension.

As a result of interactions between positively charged ions in a brine solution with the dipole of water molecules, intermolecular interactions are affected. This effect can cause a weakening of the net force caused by the water dipole moment and thus decrease the Gibbs free energy. As the Gibbs free energy is directly proportional to the surface tension, a reduction of surface tension is observed.

The subsequent increase in surface tension is due to the increase of negative charges electrolytes from chloride ions which tend to migrate to the bulk solution solvated by water molecules, leaving the surface more negative charged with oxygen-hydrogen dipole oriented.

### 4.3.2 Analysis of fluid-fluid (Brine- Oil) interactions

Based on previous results for brines with different compositions and to see whether the behaviour was affected by interactions with crude oil, fluid-fluid interactions between oil and brine at different salinities and compositions were evaluated and presented on this section.

IFT values measured for the range of salinities for SB and HB are presented in Table 4.3 and graphs are offered in Figure 4.6. Both brines showed the same trend of IFT as a function of salinity, first a decline at lower salinity (region I) and then a raise with two gradients (region II and region III). This behaviour is slightly different from the profile obtained for the surface tension of brines for different salinities discussed in the previous section. Instead of having a plateau at high salinity, the IFT increases with salinity with a gradient higher than in region II. There are some indications of a plateau for salinities between 30,000 and 40,000 ppm for SB. These results also suggest the presence of more than one mechanism affecting the resultant molecular interactions within electrolytes presents in brine solutions and acidic components in the oil.

**Table 4-3: Oil/Brine IFT for HB and SB at different salinities**

| SB | | HB | |
|---|---|---|---|
| Salinity (ppm) | Interfacial Tension (mN/m) | Salinity (ppm) | Interfacial Tension (mN/m) |
| 0 | 42.0 | 0 | 42.0 |
| 5,000 | 29.0 | 5,000 | 8.9 |
| 10,000 | 29.3 | 10,000 | 10.0 |
| 20,000 | 37.2 | 20,000 | 12.9 |
| 30,000 | 43.3 | 30,000 | 17.6 |
| 40,000 | 43.3 | 40,000 | 19.3 |
| 57,366 | 76.2 | 50,000 | 36.4 |
| | | 66,290 | 48.1 |

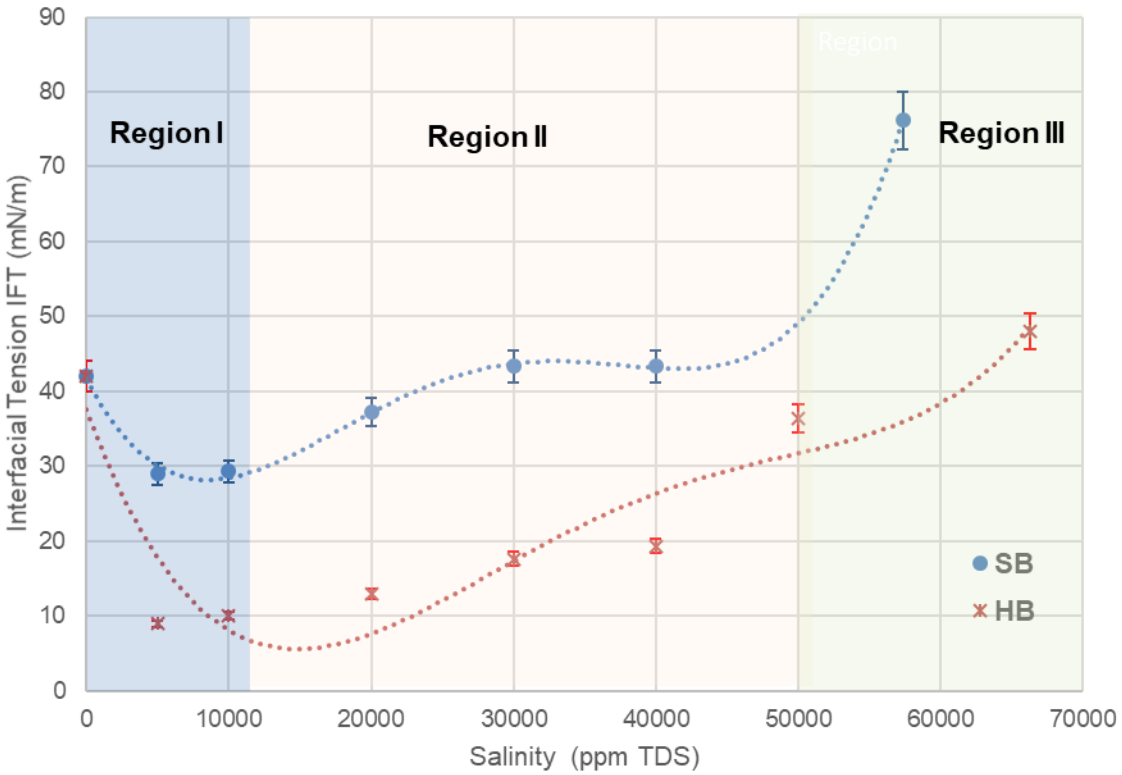


**Figure 4-6: Interfacial tension IFT Brine-Oil for HB and SB at different salinities**

HB solutions have divalent ions $Mg^{2+}$ and $Ca^{2+}$ as part of the dissolved salts $MgCl_2$ and $CaCl_2$, SB solutions contain only monovalent ions $Na^+$ and $K^+$ as part of the dissolved salts KCl and NaCl. IFT values for HB solutions are lower than for SB, indicating an effect of the divalent ions on the IFT.

These results are aligned with previous results for surface tension explained in the previous section, and also are like previous findings (Manshad *et al.*, 2016). The reduction in IFT can be associated with interactions of the ion chloride with water molecules, acting as structure breaking at lower salinity with a resultant reduction on the interfacial tension.

### 4.3.3 Analysis of interactions fluid-fluid and fluid-rock

For the study of the interactions fluids-rocks, Bentheimer core sandstone samples were used. The mineral composition of Bentheimer sandstone cores, porosity, and absolute permeability were measured. The main mineral compound in sandstones is quartz, which for Bentheimer cores is 97.5%. The content of clay is given by the content of Kaolinite. The percentage of clay is significantly low compared with quartz. The content of clay affects the chemical adsorption of the rock.

Absolute permeability values for Bentheimer core samples, determined by Darcy law correlation and using a graphic method as presented in figure 4-7, are included in table 4-4. Porosity values for each core sample are also included in table 4-4.

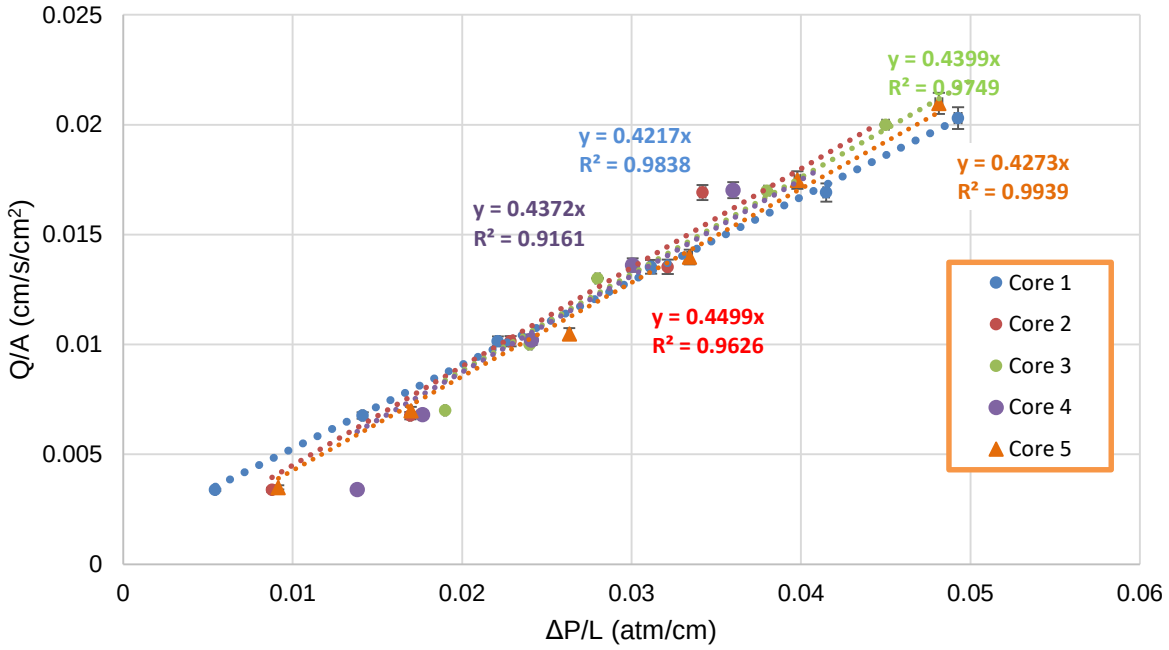


**Figure 4-7: Graphical representation of Darcy correlation to determine absolute permeability**

**Table 4-4: Absolute permeability and porosity for Bentheimer core samples**

| Sample | Porosity (%) | Absolute Permeability (mD) |
|---|---|---|
| **Core 1** | 16.4 | 422 |
| **Core 2** | 17.0 | 450 |
| **Core 3** | 17.0 | 440 |
| **Core 4** | 16.5 | 437 |
| **Core 5** | 17.6 | 427 |

The values of porosity and permeability for each core are very similar. The oil recovery factor, behaviour of relative permeability, capillary number and fractional flow of water flooding using optimal conditions of salinity required for CEOR processes were evaluated.

For that purpose, core flooding tests in sandstone were completed for the following cases:

a. Imbibition with 5.7% SB until 100% water cut in the production, followed by the injection of low salinities, one case with salinity 4.6% SB and another case with 1.5% SB salinity.
b. Imbibition with 6.6% HB until 100% water cut in the production, followed by the injection of low salinity water flooding with salinities 4.6% HB and another case with 1.5% HB salinity.

A schematic representation of the cases studied in this chapter is presented in Figure 4-8.

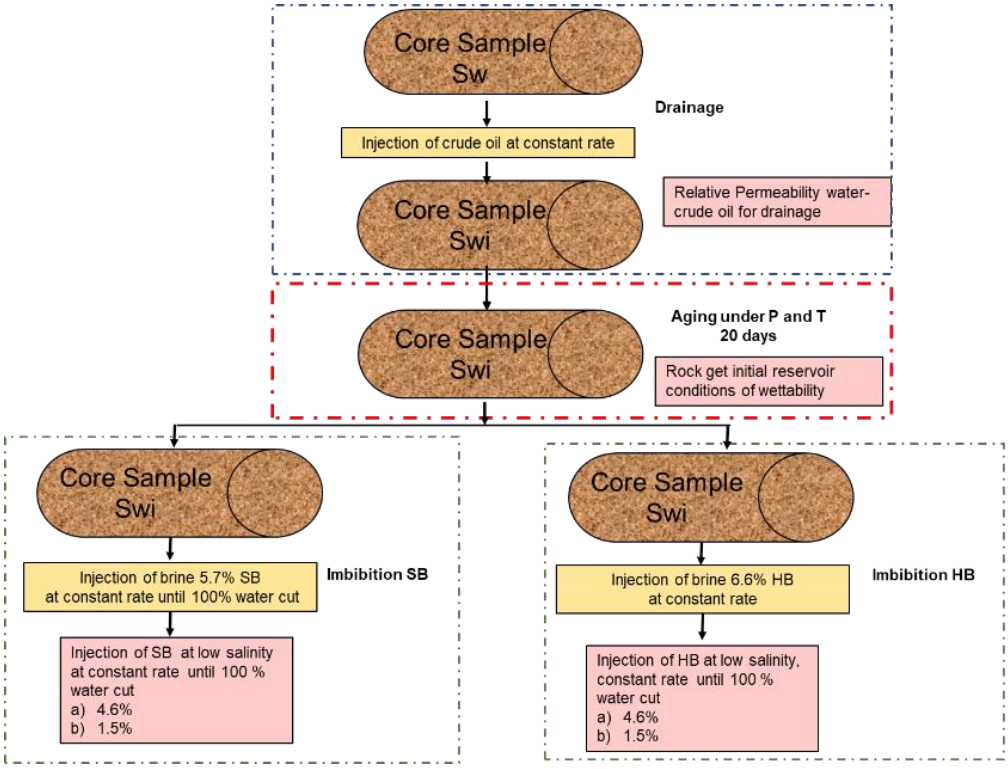


**Figure 4-8: Schematic representation of core- flooding tests with low salinity**

The low salinity of the injected water used for this part of the water flooding was determined by results of the salinity for microemulsion formation for designed chemical slugs of alkali-surfactants mixes and details are explained more in chapter 5.

#### 4.3.3.1 Oil recovery factor and effect of low salinity required for CEOR

For case (a), the oil recovery factor (RF) for the first imbibition with SB 57,000 ppm salinity was 41 % and the residual oil saturation (Sor) was 0.58. Additional RF of 1% and 3% were obtained for the imbibition process with brine with lower salinities 46,000 ppm and 15,000 ppm respectively.

For case (b), the RF for the first imbibition with SB 66,300 ppm salinity was 49% and with diluted salinities, 46,000 ppm and 15,000 ppm were 4% and 1% respectively. Detailed results are included in table 4-5. The total incremental recovery was 4% for water flooding with SB and 5% for HB. These are not huge differences at the laboratory scale but extrapolated at field scale can represent a substantial volume. Increases in oil recovery for cases (a) and (b) are presented in the graph in Figure 4-9.

The same oil recovery of 4% is achieved by the injection of 1.5% SB and 4.6% HB. Therefore, a lower salinity gradient (1.7%) is required for HB to increase the oil recovery by 4% compared to SB which requires 4.2% of reduction in salinity. SB requires to create a higher gradient with 5.7% of formation brine to increase the oil recovery. For HB the required salinity gradient to increase the recovery by 4% is small.

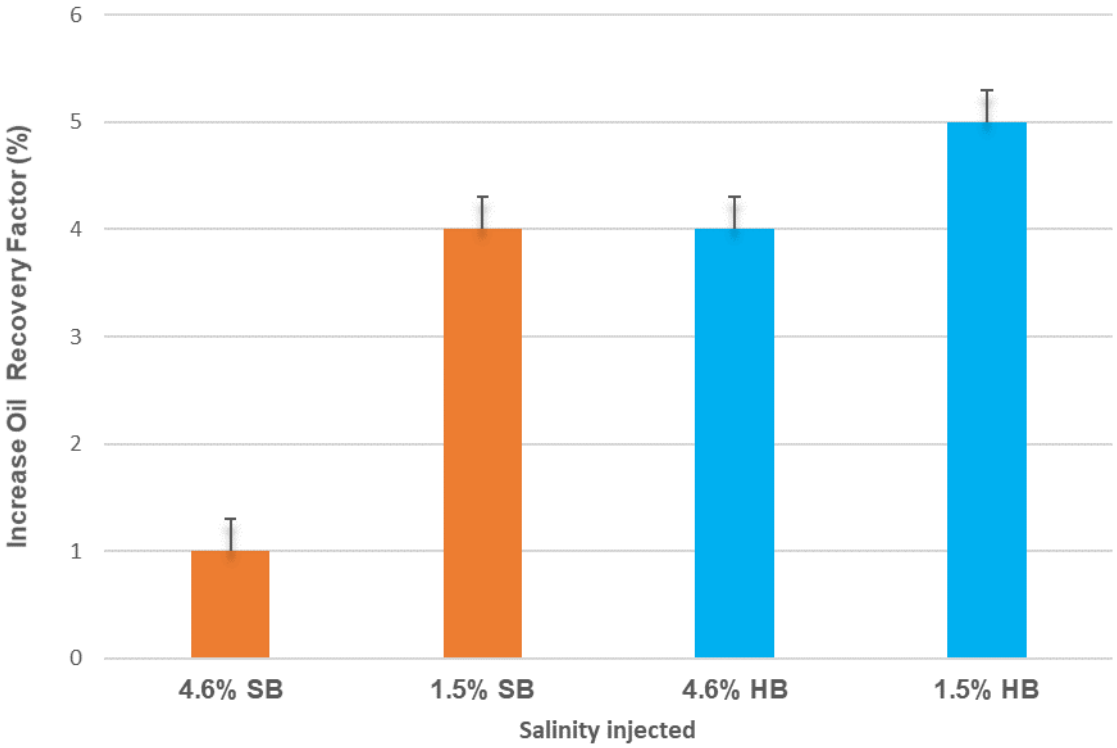


**Figure 4-9: Increase in oil recovery by salinity gradient for SB and HB**

**Table 4-5: Results from Core flooding for SB and HB with low salinity**

| Salinity used for Water flooding (% TDS) | Capillary Number Nc (x$10^{-07}$) | Recovery Factor RF | Residual Oil | Residual Oil Saturation | Displacement Efficiency $E_D$ |
|---|---|---|---|---|---|
| | | (%) | ($cm^3$) | Sro | (Fraction) |
| 5.7% SB | 0.592 | 41 | 4.38 | 0.52 | 0.416 |
| 4.6% SB | 0.817 | 42 | 4.28 | 0.51 | 0.427 |
| 1.5% SB | 1.38 | 45 | 4.08 | 0.48 | 0.461 |
| 6.6% HB | 0.939 | 49 | 3.78 | 0.45 | 0.494 |
| 4.6% HB | 2.34 | 53 | 3.58 | 0.42 | 0.528 |
| 1.5% HB | 4.01 | 54 | 3.48 | 0.41 | 0.539 |

The oil recovery obtained from the first imbibition using 6.6% HB was 8% higher than the oil recovery for 5.7% SB. For these two cases, there is no salinity gradient effect and the differences in density between the two brines HB and SB are minimal. The only appreciable difference is the content of divalent ions thus ionic composition. Different ionic composition of the different brines suggests changes in interactions between the system (brine -oil -rock) due to the different composition of the formation water. Van der Waals interactions prevail for SB, and calcium bridging interactions dominate for HB. These differences in interactions are represented in Figure 4-10.

As the crude oil for this study case is aromatic type, based on the high percentage of aromatics, the low interfacial tension of brine with divalent ions is favourable, as also reported by previous research (Kakati and Sangwai, 2017). This assumption is consistent with the results obtained for HB.

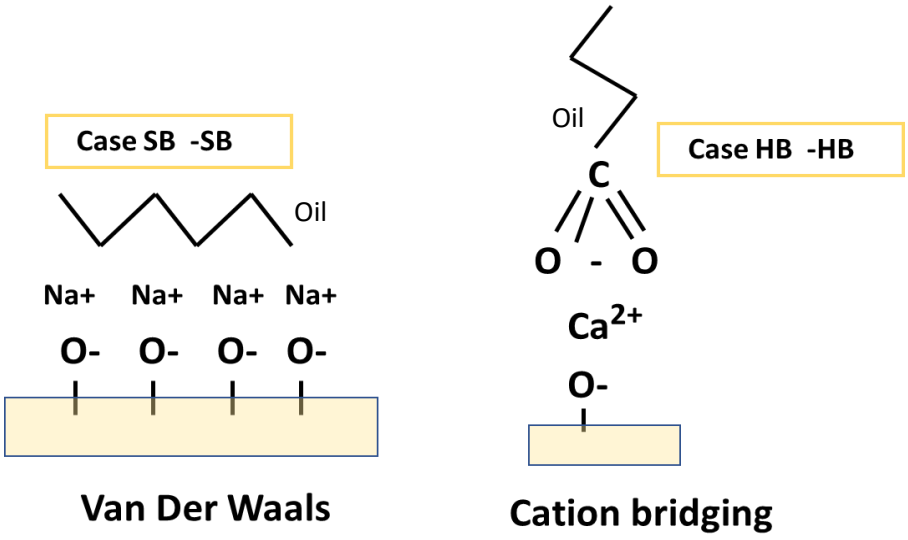


**Figure 4-10: Interactions oil-brine-water for SB and HB**
Figure adapted from literature (Lager *et al.*, 2007)

#### 4.3.3.2 Relative Permeability and effect of the low salinity required for CEOR

Endpoints for relative permeability curves were estimated from experimental results and relative permeability curves for cases (a) and (b) were adjusted using Corey correlation. Results for relative permeability of oil and water versus water saturation for SB and HB and low salinity waterflooding processes are presented in Figures 4-11 and 4-12.

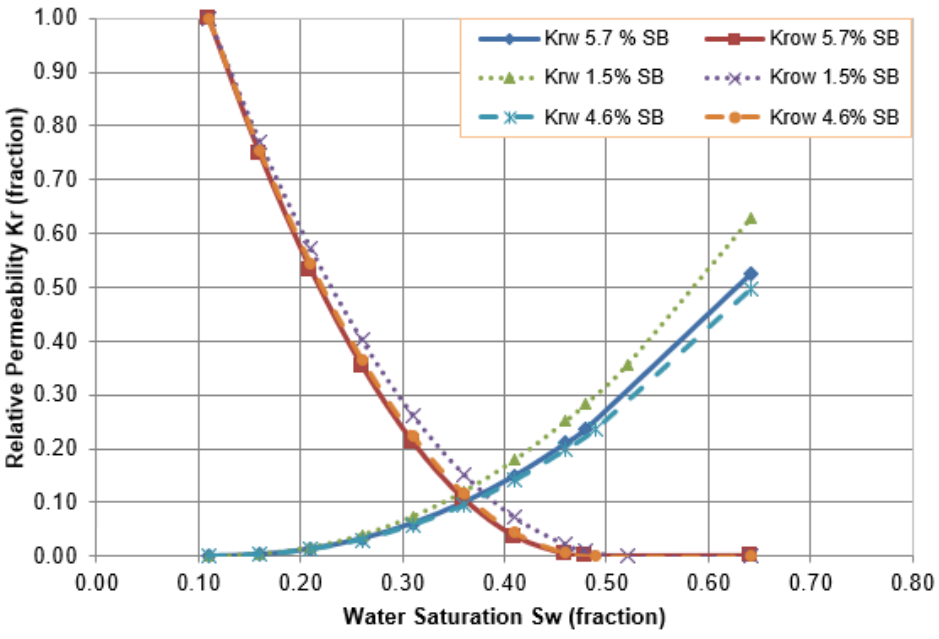


**Figure 4-11: Relative Permeability curves for SB water flooding**

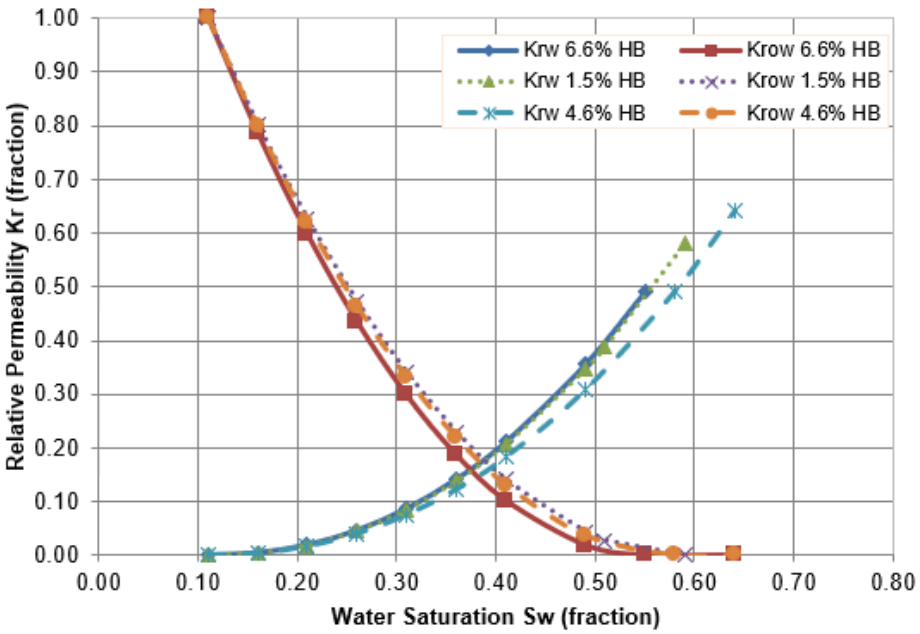


**Figure 4-12: Relative Permeability curves adjusted for HB water flooding**

The residual oil saturation decreases from 0.52 to 0.48 for SB and from 0.45 to o.41 for HB. Both relative permeability curves shift to lower residual oil saturation by the effect of the salinity gradient, and the effect is higher for HB. This effect is an indication of some changes in wettability due to interactions of fluids with the rock surface which also affects the distribution of fluid in the porous space. These results are consistent with the area of low IFT measured for HB solutions at lower salinity, which also suggest the effect of interactions fluid-fluid.

Oil relative permeability curves $k_{row}$ increase for low salinity for both SB and HB and this effect is consistent with results of residual oil saturation and oil recovery factor. However, the trend observed for water relative permeability curves $k_{rw}$ is associated with the salinity for both brines, thus decreases at 4.6% and increases at 1.5% salinity. These changes in $k_{rw}$ may be associated with interactions fluid-rock that are affecting the ionic layer adsorbed to the rock by the effect of the salinity gradient created by the injection of low salinity.

#### 4.3.3.3 Capillary Number

Capillary numbers for the different tests were calculated using IFT values measured at each salinity, flow conditions for the tests and relative permeability curves, Darcy velocity and fluid properties. Capillary number values calculated have been presented in table 4-4. A graph representing residual oil saturation as a function of capillary numbers for SB and HB is presented in Figure 4-13.

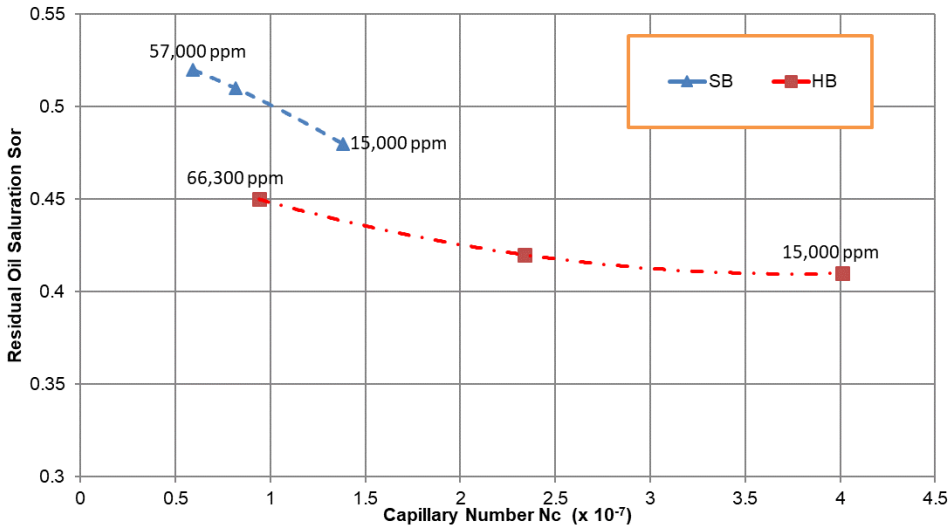


**Figure 4-13: Residual Oil Saturation versus capillary number for HB and SB**

There is a slight decrease in the residual oil saturation by changes on the capillary number by a factor of 10 by the injection of low salinity flow with both types of brine HB and SB. However, low salinity flooding with HB resulted in lower residual oil saturation than with SB. From these results is noticed the effect of the salinity on the residual oil saturation obtained after water flooding in core flooding tests. The injection of low salinity reduces the residual oil saturation and the mechanism can be associated with a reduction of IFT between oil and brine by decreasing the salinity as shown in figure 4-6.

#### 4.3.3.4 Fractional flow curves

Fractional curves were calculated based on results from core flooding experiments. There are slight differences in the fractional flow of water as a function of the water saturation for the different cases of low salinity (Figures 4-14 and 4-15). It is apparent that for SB the injection of low salinity (1.5% SB) slightly decreases the water saturation for water breakthrough, which is consistent with the increase in the relative permeability of water obtained for 1.5% SB and high recovery factor. The water saturation for water breakthroughs for HB increases for low salinity, with higher values for 4.6% HB, which is the salinity with a high recovery factor (Figure 4-15).

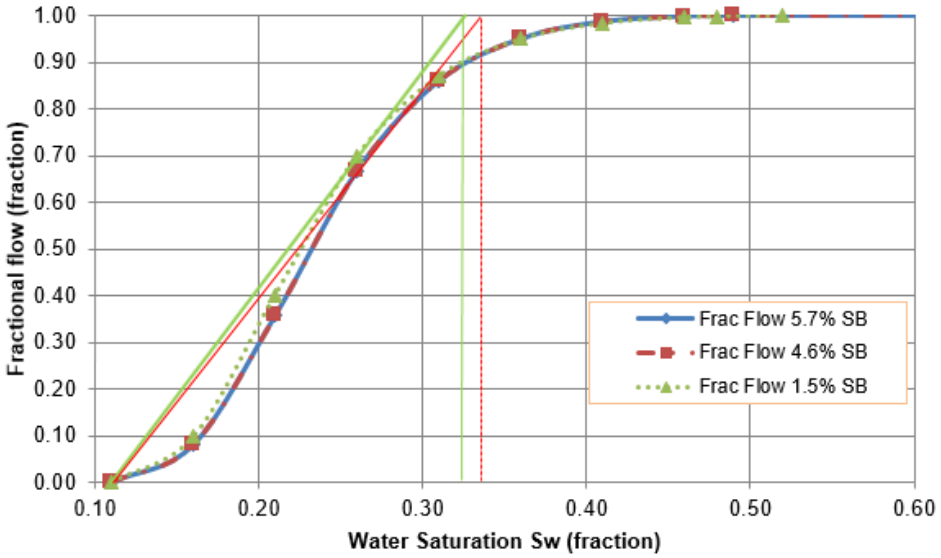


**Figure 4-14: Fractional flow curves for SB and salinity gradients**

The differences in fractional curves for SB and HB also indicates the different mechanism associated with each process. For SB both relative permeability curves increase for the optimal low salinity, which is a behaviour expected for low IFT flow. For HB the relative permeability of oil increase and the relative permeability of water decreases and increase for low salinity, which is a behaviour more associated with mobility ratio.

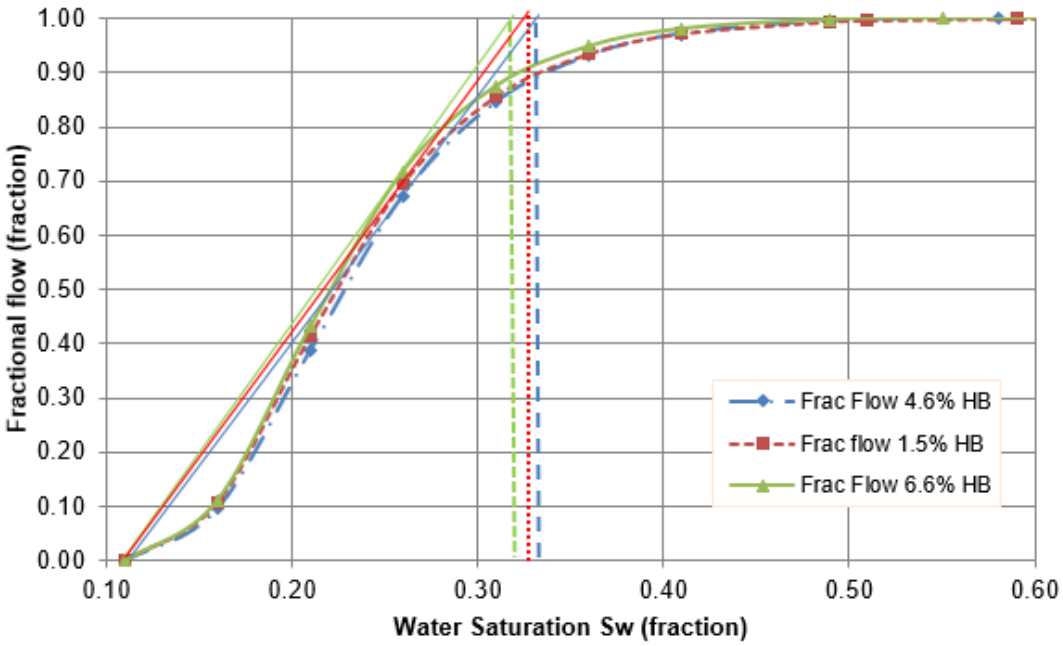


**Figure 4-15: Fractional flow curves for HB and salinity gradients**

These results evidence a slightly increase in oil recovery associated with the salinity and composition of the injected water. Also, the positive effect of divalent ions in the formation brine on the mechanism for oil recovery. It was also found that for an acidic crude oil, the injection of brine with divalent ions can be beneficial for CEOR, provided ionic interactions and mechanisms are well analysed.

The analysis of the salinity and the effect on the oil-brine-rock interactions to optimize the oil recovery factor RF are important for the design of CEOR. However, these interactions are complex and each case should be analysed separately to get the optimal RF.

# CHAPTER FIVE: STUDY OF ALKALI-SURFACTANT BEHAVIOUR AND THE EFFECT OF BRINE SALINITY AND HARDNESS

## 5.1 Introduction

This chapter presents the methodology and results of the study of the behaviour of different surfactants and their interactions with alkali for CEOR under brine with high salinity and hardness, given by the concentration of divalent cations $Ca^{2+}$ and $Mg^{2+}$.

This part of the research was aiming to:

- Study the stability of the systems brine/surfactant/oil, brine/alkali/oil, and brine/alkali/surfactant/oil in brines with high salinity and hardness.
- Evaluate the effect of salinity and brine composition on microemulsion formation for the system brine-surfactant/oil and brine-alkali –surfactant/oil.

Chemical combinations of alkali, and surfactants blends to achieve ultra-low IFT for microemulsion formation were evaluated. The ability of the chemical system to maintain the microemulsion for the range of salinity gradient between the salinity existing in the reservoir and the salinity of the injection water was also evaluated.

The effects of the chemical slug on the relative permeability, capillary number, and displacement efficiency are analysed and discussed aiming to elucidate dominant mechanisms.

Results from this study can provide some criteria to select the chemical combination for CEOR for applications in cases of brine with high salinity and with divalent cations. The systematic approach to the design of the chemical slug at a laboratory scale is also a positive outcome of this part of the project.

## 5.2 Methodology

The steps followed to complete this part of the research are included in this section and the methods were explained in chapter 3.

A series of anionic surfactants with different hydrophilic groups and hydrophobic length were evaluated, details of surfactants are presented in table 5-1. The list included three surfactants alcohol propoxy sulfate (APS), two surfactants alcohol ethoxy sulfate (AES), one surfactant methyl ester sulfonate (MES), two surfactants internal olefin sulfonate (IOS), and one non-ionic surfactant alcohol ethoxylated EO.

Likewise, alkali of different strengths (defined by the ability to form hydroxyl ions $OH^-$ on an aqueous solution) were used for the study. The use of ethylene diamine tetra-acetic acid EDTA as a complexing agent for divalent cations $Ca^{2+}$ and $Mg^{2+}$ was also evaluated. EDTA is used to prevent the precipitation of $Ca^{2+}$ and $Mg^{2+}$ hydroxides so that ASP CEOR using conventional alkali NaOH can be applied with hard brine. Details of the investigated alkalis are presented in table 5-2.

**Table 5-1: List of surfactants tested for Chemical EOR**

| Type | Surfactant Name | Formula | Chemical Formula |
|---|---|---|---|
| **Anionic** | Alcohol Propoxy Sulfate | $C_{16-17}$-13APS | $C_{\mathbf{16-17}}$-O-[$CH_2$-($CH_3$)-CH--O-]$_{\mathbf{13}}$-$SO_3^-$ Na |
| | | $C_{16-17}$-7APS | $C_{\mathbf{16-17}}$-O-[$CH_2$-($CH_3$)-CH--O-]$_7$-$SO_3^-$Na |
| | | $C_{13-14}$—7APS | $C_{\mathbf{13-14}}$-O-[$CH_2$-($CH_3$)-CH--O-]$_7$-$SO_3^-$Na |
| **Anionic** | Alcohol Ethoxy Sulfate | $C_{06-10}$-AES | $C_{\mathbf{06-10}}$-O-[$CH_2$-$CH_2$-O-]$_n$-$SO_3^-$Na |
| | | $C_{12-14}$-AES | $C_{\mathbf{12-14}}$-O-[$CH_2$-$CH_2$-O-]$_{2-3}$-$SO_3^-$Na |
| **Anionic** | Internal Olefin Sulfonate | $C_{20-24}$-IOS | R-CH-OH-$CH_2$-CH-$SO_3$-R<br>R-CH=CH-$SO_3$-R 16-25 % **R+R'=20-24** |
| | | $C_{15-18}$-IOS | R-CH-OH-$CH_2$-CH-$SO^-_3$-R<br>R-CH=CH-$SO^-_3$-R' **20-30 % R+R'=15-18** |
| **Anionic** | Methyl Ester Sulfonate | $C_{12-18}$-MES | $C_{\mathbf{12-18}}$-CH-(C-O-O-$CH_3$)$SO^-_3$Na ~20%<br>R -(CO-O-Na)$SO^-_3$Na<br>$CH_3$-$OSO_3$Na |
| **Non-ionic** | Alcohol Ethoxylate | $C_{12-15}$-7EO | $C_{\mathbf{12-15}}$-[$CH_2$-$CH_2$-O-]$_7$-OH ~ 55-65% |

**Table 5-2: List of alkalis tested for Chemical EOR**

| Type | Alkali Name | Formula |
|---|---|---|
| Strong alkali | Sodium Hydroxide | NaOH |
| Strong-Medium Alkali | Ammonium Hydroxide | $NH_4OH$ |
| Medium Alkali | Sodium-Metaborate | $NaBO_2$ |
| Weak Alkali | Sodium Hydrogen Carbonate | $NaHCO_3$ |
| Weak Alkali | Sodium Acetate | $NaO_2C_2H_3$ |
| Medium –Strong (Buffer pH=9) | Ethylene-diamine-tetracetic acid-with sodium hydroxide | EDTA/NaOH |

The steps followed to complete this part of the research are included in Figure 5-1.

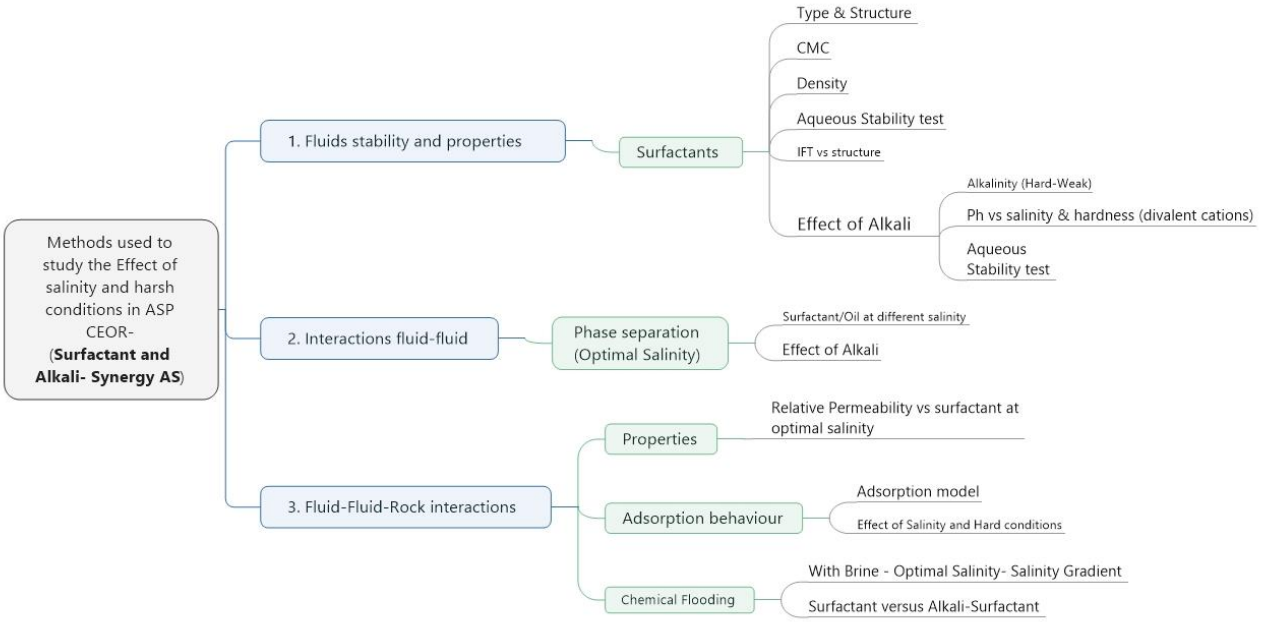


**Figure 5-1: Methodology to study the effect of brine salinity and hardness on microemulsion formation of surfactant and alkali CEOR**

In the first stage, fluids stability and properties in Figure 5-1, the stability of surfactants and alkalis solutions in brines with high salinity and hardness was evaluated to determine salinity and alkali regions of stable solutions.

The critical micellar concentration (CMC) for each surfactant was estimated experimentally. For this purpose, the surface tension (ST) of surfactant solutions at different concentrations was measured using a tensiometer (procedure described in chapter 3). Based on the CMC of each surfactant, the minimal concentration of the surfactant required for the stability test was defined.

To study the effect of alkali and interactions with surfactants for CEOR processes, a pre-selection stability analysis of alkali solutions in brine salinity and hardness was performed at laboratory scale and reservoir temperature. This study was aiming to screen alkalis, to select the salinity and alkali range of application for each formulation, and to define their suitability for applications in brines with high salinity and concentration of divalent cations.

The stability of alkalis (table 5-2) at different salinity was studied in hard (HB) and soft (SB) brines. The range of alkali concentrations used was 0.25 -0.02 mol/lt, and constant salinity for

different salinities, covering a salinity range from 5000 to 60000 ppm total dissolved solids (TDS).

The second stage corresponds to the study of the fluid-fluid interactions brine- alkali-surfactant-oil, when the aqueous phase is put in contact with the crude oil, (step number 2 in figure 5-1). The stability and effectiveness reducing IFT of the alkali, surfactants, and blends of surfactants with alkali systems are evaluated. Results are aiming to assess chemical formulations that are able to form the zone of ultra-low IFT microemulsion with a range of salinity close to the composition of the brine available at the location for injection. Interfacial tension and phase separation methods as explained in chapter 3 were used.

The third stage of the study corresponds to fluid-fluid- rock interactions at reservoir conditions, using the chemical slug (surfactant or alkali-surfactant) that show ultra-low IFT (stage 3, labelled fluid-fluid-rock interactions) and core flooding tests. To analyse physical-chemical interactions that occur between the fluids in the porous media, and how these interactions affect relative permeability curves of the oil/aqueous phase, the effect of CEOR on the oil displacement efficiency, and the adsorption of surfactant on rock samples, results from core flooding tests were studied.

## 5.3 Results and discussion

### 5.3.1 Study of stability of surfactants and alkali solutions

In this section, results from the study of conditions for stability of surfactant and alkali solutions in brine salinity and hardness are presented.

#### 5.3.1.1 Critical micellar concentration of surfactants CMC

Results of surface tension (ST) versus surfactant concentration, are presented in Figures 5-2 to 5-4. For each surfactant, the surface tension sharply drops with the increase of surfactant concentration at low surfactant concentration, until a minimum value and then remains approximately constant. The energy of surfactant solutions is reduced with surfactant concentration until a minimal surface tension with the formation of micelles. From the CMC onwards, the surface tension does not noticeably change with the increase of surfactant concentration. The critical micelle concentrations (CMC) is the concentration with the minimal value of surface tension and is very characteristic for each surfactant. Results of surface tension versus surfactant concentration, are presented in Figures 5-2 to 5-4.

CMC values for each surfactant are determined from the graph as the concentration at the inflection point and the values are presented in table 5-3, the CMC concentration of surfactant is very relevant for the initial definition of the minimal concentration of surfactant required for the chemical slug to achieve ultra-low IFT between oil and brine. As the surfactant is in the form of micelles the formation of oi/water microemulsion is favourable. (Sheng, 2010a).

**Table 5-3: CMC for different surfactants**

| Surfactant Structure | CMC (%) v/v | ST @ CMC (mN/m) |
|---|---|---|
| $C_{20-24}$-IOS | 0.025 | 29.67 |
| $C_{15-18}$-IOS | 0.025 | 32.72 |
| $C_{12-18}$-MES | 0.025 | 26.36 |
| $C_{12-15}$-7EO | 0.025 | 33.01 |
| $C_{06-10}$-AES | 0.15 | 30.03 |
| $C_{12-14}$-AES | 0.15 | 32.05 |
| $C_{16-17}$-13APS | 0.05 | 29.95 |
| $C_{16-17}$-7APS | 0.05 | 30.66 |
| $C_{13-14}$—7APS | 0.05 | 34.39 |

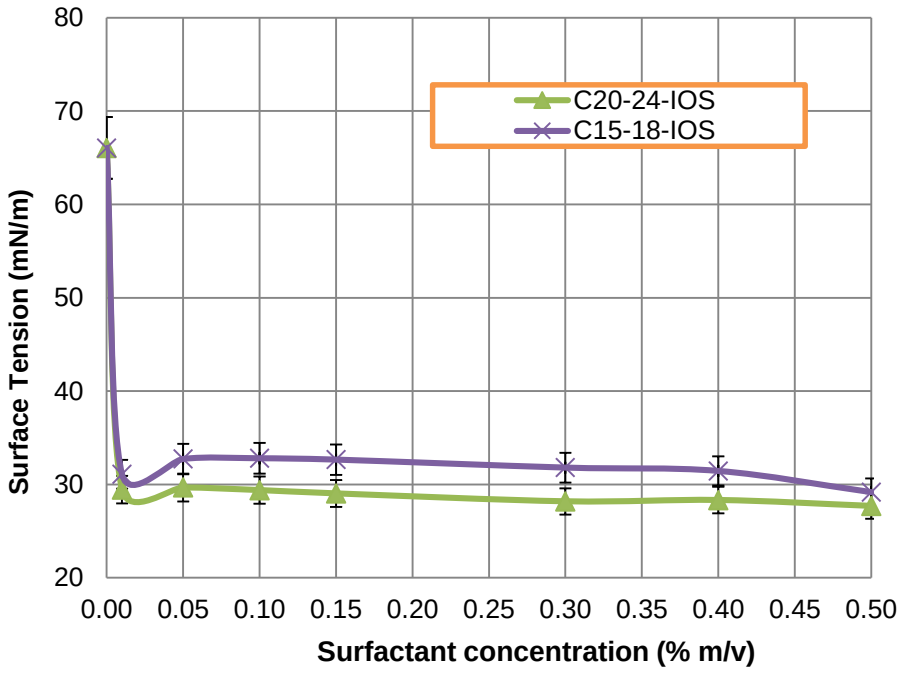


**Figure 5-2: ST versus concentration for surfactants IOS ($C_{20-24}$) and IOS ($C_{15-18}$)**

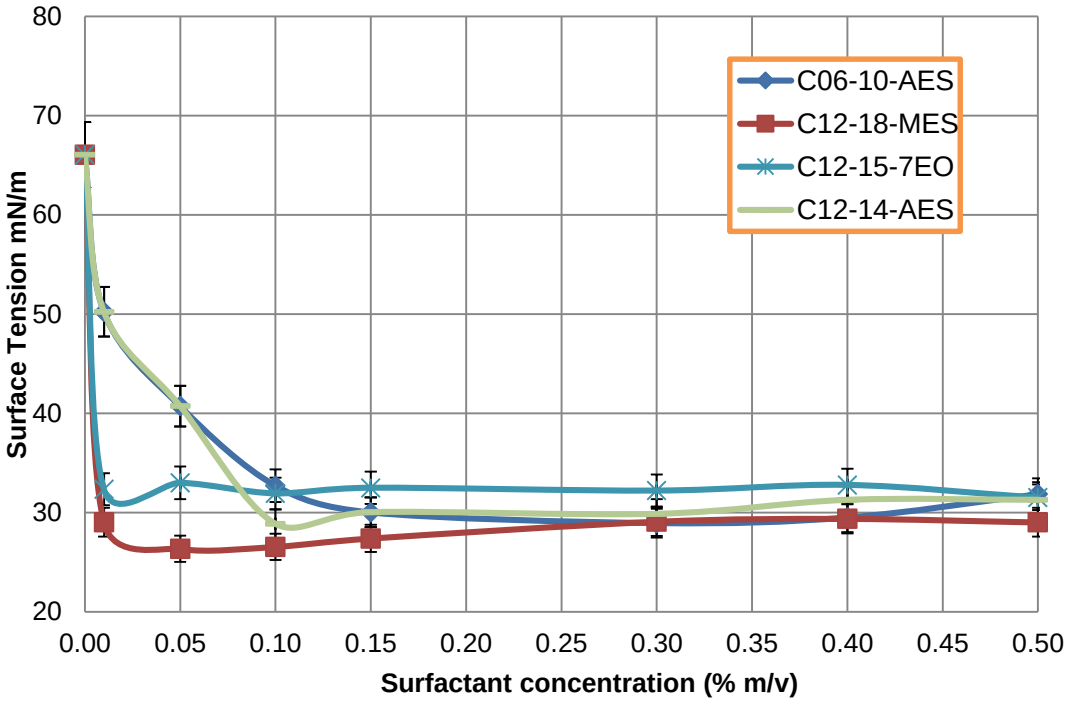


**Figure 5-3: ST versus concentration for surfactants AES ($C_{06-10}$), ($C_{12-14}$), MES ($C_{12-18}$) and EO($C_{12-15}$)**

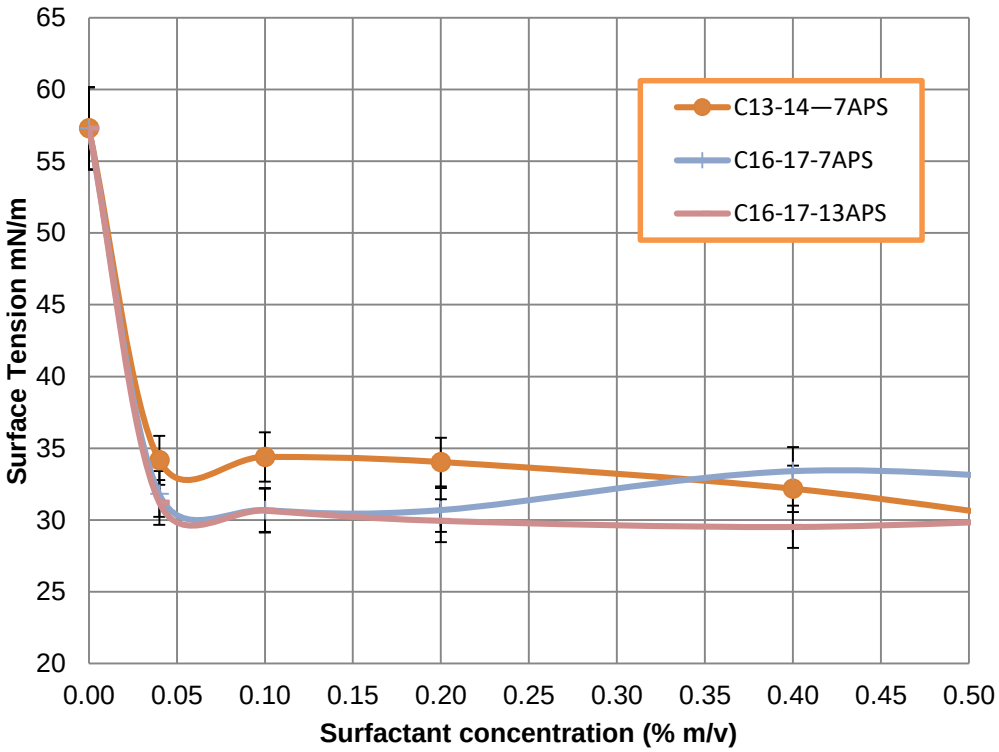


**Figure 5-4: ST versus concentration for surfactants type APS**

The critical micellar concentrations (CMC) obtained for all tested surfactants are low, yet MES ($C_{12-18}$) and EO ($C_{12-15}$) and IOS, surfactants have the lowest CMC. The surface tension of surfactant solutions has the same order of magnitude.

Surfactants type IOS have similar CMC, however, the surfactant with higher hydrophobicity ($C_{20-24}$) has slightly lower values of surface tension. The surface tension decreases with the increase in surfactant concentration to a minimal and then remains constant with similar CMC concentration. Details are presented in Figure 5-2.

Surfactants type AES show similar behaviour of surface tension versus concentration, however, the CMC for the surfactant with higher hydrophobicity ($C_{12-14}$) is slightly lower than the surfactant with low hydrophobicity ($C_{6-10}$). There is no appreciable difference in the values of surface tension. Details are included in the graph presented in Figure 5-3.

Surfactant ($C_{12-18}$) MES and ($C_{12-15}$) 7EO have similar behaviour of surface tension versus concentration; however, MES surfactant showed lower values of surface tension. The higher the hydrophobic chain the lower the surface tension is achieved. Details are also included in the graph presented in Figure 5-3.

Surfactants type APS, $C_{13-14}$—7APS, $C_{16-17}$-13APS and $C_{16-17}$-7APS, have similar behaviour of surface tension versus surfactant concentration with low and similar values of CMC; however, the surface tension for the surfactant with lower hydrophobic hydrocarbon chain, $C_{13-14}$—7APS, is higher than for surfactants with higher hydrophobic hydrocarbon chain, thus $C_{16-17}$-13APS and $C_{16-17}$-7APS. Details are included on the graph presented in Figure 5-4.

These results demonstrate that hydrophobicity has a larger impact on surface tension than hydrophilicity. The CMC for surfactants decreases with the increase of the hydrophobicity and increases with the number of polar groups in a surfactant (Wade et al., 1979).

The effect of the number of polar groups on the CMC was not noticed on this test as similar CMC and surface tension were obtained for $C_{16-17}$-13APS and $C_{16-17}$-7APS. These results indicate that the hydrophobicity of the surfactants is the main factor affecting the CMC and surface tension.

#### 5.3.1.2 Surfactant- brine interactions

Results from the stability tests showed the surfactant $C_{13-14}$—7APS is stable in SB for all the range of salinity. However, the stability in HB is limited to 4.5% TDS salinity. Samples at salinity

higher than 4.5% TDS have the formation of cloudiness. Examples of these results are presented in Figure 5-5 and 5-6.

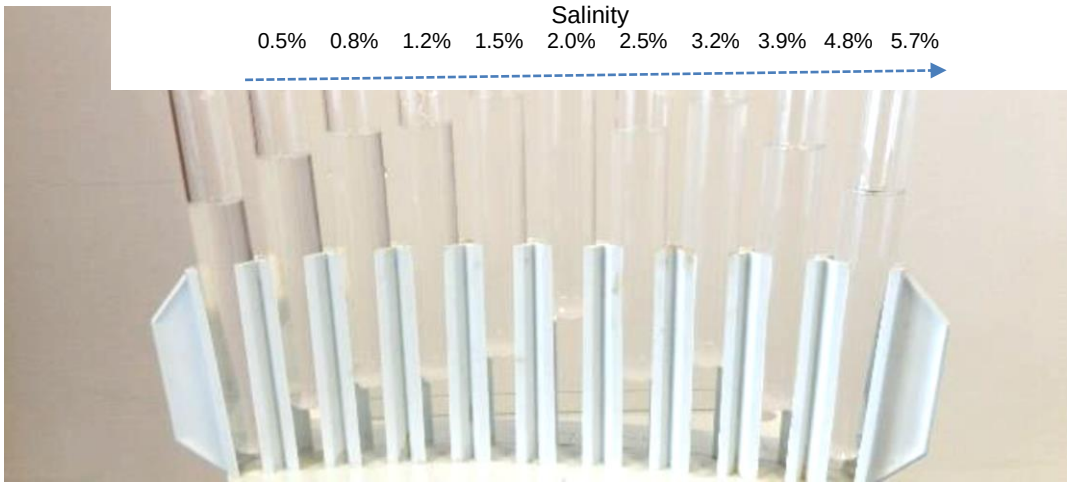


**Figure 5-5: Stability test for surfactant $C_{13-14}$—7APS at different salinities SB**

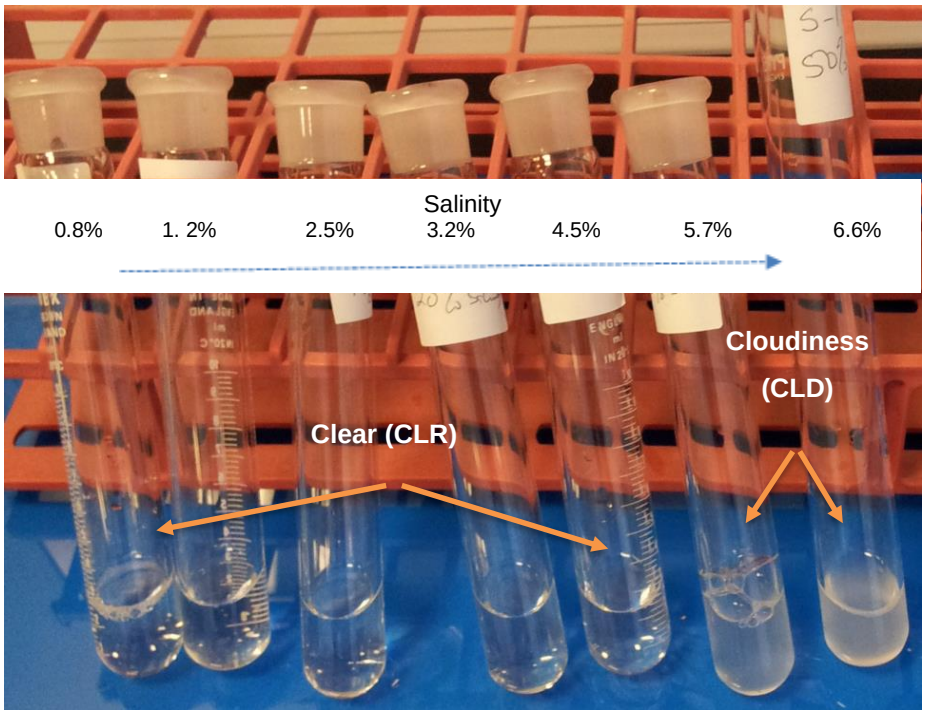


**Figure 5-6: Stability test for surfactant C13-14—7APS at different salinities HB**

Results for the evaluation of the stability of surfactants under salinity conditions and range of salinity in HB and SB are summarized in table 5-4 and a solubility graph of surfactants is represented in Figure 5-7.

**Table 5-4: Range of salinity for (0.2%) surfactants in HB and SB from stability tests**

| Surfactant | Range of salinity SB (%) | Observations | Range of salinity HB (%) | Observations |
|---|---|---|---|---|
| $C_{12-15}$-7EO | 0 – 5.7% | PPT | 0 -- 6.6% | PPT |
| $C_{12-18}$-MES | 0 – 5.7% | CLR | 0 -- 6.6% | CLR |
| $C_{06-10}$-AES | 0 – 5.7% | CLR | 0 -- 6.6% | CLR |
| $C_{12-14}$-AES | 0 – 5.7% | CLR | 0 -- 6.6% | CLR |
| $C_{15-18}$-IOS | 0 – 5.7% | CLR | 0 -- 0.3 % | CLR |
| | | | 0.3-6.6% | CLD |
| $C_{20-24}$-IOS | 0 – 5.7% | CLR | 0 -- 6.6% | CLR |
| $C_{16-17}$-13APS | 0 – 5.7% | CLR | 0 -- 1.7 % | CLR |
| | | | 1.7-6.6% | CLD |
| $C_{16-17}$-7APS | 0 – 5.7% | CLR | 0 -- 1.7 % | CLR |
| | | | 1.7-6.6% | CLD |
| $C_{13-14}$—7APS | 0 – 5.7% | CLR | 0 -- 4.5 % | CLR |
| | | | 4.5-6.6% | CLD |

Surfactant $C_{12-15}$-7EO was unstable with both HB and SB, the evidence was indicated by insoluble precipitates for all tested salinities. Similar solubility results have been reported for this type of surfactant. The number of ethylene oxide makes the surfactant more hydrophilic and enhances their solubility (Sahni *et al.*, 2010).

Surfactants type AES and $C_{12-18}$-MES showed stable aqueous solutions at the range of salinities evaluated for SB and HB.

Surfactant type IOS were stable in SB, however in HB, the surfactant with low hydrophobicity, thus $C_{15-18}$-IOS, was unstable at salinities higher than 0.3% TDS. The surfactant $C_{20-24}$-IOS was stable and had clear and stable solutions for all tested salinities.

Surfactants type APS were all stable under all the range of salinities used for SB, $C_{16-17}$-13APS, and $C_{16-17}$-7APS surfactants were unstable with HB for salinities higher than 1.7 % TDS. For salinity concentrations above 1.7% TDS salinity, precipitation was observed in all the solutions for these surfactants. $C_{13-14}$—7APS surfactant was also unstable with HB at salinities higher than 4.5 % salinity, above this concentration, precipitation was observed like for the other surfactants APS.

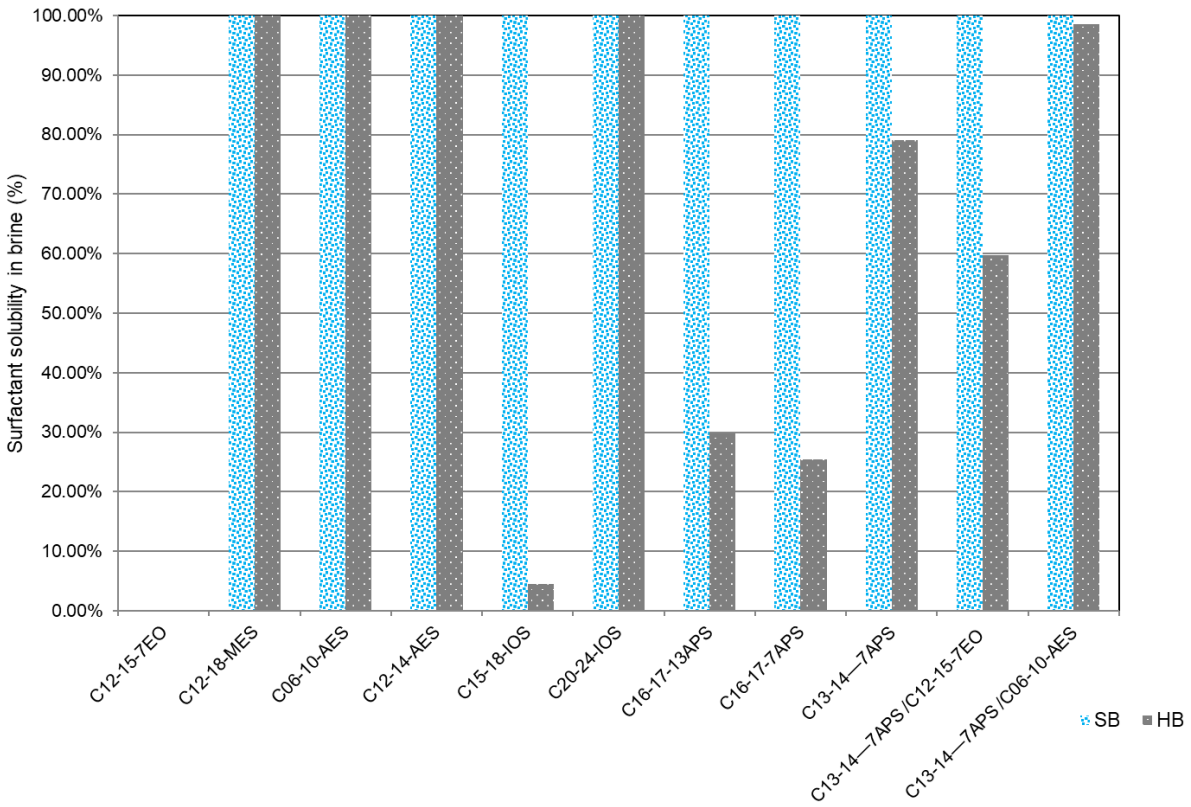


**Figure 5-7: Solubility of surfactants in synthetic SB and HB**

The effect of the number of APS groups on the stability of APS surfactants to salinity was analysed for surfactants $C_{16\text{-}17}$-13APS and $C_{16\text{-}17}$-7APS. The solubility in brine solutions was lower for the surfactant with a higher number of APS groups, thus $C_{16\text{-}17}$-13APS.

The effect of the hydrophobicity was observed by comparing $C_{13\text{-}14}$—7APS with $C_{16\text{-}17}$-7APS surfactants. The high hydrophobicity reduces the solubility of the surfactant in HB, with a small range of salinity for $C_{16\text{-}17}$-7APS than for $C_{13\text{-}14}$—7APS.

From these results is evident that divalent cations reduce the solubility of surfactants and the effect depends on surfactant structure. While surfactants type AES, MES showed good stability with SB and HB, surfactants IOS and APS present some limitations of salinity for HB.

The blends of surfactants in brine solutions showed how APS increases the solubility of ethoxylate alcohol $C_{12\text{-}15}$-7EO surfactant. Ethoxylate alcohol surfactant $C_{12\text{-}15}$-7EO was insoluble in brine with monovalent and divalent cations on the test presented on the previous section, however, when mixed in a proportion 0.2% $C_{13\text{-}14}$—7APS /0.2% $C_{12\text{-}15}$-7EO was stable at salinity up to 4% with cloudy solutions at 4.2%, similar effect has been reported by mixes of

APS surfactants with IOS type surfactants (Hirasaki et al., 2011). Alcohol ethoxy sulfate $C_{06-10}$-AES was also mixed in a proportion of 0.2% $C_{13-14}$—7APS /0.2% $C_{06-10}$-AES and mixes were stable up to 6.6% salinity.

A map of the application of surfactants based on aqueous stability results under brine salinity and hardness (concentration of divalent cations) is presented in Figure 5-8. For brines with low salinity and low concentration of divalent cations, surfactants APS with high hydrophobicity and surfactants type IOS with low hydrophobicity can be used. Surfactants type AES, MES can be used for applications with high salinity and can tolerate divalent cations. Likewise, surfactants type IOS with high hydrophobicity can tolerate divalent cations.

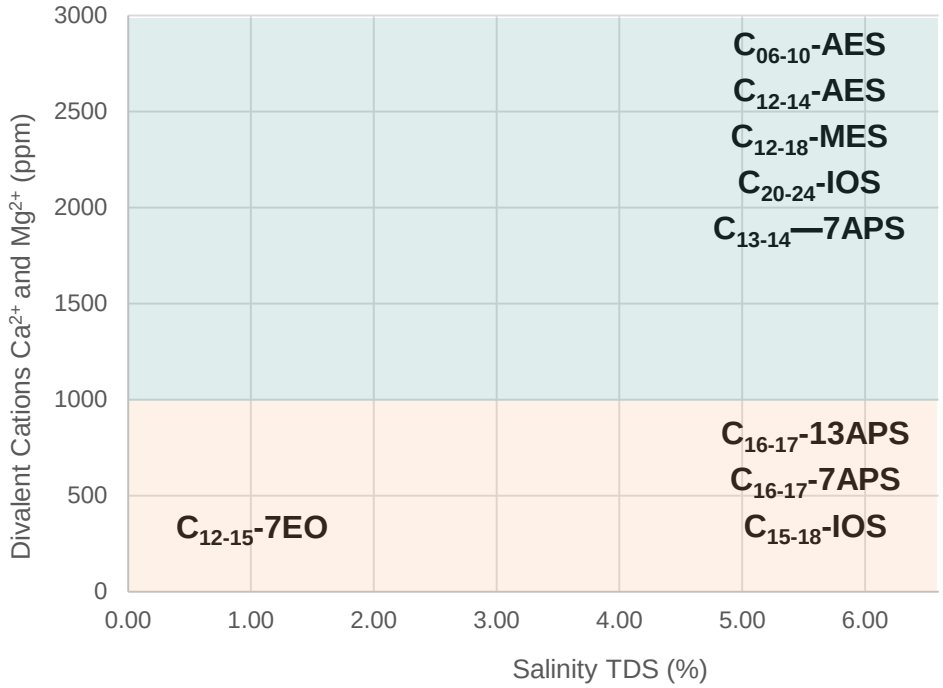


**Figure 5-8: Diagram for application of surfactants according to stability in brine salinity and concentration of divalent cations (hardness)**

#### 5.3.1.3 Alkalis-brine interactions under salinity and with divalent cations

The variations of pH for alkaline solutions with the alkali concentration for the synthetic HB used for the study are presented in Figure 5-9. While solutions of HB with strong alkalis, such as NaOH and $NH_4OH$, developed an insoluble precipitate of hydroxide for all alkali concentrations tested, solutions with medium and weak alkalis, such as $NaBO_2$, $NaHCO_3$, and $NaO_2C_2H_3$, showed clear and stable solutions and some cloudy and unstable solutions. At low

alkali concentration, solutions are more stable. Based on these results, strong alkalis NaOH and $NH_4OH$ were rejected for application with HB with divalent cations. Similar results were found by previous research (Sheng, 2010a).

Solutions of sodium acetate, $C_2H_3NaO_2$ and sodium hydrogen carbonate, $NaHCO_3$ have pH slightly alkaline, which is due to their weakness as alkalis. A minimal pH of approximately 9 is required for the saponification reaction between naphthenic acids existing in the crude oil with alkali to take place and generate a natural surfactant. Therefore, these two weak alkalis were not considered for further studies (Sheng, 2015a).

The threshold area (blue area) of stable solutions (with not precipitation) for the different alkalis in HB is presented in Figure 5-9. Solutions of $NaBO_2$ in HB were stable at low alkali concentration reaching a maximal pH of 10, therefore this alkali was considered as a good option for the ASP chemical system.

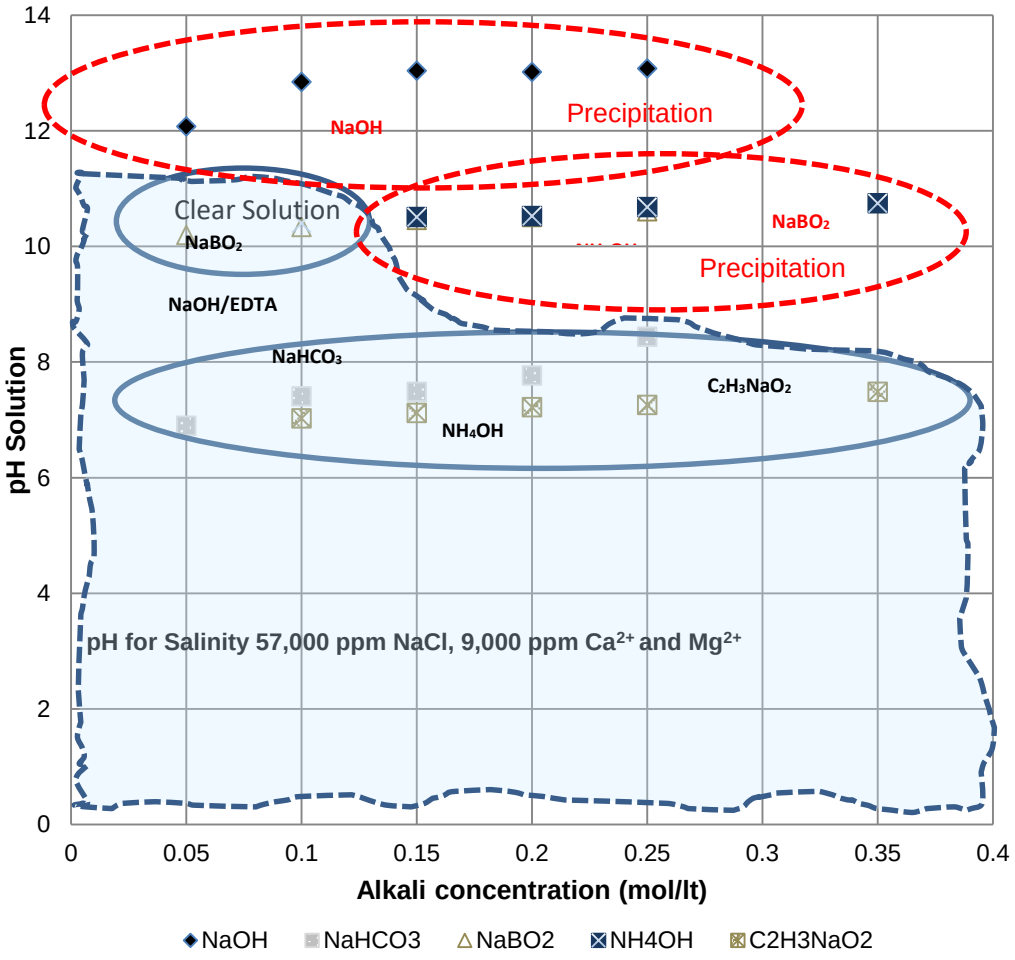


**Figure 5-9: pH of solutions of alkali at different concentration in HB with fixed salinity 57,000 ppm NaCl and 9,000 ppm $Ca^{2+}$ & $Mg^{2+}$**

Record of observations for stability tests are presented in tables 5-5 and 5-6. Examples of solutions of NaOH in HB (precipitate) and SB (clear) are presented in Figure 5-10.

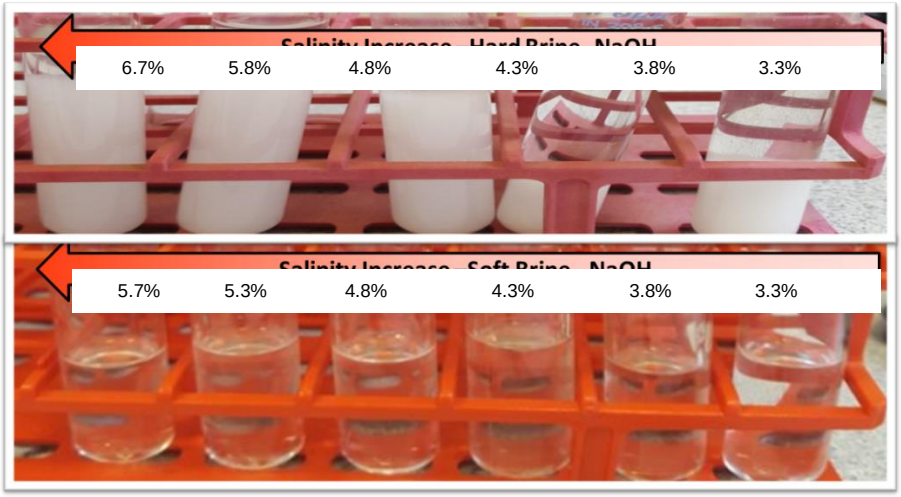


**Figure 5-10: NaOH solutions in SB (Clear Solutions)**

**Table 5-5: Stability of NaOH solutions in SB and HB**

| NaOH conc (mol/lt) | Salinity (ppm NaCl) | Divalent salts (ppm $CaCl_2$ and $MgCl_2$) | pH range | Brine | Observations |
|---|---|---|---|---|---|
| 0.25-0.05 | 57,000 | 0 | 13.5-12.5 | SB | CLR |
| 0.25-0.05 | 53,370 | 0 | 13.5-12.5 | SB | CLR |
| 0.25-0.05 | 48,260 | 0 | 13.5-12.5 | SB | CLR |
| 0.25-0.05 | 43,150 | 0 | 13.5-12.5 | SB | CLR |
| 0.25-0.05 | 38,041 | 0 | 13.5-12.5 | SB | CLR |
| 0.25-0.05 | 33,498 | 0 | 13.5-12.5 | SB | CLR |
| 0.25-0.05 | 57,000 | 9,000 | 13.6-12 | HB | PPT |
| 0.25-0.05 | 49,396 | 7,830 | 13.6-12 | HB | PPT |
| 0.25-0.05 | 41,447 | 6,570 | 13.6-12 | HB | PPT |
| 0.25-0.05 | 33,498 | 5,310 | 13.6-12 | HB | PPT |
| 0.25-0.05 | 26,117 | 4,140 | 13.6-12 | HB | PPT |
| 0.25-0.05 | 18,169 | 2,880 | 13.6-12 | HB | PPT |

*CLR: Clear solutions PPT: Precipitate*

Stability results for NaOH solutions show that there was no precipitation for any of the solutions in SB. In HB divalent cations, $Ca^{2+}$ and $Mg^{2+}$, existing in the synthetic HB are the main cause for the precipitation. The precipitates are the hydroxides of the divalent cations $Ca(OH)_2$ and $Mg(OH)_2$.

Results for $NaBO_2$ solutions in HB presented in table 5-6 indicate that at high alkali concentration there is a precipitate. Therefore, it seems to be a maximal threshold solution for the alkali concentration to complex divalent cations of about 0.1 mol/lt.

The comparison of stability for alkali solutions in HB and SB demonstrates the negative effect of divalent cations on strong alkali in brine solutions, which require special considerations in the design and evaluation of chemical formulations to avoid undesirable precipitation.

**Table 5-6: Stability of $NaBO_2$ solutions in SB and HB**

| $NaBO_2$ conc (mol/lt) | Salinity (ppm NaCl) | Divalent salts (ppm $CaCl_2$ and $MgCl_2$) | pH | Brine | Observations |
|---|---|---|---|---|---|
| 0.25 | 57,000 | 0 | 10.3 | SB | CLR |
| | 49,396 | 0 | 10.3 | SB | CLR |
| | 39,744 | 0 | 10.2 | SB | CLR |
| | 19,872 | 0 | 10.2 | SB | CLR |
| | 14,762 | 0 | 10.2 | SB | CLR |
| | 9,652 | 0 | 10.1 | SB | CLR |
| | 5,110 | 0 | 10.1 | SB | CLR |
| 0.25 | 57,000 | 9,000 | 10.3 | HB | PPT |
| | 49,396 | 7,830 | 10.3 | HB | PPT |
| | 39,744 | 6,570 | 10.4 | HB | PPT |
| | 19,872 | 3,150 | 10.4 | HB | PPT |
| | 14,762 | 2,340 | 10.5 | HB | PPT |
| | 9,652 | 1,530 | 10.6 | HB | PPT |
| | 5,110 | 810 | 10.6 | HB | PPT |
| 0.1 | 57,000 | 9,000 | 10.3 | HB | CLR |
| | 49,396 | 7,830 | 10.3 | HB | CLR |
| | 39,744 | 6,570 | 10.2 | HB | CLR |
| | 19,872 | 3,150 | 10.2 | HB | CLR |
| | 14,762 | 2,340 | 10.2 | HB | CLR |
| | 9,652 | 1,530 | 10.1 | HB | CLR |
| | 5,110 | 810 | 10.2 | HB | CLR |
| 0.02 | 57,000 | 9,000 | 9.8 | HB | CLR |
| | 49,396 | 7,830 | 9.9 | HB | CLR |
| | 39,744 | 6,570 | 9.9 | HB | CLR |
| | 19,872 | 3,150 | 10.0 | HB | CLR |
| | 14,762 | 2,340 | 10.0 | HB | CLR |
| | 9,652 | 1,530 | 10.0 | HB | CLR |
| | 5,110 | 810 | 10.0 | HB | CLR |

*CLR: Clear solutions PPT: Precipitate*

The behaviour of alkali solutions in brines for the evaluated alkalis can be explained considering the equilibrium reactions of calcium and magnesium hydroxides.

Sodium hydroxide in solutions with divalent cations reacts and form insoluble hydroxide of calcium and magnesium, and the reactions are as follow:

$$CaCl_2 + 2NaOH \rightarrow \boldsymbol{Ca(OH)_2}(ppt) + 2NaCl\,(aq) \quad (5\text{-}1)$$

$$Ca^{2+}{}_{(aq)} + 2OH^{-}{}_{(aq)} \rightarrow \boldsymbol{Ca(OH)_2}_{(ppt)} \qquad K_{sp} = 5.5\ x\ 10^{-5} \quad (5\text{-}2)$$

$$Mg^{2+}{}_{(aq)} + 2OH^{-}{}_{(aq)} \rightarrow \boldsymbol{Mg(OH)_2}_{\boldsymbol{(ppt)}} \qquad K_{sp} = 1.8\ x\ 10^{-11} \quad (5\text{-}3)$$

According to the solubility product constant (Ksp) for calcium and magnesium hydroxide, the latter will precipitate first as alkali concentration increase as is 6 order magnitude smaller. Considering the concentration of calcium and magnesium existing in the synthetic brine, the maximal concentration for alkali to avoid precipitation was calculated.

The moles of $Mg^{2+}$ and $Ca^{2+}$ calculated from the brine composition are as follow:

$[Mg^{2+}]$ =0.0401 mol

$[Ca^{2+}]$ =0.04641 mol.

By replacing those values on the equation for the solubility product, the minimal concentration of NaOH to have precipitation of $Mg(OH)_2$ is 2.12 x $10^{-5}$ mol/lt (pH=9.3) and 0.0344 mol/lt (pH= 12.5) for precipitation of $Ca(OH)_2$.

Sodium metaborate can complex divalent cations at an optimal concentration which depends on the brine composition (Liu *et al.*, 2008; Flaaten *et al.*, 2010; Bataweel, 2011). The equilibrium reaction for the formation of complex compounds of sodium metaborate solutions is as follow:

$$NaBO_2 + 6\ H_2O \text{ <=======> } Na^+ + 4\ H_2O + (B(OH)_4)^- \qquad \text{pH 9.3-11} \quad (5\text{-}4)$$

$$Ca^{2+} + (B(OH)_4)^- \text{ <=======> } Ca(B(OH)_4)^+ \qquad K=18 \quad (5\text{-}5)$$

At a higher concentration of the alkali, an amorphous precipitate with calcium and magnesium has been reported (Flaaten *et al.*, 2010). The precipitate is dissolved at higher concentration of divalent cations.

The total concentration of divalent cations $Ca^{2+}$ and $Mg^{2+}$ in the alkali-brine solution is 0.086 mol/lt. At that concentration, sodium metaborate produces stable solutions (CLEAR) without precipitation. This explains the behaviour found in table 5-6, there is a maximal concentration

of the alkali of 0.1 mol/lt required to form the complex with divalent cations. The excess of metaborate promotes the formation of complex structures and precipitation.

Ethylene-diamine-tetracetic acid EDTA was used as sequester agent of NaOH alkali solutions that showed precipitation with HB to evaluate its effectiveness as a complex agent of divalent cations calcium and magnesium. For that purpose, EDTA was added to solutions of NaOH in HB at different salinities; results are presented in table 5-7. According to observations for the different concentrations, it seems that there is also a minimal concentration of EDTA required to avoid divalent hydroxide precipitation. For the HB composition, the minimal amount of EDTA was 0.1 mol/lt and at pH ~9.5 The concentration of NaOH used was. $4.05\ x\ 10^{-5}\ mol/lt$.

**Table 5-7: Results of solutions HB –Alkali for NaOH/EDTA**

| EDTA/NaOH conc (mol/lt) | Salinity (ppm NaCl) | Divalent salts (ppm $CaCl_2$ and $MgCl_2$) | pH | Observations |
|---|---|---|---|---|
| 0.03/9.1E-04 | 57,000 | 9,000 | 10.96 | PPT |
| 0.03/9.1E-04 | 48,261 | 7,650 | 10.97 | PPT |
| 0.03/0.012 | 40,312 | 6,390 | 12.09 | PPT |
| 0.03/ 0.0151 | 32,931 | 5,220 | 12.18 | CLR |
| 0.03/ 0182 | 24,982 | 3,960 | 12.26 | CLR |
| 0.03/0.02 | 21,008 | 3,330 | 12.3 | CLR |
| 0.1/4.0E-05 | 57,000 | 9,000 | 9.6 | PPT |
| 0.1/4.0E-05 | 45,989 | 7,290 | 9.6 | PPT |
| 0.1/4.0E-05 | 38,609 | 6,120 | 9.8 | CLR |
| 0.1/4.0E-05 | 30,660 | 4,860 | 9.8 | CLR |
| 0.1/4.0E-05 | 26,685 | 4,230 | 9.8 | CLR |
| 0.2/1.1E-05 | 57,000 | 9,000 | 9.05 | CLR |
| 0.2/1.1E-05 | 48,261 | 7,650 | 9.02 | CLR |
| 0.2/1.6E-05 | 40,880 | 6,120 | 9.2 | CLR |
| 0.2/3.4E-05 | 32,931 | 5,220 | 9.6 | CLR |
| 0.2/2.0E-05 | 24,982 | 3,960 | 9.3 | CLR |
| 0.2/1.3E-05 | 17,431 | 2,763 | 9.1 | CLR |

*CLR: Clear solutions PPT: Precipitate*

Equilibrium reactions for NaOH with EDTA and divalent cations calcium and magnesium are as follow:

$NaOH + H_2O + EDTA\text{-}4H <=======> Na^{+} + OH^{-} + 3H_2O + EDTA^{-4}$ PH>8 (5-5)

$Ca^{+2} + EDTA^{-4} <=======> CaEDTA^{-2}$ $K_{eq}= 10^{10.7}$ (5-6)

$Mg^{+2} + EDTA^{-4} <=======> MgEDTA^{-2}$ $K_{eq}=10^{8.8}$ (5-7)

EDTA requires an alkali to form the complex compound with divalent cations. Therefore, the compatibility of the solution EDTA /NaOH with HB was highly affected by the concentration of divalent cations and the pH of the solution. While NaOH can react with EDTA to form the complexing form (equation 5-5), it can also react with divalent cations to form hydroxide (equations 5-2 and 5-3). The minimal concentration of EDTA required to complex the amount of calcium and magnesium was calculated as 0.09 mol/lt, however, a higher concentration was required to have an excess of EDTA thus favour the reaction (5-5). EDTA has been used as a chelating agent for divalent ions during water flooding (Mahmoud and Abdelgawad, 2015).

According to the results obtained all alkalis were compatible with SB in the range of salinity 0-5.7% TDS. It was also evidenced that strong alkalis such as NaOH, $NH_4$ in HB form insoluble precipitation by reaction with divalent cations magnesium and calcium.

EDTA can form a complex structure with divalent ions but requires the use of alkali. The combination of solutions EDTA/NaOH at 8 ≤ pH ≤9, shows clear and stable solutions in HB without hydroxide precipitation.

NaOH in excess promotes the formation of insoluble hydroxide precipitation with divalent cations. Therefore, it is important to control the pH of EDTA/NaOH to favour the formation of complexing compounds of EDTA and divalent cations.

Sodium metaborate and EDTA can be used for alkali applications with HB. However, the optimal concentration should be evaluated to determine the maximal concentration for stable solutions.

EDTA and sodium metaborate $NaBO_2$ in HB are very sensitive to the concentration of divalent cations, at pH >11 and high salinity precipitation occurs resulting in instability.

An excess of EDTA based on the concentration of divalent cations is required to favour the formation of divalent complexes with EDTA and avoid hydroxide precipitation.

### 5.3.2 Surfactant and alkali interactions in brine with oil

#### 5.3.2.1 Interfacial tension of surfactants-brine-oil system

Results from the semi-qualitative IFT test using the pendant drop method for surfactant showed that only solutions with surfactants type alcohol-propoxy sulphate (APS) can decrease the IFT with oil to ultra-low values. Surfactants $C_{06-10}$-AES, $C_{12-18}$-MES, $C_{20-24}$-IOS, and $C_{15-18}$-

IOS developed a drop with the pendant drop test that changes its shape with salinity. Results from the pendant drop method are showed in table 5-8.

As only surfactants type APS developed ultra-low IFT, they were considered as principal surfactants for CEOR under the studied conditions. The values of IFT for surfactants that develop a drop, thus $C_{06-10}$-AES, $C_{12-18}$-MES, $C_{20-24}$-IOS, and $C_{15-18}$-IOS were calculated at different salinity in SB and HB, based on the pendant drop method and drop size analysis (Figures 5-11 to 5-14). As those surfactants did not show indications of ultra-low IFT there were considered as secondary surfactants for CEOR under the conditions used for this study.

**Table 5-8: Results from surfactant screening of IFT using qualitative pendant drop method**

| Surfactant Name | IFT screening test |
|---|---|
| $C_{20-24}$-IOS | Drop |
| $C_{15-18}$-IOS | Drop |
| $C_{12-18}$-MES | Drop |
| $C_{12-15}$-7EO | Drop |
| $C_{06-10}$-AES | Drop |
| $C_{12-14}$-AES | Drop |
| $C_{16-17}$-13APS | Flow (Low IFT) |
| $C_{16-17}$-7APS | Flow (Low IFT) |
| $C_{13-14}$—7APS | Flow (Low IFT) |

IFT results for $C_{06-10}$-AES and $C_{12-18}$-MES, $C_{20-24}$-IOS and $C_{15-18}$-IOS show that the IFT decreases as salinity increases (Figures 5-11 to 5-14). Also, by comparison of the behaviour of surfactants according to their hydrophilic and hydrophobic similarities, it was noticed that for surfactants with different hydrophobicity, and common hydrophilic groups, such as $C_{06-10}$-AES and $C_{12-18}$-MES, the surfactant $C_{12-18}$-MES has lower IFT at higher salinity and the IFT is lower for SB than for HB. These two surfactants have in common the group ethoxy sulfate ES, different hydrophobic grade and an alcohol group for AES, (Figures 5-11 and 5-12). IFT for $C_{12-18}$-MES is more affected by divalent cations than $C_{06-10}$-AES, however, IFT is lower for $C_{12-18}$-MES.

IFT results for surfactants IOS show higher IFT values in HB than in SB (Figures 5-13 and 5-14), thus IFT is affected by divalent cations. The hydrophobicity affects the IFT of surfactants

IOS, with higher values for $C_{20-24}$-IOS than for $C_{15-18}$-IOS surfactant (Figures 5-17 and 5-18). However, $C_{15-18}$-IOS surfactant is unstable on HB at salinity higher than 1%.

From these results, main surfactants and secondary or co-surfactants can be selected for further tests. It was also possible to compare similar type of surfactants and understand the effect of the hydrophilic and hydrophobic groups existing in the surfactants and their behaviour under salinity. Although $C_{06-10}$-AES, $C_{12-18}$-MES, $C_{20-24}$-IOS, and $C_{15-18}$-IOS surfactants solutions in brine were stable, they did not reduce the IFT to ultra-low values in the system oil-brine.

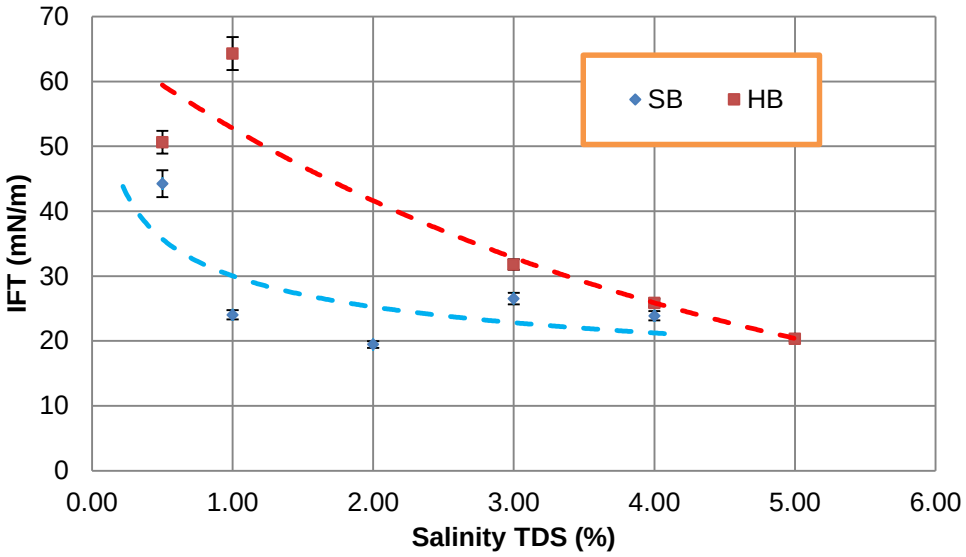


**Figure 5-11: Effect of salinity on IFT oil/brine for surfactant $C_{06-10}$-AES 0.15%**

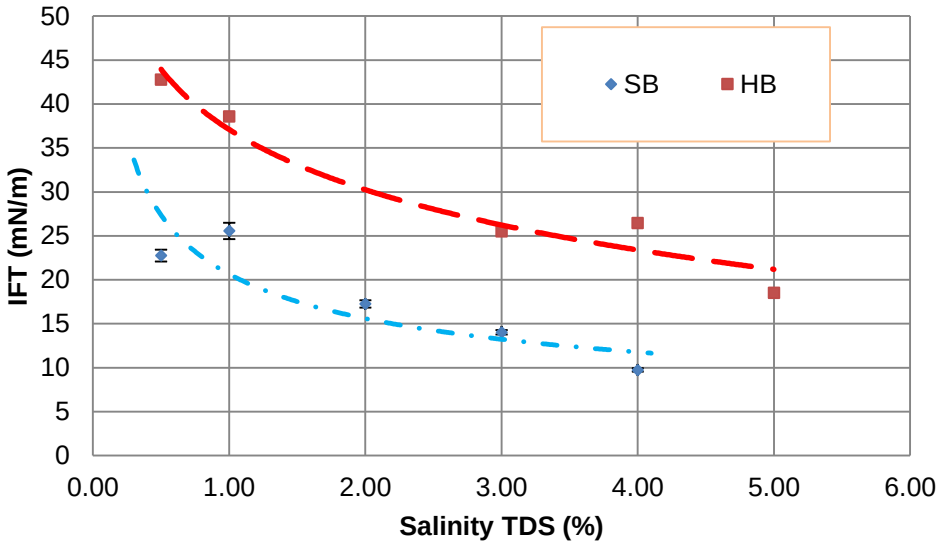


**Figure 5-12: Effect of salinity on IFT oil/brine for surfactant $C_{12-18}$-MES 0.1%**

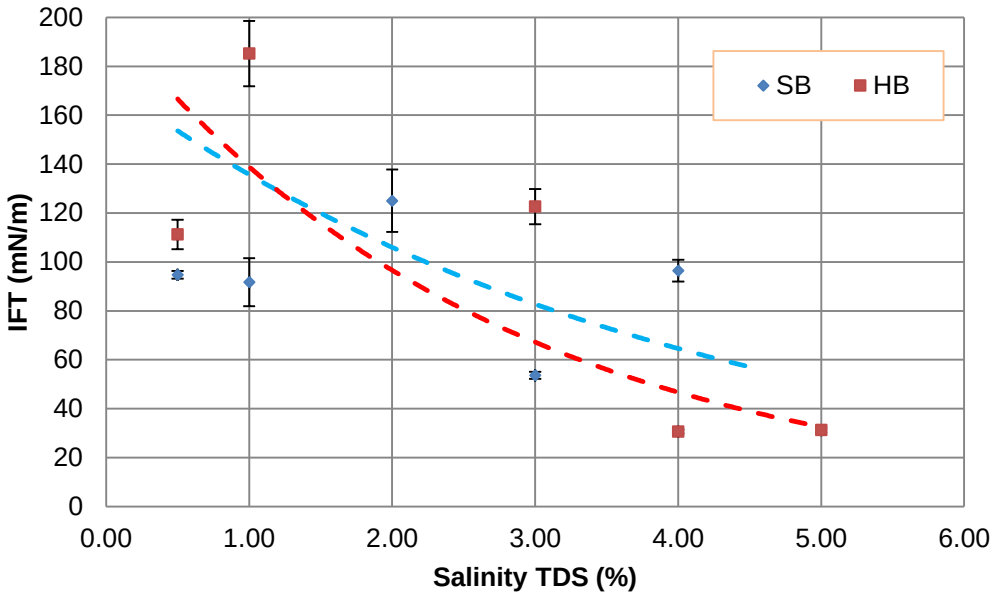


Figure 5-13: Effect of salinity on IFT oil/brine for surfactant $C_{20-24}$-IOS 0.1%

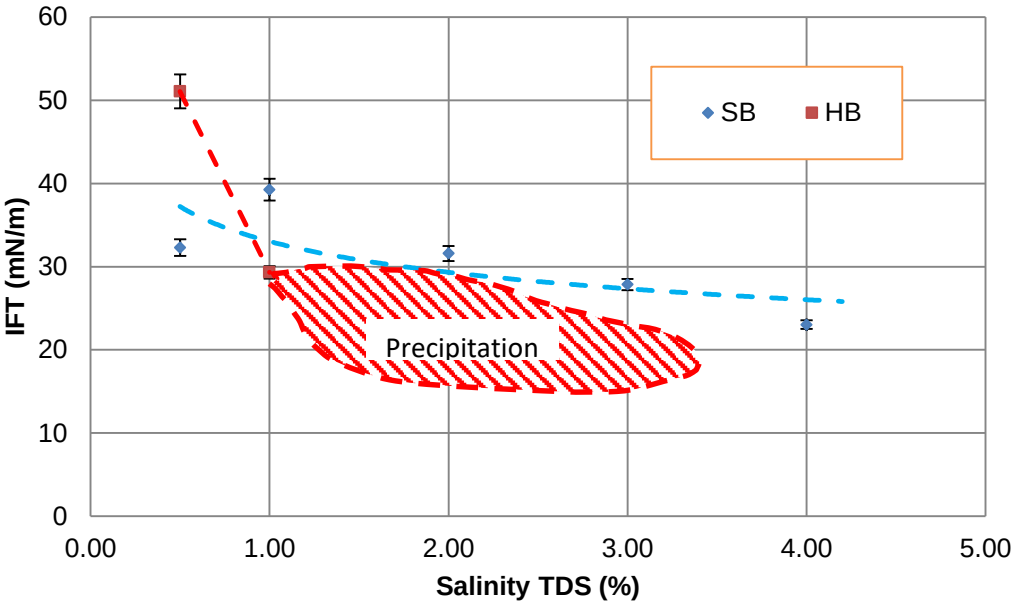


Figure 5-14: Effect of salinity on IFT oil/brine for surfactant $C_{15-18}$-IOS 0.1%

From the results discussed above, it can be appreciated the effect of the oil on the behaviour of surfactants in the system (surfactant-brine)-oil. Although AES, MES, and IOS did not show any limitations in solubility with divalent cations and have similar values of IFT in aqueous

solution, they did not achieve ultra-low salinity with oil. The limitation of solubility of $C_{15-18}$-IOS surfactant with divalent ions has changed from 1.7% to 1% TDS.

IFT was also calculated from phase separation tests and results are discussed further in this chapter in section 5-4-3.

#### 5.3.2.2 Interfacial tension alkali-brine-oil

In this section, the study of IFT in alkali-brine-oil systems is presented. IFT results from oil/brine at different salinities, using the semi qualitative pendant drop method IFT test, showed that alkali can decrease the IFT with oil to ultra-low values so that no drop can be formed. There may be some saponification reaction between the acidic compounds in the oil and the alkali developed in the system alkali-brine-oil.

Results of salinity scan of NaOH solutions in SB, EDTA/NaOH solutions in HB and $NaBO_2$ solutions in HB showed that despite all alkali having qualitative ultra-low IFT, no microemulsion was formed (Figure 5-15 to 5-17). Results for aqueous solutions of NaOH with the chelating agent EDTA (Figure 5-16) indicate not precipitation, but not microemulsion formation either.

As discussed earlier, these results demonstrated how the use of the EDTA and sodium metaborate $NaBO_2$ can help to sequester divalent cations $Ca^{2+}$ and $Mg^{2+}$ so that the system can be stable without precipitation.

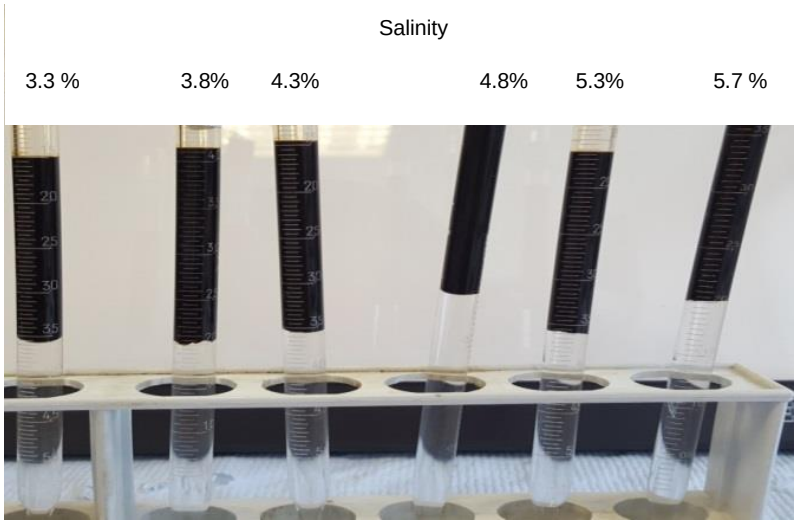


**Figure 5-15: Salinity scan for NaOH solutions in SB with Crude Oil (pH =9) at 140° F**

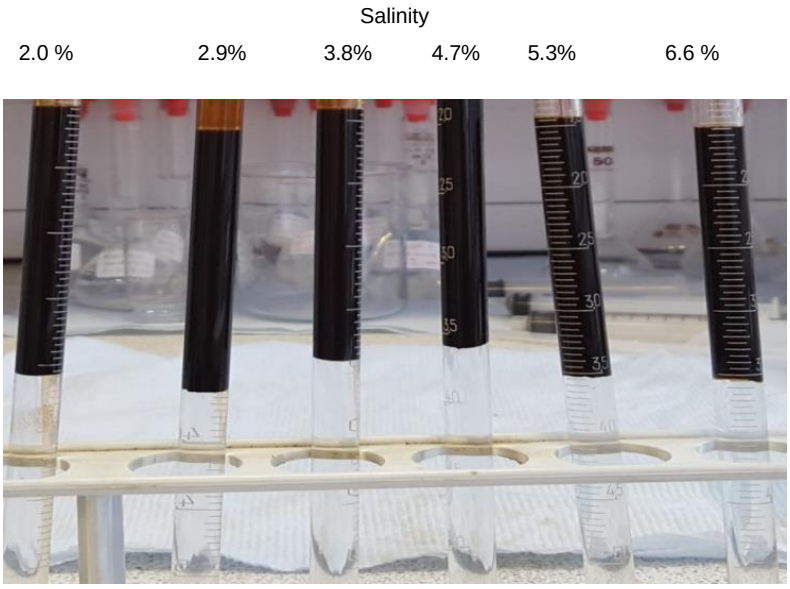


**Figure 5-16: Salinity scan for EDTA/NaOH solutions in HB with Crude Oil (pH=9) at 140º F**

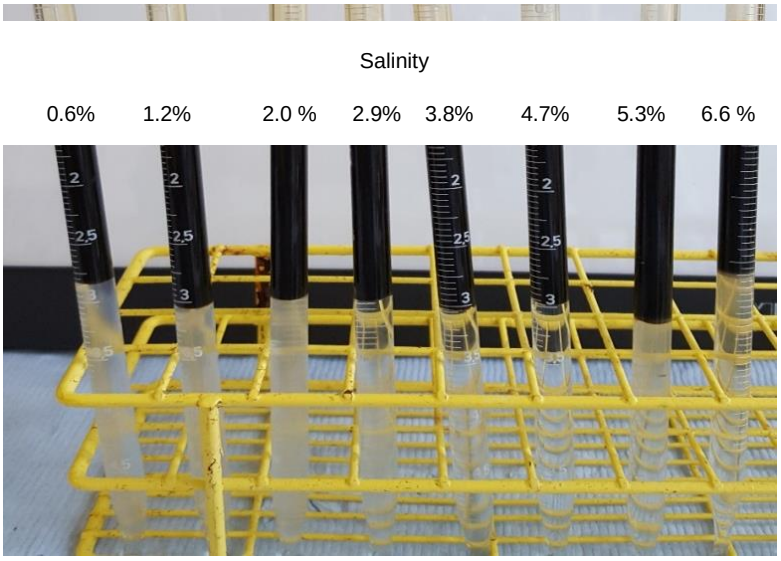


**Figure 5-17: Salinity scan for sodium metaborate solutions in HB with Crude Oil (pH=9) at 140º F**

### 5.3.2.3 Study of microemulsion formation and optimal salinity for CEOR

In this section results from phase separation tests for surfactants are evaluated. Surfactants type APS were tested as primary surfactants. Interactions between surfactant and co-surfactants, and between surfactant and alkali were also investigated. The secondary surfactants used for the tests were $C_{12\text{-}15}$-7EO and AES $C_{06\text{-}10}$-AES. $NaBO_2$ and EDTA/NaOH were the alkalis used.

#### 5.3.2.3.1 Surfactant solubility and optimal salinity for microemulsion formation

In Figure 5-18 results of phase separation or pipette test for three surfactants type APS, (from left to right $C_{13-14}$-7APS, $C_{16-17}$-7APS, and $C_{13-17}$-13APS) are presented. The salinity increases from left to right on the three sequences of pipettes.

For the surfactant $C_{13-14}$-7APS, the visual inspection of the system showed that from the second pipette from left to right, there is a clear initiation of the formation of a microemulsion at the interface. At low salinity, the oil starts taking volumetric space into the brine and this effect is developed further as the salinity increases (third pipette). It can be noticed that the emulsion starts on the aqueous phase and as the salinity increases, it moves toward the oil phase. This effect was initially described by Salager (1993) as the typical behaviour of anionic surfactants containing alcohol functional groups. When the surfactant solution is put in contact with the oil, the solubilisation occurs on the lipophilic part of the micelles, therefore the oil solution swells up into the aqueous solution and a microemulsion is created. These structures can solubilize high amounts of oil. As the salinity increases, the surfactant will be more comfortable at the oil phase as showed on sixth pipette.

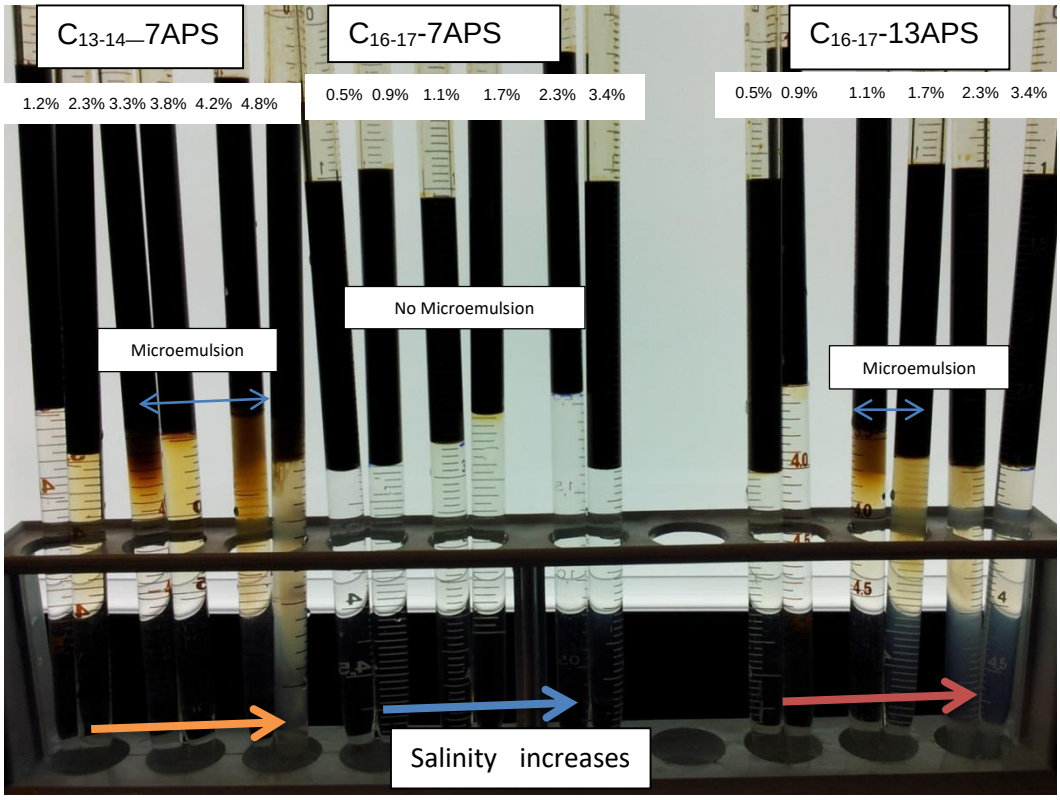


**Figure 5-18: Microemulsion formation for surfactants type APS in HB at different salinity and 140º F**

Results for the surfactant $C_{16-17}$ -7APS (middle set of 6 pipettes), did not show any indication of microemulsion, it can be inferred that in this case the surfactant is solubilized in the oil phase because the hydrophobic chain is longer ($C_{16-17}$) compared with the surfactant $C_{13-14}$— 7APS. However, with an increase in the number of functional hydrophilic groups APS from 7 to 13 as comparing surfactants $C_{16-17}$ -7APS and $C_{16-17}$-13APS, the surfactant becomes more hydrophilic and move forward to the interface oil/water and forms the microemulsion at a lower salinity than the surfactant $C_{16-17}$ -7APS.

Solubilisation ratio and relative phase volume for the different zones of phases $II^{(-)}$ (oil/water), III and $II^{(+)}$ (water/oil) were calculated with data obtained from the phase separation tests, according to the Huh method (1979), results are presented in the graphs in Figures 5-19 and 5-20. The values of solubilisation ratio are referred to ratio Vo/Vs and Vw/Vs where Vo, Vs, and Vw are the volume of oil, surfactant and brine in the microemulsion obtained from the phase separation test (or pipette test).

For the calculations of solubilisation ratio, it was assumed that all the surfactant was part of the microemulsion when this is formed. The relevance of this analysis is that allows the identification of salinity for the minimal interfacial tension (optimal salinity) and the zone of the salinity for microemulsion formation. For example, in the case presented in Figures 5-19 and 5-20, the zone of salinity for microemulsion formation is from the salinity of 2.0% to about 5.0% and the optimal salinity, where the solubility of oil Vo and brine Vw in the surfactant in the microemulsion Vs are equal, is located at 3.9%. The graph in Figure 5-20 represents first a zone identified as $II^{(-)}$ which means the surfactant is in the aqueous phase oil/water emulsion type and there is an excess of the aqueous solution. In this salinity region, the surfactant is oriented with the hydrophilic part phasing the aqueous solution and the hydrophobic part can have some drops of oil. As the salinity increases toward the optimal salinity, a middle phase microemulsion is spontaneously formed and is identified as zone III, this zone is characterized by a new structure formed by the two phases due to the modifications of interfacial strength between the oil drops emulsified in water and the surfactant, which makes possible to generate a three-phase microemulsion region (Dehghan, Masihi and Ayatollahi, 2015).

The optimal salinity is determined by a graphic method with volumes measured from experimental phase separation tests. The method depends on the ability to find the zone of microemulsion by evaluating pipette tests at different salinities keeping the ratio of oil to brine constant. Only for surfactant mixtures that form good microemulsions, the IFT can be calculated. Huh method (1979) is extensively used for surfactant selection as it is simple to use and many samples can be tested at the same time (Pope, 2011).

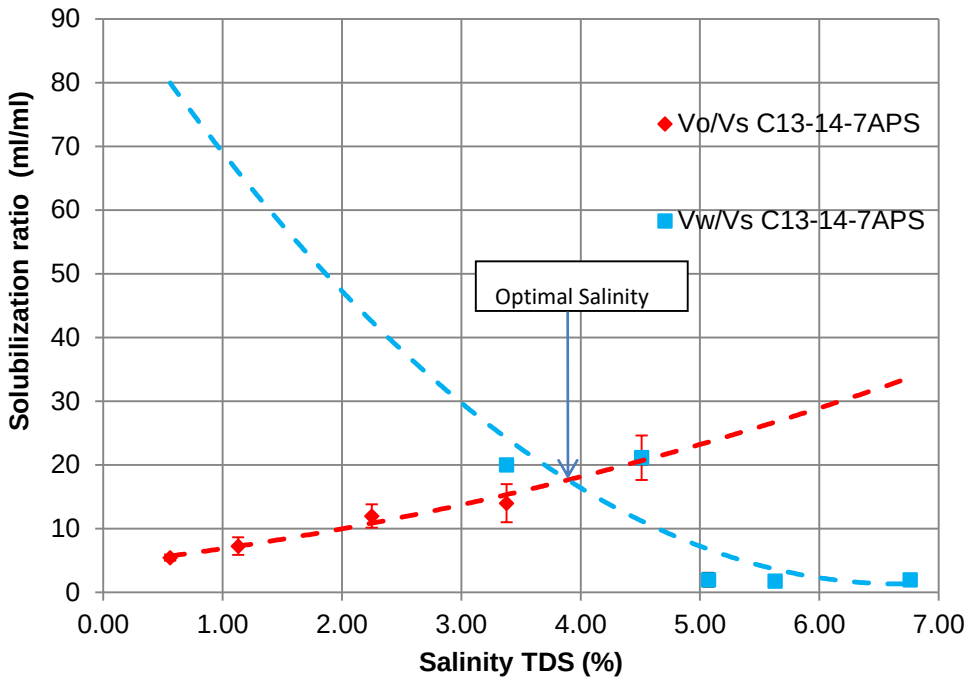


**Figure 5-19: Solubilisation ratio versus salinity for 0.2% surfactant C13-14—7APS in HB at 140º F (Optimal Salinity=3.9%)**

The effect of the surfactant structure for surfactants APS with a different number of APS hydrophilic groups and different hydrophobic chain length on the optimal salinity can be evaluated in Figures 5-19 and 5-21. $C_{13-14}$—7APS has higher optimal salinity (3.9% TDS) than $C_{16-17}$-13APS (1.5% TDS). The microemulsion formation estimated by solubility ratio for surfactant $C_{16-17}$-13APS occurs at a lower window of salinity zone III (1-2% TDS) (Figure 5-22) whereas for $C_{13-14}$—7APS occurs at a higher salinity and a wider range (2-5% TDS, Figure 5-24).

The solubilisation ratio (or volume of oil and water in the microemulsion) at the optimal salinity is higher for the surfactant $C_{13-14}$—7APS than for $C_{16-17}$-13APS. Similar results were reported by Hirasaki et al. (2008); they found that the increase in the number of propoxylated groups (APS) in a surfactant decreases the optimal salinity to form the three-phase microemulsion. This result demonstrates the length of the hydrophobic chain affects optimal salinity.

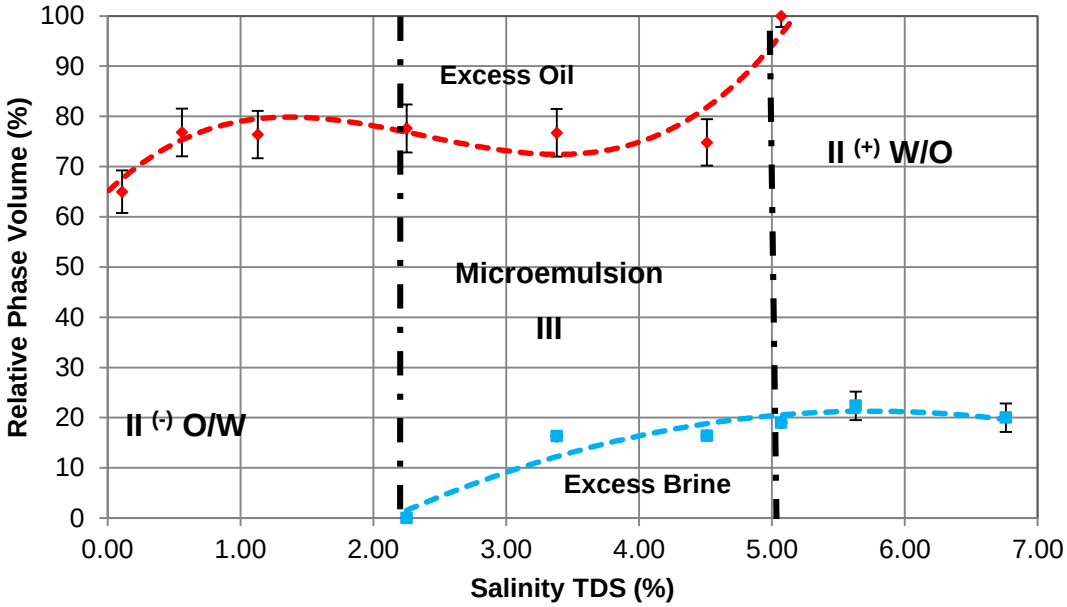


Figure 5-20: Relative phase volume versus salinity for 0.2% surfactant C13-14—7APS HB at 140° F (Salinity range 2.0% to 5.0%)

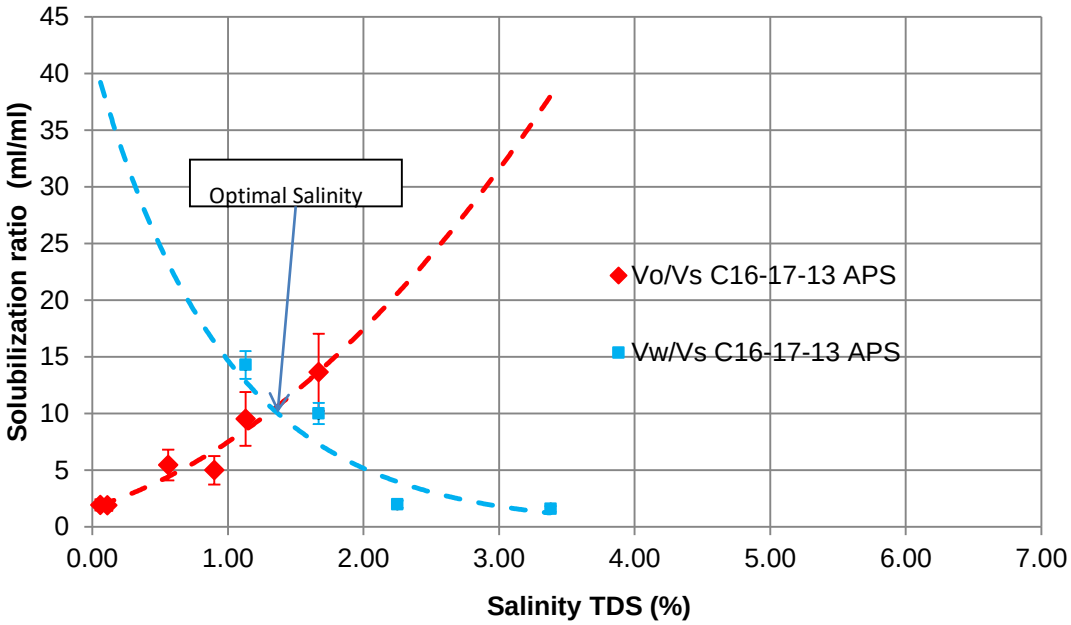


Figure 5-21: Solubilisation ratio versus salinity for 0.2% surfactant C16-17-13APS HB at 140° F (Optimal Salinity= 1.4%)

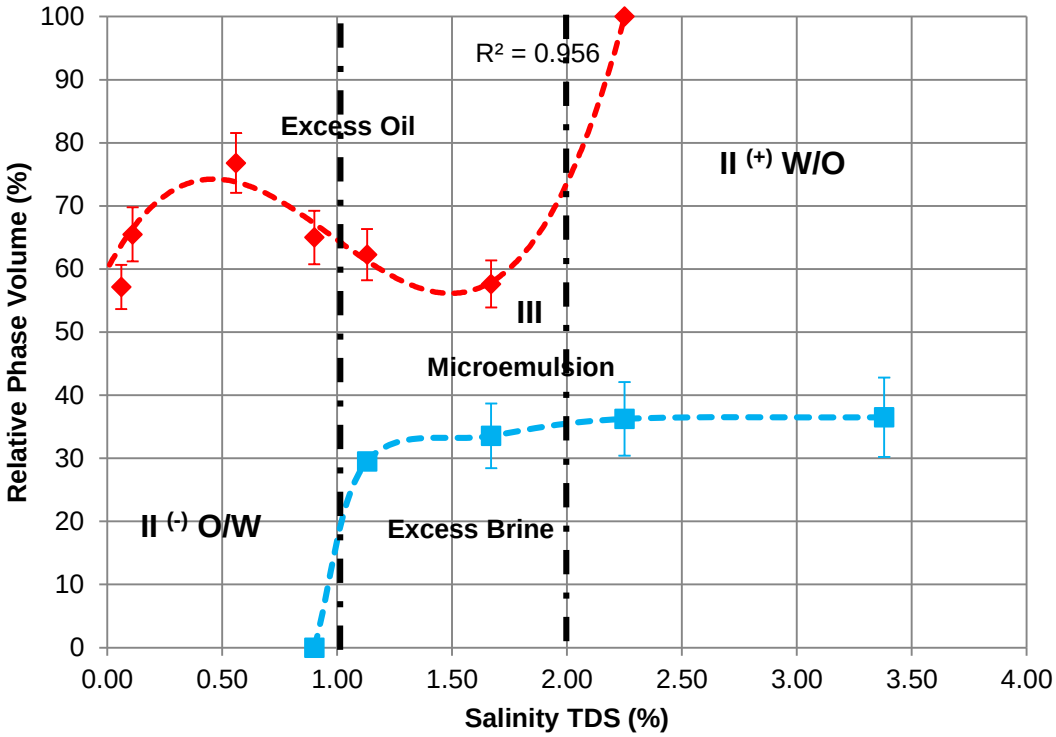


**Figure 5-22: Relative phase volume versus salinity for 0.2% surfactant C16-17-13APS HB at 140° F (Salinity range 1.0% to 2.0%)**

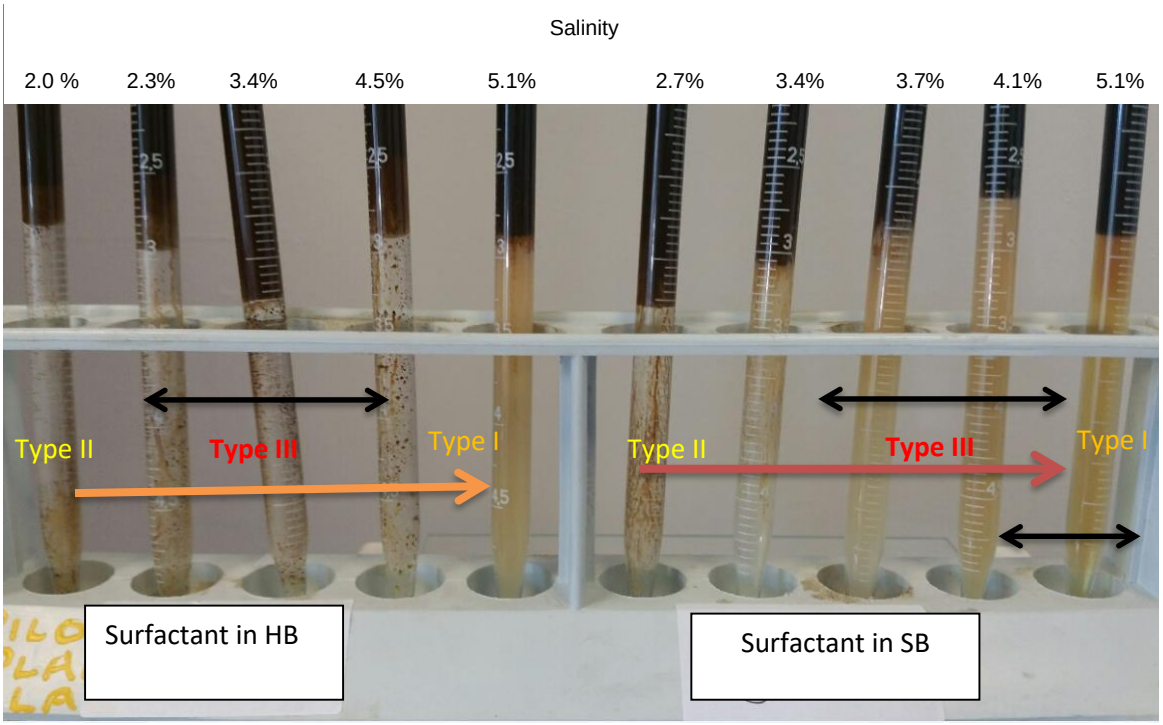


**Figure 5-23: Effect of brine composition on the microemulsion formation for surfactants C13-14—7APS at 140° F**

The presence of divalent ions in the HB reduces the optimal salinity for microemulsion formation of surfactant $C_{13-14}$—7APS as is demonstrated in figure 5-23 and by comparing Figures 5-24 (SB) and 5-19 (HB). The optimal salinity in HB is lower (3.9%) than in SB (4.2%). This effect can be due to the reduction of the solubility of the surfactant in HB due to the presence of divalent cations.

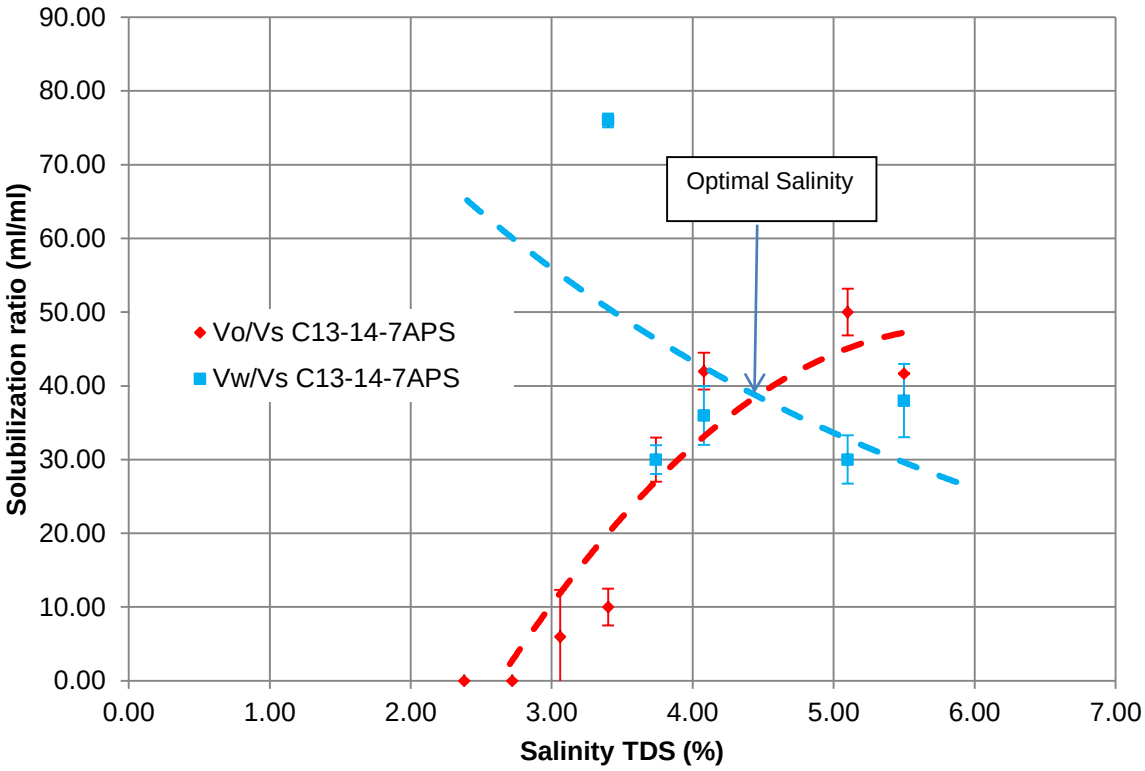


**Figure 5-24: Effect of salinity on the solubilisation ratio for 0.2% surfactant C13-14—7APS 0.3% in SB at 140º F (Optimal Salinity= 4.2 %)**

By comparison of the relative phase volume versus salinity for surfactants $C_{13-14}$—7APS in HB and SB (Figures 5-20 and 5-25 respectively), it seems the range of salinity with microemulsion formation is wider for surfactant in SB (2-5.3%) than for HB (2-5%). This difference is relevant to plan the formulation of the chemical slug, the injection and the salinity pattern for CEOR processes.

From these results, it was learned that the surfactant $C_{13-14}$—7APS has the best performance in HB and tolerate high salinity, close to the case used for this study (North Sea Reservoir

Gryphon Oilfield), therefore this surfactant was chosen as the main surfactant for further tests. Moreover, relevant aspects related to the selection of surfactants were discussed, such as solubilisation ratio, relative phase volume, and range of microemulsion for the required low IFT for CEOR processes.

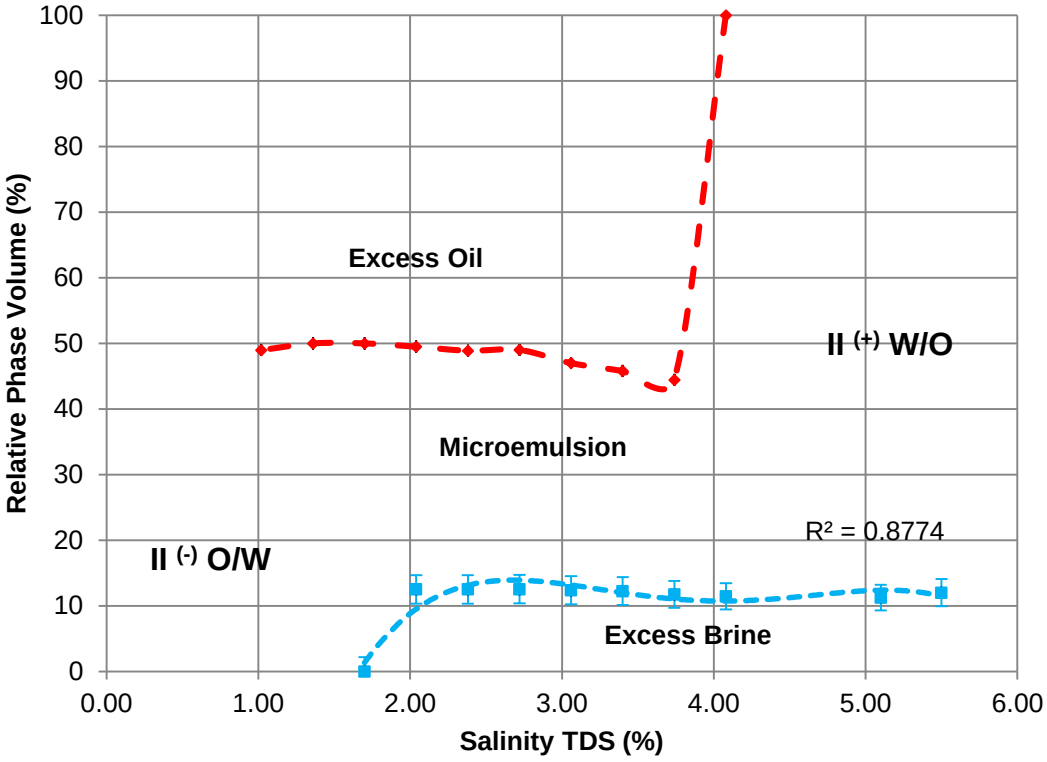


**Figure 5-25: Relative phase volume versus salinity for 0.2% surfactant $C_{13-14}$—7APS for SB at 140º F (Salinity range 2.0% to 5.3%)**

For applications of surfactants APS with brines with divalent cations, it is important to find the best balance between the number of APS groups and hydrophobic hydrocarbon chain as both have an important effect on the optimal salinity. Some important results can be summarized as follow:

- The increase in the number of APS groups reduces the solubility of surfactants in brine and the optimal salinity for microemulsion formation.
- The higher the hydrophobicity of APS surfactant, the lower the optimal salinity.
- The solubility ratio of the surfactant at the optimal salinity is higher for the most hydrophilic surfactant.

- Divalent cations reduce the optimal salinity and the salinity window for zone III microemulsion.

#### 5.3.2.3.2 Effect of interactions between blends of surfactants

In this section, the effect of blending surfactants on the formation of microemulsion in the system brine/oil, optimal salinity and interfacial tension is studied. For this purpose, two of the surfactants tested in the previous section were selected as co-surfactants to be mixes with $C_{13-14}$—7APS. Ethoxylate alcohol $C_{12-15}$-7EO, and alcohol ethoxy sulfate $C_{06-10}$-AES were used for this study (Figures 5-26 and 5-29).

Comparing the solubilized ratio curves, relative phase volume and the region for microemulsion formation and optimal salinity graphs presented in Figures 5-27 and 5-30, it can be noticed that the solubilisation ratio curves are more complex than the one obtained for a single surfactant (for example comparing with Figure 5-19). Therefore, the data points were difficult to fit with a correlation to find the optimal salinity for the system. The range of salinity for microemulsion formation is presented in figure 5-28.

Results for the system $C_{13-14}$—7APS + $C_{12-15}$-7EO on HB showed the solubilisation ratio at the optimal salinity is higher than for $C_{13-14}$—7APS alone which indicates ultra-low IFT (Figure 5-27). However, the optimal salinity (3.3% TDS) is lower than the optimal salinity obtained for $C_{13-14}$—7APS alone.

A source of error for the determination of the optimal salinity considering the trend of the solubilisation ratio may exist due to the high dispersion on experimental points. However, with a visual inspection of results the three-phase III zones of microemulsion formation were identified, one at low salinity (1.2-2.1% TDS), another at 3% TDS and another at 4.2% TDS. The salinity window for microemulsion formation for the mix $C_{13-14}$—7APS + $C_{12-15}$-7EO is (2 to 4% TDS) which is lower compared with (2 to 5% TDS) obtained for $C_{13-14}$—7APS alone (Figures 5-28 and 5-20)

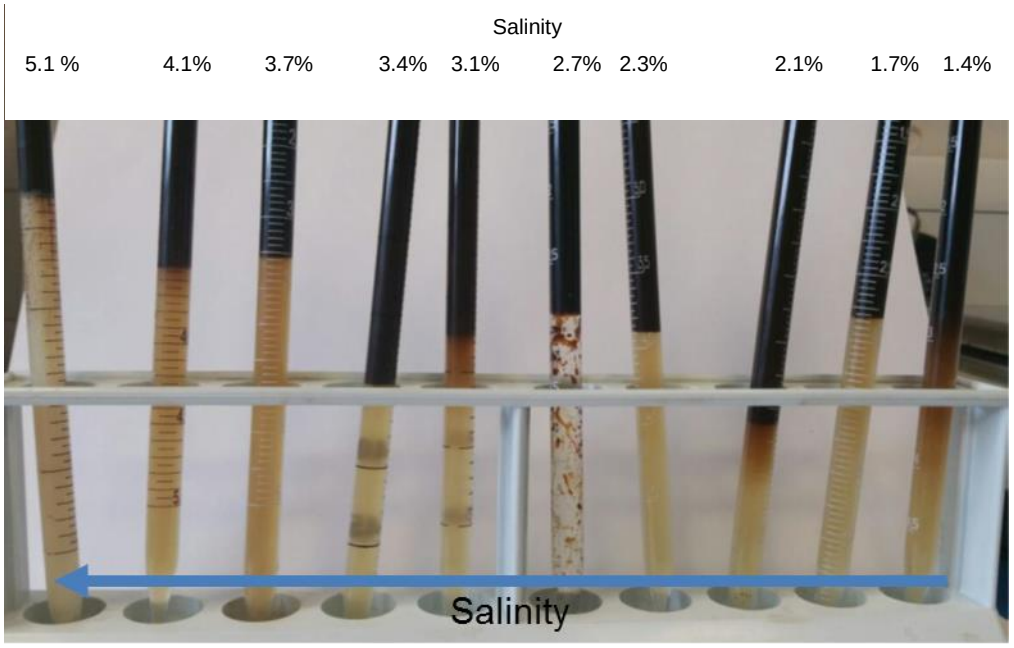


**Figure 5-26: Phase separation test for surfactants (C13-14—7APS + C12-15-7EO) at 140 °F**

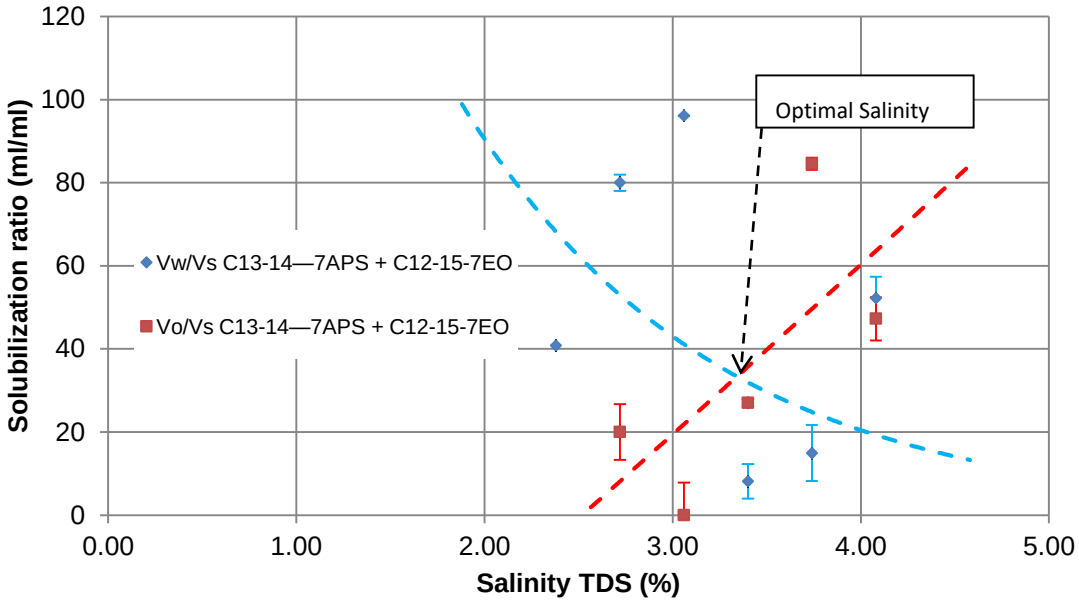


**Figure 5-27: Solubilisation ratio versus salinity for 1:1 blend of surfactants ($C_{13\text{-}14}$-7APS + $C_{12\text{-}15}$-7EO) at 140 °F (Optimal Salinity= 3.3%)**

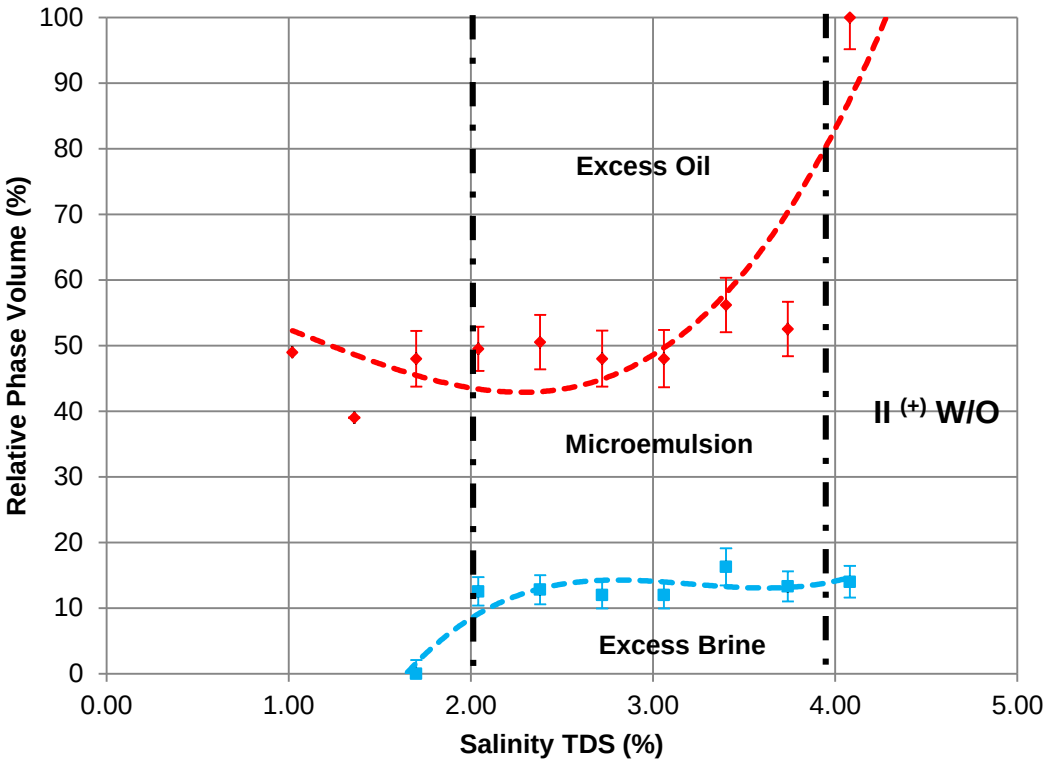


**Figure 5-28: Relative phase volume versus salinity for 1:1 blend of surfactants ($C_{13-14}$—7APS + $C_{12-15}$-7EO) at 140 °F (Salinity range 2.0% to 4.0%)**

Similarly, results for phase separation tests, solubilized ratio and relative phase volume for the combination of surfactants $C_{13-14}$—7APS + $C_{06-10}$-AES are presented in Figures 5-29 to 5-31. At low salinity, the emulsion of oil in water is predominant and gets reduced as the salinity increases up to 3.5% TDS where the surfactant is equally distributed between the oil and the brine (optimal salinity). The range of salinity for microemulsion formation for this blend of surfactants (3.4-5.2% TDS), which is lower than (2-5% TDS) obtained for $C_{13-14}$—7APS alone (Figures 5-31 and 5-20). Table 5-9 summarizes the main results obtained from phase separation tests.

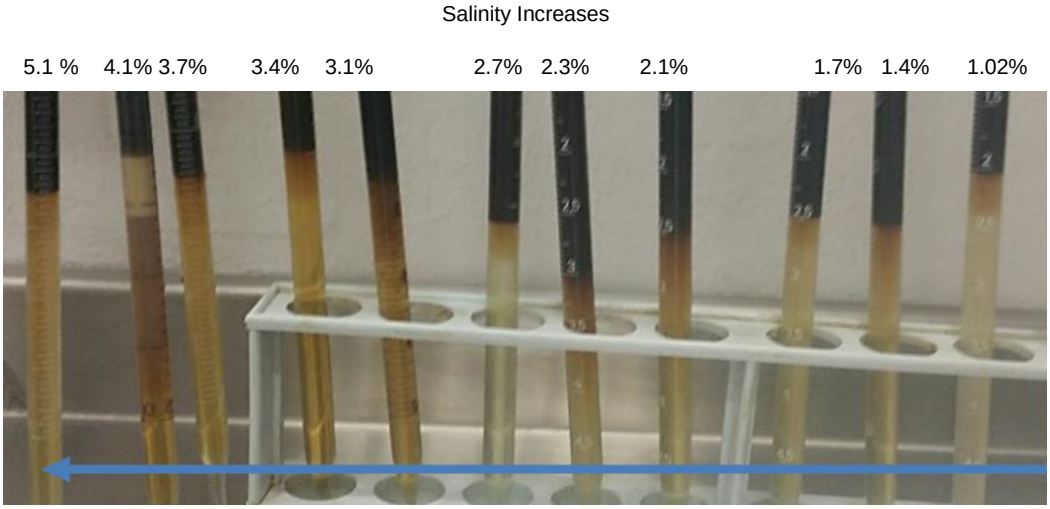


**Figure 5-29: Phase separation test for surfactants ($C_{13-14}$—7APS + $C_{06-10}$-AES) at 140 °F**

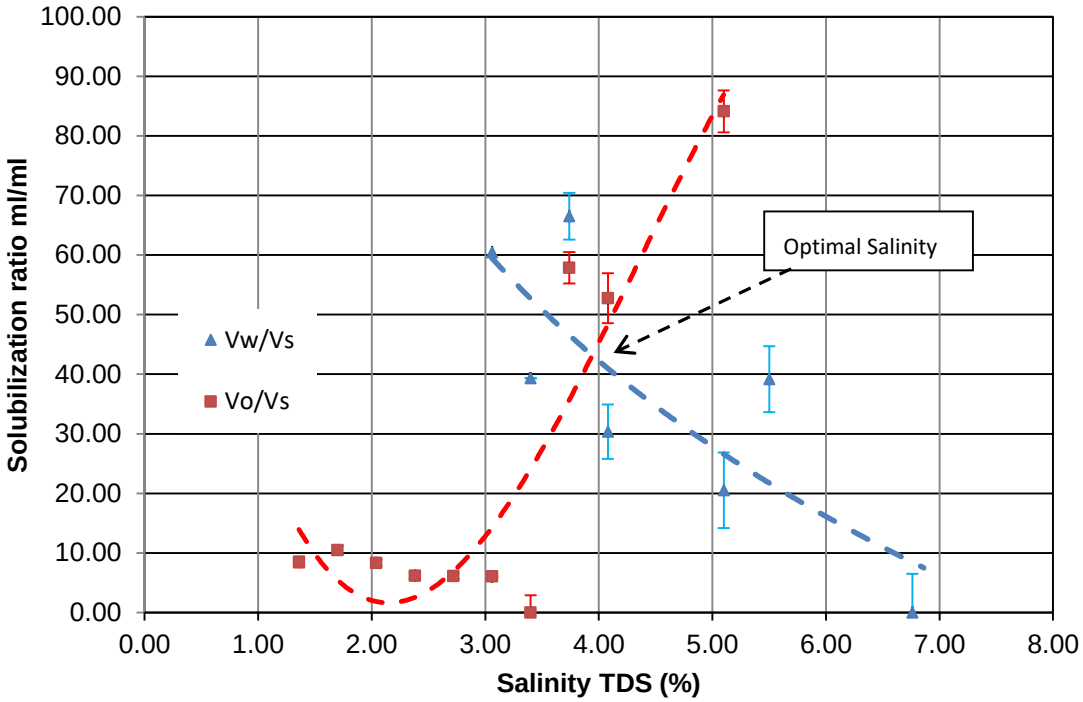


**Figure 5-30: Solubilisation ratio versus salinity for 1:1 blend of surfactants ($C_{13-14}$—7APS + $C_{06-10}$-AES) at 140 °F (Optimal Salinity= 3.75 %)**

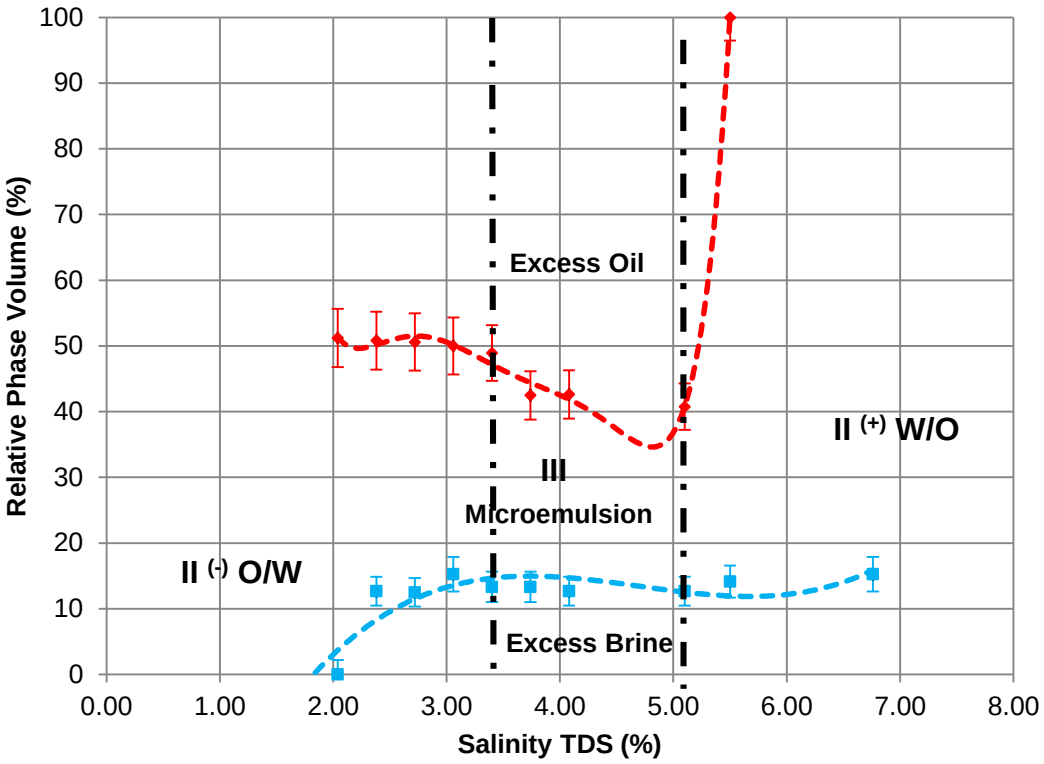


**Figure 5-31: Relative phase volume versus salinity for 1:1 blend of surfactants ($C_{13-14}$—7APS + $C_{06-10}$-AES) at 140 °F (Salinity range 3.4% to 5.2%)**

**Table 5-9: Summary of results from phase separation tests for 0.2% surfactants systems at temperature conditions (140 °F) and in SB and HB**

| System oil/brine | Optimal Salinity (%) TDS | Range of salinity (%) | Minimal IFT (mN/m) |
|---|---|---|---|
| $C_{13-14}$—7APS-HB | 3.9 | 2.8 to 4.8 | $9.26 \times 10^{-4}$ |
| $C_{13-14}$—7APS-SB | 4.4 | 2.0 to 5.3 | $2.078 \times 10^{-4}$ |
| $C_{16-17}$-13APS-HB | 1.4 | 1.1 to 2.0 | $20.8 \times 10^{-4}$ |
| $C_{16-17}$-13APS-SB | 4.8 | 3.5 to 5.2 | $9.01 \times 10^{-4}$ |
| $C_{16-17}$-7APS-HB | NA | ---- | ---------- |
| $C_{13-14}$—7APS + $C_{12-15}$-7EO-HB (Blend 1:1) | 3.3 | 2.0 to 3.8 | $2.93 \times 10^{-4}$ |
| $C_{13-14}$—7APS + $C_{06-10}$-AES-HB (Blend 1:1) | 3.8 | 3.4 to 5.2 | $1.62 \times 10^{-4}$ |

The optimal salinity and IFT of microemulsion formation for the different surfactants systems evaluated are presented in Figure 5-32 and 5-33.

The optimal salinity is higher for the surfactant $C_{13-14}$—7APS (3.9% TDS) than for the surfactant $C_{16-17}$-13APS (1.4% TDS) in HB, whereas in SB the optimal salinity for surfactant $C_{16-17}$-13APS (4.8%) is higher than for the surfactant $C_{13-14}$—7APS (4.4%).

Divalent cations reduce the salinity window of microemulsion formation for $C_{13-14}$—7APS from (2.0-5.3% TDS) in SB to (2.8-4.8%) in HB. The effect is more evident for $C_{16-17}$-13APS, from (1.1- 2.0% TDS) in HB to (3.5-5.2% TDS).

There is an effect of divalent cations in the optimal salinity which it is seems to be inversely proportional to the number of groups APS, thus the higher the number of APS groups the lower the optimal salinity. The effect of divalent cations on the solubility of the surfactant is more evident for the surfactant with higher APS groups.

These results are an indication of the effect of ionic interactions between divalent cations and propoxy sulfate (polar) groups in the surfactant, which are higher for the surfactant $C_{16-17}$-13APS, and the effect on the resultant optimal salinity. While the optimal salinity in SB for the surfactant $C_{16-17}$-13APS is higher than for the surfactant $C_{13-14}$—7APS, the difference is minor.

Mixes of surfactants $C_{13-14}$—7APS with $C_{12-15}$-7EO and $C_{06-10}$-AES have lower optimal salinity than $C_{13-14}$—7APS alone. Whereas the range of salinity of microemulsion formation for the mix of surfactants $C_{13-14}$—7APS and $C_{06-10}$-AES is moved toward high salinity, from (2.8 to 4.8%TDS) to (3.5 to 5.2%).

The co-surfactant $C_{06-10}$-AES increases the tolerance to salinity of $C_{13-14}$—7APS surfactant, moving the salinity range for microemulsion formation from (2.8 to 4.8%TDS) to (3.5 to 5.2%). This range of salinity is closer to the salinity of the brine available for injection which is very favourable considering the economic aspects of the project. This means no additional treatment of the existing brine (such as desalination, softening) is required.

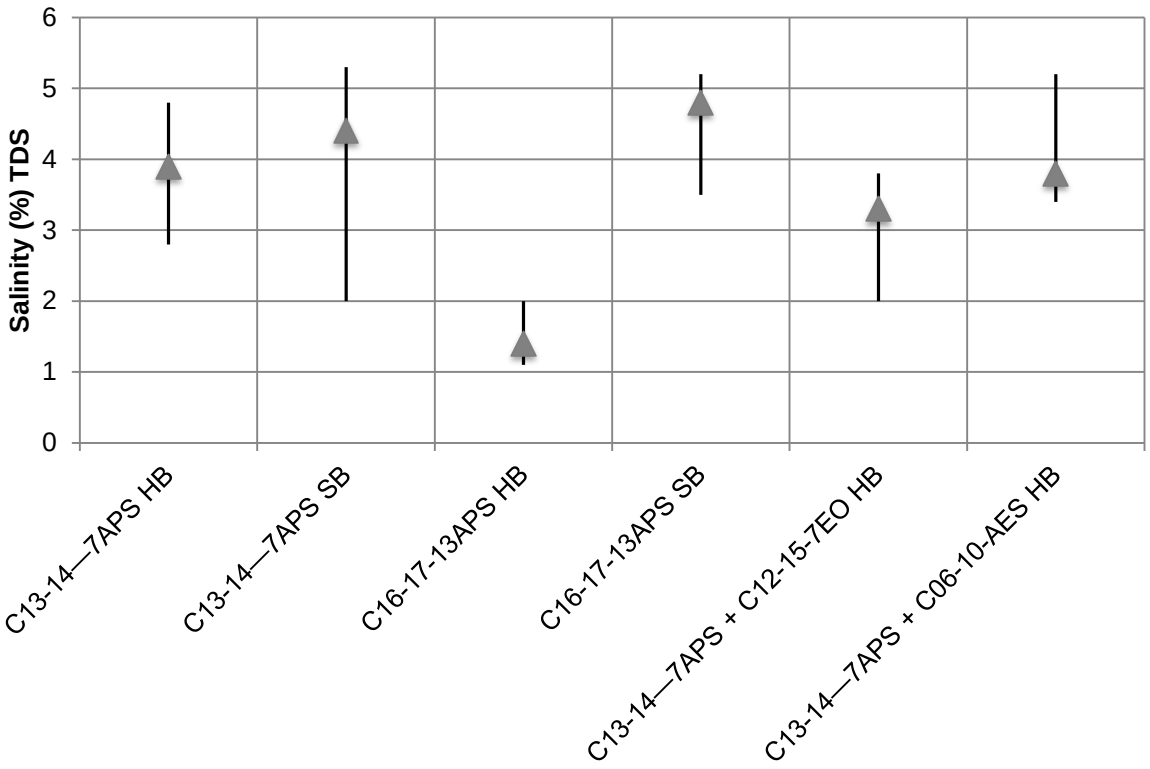


**Figure 5-32: Salinity range of microemulsion formation for surfactants solutions**

*HB: hard brine, SB: soft brine.*

Divalent cations increase the values of IFT at the optimal salinity for both surfactants $C_{16-17}$-13APS and $C_{13-14}$—7APS, and this effect is more marked for surfactant with the large number of group APS, thus $C_{16-17}$-13APS (Figure 5-33).

The addition of co-surfactant reduces the IFT of the microemulsion with a slight reduction on the optimal salinity, especially for results obtained for the co-surfactant $C_{12-15}$-7EO. The co-surfactant $C_{06-10}$-AES also reduces the IFT and move the range of salinity to higher salinities. From those results it was evident that the use of co-surfactant enhances the performance of the main surfactant in terms of its ability to reduce the IFT, keeping a similar range of salinity with minimal values of IFT.

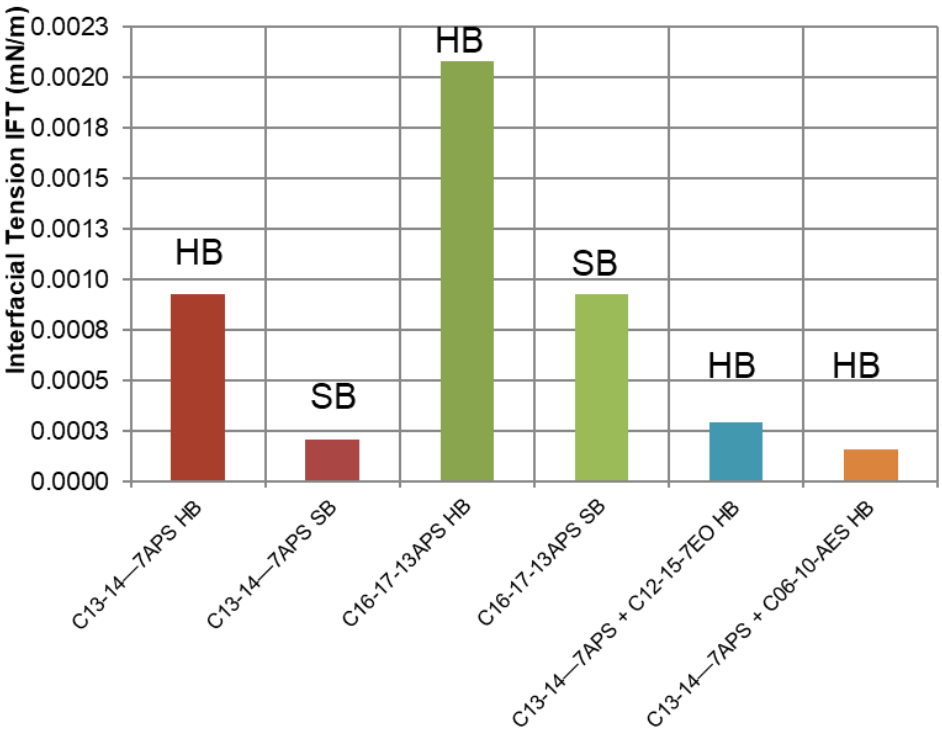


**Figure 5-33: Minimal IFT for microemulsion formation for surfactants solutions**

*HB: hard brine, SB: soft brine.*

From these results It was evidenced that mixing two different surfactants modifies the behaviour of each surfactant alone. Similar advantages from mixing surfactants have been reported (Salager et al., 2005; Hirasaki et al., 2011; Bera and Mandal, 2015). The "lipophilic linking effect" (Salager et al., 2005) can explain the decrease in IFT by co-surfactants $C_{12\text{-}15}$-7EO (Figure 5-34). The surfactant, instead of migrating to the interface oil/brine, helps to organize a thick layer of oil molecules near the interface and increases the oil solubility ratio, thus decreases IFT, like results observed for co-surfactants $C_{12\text{-}15}$-7EO and $C_{06\text{-}10}$-AES.

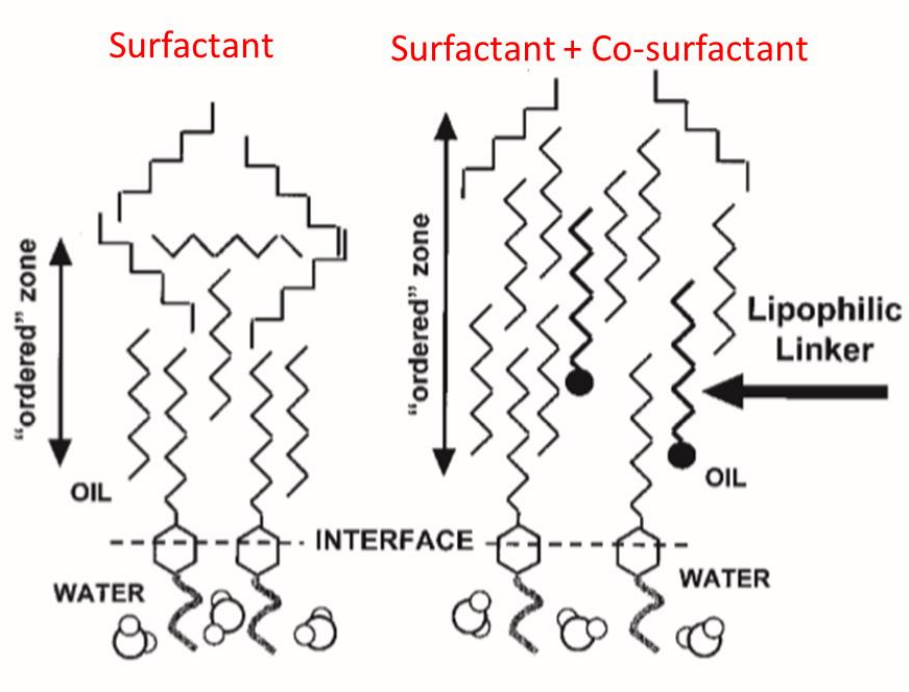


**Figure 5-34: Lipophilic linking behaviour of co-surfactants,**
adapted from Salager et al (2005)

These results demonstrated the complexity of the selection of the surfactant for the design of the chemical slug, and the dependency of the formulation on the brine and oil composition. However, based on the understanding of the characteristics of the surfactant and interactions with brine and oil, surfactant formulations can be tailored for microemulsion formation according to salinity conditions in the reservoir.

#### 5.3.2.3.3 Effect of alkali and salinity on the brine/surfactant /oil system

Results from phase separation tests for the system alkali/surfactant/oil for surfactant $C_{13\text{-}14}$—7APS are presented in this section. The following systems, using $C_{13\text{-}14}$—7APS as a surfactant (0.2%) are discussed:

a. NaOH (0.05M)- SB at 66 ºF (Figure 5-35 to 5-37)
b. NaOH (0.05M) - SB at 140 ºF. (Figure 5-38 to 5-40)
c. $NaBO_2$ (0.02M) -SB at 66 ºF. (Figure 5-41 to 5-43)
d. $NaBO_2$ (0.02M) -HB at 66 ºF. (Figure 5-44 to 5-46)
e. $NaBO_2$ (0.02M) -HB at 140º F. (Figure 5-47 to 5-49)
f. EDTA/NaOH -HB at 66 ºF. (Figure 5-50 to 5-52)
g. EDTA/NaOH -HB at 140ºF. (Figure 5-53 to 5-55)

Results of phase separation for alkalis and surfactants systems are presented in Figures 5-35 to 5-55.

Temperature affects the optimal salinity for microemulsion formation for the different systems. The optimal salinity of the chemical systems $C_{13-14}$—7APS/$NaBO_2$ (see figures for cases (d) and (e)) and $C_{13-14}$—7APS EDTA/NaOH (see figures for cases (f) and (g)) increases with temperature (2.8% to 3.2% TDS) and (3.4% to 3.6% TDS) respectively, whereas, for the $C_{13-14}$—7APS /NaOH the optimal salinity decreases with temperature (4.2% to 3.75% TDS) (see figures for cases (a) and (b)).

Divalent ions affect the optimal salinity of microemulsion formation. While the optimal salinity of $C_{13-14}$—7APS/ $NaBO_2$ increases from 1.5% to 2.8% (Figures 5-45 and 5-48), it decreases from 4.5% to 3.5% for $C_{13-14}$—7APS /NaOH (Figures 5-36 and 5-54).

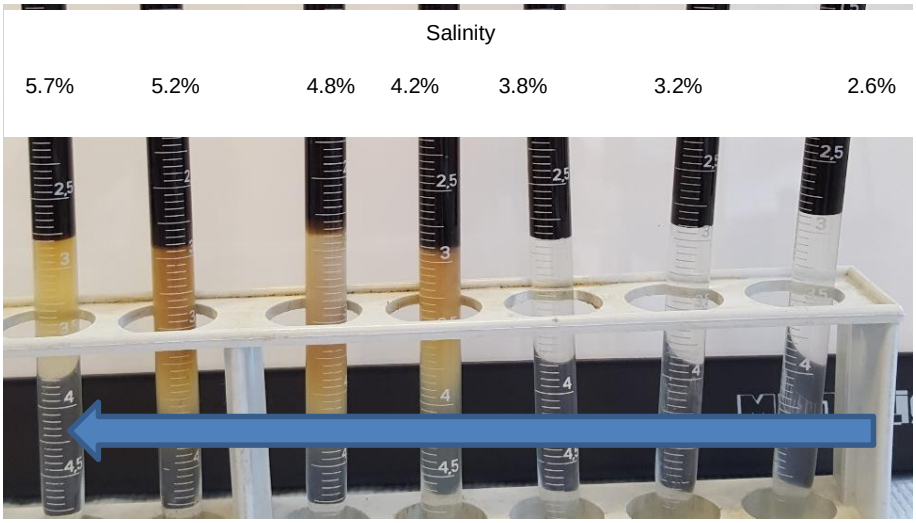


**Figure 5-35: Phase separation of NaOH/$C_{13-14}$—7APS in SB at 66 °F**

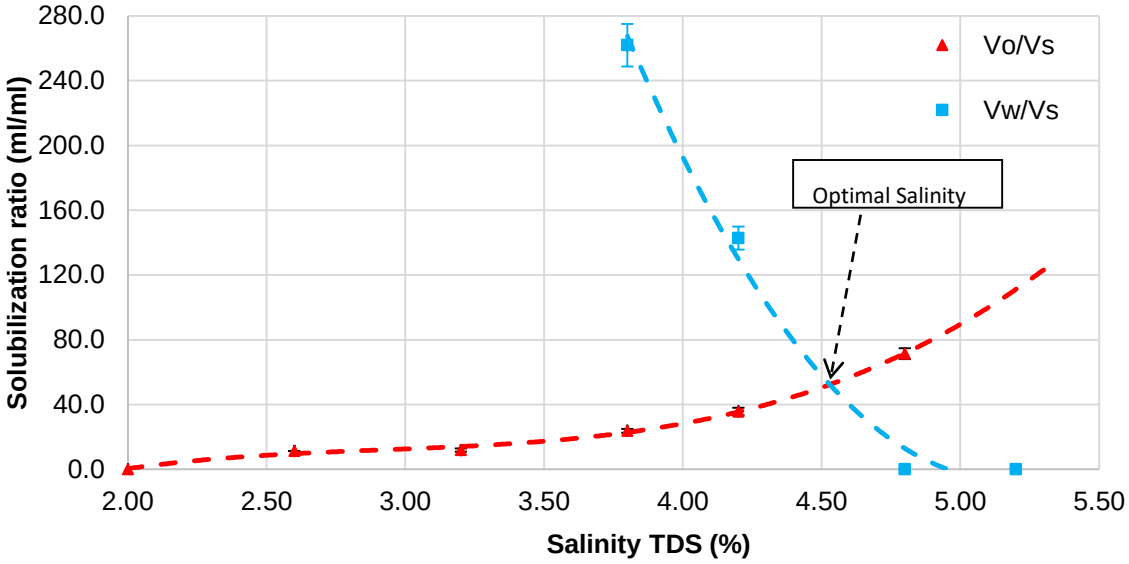


**Figure 5-36: Solubilisation ratio versus salinity of NaOH/$C_{13-14}$—7APS in SB at 66 °F (Optimal Salinity= 4.5%)**

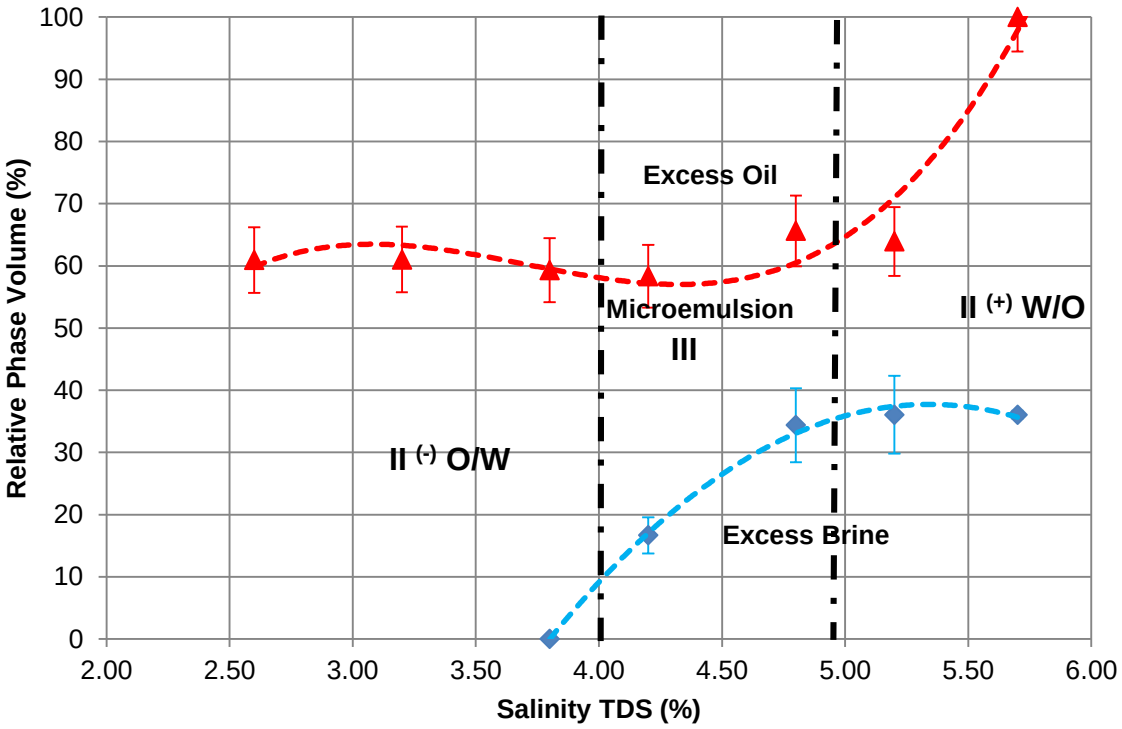


**Figure 5-37: Relative phase volume versus salinity of NaOH/$C_{13-14}$—7APS in SB at 66°F (Salinity range 4.05% to 4.7%)**

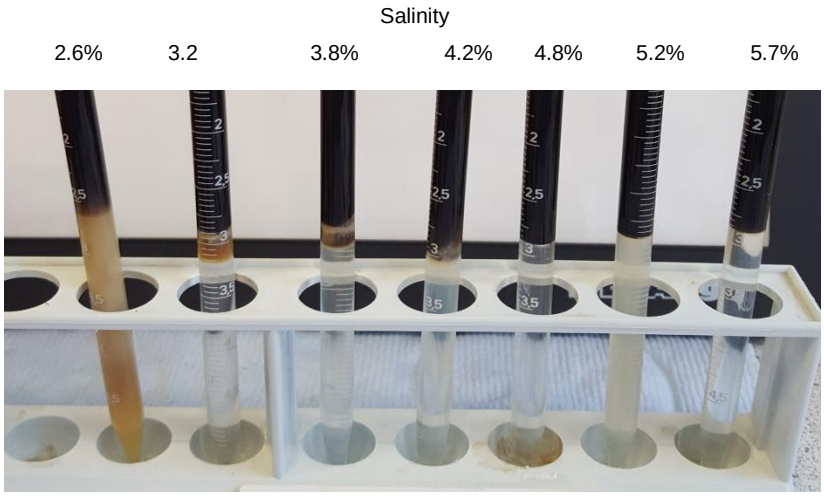


**Figure 5-38: Phase separation of NaOH/$C_{13-14}$—7APS in SB at 140 ºF**

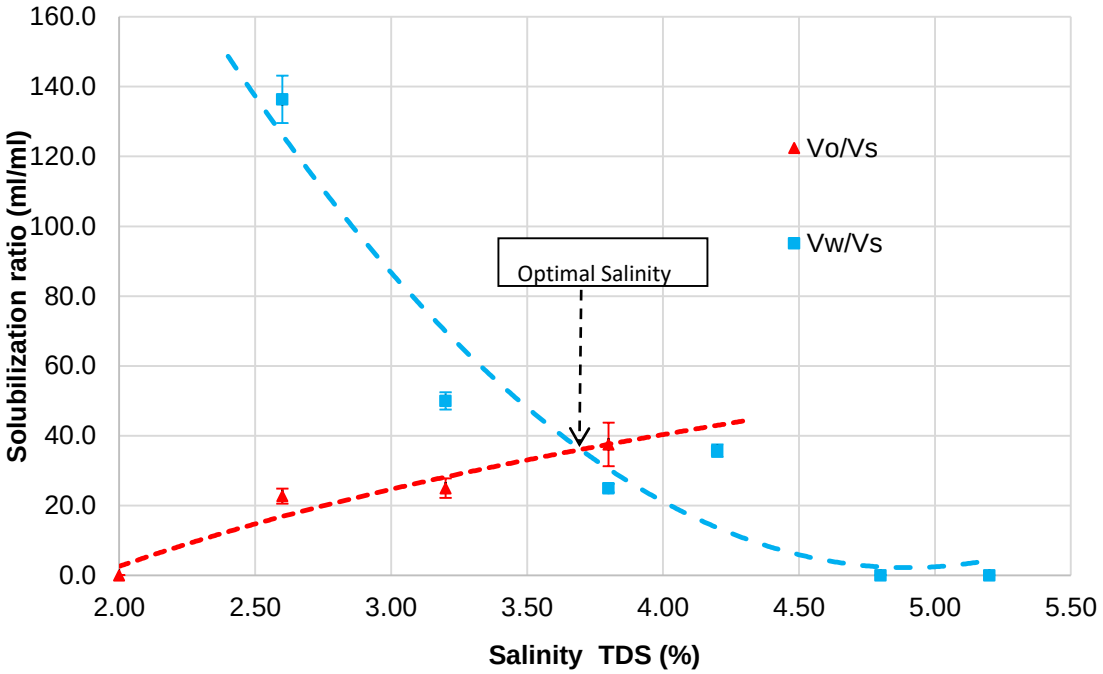


**Figure 5-39: Solubilisation ratio versus salinity of NaOH/$C_{13-14}$—7APS in SB at 140 ºF (Optimal Salinity= 3.75%)**

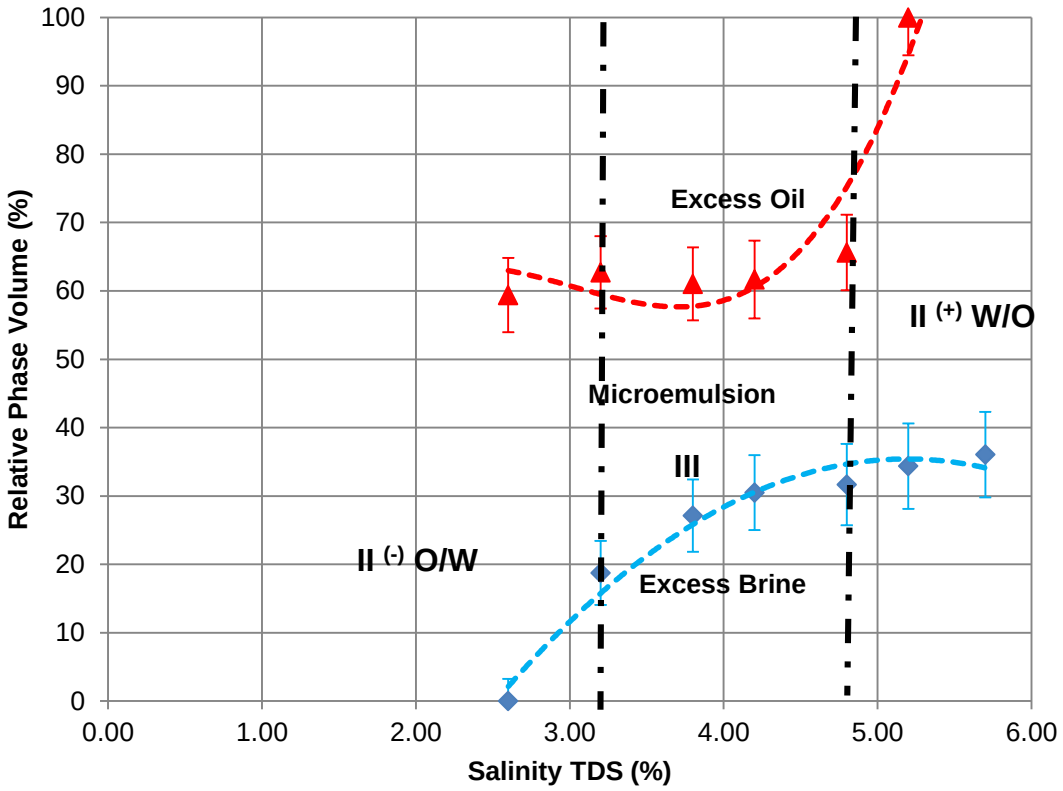


**Figure 5-40: Relative phase volume versus salinity of NaOH/$C_{13-14}$—7APS in SB at 140 °F (Salinity range 3.4% to 4.8%)**

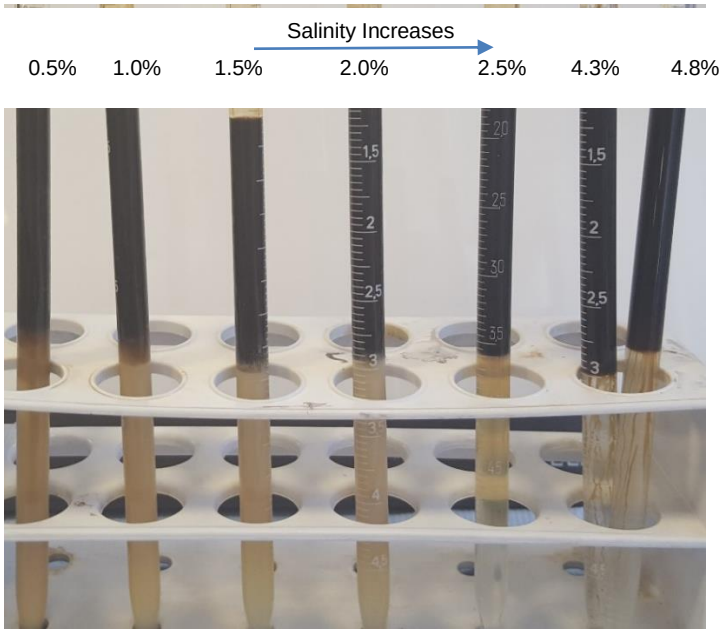


**Figure 5-41: Phase separation test for surfactants $C_{13-14}$—7APS/$NaBO_2$ in SB at 66 °F**

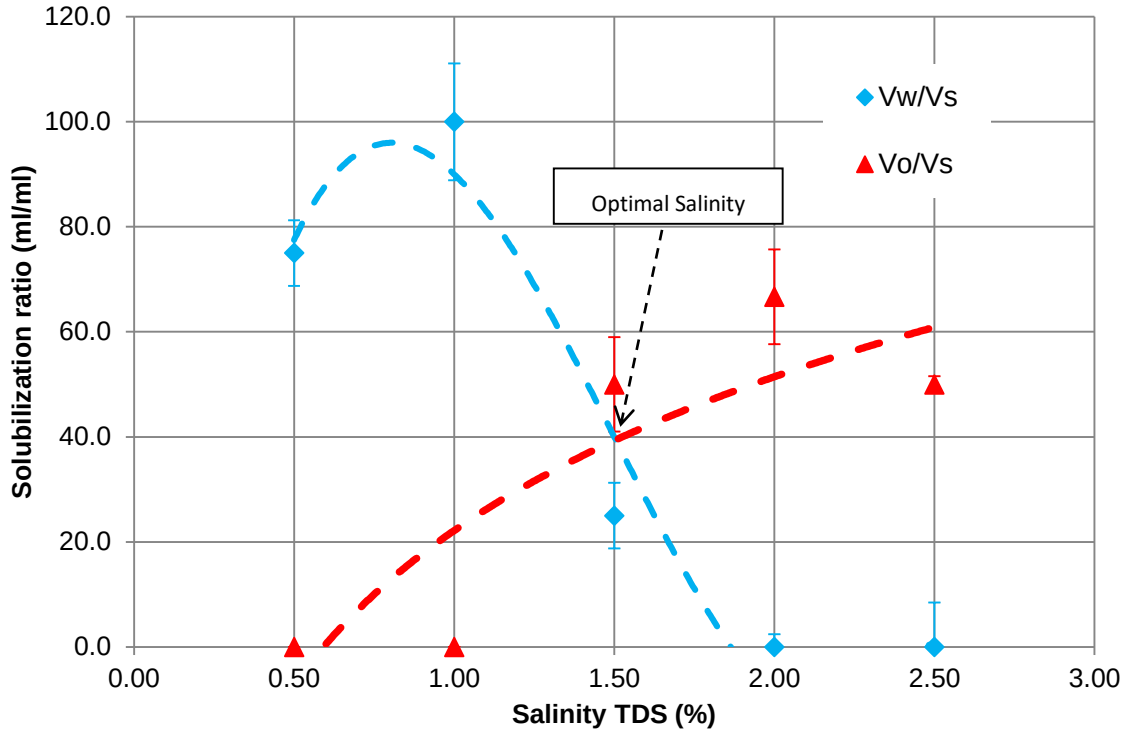


Figure 5-42: Solubilisation ratio versus salinity for $C_{13\text{-}14}$—7APS/$NaBO_2$ in SB at 66 °F (Optimal Salinity= 1.5%)

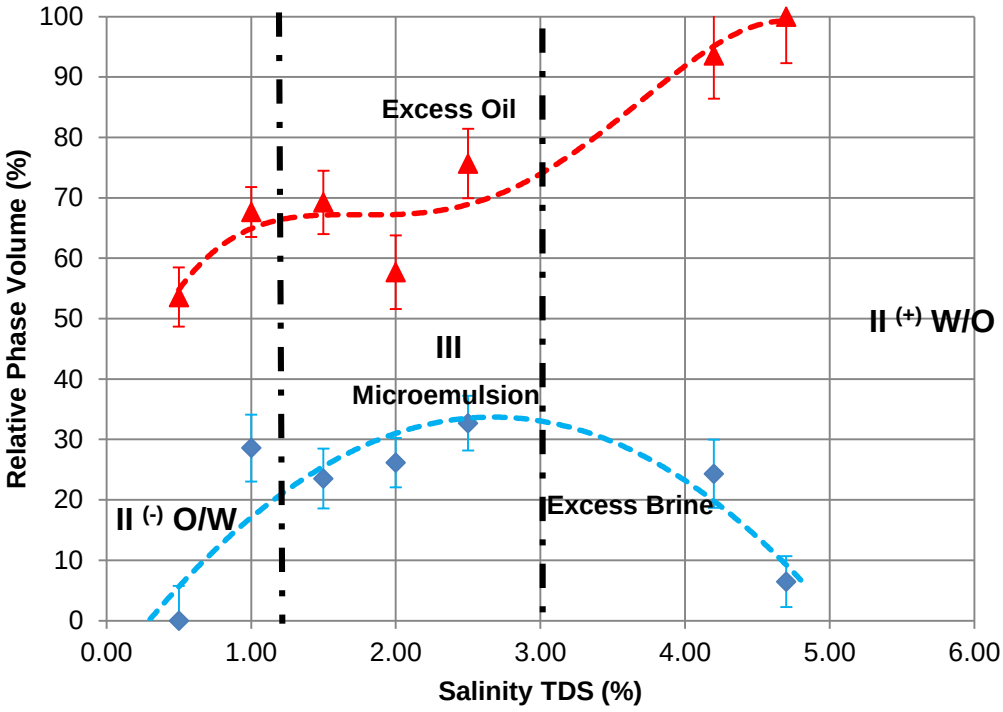


Figure 5-43: Relative phase volume versus salinity for $C_{13\text{-}14}$—7APS/$NaBO_2$ in SB at 66°F (Salinity range 1.0% to 2.5%)

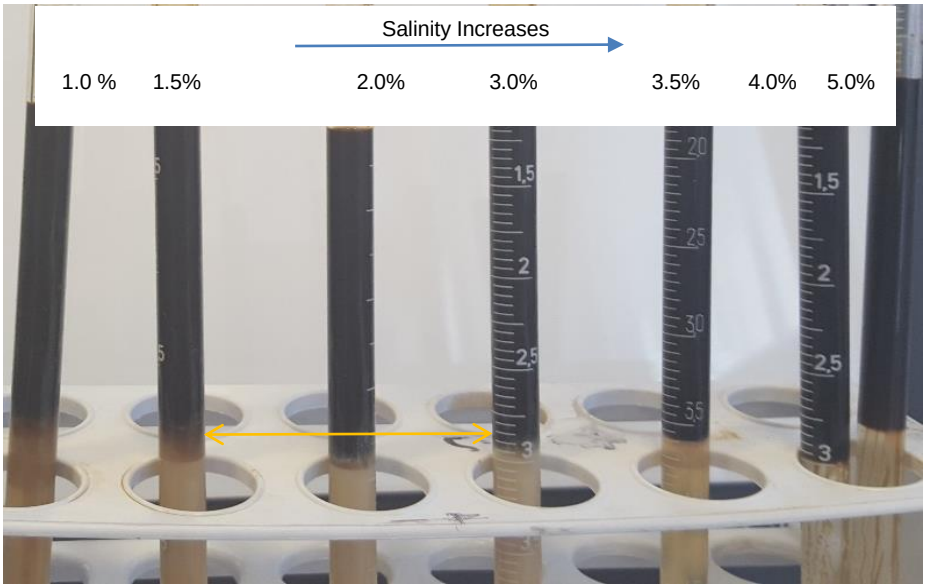


Figure 5-44: Phase separation test for $C_{13-14}$—7APS/$NaBO_2$ in HB at 66 °F

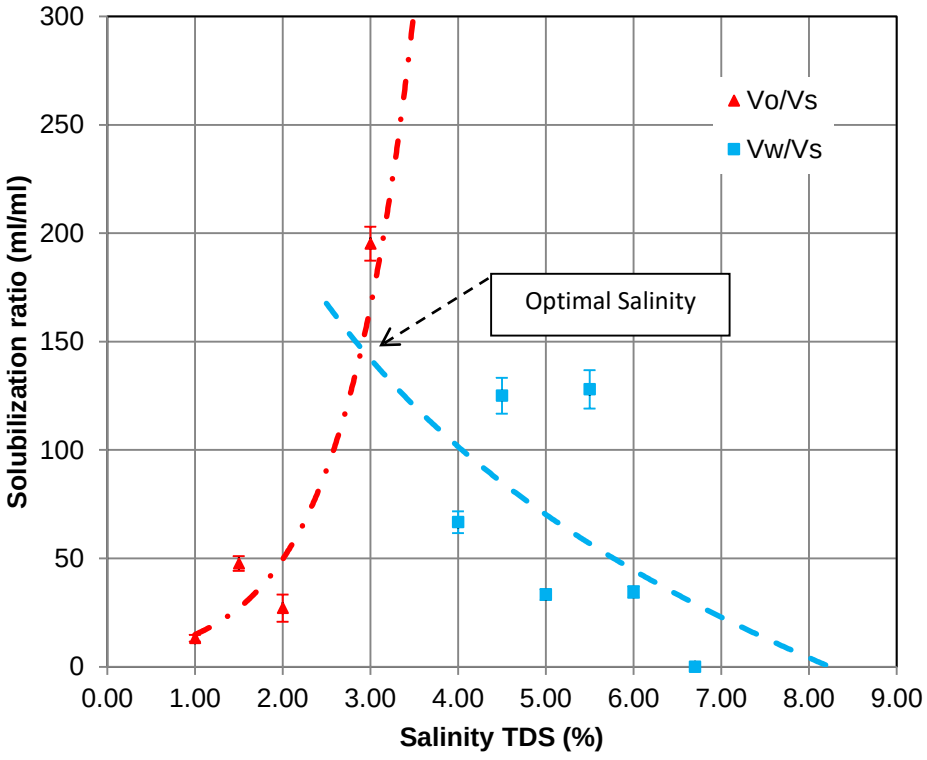


Figure 5-45: Solubilisation ratio versus salinity for $C_{13-14}$—7APS/$NaBO_2$ in HB at 66 °F (Optimal salinity=2.8%)

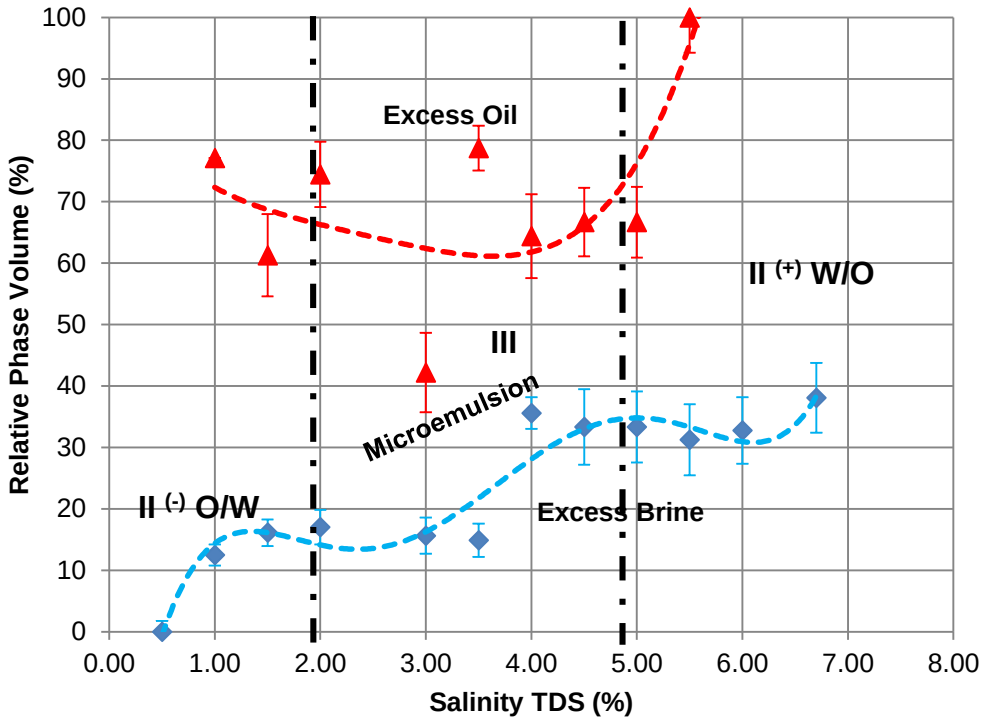


**Figure 5-46: Relative phase volume versus salinity for $C_{13\text{-}14}$—7APS/$NaBO_2$ in HB at 66°F (Salinity range 2.0% to 4.8%)**

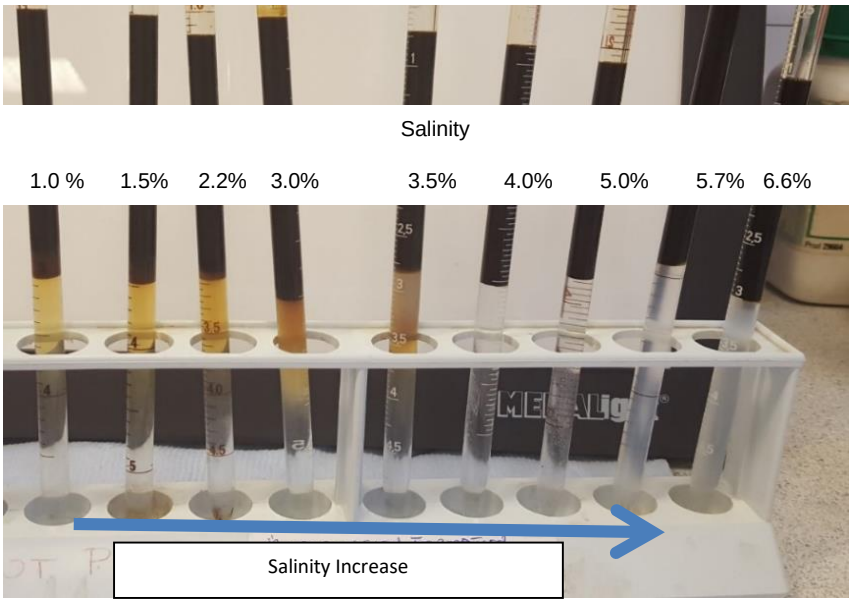


**Figure 5-47: Phase separation test for surfactants $C_{13\text{-}14}$—7APS/$NaBO_2$ in HB at 140° F**

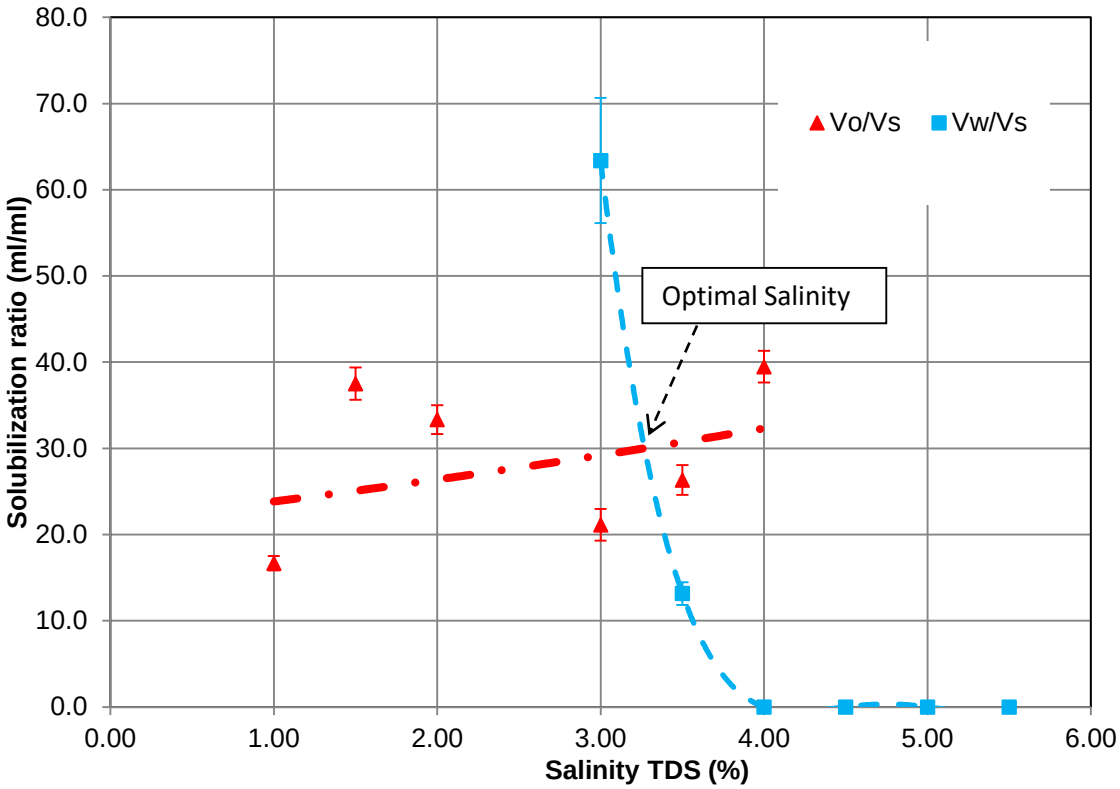


**Figure 5-48: Solubilisation ratio versus salinity for $C_{13-14}$—7APS/$NaBO_2$ in HB at 140 ºF (Optimal salinity= 3.2 %)**

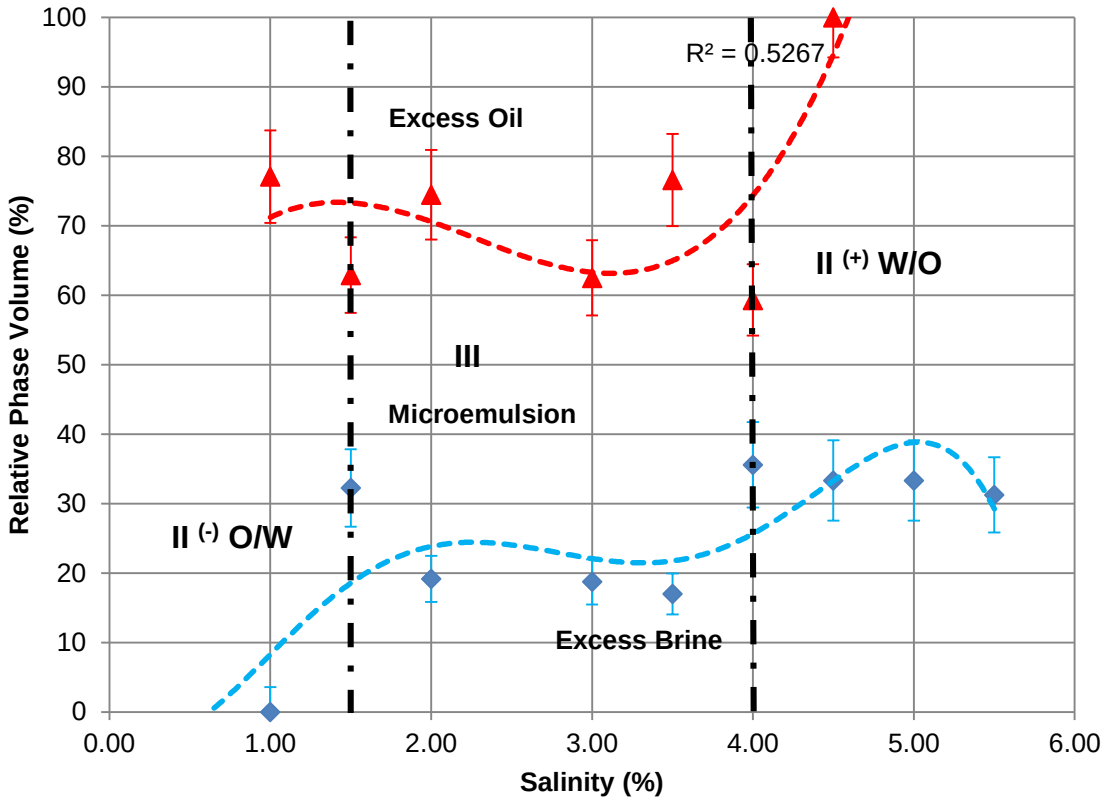


**Figure 5-49: Relative phase volume versus salinity for $C_{13\text{-}14}$—7APS/$NaBO_2$ in HB at 140 °F (Salinity range 1.5% to 4.0%)**

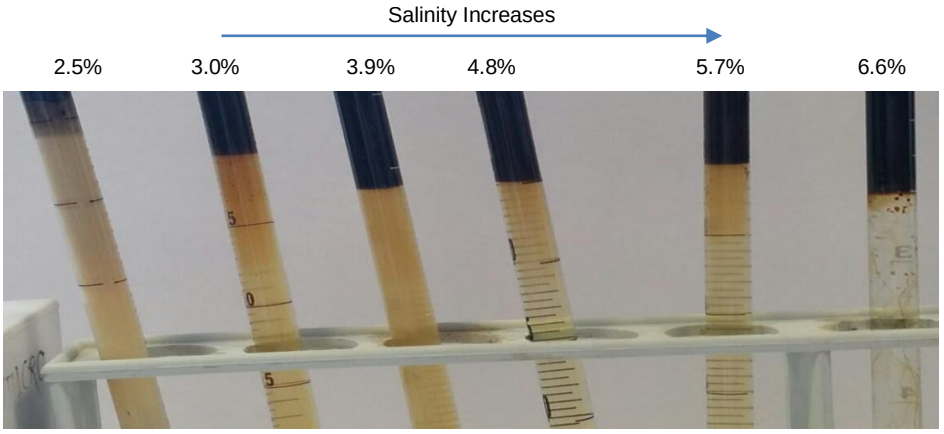


**Figure 5-50: Phase behaviour EDTA/NaOH/$C_{13\text{-}14}$—7APS on HB at 66 °F**

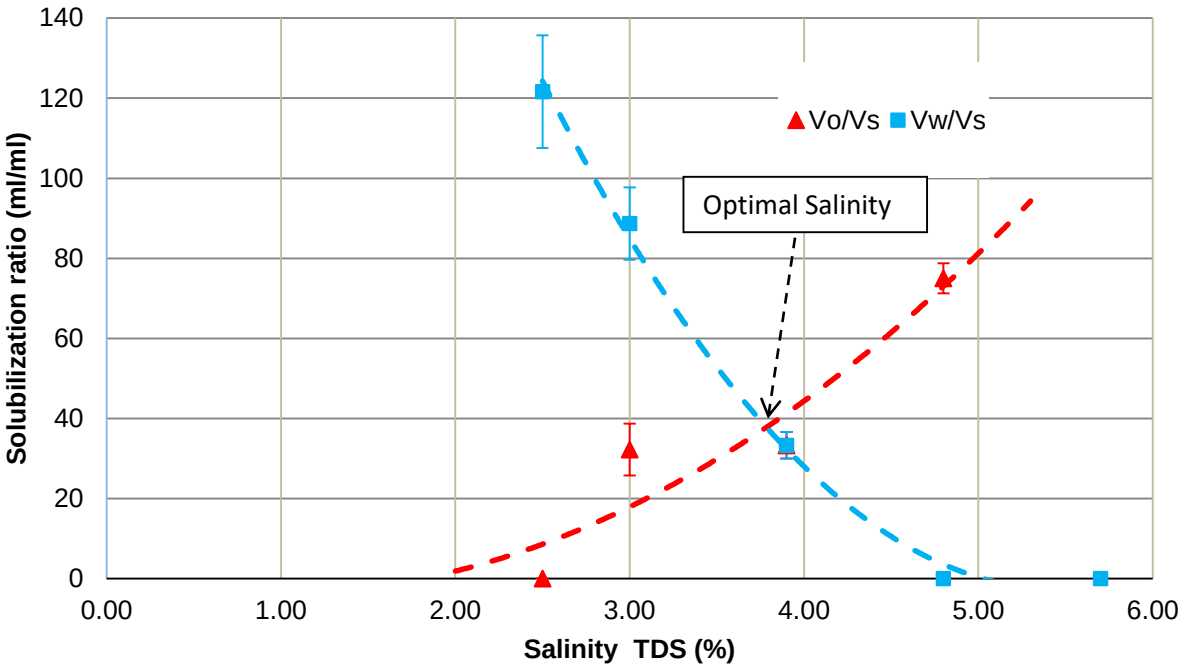


Figure 5-51: Solubilisation ratio versus salinity for EDTA/NaOH/$C_{13-14}$—7APS on HB at 66 °F (Optimal salinity=3.8%)

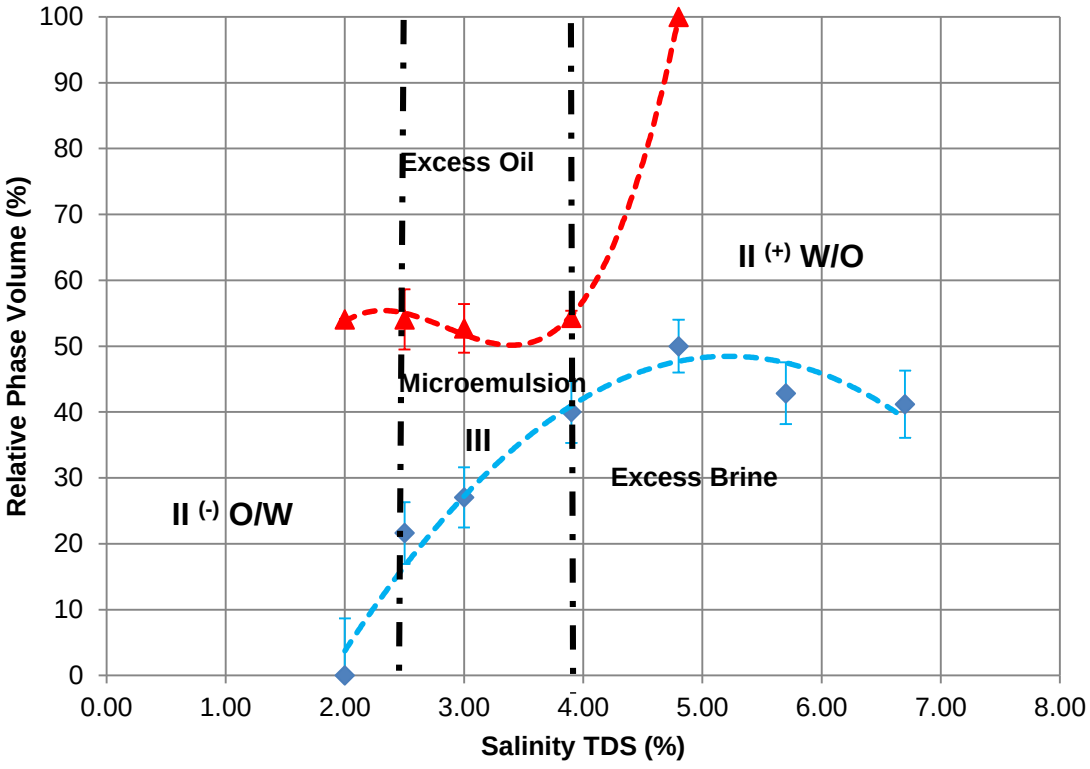


Figure 5-52: Relative phase volume versus salinity for EDTA/NaOH/$C_{13-14}$—7APS on HB at 66 °F (Salinity range 2.6% to 3.9%)

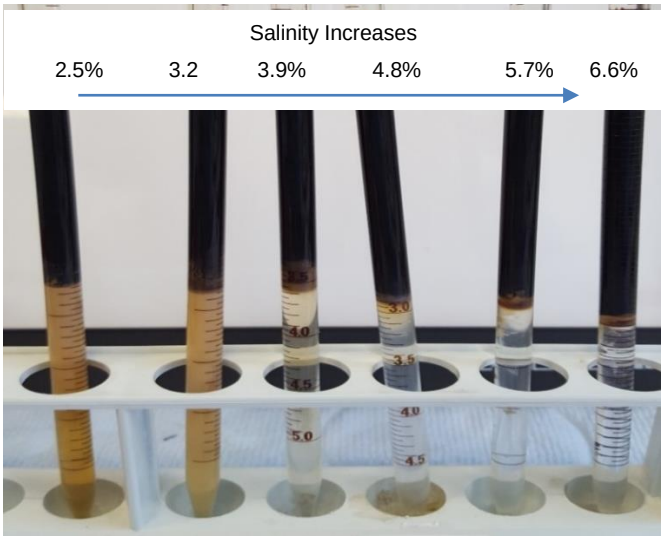


**Figure 5-53: Phase behaviour EDTA/NaOH/$C_{13-14}$—7APS on HB at 140ºF**

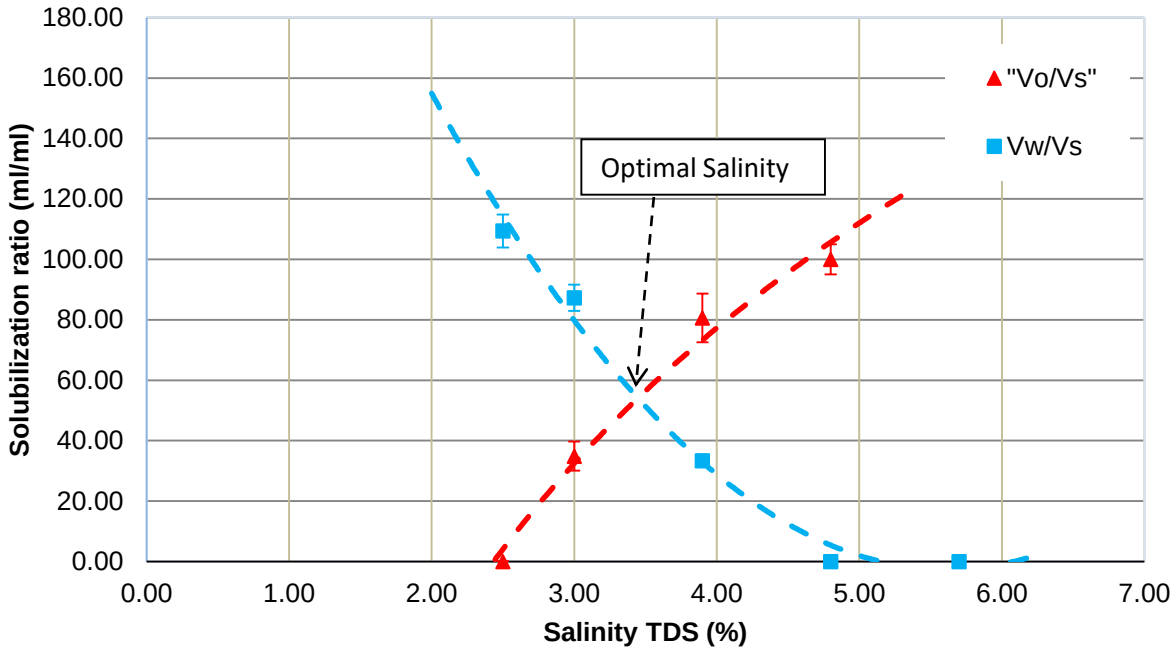


**Figure 5-54: Solubilisation ratio versus salinity for EDTA/NaOH/$C_{13-14}$—7APS on HB at 140ºF (Optimal Salinity= 3.5%)**

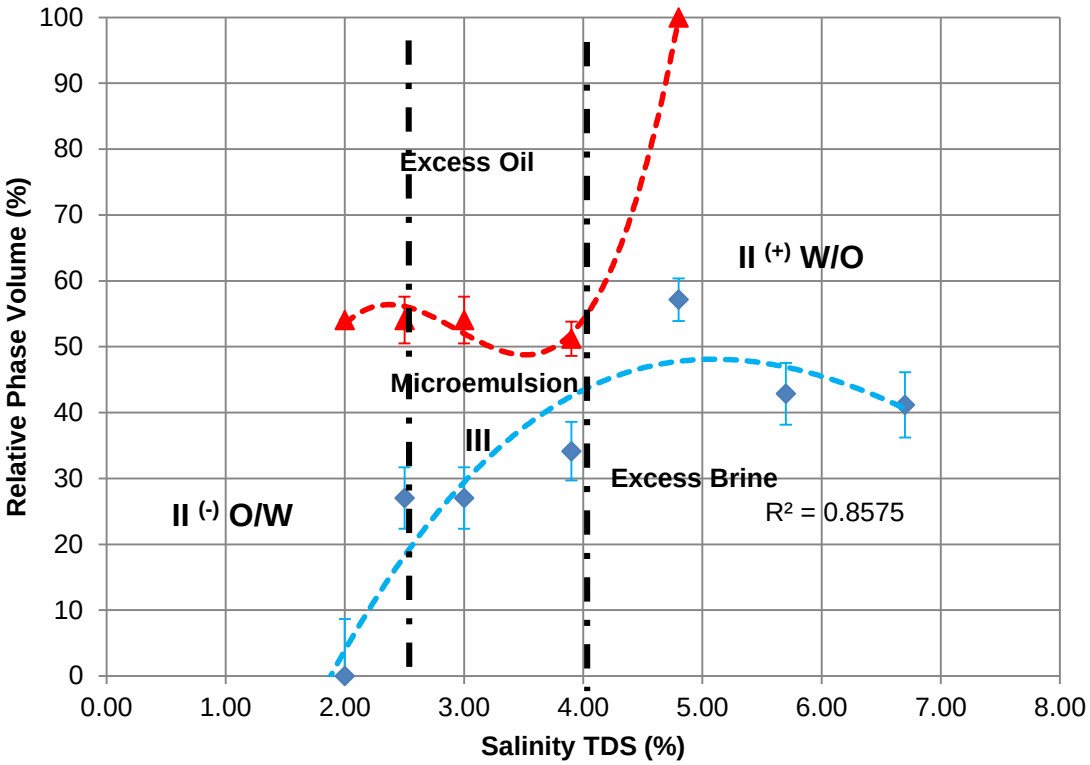


**Figure 5-55: Relative phase volume versus salinity for EDTA/NaOH/$C_{13-14}$—7APS on HB at 140ºF (Salinity range 2.5% to 4.0%)**

Optimal salinity, range of salinity and IFT calculated for all the systems described from (a) to (g) have been included in table 5-10. Also, graphical representations of these values have been presented in Figures 5-56 and 5-57.

The IFT at optimal salinity of microemulsion for all the cases is ultra-low, lower than $10^{-4}$ mN/m. IFT increases in one order of magnitude with high temperature for NaOH in SB, and $NaBO_2$ in HB. Slight changes on IFT with temperature were observed for HB NaOH/EDTA.

While $NaBO_2$ can achieve low IFT and a wide range of salinity at 60 ºF; the optimal salinity 3.4% TDS is low compared with optimal salinity obtained with the surfactant 3.9%.

Fluids-fluids interactions using EDTA/NaOH, such as IFT, range of salinity for microemulsion formation, and optimal salinity are better than for the rest of the systems. The IFT is in the order of $10^{-5}$ mN/m, the optimal salinity 3.6% TDS, and the range of optimal salinity for microemulsion formation are close to the original synthetic brine, 2.5 to 4.2% TDS.

**Table 5-10: Optimal salinity for microemulsion formation using $C_{13-14}$—7APS (0.2%) (SB) and (HB) and different alkali**

| System | Optimal Salinity (%) TDS | Temperature (ºF) | Range of salinity (%) | IFT (mN/m) |
|---|---|---|---|---|
| NaOH (0.05M) plus $C_{13-14}$—7APS -SB | 4.5 | 66 | 4.05 to 4.7 | $3.03 \times 10^{-5}$ |
| NaOH (0.05M) plus $C_{13-14}$—7APS- SB | 3.8 | 140 | 3.4 to 4.8 | $1.33 \times 10^{-4}$ |
| $NaBO_2$ (0.02M) plus $C_{13-14}$—7APS - SB | 1.5 | 66 | 2.0 to 3.4 | $1.11 \times 10^{-4}$ |
| $NaBO_2$ (0.02M) plus $C_{13-14}$—7APS - HB | 2.8 | 66 | 2.0 to 4.8 | $1.92 \times 10^{-5}$ |
| $NaBO_2$ (0.02M) plus $C_{13-14}$—7APS - HB | 3.2 | 140 | 2.0 to 4.0 | $2.45 \times 10^{-4}$ |
| EDTA/NaOH plus $C_{13-14}$—7APS - HB | 3.8 | 66 | 2.6 to 3.9 | $3.01 \times 10^{-5}$ |
| EDTA/NaOH plus $C_{13-14}$—7APS - HB | 3.5 | 140 | 2.5 to 4.2 | $5.31 \times 10^{-5}$ |

The presence of divalent ions $Ca^{2+}$ and $Mg^{2+}$ in strong alkalis requires the use of chemical components, such as $NaBO_2$ and EDTA/NaOH, able to form complex with them to avoid precipitation of their insoluble divalent hydroxides. The use of EDTA at a controlled pH of 9 with NaOH permitted the use of the alkali in hard brine without having precipitation of $Ca^{2+}$ and $Mg^{2+}$ hydroxides. The optimal salinity for the system EDTA/NaOH/ $C_{13-14}$—7APS is higher than the one obtained for $NaBO_2$/$C_{13-14}$-7APS. Optimal salinities for both systems are very close to the salinity of the SB.

The NaOH/$C_{13-14}$—7APS blend in SB has the highest optimal salinity at both temperatures (66 and 140 ºF). Whereas $NaBO_2$/$C_{13-14}$—7APS blend has a wider range of salinity for optimal conditions at 66 ºF but this range is slightly reduced at high temperature (140 ºF). The IFT increases with temperature for all the blends. $NaBO_2$/$C_{13-14}$-7APS has the lowest value of IFT (Figures 5-56 and 5-57).

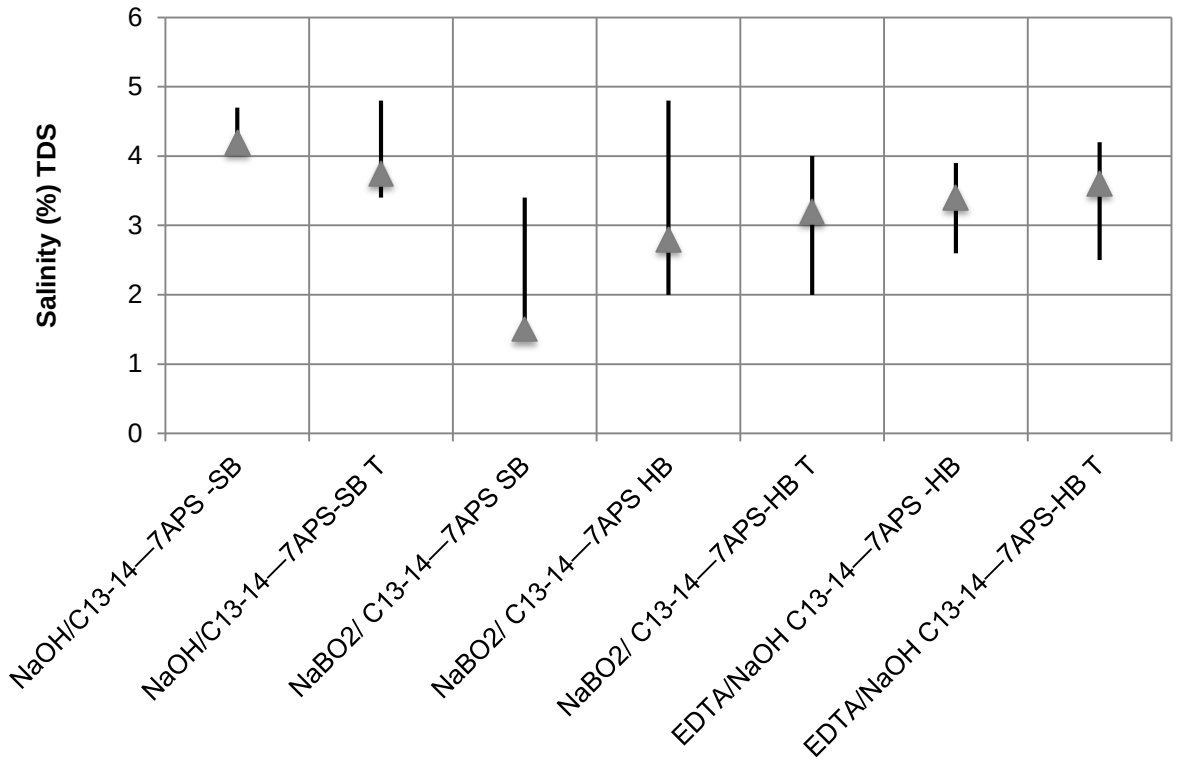


**Figure 5-56: Salinity range for microemulsion formation for alkali/surfactants solutions**

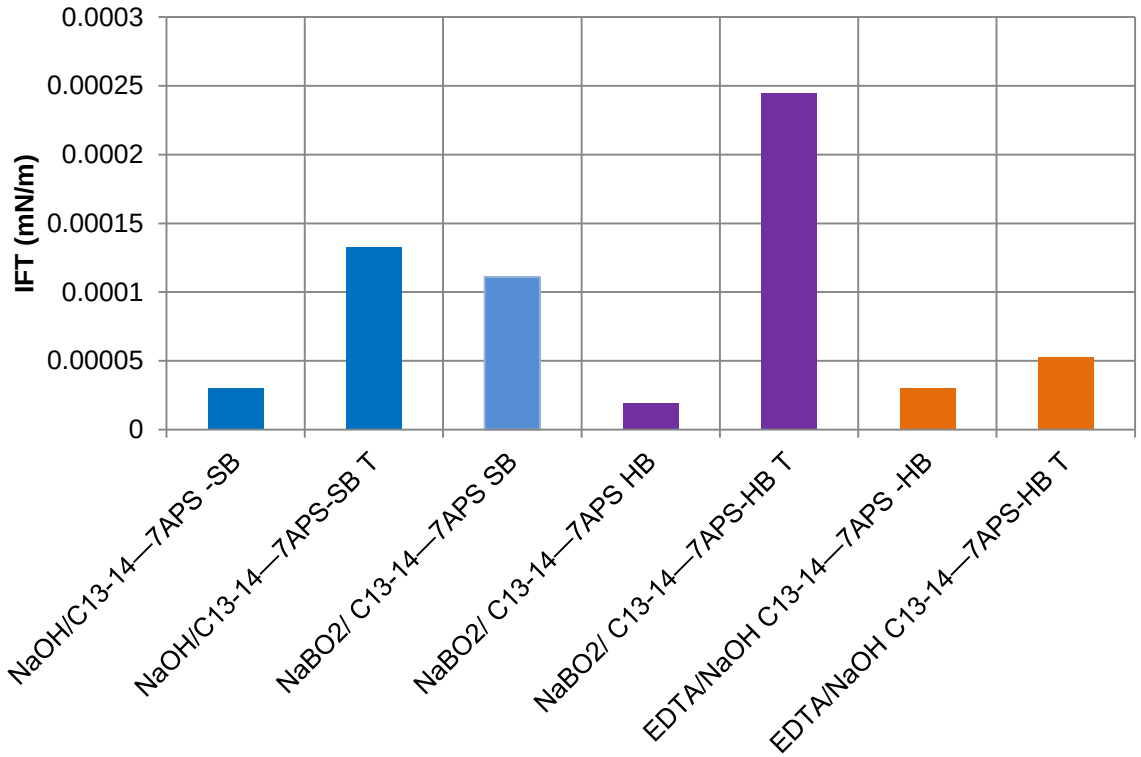


**Figure 5-57: Minimal IFT at the optimal salinity for alkali/surfactants solutions**

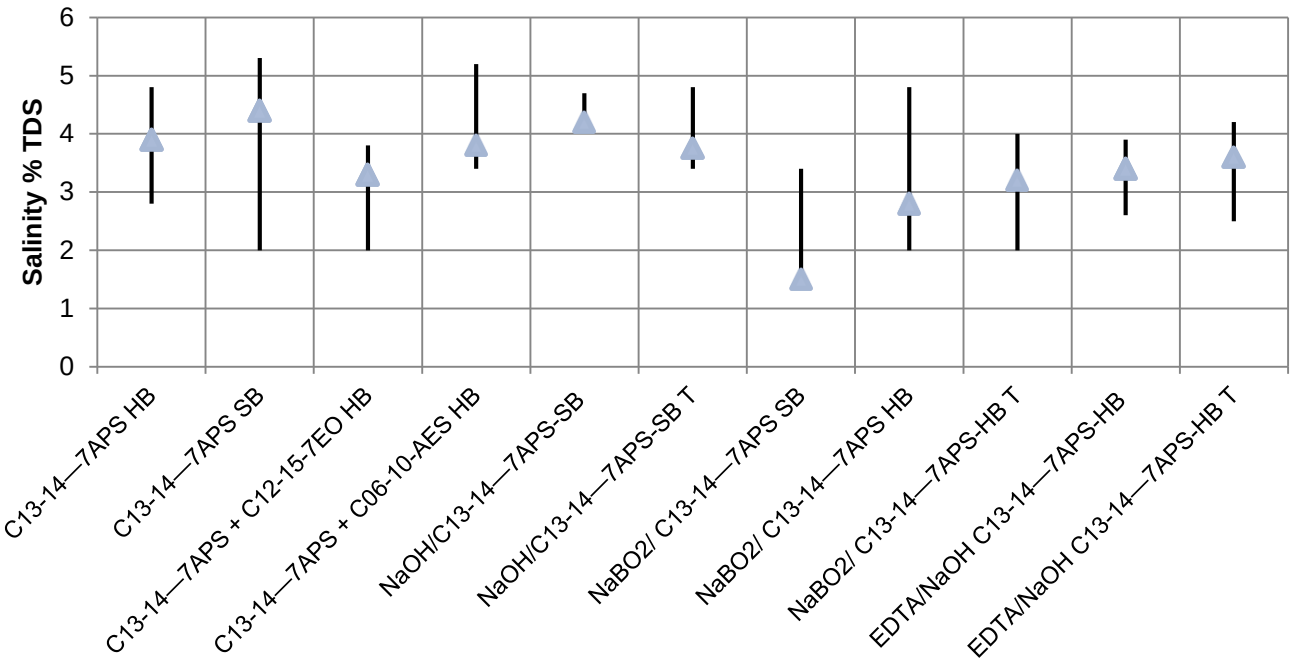


**Figure 5-58: Salinity range of microemulsion formation for surfactants, and alkali/surfactants solutions**

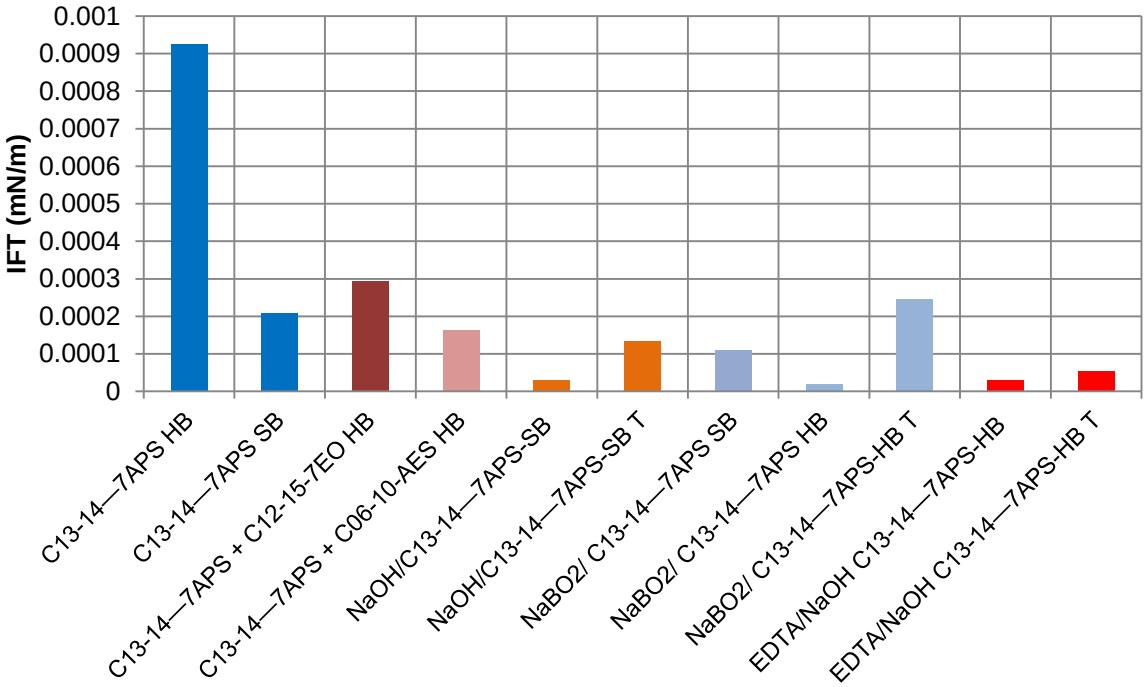


**Figure 5-59: Minimal IFT at optimal salinity for surfactant, co-surfactant and alkali/surfactants solutions**

Graphical representation of the range of salinity for microemulsion formation, optimal salinity and IFT for surfactants, blends of surfactant-co-surfactants and surfactant-alkalis are presented in Figures 5-58 and 5-59.

Comparing surfactants, co-surfactants and surfactant-alkali systems is evident that the addition of co-surfactant reduces the salinity range and the IFT of the main surfactant, with a laerger effect on the latter. Likewise, the use of alkali reduces the optimal salinity of the main surfactant, and modifies the range of optimal salinity conditions, being more noticeable at high temperature than at 60 $^{o}$F.

The salinity of the brine affects the solubility of the surfactant in the aqueous phase. There is an optimal salinity for microemulsion formation and ultra-low IFT, and this value is affected by the salinity (TDS). The optimal conditions for microemulsion formation increase with temperature as the solubility of the surfactant increases with temperature. However, the opposite effect was observed for NaOH in SB.

The concentration of divalent ions is critical for applications of CEOR. Divalent ions defined the optimal salinity of surfactants. Divalent ions also restrict the alkali selection to compounds with complexing properties to avoid precipitation. Alkali also increases the concentration of ions in the aqueous solution, therefore it has a similar effect as increasing salinity, thus reduces the solubility of surfactant in brine and reduces the optimal salinity of microemulsion formation (Sheng, 2014a).

The minimum IFT and higher optimal salinity for fluid-fluid interactions were obtained for the chemical slug formed by the blend EDTA/NaOH with the surfactant $C_{13-14}$-7APS. This result allows the use of NaOH as alkali with an optimal salinity closer to the salinity of the produced water.

The system $NaBO_2$/$C_{13-14}$-7APS is also a good alternative for applications with divalent ions. While all alkali-surfactant systems present a zone of ultra-low IFT for microemulsion formation, $NaBO_2$/$C_{13-14}$-7APS in SB is more favourable for applications at low salinity. The same system can tolerate divalent ions. NaOH/EDTA/$C_{13-14}$-7APS can also tolerate divalent ions and be applied at high salinity (Figure 5-60).

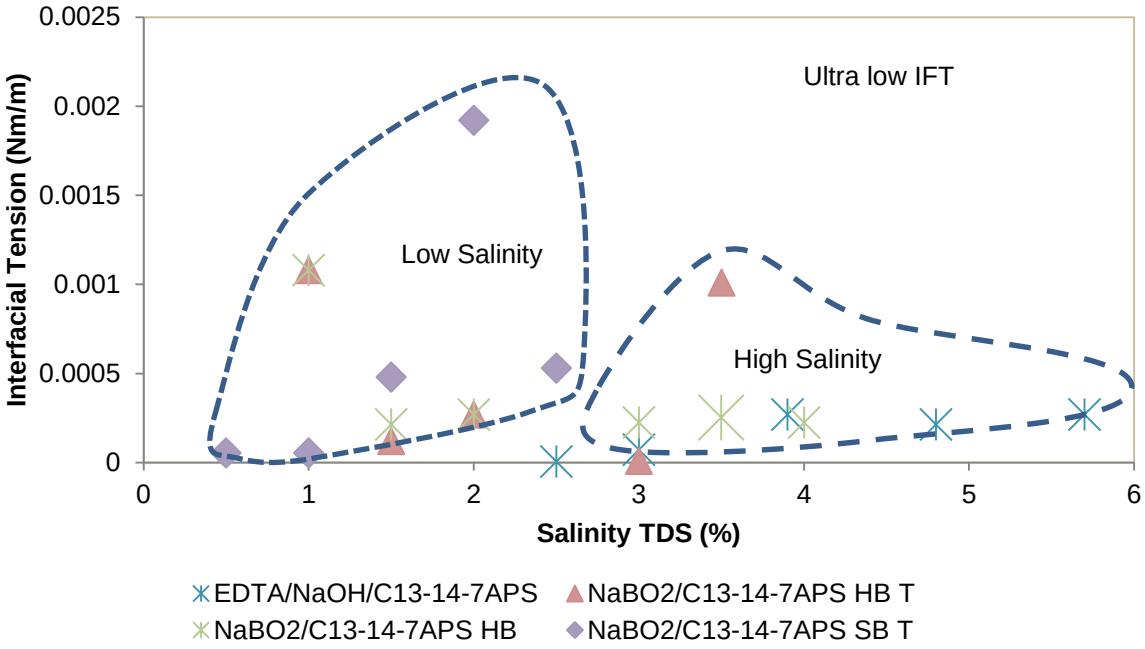


**Figure 5-60: Zone of ultra-low IFT microemulsion for alkali- surfactants solutions**

From the analysis of fluids-fluids interactions, it was possible to study the behaviour of chemicals (alkali and surfactant), also the effect of the interactions on the optimal conditions for microemulsion formation.

### 5.3.3 Study of interactions fluid –fluid –rock

In this section, the analysis of fluid-fluid and fluid-rock due to interactions during the flow of fluids through the rock is discussed based on the evaluation of core-flooding tests for waterflooding with HB and SB and the injection of chemical systems using surfactant, co-surfactant, and surfactant-alkali.

#### 5.3.3.1 Effect of surfactants and alkali-surfactant on the relative permeability

Two-phase relative permeability curves adjusted from core-flooding tests for water flooding and CEOR the process using surfactant, co-surfactant, and alkali flooding are presented in this section. Relative permeability curves are presented in Figure 5-61 and they can be identified for the following processes:

a) Water flooding with HB and $C_{16-17}$-13APS surfactant flooding at optimal salinity 1.5% using HB (1.5% HB).
b) Water flooding with SB and $C_{16-17}$-13APS surfactant flooding at optimal salinity 4.8% using SB (4.8% SB).
c) Water flooding with HB and $C_{13-14}$-7APS surfactant flooding at optimal salinity 3.9% using HB (3.9% HB).
d) Water flooding with HB and blend surfactant/co-surfactant $C_{13-14}$—7APS_$C_{06-10}$-AES flooding at optimal salinity 3.8% using HB (3.8% HB).
e) Water flooding with HB and blend NaOH/EDTA/ $C_{13-14}$—7APS surfactant flooding at optimal salinity 3.6% using HB (3.6% HB).
f) Water flooding with HB and blend $NaBO_2$/ $C_{13-14}$-7APS surfactant flooding at optimal salinity 3.2% using HB (3.2% HB).

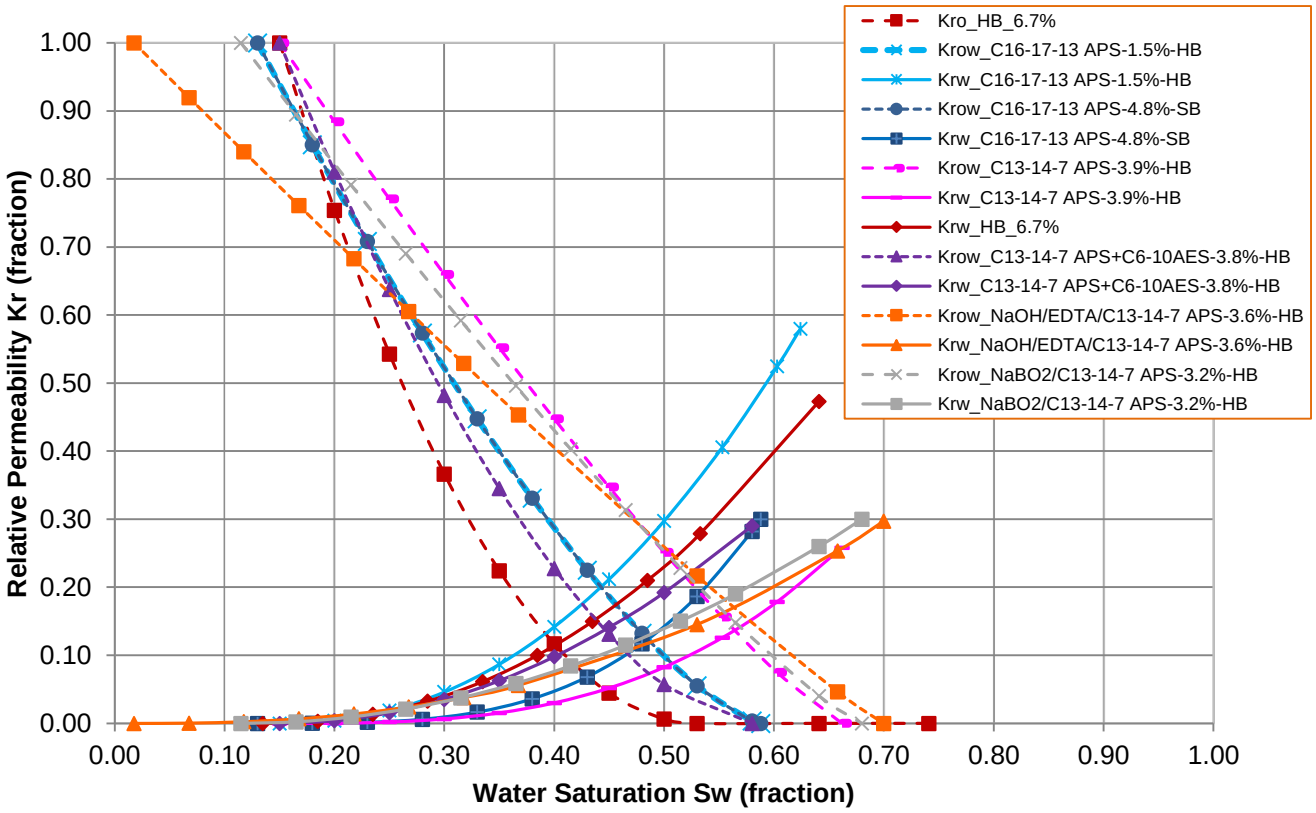


**Figure 5-61: Effect of surfactant, co-surfactant and alkali on relative permeability curves**

It is noticed that for all the chemical systems the shape of relative permeability as a function of water saturation changes by the effect of surfactant, co-surfactant, and alkali concerning water flooding with HB 6.6% TDS. These changes are indications of changes in the distribution of fluids in the porous media (Shen *et al.*, 2010). From the study of interactions fluid-fluid, it was evident the effect of chemicals on the interfacial tension by surfactants and alkali.

Oil and water relative permeability and residual oil saturation for each chemical system have been measured from the graph of Figure 5-61 and are presented in table 5-11 and Figure 5-62. Surfactants and alkali increase $k_{row}$ and reduce $S_{or}$ with slight modifications on $k_{rw}$. The higher modifications of $k_{row}$ are observed for $C_{13\text{-}14}$-7APS and alkali-surfactant systems $NaBO_2$ $C_{13\text{-}14}$—7APS HB and NaOH/EDTA $C_{13\text{-}14}$—7APS HB.

Water relative permeability $k_{rw}$ is somewhat modified according to experimental results, higher changes are obtained for surfactant $C_{16\text{-}17}$-13APS at low salinity. In this case, there are two possible effects, ionic interactions by salinity gradient due to the low salinity, and the effect of surfactant on the IFT. $k_{rw}$ and $k_{row}$ increase and Sor decreases by the effect of chemicals.

From interactions fluid-fluid as learned in the previous section, surfactants and blends of surfactants with alkali decrease the IFT between aqueous and oleic phases. This effect is noticed on changes in relative permeability curves, especially on the oil relative permeability $k_{row}$. Oil relative permeability increases due to the injection of chemical systems. The lower the interfacial tension, the more linear is the oil relative permeability curve. The oil relative permeability for alkali-surfactant chemical systems as a function of water saturation tends to be linear. Similar results have been found for many authors as reported by Sheng et al. (2010).

Surfactants modify mainly the oil relative permeability of the oil ($k_{ro}$) by decreasing the residual oil saturation *Sor* and decreasing the Corey exponent for oil (*No*) to 1, thus making the curve more linear. This is the main effect of changes in IFT fluids-fluids. As systems with alkali showed ultra-low IFT, it is consistent with the highest values of oil relative permeability observed for alkali-surfactant systems. From these results, the impact of the low IFT on the relative permeability curves and the flow of fluids in the porous media was evidenced by the analysis of core-flooding tests

**Table 5-11: Oil and water relative permeability and residual oil saturation for surfactant, co-surfactant and alkali-surfactant CEOR tests**

| Process | Kro at Sw=0.45 | Krw at Sor | Sor |
|---|---|---|---|
| | (frac) | (frac) | (frac) |
| Water flooding 6. 6% HB | 0.04 | 0.28 | 0.45 |
| $C_{16-17}$-13APS – 1.5% HB | 0.20 | 0.53 | 0.38 |
| $C_{16-17}$-13APS – 4.8% SB | 0.18 | 0.30 | 0.41 |
| $C_{13-14}$-7APS - 3.9% HB | 0.31 | 0.25 | 0.34 |
| $C_{13-14}$—7APS_$C_{06-10}$-AES 3.8% HB | 0.14 | 0.29 | 0.34 |
| $NaBO_2$ $C_{13-14}$—7APS HB | 0.31 | 0.30 | 0.32 |
| NaOH/EDTA $C_{13-14}$—7APS HB | 0.31 | 0.30 | 0.30 |

The effect of the low salinity for surfactant $C_{16-17}$-13APS – 1.5% HB is appreciated by the low value of residual oil saturation compared with $C_{16-17}$-13APS – 4.8% SB. The effect of the co-surfactant $C_{06-10}$-AES is not evident in the results.

Both alkali-surfactant systems showed similar values of $k_{row}$, $k_{rw}$ with slightly differences in Sor, however, the system NaOH/EDTA $C_{13-14}$—7APS HB reduces the initial water saturation. Additional advantages can be associated with either to interactions of EDTA with divalent ions adsorbed on the rock to promote additional oil recovery or additional effect of $OH^-$, as strong alkali on the adsorption places on the rock surface.

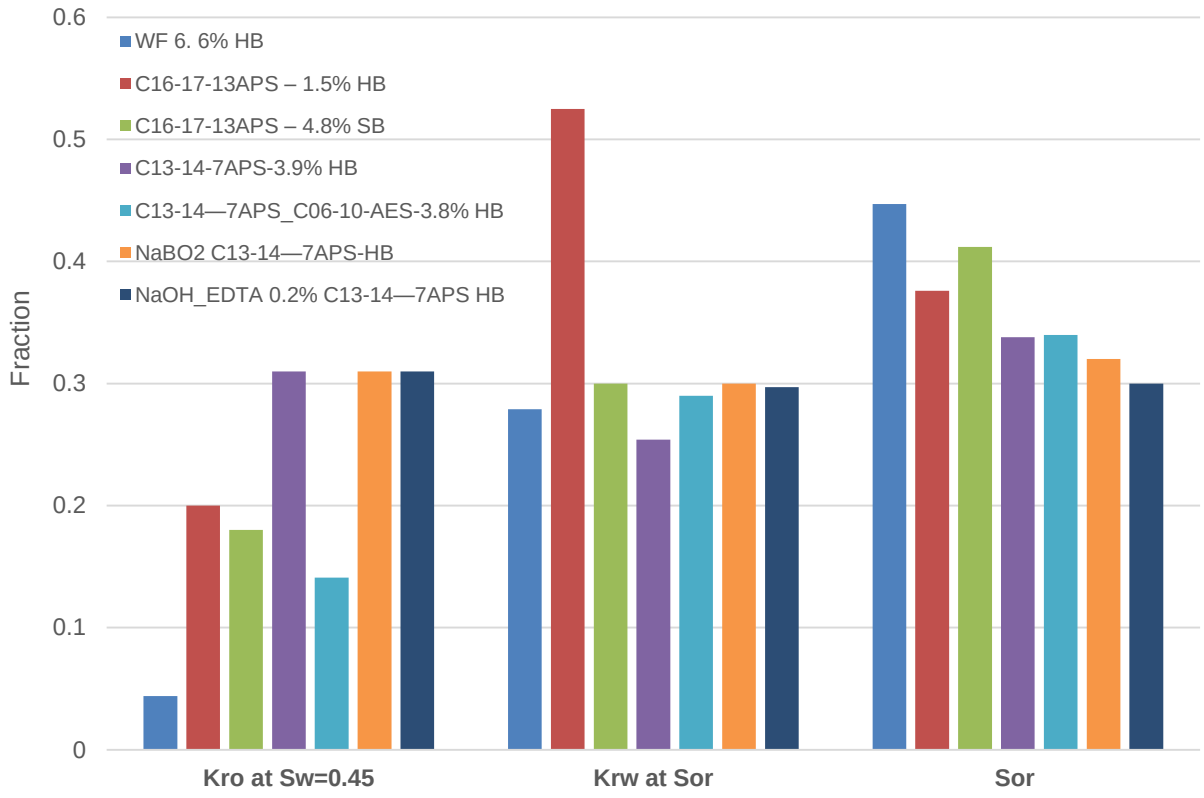


**Figure 5-62: Effect of surfactant, co-surfactant and alkali on relative permeability curves**

### 5.3.3.2 Effect of surfactants and alkali-surfactant on capillary number

Results from core flooding tests were used to calculate capillary numbers, and results have been presented in table 5-12. Residual oil saturation as a function of calculated capillary numbers is presented in Figure 5-63, this curve is called capillary desaturation curve CDC and is used in the flow equations to consider the dependence of the residual oil saturation with interfacial tension (Pope et al., 2000).

**Table 5-12: Summary of Results from core flooding for Alkali-Surfactant CEOR tests**

| Sample Bentheimer cores Porosity/Perm | Process | Capillary Number Nc | Oil Recovery Factor RF | Residual Oil Saturation | Displacement Efficiency $E_D$ |
|---|---|---|---|---|---|
| | | | (%) | Sro | $E_D$ |
| Core -500-1 (0.17/453 mD) | Water flooding 6. 7% HB | $9.39 \times 10^{-1}$ | 47 | 0.447 | 0.47 |
| | CEOR $C_{16-17}$-13APS – 1.5% HB | $2.17 \times 10^{4}$ | 56 | 0.376 | 0.56 |
| Core -500-2 (0.18/432 mD) | Water flooding 5.7% SB | $5.92 \times 10^{-1}$ | 41 | 0.518 | 0.41 |
| | CEOR $C_{16-17}$-13APS – 4.6% SB | $4.87 \times 10^{4}$ | 53 | 0.412 | 0.53 |
| Core -500-3 (0.17/450 mD) | Water flooding 6. 7% HB | $9.39 \times 10^{-1}$ | 45 | 0.471 | 0.45 |
| | CEOR $C_{13-14}$-7APS 3.9% HB | $2.17 \times 10^{5}$ | 60 | 0.338 | 0.60 |
| Core -500-4 (0.17/437 mD) | Water flooding 6.7% HB | $9.39 \times 10^{-1}$ | 46 | 0.471 | 0.46 |
| | 0.2% $C_{13-14}$—7APS_$C_{06-10}$-AES 3.8% HB | $4.87 \times 10^{4}$ | 54 | 0.317 | 0.54 |
| Core -500-5 (0.18/430 mD) | Water flooding 6. 7% HB | $9.29 \times 10^{-1}$ | 42 | 0.506 | 0.42 |
| | NaOH_EDTA 0.2% $C_{13-14}$—7APS HB | $8.50 \times 10^{5}$ | 69 | 0.300 | 0.69 |

There is a significant reduction in the residual oil saturation by the effect of surfactants and alkalis tested with changes on the capillary number by a factor of $10^4$ compared with water flooding with brine. The lowest capillary number was obtained for HB with the chemical system NaOH/EDTA $C_{13-14}$—7APS.

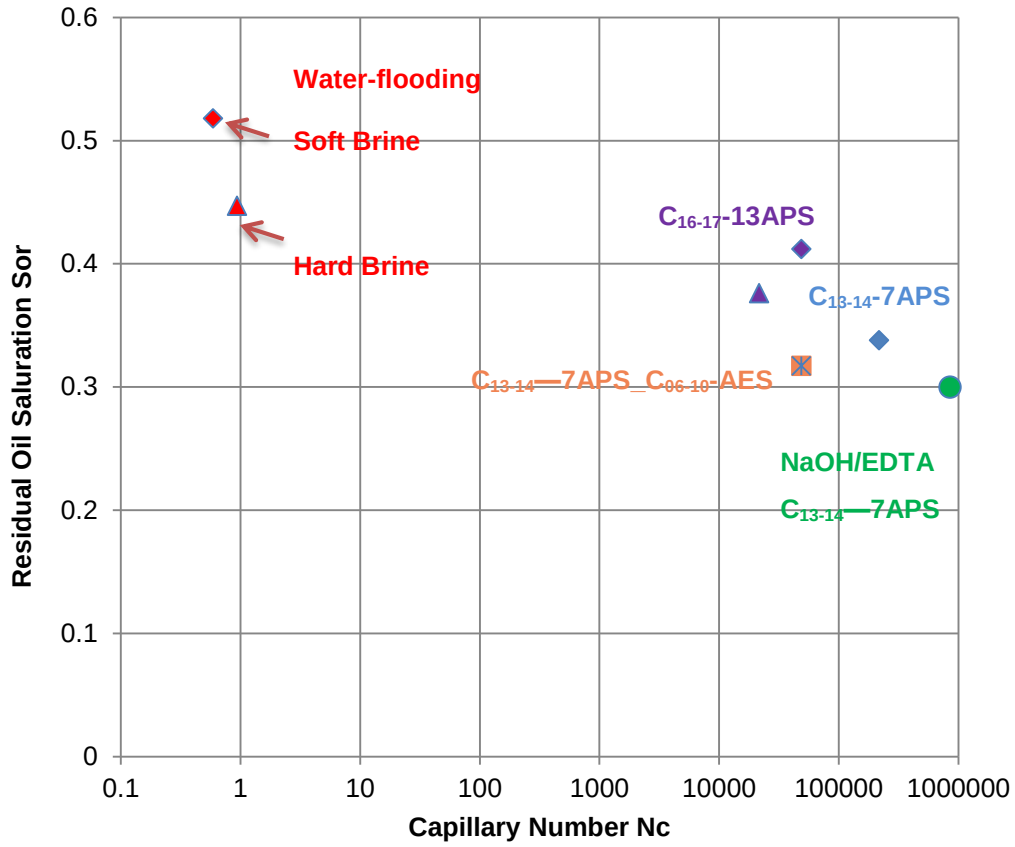


**Figure 5-63: Residual Oil Saturation versus capillary number for HB, SB and CEOR systems**

Low values of capillary numbers obtained for water flooding with HB and SB indicate that high capillary forces are the ones that drive the movement of the fluid in the porous media. These capillary forces retain drops of oil in the porous media. They are affected by different variables such as permeability, the average pore size, wettability of the rock, fluid distribution and saturation profiles. Surfactant and alkali CEOR reduce those capillary forces by reduction of the IFT, thus increase the capillary number and reduce the residual oil saturation.

These results demonstrate that surfactants, blend of surfactant with co-surfactant and alkali reduces the capillary forces that keep the oil trapped in the porous media. They can perform in terms of reducing the residual oil saturation at the microscopic level, enhancing the displacement efficiency. The best performance was found for the system NaOH/EDTA/$C_{13-14}$-7APS, increasing the RF by 12% compared with $C_{13-14}$-7APS.

The higher hydrophilicity of $C_{13-14}$—7APS compared with $C_{16-17}$-13APS improves the performance of APS surfactants for applications in high salinity with divalent ions. The addition of a small hydrophobic co-surfactant reduces the IFT and the residual oil saturation.

#### 5.3.3.3 Surfactant adsorption and effect of salinity and divalent cations

In this section, the adsorption behaviour of surfactants APS, $C_{13-14}$—7APS, $C_{16-17}$-13APS, and the blend $C_{13-14}$—7APS_$C_{06-10}$-AES is studied. Absorption isotherms using Langmuir and Freundlich (Bera *et al.*, 2013) correlations were adjusted for each surfactant and are presented in Figures 5-64 to 5-68.

Results for surfactant adsorption show that adsorption increases with surfactant concentration up to a plateau. The adsorption of surfactant increases until all adsorption places are saturated with surfactant. The adsorption of surfactant alcohol propoxy sulfate APS, shows the surfactant with a higher number of APS groups $C_{16-17}$-13APS has lower adsorption than $C_{13-14}$—7APS. Based on the number of APS groups the repulsion between the negative hydrophilic groups with the negatively charged rock surface reduces surfactant adsorption (Figures 5-64 and 5-65).

Divalent ions increase the adsorption of surfactants and the effect is higher for $C_{13-14}$—7APS surfactant. The co-surfactant $C_{06-10}$-AES decreases the adsorption of $C_{13-14}$—7APS (Figure 5-66 and Figure 5-68). This behaviour has been explained as due to the adsorption of the divalent ions $Ca^{2+}$ and $Mg^{2+}$ on the negatively charged rock acting as a link for the adsorption of anionic surfactants (Figures 5-64 and 5-66, 5-65 and 5-67).

Both behaviours of surfactant adsorption versus surfactant concentration can be represented as adsorption isotherms using Langmuir or Freundlich models (Sheng, 2010a), however a low surfactant concentration Langmuir model overestimate surfactant adsorption compare with Freundlich model. The fitting of adsorption isotherms for APS surfactants and co-surfactant is better with Freundlich model. Similar recommendations were found in the literature (Park *et al.*, 2015)

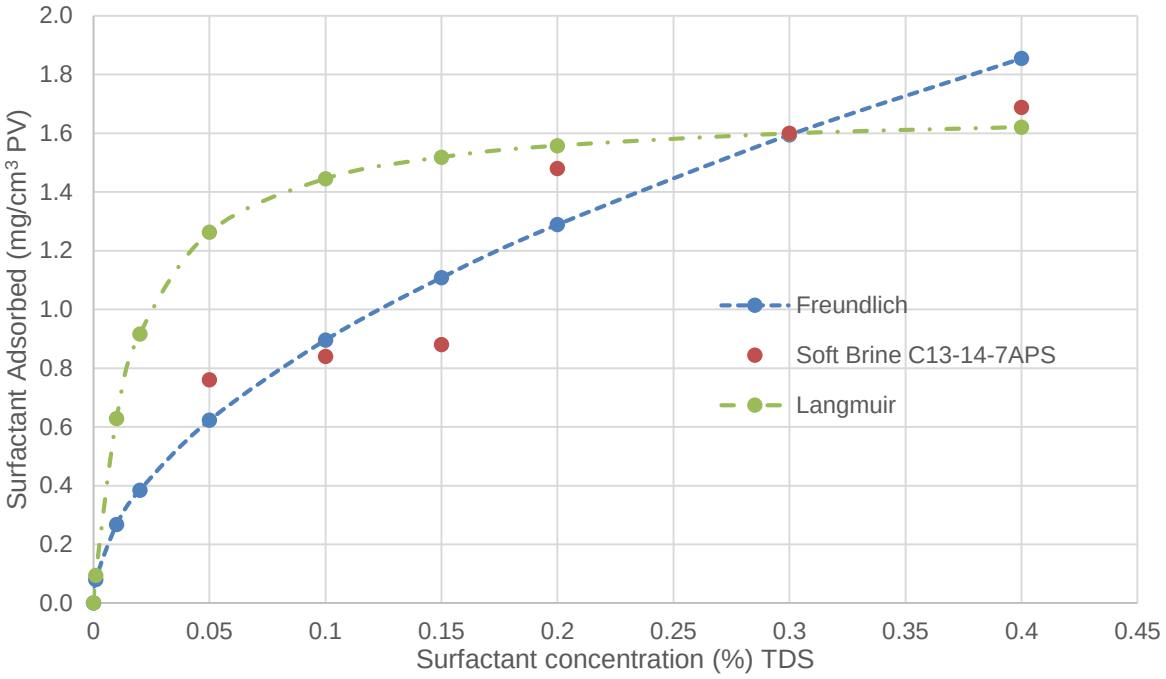


**Figure 5-64: Adsorption for surfactant $C_{13\text{-}14}$-7APS in SB and isotherm models (Freundlich and Langmuir)**

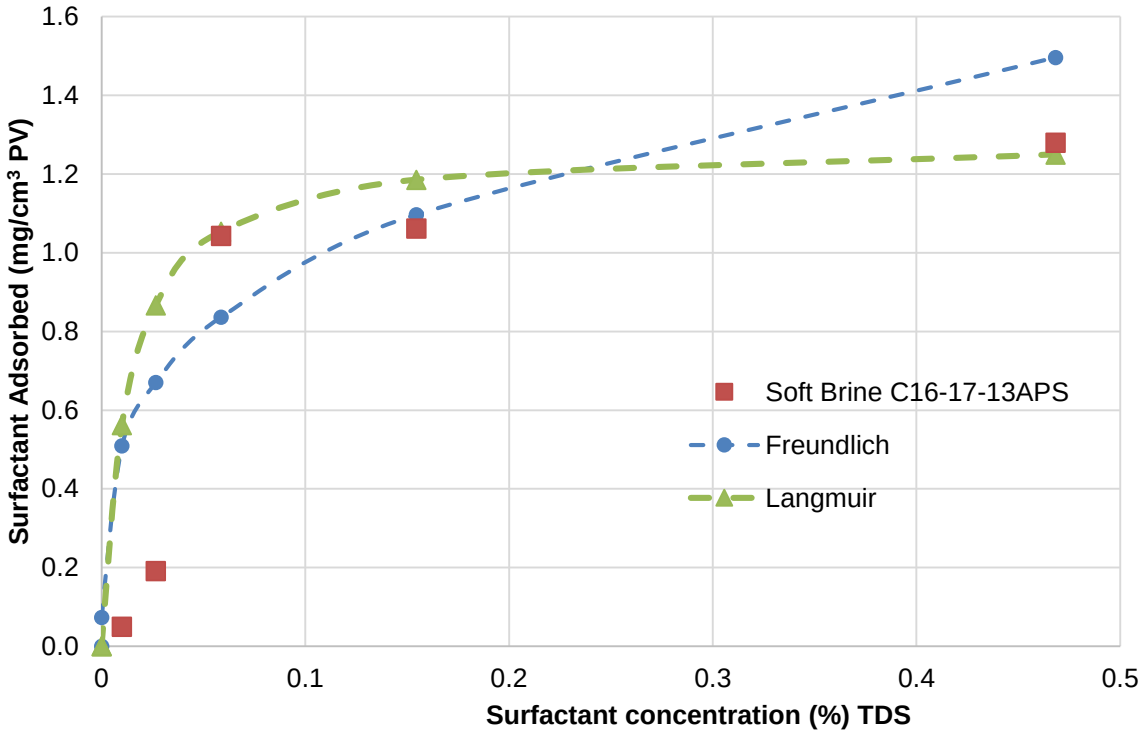


**Figure 5-65: Adsorption for surfactant $C_{16\text{-}17}$-13APS in SB and isotherm models (Freundlich and Langmuir)**

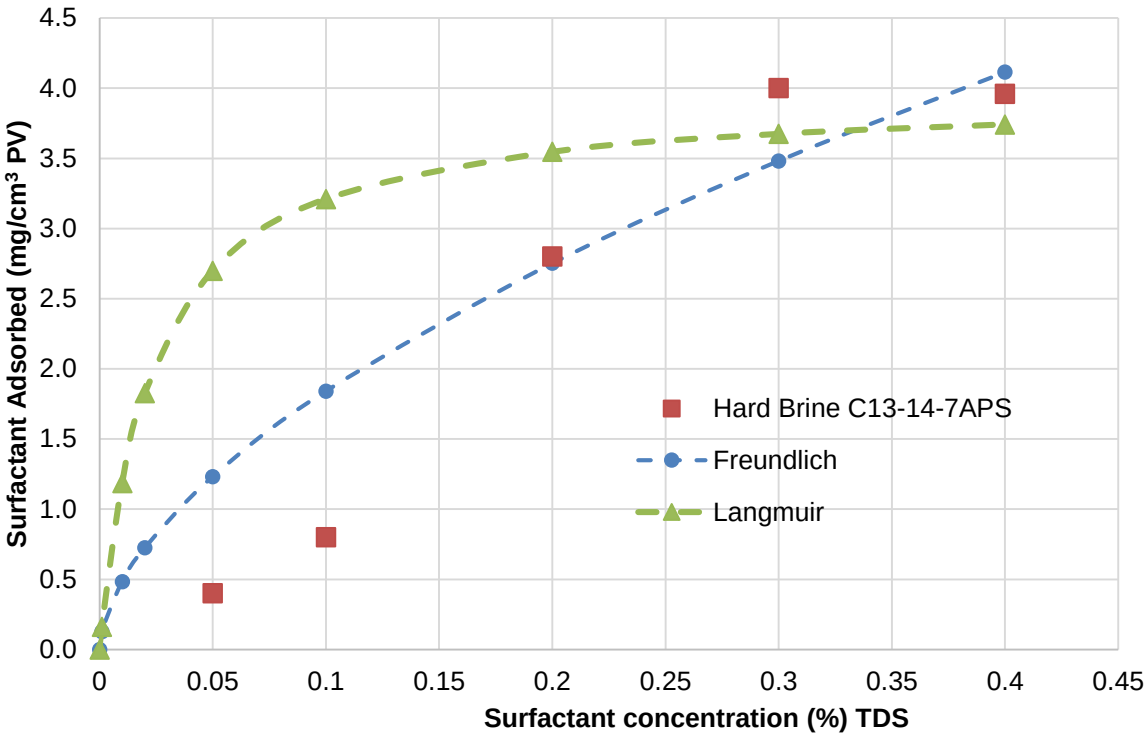


**Figure 5-66: Adsorption for surfactant $C_{13\text{-}14}$-7APS in HB and isotherm models (Freundlich and Langmuir)**

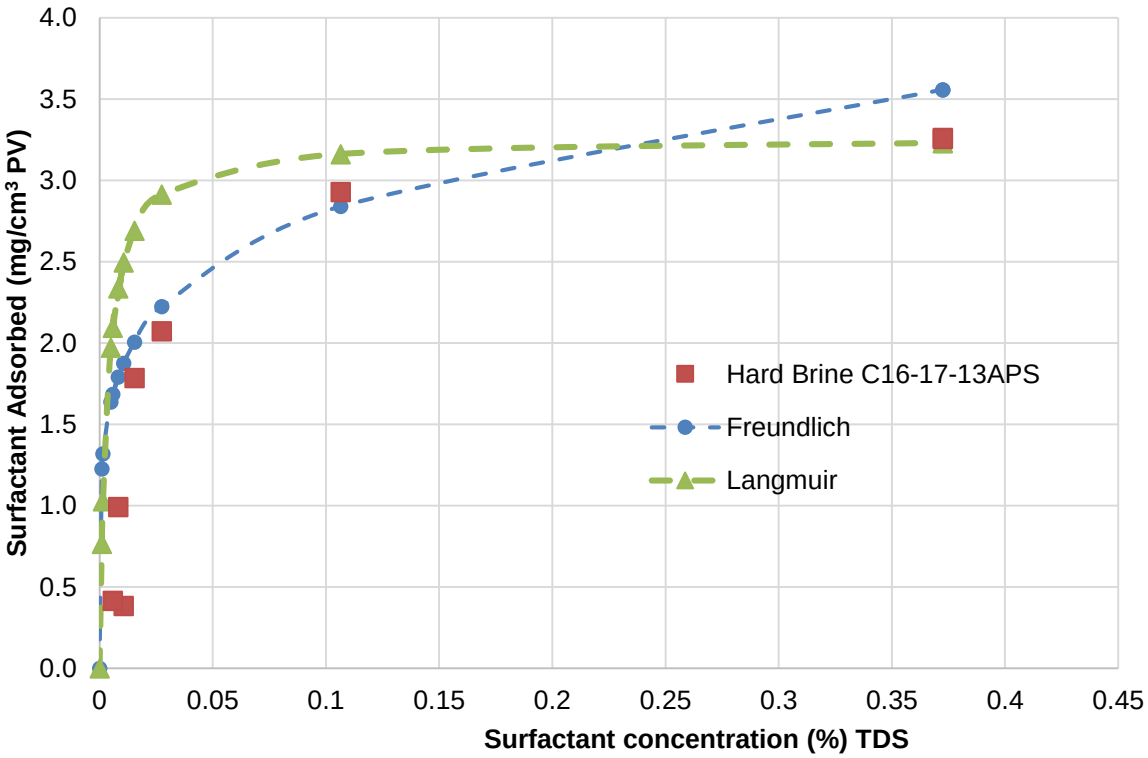


**Figure 5-67: Adsorption for surfactant $C_{16\text{-}17}$-13APS in HB and isotherm models (Freundlich and Langmuir)**

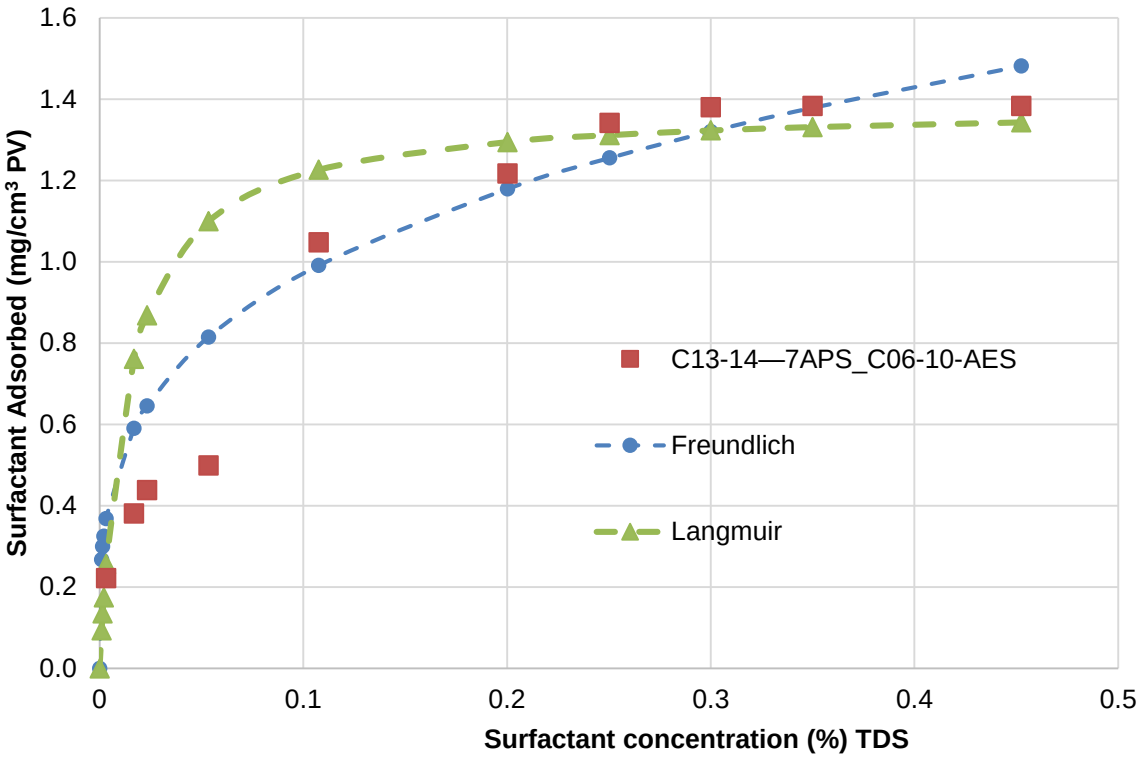


**Figure 5-68: Adsorption for surfactant $C_{13-14}$-7APS-$C_{06-10}$-AES in HB and isotherm models (Freundlich and Langmuir)**

It should be noted that the method used to analyse this surfactant adsorption is dependent on acquiring a steep calibration curve for a more accurate interpretation. The adsorption of surfactants is affected by electrostatic, chemical and associative interactions, solvation interactions (Azam *et al.*, 2013). Some sources of errors of the method are the calibration of surfactant absorbance as a function of surfactant concentration which needs to consider the salinity concentration. Any contamination of the surfactant solution will affect results. Moreover, any variation of salinity concentration needs to be included in calibration curves.

Results presented on this chapter evidence the effect of the brine on the selection of the chemical formulation, especially for applications with HB. The increase in oil recovery obtained by the synergy between alkali and surfactant and surfactant and co-surfactant and the positive effect of complexing agents such as EDTA for applications with HB was also analysed.

# CHAPTER SIX: STUDY OF POLYMERS, SURFACTANT-POLYMER AND ALKALI-SURFACTANT-POLYMER CEOR UNDER HIGH SALINITY AND HARD BRINE

## 6.1. Introduction

This chapter presents the methodology for the study of acrylamide polymers and their interactions with alkali and surfactants for SP and ASP chemical enhanced oil recovery (CEOR) under high salinity and hardness given by divalent cations $Ca^{2+}$ and $Mg^{2+}$. It also presents the results from this study, and relative permeability obtained from history matched core-flooding tests using a laboratory-scale simulation model are discussed.

This stage of the research was aiming to:

- Evaluate the comparative stability of acrylamide type polymers under brine salinity and divalent cations $Ca^{2+}$ and $Mg^{2+}$ existing in the North Sea reservoirs.
- Study the interactions of polymers with alkali and surfactant under the effect of brine salinity and hardness in SP or ASP chemicals injection systems for CEOR processes.

Results from this study contribute to the understanding of the properties and relevant mechanisms for CEOR under the effect of brine salinity and hardness. The advantages of the design parameters for the process and the synergy between chemicals for SP and ASP CEOR are also outcomes from this part of the project.

## 6.2. Methodology

The steps followed to complete this part of the research are included in this section and the methods were explained in chapter 3.

A total of 10 commercial acrylamide-based polymers were evaluated in this study. The type of polymer comprised 4 partially hydrolysed polyacrylamide (PHPA) of different molecular weight, 2 co-polymers AM-AMPS, AM-nVP and 4 Comb-type ter-polymers HMPAM. The common aspect of these polymers is that they have similar hydrolysis grade (anionic grade) and the differences are molecular weight and structure. Details of the polymers used in this study are presented in table 6-1.

**Table 6-1: Characteristics of Polymers type acrylamide with anionic charge (25-30%) used for this study**

| Polymer type | Polymer type | Molecular weight (Dalton) | Active fraction of polymer, % |
|---|---|---|---|
| Homo-Polymer Partially Hydrolyzed Polyacrylamide | PHPA -6 | High (20) | 90.0 |
| | PHPA-5 | Medium High (16) | 90.9 |
| | PHPA-4 | Medium (12) | 89.9 |
| | PHPA-3 | Low (8) | 91.2 |
| Co-Polymers | AM-AMPS | Low (8) | 90.3 |
| | AM-n-VP | Low (8) | 89.9 |
| Hydrophobic Modified Ter-polymers Polyacrylamide | HMPAM-1 | Low –Medium (9.5-12) | 88.6 |
| | HMPAM-2 | Medium High (12-16) | 88.6 |
| | HMPAM-3 | High (16-19) | 88.6 |
| | HMPAM-4 | Ultra-High (19-22) | 88.6 |

The chemical structure of the polymers studied in this part of the research is presented in Figure 6-1.

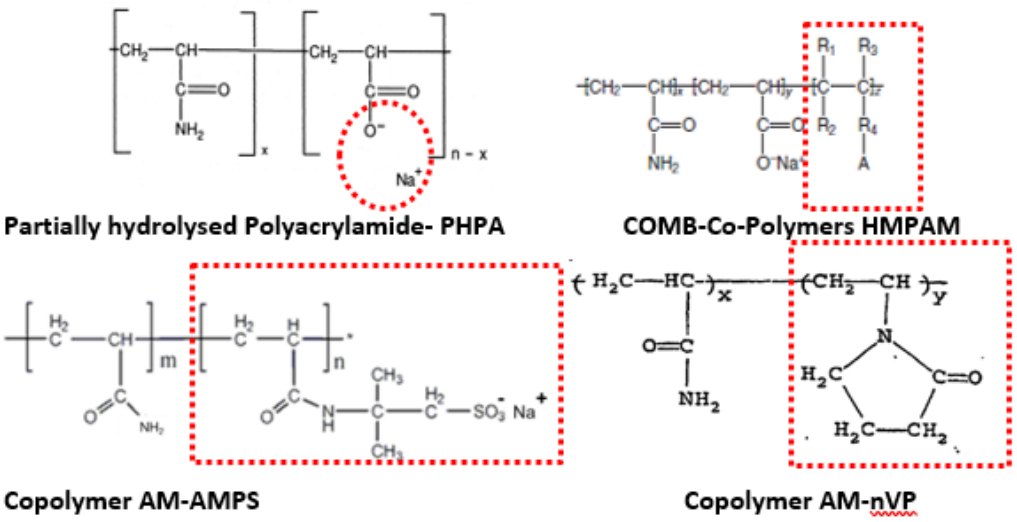


**Figure 6-1: Chemical structure of acrylamide based polymers tested**

Surfactants and alkali/surfactant systems that exhibited microemulsion formation (chapter 5) at ultra-low IFT and a large salinity range for microemulsion formation, were selected for the study. The chemical systems S and AS selected were as follow:

Two surfactants S: $C_{13\text{-}14}$—7APS + $C_{06\text{-}10}$-AES, Blend 1

Two blends AS: EDTA/NaOH/ $C_{13\text{-}14}$-7APS Blend 2

$NaBO_2$/ $C_{13\text{-}14}$-7APS. Blend 3

Two types of polymers, partially hydrolysed polyacrylamide PHPA-6 and comb-type hydrophobic modified polymer HMPAM-3 were selected at a concentration of 0.25% (2500 ppm). Polymer concentration was selected based on the minimal requirements to have a favourable viscosity for the crude oil µp > µoil to support a mobility ratio lower than one. Details are presented in Table 6-2.

**Table 6-2: Alkali, surfactant and polymer mixes tested for fluid-fluid interactions**

| Blend | Chemicals A-S-P (0.2%AS-0.25%P) | IFT (mN/m) | Range of salinity and (Optimal Salinity) (TDS) % m/v | Range of concentration for divalent Ions (Ca & Mg) % (m/v) | Csep calculated assuming a value of β=10 |
|---|---|---|---|---|---|
| Blend 1 (SP) | $C_{13\text{-}14}$—7APS + $C_{06\text{-}10}$-AES + PHPA-6 or HMPAM | $1.34 \times 10^{-3}$ | 2.8 to 4.8 (3.8) | 0.144 to 0.22 | 1.58 |
| Blend 2 (ASP) | EDTA/NaOH/ $C_{13\text{-}14}$-7APS + PHPA-6 or HMPAM | $5.31 \times 10^{-5}$ | 2.6 to 3.9 (3.6) | 0.106 to 0.18 | 1.5 |
| Blend 3 (ASP) | $NaBO_2$/ $C_{13\text{-}14}$-7APS + PHPA-6 or HMPAM | $2.45 \times 10^{-4}$ | 2.0 to 4.0 (3.2) | 0.085 to 0.169 | 1.3 |

The methodology proposed for the study is presented in Figure 6-2.

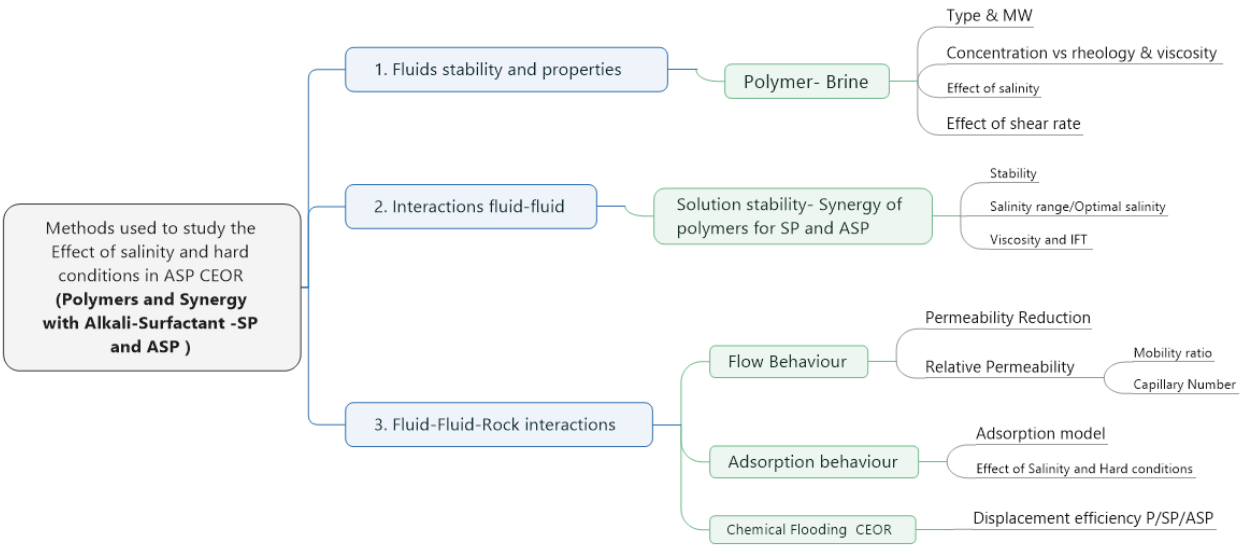


**Figure 6-2: Methodology for the study of the effect of brine salinity and hardness on optimal conditions of polymers solutions**

In the fluid stability and properties first stage, the stability and the behaviour of polymers are studied; the effectiveness of the polymer to increase the viscosity of brine solutions at different salinity and with divalent cations $Ca^{2+}$ and $Mg^{2+}$. The study of the stability of polymer solutions with brine was completed following the procedure illustrated in Figure 6-3.

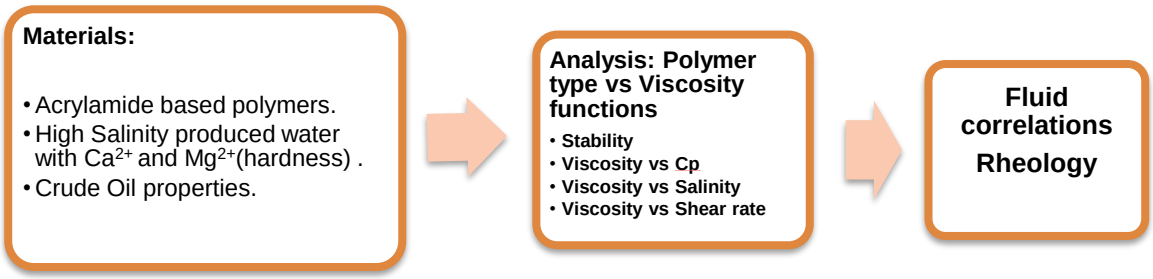


**Figure 6-3: Methodology for the study stability of polymers and effect of salinity and divalent cations**

The rheological behaviour of polymers is studied at the range of shear rate that represents reservoir flow conditions, aiming to identify differences between polymers, possible structural-relationship and categorise the required polymer concentration to obtain optimal requirements of viscosity for mobility ratio.

The concomitant effect of polymer concentration, salinity, divalent cations and the shear rate at flow conditions on the ability of the polymer to keep a favourable viscosity is assessed using mathematical correlations between the different variables. Results from this analysis are relevant to compare the effectiveness of polymers for different applications. They are also used for pressure calculations of the flow of polymer in the porous media during chemical flooding EOR processes.

To analyse the effect of salinity and divalent ions on the viscosity of the blends SP and ASP, the viscosity at different effective salinity Csep was measured for samples prepared on the range of salinity of ultra-low IFT for each blend and keeping a constant shear rate at 8 1/s.

A second stage (2 on the diagram) interactions fluids-fluids aims to study the synergy of polymers with blends of surfactant and alkali-surfactant to increase viscosity and reduce interfacial tension IFT.

The methodology followed for this part of the research is presented in Figure 6-4. Parameters to be evaluated are the viscosity, interfacial tension, and the effect of these variables on the capillary number and mobility ratio.

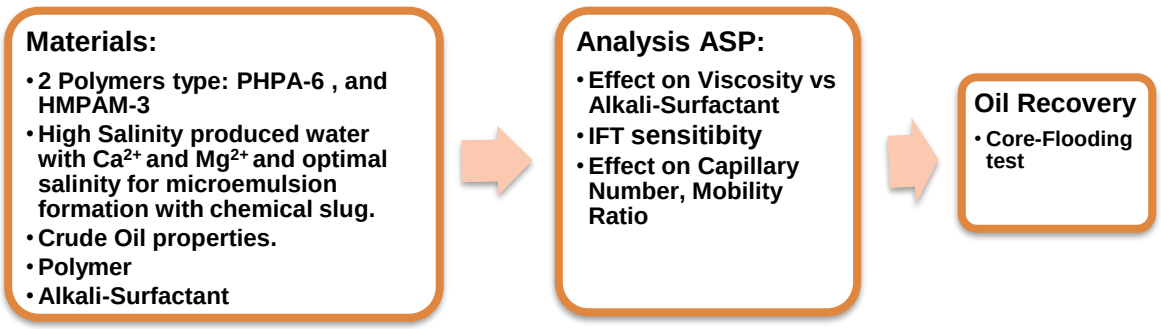


**Figure 6-4: Methodology for the study of synergy of polymers with alkali-surfactant systems and effect of brine salinity and hardness**

Phase separation tests were completed for blends of polymers with S and AS blends for chemical systems with oil in order to evaluate the effect of the chemicals interactions on the optimal salinity for minimal IFT and micro emulsion formation. For this purpose, polymers were added to each blend, on the range of salinity obtained for S and AS blends, following the method for phase separation tests explained in chapter 3.

The viscosity of the formed microemulsion was measured at fixed shear rate of 8 1/sec using the viscometer as described in chapter 3.

A stage 3 fluid-fluid-rock interactions aims to study the behaviour of polymers and the synergy with alkali and surfactant while flowing inside the porous media under reservoir conditions is completed. Results from core flooding tests were analysed to determine the behaviour of relative permeability curves for water flooding, polymer flooding P, SP and ASP under reservoir conditions. The analysis also involves a comparison of the displacement efficiency $E_D$ obtained by the injection, through core-flooding experiments of the chemical systems, thus P, SP and ASP CEOR process at laboratory scale. Results from each stage are presented and discussed in detail in the following sections.

## 6.3. Results and discussion

### 6.3.1. Fluids stability and properties of polymers and effect of brine salinity and hardness

This section presents the results of the effectiveness of polymers to increase the viscosity considering different variables. Results are offered on the following sub sections as described:

1. Section 6.3.1.1: Experimental results of the viscosity of polymers versus polymer concentrations.
2. Section 6.3.1.2: Results of the effect of salinity and divalent cations on the viscosity of polymers are presented.
3. Section 6.3.1.3: Discussion of the effect of shear rate on the viscosity of polymers.
4. Section 6.3.1.4: Study of the synergy of the effect of salinity, divalent cations and shear rate by fine-tuning of experimental data using mathematical correlations.

#### 6.3.1.1. Viscosity as a function of polymer concentration

Results show the viscosity of polymer solutions increases with polymer concentration, this can be noticed in Figures 6-5 to 6-9. Comb-type polymers, co-polymers, and PHPA polymers have similar trends and viscosity increases with polymer concentration; however, apparent viscosity values obtained for HMPAM polymers are remarkable higher than for PHPA at equivalent MW as shown in Figures 6-5 to 6-9.

Also, it can be observed that the increase of the molecular weight of polymers positively affects the viscosity of polymers solutions at the same concentration. High molecular weight (MW) results in higher viscosity. It is important to notice that as the polymer concentration increases, the difference of viscosity of the polymer solution of brine solutions is larger; showing an exponential relationship between viscosity and polymer concentration. These results are very relevant in terms of the selection of the polymer which requires a minimal concentration with favourable viscosity (Kaminsky *et al.*, 2007).

All polymer solutions require a minimal polymer concentration to have a significative effect on the viscosity of the solution. In Figures 6-5 and 6-6, this value is on the range of lower or equal to 0.1% for all polymers, however, it seems this minimal concentration depends on the type and MW of the polymer. HMPAM polymers require a low concentration to increase the viscosity (Figure 6-7). Despite co-polymers are recommended for high salinity, their viscosity

is considerably low compared to HMPAM and PHPA polymers (Figures 6-6 and 6-9), a high concentration is required for this polymer to achieve high viscosity.

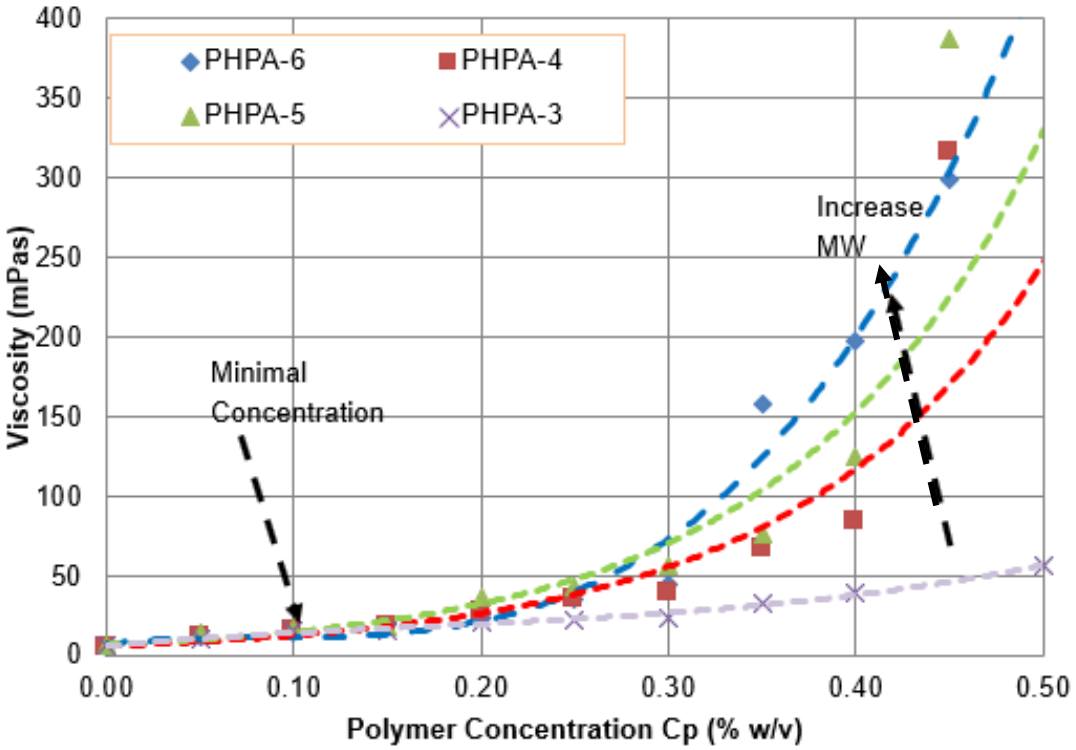


**Figure 6-5: Viscosity vs Polymer Concentration for PHPA polymer in SB 5.7% TDS (140 ºF)**

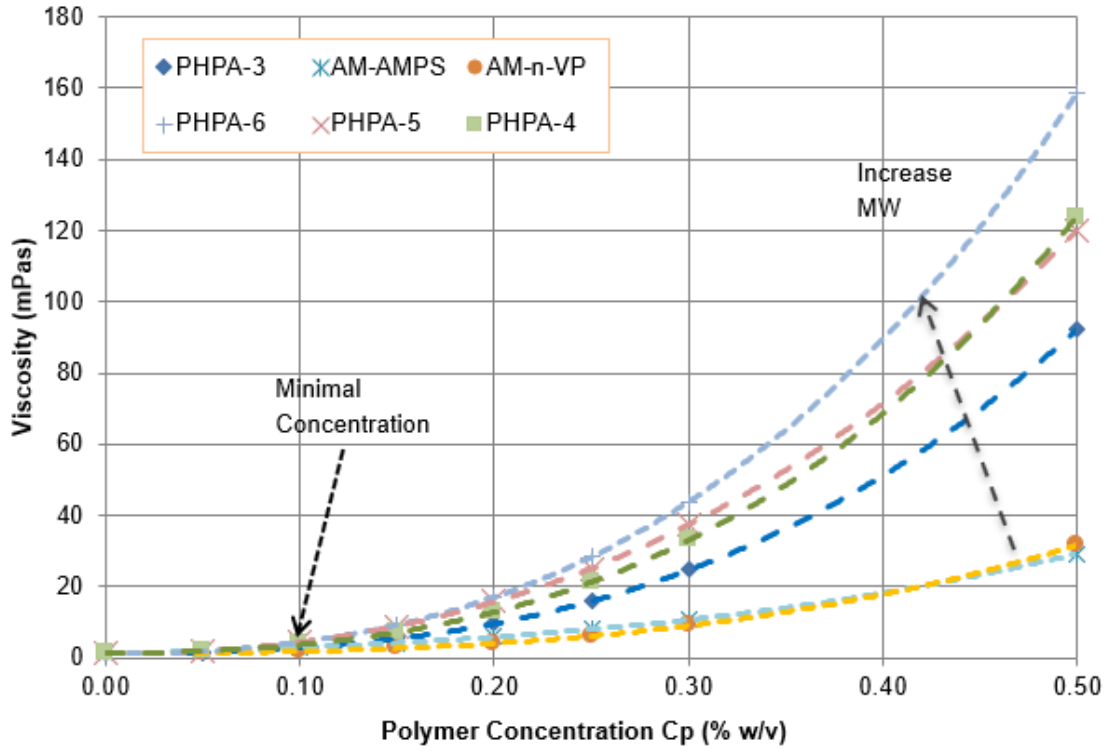


**Figure 6-6: Viscosity vs Polymer Concentration for PHPA polymer in HB 6.6% TDS (140 ºF)**

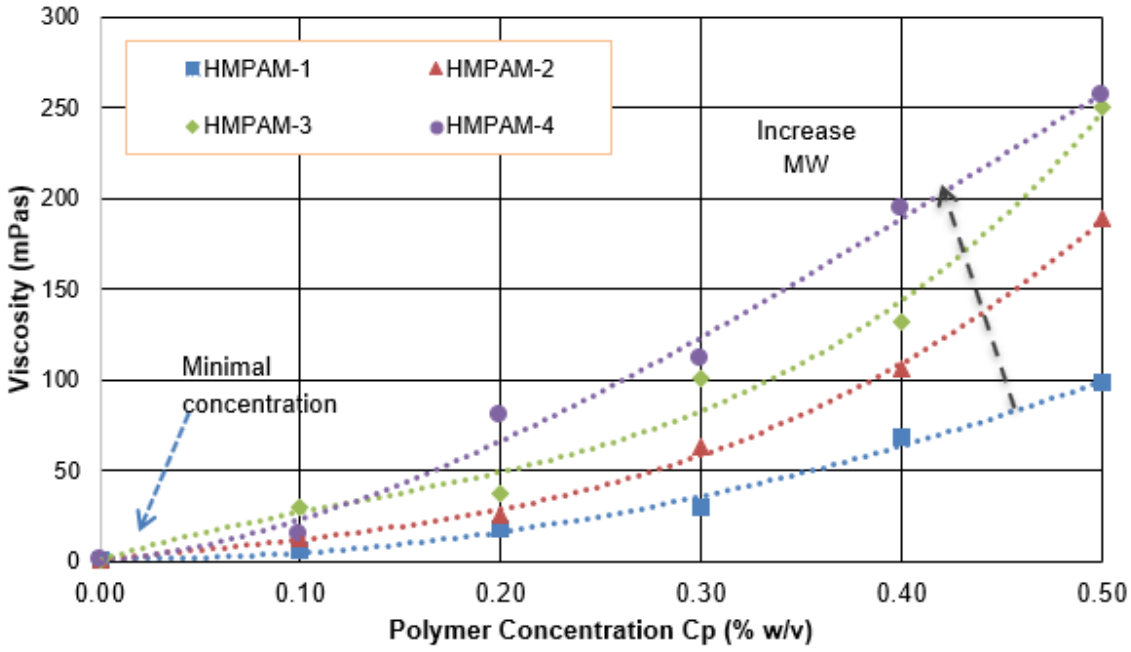


**Figure 6-7: Viscosity vs Polymer Concentration for HMPAM polymer and Co-Polymers in SB 5.7% TDS (140 ºF)**

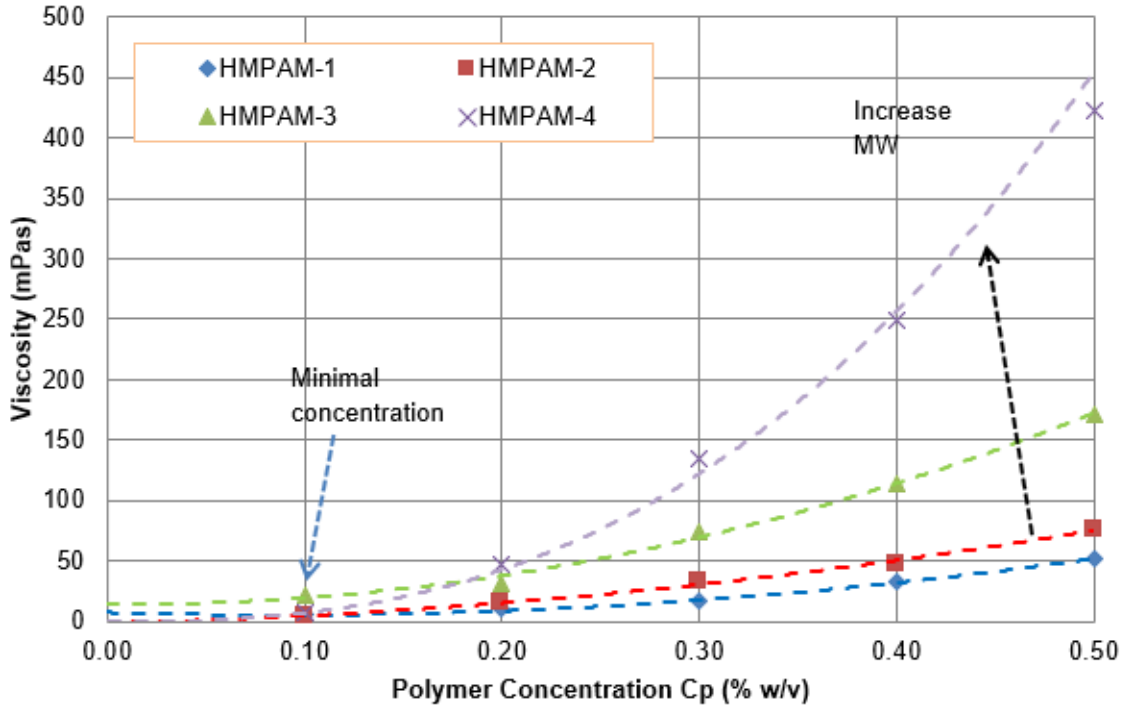


**Figure 6-8: Viscosity vs Polymer Concentration for HMPAM polymer and Co-Polymers in HB 6.6% TDS (140 ºF)**

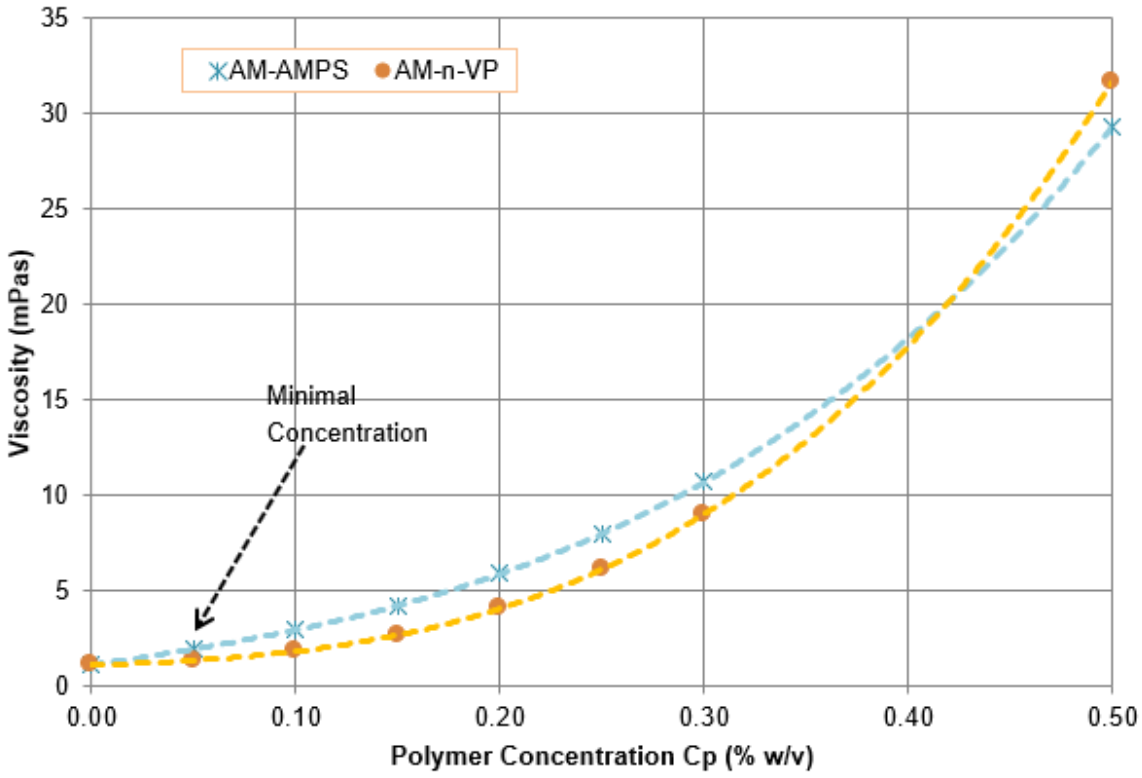


**Figure 6-9: Viscosity vs Polymer Concentration for AM-AMPS and AM-n-VP polymers in HB 6.6% TDS (140 ºF)**

#### 6.3.1.2. Polymer viscosity as a function of salinity

Salinity reduces the viscosity of polymer solutions. The viscosity measured for HMPAM is highly affected by salinity, however the apparent viscosity for these polymers is more than 30% higher than for polymers AM-AMPS, AM-n-VP and PHPA in the range of salinity evaluated. This observation concurs with results reported by the manufacturer of HMPAM polymers (www.hengju.com).

Co- polymer AM-n-VP keeps almost constant viscosity for the range of salinity evaluated, and the same behaviour was observed for the co-polymer AM-AMPS between 3.5 to 4.8 % salinity. These results can be visualized in Figure 6-10. Viscosity resistance to brines with high salinity and hardness is consistent with the behaviour reported on the literature for this type of polymers (Levitt and Pope, 2008; Vermolen *et al.*, 2011; Sheng, 2013a).

At high salinity (> 3.5 % TDS) PHPA polymers have a minimal variation on viscosity due to changes in molecular weight. However, at low salinity the variations on viscosity by changes in salinity are significative. This result is presented as regions in Figures 6-10. For PHPA, polymer viscosity is more dependent on salinity than molecular weight at high salinity.

The viscosity behaviour observed for HMPAM polymers with the increase of salinity is more complex and some differences were observed for each polymer. While there is a reduction of viscosity by the effect of salinity until about 5% TDS salinity for the two polymers with medium-high MW (HMPAM-2 and HMPAM-3), the viscosity behaviour of polymers HMPAM-1 and HMPAM-4 (Low and ultra-high MW) presents two zones with respect to salinity. The viscosity keeps steady or slightly drop for salinities lower than 4% TDS, followed by viscosity drop for salinities between 4% and 5% TDS. For all polymers, the viscosity tends to stabilize at salinity higher than 5% TDS. These results are presented in Figure 6-11.

Divalent ions $Ca^{2+}$ and $Mg^{2+}$ significantly reduce the viscosity of the polymer solution compared to monovalent ions, this effect can be noticed comparing viscosity values presented on graphs in Figures 6-5 and 6-6 for PHPA polymers and 6-7 and 6-8 for PHPAM.

Similar behaviour of viscosity as function of polymer concentration and salinity for polymer solutions has been reported (Levitt and Pope, 2008; Vermolen *et al.*, 2011; Zhu, Y. *et al.*, 2015). The increase of viscosity by polymers in aqueous solutions occurs by repulsion of existing charges along the polymer backbone which makes the polymer to extend. However, as salinity increases, ions in solutions overlap polymer charges, in a process defined as “shielding effect”. This shielding effect makes the polymer molecule to shrink as salinity

increases (Levitt and Pope, 2008). The proportion of ionic charges among the polymer skeleton is proportional to its hydrolysis grade.

From experimental results, the shielding effect is less evident in HMPAM than in PHPA polymers. The distribution of charges among the comb-polymer HMPAM is more complex compared to PHPA polymers. The backbone of HMPAM polymers includes combinations of hydrophilic and hydrophobic groups, which reduces the ionic forces and the flexibility of the molecule by steric effects. Besides, HMPAM polymers are less linear than PHPA polymers. Monomers of different functional groups as branches along the comb-polymer molecule makes the polymer structure more rigid so that the shielding effect under salinity is reduced (Zhu, Y. *et al.*, 2015).

The viscosity reduction as salinity increases for HMPAM can be explained as intra-chain interactions that can occur, with a resultant reduction on the hydrodynamic ratio of the polymer molecule. Formation of complex aggregates by inter and intra chain interactions between HMPAM polymers have been reported to occur in the presence of divalent ions (Wever *et al.*, 2011).

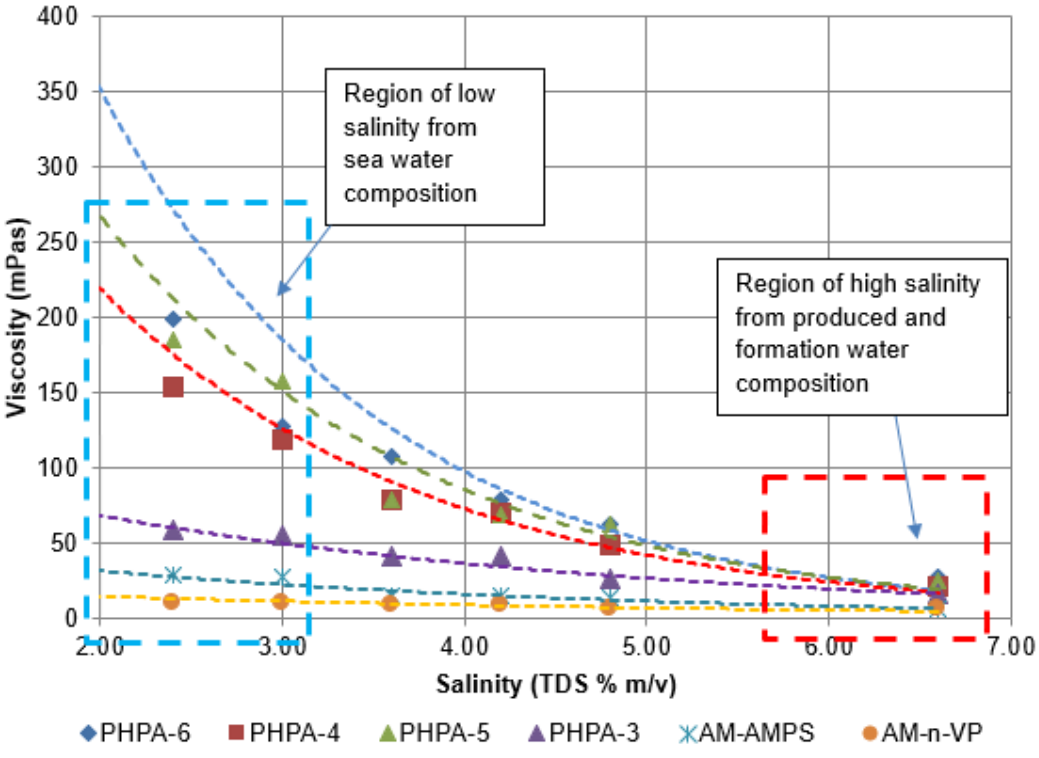


**Figure 6-10: Viscosity vs Salinity for PHPA polymers (0.25% m/v) (140 ºF)**

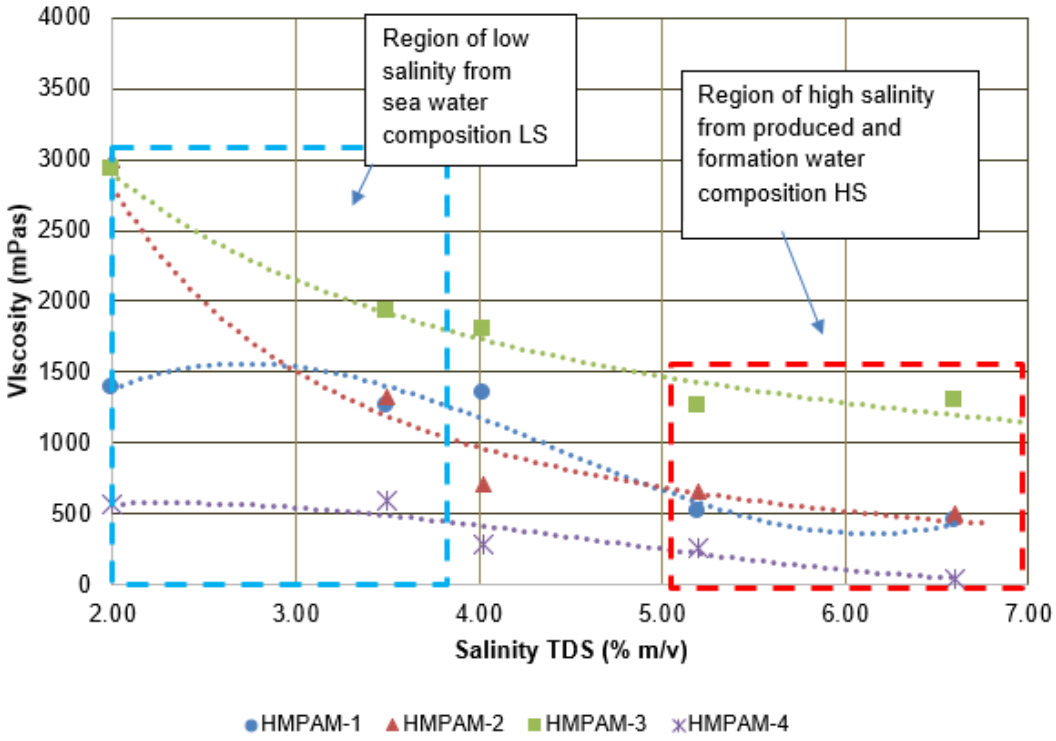


**Figure 6-11: Viscosity vs Salinity for HMPAM Comb-polymers (0.25% m/v) (140 ºF)**

Viscosity variations were investigated at two ranges of salinity, identified as high (HS-3.5-6.6% TDS) and low (LS- 0 to 3.5% TDS), from Figures 6-10 and 6-11. While viscosity of HMPAM polymers is considerably higher than the viscosity of the crude oil (21.4 cp) in both zones HS and LS, the variations of viscosity with salinity are higher than for PHPA polymers, especially for HMPAM-2 and HMPAM-3 at low salinity (Figures 6-12 and 6-13).

Comparing polymer viscosity with oil viscosity at HS and LS, it can be noticed that PHPA polymers with low molecular weight, thus PHPA-3, AM-AMPS, and AM-n-VP have less favourable viscosity for the crude oil under study. However, they can be considered for applications at low salinity. It is also noticeable that the viscosity of polymer AM-n-VP is the same for both zones LS and HS, which suggest good stability under salinity conditions. However, these polymers will require a higher concentration to increase the brine viscosity higher than crude oil.

The viscosity of the different HMPAM solutions is more affected by changes in salinity at low salinity. At high salinity, the viscosity of polymer solutions is less affected by molecular weight as most of the polymers tend to have similar low viscosity, the effect of salinity on the viscosity

of polymers is predominant for both types of polymers; this effect is called “salty effect” (Sheng, 2011).

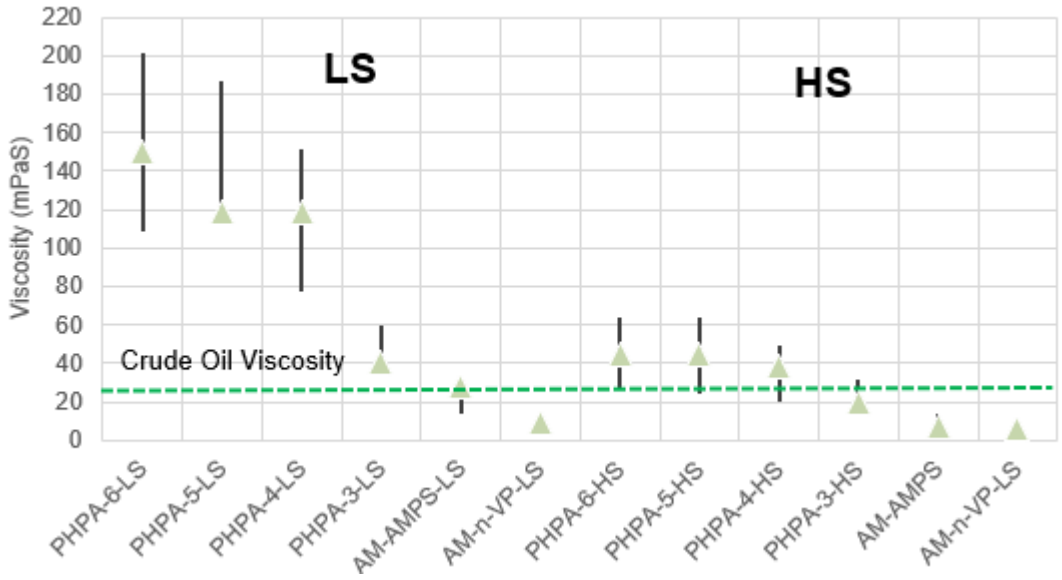


**Figure 6-12: Range of viscosity for low (LS) and high salinity (HS) for PHPA and co-polymers (0.25% m/v)**

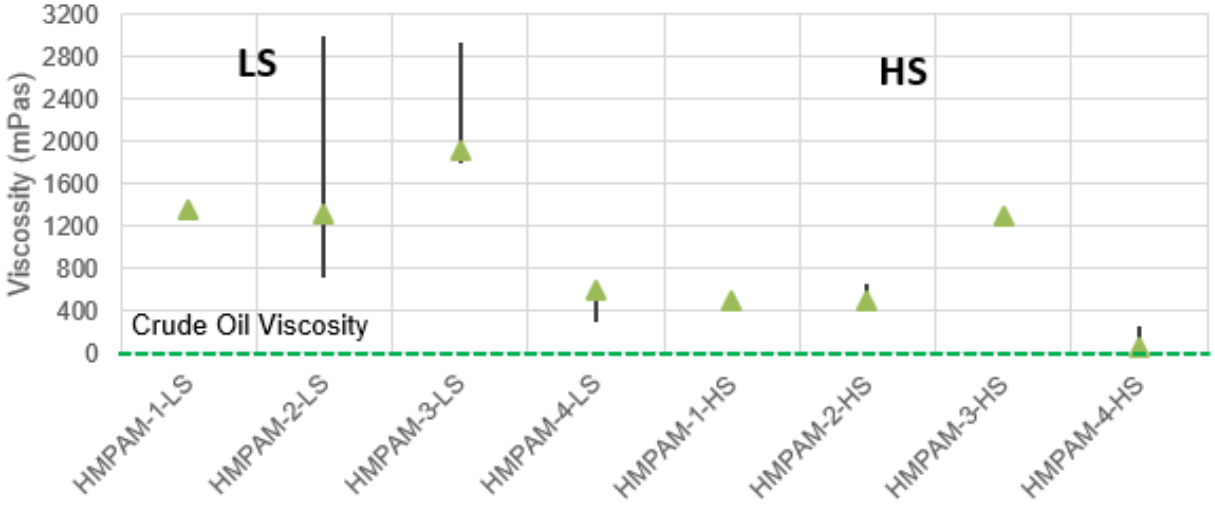


**Figure 6-13: Viscosity vs Salinity for HMPAM Comb-polymers (0.25% m/v)**

From these results, it is evident that polymers need to be tested for specific applications to assess the impact of the brine composition on the viscosity and decide on the needs for water treatment based on requirements for salinity for the chemical slug. HMPAM polymers develop viscosity at low concentration and even they are affected by salinity, yet viscosity can still be favourable for CEOR applications.

### 6.3.1.3. Polymer viscosity as a function of shear rate

On this section results from the evaluation of polymers solutions while flowing in the reservoir rock are presented.

The equivalent shear rate that represents the flow of the polymer in the porous media during core-flooding test was estimated using Karmen–Kozeny correlation (Lake,1989) for Newtonian fluids (equation 2-10). Shear rate is directly proportional to the flow rate and inversely proportional to the area of flow, a representation of the shear rate for different flow rates is presented in Figure 6-14.

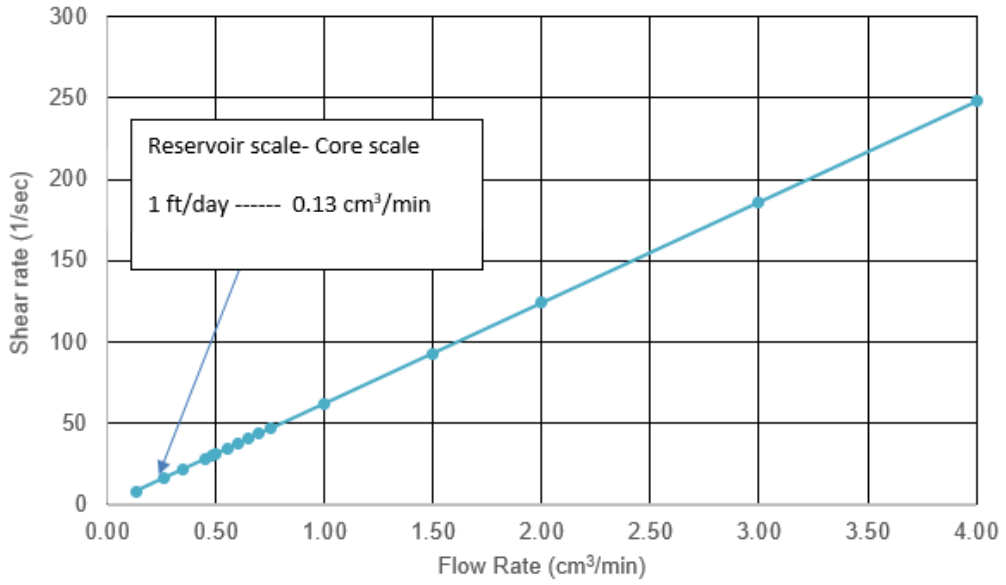


**Figure 6-14: Shear rate calculated for different flow rates using equation 6-4 and Bentheimer core samples properties.**

Shear rate as a function of permeability is presented in Figure 6-15, using an equivalent injection rate of 1ft/day (0.13 $cm^3$/min) at a laboratory scale in a 2.50 cm diameter core with an average porosity of 0.17 fraction. The average permeability of Bentheimer sandstones is 570 mD, thus the shear rate is around 8-10 1/sec. Typical shear rates expected in a reservoir are on the range of 1-10 1/sec depending on parameters such as rock permeability, porosity, and polymer flow rate (Lake, 1989).

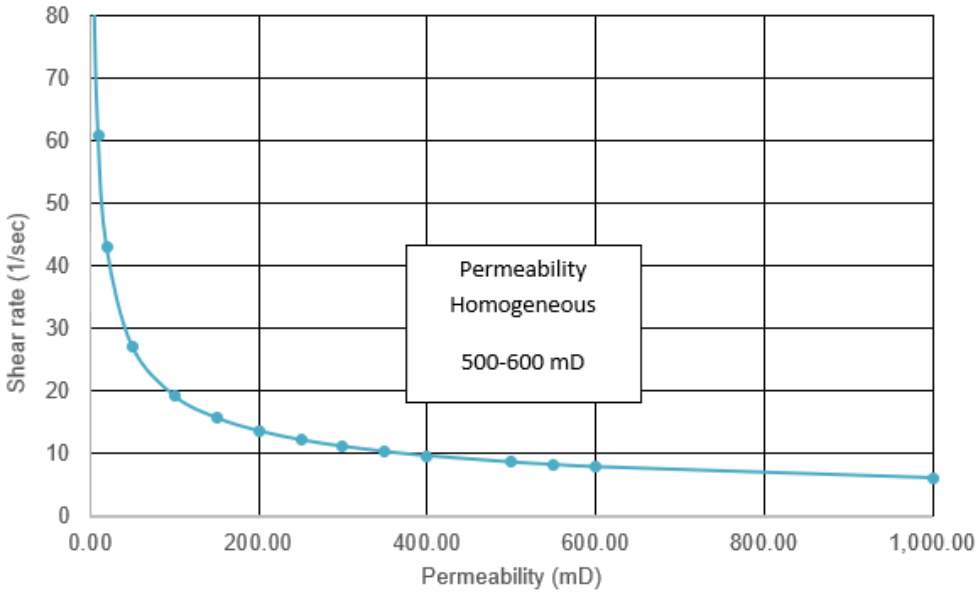


**Figure 6-15: Shear rate calculated for different permeabilities using equation 6-4 with porosity 0.17 fraction and a flow rate 0.13 $cm^3$/min and Bentheimer core samples properties.**

The viscosity of PHPA and HMPAM polymer solutions decreases with the increase of shear rate on the range 0.1 to 100 (1/sec), as shown in Figures 6-16 to 6-19, this range corresponds with permeabilities 50 to 1000 mD as presented in Figure 6-15. At low shear rates the polymer viscosity is constant as Newtonian viscosity for PHPA whereas decreases as Non-Newtonian for HMPAM, results are presented in Figures 6-16 and 6-18.

Salinity and divalent ions affect the viscosity behaviour of PHPA and HMPAM as a function of shear rate. The viscosity of PHPA polymers in HB shows Newtonian behaviour at low shear rates, followed by a zone of shear thinning, non-Newtonian behaviour viscosity at higher shear rates, details are represented in Figure 6-16. This zone of shear-thinning viscosity for PHPA polymer is different for each polymer but mainly occurs at values of shear rates lower than 10 (1/sec).

The viscosity behaviour of HMPAM solutions as a function of shear rate is shear thinning with a Newtonian behaviour region at high shear rate (indicated in Figures 6-18 and 6-19). The zone of Newtonian behaviour at low shear rate is not as evident as for PHPA polymers in the range of shear rated measured. The effect of salinity and divalent ions on the viscosity is not as significant as for PHPA polymer solutions at low shear rates (< 1 1/sec). However, at shear

rates higher than 1 (1/sec) the viscosity decreases by the effect of divalent ions, especially for polymers with high molecular weight HMPAM-3 and HMPAM-4 (Figures 6-18 and 6-19).

The effect of shear rate on the viscosity of PAM co-polymers AM-n-VP and AM-AMPS is similar PHPA; Newtonian at lower shear rate (< 10 1/sec) and non- Newtonian shear thinning behaviour at shear rates higher than 10 (1/sec) as is shown in Figures 6-16 and 6-17. The viscosity of HMPAM polymers solutions is more affected by shear rate than the viscosity for PHPA and co-polymer solutions. (Figures 6-16 and 6-18).

Similar effects of shear on polymer viscosity have been reported in previous research (Levitt, 2009; Sheng, 2011).

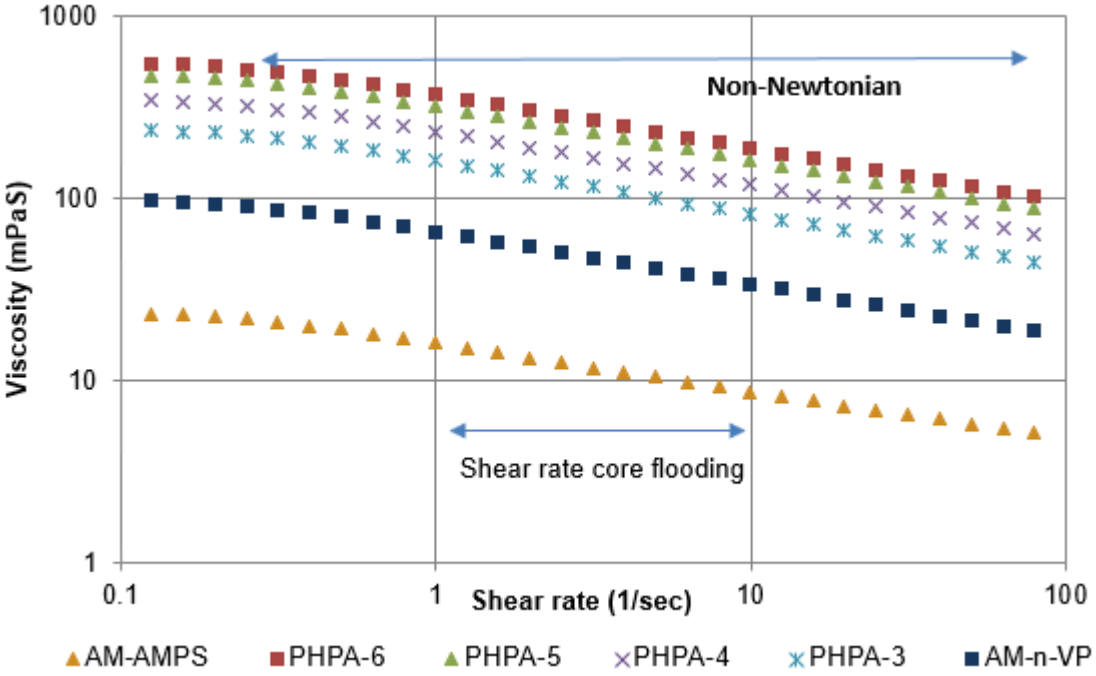


**Figure 6-16: PHPA and Co-Polymers Viscosity vs Shear rate 0.25% Polymer concentration SB 5.7% TDS non-divalent ions**

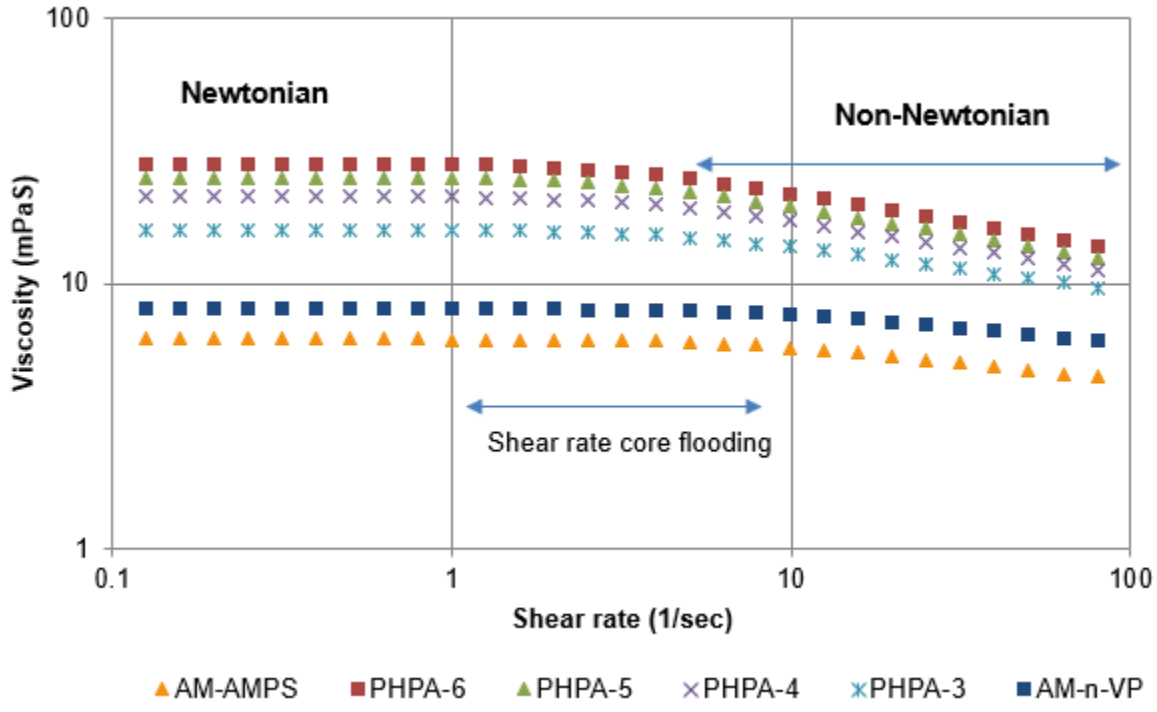


**Figure 6-17: PHPA and Co-Polymers Viscosity vs Shear rate 0.25% Polymer concentration HB 6.6% TDS**

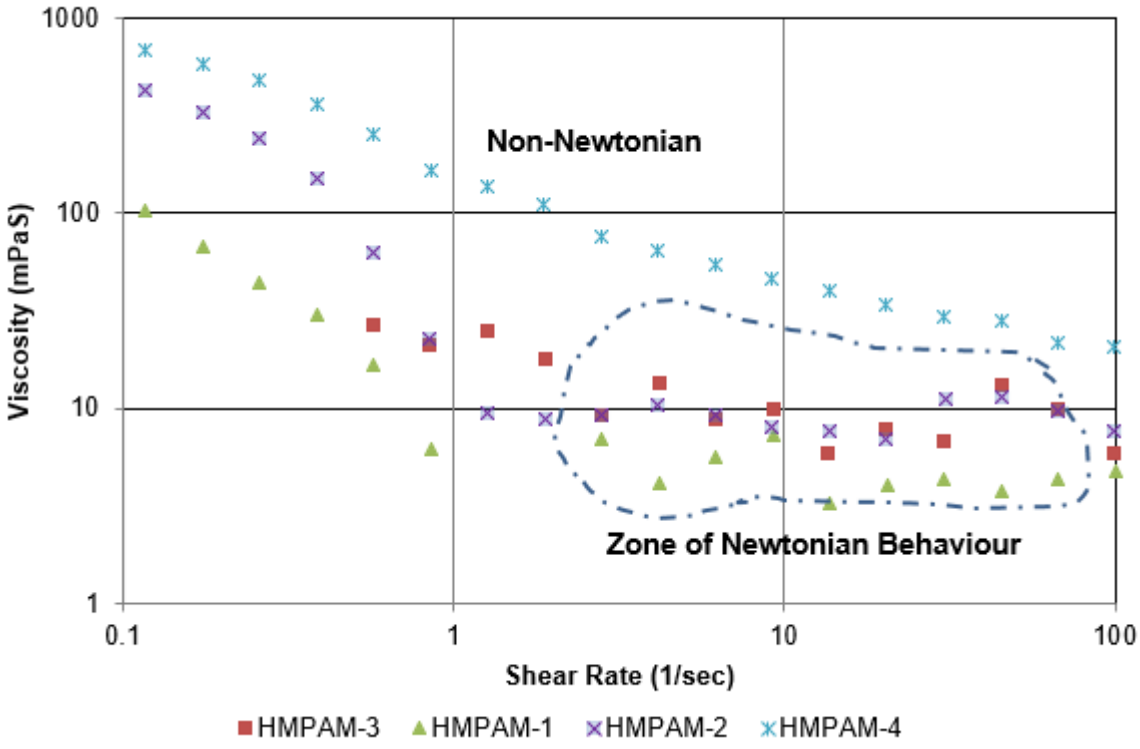


**Figure 6-18: HMPAM Viscosity vs Shear rate SB 5.7% TDS**

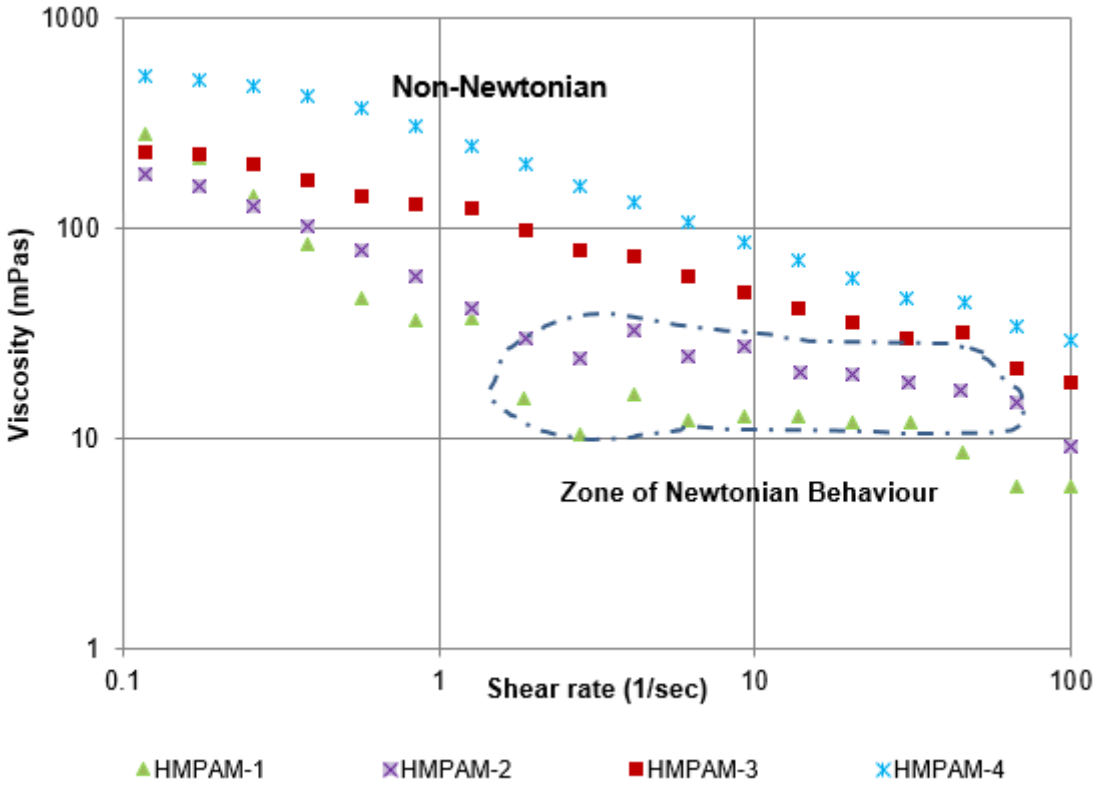


**Figure 6-19: HMPAM Viscosity vs Shear rate HB 6.6% TDS**

These results show the importance of predicting how the viscosity of polymer solutions are affected by flow conditions and the effect of salinity and divalent cations $Ca^{2+}$ and $Mg^{2+}$ of the injection and formation brine.

#### 6.3.1.4. Analysis of combined effect of polymer concentration, shear rate, salinity and divalent cations on polymer viscosity

Results from rheological tests for polymers presented on the previous sub section are relevant to analyse the behaviour of polymers under the different variables existing during the CEOR process, such as changes in concentration by polymer adsorption, deformation of fluid by shear rate, and interaction with salinity existing in the reservoir and used on the preparation of polymer solutions, a comparative studied of polyacrylamide.

The effect of combined variables on the resultant viscosity of polymers was analysed based on the fine tuning of parameters of the Flory-Huggins and Meter and Bird correlation (1964) as cited by Sheng (2011) (chapter 2- equation 2-43). These correlations include the dependence of polymer viscosity with polymer concentration and shear rate. The fitting of the value of polymer viscosity at zero shear rate $\mu_{p0}$ in both correlations, allowed the adjustment

of empirical parameters of both equations for each polymer. A protocol was followed and included in the appendix 1, parameters are presented in tables 6-4 to 6-7.

**Table 6-3: Parameters of PHPA polymers for Flory-Huggins correlation**
(Centeno *et al.*, 2017)

| | PHPA-6 | PHPA-5 | PHPA-4 | PHPA-3 | AM-n-VP | AM-AMPS |
|---|---|---|---|---|---|---|
| $A_{p1}$ | 3 | 0 | 11 | 2 | 4 | 17 |
| $A_{p2}$ | 350 | 435 | 143 | 124 | 22 | 14 |
| $A_{p3}$ | 1200 | 545 | 1000 | 654 | 232 | 147 |
| $C_{sep}$ (meq/cm$^3$) | 3.06 | 3.07 | 2.7458 | 2.7458 | 2.72 | 2.37 |
| $S_p$ | -0.49 | -0.47 | -0.43 | -0.36 | -0.31 | -0.24 |
| $\mu_w$ (mPas) | 1.14 | 1.14 | 1.14 | 1.14 | 1.14 | 1.14 |

**Table 6-4: Parameters of 2500 ppm HMPAM polymers for Flory-Huggins correlation**
(Centeno *et al.*, 2017)

| | HMPAM-1 | HMPAM-2 | HMPAM-3 | HMPAM-4 |
|---|---|---|---|---|
| $A_{p1}$ | 50 | 180 | 600 | 70 |
| $A_{p2}$ | 45 | 1000 | 900 | 1080 |
| $A_{p3}$ | 500 | 1000 | 2200 | 2800 |
| $C_{sep}$ (meq/cm$^3$) | 2.978 | 1.889 | 2.875 | 1.779 |
| $S_p$ | -1.256 | -3.118 | -1.633 | -1.018 |
| $\mu_w$ (mPas) | 1.97 | 1.14 | 1.17 | 1.17 |

**Table 6-5: Parameters of 2500 ppm PHPA polymers in HB for Meter's correlation**
(Centeno *et al.*, 2017)

| | PHPA-6 | PHPA-5 | PHPA-4 | PHPA-3 |
|---|---|---|---|---|
| $\mu o$, (mPas) | 28.41 | 25.16 | 21.31 | 15.92 |
| $\mu\infty$, (mPas) | 1.14 | 1.14 | 1.14 | 1.14 |
| $P\alpha$ | 1.72 | 1.72 | 1.69 | 1.68 |
| $(1- P\alpha) = n$ | 0.72 | 0.72 | 0.69 | 0.68 |
| $\gamma_{1/2}$ (1/sec) | 58.76 | 58.76 | 68 | 90 |

**Table 6-6: Parameters of 2500 ppm HMPAM polymers in HB for Meter's correlation** (Centeno *et al.*, 2017)

| | AM-AMPS | AM-n-VP | HMPAM-1 | HMPAM-2 | HMPAM-3 | HMPAM-4 |
|---|---|---|---|---|---|---|
| | 8.02 | 6.16 | 335.6 | 218 | 293 | 659 |
| $\mu^{\infty}$, (mPas) | 1.14 | 1.14 | 6.5 | 10 | 1.14 | 2.5 |
| Pα | 1.9 | 1.95 | 2.9 | 2.3 | 1.59 | 1.74 |
| (1- Pα) =n | 0.9 | 0.95 | 1.9 | 1.3 | 0.59 | 0.74 |
| $\gamma_{1/2}$ (1/sec) | 180 | 140 | 0.22 | 0.36 | 0.75 | 0.88 |

The effect of divalent ions and salinity, assessed by the factor $S_p$, is higher for HMPAM than for PHPA polymers. $S_P$ also seems to be associated with the MW of polymers HMPAM, as the effect is low for polymers with high MW (HMPAM-4). Except for polymer HMPAM-1, $S_p$ values decrease with the molecular weight. The higher values of $S_p$ are obtained for polymers HMPAM-2 and HMPAM-3 which is consistent with the high variations on viscosity with changes in salinity obtained for this polymer (Figure 6-11). Dependence of viscosity with salinity and divalent ions respect to molecular weight is opposite for PHPA and co-polymers. $S_p$ increases with the MW.

The parameter Pα is an indication of the rheological behavior of the polymer in the middle zone of shear thinning viscosity. The factor (Pα-1) is equal to the rheological behavior index (*n)*. Pα values are higher than 1 for all polymers.

The Pα factors for PHPA polymers have similar values and slightly increase with the MW of the polymer. For HMPAM polymers, Pα values are higher for polymers HMPAM-1 and HMPAM-2, indicating less shear thinning effect on the viscosity than for HMPAM-3 and HMPAM-4. Pα values are low for polymers with higher MW polymers, thus HMPAM-3 and HMPAM-4, these results are consistent with the graph of Figure 6-19.

AM-AMPS and AM-n-VP have a rheological index close to 1, which indicates Newtonian behavior. Those results are consistent with the information presented in Figure 6-17. The viscosity as a function of shear rate for PHPA, AM-AMPS and AM-n-VP show a similarly large range of shear rate with Newtonian behavior, thus the viscosity does not depend on shear rate, whereas the viscosity of HMPAM depends on shear rate, and the behavior is affected by the size of polymer molecules.

Comparing adjusted $\gamma_{1/2}$ parameters for PHPA and co-polymers with HMPAM polymers, higher values were obtained for PHPA than for HMPAM polymers. This result indicates that PHPA polymers have lower relaxation time than HMPAM polymers. The greater the $\gamma_{1/2}$ nominal value is for a polymer, the less relevant is the effect of shear rate on the viscosity of polymer solutions as the relaxation time is short. PHPA polymers behave as Newtonian in a

range of low shear rates < 5 (1/s) whereas HMPAM polymers behave as no-Newtonian on the range of shear rate evaluated. While for PHPA polymers the value of γ ½ decrease with the molecular weight of the polymer, opposite results are found for HMPAM, thus γ ½ values increase with the MW of the polymer. Results for Co-polymers AM-AMPS and AM-nVP are very similar than for PHPA polymers, due to the Newtonian behavior in most of the range of shear rate used for viscosity tests.

The viscosity correlations calculated as a function of shear rate from the adjustment of the experimental parameters are very close for PHPA and acceptable for HMPAM polymers with some deviations at high shear rates. It is important to notice some differences between measured values and the values estimated by the rheological parameters found for polymers HMAPM-1 and HMPAM-2 between shear rates (8-90 1/sec). The mathematical correlation underestimate polymer viscosities; at low shear rates experimental and fitted values are very similar (Figures 6-20 and 6-21)

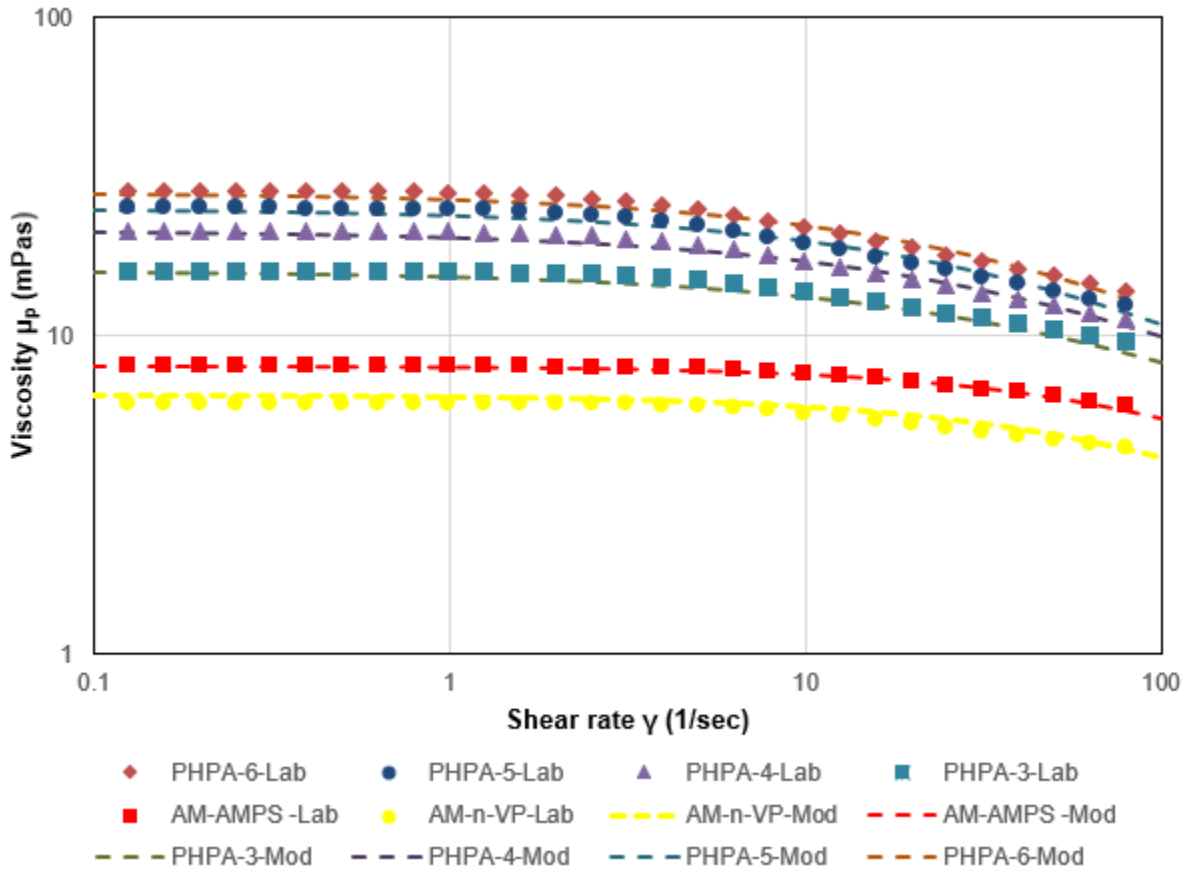


**Figure 6-20: Viscosity versus shear rate based on adjusted parameters for PHPA and co-polymers**

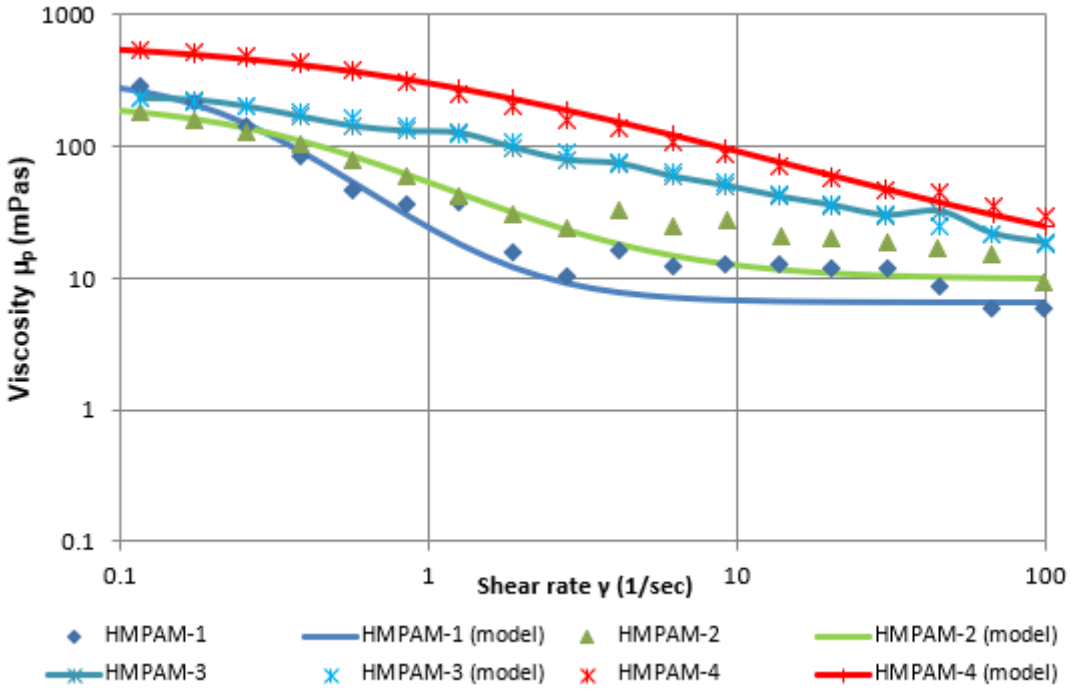


**Figure 6-21: Viscosity versus shear rate based on adjusted parameters for HMPAM polymers**

These results evidence differences in the rheological behaviour of polymers PHPA and HMPAM. The model assumes a viscosity of polymer close to the viscosity of brine at a high shear rate for the variable $\mu_\infty$, which underestimates experimental values with HMPAM polymers. However, for polymers HMPAM-1 and HMPAM-2 the viscosity at high shear rate had to be assumed as 6.5 and 10 mPa-s respectively to match mathematical correlations. An underestimated polymer viscosity would predict an under-performance of the polymer compared to the experimental behaviour. Results obtained for polymer viscosity versus concentration considering the effect of shear rate salinity and divalent cations $Ca^{2+}$ and $Mg^{2+}$ were verified for PHPA and HMPAM polymers and the values were very close (Figures 6-22 and 6-23).

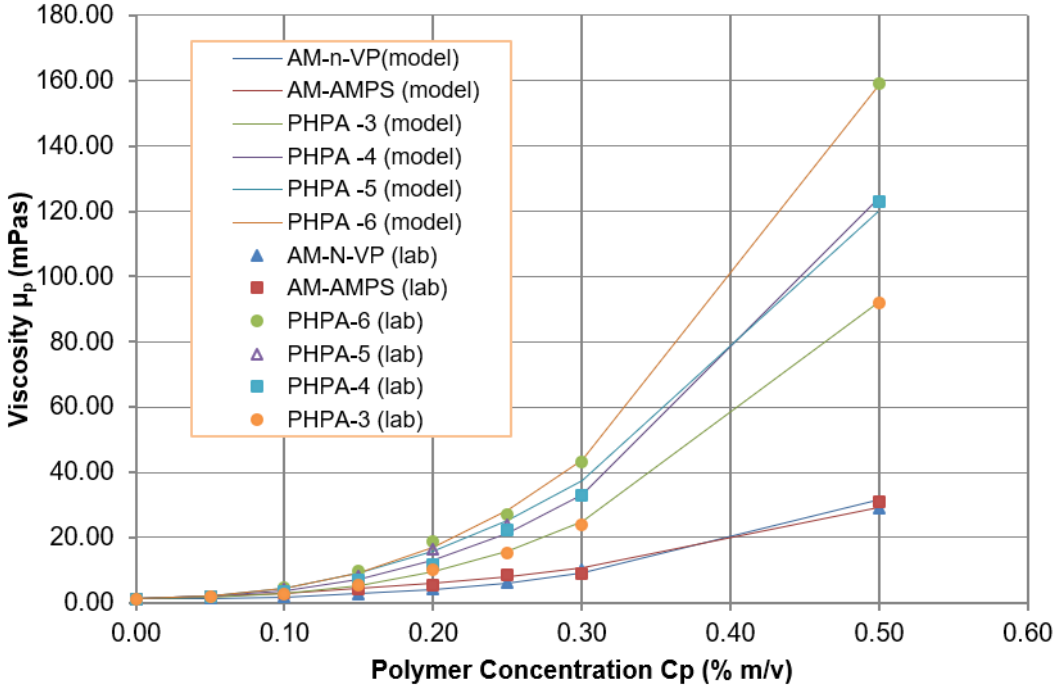


**Figure 6-22: Viscosity vs Polymer Concentration for PHPA polymers and Co-Polymers on HB 6.6% TDS determined by mathematical correlations**

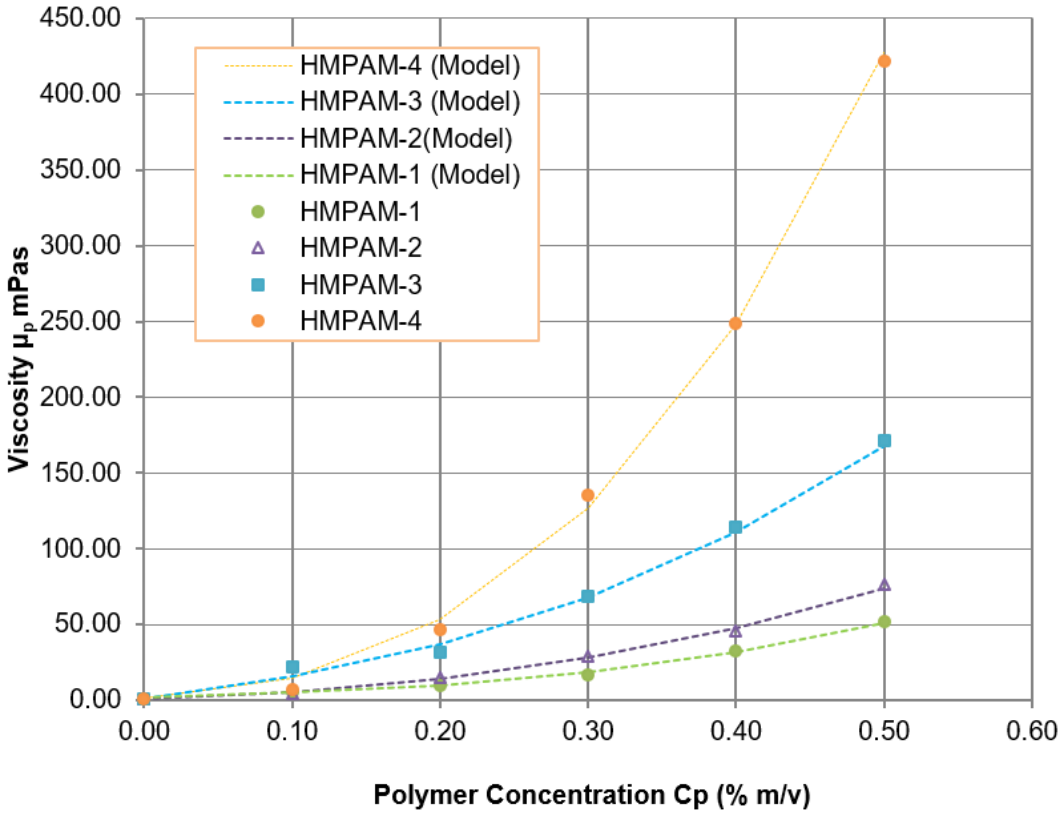


**Figure 6-23: Viscosity vs Polymer Concentration for HMPAM polymers in HB 6.6% TDS determined by mathematical correlations**

Despite HMPAM polymers are highly affected by salinity, they are able to develop viscosities 30% higher than PHPA polymers. The structure and size of acrylamide type polymers affect their viscosity behaviour in aqueous solutions. Moreover, polymer viscosity is reduced by salinity and divalent cations $Ca^{2+}$ and $Mg^{2+}$, and the mechanism is associated with ionic interactions within existing charges among the polymer molecule and with ions in the solution. These ionic interactions are more complex for HMPAM. The shear rate also affects polymer viscosity with more effect on HMPAM polymers.

### 6.3.2. Fluid –fluid interactions for SP or ASP under brine salinity and hardness

In this section, further evaluation of surfactants and alkali are presented from the study of the chemicals interactions of SP and ASP systems. The aim of this stage was to evaluate the effect of combining polymers with the selected alkali-surfactant chemical system (explained in the previous chapter) and the effect of salinity and divalent cations on the viscosity and IFT of SP and ASP systems.

Results are presented on the following subsections as described:

1. Section 6.3.2.1: Stability and properties of chemical systems.
2. Section 6.3.2.2: Analysis of the effect of salinity range and optimal salinity on viscosity.
3. Section 6.3.2.3: Study of IFT microemulsion formation and viscosity for SP and ASP.

#### 6.3.2.1. Stability and properties of alkali, surfactant and polymer for ASP CEOR

Results from stability tests showed no visual indication of cloudiness or precipitate for all blends of brine-alkali-surfactant or brine-surfactant with polymers.

Apparent viscosity of blend 1 and 2 with both polymers are slightly lower than the viscosity of polymer solutions, however, changes on viscosity are more obvious for blend 1 with PHPA polymer and for blends 2 and 3 for HMPAM polymers. These changes in viscosity for both polymers indicate some physical interactions between chemicals in the aqueous solution as presented on graphs in Figures 6-24 and 6-25.

Apparent viscosity of PHPA-6 solutions is slightly higher than the viscosity of the crude oil for shear rates lower than 10 (1/s), however, the blends of PHPA-6 with SP and ASP show slightly lower values of viscosity (Figure 6-24). The viscosity also tends to behave as Newtonian by the effect of alkali and surfactant. Apparent viscosity of PHPAM-3 is significantly higher than the viscosity of the crude oil at shear rates lower than 10 (1/sec), and lower at shear rates

above that value. The no Newtonian behaviour of the viscosity is not affected by the chemical blends.

From these results is observed that alkali and surfactants reduce the viscosity and can change the rheological behaviour of polymers from pseudo plastic to Newtonian. These changes have implications on the mobility ratio.

The calculated shear rate that represent the flow of fluids on Bentheimer sandstone cores (Figure 6-14) was equivalent to 8 (1/s) shear rate, thus at this shear rate the viscosity of the SP (blend1-polymer) and ASP (blend 2- polymer and blend 3-polymer) is slightly lower than the viscosity of the crude oil.

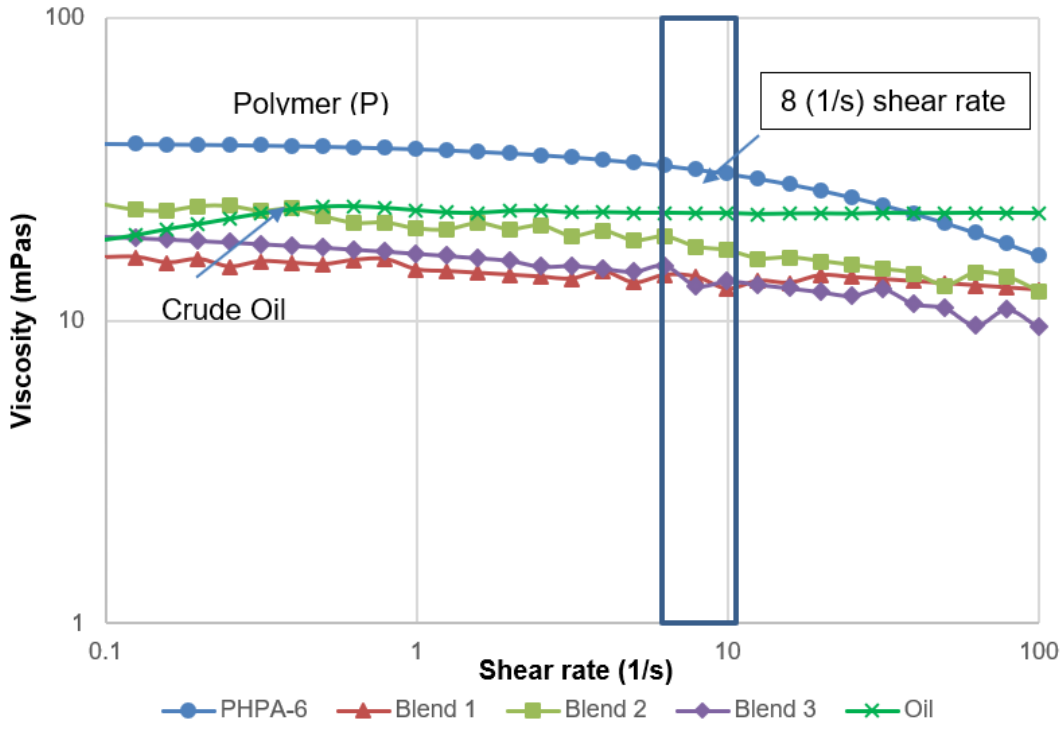


**Figure 6-24: Viscosity of SP and ASP for polymer PHPA-6**

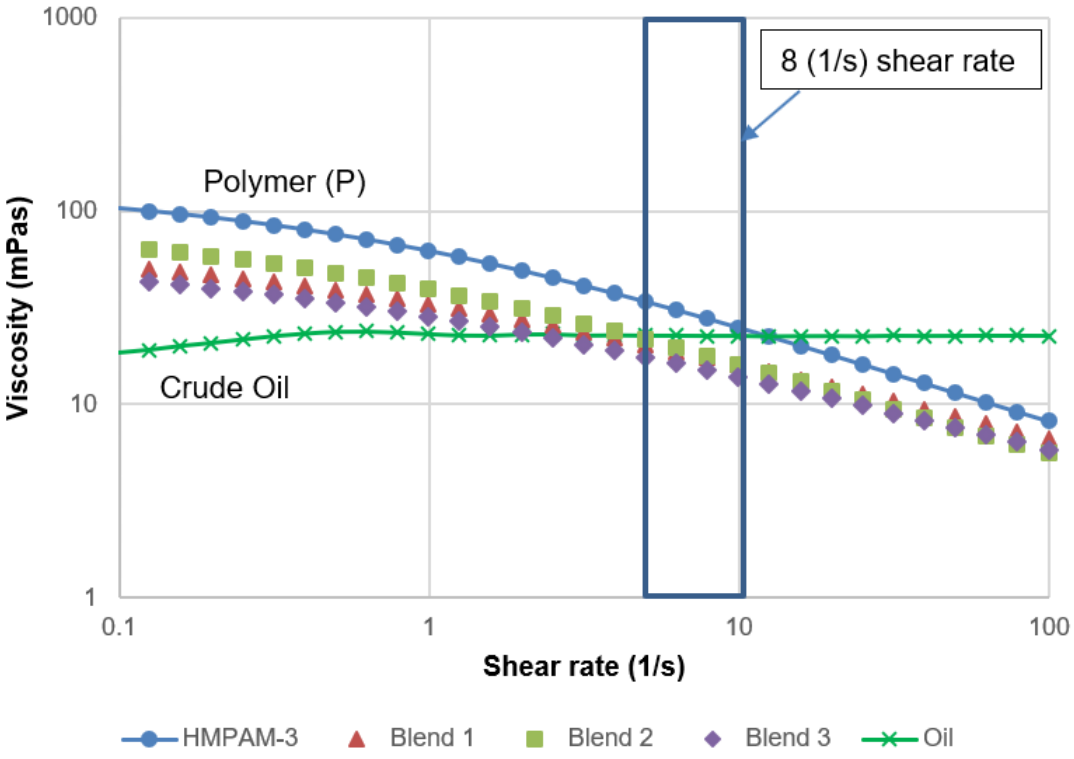


**Figure 6-25: Effect of surfactant and alkali in polymer HMPAM-3 at optimal salinity**

### 6.3.2.2. Effect of salinity range and optimal salinity on viscosity

The effective salinity Csep affects the viscosity of blends, especially at low salinity (Csep 1.3). (Figure 6-26). The viscosity behaviour for SP and ASP blends at hard conditions is not too different as values of Csep are very close (1.5 and 1.58). At low salinity, while the viscosity of the SP (blend 1) with polymer HMPAM is more favourable for the crude oil, ASP with EDTA (blend 2) with PHPA-6 polymer shows the best viscosity. At high salinities, equivalent to Csep 1.5 and 1.58, (36,000 -38,000 ppm), there are no remarkable differences between SP and ASP respect to the viscosity of the crude oil. These results evidence that alkali and surfactant affect the viscosity of polymers and the effect is more evident at low salinity. At high salinity, the viscosity is dominated by ionic interactions by the effect of salinity as there was not a significant difference between the viscosity for the different blends.

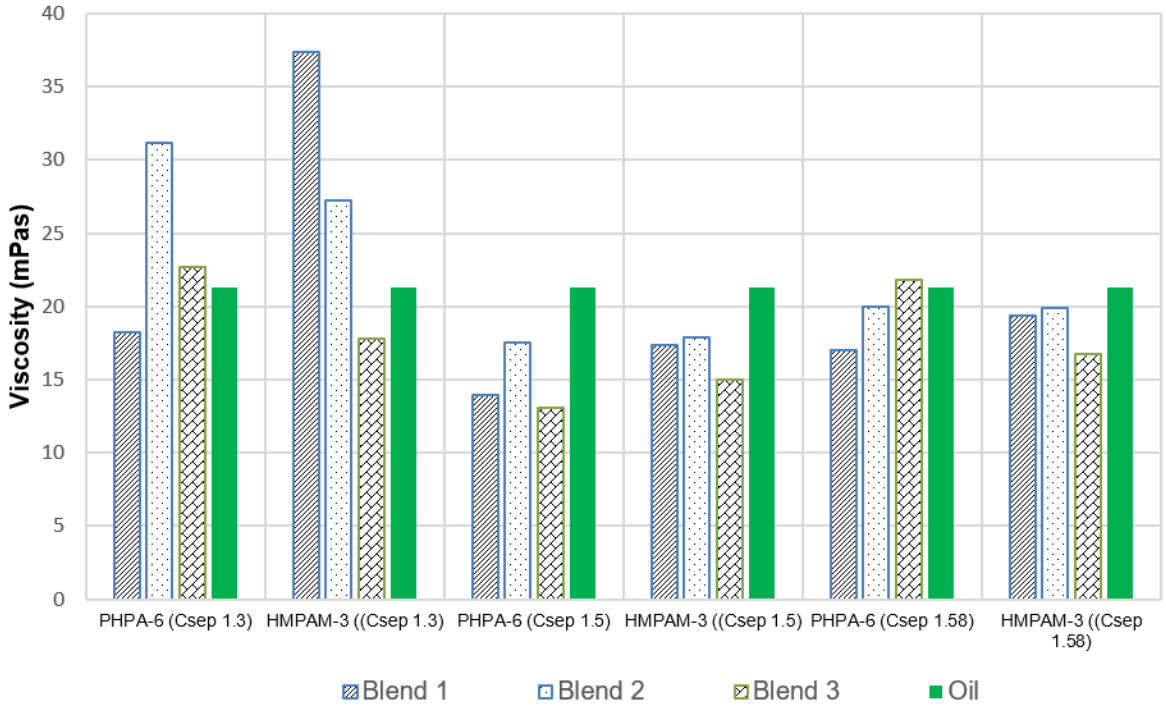


**Figure 6-26: Viscosity of SP (blend 1) and ASP (blends 2 and 3) at different effective salinity (Csep)**

The viscosity of blend 1 with polymer HMPAM-3 is higher than with PHPA-6 at low salinity, and the differences decrease at high salinity. The increase on viscosity of blends surfactant-polymer is due to the aggregate polymer –surfactant which makes a bigger molecule, however depending on the balance of charge between the molecule and counter ions existing in the solution, the shielding effect, and net charges will govern the final orientation and hydrodynamic size of the polymer with resultant viscosity (Kwak, 1998). Interactions between surfactants and hydrophobic polymers, such as HMPAM are more complex, due to the possible combination of interactions between different hydrophobic chains existing along the polymer backbone with the surfactant, which can form a complex structure which favour higher viscosities compared with the resultant of surfactants with homo-polymers (Kwak, 1998), such as PHPA.

### 6.3.2.3. Study of IFT micro emulsion formation and viscosity for SP and ASP

Results from phase separation tests showed that the addition of polymer to alkali-surfactant does not affect the optimal salinity for micro emulsion formation for blends of surfactant and alkali systems whereas the minimal IFT obtained for the three-phase microemulsion was

slightly higher than the one obtained for surfactant and alkali-surfactant without polymer. The adjusted map of ultra-low IFT of micro emulsion formation versus salinity is presented in Figure 6-27.

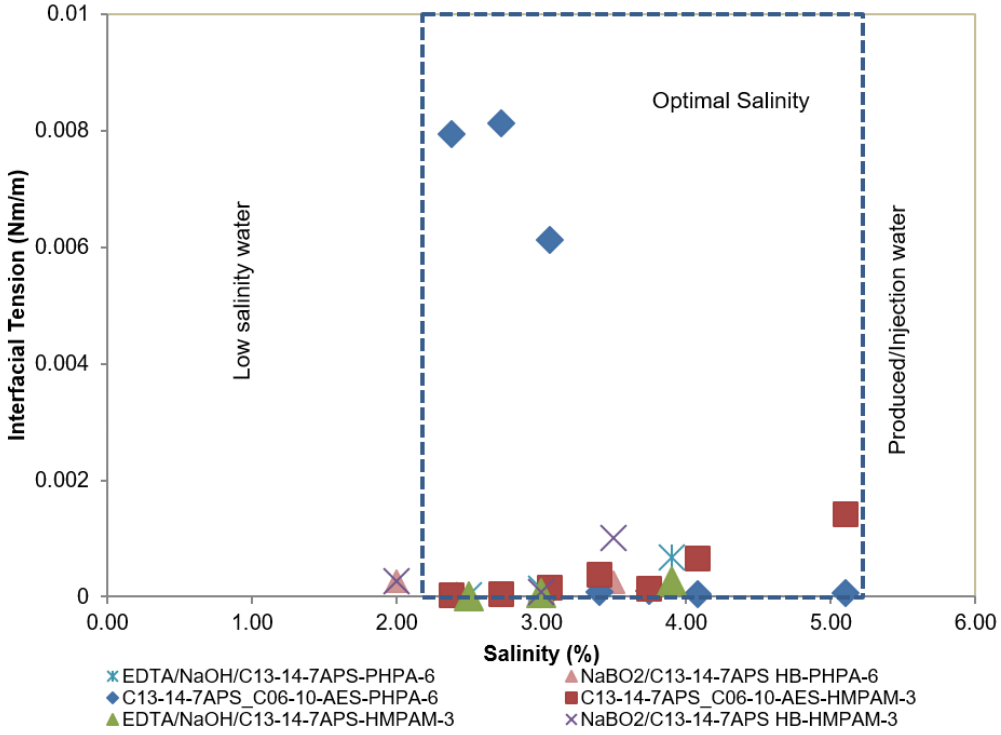


**Figure 6-27: Zones of ultra-low salinity for SP and ASP CEOR solutions**

The variations on viscosity and IFT due to interactions of surfactants with polymers have been reported in previous research (Yan and Xiao, 2004; Wu, X. *et al.*, 2015; ZHU, Youyi *et al.*, 2012; Kwak, 1998). The increase on the IFT of surfactants by the addition of ionic polymer has been explained by two types of interactions that can occur between ionic polymers and surfactants, which are hydrophobic and electrostatic (Kwak, 1998; Wu, X. *et al.*, 2015); the resultant effect on the IFT depends on the structure and ionic charge of the polymer and surfactant, and also on the ionic content of the solution, given by brine salinity and the content of divalent cations (hardness).

The viscosity of the resultant microemulsion formed on phase separations tests for chemical blends, at the optimal salinity measured at 8 (1/s) shear rate, are higher than the viscosity of the polymer and the oil. This effect makes the mobility ratio more favourable for the displacement of the trapped crude oil (Figure 6-28).

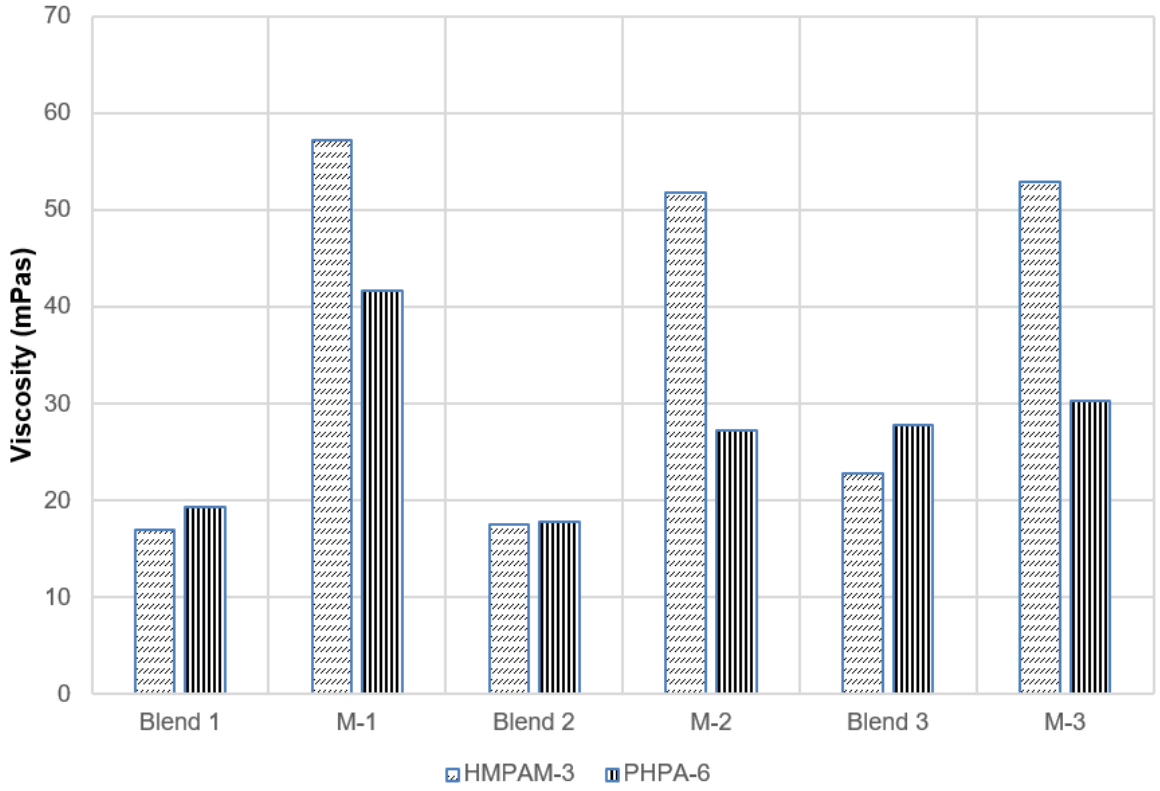


**Figure 6-28: Effect of interactions surfactant and alkali with polymer SP and ASP on the microemulsion viscosity**

The synergy of SP and ASP CEOR in the oil recovery is associated with the viscosity augmentation and the reduction of IFT (ZHU, Youyi *et al.*, 2012; Han *et al.*, 2013). However, the major concerns associated with microemulsions are the formation of stable microemulsion with ultra-high viscosity as high viscosities can promote undesirable high flowing pressures, increase the retention of surfactants in the porous media and affect the flow of chemicals inside the porous media. The use of solvent or co-surfactant is recommended to reduce the viscosity of microemulsions (Bera and Mandal, 2015; Walker *et al.*, 2012; Sheng, 2010a). It was also noticed higher viscosity for microemulsions with polymer HMPAM-3, this effect can be due to the complexity of the structure and charge distribution on this type of polymer, which can form ionic interactions inter and intra-molecular with surfactants.

### 6.3.3. Study of fluid-fluid-rock interactions for polymers P, SP and ASP, effect of brine salinity and hardness

Results on this section are presented on the following sub sections as described:

1. Section 6.3.3.1: Acrylamide type polymers PHPA and HMPAM.
2. Section 6.3.3.2: Effect of polymer interactions with surfactant and alkali-surfactant for SP and ASP CEOR.

### 6.3.3.1. Acrylamide type polymers PHPA and HMPAM

#### 6.3.3.1.1. Relative permeability and mobility control factors

The injection of polymer reduces the relative permeability of water compared with water-flooding but does not affect the relative permeability of oil (Figure 6-29). It is also observed that the reduction in the water relative permeability is associated with the size of the polymer molecule, represented by the molecular weight MW.

The permeability reduction factor $R_k$ increases with the molecular weight of the polymer. $R_k$ is related to the size of the polymer molecule as the value increases with the molecular weight of polymers PHPA, except for PHPA-5 polymer. Polymers PHPA-5 and HMPAM-3 have similar values of $R_k$ as they have similar molecular weight. The displacement efficiency of the oil in the core samples is improved with the increase on the permeability reduction factor $R_k$ by polymers, results are presented in Table 6-7.

As the resistant factor $R_f$ represents the combination of permeability reduction and increase of viscosity by polymer, it is apparent that not only the molecular weight affects the value but also how the molecule of polymer is orientated in the brine solution, which is also affected by ionic interactions within molecules of polymer (Table 6-7). The mobility ratio M is lower than one by the injection of polymers.

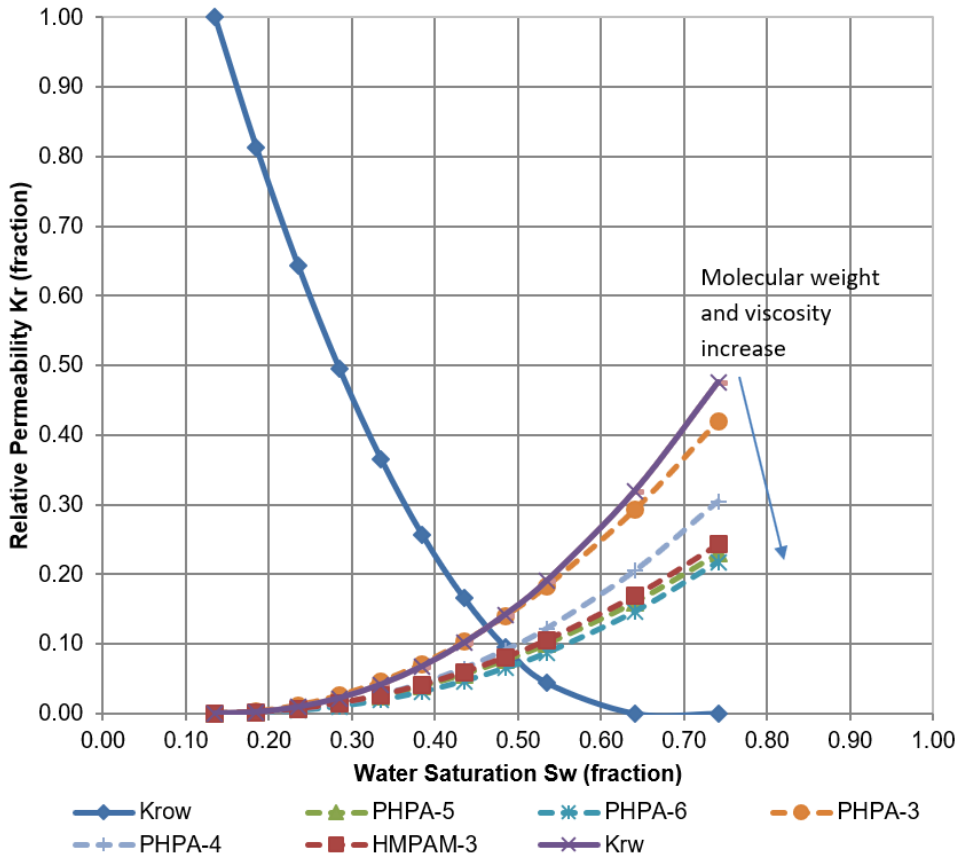


**Figure 6-29: Comparison of relative permeability of polymer flooding and water flooding**

**Table 6-7: Mobility control factors for polymers**

| Polymer | Permeability reduction Factor Rk (fraction) | Viscosity Polymer (mPas) (4 1/s) | Viscosity ratio $\mu_p/\mu_w$ | Resistance Factor Rf (fraction) | Mobility Ratio M |
|---|---|---|---|---|---|
| PHPA-3 | 1.09 | 13.4 | 10.31 | 11.23 | 0.005-6.45 |
| PHPA-4 | 1.56 | 18.1 | 13.92 | 21.71 | 0.002-3.27 |
| PHPA-5 | 2.00 | 21.2 | 16.31 | 32.62 | 0.002-2.28 |
| PHPA-6 | 2.18 | 23.9 | 18.38 | 40.07 | 0.001-1.76 |
| HMPAM-3 | 1.88 | 14.8 | 11.38 | 21.39 | 0.003-3.47 |

From results, it is noticed that the mobility ratio is lower than one (M < 1) for polymer injection for water saturations below 0.5, and the range of saturation for low mobility ratio is associated with the molecular weight of the polymer. PHPA-6 polymer has the lowest mobility ratio and the highest rage of water saturation with M < 1. Details are presented in Figure 6-30. It is also noticed the area of low mobility ratio (M<1), which is associated with favourable oil recovery

and piston-like displacement, has a threshold value for water saturation of 0.5, which is the point where the relative permeability of water and oil have similar values, represented on the graph shown in Figure 6-30. Reduction of mobility increase the oil displacement efficiency (Figure 6-31)

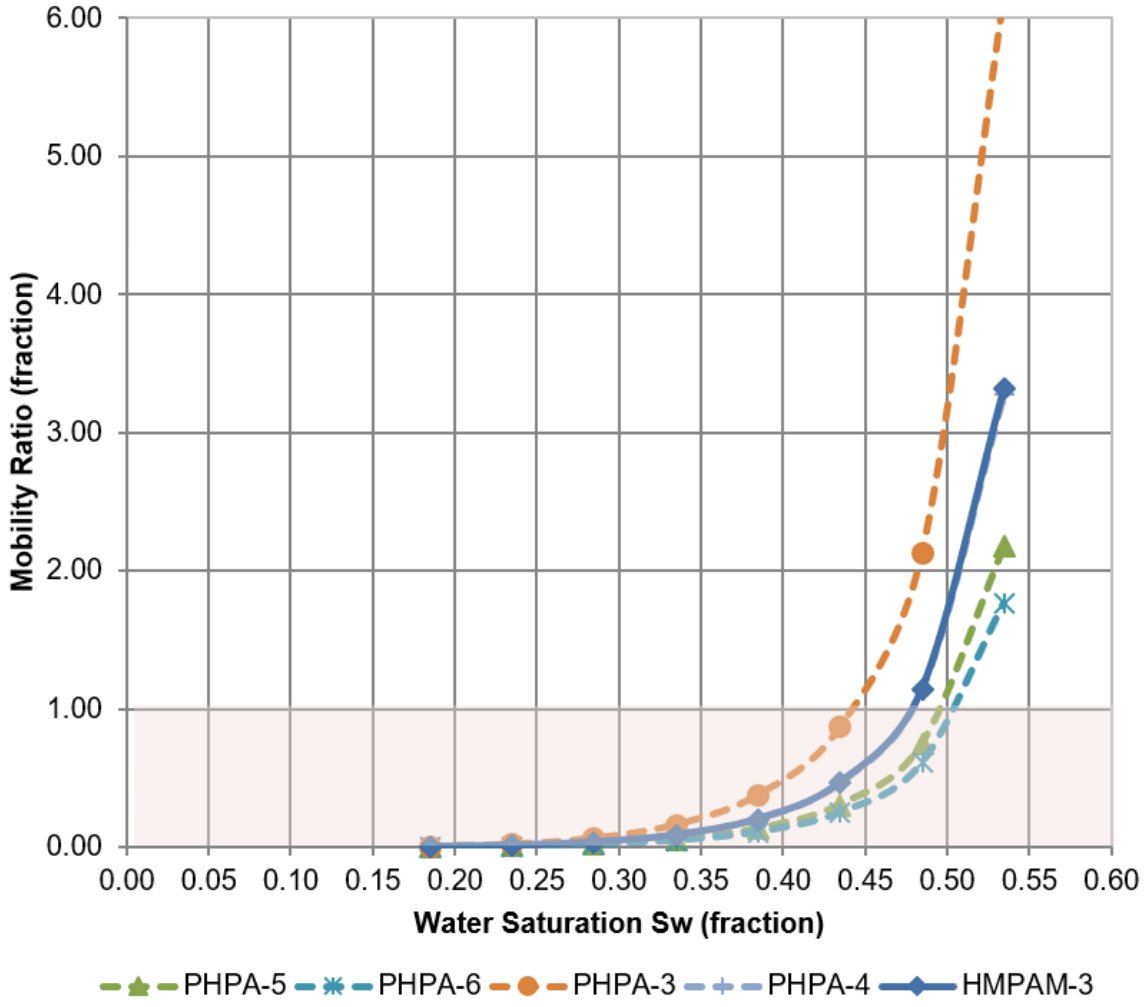


**Figure 6-30: Mobility ratio M for polymers**

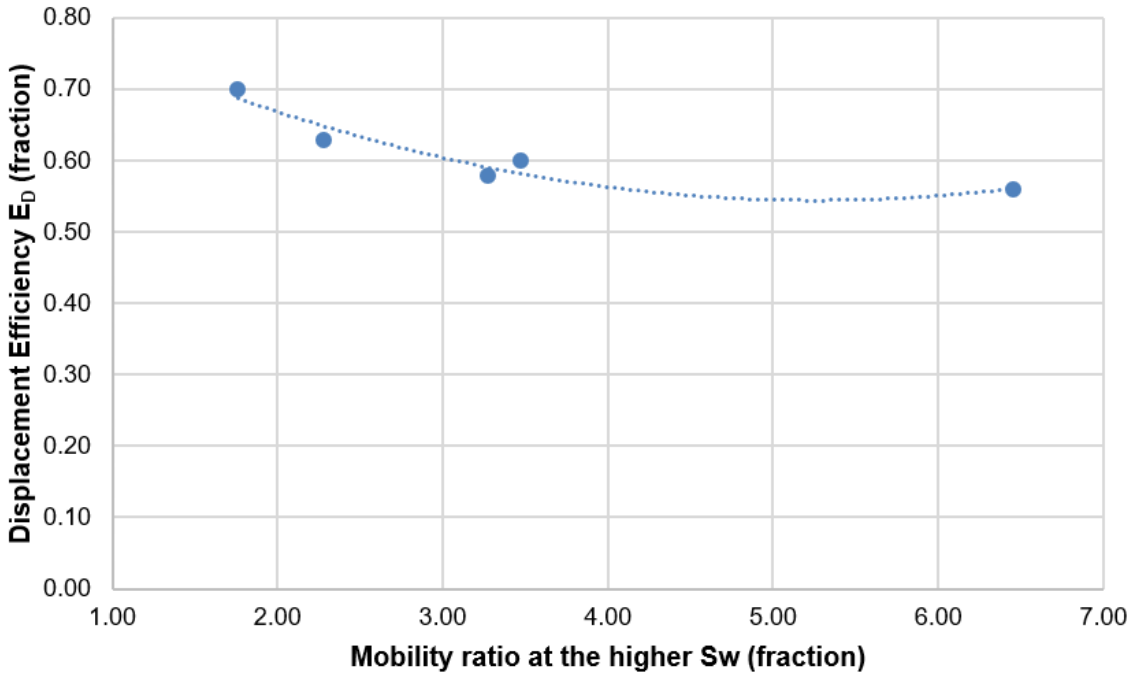


**Figure 6-31: Displacement Efficiency $E_D$ versus mobility ratio**

The displacement efficiency increases with the increase of Rk and Rf and is more sensitive to permeability reduction factor than to the resistant factor as shown by comparing the behaviour of displacement efficiency displayed in Figures 6-32 and 6-33, there is a quadratic relationship between displacement efficiency and Rk and Rf. The highest displacement efficiency was related to the resistant factor and permeability reduction factor for PHPA-6 polymer.

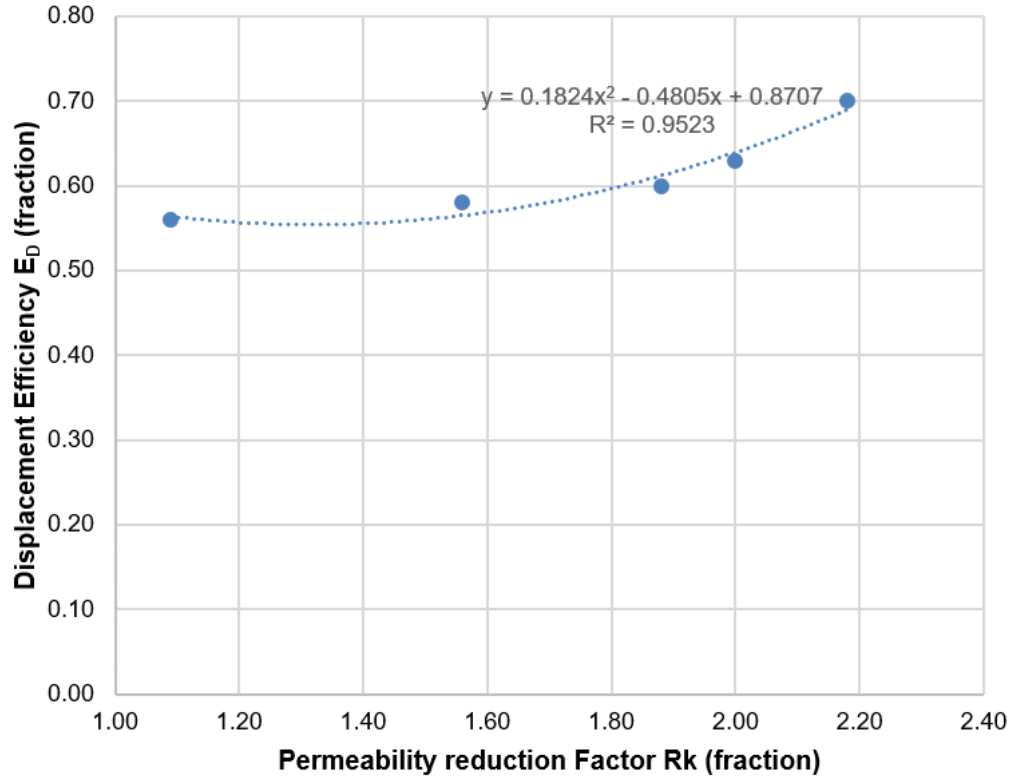


Figure 6-32: Displacement efficiency versus permeability reduction factor Rk

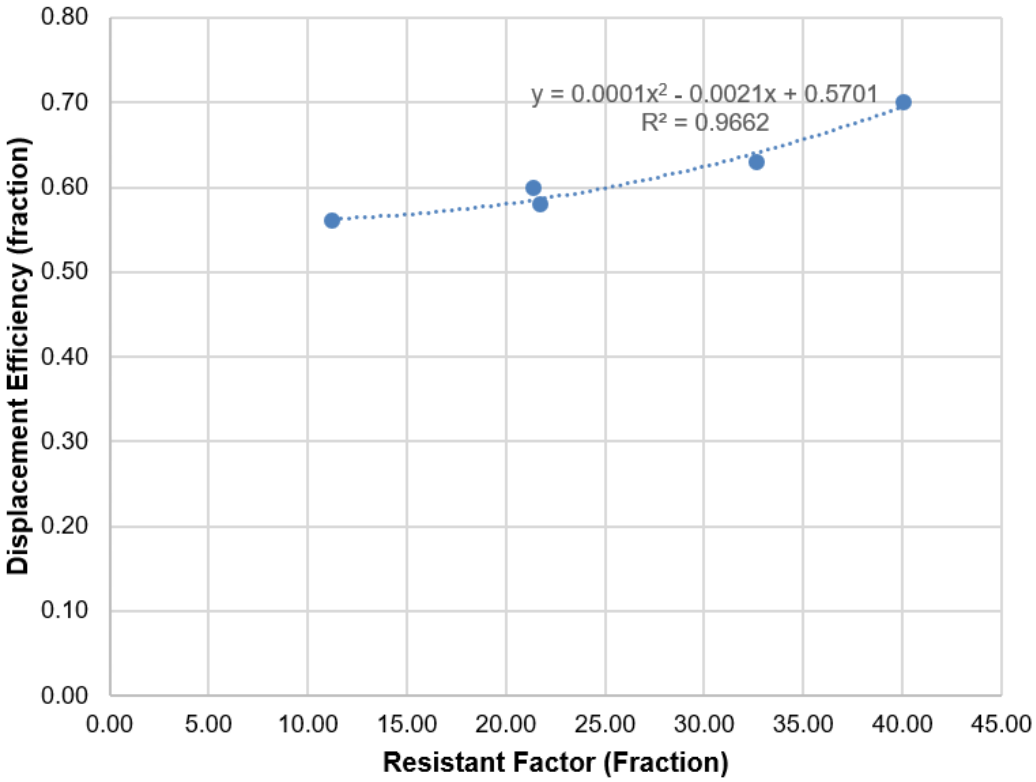


Figure 6-33: Displacement efficiency versus resistant factor Rf

From these results, it was noticed that polymers reduce relative permeability and increase the viscosity of the displacing fluid. As a result, the mobility ratio M is also reduced. The combined effect of relative permeability and viscosity increases the oil displacement efficiency (Figure 6-31 and 6-33)

Permeability reduction is due to the adsorption of polymers as a single layer which reduces the effective pore size and the permeability of the porous media (Hirasaki and Pope, 1974; Mishra et al., 2014). While adsorption is affected by polymer concentration, retention is affected by the effective size of the polymer molecule.

#### 6.3.3.1.2. Fractional flow curves and production profile for polymers

Fractional curves for water flooding and polymer flooding have an S shape which include an inflection point at intermediate values of saturation; the saturation value of the inflection point depends on the mobility ratio. For polymers, the inflection point moves towards high water saturation as the mobility ratio decreases. As a result, the polymer can displace more of the mobile oil and the displacement profile is piston-like with a better displacement efficiency. Results from the graphical determination of the point of water breakthrough and the average saturation behind the displacement front inside the core at that point are presented in Table 6-8.

As the fractional curve concave forward at higher saturation, the point of breakthrough is close to the water saturation that corresponds with the maximal point to recover all the mobile oil. Polymers increase the displacement efficiency by a range of 11% to 25% which is seems to be related to the molecular weight. Higher values were obtained for polymer PHPA-6 followed by polymer PHPA-4 and HMPAM-3.

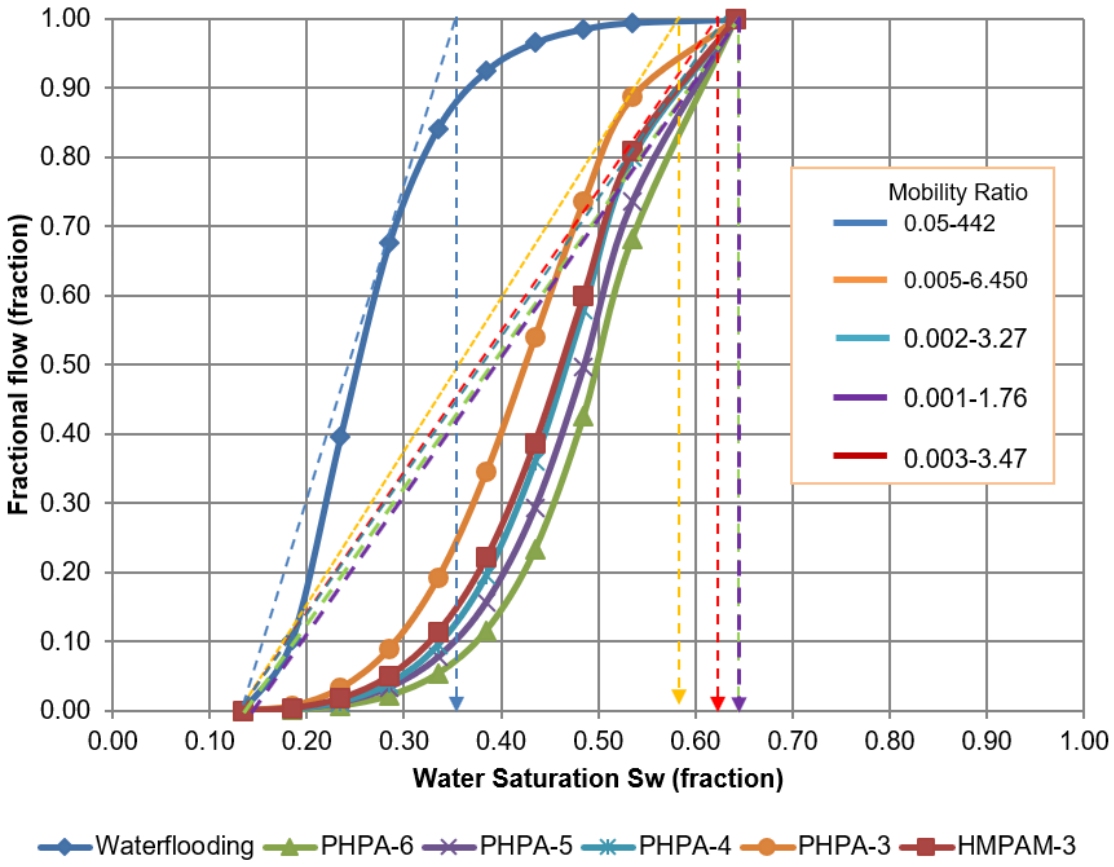


**Figure 6-34: Fractional flow curves for polymers, effect of mobility ratio**

**Table 6-8: Results from water flooding and Polymer CEOR**

| Chemical | Resistance Factor Rf (fraction) | Mobility ratio M | Water Breakthrough (Graphical) (Sbt) Sw | Displacement Efficiency $E_D$ (fraction) | | |
|---|---|---|---|---|---|---|
| | | | | Water-flood | Polymer | Total |
| PHPA-3 | 11.23 | 1.35-1.55 | (0.525) 0.575 | 0.451 | 0.111 | 0.56 |
| PHPA-4 | 21.71 | 1.01-1.17 | (0.525) 0.625 | 0.342 | 0.234 | 0.58 |
| PHPA-5 | 32.62 | 0.84-1.01 | (0.641) 0.641 | 0.470 | 0.159 | 0.63 |
| PHPA-6 | 40.07 | 0.75-0.89 | (0.641) 0.641 | 0.450 | 0.251 | 0.70 |
| HMPAM-3 | 21.39 | 0.41-1.44 | (0.525) 0.625 | 0.441 | 0.161 | 0.60 |

#### 6.3.3.1.3. Pressure profiles for polymers

Profiles of pressure and production of oil and water for injection of polymers PHPA-6 and HMPAM-3 are presented in Figures 6-35 and 6-36; for both graphs there is a reduction of pressure while oil is displaced by water during water flooding until the point of water breakthrough, represented by a zone of low pressure, then as polymer is injected, the pressure raise by the effect of the higher viscosity and the accumulation of oil, and during the displacement of oil there is another zone of reduction on pressure with an increase of water cut.

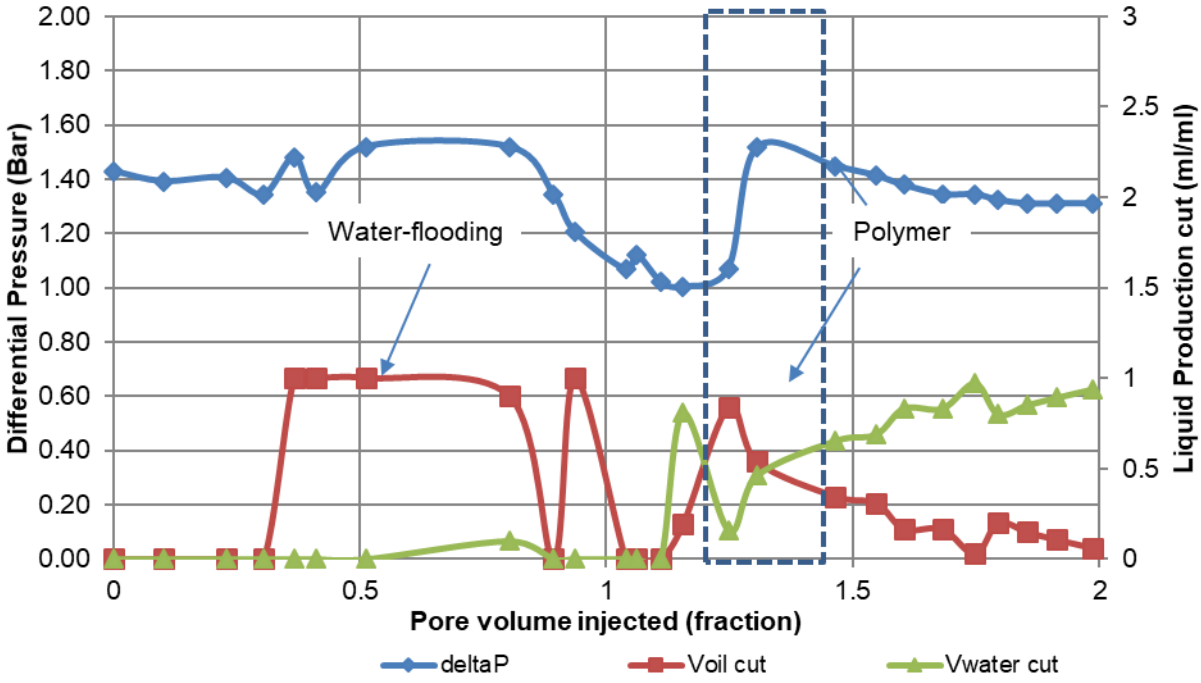


**Figure 6-35: Pressure and production profile for water flooding and PHPA-6 CEOR**

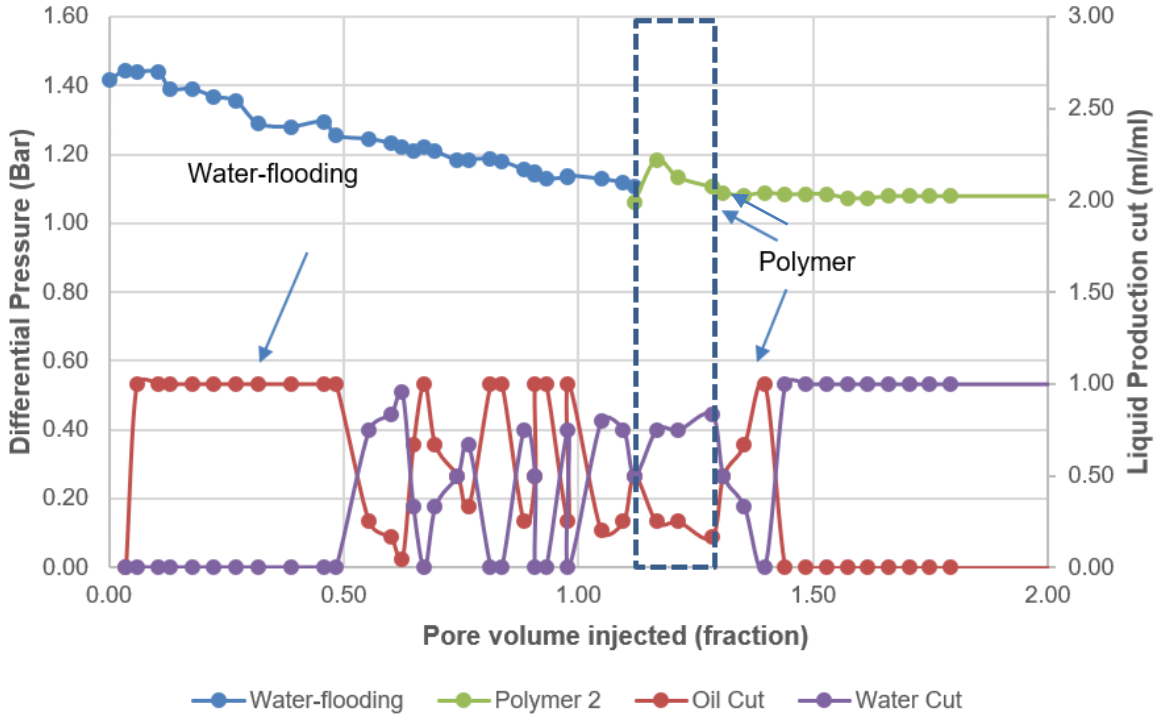


**Figure 6-36: Pressure and production profile for water flooding and HMPAM-3 CEOR**

The production profile for water- flooding at the beginning of the test is piston-like until the water overcome the oil and water breakthrough occurs, this point is when the displacement has reached about 0.5 pore volume, the reduction of pressure continues with the increase of water cut raise until 81-100%, then the injection of polymer reduces the water cut and allows additional production of oil. Similar production profiles were obtained for both polymers as presented in Figures 6-38 and 6-39 with differences in additional oil recovery by each polymer of 9%. There are some discrepancies observed on the oil displacement by the injection of the two polymers, with a delay on production for polymer HMPAM-3, these differences can be associated either with rock-fluid interactions of the polymers inside the porous media or with delays related with the dead volume in the core-flooding test or the manual production method used for the experiment. Another possible cause of that delay may be associated with polymer adsorption in the rock.

From the evaluation of polymer as a standalone method, it was learned that polymers can efficiently perform displacing the mobile oil, and the drive mechanisms are associated with viscosity and the ability of the polymer to modify the relative permeability of the displacing fluid in the porous media. High viscosity favours the recovery of mobile oil. Based on the analysis

of fractional flow curves there were no appreciable differences between PHPA-5, PHPA-6 and HMPAM-3, as all can get high oil recovery.

#### 6.3.3.2. Effect of polymer interactions with surfactant and alkali-surfactant for SP and ASP CEOR.

In this section results from the combination of polymers with surfactant and alkali –surfactant blends are discussed based on the dynamic behaviour in the porous media.

##### 6.3.3.2.1. Relative permeability and mobility control factors

Relative permeability curves for the blends SP and ASP obtained for water flooding and CEOR core-flooding tests for the blends 1 to 3 with polymers are presented in Figure 6-37. For all blends, the oil relative permeability curves versus water saturation increase compared to water flooding at the same water saturation. However, water relative permeability values decrease for CEOR. These aspects are an indication of the combined effect of viscosity and IFT on the permeability of fluids in the porous media.

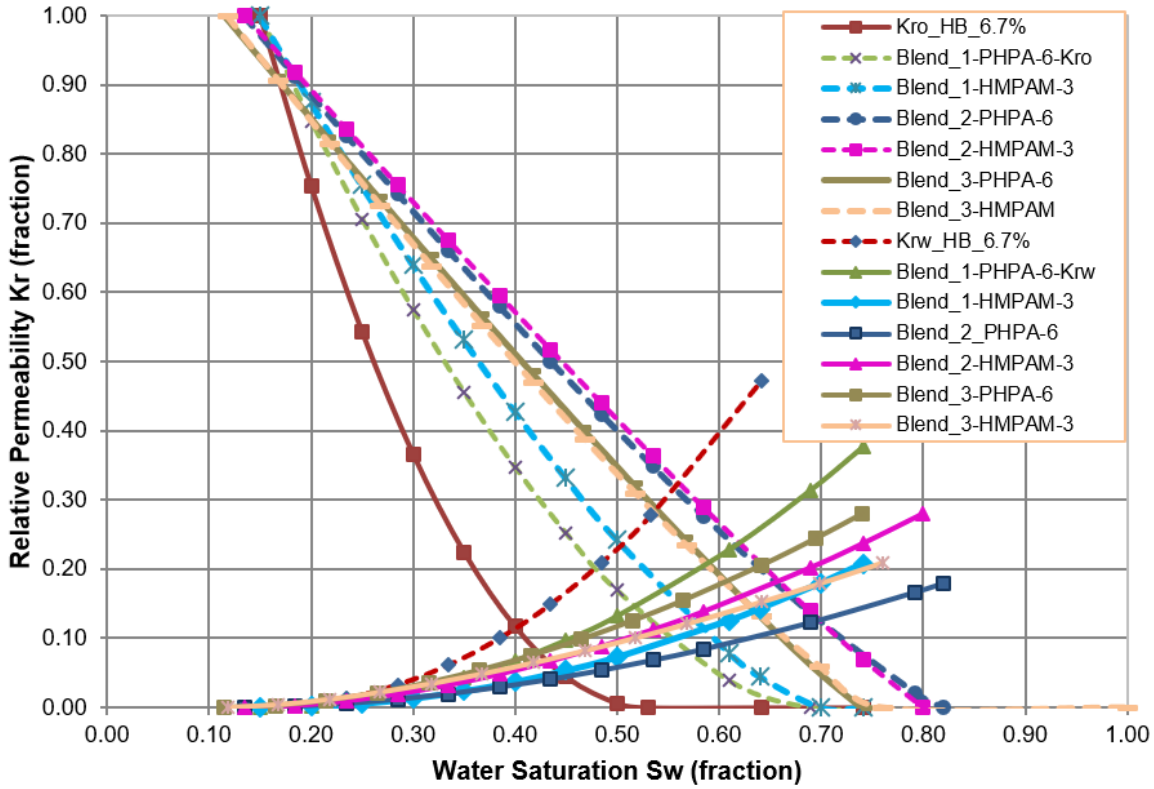


Figure 6-37: Relative permeability of water flooding and SP and ASP CEOR

There is the permeability reduction of water as displacing fluid in both SP and AS by the increase of viscosity given by the polymer and microemulsion. The effect of the interfacial tension on the release of the trapped oil by changing its relative permeability $k_{ro}$ is also observed (Figure 6-37). Relative permeability functions also get more linear for ASP blends. The synergy of SP and ASP on relative permeability curves is more marked for ASP (blends 2 and blend 3) than for SP.

By analysis of the displacement cross point, where relative permeability oil and water have equal value of permeability, as the cross point tends to higher values of water saturation Sw, the residual oil saturation Sor tends to lower values. The higher point for water saturation and lower Sor are obtained for the ASP blend 2, followed by ASP blend 3 and SP blend 1. These results indicate the effect of alkali on wettability change (Table 6-9 and in Figure 6-38).

**Table 6-9: Results from water flooding and Polymer CEOR**

| Chemical System | Sw at the cross point (fraction) | Sor (fraction) |
|---|---|---|
| Water flooding | 0.4 | 0.47 |
| Blend-1-PHPA-6 | 0.52 | 0.31 |
| Blend-1-HMPAM-3 | 0.58 | 0.3 |
| Blend-2-PHPA-6 | 0.68 | 0.18 |
| Blend-2-HMPAM-3 | 0.66 | 0.2 |
| Blend-3-PHPA-6 | 0.62 | 0.26 |
| Blend-3-HMPAM-3 | 0.63 | 0.24 |

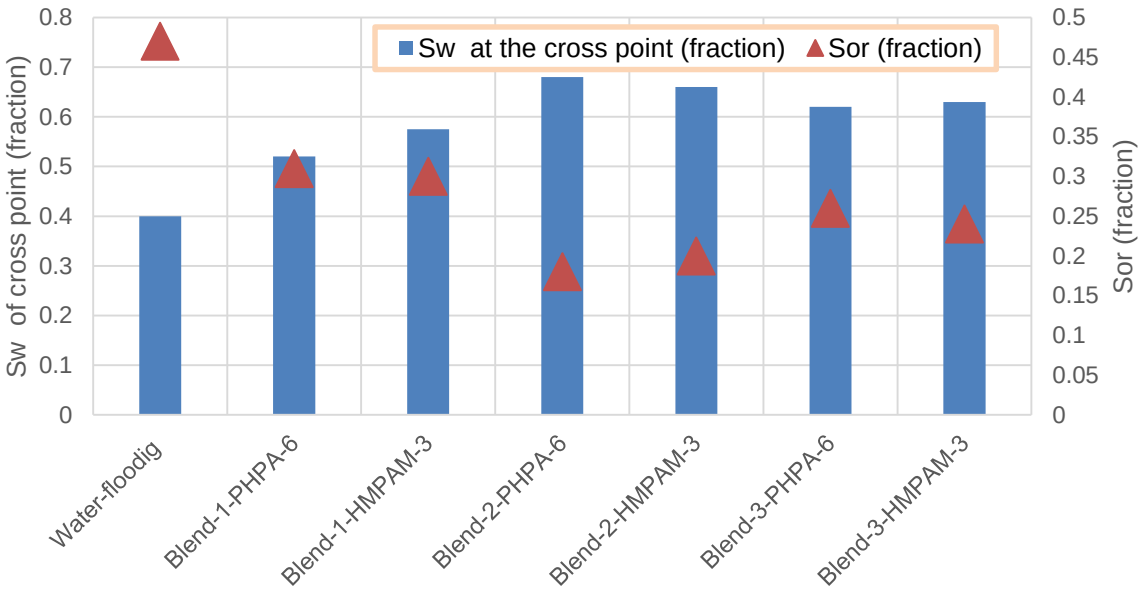


**Figure 6-38: Water Saturation at the cross point of relative permeability of water and oil and irreducible oil saturation for water flooding, SP and ASP CEOR**

The analysis of changes in relative permeability curves of oil and water revealed they both tend to be more linear for ASP than for SP and water flooding. Besides, there are some differences between the shape of the oil relative permeability curves for the same blend, for example for blend1, there are differences between PHPA-6 and HMPAM-3, with the latter one with higher values, possible associated with rock-fluid interactions. The more linear the relative permeability curve is, the lower is the residual soil for the flow at low IFT with an increase in relative permeability and a reduction in the residual oil. There are differences in the effect of polymers on the water relative permeability, and the difference is higher for SP (blend 1) than for ASP (blends 2 and 3). A comparison of the behaviour of relative permeability curves for water and oil are presented in Figures 6-39 and 6-40.

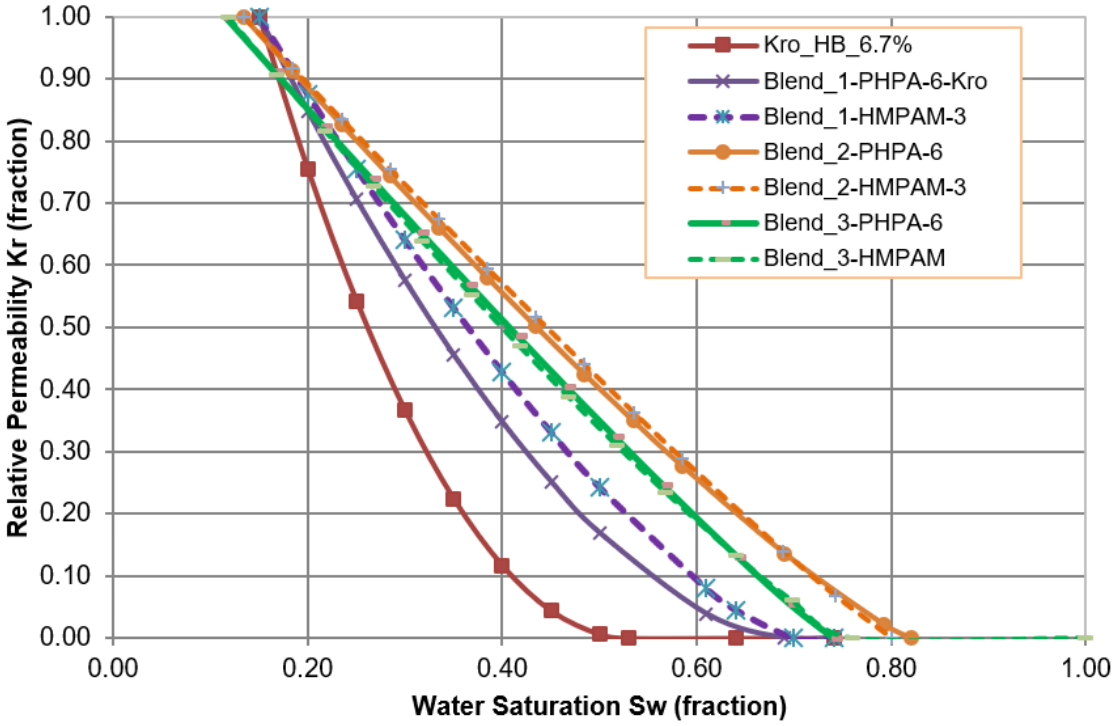


Figure 6-39: Relative permeability of oil for SP and ASP CEOR

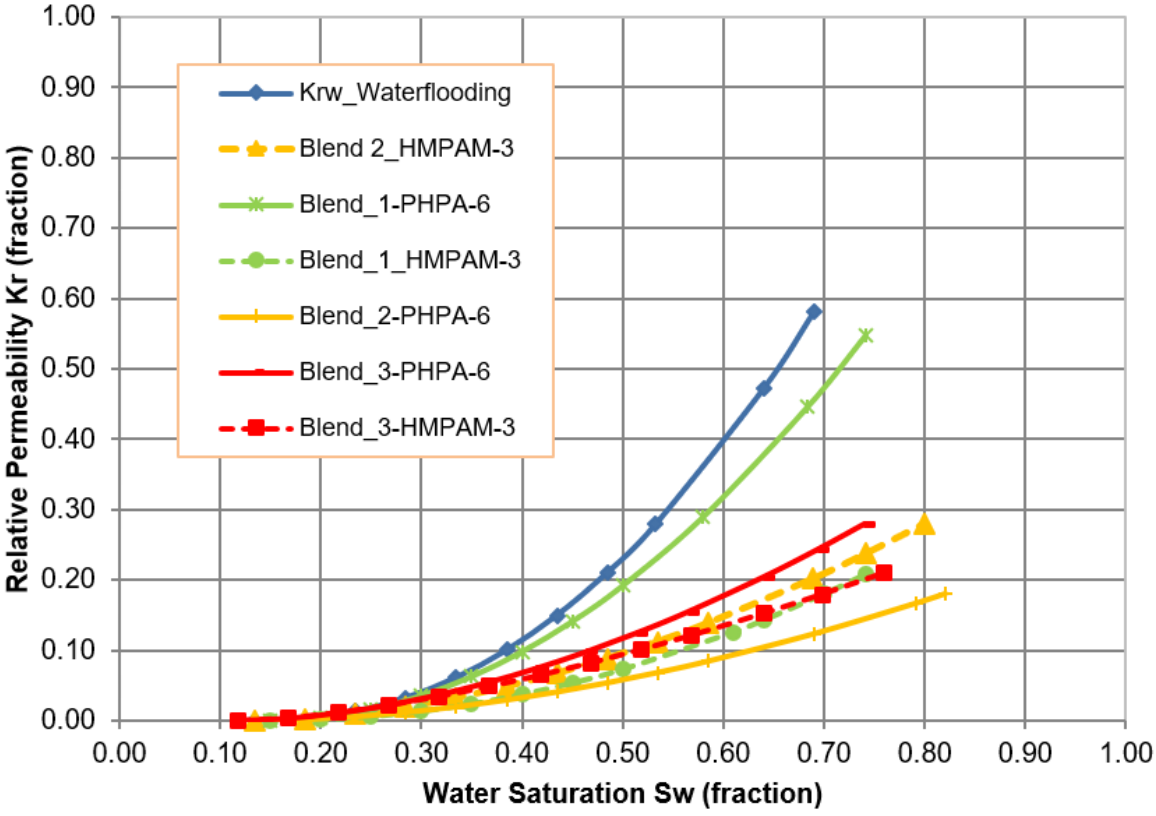


Figure 6-40: Relative permeability of water for SP and ASP CEOR

Results of displacement efficiency as a function of relative permeability of water and oil presented in Figure 6-41 show how the displacement efficiency $E_D$ increases with the increase of oil relative permeability whereas the effect of water relative permeability on $E_D$, shows the maximal displacement efficiency at water relative permeability values close to 0.1.

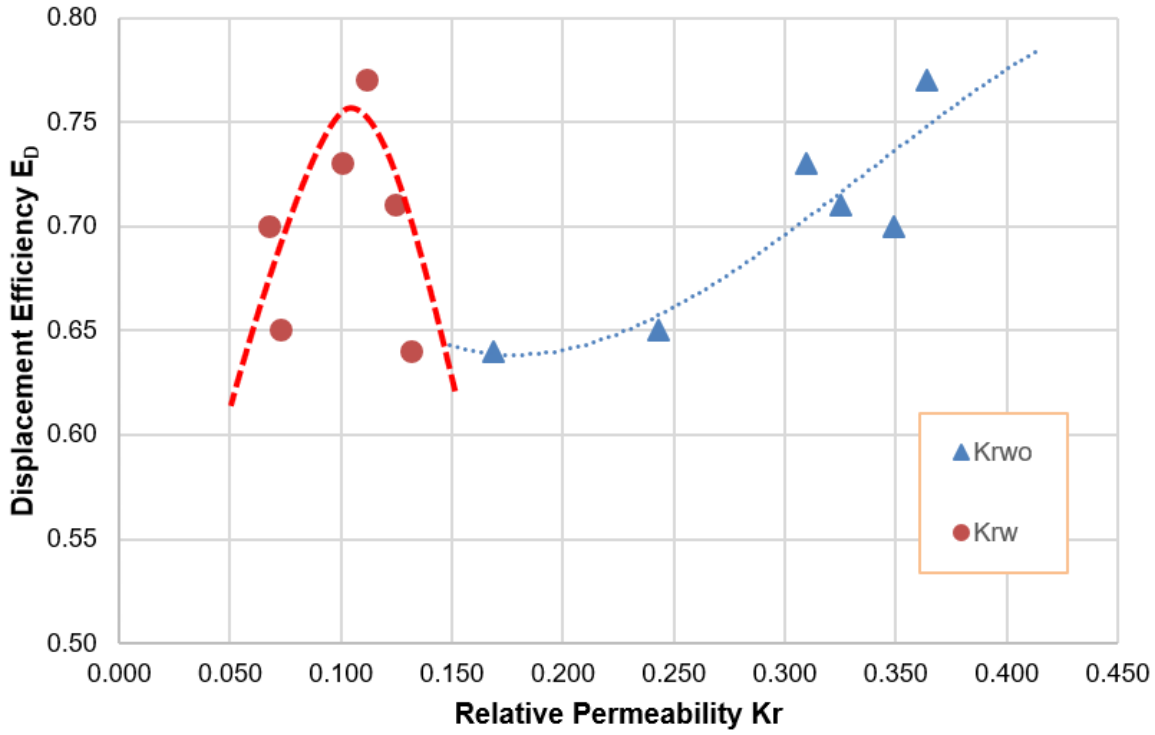


**Figure 6-41: Effect of relative permeability of water and oil on the displacement efficiency for SP and ASP CEOR**

The mobility ratio of CEOR SP and ASP is lower than one, favourable for displacement efficiency until values of water saturation higher than 0.5 (better than for water flooding or polymer flooding), with higher values for ASP (blends 2 and 3) than for SP (blend 1) blends for both polymers. The higher value of the threshold for water saturation with low M is obtained for blend 2 with NaOH and EDTA. These results are presented in Figure 6-42.

To analyse the contribution of chemicals on the displacement efficiency, combinations of variables evaluated are presented in graphs in Figures 6-43 through 6-45. It can be noticed the displacement efficiency is not substantially affected by the mobility ratio at a laboratory scale (Figure 6-43). The resistance factor $R_f$ and residual factor $R_k$ affects the mobility ratio, whereas they do not appreciably change the displacement efficiency (Figures 6-44 and 6-45).

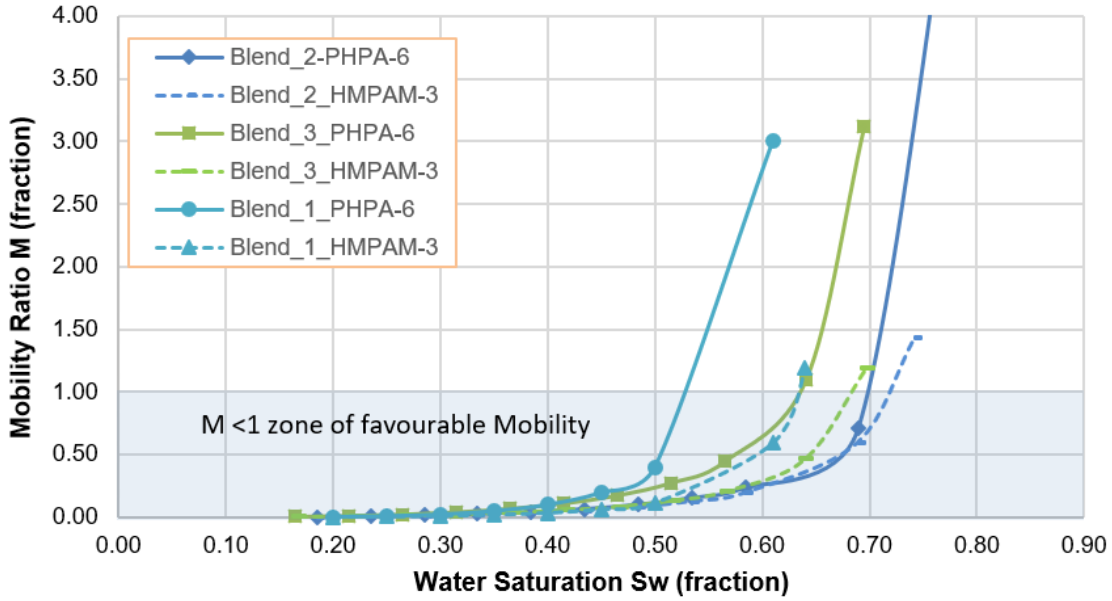


Figure 6-42: Mobility ratio for SP and ASP CEOR

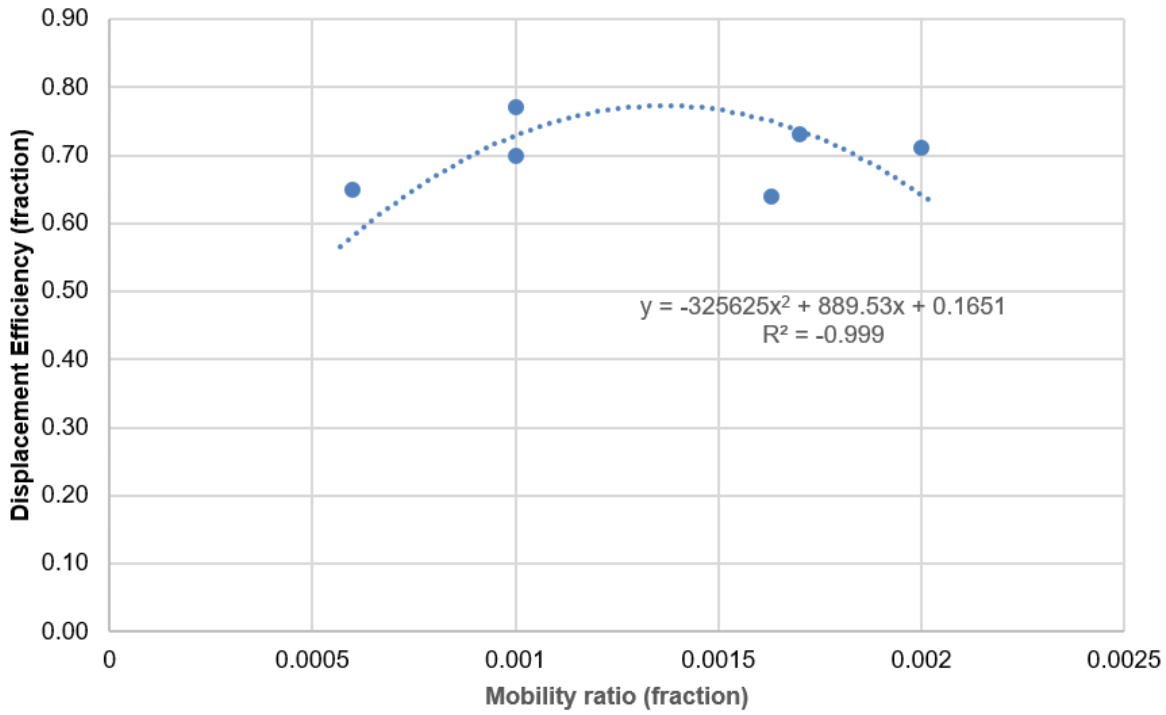


Figure 6-43: Effect of Mobility ratio on displacement efficiency for SP and ASP CEOR

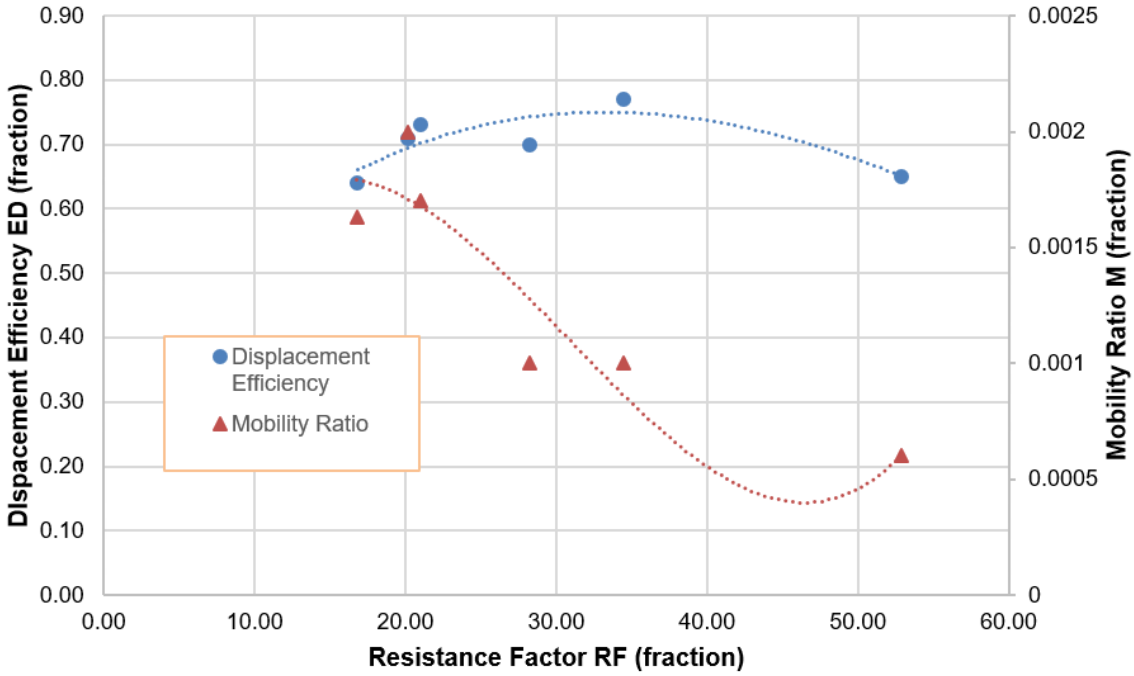


**Figure 6-44: Effect of resistant factor Rf on displacement efficiency and Mobility ratio for SP and ASP CEOR**

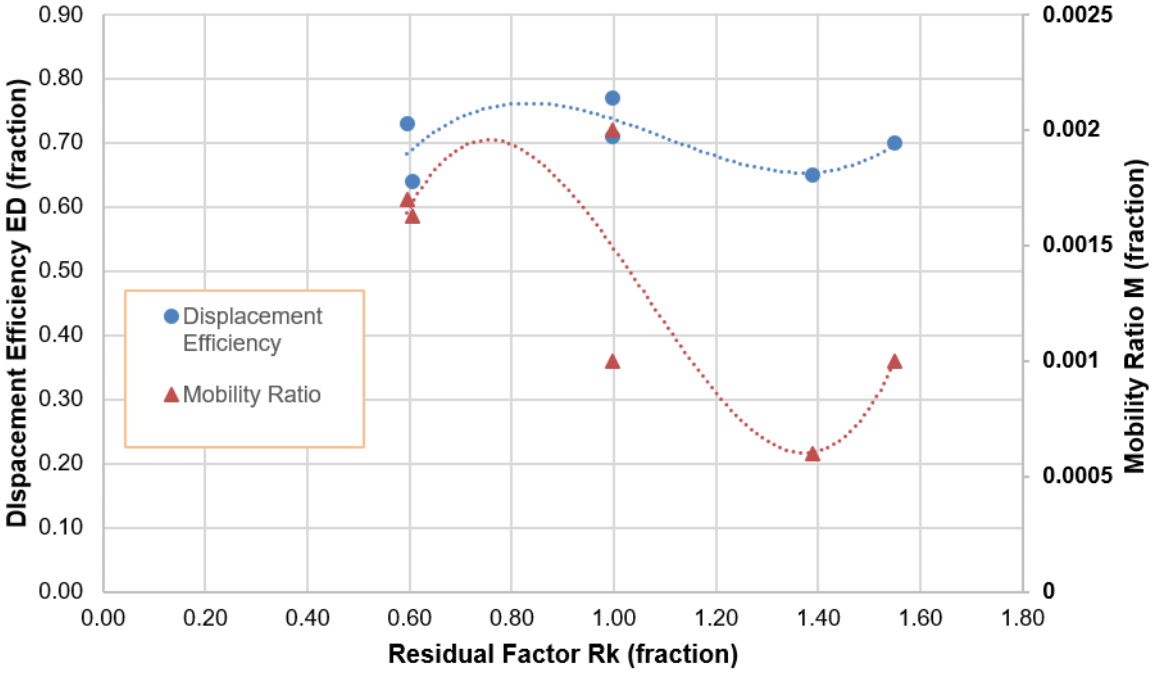


**Figure 6-45: Effect of residual factor Rk on displacement efficiency and Mobility ratio for SP and ASP CEOR**

#### 6.3.3.2.2. Effect of SP, ASP on capillary number Nc

The capillary number and mobility ratio are important parameters to assess the performance of CEOR, and the effect is more relevant for surfactant applications. After analysing the values of relative permeability of water and oil at a fixed water saturation Sw=0.5, which is the point after CEOR is injected, as a function of capillary number, it was observed that while the relative permeability of oil decreases until a minimal and then increases with capillary number, the relative permeability of polymer –brine is not significantly affected by changes in the capillary number and have values lower than the relative permeability of oil. These results are presented in Figure 6-46.

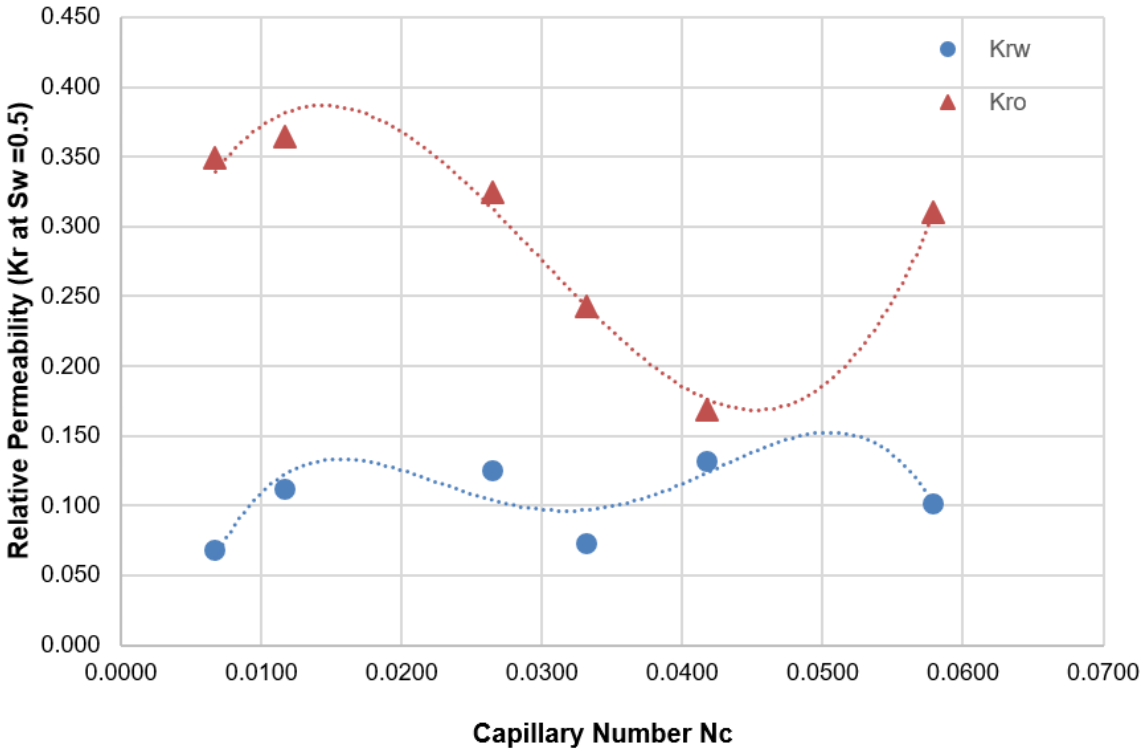


**Figure 6-46: Effect of capillary number Nc on the relative permeability of water and oil at water saturation Sw=0.5**

Changes in capillary number affect more the relative permeability of oil, which is consistent with the effect of interfacial tension on the reduction of the residual oil saturation and the contribution to the correlation between the residual oil saturation and the capillary number (Sheng, 2010a), this effect favours the mobility of oil trapped inside the porous media. According to previous research, there are critical values of IFT which define the grade of the changes in relative permeability results by the IFT reduction (Shen *et al.*, 2005). Interfacial

tension also affects the values of the n exponents, thus $n_w$ and $n_0$ on the relative permeability curves.

Results of the oil recovery factor and displacement efficiency of oil by the different tests are reported in Table 6-10. Displacement efficiency increases with the capillary number and all the blend tested have a high capillary number compared to water flooding (Figure 6-47). Both SP and ASP have favourable recovery compared with water flooding as their capillary number are 6 order of magnitude higher than water flooding and also have ultra-low values of IFT ($\sigma_{o/w}$). The maximal displacement efficiency obtained for CEOR S, SP and ASP is in the following order: (64-65%) SP, (70-77%) ASP.

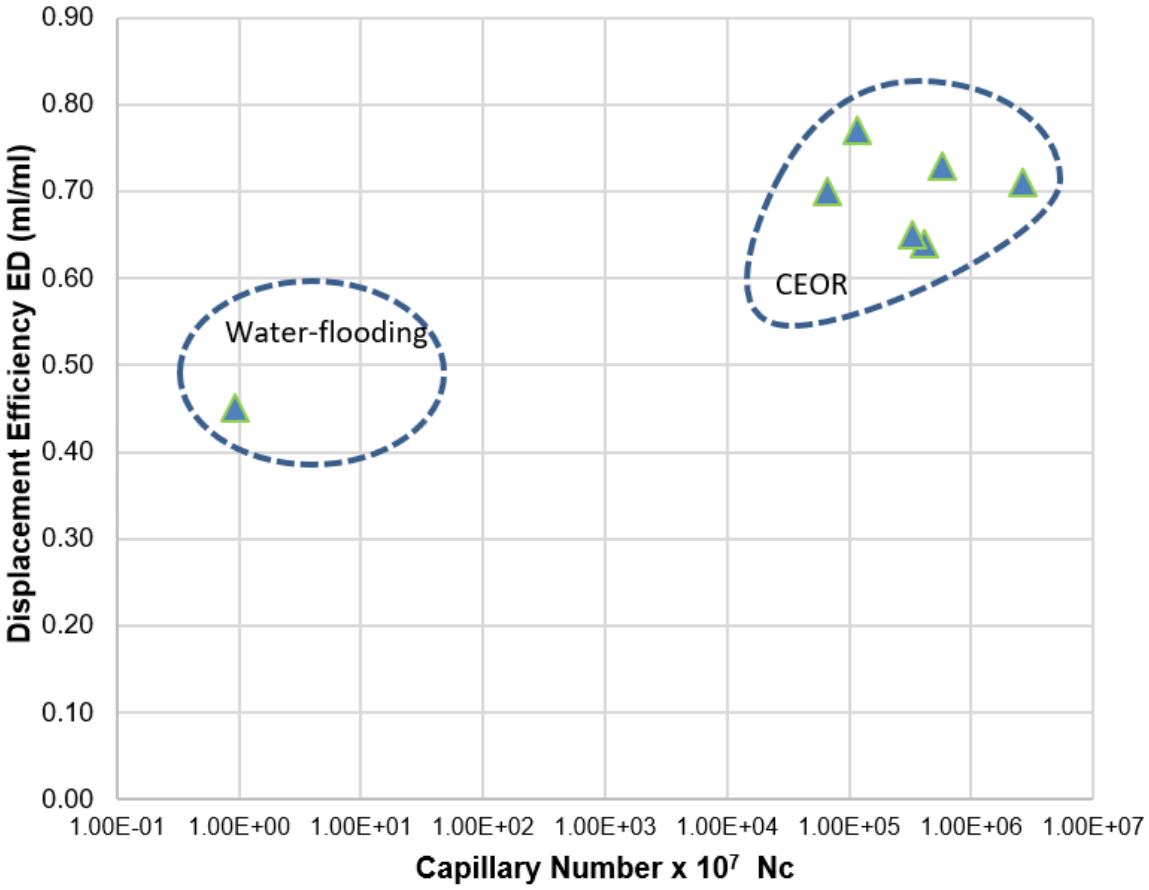


**Figure 6-47: Effect of capillary number on displacement efficiency**

From these results, it is inferred that at optimal salinity of ultra-low microemulsion, the effect of the IFT and capillary number govern the mechanism for ASP, the effect of alkali-surfactant is the more important. It is important to mention that this can be true at a microscopic scale but not a macroscopy scale where the advantage of polymer is associated with sweeping. The

higher values of displacement efficiency are obtained for ASP CEOR with polymer HMPAM-3. The synergy ASP is evidenced by these results.

#### 6.3.3.2.3. Fractional flow curves for SP and ASP CEOR

Fractional flow curves show the effect of SP and ASP on the displacement of fluids in the core sample for water flooding and CEOR with SP (blend 1) and ASP (blends 2 and 3). The curves are concave towards high water which indicates in some cases a total recovery of the mobile fluid. The water breakthrough moves toward high-water saturation with the highest for blends with polymer HMPAM-3. These results show the combined effect of ultra-low interfacial tension of surfactant to reduce the residual oil saturation to the minimal mobile fluid and the viscosity of the microemulsion and polymer on the fractional flow curve. The results are presented in Figure 6-48. While PHPA-6 polymer as standalone shows better performance than HMPAM-3 polymer, the interaction with surfactant and alkali surfactant for SP and ASP show better results for HMPAM-3. The effect of the microemulsion formation improves the performance of polymers.

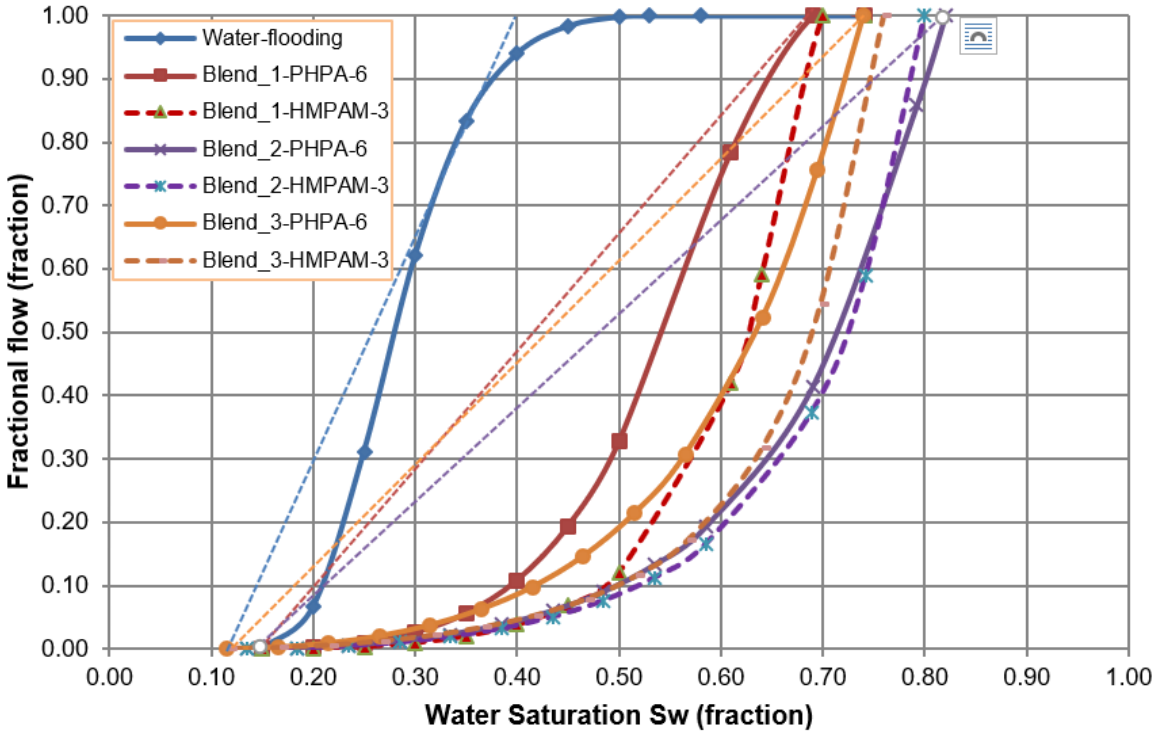


Figure 6-48: Fractional flow behaviour for SP and ASP CEOR

At the optimal salinity, the viscosity of the microemulsion is reported to be 5 times higher than either water or oil viscosity, however the emulsion viscosity also depends on the proportion of each phase, being close to brine for lower proportion of oil in the microemulsion and close to the viscosity of oil for microemulsions with high proportion of oil (Lu *et al.*, 2013).

Changes in the oil and water relative permeability affect the oil displacement efficiency, however, increase in oil relative permeability was more evident. Despite the effect of IFT is well recognized as an increase in both relative permeability, water and oil (Shen *et al.*, 2005; Amaefule and Handy, 1982), the results show that water relative permeability decreases for SP and ASP blends, the effect of polymer on the synergy SP and ASP affects the behaviour of water relative permeability.

#### 6.3.3.2.4. Pressure profile for SP and ASP CEOR

The pressure profile for water flooding and CEOR for SP and ASP shows as during the injection of brine (Figure 6-49 to 6-51), pressure increases gradually and remain high for about 0.5 pore volume (PV) of injected fluid and then decreases until a constant value after 1 PV has been displaced, due to the depletion of oil in the core sample, leaving the trapped oil behind the displaced front of fluid. Moreover, during the CEOR injection, the pressure rapidly increases again until a maximum point, higher than the pressure observed during the water flooding, and then a pressure declines with the displacement process until another constant pressure at about 2.5- 3 PV displaced by injected fluid. This pressure behaviour during CEOR injection can be explained as due to the formation of an oil bank due to the reduction in IFT, following by a viscous displacement enhanced by emulsification of the SP and ASP at the optimal salinity (Shen *et al.*, 2009). The final pressure after the displacement of CEOR slug is higher than the pressure for water flooding. This incremental pressure is due to the effect of SP and ASP fluid-fluid and rock-fluids interactions, such as the viscosity of the microemulsion SP and ASP and the dynamic effect on adsorption and retention that occurs while flowing inside the rock.

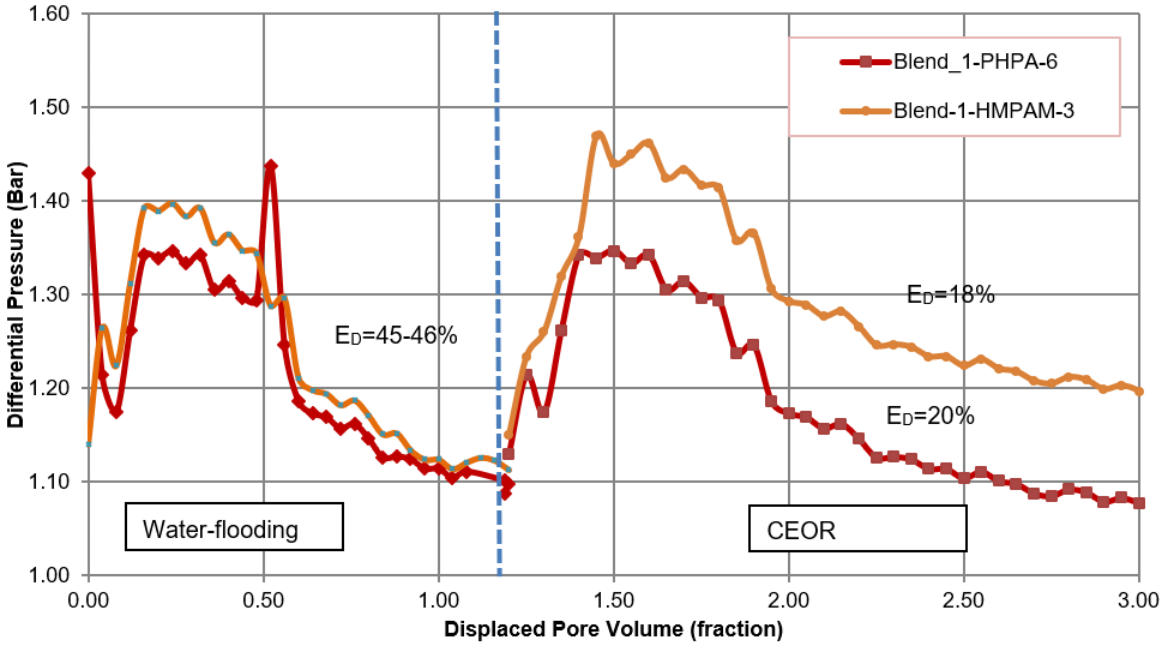


Figure 6-49: Core-flooding pressure profile for SP (Blend-1-PHPA-6 an HMPAM-3)

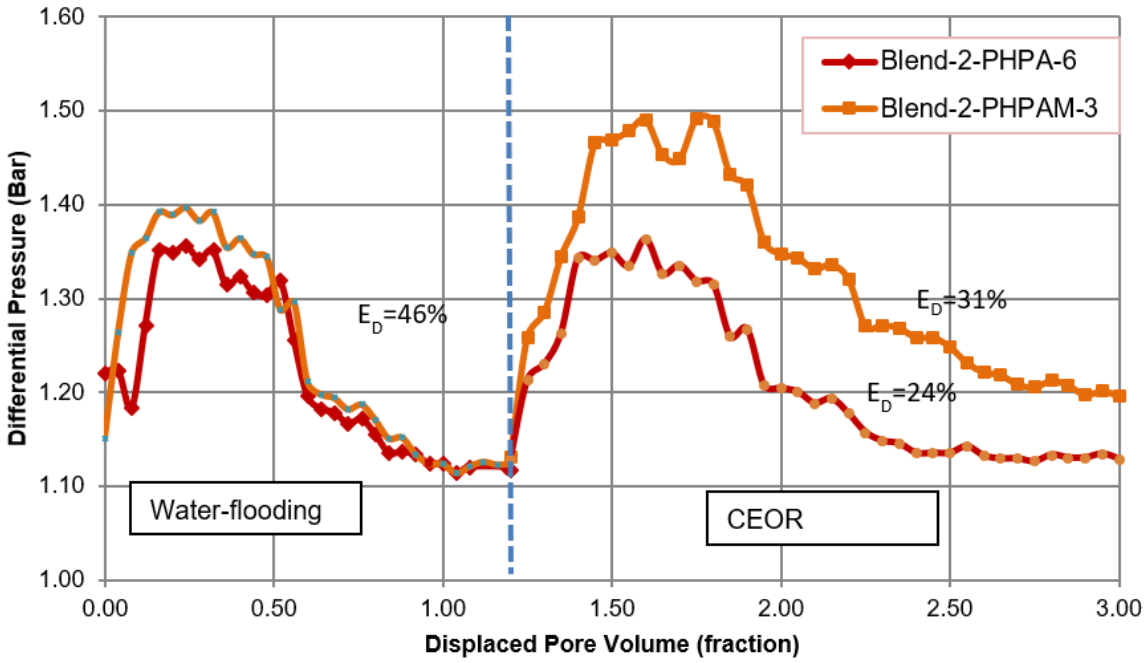


Figure 6-50: Core-flooding pressure profile for ASP (Blend-2-PHPA-6 an HMPAM-3)

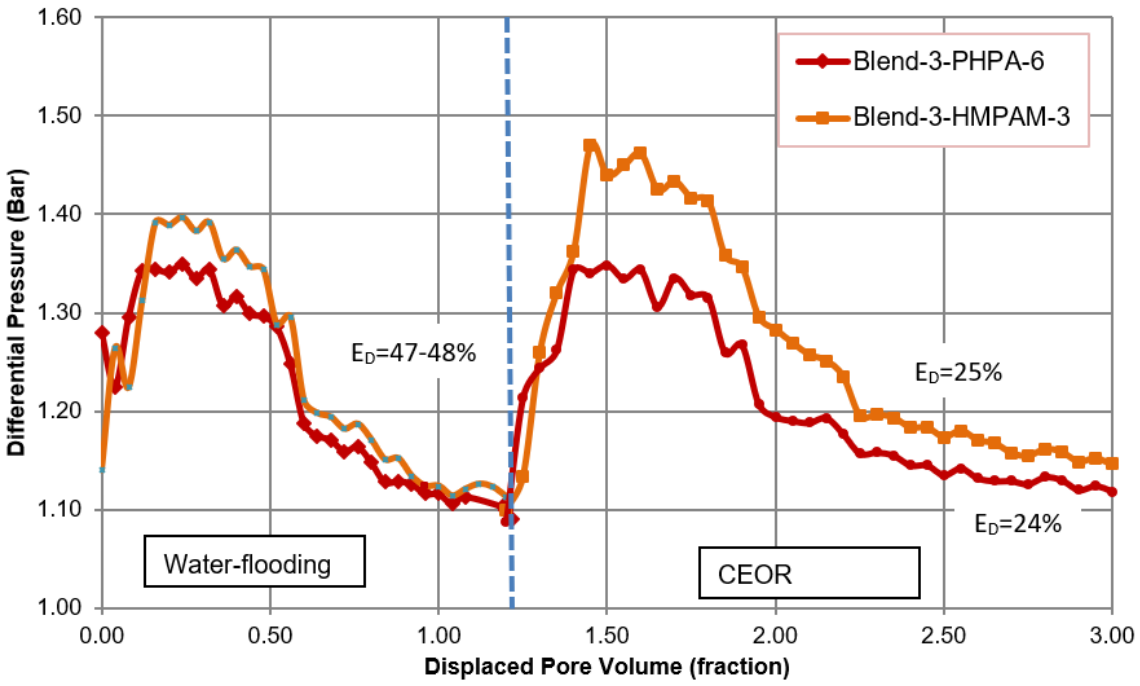


**Figure 6-51: Core-flooding pressure profile for ASP (Blend-3-PHPA-6 an HMPAM-3)**

The pressure profile of injection for blends with hydrophobic modified polymer HMPAM-3 is higher than for PHPA-6, with larger differences for SP-blend 2. By the analysis of the oil displacement efficiency $E_D$ obtained for water flooding for these experiments (Table 6-10), there are some differences and the range of 45% to 48% obtained for blend 2. These differences can be associated with the fact that the optimal salinity of blend 3 is lower than blend 1 and 2. The interactions SP increase the $E_D$ by 18%-20% and the ASP by 24-31%. An increase in pressure is associated with oil displacement and it is represented by results of displacement efficiency $E_D$. Comparing the differences in recovery, it is noticed the advantages of the synergy ASP on the displacement efficiency. Optimal results are obtained for blend-2-HMPAM-3, with the use of alkali and EDTA compared to SP with 5-7% additional recovery.

**Table 6-10: Results from water flooding HB (WF-HB) and SP and ASP CEOR**

| Sample Bentheimer cores | Process | Capillary Number Nc | Resistance Factor $R_F$ | Mobility Ratio M | Oil Recovery Factor ORF | Residual Oil Saturation | Displacement Efficiency $E_D$ |
|---|---|---|---|---|---|---|---|
| | | | Fraction | Fraction | (%) | Sro | $E_D$ |
| Core-500-6 | WF-HB 6.6% | $9.39x10^{-08}$ | 16.82 | 0.00163-3.0 | 46 | 0.47 | 0.46 |
| | Blend 1-PHPA-6 | $4.18 x10^{-02}$ | | | 64 | 0.31 | 0.64 |
| Core -500-7 | WF-HB 6.6% | $9.39x10^{-08}$ | 52.93 | 0.0006-1.19 | 45 | 0.47 | 0.45 |
| | Blend 1-HMPAM-3 | $3.32 x10^{-02}$ | | | 65 | 0.20 | 0.65 |
| Core -500-8 | WF-HB 6.6% | $9.39x10^{-08}$ | 28.20 | 0.001-6.05 | 46 | 0.47 | 0.46 |
| | Blend 2-PHPA-6 | $6.67 x10^{-02}$ | | | 70 | 0.30 | 0.70 |
| Core -500-9 | WF-HB 6.6% | $9.39x10^{-08}$ | 34.44 | 0.001-1.43 | 46 | 0.47 | 0.46 |
| | Blend 2-HMPAM-3 | $1.2 x10^{-02}$ | | | 77 | 0.20 | 0.77 |
| Core -500-9 | WF-HB 6.6% | $9.39x10^{-08}$ | 20.13 | 0.002-3.11 | 47 | 0.47 | 0.47 |
| | Blend 3-PHPA-6 | $2.56 x10^{-02}$ | | | 71 | 0.26 | 0.71 |
| Core -500-10 | WF-HB 6.6% | $9.39x10^{-08}$ | 21.03 | 0.0017-1.19 | 48 | 0.46 | 0.48 |
| | Blend 3-HMPAM-3 | $5.79 x10^{-02}$ | | | 73 | 0.24 | 0.73 |

### 6.3.4. Study of displacement efficiency of P, SP and ASP CEOR, and the role of salinity

This section presents the analysis within the variables: Sor, IFT, and Nc obtained from core flooding tests for S, AS, SP and ASP CEOR and low salinity (LS) systems. The form of an existing correlation between Sor and interfacial tension reported from previous research was used to fit the values, the correlation has the following equation (Shen *et al.*, 2010):

$$S_{or} = \frac{\sigma^{1.5}}{A\sigma^{1.5}+B} \quad (6\text{-}11)$$

Where σ is the interfacial tension IFT, and the constants A and B are parameters related to experimental conditions and rock properties.

From results showed in Figure 6-52, there were no single values for the constants A and B able to fit all experimental points using equation 6-11, examples of 3 sets of values for A and B are shown in Figure 6-52. The range of values for the constant that can represent the set of experiments are A=2.02 -2.1 and B=2.2 x $10^{-06}$-2.0 x $10^{-06}$. The value for A is on the same order of magnitude and close to the value reported on the reference (Shen *et al.*, 2010), however, the fitted value for B is remarkable lower in 5 or 6 orders of magnitude. The low salinity process reduces Sor, therefore move the capillary desaturation curve to lower values of Sor (points at IFT lower than 10 mN/m) in Figure 6-52.

As experimental points are missing in the region of interfacial tension close to the deflection zone in the graph, and the points at ultra-low interfacial tension are dispersed at low residual oil saturation, it is difficult to predict the best fitting for parameters A and B. Moreover, the effect of the salinity on the recovery of water flooding is not considered on the mathematical correlation. The minimal residual oil saturation is 0.4, which is the minimum value reported for Berea sandstone rocks (Lake, 1989).

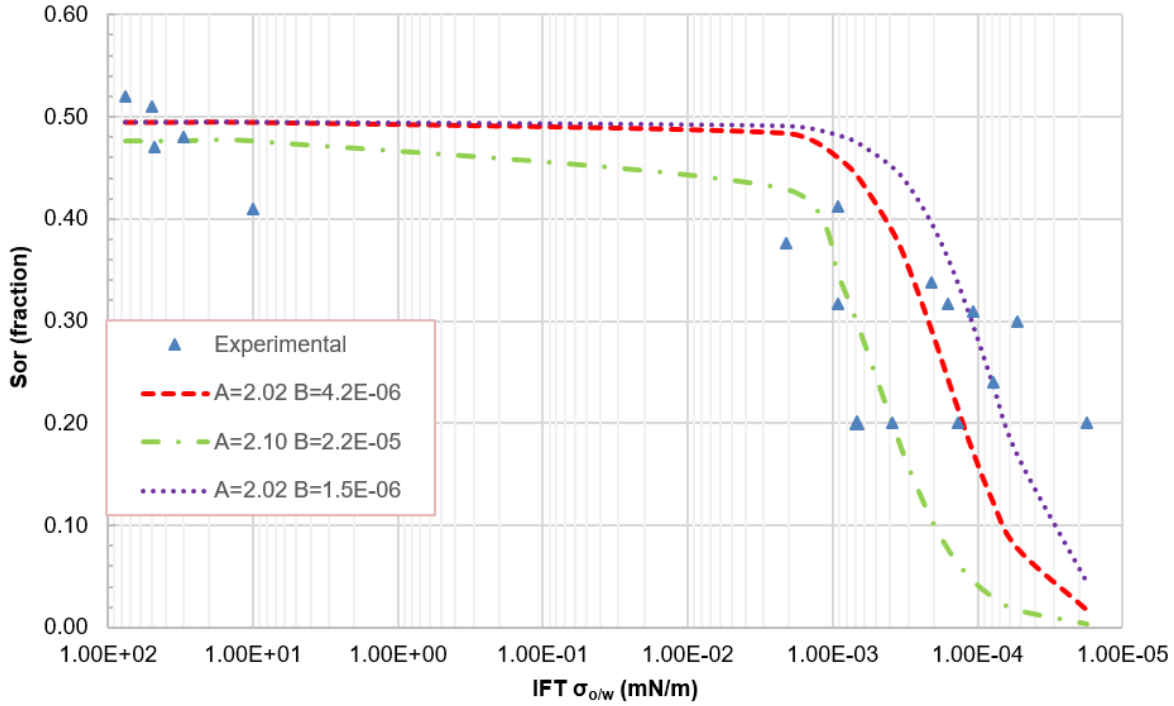


**Figure 6-52: Sor versus IFT for water flooding, S, AS, SP and ASP CEOR**

Capillary number curves were calculated using the fitted equation and results are presented in Figure 6-53. The residual oil saturation is not affected by the interfacial tension or equivalent capillary number until a value defined as the critical capillary number Nc_cr (Lake, 1989), where there is a deflection on the curve and Sor decreases with the increase of capillary number. The critical initial point of IFT from experiments was 0.002 mN/m and Nc above 1 x $10^{-03}$. For IFT lower than 0.002 mN/m, Sor is very sensitive to changes in IFT. According to the correlation model, there is another point of IFT where Sor is less sensitive to changes of IFT; however, the minimal Sor obtained for the conditions tested was 0.2.

As the capillary number represents the balance between viscous and capillary driving forces for the displacement of fluids in the porous media (Guo, H. *et al.*, 2015), it was demonstrated that the effect of the IFT on the SP and ASP reduces the Sor and increases the oil displacement efficiency for SP and ASP CEOR (Figure 6-53).

The final shape of the curve Sor versus capillary number and the critical capillary number Nc is associated with the type of rock, pore size distribution, relative permeability, and wettability. Capillary desaturation curves for the wetting and non-wetting phase are critical for the analysis of the fluid's distribution during CEOR processes.

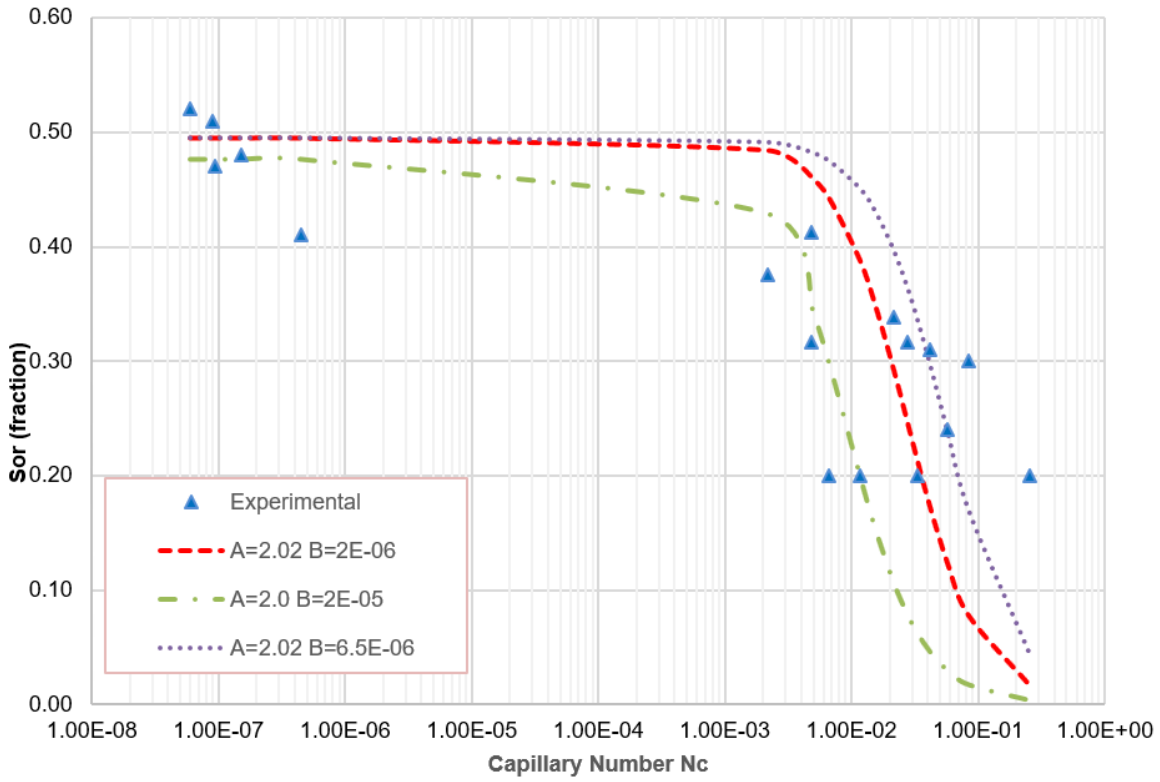


**Figure 6-53: Sor versus Nc for water flooding, S, AS, SP and ASP CEOR**

All optimal salinity values obtained from phase separation tests are lower than the salinity of the production brine available for injection. This result adds a requirement of the provision of SB for the preparation of the chemical slug of a CEOR project.

Comparing the combined effect of the brine composition, salinity gradient, and divalent cations $Ca^{2+}$ and $Mg^{2+}$ on the displacement efficiency ($E_D$) of water –flooding, it is noticed that $E_D$ is slightly increased by decreasing salinity and divalent ions (or divalent cations $Ca^{2+}$ and $Mg^{2+}$). An increase of 5% in oil recovery was achieved by decreasing the salinity by 5.1% TDS and 0.7% on divalent salts whereas 4% is obtained by the same salinity gradient with SB and not divalent ions (Figure 6-54).

There is a remarkable enhanced of $E_D$ by CEOR compared with water flooding. Results showed an increase of 15% injecting surfactant, 18-20% using SP and 30% using ASP. By adding only polymer, the displacement efficiency increases by a maximum of 25% using PHPA-6 and 15% for HMPAM-3. According to these results the displacement efficiency is ASP > P > AS>SP > LS > WF.

Similar differences in oil recovery have been reported from laboratory evaluation of CEOR (Ibrahim *et al.*, 2006). The salinity and divalent cations $Ca^{2+}$ and $Mg^{2+}$ limit the chemical formula and optimal salinity required for CEOR applications with a maximal concentration of divalent salts of 0.52% TDS and optimal salinity between 3.6 to 3.8% TDS (Figure 6-54).

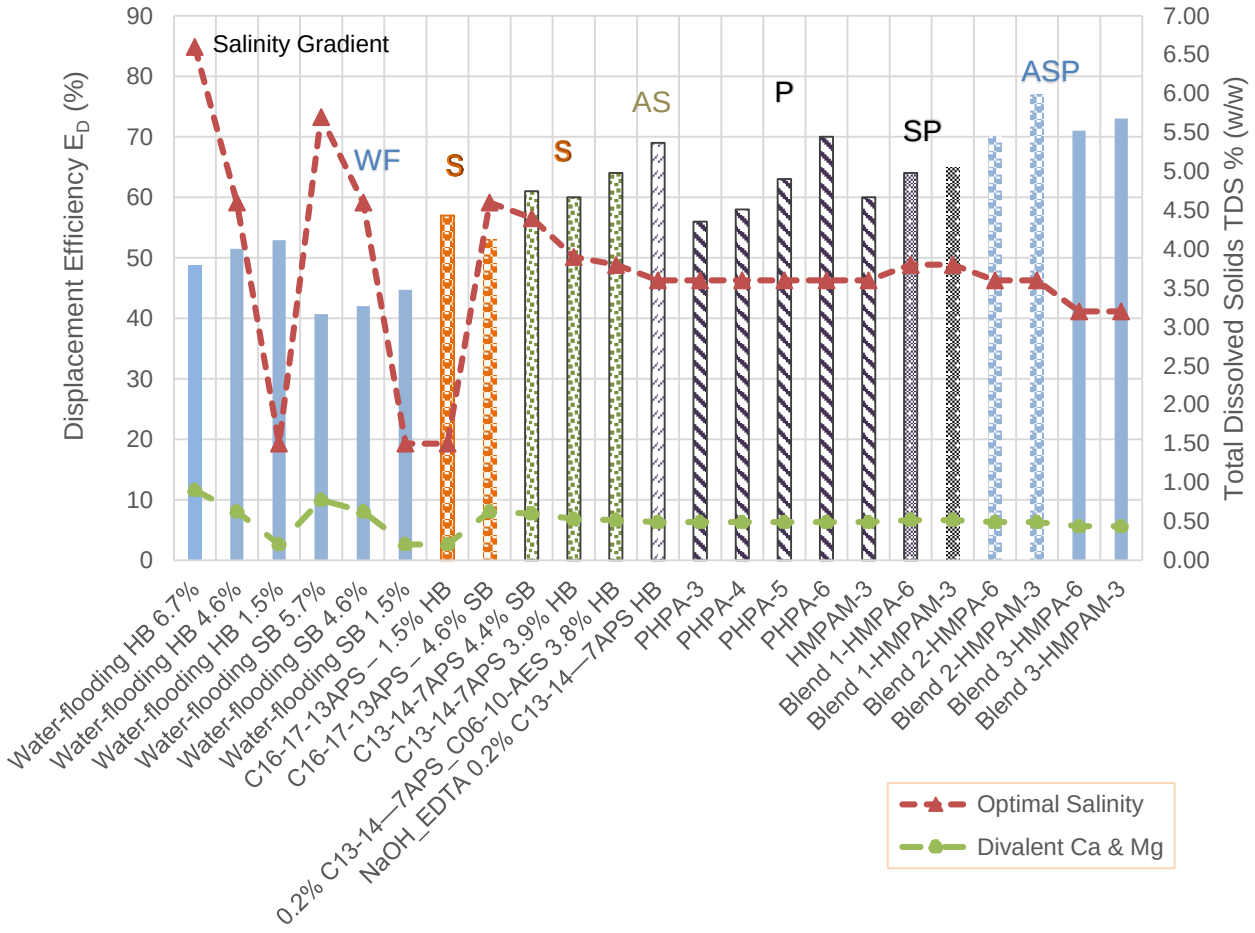


**Figure 6-54: Comparison of oil displacement efficiency for water flooding, low salinity, S, AS, P, SP and ASP CEOR, optimal salinity and divalent ions**

While S and AS CEOR processes increase $E_D$, the advantage of adding polymer shows incremental values (Figure 6-54). It is also noticed that the optimal salinity for the synergy CEOR determined by experiments is closed to the salinity of the seawater, which is also available for offshore CEOR applications. The role of salinity on the selection and performance of CEOR is defined by the optimal salinity of microemulsion and requirements for brine composition. The concentration of divalent ions is limited to 0.52% TDS (5,200 ppm), here the inclusion of divalent ions on requirements of screening for CEOR reported (Manrique *et al.*, 2010; Alvarado and Manrique, 2010).

# CHAPTER SEVEN: CONCLUSIONS AND RECOMMENDATIONS

## 7.1. Conclusions and contribution to knowledge

This project aimed to address the mechanisms and problems considered for the design of ASP CEOR in brines with high salinity and divalent cations or hardness. Interactions fluid-fluid and fluid-rock for the systems brine/oil, surfactant-brine/oil, alkali-surfactant-brine-oil, surfactant-polymer/oil, and alkali-surfactant-polymer/oil were studied at laboratory scale using Bentheimer sandstone core samples.

Several ionic interactions control the properties of the chemical slug and the effectiveness of the CEOR process. It was also evident that displacement tests using core-flooding and simulation of different cases are also required to understand the different interactions within the system fluid-fluid-rock and adjust experimental results at laboratory scale.

Salinity and divalent cations affect the IFT of the brine/oil interactions. The IFT declines at low salinity and then it raises at higher salinity, with two inflection points well identified at 5,000 ppm TDS and 40,000 ppm TDS. The presence of divalent cations has a higher effect than monovalent ions on decreasing IFT at lower salinity.

Divalent ions in the formation water affect the interactions brine/oil/rock and increase the oil recovery factor. There is an optimal salinity gradient during water flooding to favours maximal oil recovery, this salinity gradient was 1.4% TDS for HB and 4.2% TDS for SB.

Oil relative permeability curves for the system brine/oil/rock increase by the effect of the salinity gradient, whereas water relative permeability curves decrease at low salinity gradient and increase at a high salinity gradient. An expansion effect on the ionic layer adsorbed to the rock surface may be the cause of the effect of the low salinity gradient. At high salinity gradient, the proposed mechanism is the ion exchange of divalent cations $Ca^{2+}$ and $Mg^{2+}$ adsorbed on the rock by monovalent $Na^{+}$ in the injected brine, expanding the ionic layer on the rock surface.

The residual oil saturation as a function of the capillary number showed there is an effect of the salinity gradient and brine composition on the residual oil saturation. Capillary desaturation curves not only are affected by the type of rock, but also by the composition of formation water and the injected brine.

From the study of the surfactant-brine-oil and alkali-surfactant-brine-oil interactions, the complexity of the design of the chemical slug was evident, especially for interactions with alkali. The effect of brine salinity and hardness on the behaviour of surfactants and alkali is

revealed by the effect on the changes in the range of solubility and the optimal salinity of ultra-low three phase microemulsion.

Either surfactants with a short hydrophobic chain or a low number of alcohol alkoxy -sulfate (APS) can be used for formulations of surfactants slugs at high salinity. Long hydrophobic chain internal olefin sulfonate (IOS) surfactants also favour applications at high salinity and can be used as co-surfactants.

The combination of ethoxylated alcohol $C_{12-15}$-7EO and APS ($C_{13-14}$—7APS) surfactants increases the range of salinity and stability of the mixed system. The solubilisation ratio and IFT of surfactant $C_{13-14}$—7APS in the system brine/oil was enhanced by the co-surfactant $C_{06-10}$-AES.

The optimal salinity for microemulsion formation of surfactants depends on the ionic composition of the brine used for the preparation of the chemical slug. Divalent ions in the HB reduce the optimal salinity for the formation of the ultra-low IFT microemulsion for surfactant compared with SB. High salinity also restricts the use of the surfactant alcohol ethoxylated $C_{12-15}$-7EO.

Divalent ions react with alkali to form insoluble divalent hydroxides; this effect limits the pH of alkali-surfactant slugs to 9 (pH≤ 9). Salinity and ion composition determine the mechanism for alkali in terms of the formation of the natural surfactant as the reaction requires a pH > 9.

EDTA forms complexing structures with divalent ions $Ca^{2+}$ and $Mg^{2+}$, allowing the use of NaOH at controlled pH ≤ 9. The combination alkali-surfactant-EDTA showed the highest displacement efficiency from core-flooding experiments. EDTA is a promising additive for applications with divalent ions, however, the formulation is very sensitive to pH.

Surfactants reduce the interfacial tension (IFT) between oil/brine to ultra-low values and increase the oil displacement efficiency. Chemical adsorption of surfactants is affected by salinity. Co-surfactant $C_{06-10}$-AES reduces the adsorption of $C_{13-14}$—7APS. Absorption isotherms for surfactants and co-surfactants were better represented by Freundlich model.

It was found that polymers viscosity increases with polymer concentration and the effect is larger for HMPAM polymers. For both types of polymers (PHPA & HMPAM), the high molecular weight makes polymers more sensitive to salinity changes. This effect is stronger for HB. The viscosity of HMPAM polymers was less affected by polymer concentration compared with similar conditions for PHPA polymers.

While HMPAM behaves as a non-Newtonian shear-shining fluid, PHPA behaves as Newtonian at low shear rates (lower than 1 1/sec) and as non-Newtonian at intermediate shear rates (1-10 1/s). These differences need to be taken into consideration for the flow behaviour of polymer flooding and mobility ratio.

Published mathematical correlations were fine-tuned using experimental data to evaluate polymer viscosity as a function of polymer concentration, salinity and shear rate, and there was a good match for PHPA polymers however the correlation underestimates the viscosity of HMPAM polymers at high shear rate. The assumption of polymer viscosity similar to water viscosity at a high shear rate for polymers used in these correlations needs to be reviewed for HMPAM. HMPAM polymers are more sensitive to salinity changes and shear rate than PHPA polymer. However, PHPAM keeps a favourable mobility ratio under high salinity and shear rates.

Polymers reduce the mobility of the displacing fluid and the mobility ratio by permeability reduction and viscosity augmentation. The effect is reflected in the displacement efficiency $E_D$. Results from core-flooding CEOR tests with polymers demonstrated the advantages of this process with a maximal increase of 25% over water flooding for PHPA-6 and 16% for PHPAM-3.

The combination of polymers with AS shows that alkali-surfactant blends reduce polymer viscosity with small modifications in the rheological behaviour, turning the polymer behaviour to Newtonian from non-Newtonian. The viscosity of ASP microemulsion is remarkably different compared with AS microemulsions; the interfacial tension of ASP slugs is slightly increased by the polymer, but there is no appreciable change in the optimal salinity.

Results from core flooding tests for surfactant-polymers and alkali-surfactant-polymer demonstrate the advantages of using ASP for applications in divalent cations by using the complexing agent EDTA and keeping a buffer pH of 9 with the alkali. The use of EDTA with a controlled pH allowed the use of alkali for brine with concentration of divalent ions higher than 1,500 ppm.

The stability of chemicals in brine solution is limited by the concentration of divalent ions and not by the total salinity. Chemicals have good solubility in NaCl brines. High salinity affects the molecular interactions and reduces the viscosity of polymers; the effect is higher for hard brine with divalent ions.

The advantages of the synergy of SP and ASP were demonstrated on the displacement efficiency with a maximal increase of 30% for ASP with NaOH and EDTA. However, stoichiometry calculations are required to control equilibrium reactions involved in the process.

While the mechanism of polymer flooding is associated with mobility ratio, it was demonstrated the predominant effect of IFT on the displacement efficiency of SP and ASP systems for CEOR, which indicate the mechanism is dominated by the changes in the capillary number Nc.

The capillary desaturation curve, CDC, was obtained for chemical systems by adjusting an existing correlation between residual oil saturation (Sor) and IFT and Nc using experimental results from core-flooding tests and good agreement was obtained. This CDC correlation is required to calculate the oil saturation at different times during the fluid displacement inside the porous media.

The recovery factor of HMPAM-3 polymer as part of SP and ASP was better than for polymer PHPA-6. SP CEOR adds 19% oil recovery over water flooding, ASP adds 31% for blend 3 and 33% for blend 2. There are not significant differences between the oil recovery for SP and ASP. The tolerance to divalent ions is limited to 0.52% TDS, hence the importance of divalent ions on requirements of screening for CEOR processes.

### 7.2. Contribution to knowledge

This research presents a detailed study of the fluid-fluid and fluid-rock interactions that affect the design of SP and ASP CEOR at a microscopic scale.

The study proposes a systematic analysis of standalone methods, and the synergy of combined methods on the system fluid-fluid–rock for a sandstone rock.

Mathematical correlations that combined the effect of concentration, salinity and shear rate on polymer viscosity were fine-tuned using experimental results.

The methodology presented can define the range of applicability and conditions of CEOR at laboratory scale for oilfield applications.

### 7.3. Recommendations and future work

For this study reservoir conditions similar to an offshore, sandstone reservoir, with a constant temperature of 140 ºF were considered. The study can be extended to further evaluation at higher temperatures.

The control of precipitation by using EDTA can be explored more in detail, by the evaluation of solutions with alkalis of different strengths for applications with divalent ions. Besides, the analysis of the interactions EDTA-Rock with divalent ions adsorbed on the rock and the effect on the displacement efficiency also require further study.

.

# CHAPTER EIGHT: REFERENCES


Aghaeifar, Z., Puntervold, T., Strand, S., Austad, T., Maghsoudi, B. and Ferreira, J. d. C. (2018) Low Salinity EOR Effects After Seawater Flooding in a High Temperature and High Salinity Offshore Sandstone Reservoir, in: *SPE Norway One Day Seminar,* Society of Petroleum Engineers.

Al Adasani, A. and Bai, B. (2011) Analysis of EOR projects and updated screening criteria, *Journal of Petroleum Science and Engineering,* 79 (1), pp. 10-24. DOI: //doi.org/10.1016/j.petrol.2011.07.005.

Al Hashmi, A. R., Al Maamari, R. S., Al Shabibi, I. S., Mansoor, A. M., Zaitoun, A. and Al Sharji, H. H. (2013) Rheology and mechanical degradation of high-molecular-weight partially hydrolyzed polyacrylamide during flow through capillaries, *Journal of Petroleum Science and Engineering,* 105 , pp. 100-106. DOI: //doi.org/10.1016/j.petrol.2013.03.021.

Al-Bahar, M. A., Merrill, R., Peake, W., Jumaa, M. and Oskui, R. (2004) Evaluation of IOR potential within Kuwait, in: *Abu Dhabi International Conference and Exhibition,* Society of Petroleum Engineers.

Aliyu, S. (2009) Assessment of compositional heterogeneities of core samples from harding (9/23b-10) and gryphon (9/18b-17) oil columns, *Journal of Applied Sciences,* 9 (22), pp. 4032-4037.

Al-Mjeni, R., Arora, S., Cherukupalli, P., Van Wunnik, J., Edwards, J., Felber, B. J., Gurpinar, O., Hirasaki, G. J., Miller, C. A. and Jackson, C. (2010) Has the time come for EOR, *Oilfield Review,* 2011 (22), pp. 4.

Alvarado, V. and Manrique, E. (2010) Enhanced oil recovery: An update review, *Energies,* 3 (9), pp. 1529-1575.

Amaefule, J. O. and Handy, L. L. (1982) The effect of interfacial tensions on relative oil/water permeabilities of consolidated porous media, *Society of Petroleum Engineers Journal,* 22 (03), pp. 371-381.

American Petroleum Institute (1998) *Recommended practices for core analysis.* .

Anderson, D. R., Bidner, M. S., Davis, H. T., Manning, C. D. and Scriven, L. E. (1976) Interfacial Tension and Phase Behavior in Surfactant-Brine-Oil Systems, *SPE Improved Oil Recovery Symposium,* , pp. 12. DOI: 10.2118/5811-MS.

Anderson, W. (1986) Wettability literature survey-part 2: Wettability measurement, *Journal of Petroleum Technology,* 38 (11), pp. 1,24-1,262.

Arihara, N., Yoneyama, T., Akita, Y. and XiangGuo, L. (1999) Oil recovery mechanisms of alkali-surfactant-polymer flooding, in: *SPE Asia Pacific Oil and Gas Conference and Exhibition,* Society of Petroleum Engineers.

Askarinezhad, R. (2010) A new statistical approach to pore/throat size distribution of porous media using capillary pressure distribution concept, *Journal of Petroleum Science and Engineering,* 75 (1-2), pp. 100-104.

Ayirala, S., Al-Enezi, S. and Al-Yousef, A. (2017) A state of the art review to develop novel workflow for microscopic scale understanding of advanced water flooding mechanisms in carbonates, *Journal of Petroleum Science and Engineering,* 157 , pp. 530-546. DOI: 10.1016/j.petrol.2017.07.038.

Ayirala, S. and Yousef, A. (2014) Injection Water Chemistry Requirement Guidelines for IOR/EOR, in: SPE. DOI: 10.2118/169048-MS.

Azam, M. R., Tan, I. M., Ismail, L., Mushtaq, M., Nadeem, M. and Sagir, M. (2013) Static adsorption of anionic surfactant onto crushed berea sandstone, *Journal of Petroleum Exploration and Production Technology,* 3 (3), pp. 195-201. DOI: 10.1007/s13202-013-0057-y.

Bala, G. A., Duvall, M. L., Jackson, J. D. and Larsen, D. C. (1992) A flexible low-cost approach to improving oil recovery from a (very) small Minnelusa Sand reservoir in Crook County, Wyoming, in: *SPE/DOE Enhanced Oil Recovery Symposium,* Society of Petroleum Engineers.

Bataweel, M. A. (2011) *Enhanced Oil Recovery in High Salinity High Temperature Reservoir by Chemical Flooding.* Ph. D. dissertation, Texas A&M University, Texas, USA.

Bataweel, M. A. and Nasr-El-Din, H. A. (2012) ASP vs. SP flooding in high salinity/hardness and temperature in sandstone cores, in: *SPE EOR Conference at Oil and Gas West Asia,* Society of Petroleum Engineers.

Bazin, B., Tabary, R., Douarche, F., Moreau, P. and Oukhemanou, F. (2013) Impact of difficult environments on chemical flooding performance, in: *Saint Petersburg Russia - From Fundamental Science to Deployment: 17th European Symposium on Improved Oil Recovery, IOR,* .

Bera, A., Kumar, T., Ojha, K. and Mandal, A. (2013) Adsorption of surfactants on sand surface in enhanced oil recovery: Isotherms, kinetics and thermodynamic studies, *Applied Surface Science,* 284 , pp. 87-99.

Bera, A. and Mandal, A. (2015) Microemulsions: a novel approach to enhanced oil recovery: a review, *Journal of Petroleum Exploration and Production Technology,* 5 (3), pp. 255-268. DOI: 10.1007/s13202-014-0139-5.

Bera, A., Ojha, K., Mandal, A. and Kumar, T. (2011) Interfacial tension and phase behavior of surfactant-brine–oil system, *Colloids and Surfaces A: Physicochemical and Engineering Aspects,* 383 (1), pp. 114-119. DOI: //doi.org/10.1016/j.colsurfa.2011.03.035.

Berger, P. D. and Lee, C. H. (2006) Improved ASP process using organic alkali, in: *SPE/DOE Symposium on Improved Oil Recovery,* Society of Petroleum Engineers.

Boardman, R. S., Moore, L. J., Julian, M. H., Bilbrey, D. G. and Moore, J. S. (1982) Design and implementation of four enhanced recovery projects in Bay Fields of South Louisiana, in: *SPE Enhanced Oil Recovery Symposium,* Society of Petroleum Engineers.

Bourrel, M., Morel, D. C., Gauer, P. R., Levitt, D. and Chamerois, M. (2011) The Effect of a Non-Negative Salinity Gradient on ASP Flood Performance, in: SPE. DOI: 10.2118/144938-MS.

Centeno, M. A., Diaz, P. and Breda, A. (2017) Comparative Study of Polyacrylamide Co-polymers for EOR at High Salinity Conditions “Laboratory and Simulation, in: *IOR 2017-19th European Symposium on Improved Oil Recovery.*

Chang, H. (2013) Chapter 10 - ASP Process and Field Results, *Enhanced Oil Recovery Field Case Studies,* , pp. 203-249.

Chen, Z., Zhao, X., Wang, Z. and Fu, M. (2015) A comparative study of inorganic alkaline/polymer flooding and organic alkaline/polymer flooding for enhanced heavy oil recovery, *Colloids and Surfaces A: Physicochemical and Engineering Aspects,* 469 , pp. 150-157.

Chou, S. I. and Shah, D. O. (1981) The optimal salinity concept for oil displacement by oil-external microemulsions and graded salinity slugs, *Journal of Canadian Petroleum Technology,* 20 (03), pp. 10. DOI: 10.2118/81-03-08.

Computer Modeling Group Ltd (2015) *CMG-STARS User’s Manual.* .

Computer Modeling Group Ltd. (2015) *Winprop User’s Manual.* .

Craig, F. F. (1971) *The reservoir engineering aspects of waterflooding.* HL Doherty Memorial Fund of AIME New York.

Dake, L. P. (2001) *The practice of reservoir engineering (revised edition).* Elsevier.

Dang, C. T. Q., Nghiem, L. X., Chen, Z. J. and Nguyen, Q. P. (2013) Modeling low salinity waterflooding: ion exchange, geochemistry and wettability alteration, in: *SPE Annual Technical Conference and Exhibition,* Society of Petroleum Engineers.

de Melo, M. A., Holleben, C. R., Silva, I. G., de Barros Correia, A., Silva, G. A., Rosa, A. J., Lins Jr, A. G. and de Lima, J. C. (2005) Evaluation of polymer-injection projects in Brazil, in: *SPE Latin American and Caribbean Petroleum Engineering Conference,* Society of Petroleum Engineers.

Delshad, M., Han, C., Veedu, F. K. and Pope, G. A. (2013) A simplified model for simulations of alkaline–surfactant–polymer floods, *Journal of Petroleum Science and Engineering,* 108 , pp. 1-9.

Demin, W., Jiecheng, C., Junzheng, W., Zhenyu, Y. and Yuming, Y. (1999) Summary of ASP pilots in Daqing oil field, in: *SPE Asia Pacific Improved Oil Recovery Conference,* Society of Petroleum Engineers.

DeZabala, E. F., Vislocky, J. M., Rubin, E. and Radke, C. J. (1982) A chemical theory for linear alkaline flooding, *Society of Petroleum Engineers Journal,* 22 (02), pp. 245-258.

Dickson, J. L., Leahy-Dios, A. and Wylie, P. L. (2010) Development of improved hydrocarbon recovery screening methodologies, in: *SPE Improved Oil Recovery Symposium,* Society of Petroleum Engineers.

Doll, T. E. (1988) Performance Data Through 1987 of the Isenhour Unit, Sublette County, Wyoming, Polymer-Augmented Alkaline Flood, in: *SPE Rocky Mountain Regional Meeting,* Society of Petroleum Engineers.

dos Santos, A. P., Diehl, A. and Levin, Y. (2010) Surface tensions, surface potentials, and the hofmeister series of electrolyte solutions, *Langmuir,* 26 (13), pp. 10778-10783. DOI: 10.1021/la100604k.

Drelich, J., Fang, C. and White, C. L. (2002) Measurement of interfacial tension in fluid-fluid systems, *Encyclopedia of Surface and Colloid Science,* 3 , pp. 3158-3163.

Flaaten, A., Nguyen, Q., Pope, G. and Zhang, J. (2008) A systematic laboratory approach to low-cost, high-performance chemical flooding, in: *SPE Symposium on Improved Oil Recovery,* Society of Petroleum Engineers.

Flaaten, A., Nguyen, Q., Zhang, J., Mohammadi, H. and Pope, G. (2010) Alkaline/surfactant/polymer chemical flooding without the need for soft water, *SPE Journal,* 15 (01), pp. 184-196.

Gharbi, R. B. C. (2000) An expert system for selecting and designing EOR processes, *Journal of Petroleum Science and Engineering,* 27 (1), pp. 33-47. DOI: //doi.org/10.1016/S0920-4105(00)00049-8.

Glover, P. W. (2002) *Formation evaluation.* Université Laval: Québec, Canada.

Gogarty, W. B. (1976) Status of surfactant or micellar methods, *Journal of Petroleum Technology,* 28 (01), pp. 93-102.

Government of Western Australia. All rights reserved. (2017) *Understanding Salinity.* .

Goyal, K. L., Gupta, R. K., Nanda, S. K., Paul, A. K. and Sharma, P. (1991) Performance Evaluation of Caustic Pilot Project of North Gujarat Oil Field, India, in: *Middle East Oil Show,* Society of Petroleum Engineers.

Graue, D. J. and Johnson Jr, C. E. (1974) Field trial of caustic flooding process, *Journal of Petroleum Technology,* 26 (12), pp. 1,35-1,358.

Gregersen, C. S., Kazempour, M. and Alvarado, V. (2013) ASP design for the minnelusa formation under low-salinity conditions: Impacts of anhydrite on ASP performance, *Fuel,* 105 , pp. 368-382. DOI: //doi.org/10.1016/j.fuel.2012.06.051.

Guo, B. and Schechter, D. S. (1997) A simple and accurate method for determining low IFT from pendant drop measurements, in: *International Symposium on Oilfield Chemistry,* Society of Petroleum Engineers.

Guo, H., Dou, M., Hanqing, W., Wang, F., Yuanyuan, G., Yu, Z., Yansheng, W. and Li, Y. (2015) Review of capillary number in chemical enhanced oil recovery, in: *SPE Kuwait Oil and Gas Show and Conference,* Society of Petroleum Engineers.

Gurgel, A., Moura, M., Dantas, T., Neto, E. B. and Neto, A. D. (2008) A review on chemical flooding methods applied in enhanced oil recovery, *Brazilian Journal of Petroleum and Gas,* 2 (2).

Hadia, N. J., Ashraf, A., Tweheyo, M. T. and Torsæter, O. (2013) Laboratory investigation on effects of initial wettabilities on performance of low salinity waterflooding, *Journal of Petroleum Science and Engineering,* 105 , pp. 18-25. DOI: //doi.org/10.1016/j.petrol.2013.03.014.

Han, M., AlSofi, A., Fuseni, A., Zhou, X. and Hassan, S. (2013) Development of chemical EOR formulations for a high temperature and high salinity carbonate reservoir, in: *IPTC 2013: International Petroleum Technology Conference,* .

Healy, R. N., Reed, R. L. and Stenmark, D. G. (1976) Multiphase microemulsion systems, *Society of Petroleum Engineers Journal,* 16 (03), pp. 147-160.

Hernandez, C., Chacon, L. J., Lorenzo, A., Baldonedo, A., Jie, Q., Dowling, P. C. and Pitts, M. J. (2001) ASP system design for an offshore application in the La Salina Field, Lake Maracaibo, in: *SPE Latin American and Caribbean petroleum engineering conference,* Society of Petroleum Engineers.

Hilner, E., Andersson, M. P., Hassenkam, T., Matthiesen, J., Salino, P. A. and Stipp, S. L. S. (2015) *The effect of ionic strength on oil adhesion in sandstone – the search for the low salinity mechanism.* The Author(s).

Hirasaki, G., Miller, C. and Puerto, M. (2011) Recent advances in surfactant EOR, *SPE Journal,* 16 (04), pp. 889-907. DOI: 10.2118/115386-PA.

Hirasaki, G., van Domselaar, H. R. and Nelson, R. C. (1983) Evaluation of the salinity gradient concept in surfactant flooding, *Society of Petroleum Engineers Journal,* 23 (03), pp. 486-500. DOI: 10.2118/8825-PA.

Hirasaki, G. and Pope, G. (1974) Analysis of factors influencing mobility and adsorption in the flow of polymer solution through porous media, *Society of Petroleum Engineers Journal,* 14 (04), pp. 337-346.

Hongyan, W., Xulong, C., Jichao, Z. and Aimei, Z. (2009) Development and application of dilute surfactant–polymer flooding system for shengli oilfield, *Journal of Petroleum Science and Engineering,* 65 (1-2), pp. 45-50.

Hua, Z., Li, M., Ni, X., Wang, H., Yang, Z. and Lin, M. (2016) Effect of injection brine composition on wettability and oil recovery in sandstone reservoirs, *Fuel,* 182 , pp. 687-695.

Ibrahim, Z. B., Manap, A. A. A., Hamid, P. A., Hon, V. Y., Lim, P. H. and Wyatt, K. (2006) Laboratory aspect of chemical EOR processes evaluation for Malaysian oilfields, in: *SPE Asia Pacific Oil & Gas Conference and Exhibition,* Society of Petroleum Engineers.

Jamaloei, B. Y. (2009) Insight into the Chemistry of Surfactant-Based Enhanced Oil Recovery Processes, in: , pp. 1-10.

Jerauld, G. R., Webb, K. J., Lin, C. and Seccombe, J. (2006) Modeling low-salinity waterflooding, in: *SPE Annual Technical Conference and Exhibition,* Society of Petroleum Engineers.

Kakati, A. and Sangwai, J. S. (2017) Effect of monovalent and divalent salts on the interfacial tension of pure hydrocarbon-brine systems relevant for low salinity water flooding, *Journal of Petroleum Science and Engineering,* 157 , pp. 1106-1114. DOI: //doi.org/10.1016/j.petrol.2017.08.017.

Kalwar, S. A. and Elraies, K. A. (2014) A rheological study of polymer using precipitation inhibitor, alkali, and surfactant for high salinity in carbonate reservoirs, *Petroleum Science and Technology,* 32 (19), pp. 2329-2336. DOI: 10.1080/10916466.2013.823995.

Kaminsky, R. D., Wattenbarger, R. C., Szafranski, R. C. and Coutee, A. (2007) Guidelines for polymer flooding evaluation and development, in: *International petroleum technology conference,* International Petroleum Technology Conference.

Karpan, V., Farajzadeh, R., Zarubinska, M., Dijk, H., Matsuura, T. and Stoll, M. (2011) Selecting the "Right" ASP Model by History Matching Coreflood Experiments, in: Kuala Lumpur, Malaysia: Society of Petroleum Engineers, pp. 12.

Keelan, D. K. (1972) Core Analysis Techniques and Applications, in: Columbus, Ohio: Society of Petroleum Engineers, pp. 16.

Khanamiri, H. H., Torsæter, O. and Stensen, J. Å (2015) Experimental study of low salinity and optimal salinity surfactant injection, in: *EUROPEC 2015,* Society of Petroleum Engineers.

Kokal, S. and Al-Kaabi, A. (2010) Enhanced oil recovery: Challenges & opportunities, *World Petroleum Council: Official Publication,* 64 .

Konopnicki, D. T. and Zambrano, L. G. (1984) Application of the Alkaline Flooding Process in the Torrance Field, in: *SPE Enhanced Oil Recovery Symposium,* Society of Petroleum Engineers.

Kotlar, H. K., Selle, O. and Torsaeter, O. (2007) Enhanced oil recovery by comb flow: Polymer floods revitalized, in: *International Symposium on Oilfield Chemistry,* Society of Petroleum Engineers.

Kronberg, B., Holmberg, K. and Lindman, B. (2014) Surface chemistry of surfactants and polymers.

Kumar, S. and Mandal, A. (2016) Studies on interfacial behavior and wettability change phenomena by ionic and nonionic surfactants in presence of alkalis and salt for enhanced oil

recovery, *Applied Surface Science,* 372 , pp. 42-51. DOI: //doi.org/10.1016/j.apsusc.2016.03.024.

Kwak, J. C. (1998) *Polymer-surfactant systems.* CRC Press.

Lager, A., Webb, K. J. and Black, C. (2007) Impact of brine chemistry on oil recovery, in: *IOR 2007-14th European Symposium on Improved Oil Recovery,* .

Lake, L. W. (1989) *Enhanced oil recovery.* Old Tappan, NJ; Prentice Hall Inc.

Law, S., McDonald, A., Fellows, S., Reed, J. and Sutcliffe, P. G. (2015) Influence of clay content and type on oil recovery under low salinity waterflooding in North Sea reservoirs, in: *SPE Offshore Europe Conference and Exhibition,* Society of Petroleum Engineers.

Leroy, P., Lassin, A., Azaroual, M. and André, L. (2010) Predicting the surface tension of aqueous 1:1 electrolyte solutions at high salinity, *Geochimica Et Cosmochimica Acta,* 74 (19), pp. 5427-5442. DOI: //doi.org/10.1016/j.gca.2010.06.012.

Levitt, D. (2006) *Experimental evaluation of high performance EOR surfactants for a dolomite oil reservoir.* University of Texas at Austin.

Levitt, D., Pope, G. and Jouenne, S. (2011) Chemical degradation of polyacrylamide polymers under alkaline conditions, *SPE Reservoir Evaluation & Engineering,* 14 (03), pp. 281-286.

Levitt, D. and Pope, G. (2008) Selection and Screening of Polymers for Enhanced-Oil Recovery, in: SPE.

Liu, S. (2008) *Alkaline Surfactant Polymer enhanced oil recovery process.* Rice University.

Liu, S., Zhang, D., Yan, W., Puerto, M., Hirasaki, G. J. and Miller, C. A. (2008) Favorable attributes of alkaline-surfactant-polymer flooding, *SPE Journal,* 13 (01), pp. 5-16. DOI: 10.2118/99744-PA.

Lu, J., Pope, G. and Weerasooriya, U. (2013) Stability Investigation in Low-Tension Surfactant Floods, in: *SPE International Symposium on Oilfield Chemistry,* Society of Petroleum Engineers.

Mahmoud, M. A. and Abdelgawad, K. Z. (2015) Chelating-agent enhanced oil recovery for sandstone and carbonate reservoirs, *SPE Journal,* 20 (03), pp. 483-495. DOI: 10.2118/172183-PA.

Manrique, E. J., Muci, V. E. and Gurfinkel, M. E. (2007) EOR field experiences in carbonate reservoirs in the united states, *SPE Reservoir Evaluation & Engineering,* 10 (06), pp. 667-686.

Manrique, E. J., Thomas, C. P., Ravikiran, R., Izadi Kamouei, M., Lantz, M., Romero, J. L. and Alvarado, V. (2010) EOR: Current Status and Opportunities, in: Tulsa, Oklahoma, USA: Society of Petroleum Engineers, pp. 21.

Mansell, M. and Dean, A. A. (1994) Gryphon Water Injection: Reinfection Of Produced Water Supplemented By An Overlying Aquifer, in: *Offshore Technology Conference,* Offshore Technology Conference.

Manshad, A. K., Olad, M., Taghipour, S. A., Nowrouzi, I. and Mohammadi, A. H. (2016) Effects of water soluble ions on interfacial tension (IFT) between oil and brine in smart and carbonated smart water injection process in oil reservoirs, *Journal of Molecular Liquids,* 223 , pp. 987-993.

Mansour, A. M., Al-Maamari, R. S., Al-Hashmi, A. S., Zaitoun, A. and Al-Sharji, H. (2014) In-situ rheology and mechanical degradation of EOR polyacrylamide solutions under moderate shear rates, *Journal of Petroleum Science and Engineering,* 115 , pp. 57-65. DOI: //doi.org/10.1016/j.petrol.2014.02.009.

Marcus, Y. (2016) *Ionic liquid properties From Molten Salts to Room Temperature.* Springer.

Mayer, E. H. and Breit, V. S. (1986) Alkaline flood prediction studies, ranger VII pilot, wilmington field, california, *SPE Reservoir Engineering,* 1 (01), pp. 9-22.

Mayer, E. H., Berg, R. L., Carmichael, J. D. and Weinbrandt, R. M. (1983) Alkaline injection for enhanced oil recovery - A status report, *Journal of Petroleum Technology,* 35 (01), pp. 209-221. DOI: 10.2118/8848-PA.

Misak, M. D. (1968) Equations for determining 1/H versus S values in computer calculations of interfacial tension by the pendent drop method, *Journal of Colloid and Interface Science,* 27 , pp. 141-142.

Mishra, S., Bera, A. and Mandal, A. (2014) Effect of polymer adsorption on permeability reduction in enhanced oil recovery, *Journal of Petroleum Engineering,* 2014 .

Moeini, F., Hemmati-Sarapardeh, A., Ghazanfari, M., Masihi, M. and Ayatollahi, S. (2014) Toward mechanistic understanding of heavy crude oil/brine interfacial tension: The roles of salinity, temperature and pressure, *Fluid Phase Equilibria,* 375 , pp. 191-200. DOI: //doi.org/10.1016/j.fluid.2014.04.017.

Mohammad Salehi, M., Omidvar, P. and Naeimi, F. (2017) Salinity of injection water and its impact on oil recovery absolute permeability, residual oil saturation, interfacial tension and capillary pressure, *Egyptian Journal of Petroleum,* 26 (2), pp. 301-312. DOI: 10.1016/j.ejpe.2016.05.003.

Mohammadi, H. and Jerauld, G. (2012) Mechanistic modeling of the benefit of combining polymer with low salinity water for enhanced oil recovery, in: *SPE Improved Oil Recovery Symposium,* Society of Petroleum Engineers.

Mohammed, M. and Babadagli, T. (2015) Wettability alteration: A comprehensive review of materials/methods and testing the selected ones on heavy-oil containing oil-wet systems, *Advances in Colloid and Interface Science,* 220 , pp. 54-77. DOI: //doi.org/10.1016/j.cis.2015.02.006.

Mohnot, S. M., Bae, J. H. and Foley, W. L. (1987) A study of mineral/alkali reactions, *SPE Reservoir Engineering,* 2 (04), pp. 653-663. DOI: 10.2118/13032-PA.

Muggeridge, A., Cockin, A., Webb, K., Frampton, H., Collins, I., Moulds, T. and Salino, P. (2014) Recovery rates, enhanced oil recovery and technological limits, *Philosophical Transactions of the Royal Society A: Mathematical, Physical and Engineering Sciences,* 372 (2006), pp. 20120320. DOI: 10.1098/rsta.2012.0320.

Nasralla, R. A. and Nasr-El-Din, H. A. (2014) Impact of cation type and concentration in injected brine on oil recovery in sandstone reservoirs, *Journal of Petroleum Science and Engineering,* 122 , pp. 384-395. DOI: //doi.org/10.1016/j.petrol.2014.07.038.

Nelson, P. (2009) Pore-throat sizes in sandstones, tight sandstones, and shales, *AAPG Bulletin,* 93 (3), pp. 329-340. DOI: 10.1306/10240808059.

Nelson, R. (1982) The salinity-requirement diagram - A useful tool in chemical flooding research and development, *Society of Petroleum Engineers Journal,* 22 (2), pp. 259-270. DOI: 10.2118/8824-PA.

Nelson, R., Lawson, J., Stegemeier, G. and Thigpen, D. (1984) Cosurfactant-enhanced alkaline flooding, in: United States: .

Nimmo, J. R. (2004) Porosity and pore size distribution, *Encyclopedia of Soils in the Environment,* 3 (1), pp. 295-303.

OGA (2016) *Enhanced Oil Recovery Strategy.* Available from: “Available from” — https://www.ogauthority.co.uk/media/1143/eor_strategy_final-2016.pdf [Accessed 09/07/2019].

Olajire, A. A. (2014) Review of ASP EOR (alkaline surfactant polymer enhanced oil recovery) technology in the petroleum industry: Prospects and challenges, *Energy,* 77 , pp. 963-982. DOI: //doi.org/10.1016/j.energy.2014.09.005.

Pabón, R. and de Souza Filho, C. (2019) Crude oil spectral signatures and empirical models to derive API gravity, *Fuel,* 237 , pp. 1119-1131.

Park, S., Lee, E. S. and Sulaiman, W. R. W. (2015) Adsorption behaviors of surfactants for chemical flooding in enhanced oil recovery, *Journal of Industrial and Engineering Chemistry,* 21 , pp. 1239-1245. DOI: //doi.org/10.1016/j.jiec.2014.05.040.

Pei, H., Zhang, G., Ge, J., Jin, L. and Ma, C. (2013) Potential of alkaline flooding to enhance heavy oil recovery through water-in-oil emulsification, *Fuel,* 104 , pp. 284-293. DOI: //doi.org/10.1016/j.fuel.2012.08.024.

Pei, H., Zhang, G., Ge, J., Zhang, L. and Wang, H. (2014) Effect of polymer on the interaction of alkali with heavy oil and its use in improving oil recovery, *Colloids and Surfaces A: Physicochemical and Engineering Aspects,* 446 , pp. 57-64.

Petersen, P. B. and Saykally, R. J. (2005) Adsorption of ions to the surface of dilute electrolyte solutions: The Jones−Ray effect revisited, *Journal of the American Chemical Society,* 127 (44), pp. 15446-15452. DOI: 10.1021/ja053224w.

Petersen, P. B. and Saykally, R. J. (2004) Confirmation of enhanced anion concentration at the liquid water surface, *Chemical Physics Letters,* 397 (1), pp. 51-55. DOI: //doi.org/10.1016/j.cplett.2004.08.049.

Pitts, M. J., Wyatt, K. and Surkalo, H. (2004) Alkaline-Polymer Flooding of the David Pool, Lloydminster Alberta, in: *SPE/DOE Symposium on Improved Oil Recovery,* Society of Petroleum Engineers.

Pope, G. (2011) Recent developments and remaining challenges of enhanced oil recovery, *Journal of Petroleum Technology,* 63 (07), pp. 65-68.

Pope, G. and Delshad, M. (2000) Volume I: User's guide for UTCHEM-9.0, A three-dimensional chemical flood simulator, *Reservoir Engineering Research Program, University of Texas at Austin, Austin, TX, USA,* .

Pope, G. and Nelson, R. (1978) A chemical flooding compositional simulator, *Society of Petroleum Engineers Journal,* 18 (5), pp. 339-354. DOI: 10.2118/6725-PA.

Pope, G., Tsaur, K., Schechter, R. and Wang, B. (1982) The effect of several polymers on the phase behavior of micellar fluids, *Society of Petroleum Engineers Journal,* 22 (06), pp. 816-830. DOI: 10.2118/8826-PA.

Pouryousefy, E., Xie, Q. and Saeedi, A. (2016) Effect of multi-component ions exchange on low salinity EOR: Coupled geochemical simulation study, *Petroleum,* 2 (3), pp. 215-224.

RezaeiDoust, A., Puntervold, T. and Austad, T. (2010) A discussion of the low-salinity EOR potential for a North Sea sandstone field, in: *SPE Annual Technical Conference and Exhibition,* Society of Petroleum Engineers.

Rilian, N. A., Sumestry, M. and Wahyuningsih, W. (2010) Surfactant Stimulation to Increase Reserves in Carbonate Reservoir" A Case Study in Semoga Field", in: *SPE EUROPEC/EAGE Annual Conference and Exhibition,* Society of Petroleum Engineers.

Riswati, S. S., Bae, W., Park, C., Permadi, A. K., Efriza, I. and Min, B. (2019) Experimental analysis to design optimum phase type and salinity gradient of alkaline surfactant polymer flooding at low saline reservoir, *Journal of Petroleum Science and Engineering,* 173 , pp. 1005-1019. DOI: //doi.org/10.1016/j.petrol.2018.09.087.

Saboorian-Jooybari, H., Dejam, M. and Chen, Z. (2015) Half-century of heavy oil polymer flooding from laboratory core floods to pilot tests and field applications, in: *SPE Canada heavy oil technical conference,* Society of Petroleum Engineers.

Sahni, V., Dean, R., Britton, C., Kim, D., Weerasooriya, U. and Pope, G. (2010) The role of co-solvents and co-surfactants in making chemical floods robust, in: *SPE Improved Oil Recovery Symposium,* Society of Petroleum Engineers.

Salager, J., Antón, R. E., Sabatini, D. A., Harwell, J. H., Acosta, E. J. and Tolosa, L. I. (2005) Enhancing solubilization in microemulsions—state of the art and current trends, *Journal of Surfactants and Detergents,* 8 (1), pp. 3-21.

Sandrea, R. and Dharod, D. (2016) Approach screens reservoir candidates for EOR, *Oil & Gas Journal,* 114 (4), pp. 48-52.

Saxena, N., Kumar, A. and Mandal, A. (2019) Adsorption analysis of natural anionic surfactant for enhanced oil recovery: The role of mineralogy, salinity, alkalinity and nanoparticles, *Journal of Petroleum Science and Engineering,* 173 , pp. 1264-1283. DOI: //doi.org/10.1016/j.petrol.2018.11.002.

Shah, B. N., Lawrence, G., Willhite, P. and Green, D. W. (1978) The effect of inaccessible pore volume on the flow of polymer and solvent through porous media, in: *SPE Annual Fall Technical Conference and Exhibition,* Society of Petroleum Engineers.

ShamsiJazeyi, H., Verduzco, R. and Hirasaki, G. J. (2014) Reducing adsorption of anionic surfactant for enhanced oil recovery: Part I. competitive adsorption mechanism, *Colloids and Surfaces A: Physicochemical and Engineering Aspects,* 453 , pp. 162-167. DOI: //doi.org/10.1016/j.colsurfa.2013.10.042.

Sharma, H., Dufour, S., Arachchilage, Gayani W. P. Pinnawala, Weerasooriya, U., Pope, G. A. and Mohanty, K. (2015) Alternative alkalis for ASP flooding in anhydrite containing oil reservoirs, *Fuel,* 140 , pp. 407-420. DOI: //doi.org/10.1016/j.fuel.2014.09.082.

Shen, P., Wang, J., Yuan, S., Zhong, T. and Jia, X. (2009) Study of enhanced-oil-recovery mechanism of alkali/surfactant/polymer flooding in porous media from experiments, *Spe Journal,* 14 (02), pp. 237-244.

Shen, P., Zhu, B., Li, X. and Wu, Y. (2010) An experimental study of the influence of interfacial tension on water–oil two-phase relative permeability, *Transport in Porous Media,* 85 (2), pp. 505-520.

Shen, P., Zhu, B. and Wu, Y. (2005) The influence of interfacial tension on water-oil two-phase relative permeability, in: *SPE/DOE Symposium on Improved Oil Recovery,* 2006/1/1/Society of Petroleum Engineers.

Sheng, J. (2014a) A comprehensive review of alkaline–surfactant–polymer (ASP) flooding, *Asia-Pacific Journal of Chemical Engineering,* 9 (4), pp. 471-489. DOI: 10.1002/apj.1824.

Sheng, J. (2013a) A Comprehensive Review of Alkaline-Surfactant-Polymer (ASP) Flooding, in: Monterey, California, USA: Society of Petroleum Engineers, pp. 20.

Sheng, J. (2017) Critical review of alkaline-polymer flooding, *Journal of Petroleum Exploration and Production Technology,* 7 (1), pp. 147-153.

Sheng, J. (2014b) Critical review of low-salinity waterflooding, *Journal of Petroleum Science and Engineering,* 120 , pp. 216-224. DOI: //doi.org/10.1016/j.petrol.2014.05.026.

Sheng, J. (2013b) *Enhanced oil recovery field case studies.* Waltham, MA: Gulf Professional Publishing.

Sheng, J. (2015a) Investigation of alkaline–crude oil reaction, *Petroleum,* 1 (1), pp. 31-39.

Sheng, J. (2010a) *Modern chemical enhanced oil recovery: theory and practice.* Gulf Professional Publishing.

Sheng, J. (2010b) Optimum phase type and optimum salinity profile in surfactant flooding, *Journal of Petroleum Science and Engineering,* 75 (1), pp. 143-153. DOI: //doi.org/10.1016/j.petrol.2010.11.005.

Sheng, J. (2015b) Status of alkaline flooding technology, *J Petrol Eng Technol,* 5 (1), pp. 44-50.

Sheng, J. (2015c) Status of surfactant EOR technology, *Petroleum,* 1 (2), pp. 97-105.

Shepherd, A. G., Faber, M. J. and Bouwmeester, R. (2013) Systematic Investigation of Formulation for Chemical EOR: Back to Basics Production Chemistry Approach, in: *SPE Enhanced Oil Recovery Conference,* Society of Petroleum Engineers.

Somasundaran, P. and Krishnakumar, S. (1997) Adsorption of surfactants and polymers at the solid-liquid interface, *Colloids and Surfaces A: Physicochemical and Engineering Aspects,* 123 , pp. 491-513.

Spildo, K., Sun, L., Djurhuus, K. and Skauge, A. (2014) A strategy for low cost, effective surfactant injection, *Journal of Petroleum Science and Engineering,* 117 , pp. 8-14. DOI: //doi.org/10.1016/j.petrol.2014.03.006.

Strand, S., Puntervold, T. and Austad, T. (2016) Water based EOR from clastic oil reservoirs by wettability alteration: A review of chemical aspects, *Journal of Petroleum Science and Engineering,* 146 , pp. 1079-1091. DOI: //doi.org/10.1016/j.petrol.2016.08.012.

Taber, J., Martin, F. D. and Seright, R. S. (1997a) EOR screening criteria revisited-part 1: Introduction to screening criteria and enhanced recovery field projects, *SPE Reservoir Engineering,* 12 (03), pp. 189-198.

Taber, J., Martin, F. D. and Seright, R. S. (1997b) EOR screening criteria Revisited—Part 2: Applications and impact of oil prices, *SPE Reservoir Engineering,* 12 (03), pp. 199-206. DOI: 10.2118/39234-PA.

Tang, G. Q. and Morrow, N. R. (1997) Salinity, temperature, oil composition, and oil recovery by waterflooding, *SPE Reservoir Engineering,* 12 (04), pp. 269-276.

Thomas, S. (2008) Enhanced oil recovery - an overview, *Oil & Gas Science and Technology - Rev.IFP,* 63 (1), pp. 9-19. Available from: https://doi.org/10.2516/ogst:2007060.

Tichelkamp, T., Teigen, E., Nourani, M. and Øye, G. (2015) Systematic study of the effect of electrolyte composition on interfacial tensions between surfactant solutions and crude oils, *Chemical Engineering Science,* 132 , pp. 244-249.

Unalmiser, S. and Funk, J. J. (1998) Engineering core analysis, *Journal of Petroleum Technology,* 50 (04), pp. 106-114. DOI: 10.2118/36780-JPT.

Veerabhadrappa, S. K., Urbissinova, T., Trivedi, J. J. and Kuru, E. (2011) Polymer screening criteria for EOR application-a rheological characterization approach, in: *SPE Western North American Region Meeting,* Society of Petroleum Engineers.

Vermolen, E., Van Haasterecht, M. J., Masalmeh, S. K., Faber, M. J., Boersma, D. M. and Gruenenfelder, M. A. (2011) Pushing the envelope for polymer flooding towards high-temperature and high-salinity reservoirs with polyacrylamide based ter-polymers, in: *SPE middle east oil and gas show and conference,* Society of Petroleum Engineers.

Vledder, P., Gonzalez, I. E., Carrera Fonseca, J. C., Wells, T. and Ligthelm, D. J. (2010) Low salinity water flooding: proof of wettability alteration on a field wide scale, in: *SPE Improved Oil Recovery Symposium,* Society of Petroleum Engineers.

Wade, W. H., Morgan, J. C., Vasquez, E., Salager, J. L. and Schechter, R. S. (1979) Optimum formulation of surfactant/water/oil systems for minimum interfacial tension or phase behavior, *Society of Petroleum Engineers Journal,* 19 (2), pp. 107-115. DOI: 10.2118/7054-PA.

Walker, D., Britton, C., Kim, D. H., Dufour, S., Weerasooriya, U. and Pope, G. A. (2012) The impact of microemulsion viscosity on oil recovery, in: *SPE Improved Oil Recovery Symposium,* Society of Petroleum Engineers.

Wang, F., Kong, D., Guo, H., Li, Y., Li, B. and Li, Y. (2017) Lessons Learned From ASP Flooding Tests in China, in: Society of Petroleum Engineers.

Wang, J. and Dong, M. (2009) Optimum effective viscosity of polymer solution for improving heavy oil recovery, *Journal of Petroleum Science and Engineering,* 67 (3), pp. 155-158. DOI: 10.1016/j.petrol.2009.05.007.

Wang, Z., Le, X., Feng, Y. and Zhang, C. (2013) The role of matching relationship between polymer injection parameters and reservoirs in enhanced oil recovery, *Journal of Petroleum Science and Engineering,* 111 , pp. 139-143. DOI: //doi.org/10.1016/j.petrol.2013.07.011.

Wei, B., Lu, L., Pu, W., Jiang, F., Li, K., Sun, L. and Jin, F. (2017) From phase behavior to understand the dominant mechanism of Alkali-Surfactant-Polymer flooding in enhancing heavy oil recovery, *Journal of Surfactants and Detergents,* 20 (2), pp. 355-366.

Wever, D. A. Z., Picchioni, F. and Broekhuis, A. A. (2011) Polymers for enhanced oil recovery: A paradigm for structure–property relationship in aqueous solution, *Progress in Polymer Science,* 36 (11), pp. 1558-1628. DOI: //doi.org/10.1016/j.progpolymsci.2011.05.006.

Wu, X., Han, M., Zahrani, B. H. and Guo, L. (2015) Effect of Surfactant-Polymer Interaction on the Interfacial Properties for Chemical EOR, in: Manama, Bahrain: Society of Petroleum Engineers, pp. 9.

Wu, Y., Shuler, P. J., Blanco, M., Tang, Y. and Goddard, W. A. (2005) A study of branched alcohol propoxylate sulfate surfactants for improved oil recovery, in: *SPE Annual Technical Conference and Exhibition,* Society of Petroleum Engineers.

Xie, J., Chung, B. C. and Leung, L. (2008) Design and Implementation of a Caustic Flooding EOR Pilot at Court Bakken Heavy Oil Reservoir, in: Calgary, Alberta, Canada: Society of Petroleum Engineers, pp. 7.

Xie, X., Weiss, W. W., Tong, Z. J. and Morrow, N. R. (2005) Improved oil recovery from carbonate reservoirs by chemical stimulation, *SPE Journal,* 10 (03), pp. 276-285.

Yan, P. and Xiao, J. (2004) Polymer–surfactant interaction: Differences between alkyl sulfate and alkyl sulfonate, *Colloids and Surfaces A: Physicochemical and Engineering Aspects,* 244 (1), pp. 39-44. DOI: //doi.org/10.1016/j.colsurfa.2004.06.023.

Yang, D., Wang, J., Jing, L., Feng, Q. and Ma, X. (2010) Case Study of Alkali-Polymer Flooding with Treated Produced Water, in: *SPE EOR Conference at Oil & Gas West Asia,* Society of Petroleum Engineers.

Yang, H. D. and Wadleigh, E. E. (2000) Dilute surfactant IOR-design improvement for massive, fractured carbonate applications, in: *SPE International Petroleum Conference and Exhibition in Mexico,* Society of Petroleum Engineers.

Zerpa, L. E., Queipo, N. V., Pintos, S. and Salager, J. (2005) An optimization methodology of alkaline–surfactant–polymer flooding processes using field scale numerical simulation and multiple surrogates, *Journal of Petroleum Science and Engineering,* 47 (3), pp. 197-208. DOI: //doi.org/10.1016/j.petrol.2005.03.002.

Zhang, D., Liu, S., Yan, W., Puerto, M., Hirasaki, G. and Miller, C. (2006) Favorable Attributes of Alkali-Surfactant-Polymer Flooding, in: Tulsa, Oklahoma, USA: Society of Petroleum Engineers, pp. 13.

Zhang, J., Wang, K., He, F. and Zhang, F. (1999) Ultimate evaluation of the alkali/polymer combination flooding pilot test in XingLongTai oil field, in: *SPE Asia Pacific Improved Oil Recovery Conference,* Society of Petroleum Engineers.

Zhu, Y., Lei, M. and Zhu, Z. (2015) Development and performance of salt-resistant polymers for chemical flooding, in: *SPE Middle East Oil and Gas Show and Conference, MEOS, Proceedings,* , pp. 2559-2572.

Zhu, Y. Y., Luo, W. L., Jian, G. Q., Wang, C. A., Hou, Q. F. and Niu, J. L. (2012) Development and performance of water soluble salt-resistant polymers for chemical flooding, in: *Advanced Materials Research,* Trans Tech Publ, pp. 227-235.

ZHU, Y., ZHANG, Y., NIU, J., LIU, W. and HOU, Q. (2012) The research progress in the alkali-free surfactant-polymer combination flooding technique, in: , pp. 371-376.

Zubari, H. K. and Sivakumar, V. C. (2003) Single well tests to determine the efficiency of alkaline-surfactant injection in a highly oil-wet limestone reservoir, in: *Middle East Oil Show,* Society of Petroleum Engineers.

# Appendix A

## 9.1 Protocol followed to fine tune parameters of the Flory-Huggins and Meter and Bird correlation

The effect of combined variables on the resultant viscosity of polymers was analysed based on the fine tuning of parameters of the Flory-Huggins (included in chapter 2- equations 2-41 and 2-42) and Meter and Bird correlation (1964) as cited by Sheng (2011) (chapter 2- equation 2-43).

1. From Flory-Huggins correlation (included in chapter 2- equations 2-41 and 2-42), an expression to calculate the variable $S_p$ was derived as follow:

$$\frac{\mu_p^0-\mu_w}{\mu_w} = (A_{p1}C_p + A_{p2}C_p^2 + A_{p3}C_p^3)C_{sep}^{S_p} \quad (9\text{-}1)$$

2. A graphical representation of the relation of viscosities $\frac{\mu_p^0-\mu_w}{\mu_w}$ versus the effective salinity $C_{sep}$ in a log-log scale was fitted to linear trend line with an R square value close to 1.
3. Determination of Sp parameter from the slope of the graph, an example is presented in Figure 9-1 below. The Sp parameter represents the dependency of the apparently viscosity with salinity on equation 9-1, the values obtained are negative which demonstrate a reduction of viscosity by the effect of salinity. The slope on the example in Figure 9-1 is -0.357 as the graphs is in a log-log scale.

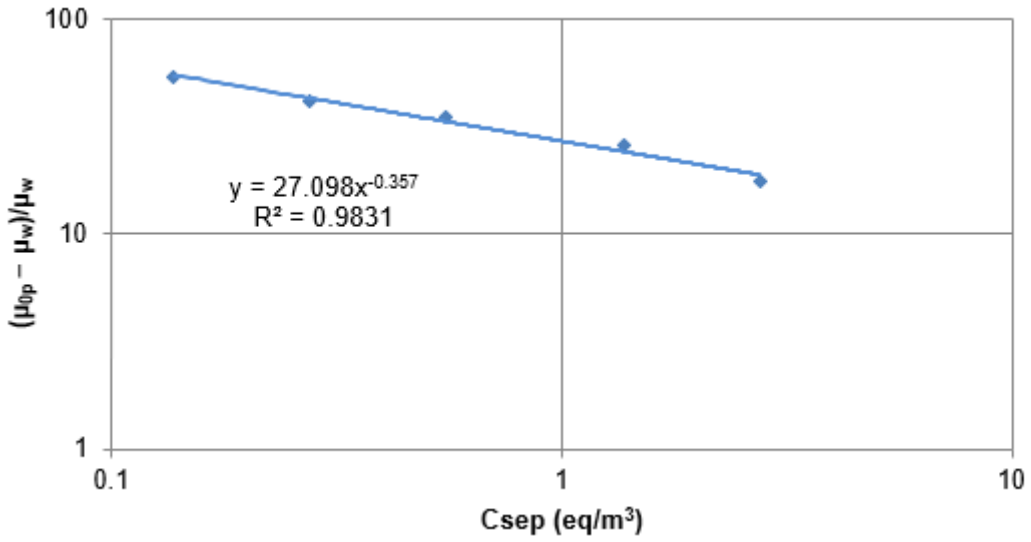


**Figure 9-1: Log-Log graph of $\frac{\mu_p^0-\mu_w}{\mu_w}$ versus Csep used to determine the value of Sp= -0.357 with a value of βp=10.2 for PHPA-3 polymer**

4. A third order polynomial adjustment of polymer viscosity versus polymer concentration is performed to estimate AP1, AP2, AP3 of the polynomial correlation of equation 9-1. Example for polymer HMPAM-4 is showed in Figure 9-2.

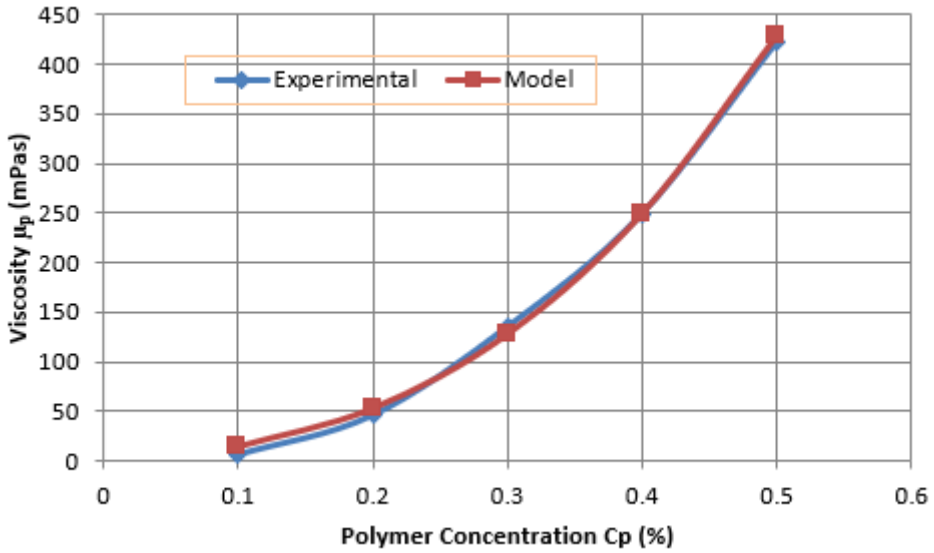


**Figure 9-2: Viscosity vs Polymer Concentration measured and calculated for HMPAM-4 polymer**

5. Graphical representation of apparent viscosity ($\mu_p$) versus shear rate $\gamma$ for the different polymers and fitting the value of $\gamma_{1/2}$ that will minimize the differences in viscosity $\mu_{p0}$ calculated by using Meter's equation (chapter 2- equation 2-43) (Meter and Bird, 1964) and Flory-Huggins correlations, equation 6-1. An example is presented in Figure 9-3 for HMPAM-4 with fitting parameters for the model curve included in Table 9-1.

**Table 9-1: Fitting values of Pα, $\gamma_{1/2}$ and $\gamma_c$ for polymer HMPAM-4**

| | | |
|---|---|---|
| **$\mu_w$** | **2.5** | **cp** |
| **μ0** | **659** | **cp** |
| **Pα** | **1.74** | |
| **$\gamma_{1/2}$** | **0.88** | **1/sec** |

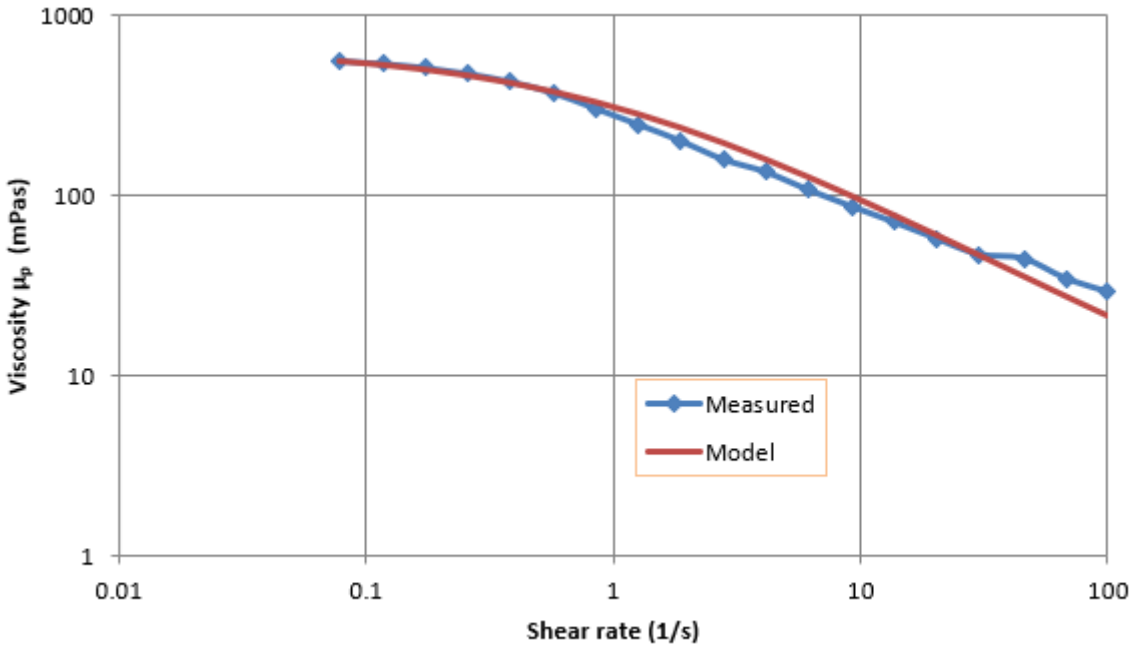


**Figure 9-3: Log-Log graph of viscosity versus shear rate in order to determine the value of Pα, $\gamma_{1/2}$ for polymer HMPAM-4 polymer**

The value of $\gamma_{1/2}$ is relevant as the inverse of its value is an indication of the relaxation time or time factor of polymer λ, which is an indication of how the polymer release the stress under constant strain or how the polymer viscosity is affected by shear rate. The higher the value of $\gamma_{1/2}$ is, the less the viscosity is affected by shear rate (Veerabhadrappa *et al.*, 2011; Al Hashmi *et al.*, 2013).

## 9.2 PVT Data for the crude oil

### Summary of PVT Data - Physically Recombined Reservoir Fluid

**Partial Constant Composition Expansion at 140°F**

| | |
|---|---|
| Bubble point pressure | 2430 psig |
| Density at saturation pressure | 0.8576 g cm-3 |

**Separator Test Data**

| Pressure (psig) | Temperature (°F) | Formation Volume Factor Bofb (1) | Total Solution Gas-oil ratio (scf/bbl) Rsfb (2) | Stocktank Oil Density (g cm-3) |
|---|---|---|---|---|
| 2430 | 140 | 1.114 | 245 | |
| 149 | 113 | | | |
| 0 | 60 | | | 0.9269 (API =21.0°) |

### Compositional Analysis of Physically Recombined Reservoir Fluid to C36+

| | Component | Mole % | Weight % |
|---|---|---|---|
| $H_2$ | Hydrogen | 0.00 | 0.00 |
| $H_2S$ | Hydrogen sulphide | 0.00 | 0.00 |
| $CO_2$ | Carbon dioxide | 0.94 | 0.20 |
| $N_2$ | Nitrogen | 0.05 | 0.01 |
| $C_1$ | Methane | 36.90 | 2.91 |
| $C_2$ | Ethane | 2.06 | 0.31 |
| $C_3$ | Propane | 0.36 | 0.08 |
| $iC_4$ | i-Butane | 0.10 | 0.03 |
| $nC_4$ | n-Butane | 0.16 | 0.04 |
| $C_5$ | neo-Pentane | 0.01 | 0.00 |
| $iC_5$ | i-Pentane | 0.07 | 0.02 |
| $nC_5$ | n-Pentane | 0.07 | 0.03 |
| $C_6$ | Hexanes | 0.14 | 0.06 |
| | Me-Cyclo-pentane | 0.07 | 0.03 |
| | Benzene | 0.01 | 0.00 |
| | Cyclo-hexane | 0.09 | 0.04 |
| $C_7$ | Heptanes | 0.14 | 0.07 |
| | Me-Cyclo-hexane | 0.11 | 0.06 |
| | Toluene | 0.02 | 0.01 |
| $C_8$ | Octanes | 0.17 | 0.10 |
| | Ethyl-benzene | 0.02 | 0.01 |
| | Meta/Para-xylene | 0.01 | 0.01 |
| | Ortho-xylene | 0.04 | 0.02 |
| $C_9$ | Nonanes | 0.32 | 0.20 |
| | Tri-Me-benzene | 0.10 | 0.06 |
| $C_{10}$ | Decanes | 1.14 | 0.80 |
| $C_{11}$ | Undecanes | 1.90 | 1.37 |
| $C_{12}$ | Dodecanes | 2.65 | 2.10 |
| $C_{13}$ | Tridecanes | 3.19 | 2.75 |
| $C_{14}$ | Tetradecanes | 3.56 | 3.33 |
| $C_{15}$ | Pentadecanes | 3.83 | 3.89 |
| $C_{16}$ | Hexadecanes | 3.57 | 3.90 |
| $C_{17}$ | Heptadecanes | 3.13 | 3.65 |
| $C_{18}$ | Octadecanes | 3.07 | 3.79 |
| $C_{19}$ | Nonadecanes | 2.97 | 3.84 |
| $C_{20}$ | Eicosanes | 2.65 | 3.59 |
| $C_{21}$ | Heneicosanes | 2.41 | 3.46 |
| $C_{22}$ | Docosanes | 2.16 | 3.25 |
| $C_{23}$ | Tricosanes | 1.91 | 3.00 |
| $C_{24}$ | Tetracosanes | 1.76 | 2.86 |
| $C_{25}$ | Pentacosanes | 1.55 | 2.64 |
| $C_{26}$ | Hexacosanes | 1.43 | 2.52 |
| $C_{27}$ | Heptacosanes | 1.28 | 2.35 |
| $C_{28}$ | Octacosanes | 1.30 | 2.49 |
| $C_{29}$ | Nonacosanes | 1.23 | 2.44 |
| $C_{30}$ | Triacontanes | 1.17 | 2.41 |
| $C_{31}$ | Hentriacontanes | 1.05 | 2.22 |
| $C_{32}$ | Dotriacontanes | 0.93 | 2.04 |
| $C_{33}$ | Tritriacontanes | 0.83 | 1.88 |
| $C_{34}$ | Tetratriacontanes | 0.76 | 1.76 |
| $C_{35}$ | Pentatriacontanes | 0.69 | 1.66 |
| $C_{36+}$ | Hexatriacontanes plus | 5.92 | 25.71 |
| | Totals : | 100.00 | 100.00 |

Note: 0.00 means < 0.005.

## 9.3 Results from history match of core-flooding using simulation model

The core flooding experiments were simulated using the software CMG START. A 2D model at a laboratory scale was built as explained in chapter 3. The experimental core-flooding tests were simulated in order to history match experimental results and compare saturation profile of the samples for the different cases. The cases evaluated are presented as follow:

a- Water-flooding with HB followed by surfactant flooding $C_{16-17}$- 13 APS at optimal salinity 1.5% using HB, Figure 9-4.

b- Water-flooding with SB followed by surfactant flooding $C_{16-17}$- 13 APS and surfactant flooding at optimal salinity 4.6% for SB, Figure 9-5.

c- Water-flooding with HB followed by surfactant flooding $C_{13-14}$- 7 APS at optimal salinity 3.9% for HB, figure 9-6.

d- Water-flooding with HB followed by the blend surfactant/co-surfactant flooding at optimal salinity for HB, figure 9-7.

e- Water-flooding with HB and alkali/surfactant/EDTA flooding at optimal salinity for HB, Figure 9-8.

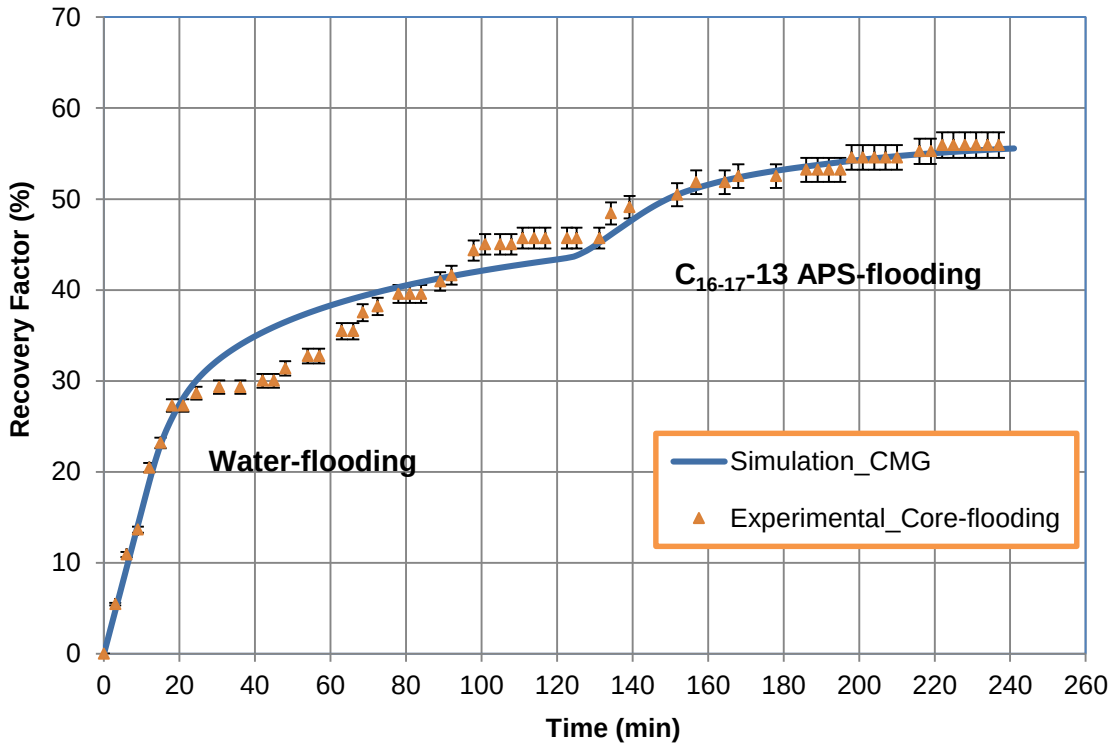


**Figure 9-4: History matched of core-flooding and 2D simulation for recovery factor for water-flooding with HB and CEOR using surfactant $C_{16-17}$- 13 APS at optimal salinity 1.5%**

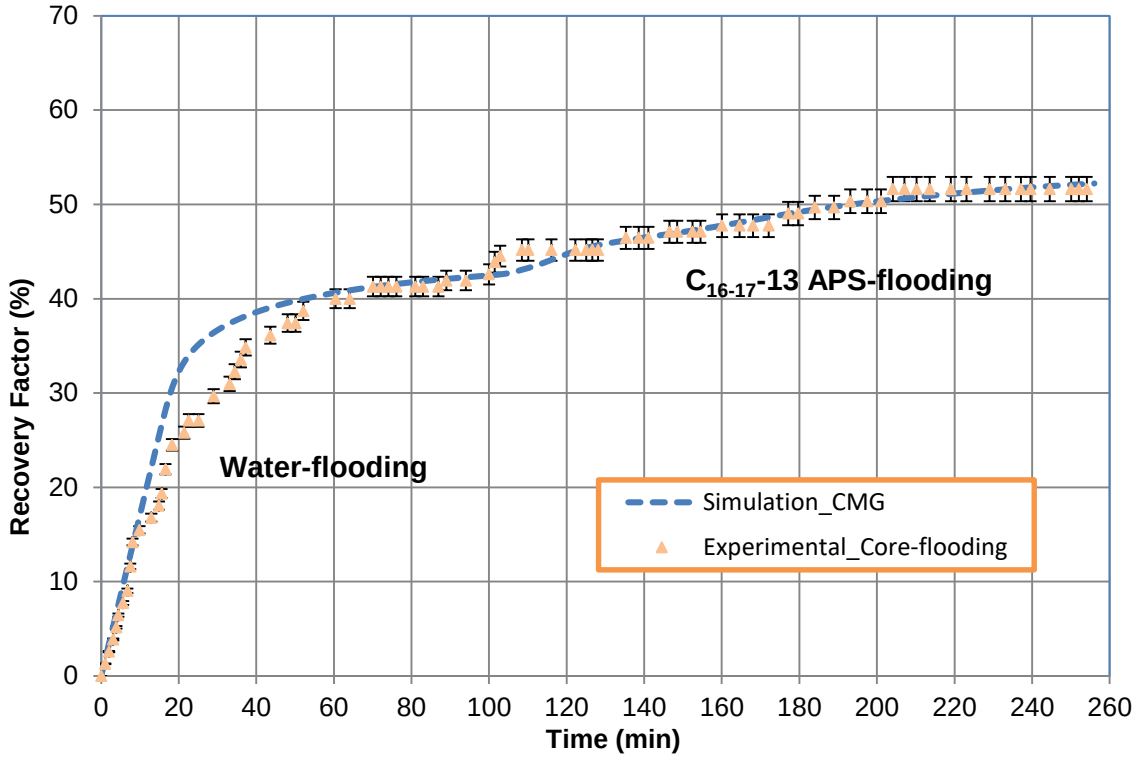


Figure 9-5: History matched of core-flooding and 2D simulation for recovery factor for water-flooding with SB and CEOR using surfactant $C_{16-17}$-13 APS at optimal salinity 4.6%

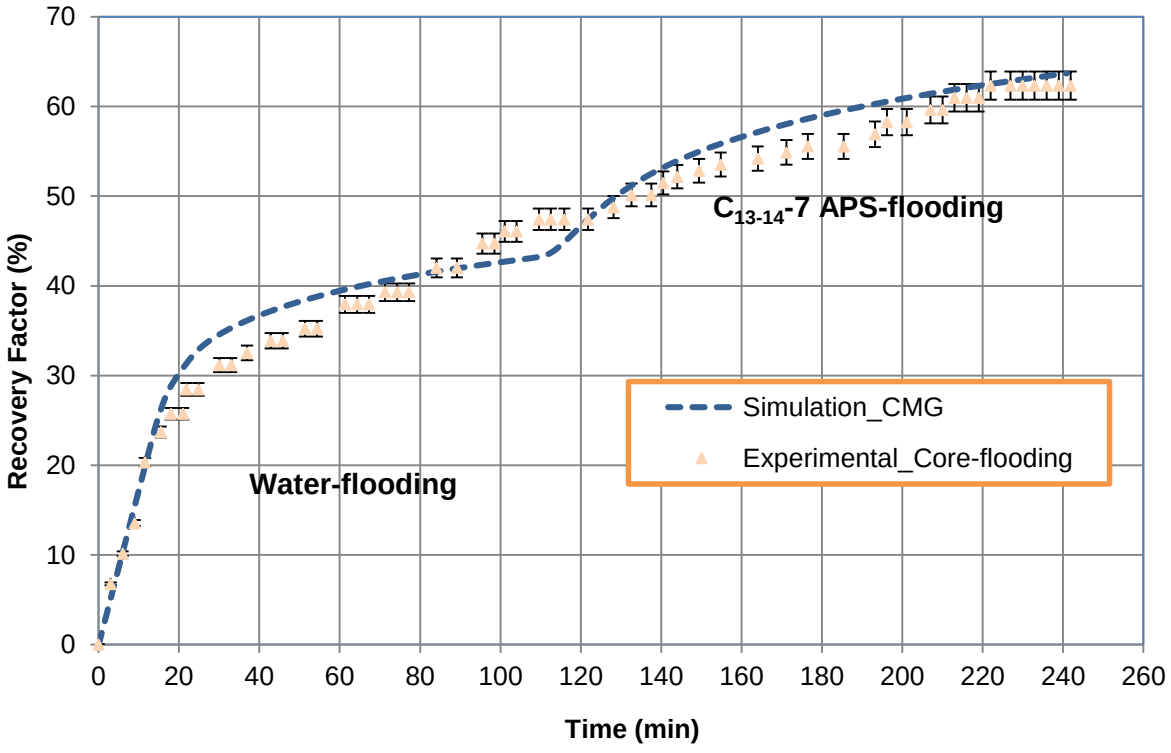


Figure 9-6: History matched of core-flooding and 2D simulation for recovery factor for water-flooding with HB and CEOR using surfactant C13-C14- 7 APS at optimal salinity 3.9%

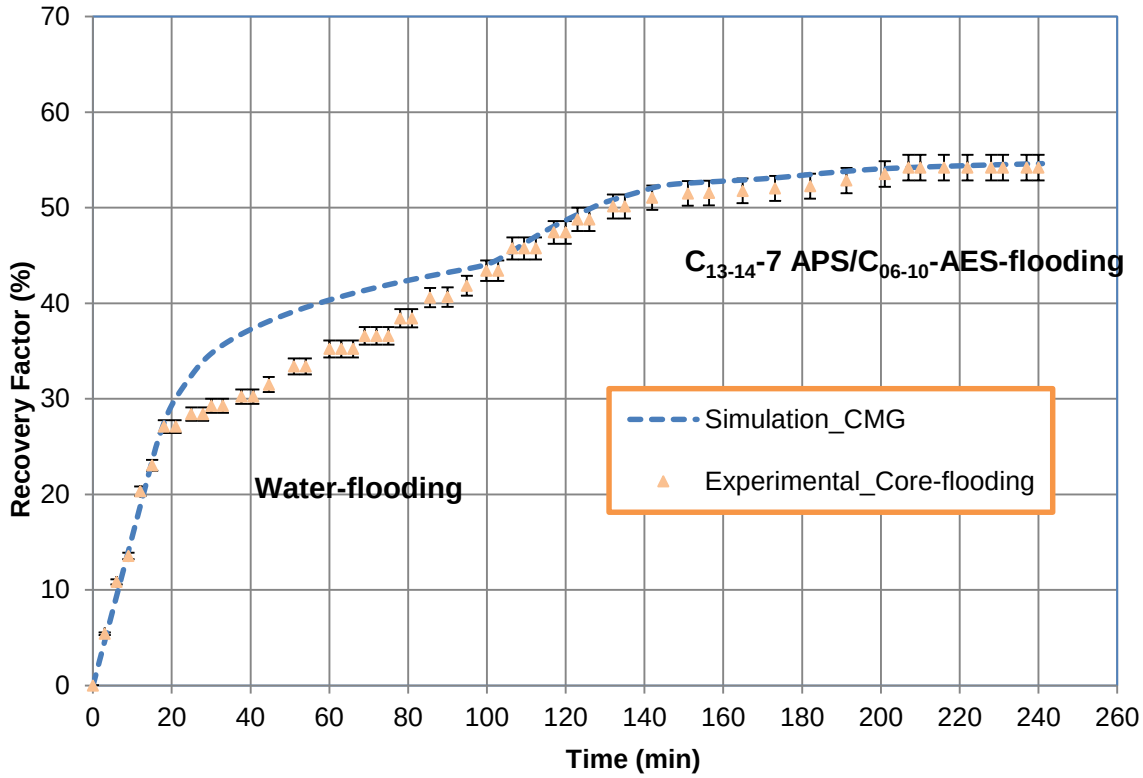


Figure 9-7: History matched of core-flooding and 2D simulation for recovery factor for water-flooding with HB and CEOR using surfactant C13-14—7APS_C06-10-AES HB at optimal salinity 3.8%

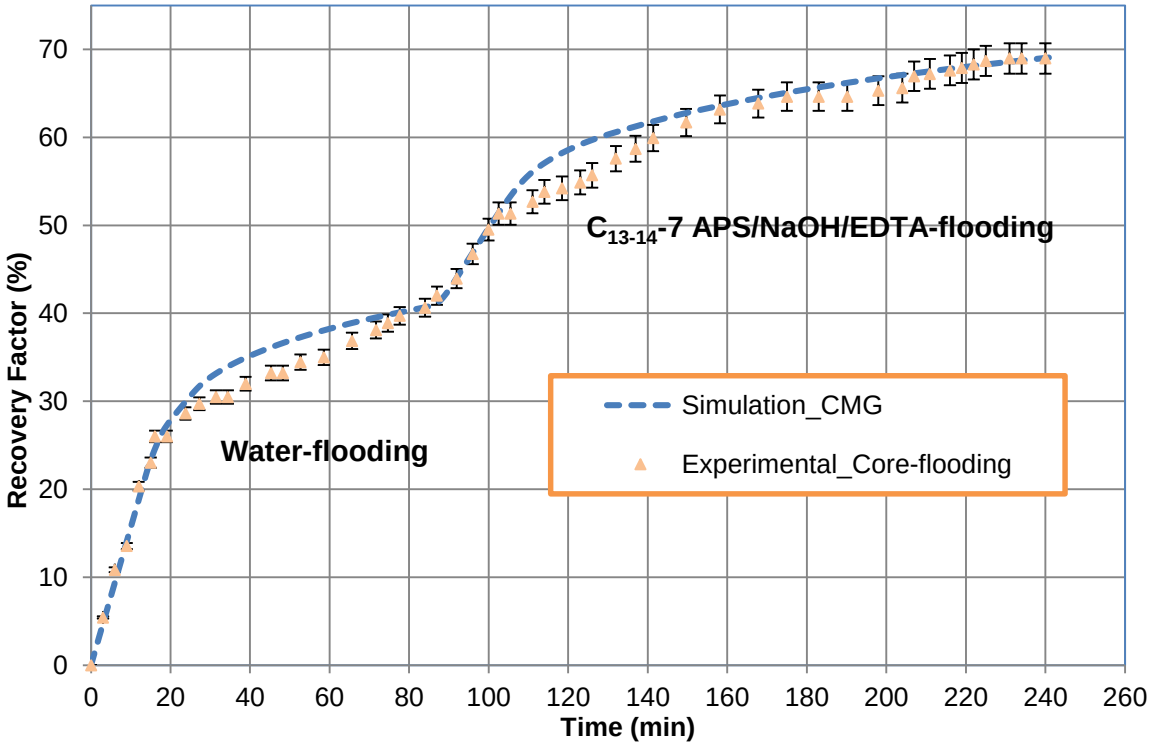


Figure 9-8: History matched of core-flooding and 2D simulation for recovery factor for water-flooding with HB and CEOR using surfactant C13-14—7APS HB with NaOH/EDTA, at optimal salinity 3.5%